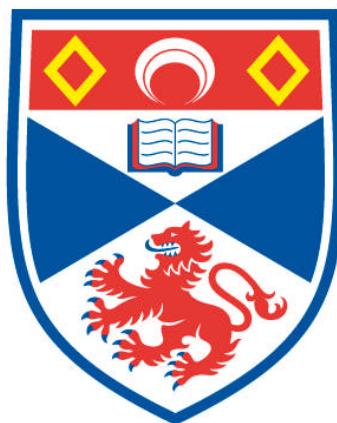


**EMERGENCE IN COMPLEX SYSTEMS BASED ON
SYNTHETIC REPLICATORS**

Juergen Huck

**A Thesis Submitted for the Degree of PhD
at the
University of St Andrews**



2011

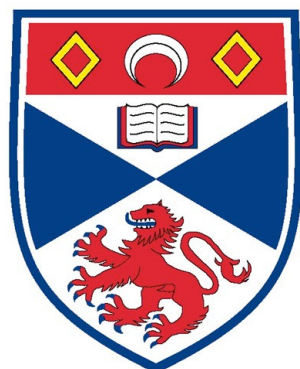
**Full metadata for this item is available in
Research@StAndrews:FullText
at:**

<http://research-repository.st-andrews.ac.uk/>

Please use this identifier to cite or link to this item:

<http://hdl.handle.net/10023/3067>

This item is protected by original copyright



Emergence in Complex Systems Based on Synthetic Replicators

by

Juergen Huck

A thesis submitted to the School of Chemistry, University of St Andrews,
for the degree of Doctor of Philosophy,
June 2011

1. Candidate's declarations:

I, Juergen Huck, hereby certify that this thesis, which is approximately 80,000 words in length, has been written by me, that it is the record of work carried out by me and that it has not been submitted in any previous application for a higher degree.

I was admitted as a candidate for the degree of PhD in February 2007; the higher study for which this is a record was carried out in the University of St Andrews between 2007 and 2010.

Date 15/7/2011 signature of candidate

2. Supervisor's declaration:

I hereby certify that the candidate has fulfilled the conditions of the Resolution and Regulations appropriate for the degree of PhD in the University of St Andrews and that the candidate is qualified to submit this thesis in application for that degree.

Date 15/7/2011 signature of supervisor

3. Permission for electronic publication: *(to be signed by both candidate and supervisor)*

In submitting this thesis to the University of St Andrews we understand that we are giving permission for it to be made available for use in accordance with the regulations of the University Library for the time being in force, subject to any copyright vested in the work not being affected thereby. We also understand that the title and the abstract will be published, and that a copy of the work may be made and supplied to any bona fide library or research worker, that my thesis will be electronically accessible for personal or research use unless exempt by award of an embargo as requested below, and that the library has the right to migrate my thesis into new electronic forms as required to ensure continued access to the thesis. We have obtained any third-party copyright permissions that may be required in order to allow such access and migration, or have requested the appropriate embargo below.

The following is an agreed request by candidate and supervisor regarding the electronic publication of this thesis:

(iii) Embargo on all printed copy and electronic copy for the same fixed period of 2 years on the following ground(s):

Publication would preclude future publication;

Date 15/7/2011 signature of candidate

signature of supervisor

Acknowledgements

First of all, I would very much like to thank Prof. Douglas Philp for the opportunity to become a part of his work group and to conduct research in the fascinating field of Systems Chemistry. It is only thanks to his guidance and constant motivation, that the last four years have been so exceptionally successful. With an open ear for problems of all kind, he was more than just an academic supervisor.

I also owe thanks to the technical staff of the School of Chemistry: Caroline Horsburgh for the performance of all mass spectrometry analyses, Catherine Botting for the performance of MALDI spectrometry and, in particular, Melanja Smith and Dr. Tomas Lebl for their help with NMR spectroscopy.

Big thanks goes to all members of the Philp group: Evan Wood for his previous work on multicycles; Jan Sadownik and his wife Marta for the first months in St Andrews, especially the youtube parties; Annick Vidonne for countless lunchtime discussions about science and life, for sharing her precious absinth with me and for being very Swiss when it came to lab organisation; Vicente Del Amo for his advice on synthetic problems, the time spend at the conference in Groningen and seeing him rolling on the floor in celebration of a Spanish victory during the Euro; Craig Robertson for his advice on a million and one computational and technical problems, for being an excellent personal guide to Scotland and, most importantly, for being fortunate to see him become a husband to Jen and a proud father to gorgeous Aaron; Izzaty Hassan for her cheerful character, the amazingly delicious dinners and the prospect of meeting her again soon in Malaysia; Harry MacKenzie for making me feel very, very old with his youthful enthusiasm; Lukasz Cieslak for delivering outstanding Polish quality and for being a genuinely nice guy, and all project students for the effort they have put into their projects especially Gabrielle Robson and Jon Osler.

Looking back at four fantastic years in St Andrews, many special thanks go to Gary, Nicolas and Paul who kept me grounded not only on a Friday night. A massive 'thank you' also goes to: Jason, Peter & Marzia, Wouter & Caroline, Nelly, Nikos, Jan, Scott, Simon, Gil, Bianca and Dirk.

I am very grateful to Volker for always having been there for me over the last years even though we have lived 7000 miles apart (that's linear distance).

To Ilaria, work colleague, friend and woman I love, you should always know: Mi piace tu, mi piace solo tuuu! I am looking forward to the year 2012 and every second thereafter...

Last but not least, I would like to express my gratitude to my parents and my brothers, Gernot and Holger.

Abbreviations

Ac	acetyl
B3LYP	Becke, 3 parameter, Lee, Yang and Parr
C	Cytidine
calc.	calculated mass
CI	chemical ionisation
d	doublet
DCC	dynamic covalent chemistry
DCL	dynamic combinatorial library
decomp.	decomposed
DMF	dimethylformamide
DMSO	dimethyl sulfoxide
DNA	deoxyribonucleic acid
EDTA	ethylenediaminetetraacetic acid
EM	effective molarity
ES	electrospray
Et	ethyl
g	gram(s)
G	Guanosine
h	hour(s)
HMTA	hexamethylenetetramine
HRMS	high resolution mass spectrometry
K _a	association constant
K _d	dissociation constant
lit.	literature
M	molar
m	multiplet
m.p.	melting point
MALDI	matrix-assisted laser desorption/ionisation

Me	methyl
MHz	megahertz
min	minute(s)
mL	milliliter
mM	millimolar
mmol	millimol
MS	mass spectroscopy
NBS	N-bromosuccinimide
NMR	nuclear magnetic resonance
o	ortho
p	para
Ph	phenyl
PTSA	p-toluenesulphonic acid
r.t.	room temperature
RNA	ribonucleic acid
s	second(s) / singlet
sat.	saturated
t	time / triplet
TFA	trifluoroacetic acid
THF	tetrahydrofuran
TMEDA	tetramethylethylenediamine
TS	transition state
UV	ultraviolet

Abstract

Biopolymers with defined recognition pattern were used to generate the first artificial replicating systems. Stripping down these systems to their most fundamental properties allowed to move away from the biological origins to construct replicators consisting of simple organic molecules. These systems have proven highly instructive for the in-depth understanding of the main requirements for the targeted development of efficient replicators. With this knowledge at hand, it is now possible to combine several replicators for the formation of molecular networks, and to use the unique properties of replication to manipulate these networks by external stimuli.

In the thesis presented, the investigation of a family of self-replicators culminated in the successful construction of several examples of a multicyclic system in which four building blocks are able to react *via* two autocatalytic and two reciprocal pathways. Owing to the connectivity in this reaction system, it was demonstrated that its outcome can be influenced in a programmable manner by the addition of informational template. Some of the responses can be deduced directly from the functioning of the individual systems, others however are to be classified as emergent properties of the network. Upon elucidation of the multicyclic systems, it became apparent that working in closed reaction systems puts intrinsic boundaries on the possibility to bias the outcome of the reaction network. This limitation prevented the extinction of the inferior type of replicators even under highly unfavourable conditions and instead always led to coexistence for all species.

1.	Introduction	1
1.1	The biological origins of replication	1
1.2	Models of self-replication	3
1.3	Kinetic theory of replication	5
1.4	Artificial replicators based on oligonucleotides	8
1.5	Peptide replicators	12
1.6	Synthetic replicators	21
1.7	Systems Chemistry	35
1.8	Design principles and objectives	40
2.1	The recognition event	40
2.2	Template geometry restraints	41
2.3	The chemical reaction suitable for self-replication	41
2.4	Kinetic investigations of replicating systems	44
2.5	The design of a multicyclic replicating system	46
3.	Structure-dependent reactivity in a family of self-replicators	53
3.1	Design of a library of nitrones and maleimides	53
3.2	Synthesis of nitrones 70 and 71	56
3.3	Synthesis of maleimides 72, 73 and 74	57
3.4	Kinetic analysis	59
3.4.1	Reaction of maleimide 72 with nitrone 70	63
3.4.2	Reaction of maleimide 72 with nitrone 71	66
3.4.3	Reaction of maleimide 73 with nitrone 70	70
3.4.4	Reaction of maleimide 73 with nitrone 71	72
3.4.5	Reaction of maleimide 74 with nitrone 70	75
3.4.6	Reaction of maleimide 74 with nitrone 71	79
3.5	Comparison of the analysed systems	81
3.5.1	Comparison of the bimolecular rates	84
3.5.2	Comparison of the free energies of connection	85
3.5.3	Comparison of the effective molarities	86
3.6	Summary	87
4.	Fine-tuning the activity by changing the strength of recognition	89
4.1	Choice of recognition sites	89
4.2	Choice of test reactions	90
4.2.1	Variable substitution pattern on the maleimide building block	90
4.2.2	Variable substitution pattern on the nitrone building block	93
4.3	Determination of association constants	95
4.4	Screening the set of maleimides 72, 66, 100 and 101	96
4.4.1	Reaction of the set of maleimides with nitrone 70	96
4.4.2	Fitting and analysis	98
4.4.3	Reaction of the set of maleimides with nitrone 71	99
4.4.4	Fitting and analysis	101
4.5	Screening the set of nitrones 116, 117, 118 and 119	103
4.5.1	Reaction of the set of nitrones with maleimide 33	103

4.5.2	Fitting and analysis	105
4.5.3	General calculations for a self-replicating system	107
4.5.4	Reaction of the set of nitrones with maleimide 120	110
4.5.5	Fitting and analysis	112
4.5.6	General calculations for an AB system	116
4.6	Summary and conclusion	120
5.	Controlling replicating activity with a reversible proton switch	122
5.1	Using changes in pH to reversibly block recognition	122
5.2	Synthesis of maleimide H-72	123
5.2.1	Reactivity of maleimide H-72	125
5.3	Kinetic analysis of a pH triggered self-replicating system	127
5.4	Controlling a self-replicating reaction with a reversible pH switch	131
5.5	pH controlled competition between an AB and a self-replicating system	133
5.6	pH controlled temporal separation of a SR from a coexisting AB system	137
5.7	Interpretation of the pH switch reactions as NAND logic gate	139
6.	Replicating networks of three and more building blocks	143
6.1	Designing systems of increased complexity	143
6.2	Analytical requirements	143
6.3	The reagent pool	144
6.4	Individual analysis of the replicators with fluorine tags	146
6.4.1	Reaction of maleimide 72 with nitrone 141	146
6.4.2	Reaction of maleimide 72 with nitrone 142	147
6.4.3	Reaction of maleimide 74 with nitrone 141	149
6.4.4.	Reaction of maleimide 74 with nitrone 142	150
6.4.5	Comparison of the fluorinated systems and influence of the tag	152
6.5	Competition scenarios	152
6.5.1	System I: maleimide 72 with nitrones 141 and 142	152
6.5.2	Fitting and simulation	157
6.5.3	Coupling the competition scenario to a DCL	160
6.5.4	Scenario II: maleimides 72 and 74 with nitrone 142	167
6.5.5	Scenario III: maleimide 74 with nitrones 141 and 142	170
6.5.6	Scenario IV: maleimides 72 and 74 with nitrone 141	173
6.5.7	A four component network	175
6.6	General conclusions	179
7.	Multicyclic replicating systems	182
7.1	Computational analysis of a multicyclic system	182
7.2	Using <i>trans</i> -59b as preset replicator in the design of a multicyclic system	185
7.3	Using <i>trans</i> -161 as replicator in the design of a multicyclic system	188
7.4	A multicyclic system based on <i>trans</i> -59b and <i>trans</i> -161	190
7.5	Analysis of the multicyclic system based on <i>trans</i> -59b and <i>trans</i> -161	195
7.6	Instructing the multicyclic system	198
7.6.1	Addition of 20 mol-% reciprocal template <i>trans</i> -69	198
7.6.2	Addition of 20 mol-% autocatalytic template <i>trans</i> -161	201

7.6.3	Addition of 20 mol-% autocatalytic template <i>trans</i> -59b	204
7.6.4	Summary of the doping experiments	207
7.7	Recycling experiments	209
7.8	Imbalance reaction	211
7.9	Creating an imbalance by changing the recognition site	217
7.10	Using <i>trans</i> -149 as autocatalyst in the multicyclic system	218
7.11	Using <i>trans</i> -147 as autocatalyst in the multicyclic system	225
7.12	Using <i>cis</i> -170 as AB system in the multicyclic system	230
7.13	Summary of results	235
8.	Future work	238
8.1	Systems including maleimide 73	238
8.2	Developing a dynamic multicyclic system	240
8.3.	Developing a multicyclic imine system	242
8.4	Chemical waves	244
9.	Conclusion	247
10.	Experimental	250
10.1	General procedures	250
10.2	NMR spectroscopy	251
10.2.1	Kinetic measurements using ¹ H NMR spectroscopy	251
10.2.2	Kinetic measurements using ¹⁹ F NMR spectroscopy	253
10.3	Determination of binding constants	255
10.4	Kinetic simulation and fitting	255
10.5	Molecular modelling	256
10.6	Synthetic procedures	257
	Appendix	312
	References	328

1. Introduction

1.1 The biological origins of replication

The elucidation of the DNA structure is widely considered to be one of the major scientific discoveries of the 20th century.^[1,2] The intriguing beauty and simplicity of its helical arrangement has rapidly become an icon for the field of molecular biology and has fascinated an audience far beyond the academic community.^[3,4]

DNA is the centrepiece for the phenomena we call Life,^[5-8] since its interplay with RNA creates the proteins and enzymes that are indispensable for maintaining all essential functions in the cell. Not only does DNA act as storage for the information needed to instruct the synthesis of such entities, but its ability to copy itself by replication allows Life to propagate and evolve.^[9-11] In this replicating process, each strand of the double-helix serves as a template for the formation of the complementary partner strand.^[12] Even though DNA replication is conceptually simple, its actual performance in the cell involves the help of a plethora of enzymes.^[13,14] It is therefore considered highly unlikely that the complex network of interactions found today in biological systems has already existed at the dawn of Life, but that it gradually evolved from a much simpler construct.

Since the discovery of catalytically active RNA,^[15-20] especially its central function in the ribosome,^[21] the notion of an 'RNA world' has found wide-spread approbation.^[22-24] In this scenario, RNA not only precedes DNA as the central informational biopolymer for the storage and transmission of genetic information, but RNA is also assumed to have conducted all enzymatic tasks^[25] until it was gradually^[26-29] displaced by proteins which possess much higher structural flexibility and generate the incomparable substrate specificity found today in many enzymes. Even though this concept has attracted a lot of attention and much progress has been made regarding the prebiotic synthesis of the nucleotide building blocks,^[30-35] their activation towards oligomerisation with the correct 3'-5' linkage and their templated reaction to form oligonucleotides of sufficient length to conduct catalytic tasks^[36-38] using clay material,^[39-42] many fundamental problems such as the susceptibility of RNA to hydrolytic cleavage in aqueous solution still poses scientific challenges.

Despite these limitations, the possibility of using RNA as a rudimental basis to mimic Life's most important feature, replication of genetic information with the potential generation of superior mutants to allow the evolution and survival of a species, has intrigued many scientists. Since RNA can be both template in the replication process and act as a polymerase for the formation of long RNA strands, Szostak *et al.* have proposed the existence

of an RNA replicase.^[43] Their idea is based on an RNA duplex structure which can dissociate to release two strands, one of which can fold to adopt a secondary structure to function as a replicase, whereas the complementary strand acts as a template for a primer extension reaction catalysed by the replicase analogous to the functioning of the Taq polymerase in the polymerase chain reaction.^[44,45] Once the extension of the primer using activated nucleotide monomers or short oligomers is completed, the replicase can dissociate and the newly formed duplex can re-enter the reaction cycle. In order to ensure self-replication of the initial duplex, both strands need to possess the ability to alternatively act as template and replicase.

No matter how fascinating the idea of such system might be, its realisation in the near future seems unlikely. The usage of self-replicating vesicles^[46] as reaction containers might indeed allow for the compartmentalisation^[47,48] of all necessary entities in a defined space and the development of a replicase with high fidelity for copying its own sequence has seen some impressive progress,^[49] however, more fundamental questions such as how to separate the RNA duplex or under what conditions the folding of the individual strand into the replicase can take place remain unanswered.

The group of Joyce has set out to explore the feasibility of a scenario that circumvents the necessity of a replicase. Their non-enzymatic approach condenses Szostak's scheme to its most essential feature: an RNA duplex that can make copies of itself. Central for this venture was the development of an efficient RNA ligase that can bind two oligonucleotide substrates and join them together.^[50] Building on this ribozyme design, a self-replicating variant was developed in which the newly formed RNA strand is identical to the RNA ligase that catalyses its formation.^[51,52] Efforts to establish a framework based on two cross-complementary RNA strands^[53] recently culminated in a system in which two RNA ligase enzymes catalyse each other's formation from a total of four oligomeric RNA subunits.^[54]

With their work, Joyce *et al.* are bridging the gap between enzymatic RNA replication as envisaged by Szostak and the construction of replicating systems based on simple molecules. Using biology as a blueprint, chemists have started to explore molecular self-replication to establish the minimal requirements for translating the principles into synthetic systems and to elucidate whether relatively simple chemical structures are able to mimic the ability of nucleic acids to store and transmit information on a molecular level.^[55-58] Additionally, the concept of making exact copies of a chemical entity in a non-linear fashion could have a significant impact on the fabrication of molecular architectures on the nanometer scale.^[59]

The last 25 years have seen the development of a considerable amount of non-enzymatic synthetic replicating systems based on nucleic acids, peptides and small organic

molecules.^[60-68] Even though the chemical natures of these structures are intrinsically different, when it comes to analysing their replicating properties, the same rules hold for all of them. In the following sections, the two fundamental mechanisms of replication are presented and a concise theoretical analysis is given. Ultimately, a comprehensive overview over the history of synthetic self-replicators including most recent developments is provided.

1.2 Models of self-replication

Almost all of the examples of synthetic self-replicators reported during the past 25 years are based on the minimal model shown in **Figure 1a**.^[69] This minimal model of self-replication contains two distinct recognition-mediated reaction channels. Compounds **A** and **B** bear complementary recognition sites and so, they can associate with each other to form a binary complex, $[A \cdot B]$. Within this complex, **A** and **B** are preorganised with respect to each other and the reaction between them is pseudo-intramolecular. The product of this reaction is a closed template T_{inactive} in which the recognition used to assemble the binary complex lives on in the template. Thus, although rate acceleration is achieved by this mechanism, this template is inert catalytically.

Alternatively, the system can exploit an autocatalytic cycle. In this case, **A** and **B** bind reversibly to the open template T_{AB} to form a catalytic ternary complex $[A \cdot B \cdot T_{\text{AB}}]$. In a manner similar to the $[A \cdot B]$ complex, the reaction between **A** and **B** is also rendered pseudo-intramolecular. Bond formation occurs between **A** and **B** to give the product duplex $[T_{\text{AB}} \cdot T_{\text{AB}}]$, which then dissociates to return two molecules of T_{AB} to the start of the autocatalytic cycle. Thus, assuming the open template T_{AB} presents its recognition sites in the correct orientation, it can act as a template for its own formation, transmitting molecular information through the formation of identical copies of itself. Self-replication is therefore a subset of autocatalytic reactions.^[70,71] In an autocatalytic reaction, the product formed in the reaction mixture is a catalyst for the same reaction. A system in which self-replication is operating can be defined as an autocatalytic reaction capable of transmitting structural information. This information can be stored as constitution or configuration. Key design elements in this model of replication are a) minimisation of reaction flux through the binary complex reaction channel and b) inefficient autocatalysis through product inhibition arising from an excessively stable product duplex $[T_{\text{AB}} \cdot T_{\text{AB}}]$.

The model of self-replication discussed thus far involves self-complementary structures. However, template effects in a replication cycle can also operate in a reciprocal sense. In a minimal system, the template is self-complementary, whereas in a reciprocal

system a pair of templates are complementary to each other. Therefore, reciprocal replicating systems rely on two interlinked crosscatalytic cycles in which the two templates catalyse the formation of each other. The processes involved in reciprocal replication are encapsulated schematically in **Figure 1b**.

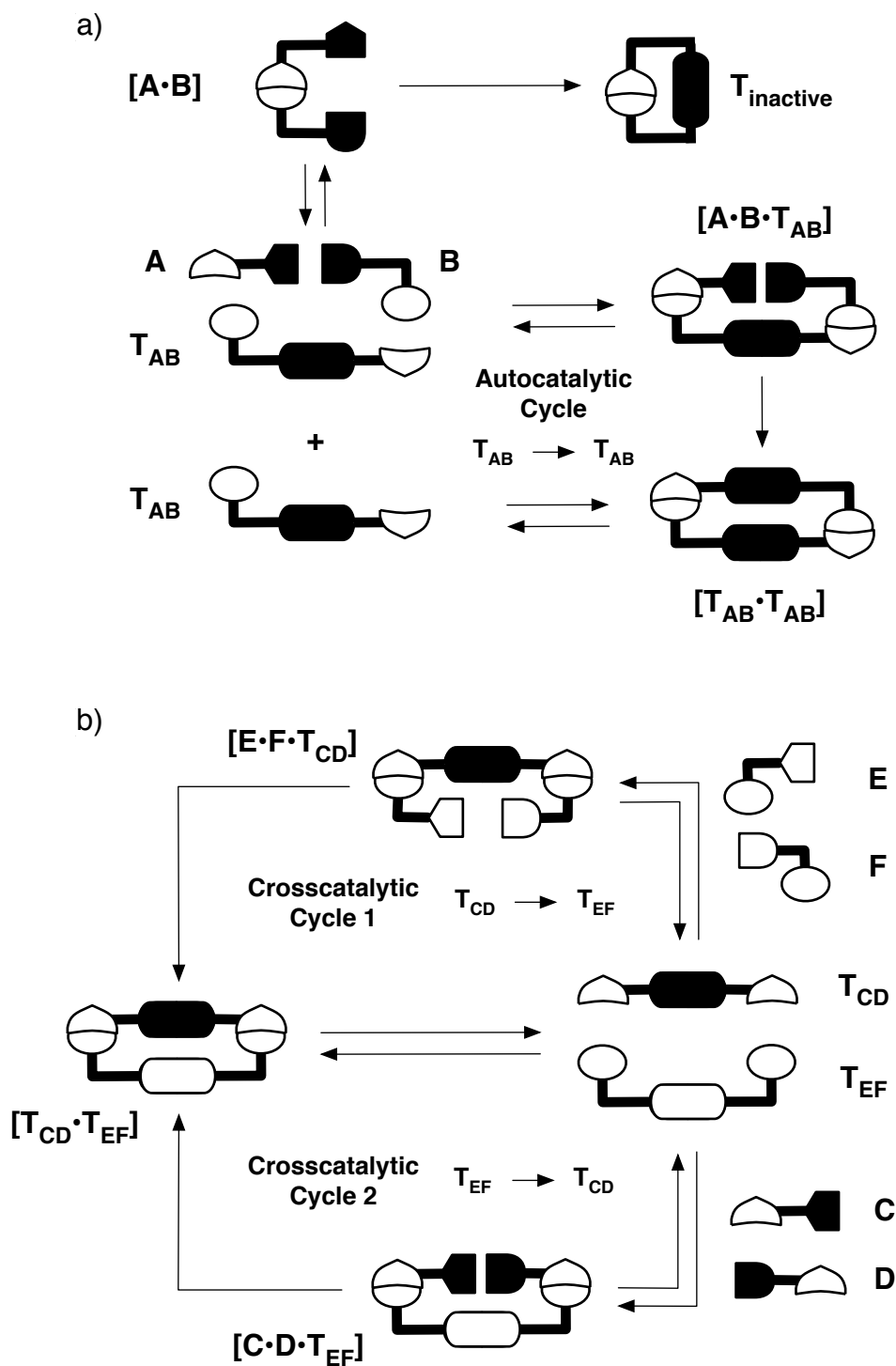


Figure 1.1 Schematic model for the functioning of a) an autocatalytic system and b) a crosscatalytic system.

In these systems, compounds **C** and **D** can react to form the template T_{CD} , and, similarly, compounds **E** and **F** can react to form template T_{EF} . Since the four reactive partners bear appropriate recognition sites and since T_{CD} and T_{EF} are mutually complementary, T_{CD} is capable of assembling **E** and **F** into the ternary complex $[E \cdot F \cdot T_{CD}]$. This ternary complex intramolecularises the reaction between **E** and **F** and, hence, catalyse the formation of T_{EF} . Similarly, T_{EF} is capable of assembling **C** and **D** into the ternary complex $[C \cdot D \cdot T_{EF}]$ and, hence, catalyses the formation of T_{CD} . These two interlinked crosscatalytic cycles represent a formal reciprocal replication cycle.^[72,73] It is, however, important to note that the complexity of this system can increase dramatically depending on the nature of the chemical reaction which forms the two templates. In the case where the reaction between **C** and **D** and the reaction between **E** and **F** are orthogonal, only one reciprocal replication cycle is present in the system. However, if **C** can react with **E** and **D** with **F**, three replication cycles are possible: two minimal replication cycles – T_{CE} and T_{DF} may self-replicate – and the original reciprocal replication cycle $T_{CD} \rightarrow T_{EF}$ and $T_{EF} \rightarrow T_{CD}$. Additionally, the minimal replicators T_{CE} and T_{DF} may crosscatalyse the formation of each other.

1.3 Kinetic theory of replication

Kinetic simulation of the behaviour of a minimal replicator can provide some insight into the various processes which operate these systems. The fitting of experimental data to kinetic models allows the determination of important thermodynamic and kinetic parameters within the system including rate constants for reactions and equilibrium constants for recognition processes. A series of simplified kinetic models to describe the behaviour of artificial self-replicating systems were first introduced^[69] in a seminal paper by von Kiedrowski. The simplest of these models is a purely autocatalytic reaction (**Figure 1.2**) with a variable reaction order for the product – known as the autocatalytic reaction order p . The parameter p describes the autocatalytic behaviour of the system and determines the type of the autocatalytic growth curve. In real systems, the value of p is expected to lie between 0.5 and 1. At the two extremes, a value of $p = 0.5$ denotes a self-replicating system that obeys the ‘square root law’. In this situation, the dissociation rate of the template duplex $[T \cdot T]$ is limiting overall. The concentration *vs* time profile of such reaction shows parabolic growth (**Figure 1.2a**). However, if dissociation of the product duplex is not rate limiting, the value of p will tend to 1. In that case, the dissociation of the product duplex is rapid compared to other processes in the system and the concentration *vs* time profile of the reaction shows exponential growth (**Figure 1.2b**). The calculated concentration *vs* time profiles shown in

Figure 1.2 demonstrate clearly that the change of the autocatalytic reaction order p produces a dramatic effect on the shape of the profiles. It is worth noting that the maximum rate of reaction for a self-replicating system, parabolic or exponential, does not occur at $t = 0$. Instead, it occurs at some later point in the reaction and is associated with a particular concentration of **T**. These parameters can be accessed readily by exploiting a rate *vs* time profile (dashed lines, **Figure 1.2**), which is simply the first derivative of the concentration *vs* time profile.

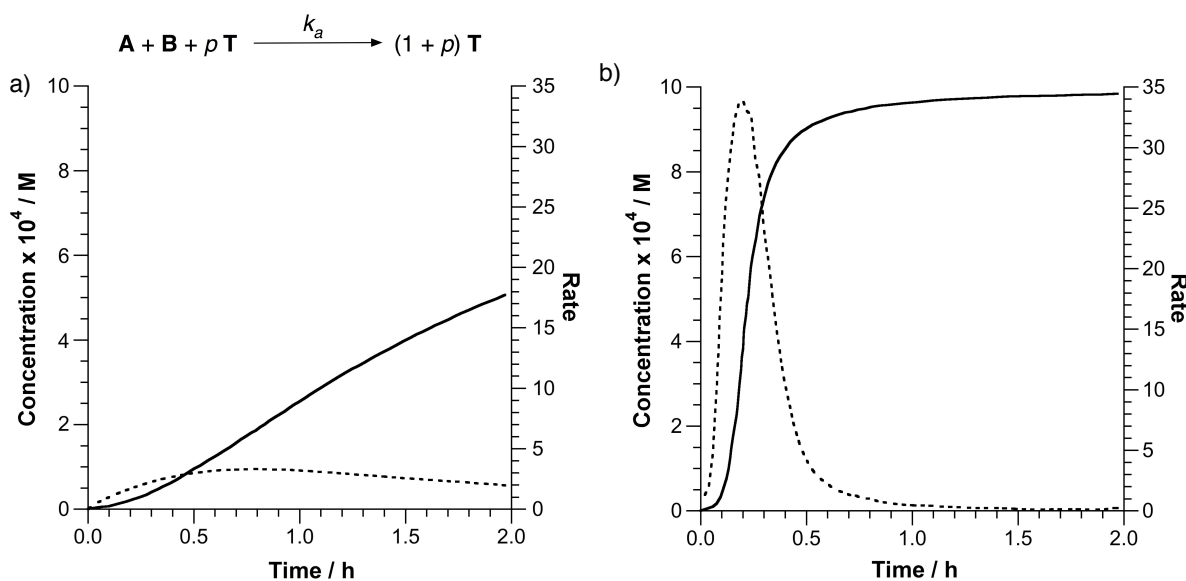


Figure 1.2 Computed concentration *vs* time (solid lines) and rate *vs* time (dashed lines) profiles for a) an autocatalytic system with reaction order $p = 0.5$ showing parabolic growth and b) an autocatalytic system with reaction order $p = 1$ exhibiting exponential growth.

The concentration *vs* time profiles shown in **Figure 1.2** illustrate purely autocatalytic systems, which are rarely representative of real experimental systems. **Figure 1.3** shows the corresponding growth curves when formation of template molecules through the bimolecular channel is taken into account. The autocatalytic efficiency ϵ , which is the ratio of the template-catalysed rate constant, k_a , over the template-independent rate constant, k_b , measures the relative contribution of the pathway involving **T** to the observed rate of reaction. A sigmoidal shape only becomes apparent in the concentration *vs* time profile above a critical value of ϵ . Indeed, some experimental systems do not display sigmoidal production of the template even though an autocatalytic pathway is present within the system.

In practice, one of the easiest ways to discern whether a replicator is parabolic or exponential is to follow the formation of product **T** in the presence of three different amounts of preformed template at the start of the reaction (normally between 2 and 10 % of the initial

concentration of the precursors). Typically, the concentration of template added is doubled when proceeding to the next experiment. In the parabolic case, the initial rate of formation of **T** scales as $1 : \sqrt{2} : \sqrt{4}$ upon addition of increasing amounts of **T**. In the exponential case, the initial rate of formation of **T** scales as $1 : 2 : 4$.

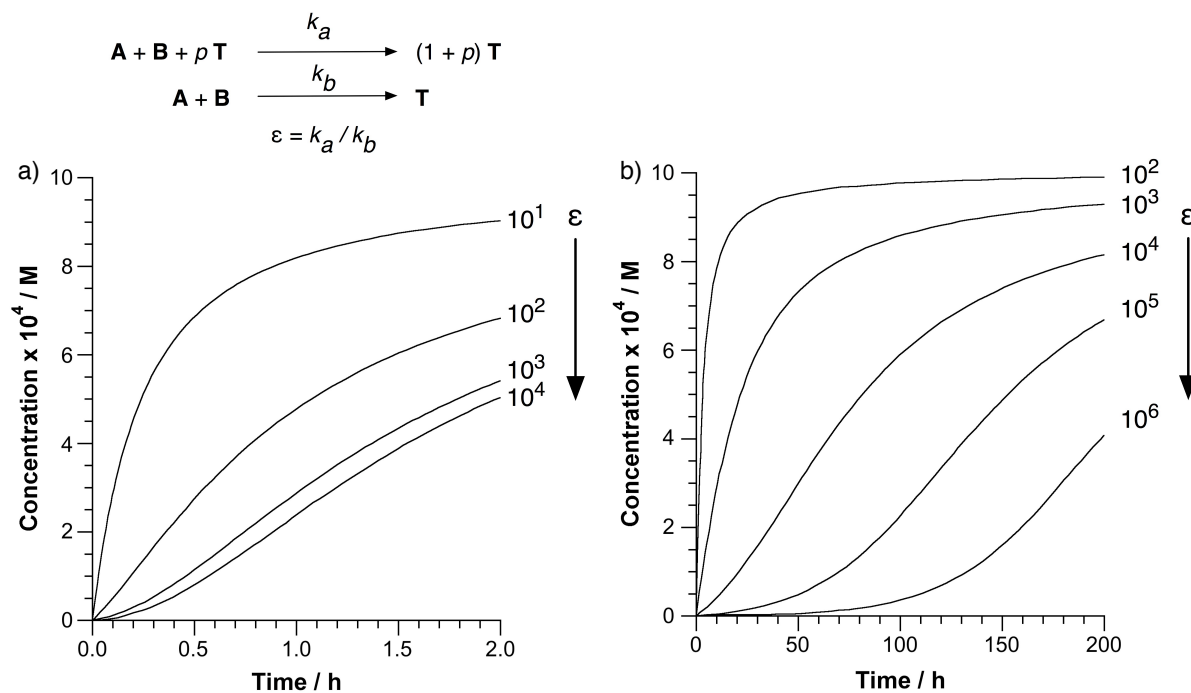


Figure 1.3 Computed concentration *vs* time profiles for various values of catalytic efficiencies ε for a) an autocatalytic system with reaction order $p = 0.5$ and b) an autocatalytic system with the reaction order $p = 1$. The sigmoidal shape of the profile is only visible above a certain value for ε .

Often, the course of a reaction is followed by NMR spectroscopy, and so kinetic data for the system is usually based on the monitoring of NMR integrals. However, the changes in the observed chemical shifts for the various species present in solution during the course of the reaction are not taken into account. By contrast, thermodynamic parameters for the supramolecular complexes involved is usually derived from independent NMR titration experiments. Von Kiedrowski recently introduced^[74] a kinetic method ('kinetic NMR titration'), which combines analysis of integral and chemical shift changes, to harvest kinetic and thermodynamic information from the same experiment.

Reinhoudt and co-workers advocate^[75] the use of complete kinetic modelling. In their approach, numerical integration of a complete set of differential rate laws which describe all pathways, both reversible and irreversible, within the system is used to obtain detailed information about the relative importance of each potential reaction pathway. This approach has proven extremely useful in several cases, particularly in our laboratory.

1.4 Artificial replicators based on oligonucleotides

In 1986, von Kiedrowski first demonstrated enzyme-free self-replication using a pair of trideoxynucleotides that condense to form a product consisting of six nucleotides (**Figure 1.4**).^[76] By choosing a palindromic pattern of nucleic acids, this product can act as a template for its own formation. Previous work by Inoue *et al.* demonstrated the feasibility of using a C-C-G-C-C template to form the corresponding G-G-C-G-G strand from activated guanosine (G) and cytidine (C) building blocks.^[77] In order to exploit the favourable association between these two nucleic acids, the self-replicating system was designed using motifs of these pentameric sequences. Trideoxynucleotide **1** bears the sequence C-C-G with its 5'-terminus protected as methyl ether. Its reactive partner **2** possesses the structure C-G-G with an *o*-chlorophenyl group as protecting group in 3'-position. Ligation of both fragments through the unprotected end groups leads to the formation of product **3** with its palindromic sequence, C-C-G-C-G-G. Water-soluble 1-(3-dimethylaminopropyl)-3-ethylcarbodiimide (CDI) was used to activate the 3'-phosphate of **1** to its carbodiimide form and increase its reactivity towards nucleophilic attack of the 5'-hydroxy group of **2**.

Once the template has formed in a bimolecular fashion, **3** can act as a template to assemble both starting fragments in a ternary complex. The specific pattern of hydrogen bonds allows optimal interaction in the complex only when both fragments are orientated with their reactive sites towards each other. This specific geometric arrangement promotes the condensation reaction in the ternary complex and accelerates the rate of product formation. In a consecutive analysis, von Kiedrowski showed that the autocatalytic activity is indeed highest for the given set of trideoxynucleotides.^[78] Variations of only one position from C to G, or vice versa, in **1** led to a significant decrease of catalytic activity. In general, the sensitivity of the system for mismatched pairs is more pronounced for nucleic acid residues close to the reactive site and mismatches between two guanosine moieties have less consequences on the stability of the ternary complex than mismatch pairs of cytidine.

Addition of preformed hexameric template product at the start of the reaction showed an increase in initial rate with increasing amount of dopant. Kinetic analysis of the data provided a value of 0.48 for *p*, which suggests that strong association between the two strands in the product duplex limits severely their separation. Since only free template is catalytically active, its self-aggregation prevents the system from exponential growth.

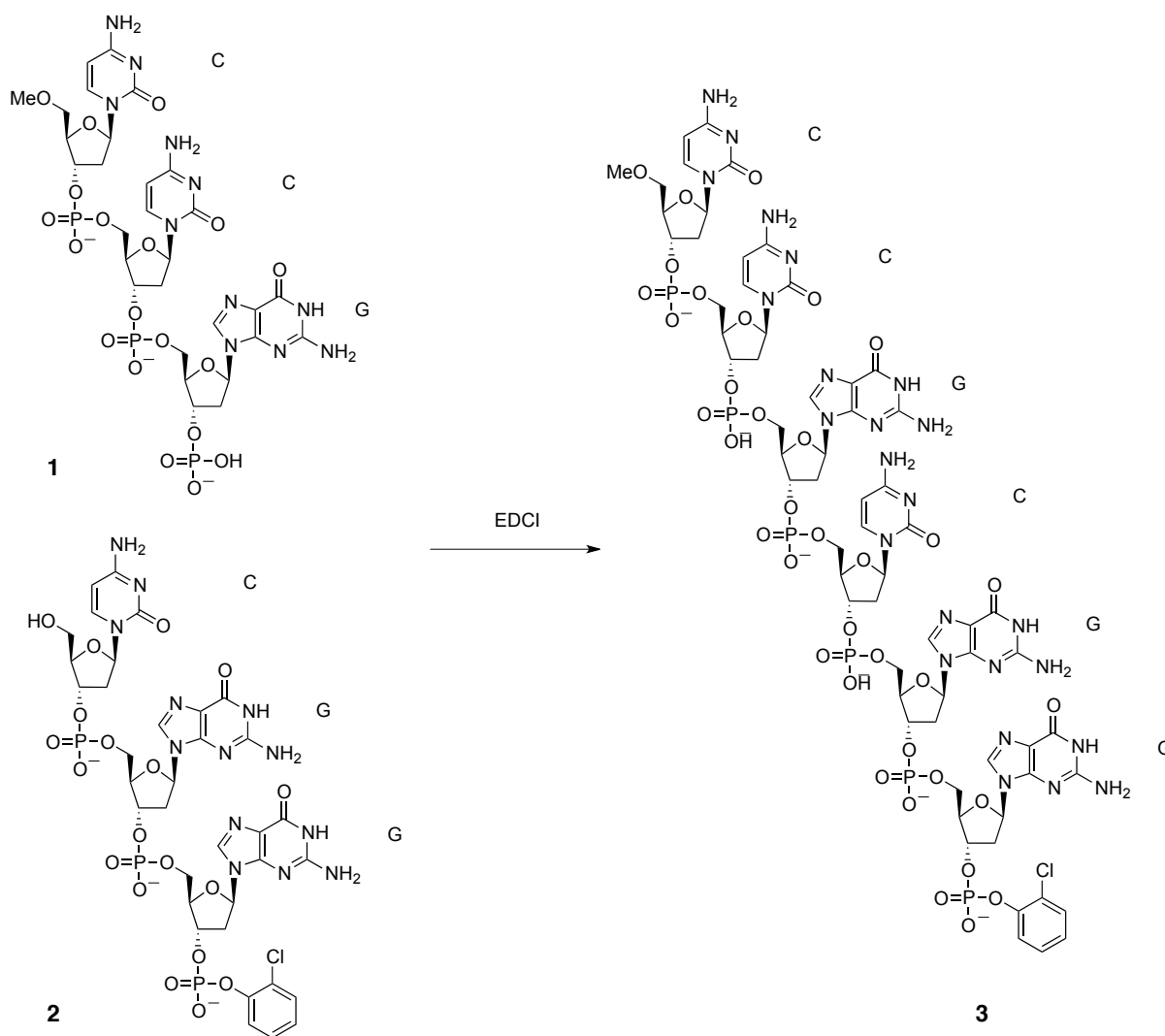


Figure 1.4 The palindromic hexadeoxynucleotide 3 is capable of templating its own formation from a nucleophilic trideoxynucleotide 1 and an electrophilic trideoxynucleotide 2. EDCI = 1-ethyl-3-(3'-dimethylaminopropyl)carbodiimide.

The results of the investigation of the autocatalytic formation of a tetranucleotide triphosphoamidate underlined von Kiedrowski's empirical law by which in systems with strong product inhibition the reaction rate depends on the square root of the total concentration of present template.^[79] Additionally, relatively fast background reactions in both systems prevented the formation of the expected sigmoidal rate profile. It was not until the hydroxy group in 2 was replaced with an amine group to form a 3'-5'-phosphoamidate bond during ligation, that the rate of the template-dependent formation of product was strengthened in respect to the bimolecular background pathway and the sigmoidal rate profile expected for autocatalytic processes became visible.^[80] Calculating the kinetic effective molarity for this very system gave a value of 420. The system based on tetranucleotides performed slightly worse ($\epsilon = 340$) but still better than the first system based on synthetic organic molecules ($\epsilon = 80$, *vide infra*).

An intriguing example of avoiding product inhibition was presented by Li *et al.*^[81] In their protocol, they exploit the pH dependent assembly of complementary DNA strands in duplex or triplex structures. At pH 6, two complementary strands entirely consisting of either purines or pyrimidines form a double-helix which has the ability to associate two complementary DNA fragments and enhance their ligation to form a triplex structure. Consecutive dissociation of the newly formed triple-helix can be achieved by increasing the pH to 7. Under these conditions, the triplex structure becomes thermodynamically unfavourable and splits into a duplex and a single strand. This single strand can then act as a template for the ligation of a second set of DNA fragments to generate another DNA duplex that can in turn undergo further replicating cycles. Choosing a palindromic structure for both purine and pyrimidine strand allowed for the formation of an identical copy of the starting DNA duplex in one cycle.

Another iterative approach to generate an exponential self-replicating system combines solid-phase chemistry with chemical replication of oligonucleotides.^[82] At the start of the reciprocal version of this procedure, two complementary oligonucleotide templates are immobilised onto a solid support. Appropriate nucleotide building blocks can then be recognised on the templates and reacted to form copies of both strands. Treatment of the duplexes with polar solvents leads to their separation and the freed product molecules can then be connected onto the solid support to start a second cycle of replication. In principal, this protocol also holds for self-complementary oligonucleotide templates. Analysis of a reciprocal model system confirmed the exponential mode of amplification for both oligonucleotide templates.

As the ultimate target, non-enzymatic replication of oligonucleotides using single nucleotides as building blocks is envisaged. The integration of several interconnected replication cycles to form a template from three building blocks can be considered as the first step in this direction.^[83] In order to achieve this aim, von Kiedrowski's original hexadeoxynucleotide template C-C-G-C-G-G was cut into three segments of different length, C-C-G, C-G and G. The two smaller fragments were both equipped with an amine group on their 5'-terminus to ensure formation of a 3'-5'-phosphoamidate bond. Protection of the 5'-terminus of the C-C-G fragment and the 3'-position of the deoxyguanosinephosphate G limited the number of possible ligation products. As a consequence of its palindromic character, the formation of 'wrong' template C-C-G-G from C-C-G and G was favoured in the native reaction of all three building blocks. However, once a certain amount of 'correct' template, C-C-G-C-G-G, had formed, suitable smaller precondensed building blocks such as C-C-G-C-G and C-G-G, were employed to autocatalytically generate more final hexameric

product. Doping with preformed template initially stimulated the templated ligation of C-C and C-G and consequent incorporation of G led to an enhanced formation of final product. Overall, a catalytic network with a total of six directed interactions could be derived giving just a small glimpse at the degree of complexity that can be found in such systems.

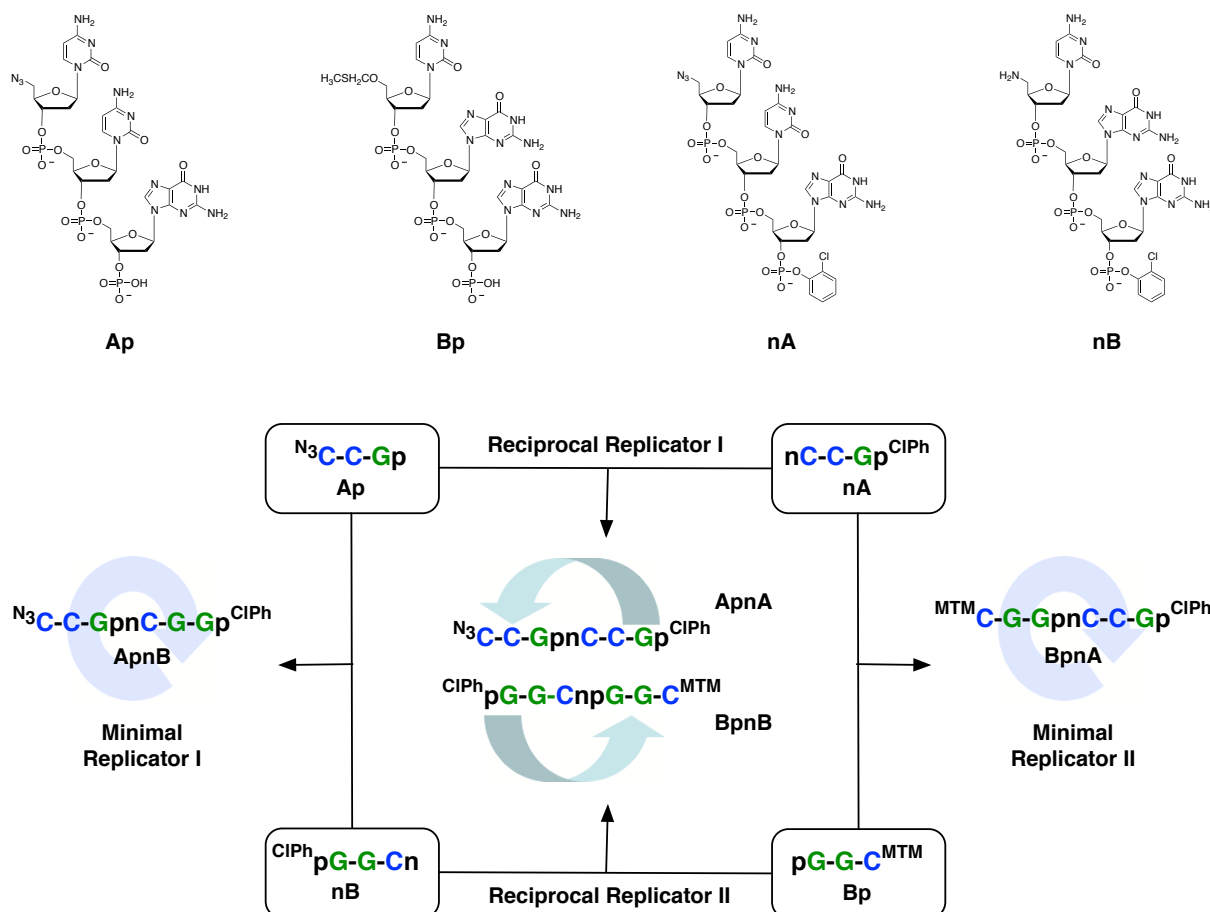


Figure 1.5 Reaction network based on the interaction of trideoxynucleotide derivatives **Ap**, **Bp**, **nA** and **nB** to give four possible hexameric 3'-5'-phosphoramidates by combinatorial synthesis *via* autocatalytic (**ApnB** and **BpnA**) or crosscatalytic pathway (**ApnA** and **BpnB**).

In this context, an ingenious modification of the original pair of von Kiedrowski's nucleotides led to a network of interdependent auto- and crosscatalytic replicators.^[84,85] The four building blocks used for this purpose are depicted in **Figure 1.5**. Fragments **Ap** and **nB** are identical to the self-replicating system described previously except for the azide protecting group in the 5'-terminus of **Ap** instead of the original methyl ether. Moving the protecting groups in both fragments from one end to the other, gives rise to structures **nA** and **Bp** which can react to form an equally efficient self-replicating system **BpnA**. Moreover, recombination of all four components opened a third reaction pathway. The reaction between **nA** and **Ap** gave rise to a template **nAAp** with a sequence complementary to the one found

in the product **nBBp** between **nB** and **Bp**. This reciprocal relationship leads to the generation of a crosscatalytic cycle in which both templates catalyse the formation of its partner. Since all catalytic pathways proceed through ternary complexes of very similar stability, the native reaction between all four starting compounds gave rise to all four possible products in nearly equal amounts. Doping a fresh solution of reagents with preformed product showed selfish amplification in the case of both self-complementary templates whereas adding crosscatalytic template led to amplification of the corresponding complementary strand.

1.5 Peptide replicators

Replication processes ensure the transmission of information in biological systems. Biopolymers such as RNA or DNA employ a precise pattern of oligonucleotides as their means of storing and passing down information from one generation to another. Peptides are another class of biopolymers that were explored as a platform for the development of self-replicating structures.^[86,87] Compared with systems based on oligonucleotides, polypeptides do not possess the self-complementarity of nucleic acids and are usually not found to adopt a helical arrangement. However, since protein structures can avail themselves of a pool of 22 amino acid building blocks, the structural diversity of the biopolymer is considerably larger than for nucleotides.

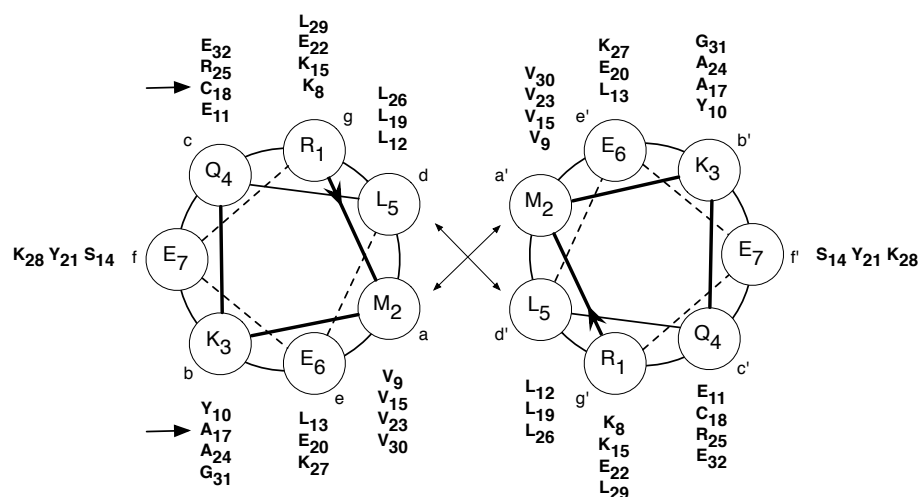


Figure 1.6 Helical-wheel diagram of the template peptide in the dimeric α -helical coiled-coil configuration emphasising the heptad repeat motif. The interhelical recognition surface consists of amino acids allowing for hydrophobic packing interactions (positions *a* and *d*) and electrostatic interactions (positions *e* and *g*). Amino acids at positions *b*, *c* and *f* lie on the solvent-exposed surface of the helical structure and do not participate in the molecular recognition processes. Arrows indicate the ligation site between a cysteine and an alanine residue.

In 1996, Ghadiri *et al.* presented^[88,89] a platform for the investigation of self-replicating peptides based on the coiled-coil domain of the yeast transcription factor GCN4 (**Figure 1.6**).

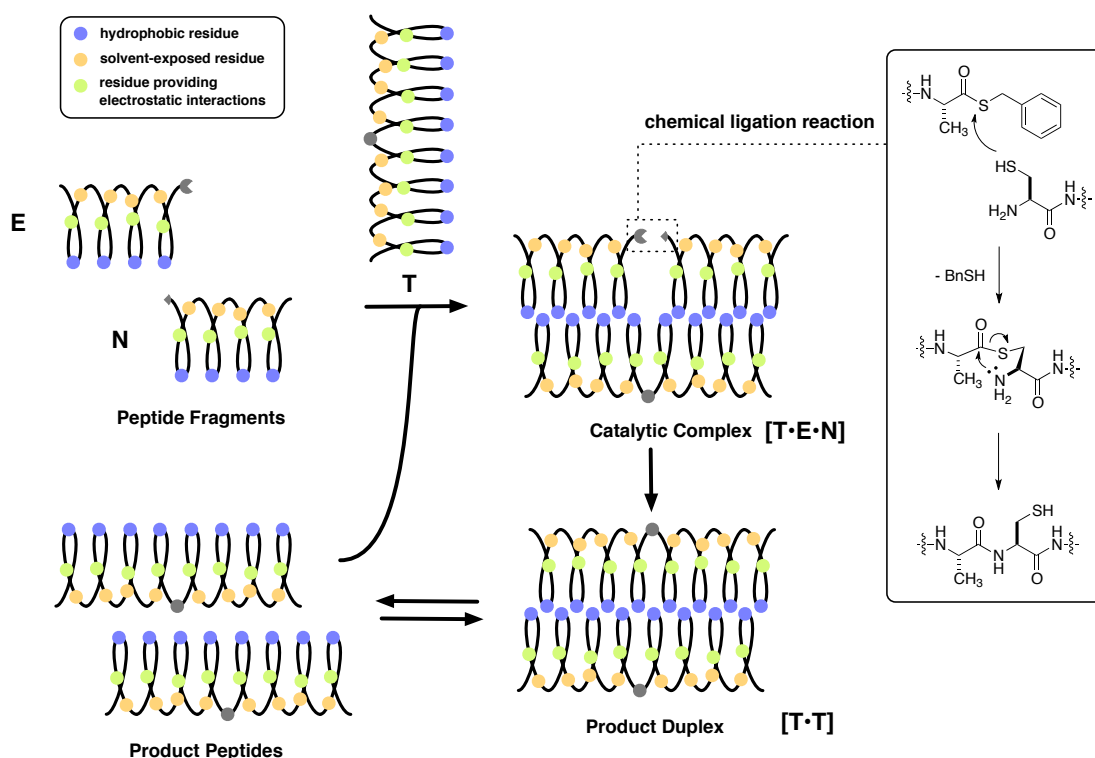


Figure 1.7 Schematic representation of the minimal autocatalytic reaction cycle for the self-replicating α -helical peptide. The electrophilic and nucleophilic peptide fragments E and N are recognised by template T through interhelical hydrophobic interactions to form catalytic complex [T·E·N]. Subsequent chemical ligation produces an identical copy of the template which remains bound in the product duplex. Dissociation releases the two templates which can then undergo further catalytic cycles. The inset depicts the mechanism of the amide bond formation which includes a transthioesterification between the activated C-terminus of electrophile E and the N-terminal cysteine side chain of nucleophile N as a first step. Rapid rearrangement of the intermediate thioester gives rise to the final amide bond.

In this motif, an identical pair of parallel α -helical peptides wrap around one another with a slightly left-handed superhelical twist. As shown in the helical-wheel diagram, the peptide exhibits a seven-residue repeat (*abcdefg*). Recognition between both strands is promoted through non-polar residues at position *a* and *d* forming a specific hydrophobic interface. Residues at the flanking positions *e* and *g* promote a secondary level of recognition through electrostatic interactions whereas positions *b*, *c* and *f* are exposed to the solvent and of minor importance for the stability of the coiled-coil arrangement. Compared to the original structure found in the yeast transcription factor, an optimisation of the binding interaction in the hydrophobic recognition domain was achieved by replacing an asparagine group in position 16 with valine. The removal of the polar group significantly increased the

stability of the helical structure and allowed the peptide to equilibrate between two and three stranded species. During the templated process, ligation of two subunits proceeded by reacting the activated C-terminus of the electrophilic peptide fragment E with the cysteine side chain at the N-terminal of the nucleophilic peptide fragment N (**Figure 1.7**). The intermediate thiolester was found^[90] to rearrange rapidly to form the final ligation product.

The self-replicating nature of Ghadiri's initial peptide structure was confirmed by doping experiments. Addition of an increasing amount of template at the start of the reaction was shown to increase significantly the initial rate of product formation. Control experiments were carried out in a solution of guanidinium hydrochloride, a chaotropic reagent which was found to cause denaturation of proteins by interrupting the stabilising intramolecular interactions. Running experiments of E and N under such conditions with and without initially added template clearly established the template-directed nature of the native experiment, since both reactions proceeded with significantly slower rates. In order to investigate the necessity of binding both subunits onto the template to achieve full catalytic activity, two crippled peptide subunits, E* and N*, bearing a glutamic acid residue in the recognition interface were designed. Introduction of a hydrophilic group led to severe destabilisation of recognition between the peptide fragments. Respective reaction of E with N* and E* and N gave rise to two mutant templates which both failed to show any rate enhancement for the native reaction between N and E.

In addition, two further variants, E' and N', were synthesised in which residues in the hydrophobic core were replaced with alanine. Even though alanine does not bear any destabilising side-chains, this highly conservative replacement proved to eliminate all autocatalytic activity. Reactions between E' and N as well as E and N' did not show any template-directed acceleration upon addition of both alanine-modified or native template. This remarkably high fidelity towards sequence variations was later explored in investigations of more complex systems of interacting replicators.

Kinetic analysis of the experimental data gave rise to a *p* value of 0.63 which is slightly higher than in oligonucleotide systems. This finding suggests that self-replicators on the basis of peptides suffer less from product inhibition than oligonucleotides. Furthermore, there might be a significant contribution of catalytically active product duplexes which are able to associate two subunits in a quaternary complex. All things considered, the authors could convincingly demonstrate the efficiency of their replicating peptide structure and shed light on the mechanism which clearly indicated the necessity for both subunits to be bound onto the template structure(s) to form a ternary and/or quaternary complex.

Apart from the design of self-replicating systems, the authors were able to successfully apply their concept in the construction of a peptide template that was found to very efficiently catalyse the ligation of various peptide subunits.^[91]

Contemporaneous, the group of Chmielewski presented some intriguing work on the manipulation of the efficiency of self-replicating peptides by external triggers. As a platform for their work, they exploited the same coiled-coil arrangement and ligation reaction as Ghadiri *et al.* In their initial contribution, they presented the design of a self-replicating peptide ($\mathbf{E1} + \mathbf{E2} \rightarrow \mathbf{E1E2}$) whose efficiency could be modulated by variation of pH.^[92] Recognition between both strands was ensured by creating a hydrophobic core consisting entirely of leucine residues. The key structural change was performed on the positions *e* and *g* which contribute to the stability of the duplex through electrostatic interactions. All such residues were replaced with glutamic acid (Glu) units, thus the strength of electrostatic repulsion could now be tuned by varying the pH value. Under acidic conditions, protonation of the Glu side chain was found to stabilise the coiled-coil formation whereas under physiological conditions, the deprotonated acid functionality caused sufficient repulsion to prevent the formation of the helical structure. Circular dichroism spectroscopy was applied to confirm the helical content of the peptide and was in agreement with the obtained results. Accordingly, the efficiency of the self-replicating peptide was found to vary in a pH-dependent manner. At pH values above 4, no autocatalytic activity was found for the formation of the peptide. Only at a pH value of 4 did the system start to behave autocatalytically. However, the reactivity of the ligation reaction was also found to decrease by lowering the pH value preventing efficient self-replicating activity in pH regimes lower than 3.

Having established the crucial role of the flanking positions on the stability of the coiled-coil structure, the authors presented a second system ($\mathbf{K1} + \mathbf{K2} \rightarrow \mathbf{K1K2}$) in which all glutamic acid residues at the flanking positions were replaced by lysines.^[93] Since the amine group is protonated at acidic and neutral pH, the formation of the coiled-coil conformation is prevented due to electrostatic repulsion. Increasing the pH or working at neutral conditions with high concentrations of shielding counterions was expected to minimise the repulsive forces and allow formation of the coiled-coil arrangement. Accordingly, addition of increasing amounts of NaClO₄ at pH 7.5 was shown to enhance the formation of the peptide in an autocatalytic fashion. Doping experiments with preformed peptide template showed the expected increase in initial rate and kinetic analysis provided an effective molarity of 280 for the best system.

In combining both replicators, Chmielewski *et al.* created a four-component system in which, under certain conditions, auto- and crosscatalysis coexist.^[94] At physiological conditions, next to the native replicators bearing glutamic acid groups (**E1E2**) and lysine residues (**K1K2**) in the flanking positions, two recombinant mutants (**E1K2** and **E2K1**) were found to be efficient templates for their own formation. Similar to the example based on oligonucleotides, this system allowed for the selective amplification of one or more of the products by instructing the reaction mixture with preformed template. Both crosscatalytic templates (**E1E2** and **K1K2**) and both autocatalysts (**E1K2** and **E2K1**) showed high fidelity for their reciprocal and own formation, respectively. Besides these expected interactions, a number of crosscatalytic activities between the native peptides and their mutants were found. For example, **K1K2** was found to catalyse the formation of **K1E2**. Since mutant peptides aggregate in an antiparallel conformation, it is possible to imagine a dimeric **K1E2** template that can bind fragments **K1** and **K2** onto its negatively charged surface leading to a trimeric product complex. Additionally, variations in the environment proved to have a major impact on the formation of products. Working at high salt concentration promoted the formation of the replicator bearing only lysine groups (**K1K2**) whereas lowering the pH yielded the above-mentioned replicator (**E1E2**) with acidic side-chains.

Another focus of research aimed at increasing the efficiency of peptide replicators. The efficiency of self-replicating systems can be tuned by increasing the stability of the ternary complex and/or destabilising the final product duplex. The latter was achieved by shortening the chain length of the native sequence of replicator **E1E2**.^[95] As a consequence, the interaction in the hydrophobic core of this new design is reduced leading to a decreased stability of the coiled-coil helix preventing strong product inhibition. The catalytic efficiency of this shortened version was calculated to be in the range of 1×10^5 , a value about two to four magnitudes higher than in other self-replicating systems, and a p value of 0.91 was found.

Instead of shortening the peptide sequence, the same authors presented a structure **Ep** in which the incorporation of a proline residue close to the reactive side showed a pronounced destabilising effect on the stability of the product template without altering the interactions between the subunits and the template (**Figure 1.8**).^[96] The resulting proline-modified structure was indeed found to possess a destabilising kink and the effective molarity in the autocatalytic process as well as the p value were established to be similar to the shortened peptide ($\epsilon = 3.2 \times 10^4 \text{ M}^{-1}$ and $p = 0.91$).

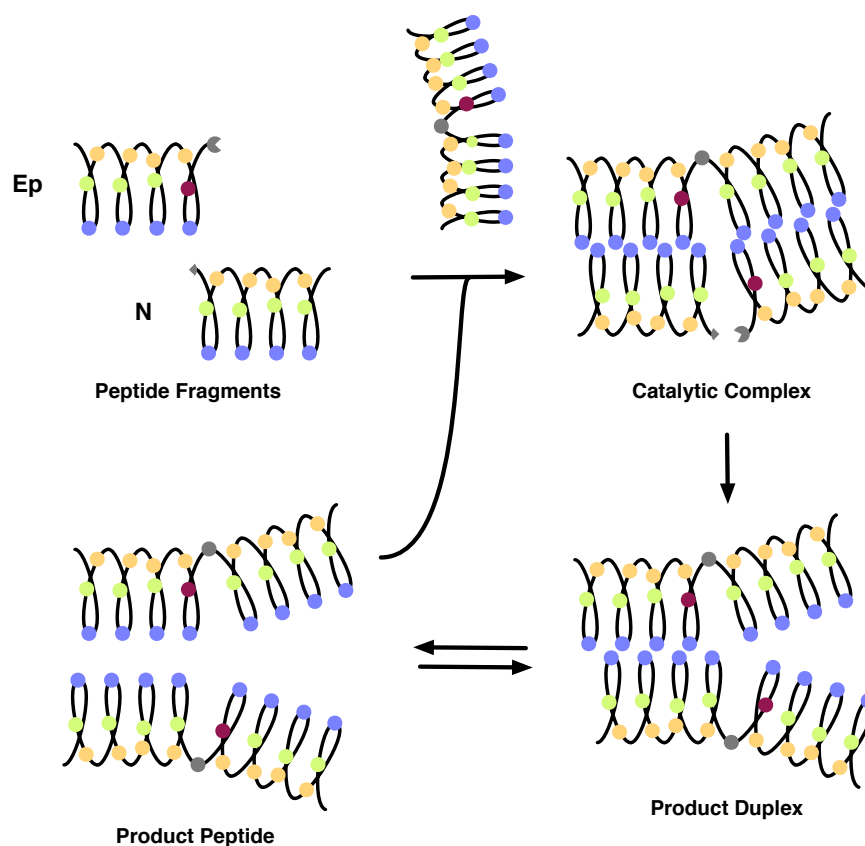


Figure 1.8 Introduction of a proline residue (red residue in **Ep**) alters the geometry of the template thereby decreasing the hydrophobic interactions in the product duplex which favours its dissociation and promotes highly efficient peptide replication.

Based on their initial design, Ghadiri *et al.* presented a network in which two replicators were found to autocatalyse their own formation but also crosscatalyse the formation of the partner (**Figure 1.9**).^[97] Both replicators employ the same electrophilic subunit **E** but vary in the constitution of the hydrophobic core of the nucleophile. Fragment **N1** was identical to the initial structure bearing valine and leucine residues giving rise to peptide replicator **R1** whereas in fragment **N2** all valine groups were replaced with isoleucine residues. This rather conservative variation was yet expected to affect profoundly the stability of the coiled-coil conformation. However, subunits **E** and **N2** were found to generate self-replicating peptide **R2**, even though it proved less efficient than **R1**. In the native reaction between an equimolar amount of **E** and both nucleophiles **N1** and **N2**, the original replicator **R1** predictably dominated in the product pool. However, isolated analysis of both replicators showed not only pronounced template effects for the doping with the native template peptide but stated an even higher crosscatalytic impact upon addition of the opposite template. Under these circumstances, both replicators were found to exist in a symbiotic relationship in which production of one species promotes the production of the other in an even greater extent. Such beneficial relationship is reminiscent of a hypercycle,

[98-100] in which two autocatalytic species are closely connected through an additional crosscatalytic relationship that allows both members to compete more efficiently for existing resources than any member on its own.

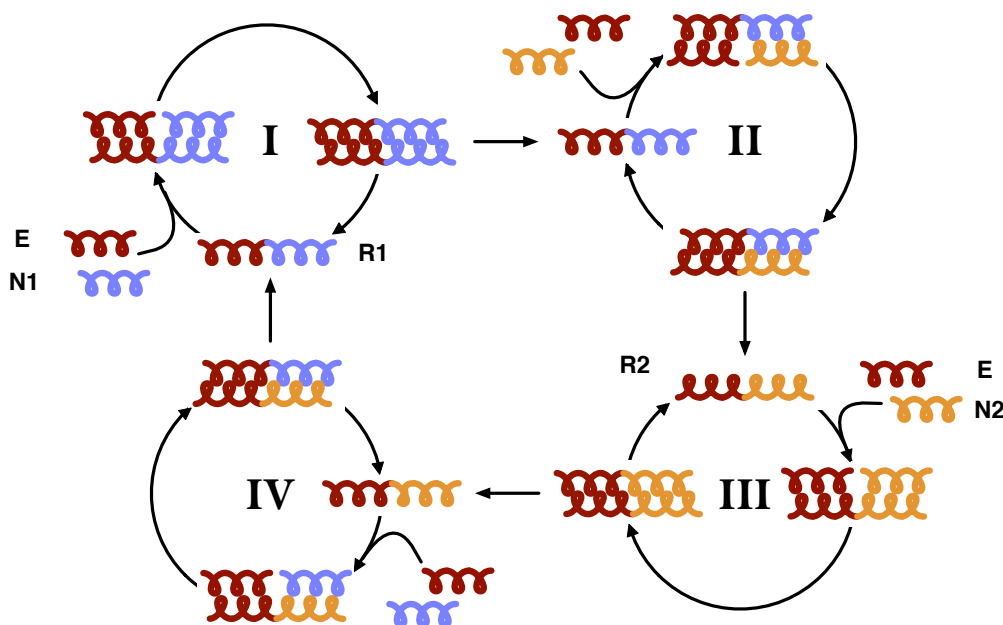


Figure 1.9 Schematic representation of a hypercyclic system based on two self-replicating peptides. Autocatalytic formation of replicator **R1** from fragments **E** and **N1** and replicator **R2** from **E** and **N2** proceed *via* cycles **I** and **III**, respectively. Cycles **II** and **IV** represent the positive crosscatalytic relationship in which **R1** catalyses the formation of **R2** and *vice versa* to form the hypercycle in which the replicators positively regulate each others' production.

Another intriguing example of peptide interaction inspired by phenomena found in nature was conducted by combining the original peptide self-replicator **T** with a set of single residue mutant electrophile and nucleophile (**Figure 1.10**).^[101] The subunits were altered by replacing valine and leucine with an alanine residue in position 9 and 26 of the electrophile (**E_{9A}**) and nucleophile (**N_{26A}**), respectively. These conservative replacements were already shown to have a dramatic effect on the autocatalytic and crosscatalytic efficiencies of the product peptides. No significant template-assisted catalysis upon addition of **T**, **T_{9A}** and **T_{26A}** was stated for the reaction of **E_{9A}** with **N** and **E** with **N_{26A}**. Accordingly, in a reaction mixture composed of equimolar amounts of **E**, **E_{9A}**, **N** and **N_{26A}**, native replicator **T** was found to dominate the product pool.

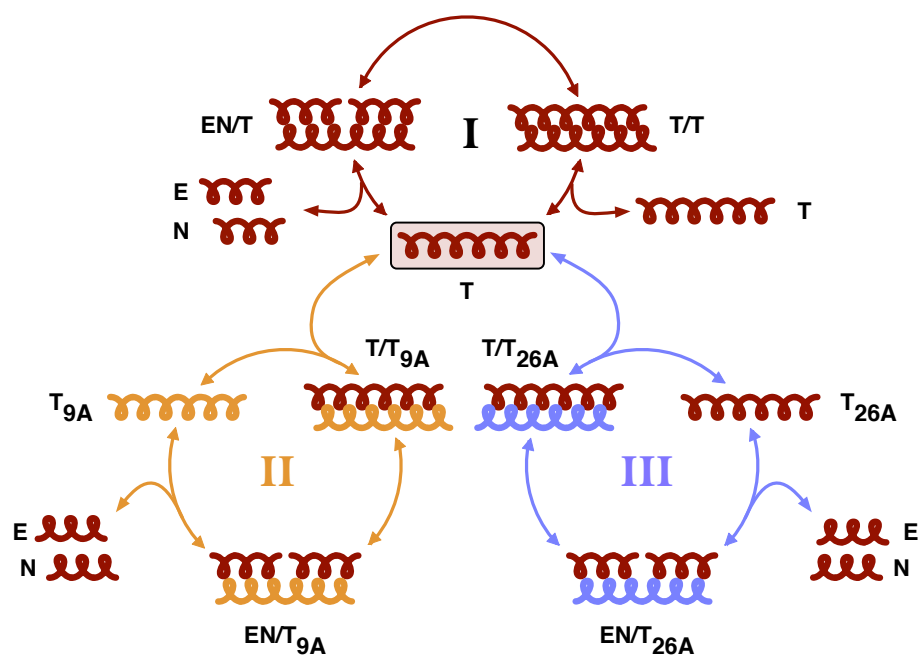


Figure 1.10 Schematic representation of a replicating network exhibiting dynamic error-correction properties. Template T is formed in an autocatalytic manner from building blocks E and N (cycle I) but is also catalysed by mutant templates T_{9A} (orange, cycle II) and T_{26A} (blue, cycle III) which in turn do not possess any catalytic ability for their own formation.

Dissecting the various catalytic relationships in this system showed that the native replicator was not only formed through the established autocatalytic cycle but both mutant templates were also able to crosscatalyse its formation. This imbalanced relationship could be explained by comparing the stability of the ternary pre-ligation complex to the corresponding catalyst dimer. In reactions in which unmodified template aims to ligate an unmodified fragment with a mutant subunit, destabilisation in the hydrophobic core in the ternary complex prevents any catalytic activity. Addition of mutant template to the original fragments creates a situation in which destabilisation affects both the ternary complex and the catalyst dimer. The resulting increase in dissociated free product was expected to compensate for the reduced stability of the catalytic species. In summary, Ghadiri *et al.* have created a network in which an autocatalytic template exploits two mutant templates to enhance its own formation through two further crosscatalytic pathways without contributing to their formation. This selfish behaviour reminds of biological systems in which errors in the replicating process leads to the formation of closely-related mutants. Correction of the committed error can only occur if the replicating activity of the mutant species proves inferior to the original structure.

The homochirality in biological systems is believed to be of utmost importance for the generation and maintenance of living matter.^[102] Its emergence from a pool of prebiotic building blocks is thought to have proceeded by non-linear amplification of an infinitesimal

imbalance for one of the isomers.^[103-105] Replication with its feedback loop potentially provides exponential growth and features prominently in the discussion of the origin of homochirality.^[106,107] In order to maintain and transfer the stereochemical information from one generation to the next, the replication process needs to be chiroselective. This means that in the autocatalytic process the homochiral template must only instruct the synthesis of a species of the same handedness.

Using a peptide structure very closely related to their original example, Ghadiri *et al.* showed how a replicator can selectively amplify homochiral sequences.^[108] For this purpose, the electrophilic **E** and nucleophilic **N** peptide fragments were synthesised in their enantiopure form. **E^L** and **N^L** were composed entirely of natural L-amino acids where **E^D** and **N^D** contained only unnatural D-amino acids. In a subsystem of **E^L** with both nucleophilic units only the homochiral replicator **T^{LL}** showed autocatalytic activity, whereas the heterochiral species **T^{DL}** remained catalytically inactive. Unfortunately, the authors provide no evidence whether the corresponding homochiral template **T^{DD}** was found to self-replicate. They however did establish that replacing one amino acid in the homochiral template **T^{LL}** with its stereochemical partner shuts down all autocatalytic pathways. Hence, the investigated single stereochemical mutants proved to be efficient catalysts for the formation of the homochiral peptide template. This finding complements the results for the dynamic error correction in single alanine mutants on a stereochemical level and was termed 'dynamic stereochemical editing' by the authors.

Within a surprisingly short time, a deep insight into the basics of peptide replication was gained and this knowledge was applied to create a remarkable number of systems with several interacting peptide replicating units. With these sophisticated protocols at hand, the group of Ghadiri took the concept one step further by designing and investigating a molecular network of nine peptide replicators.^[109] In this network, every replicator is formed through ligation of one of nine possible electrophilic fragments with one nucleophile. Variation between alanine, glutamic acid and lysine were allowed in two positions in the electrophilic fragments to create the nine variants. Reaction of all nine electrophilic fragments with the common nucleophile produced nine peptide templates. Their auto- and crosscatalytic abilities were computed based on the stability of the substrate-template transition-state and probed experimentally. In the derived network architecture, three kinds of directed catalytic interactions could be established. Templates could promote their own formation through an autocatalytic pathway, they could serve as a template for the formation of a second structure or they could exploit another peptide template for their own formation.

A subsystem of this molecular network, namely T_1 , T_3 , T_4 , T_5 and T_7 , showed pronounced interaction among its members and was used to generate three examples of a molecular logic gate (**Figure 1.11**).^[110] Instructing the network by adding preformed peptide template changed the output of an interconnected species. For instance, addition of either T_3 , T_4 or both led to a significant increase for the formation of template T_7 simulating an OR logic operation.

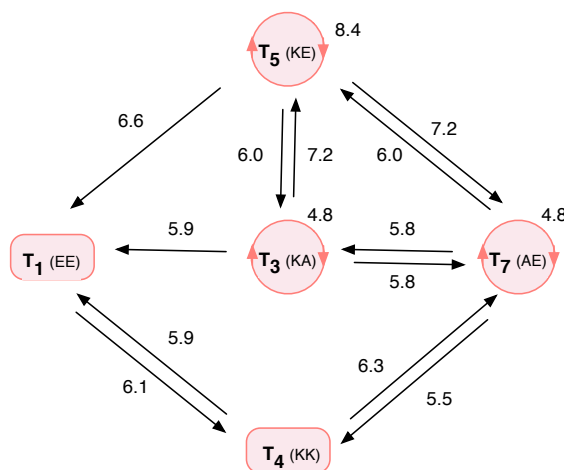


Figure 1.11 Schematic representation of a network of replicating peptides. Each node in the graph represents a particular peptide template or product (T_1 , T_3 , T_4 , T_5 and T_7) and the arrows indicate the relationship between the nodes pointing from the template to the product. Circular nodes represent peptide templates with autocatalytic ability (T_3 , T_5 and T_7). The templates can be identified according to the two amino acid code giving in parenthesis. Numbers next to the templates or the arrows represent theoretical estimation of the relative efficiency of the depicted pathway and were estimated on the basis of the calculated difference in the stability of the trimeric product species.

Recently, the alignment of peptides consisting of alternating hydrophilic and hydrophobic amino acid residues into ordered β -sheet assemblies was used as a platform for the design of a novel type of self-replicating peptide structures.^[111] It was shown that existing β -sheet aggregates of an amphiphilic peptide **P** can act as a template for the association of two smaller peptide fragments, **N** and **E**, which react to form a new molecule of **P**. This copy is consecutively incorporated into the β -sheet and the extended aggregate can then undergo further catalytic cycles.

1.6 Synthetic replicators^[112,113]

In 1990, Rebek *et al.* presented a self-replicating system made up entirely of synthetic building blocks (**Figure 1.12**).^[114] With their expertise in designing receptors for biological molecules, they reasoned that connecting both recognition partners by a suitable covalent

linker would give rise to a molecular structure that can self-replicate. For this purpose, they exploited the association through hydrogen bonding between a maleimide moiety based on Kemp's triacid^[115] (in **4**) and adenosine (in **5**). The formation of an amide between an activated pentafluorophenyl ester on maleimide **4** and a primary amine connected to the adenine structure **5** was chosen as the chemical reaction to create the covalent bond in the self-complementary template **6**. In order to avoid recognition-mediated reactions through a binary complex, a naphthalene spacer was incorporated into structure **4**. Initial problems with strong product inhibition were overcome by introducing a sterically demanding ribose sugar into **5**. This group was shown to induce a slight kink into the structure of product **6** thereby reducing the stability of its duplex structure.

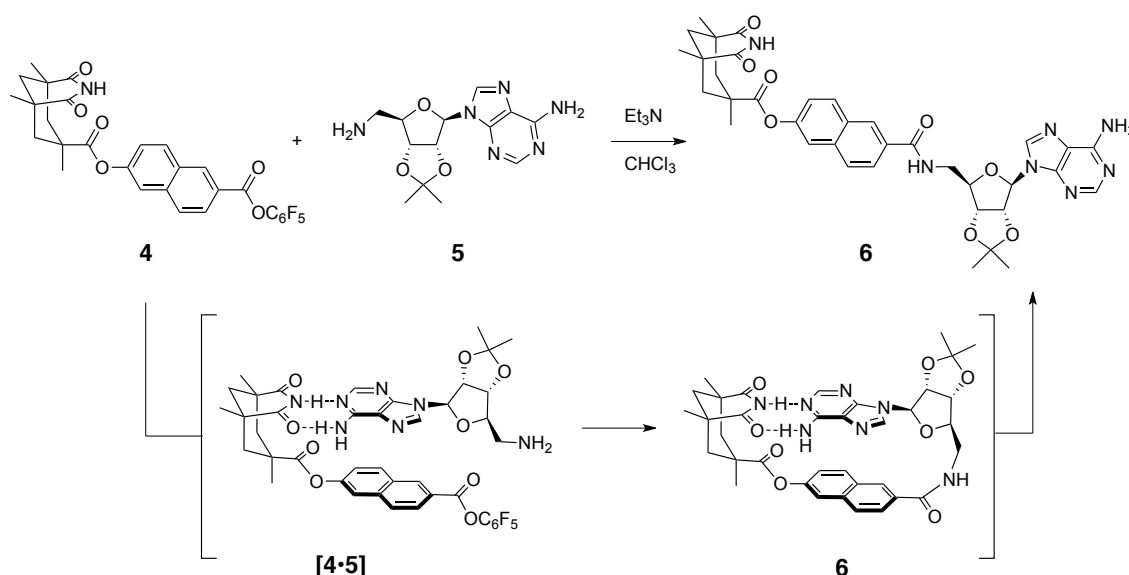


Figure 1.12 The recognition between the Kemp's triacid imide in the activated ester **4** and the adenine base in **5** drives the formation of template **6** either through the binary complex **[4·5]** or through the corresponding **[4·5·6]** complex (shown as pathway **III** in Figure 1.13).

The amide bond formation of the self-complementary structure **6** was shown to be enhanced by addition of preformed product. Control experiments with recognition disabled compounds showed significantly lower reactivity. A kinetic analysis by von Kiedrowski calculated the kinetic efficient molarity ϵ to be around 80.^[80]

Rate-enhancements of over 40% were assigned to the generation of a ternary complex in which a product molecule acts as a template to assemble both starting compounds to facilitate their reaction by bringing the reactive sites, the primary amine and the pentafluorophenyl ester, in close proximity (**Figure 1.13**, pathway **III**). After bond formation, the duplex structure dissociates into two catalytically active template molecules. Next to this

autocatalytic mode, two further reaction pathways were assumed to occur (**Figure 1.13**, pathway **I** and **II**).^[116] Firstly, both compounds can react in a bimolecular fashion without making use of their recognition sites. Furthermore, despite the incorporation of a naphthalene spacer, the formation of a binary complex between both reactive partners deemed possible. In this case, fixation of the adenine in the imide pocket brings both reactive sites in close proximity and allows a rate-enhanced pseudo-intramolecular aminolysis to form the *cis*-amide which can subsequently isomerise to the more stable *trans*-amide product.

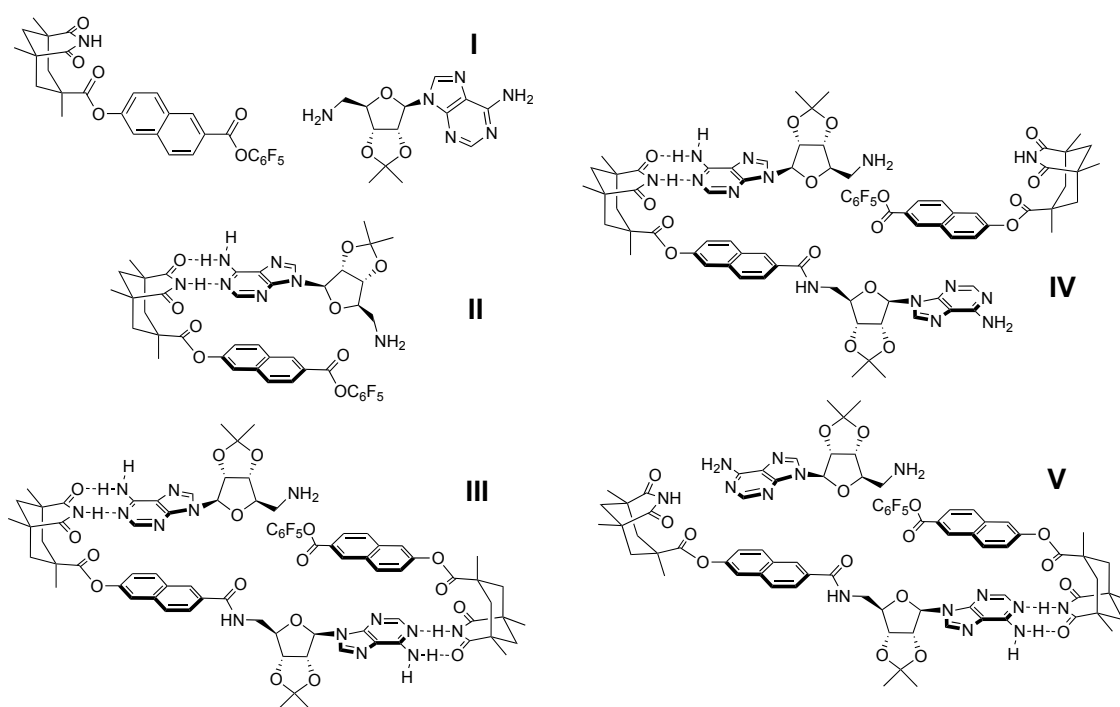


Figure 1.13 The five pathways which contribute to the observed kinetics of the Rebek replicator shown in **Figure 1.12**: the background reaction (**I**), the AB complex (**II**), the ternary complex (**III**), the reaction between the activated amine (by the bonded template) with free ester (**IV**), and the reaction between the activated ester (by the bonded template) with free amine (**V**).

Rebek's results were questioned by Menger who thought to be able to explain the observed rate-enhancements by simple amide catalysis.^[117-120] He published an alternative mechanism (**Figure 1.13**, pathway **V**) in which only one recognition event was necessary to hold the reactive partners in place for the reaction. By stabilising the tetrahedral intermediate through hydrogen bonding, this intermediate step would also explain the observed catalytic effect.

However, it was not until Reinhoudt *et al.* subjected Rebek's system to an exhaustive kinetic analysis.^[75] In the resumé of their investigations,^[75] they declared the presence of five reaction pathways that all contribute to the formation of product (**Figure 1.13**). In addition to

the three pathways proposed by Rebek, they could verify the existence of Menger's activated bimolecular species as well as the presence of a related bimolecular species, in which the ester is preorganised on the template to react with unbound amine (pathway IV).

Comparison of rates led to the conclusion that the highest contribution comes from Menger's activated bimolecular pathway, however, results proved to be highly dependent on the concentration at which the experiments were conducted. As a matter of fact, both parties could save their face, but this example shows that a clean kinetic analysis of a potential self-replicating system and the execution of the right control experiments are absolutely crucial.

At the time of Reinhoudt's resolving paper, Rebek had already presented a modified version of his initial self-replicating system (**Figure 1.14**). Using a biphenyl moiety as a prolonged spacer instead of the original naphthalene backbone led to the observation of sigmoidal growth.^[121] By extending the spacer length, reaction through the binary complex is suppressed giving way to the self-replicating mode with its characteristic sigmoidal rate profile.

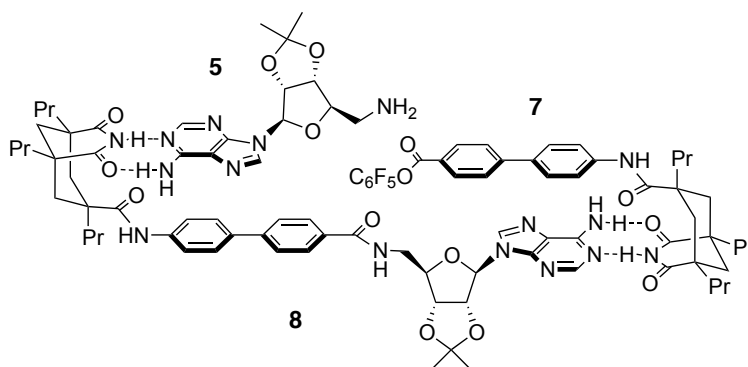


Figure 1.14 The longer biphenyl spacer present in activated ester 7, when compared to the naphthyl spacer present in 4 (**Figure 1.12**), ensures that template 8 is formed principally by the reaction through the ternary complex [5·7·8] shown.

In order to optimise the binding event between the adenine moiety and its receptor, Rebek *et al.* created^[122,123] a second structure in which the adenine moiety was simultaneously recognised through both Watson-Crick and Hoogsteen hydrogen bonding (**Figure 1.15**). A cleft-like structure of two imides attached to a biphenylcarbazole backbone was designed and investigated. In this new structure, recognition of the adenine structure occurs simultaneously through the two imides by both binding modes. In addition, pronounced π - π interactions between the adenine and the biphenylcarbazole further optimise the binding event. However, increasing the association constant did not lead to the

expected enhanced self-replicating activity of the novel system. Instead, the reactivity was hampered by strong association in the product duplex.

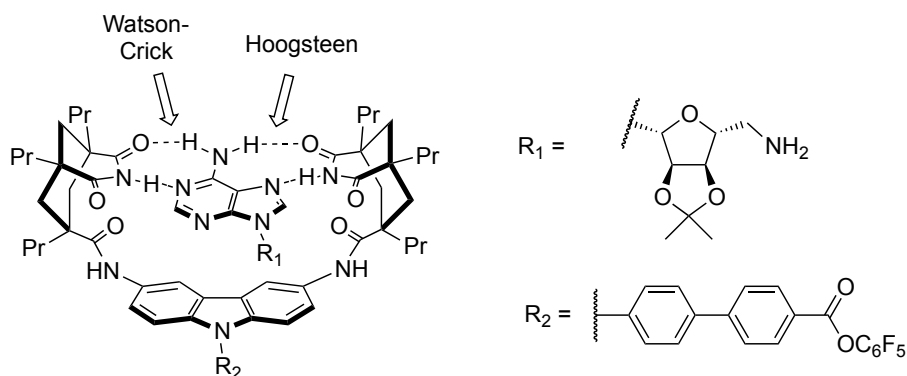


Figure 1.15 A combination of Watson–Crick and Hoogsteen hydrogen bonding patterns permit the recognition between the adenine and the diimide.

Having increased the association between the adenine and the diimide cleft structure, Rebek *et al.* were able to establish crosscatalytic protocols in which a presynthesised bis (diimide) structure was found to be able to catalyse the condensation of two adenine molecules through amide bond formation.^[124,125] In reverse, this bis(adenine) structure acted as a reciprocal template for the formation of the original diimide template, thus completing a crosscatalytic replicating cycle. However, strong autocatalytic pathways between the recombinant amine and ester variants prevented an investigation of the pure reciprocal system.^[126]

Besides optimisation of their efficiency, Rebek aimed at incorporating self-replicating systems into more complex scenarios to mimic biological features such as mutation and evolution. For instance, manipulation the outcome of a competition reaction between two self-replicators by external trigger was demonstrated using two variants of the replicating system bearing the biphenyl spacer.^[127] In the original system, recognition between the adenine moiety and the ester imide can occur by both Watson-Crick and Hoogsten mode. When blocking the exocyclic adenine amine with a protecting group such as benzyloxycarbonyl, hydrogen bonding through the Watson-Crick mode is severely disfavoured and association to the imide ester occurs mainly through Hoogsten binding generating a comparably less efficient self-replicating system. Introduction of a structurally very similar photolabile *o*-nitrobenzyloxycarbonyl group has the same impact on the efficiency of the system. In fact, combining biphenyl imide ester with both protected species showed that the two self-replicators not only catalyse their own formation but they also act

as templates for the formation of its partner. A competition experiment was conducted in which both protected adenine structures were allowed to react with a limited amount of active ester. Both replicators proved nearly equally efficient, however, irradiation of the solution removed the photolabile *o*-nitrobenzyloxycarbonyl protecting group converting it into the original adenine structure with free exocyclic amine. By releasing the free amine, the original replicator is regenerated and binding of the adenine to the imide moiety can again proceed through both modes, leading to a self-replicating system with increased efficiency. When more fresh reagent is added to the reaction mixture, the unprotected replicator now quickly starts to dominate the product pool. This model experiment shows how an external trigger can induce a structural change in an existing replicator to create an even more potent mutant species.

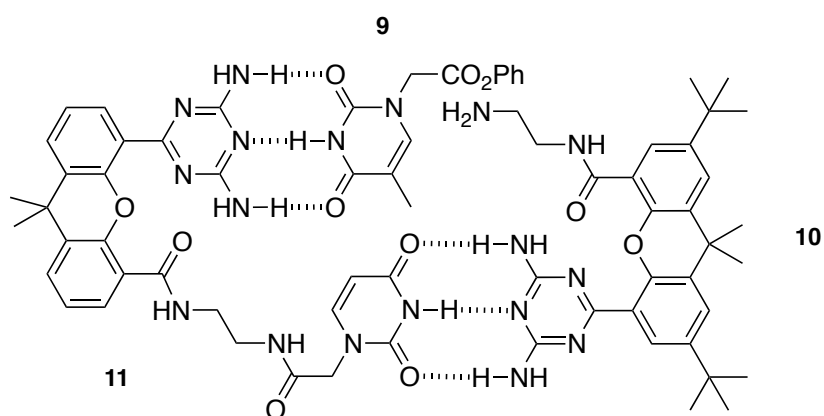


Figure 1.16 A self-replicating system between ester **9** and amine **10** to give amide **11** based on a diaminotriazine/thymine recognition motif.

Another self-replicating system was based on the well-defined pattern of hydrogen bonds between thymine and diaminotriazine (**Figure 1.16**).^[128,129] The thymine moiety in **9** was equipped with an activated ester which can react with the amine in **10** to form the amide bond in template **11**. The xanthene backbone in **10** and **11** assured the appropriate geometry for the assembly of both starting fragments on the product template to form the ternary complex necessary for self-replicating activity. As demonstrated in other systems, self-replication was stated through doping experiments. Adding a fixed amount of preformed template increased the rate of product formation whereas applying recognition-inhibited template molecules did not exhibit any increase in rate. Recently, this recognition motif was revisited to design two self-replicating systems in which the newly formed bond consisted of a thiourea^[130] or imidazolidine^[131] moiety. The final template structures were then tested as organocatalysts in a Michael addition, hydrogenation and Friedel-Crafts alkylation.

A combination of the original adenine replicator with the thymine based replicator allowed the performance of crossover experiments.^[132] Since both systems rely on amide bond formation, a set of all four starting blocks can potentially lead to two additional recombinant replicating systems. Adenine amine **5** was found to react with thymine ester **9** to give rise to an exceptionally efficient self-replicator. This efficiency is owed to the appropriate orientation of recognition and reactive sites in the ternary complex. However, a combination of both larger fragments, ester **4** and amine **10**, generated a template which did not possess the right geometry to promote self-replication.

An intriguing example of a structurally very simple self-replicating system utilises amidinium-carboxylate salt bridges to enhance the catalytic condensation of an aniline structure with a benzaldehyde derivative (**Figure 1.17**).^[133] Several structures with various substituents in para-position to the recognition sites have been investigated. For instance, autocatalysis was established in the formation of anil **14** from aniline **12** and aldehyde **13**. Adding preformed template to the reaction mixture increased the initial rate of product formation and the obtained experimental data was in accordance with the square-root model.

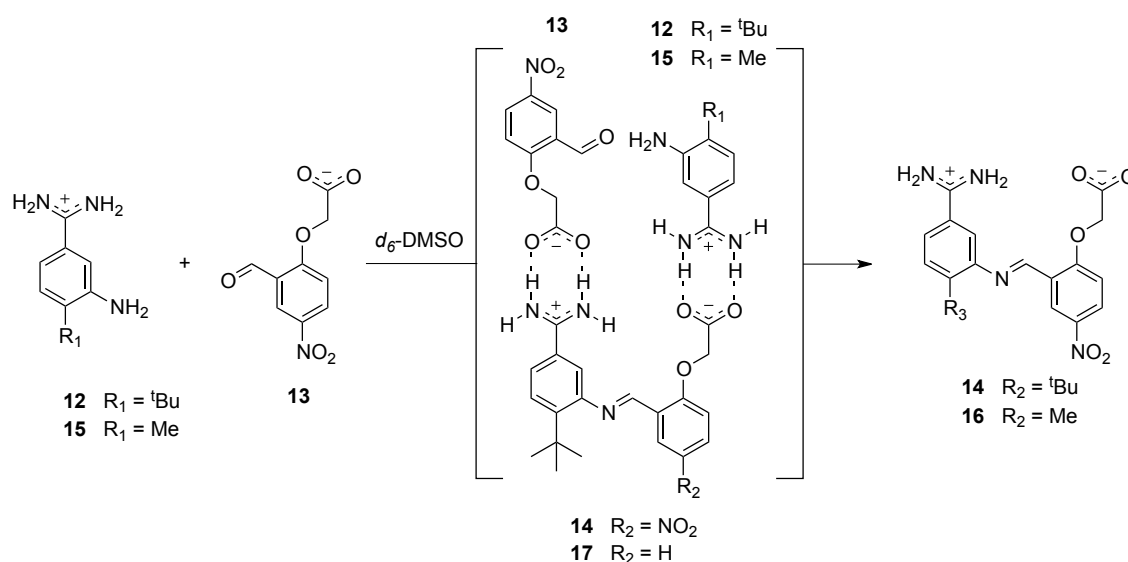


Figure 1.17 A series of auto- and crosscatalytic templates can be formed by combinations of amines **12** and **15** with aldehyde **13**.

More interestingly, anil **17** was found to crosscatalyse the condensation of amine **15** and aldehyde **13** to form **16** with a first-order relationship, hence addition of preformed template of **17** led to a proportional increase in formation of **16**. Crucial for such behaviour are different stabilities of the ternary and the product duplex. In case of a stable duplex,

strong association leads to a square-root dependence of rate with respect to the total template concentration. However, if the product duplex proves less stable than the ternary complex of building blocks and template, the system can reach its full catalytic potential.

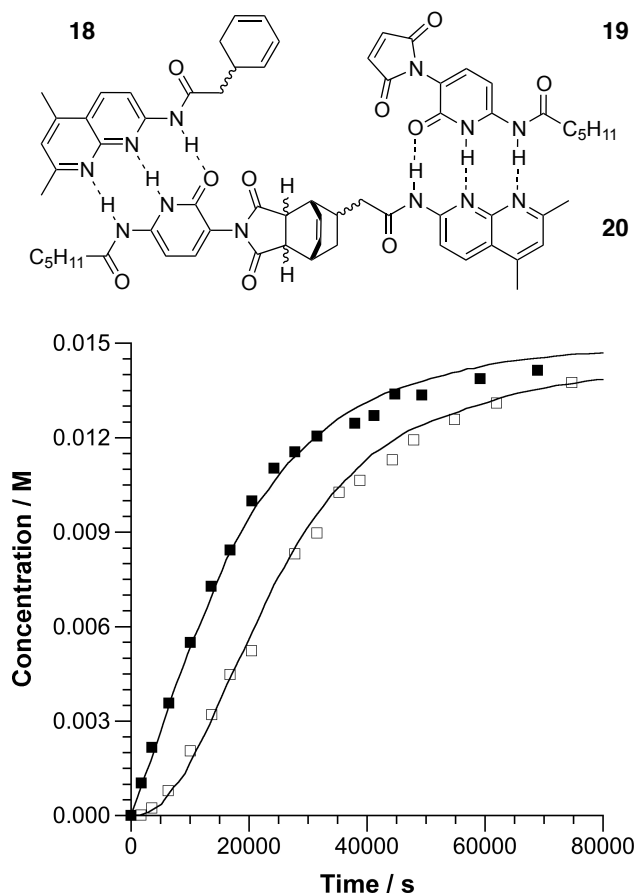


Figure 1.18 Diels–Alder cycloadduct **20** can assemble the chiral diene **18** and maleimide **19** in a catalytically active ternary complex. This complex is the dominant reactive species in the formation of **20** in CD_2Cl_2 at 25 °C (open squares in graph). The addition of 5 mol-% of **20** to the reaction mixture (filled squares in graph) removes the lag period from the concentration *vs* time profile demonstrating that **20** is a catalyst for its own formation. Data taken from ref. [134].

A replicating system of simple organic molecules with surprisingly high p value was presented by Wang and Sutherland in 1997 (**Figure 1.18**).^[134] In their design, they exploit the directed recognition through hydrogen bonding between an amido naphthyridine **18** and an amido pyridone moiety **19**. As chemical reaction to join both fragments together, the authors chose the Diels-Alder reaction between a maleimide and a cyclohexadiene. Reacting both recognition-enabled compounds showed a sigmoidal rate profile for the formation of product **20**. Doping a mixture of reactants with presynthesised template **20** confirmed the autocatalytic mechanism of the reaction by overcoming the initial lag period with maximum rate at the beginning of the reaction. Experiments with recognition-enabled reagents showed

significantly lower conversions by solely forming the products *via* bimolecular pathways. Fitting of the obtained results provided a value of 0.8 for p as best approximation. This value is somewhat higher than for other systems based on oligonucleotides or simple organic molecules. Steric repulsion between the methyl group on the naphthyridine **18** with the alkyl group of the pyridone side-chain in **19** caused some inhibition of the binding event leading to a relatively low association constant. This rejection was also expected to exist in the product reducing the stability of the duplex. With the equilibrium shifting away from the catalytically inert duplex structure, more free template becomes available thereby increasing the autocatalytic efficiency. Furthermore, this replicating system can potentially form four possible diastereoisomers, but it was not until recent, that the stereochemical features of a slightly modified variant was thoroughly analysed by von Kiedrowski *et al.*^[135]

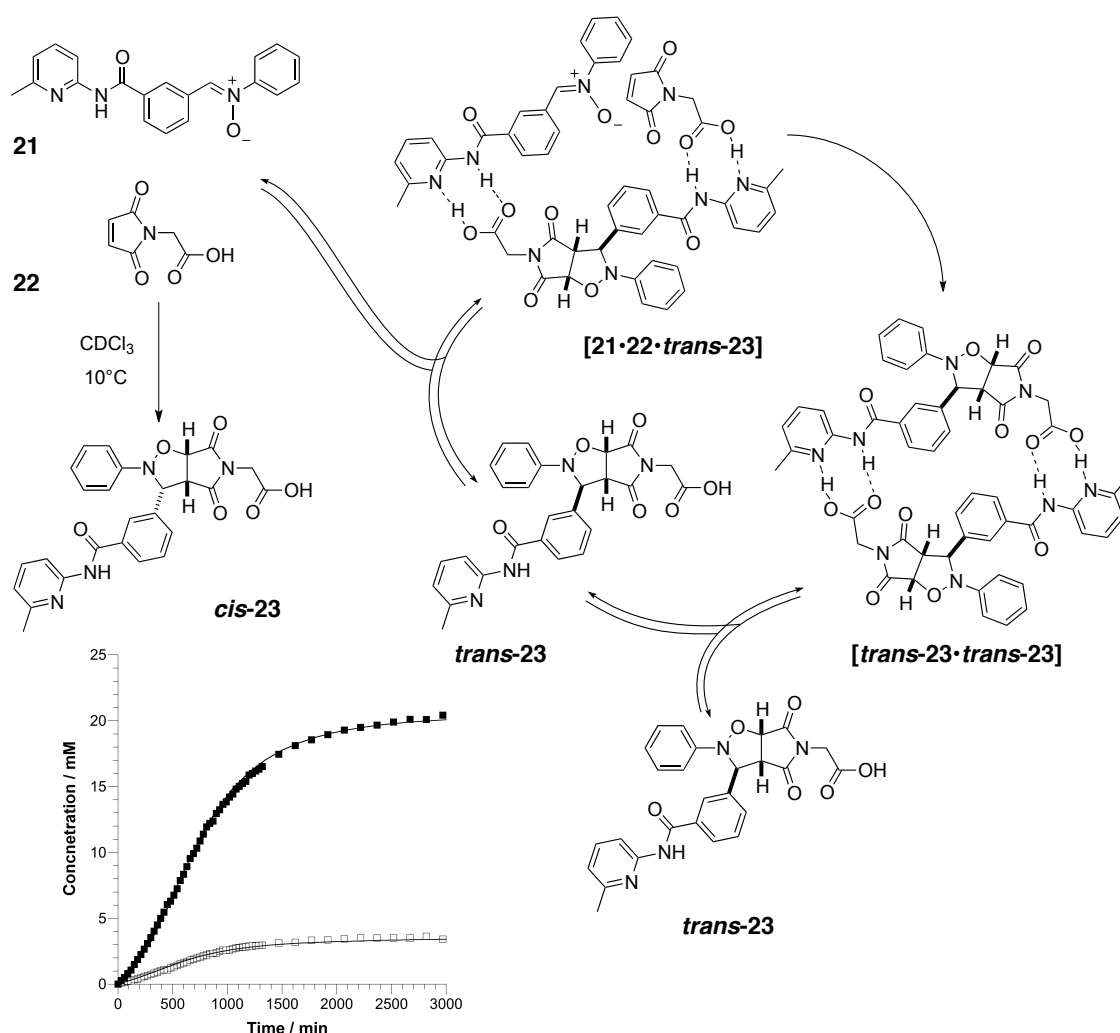


Figure 1.19 Reaction of nitron **21** with maleimide **22** in CDCl₃ at 10 °C gives rise to two diastereoisomeric cycloadducts – *cis*-**23** and *trans*-**23**. While *cis*-**23** does not exhibit appreciable recognition-mediated reactivity (filled triangles in graph), the formation of *trans*-**23** (filled squares in graph) exhibits a sigmoidal concentration *vs* time profile and further experiments confirm the operation of the autocatalytic cycle mediated by the ternary complex [21·22·*trans*-23] in this system.

Self-replicating processes based on simple organic molecules may allow the transfer of chemical information to be passed on through the regio- and stereoselectivity of the template catalysed bond formation. A self-replicating system in which stereochemical information was transmitted faithfully to the formed template within the reactive ternary duplex was demonstrated using the 1,3-dipolar cycloaddition between nitrone **21** and maleimide **22** (**Figure 1.19**).^[136] This reaction generally proceeds slow and with low selectivity for the formation of the two possible diastereoisomers of **23**. Both isomers can be distinguished by the relative orientation of the three protons attached to the bicyclic ring system. In the case of *cis*-**23**, all protons point to the same side in respect to the bicycle whereas in cycloadduct *trans*-**23** the proton on the isoxazolidine ring is orientated away from the protons at the ring junction. In a simple bimolecular reaction, the *trans*-isomer is usually formed in a ratio of about 3:1 over the *cis*-isomer. In order to allow recognition events to take place, **21** and **22** were equipped with an amidopyridine and a complementary acid functionality, respectively. The reaction of both compounds gave rise to two diastereoisomeric products *trans*-**23** and *cis*-**23** in a ratio of 7:1. As comparison, the reaction-inhibited reaction between **24**, the methyl ester of **22**, and **21** proceeded at much slower rate giving rise to a diastereoisomeric mixture of the isoxazolidines with a ratio of only 4:1 for the *trans*-isomer after the same time (**Figure 1.20**).

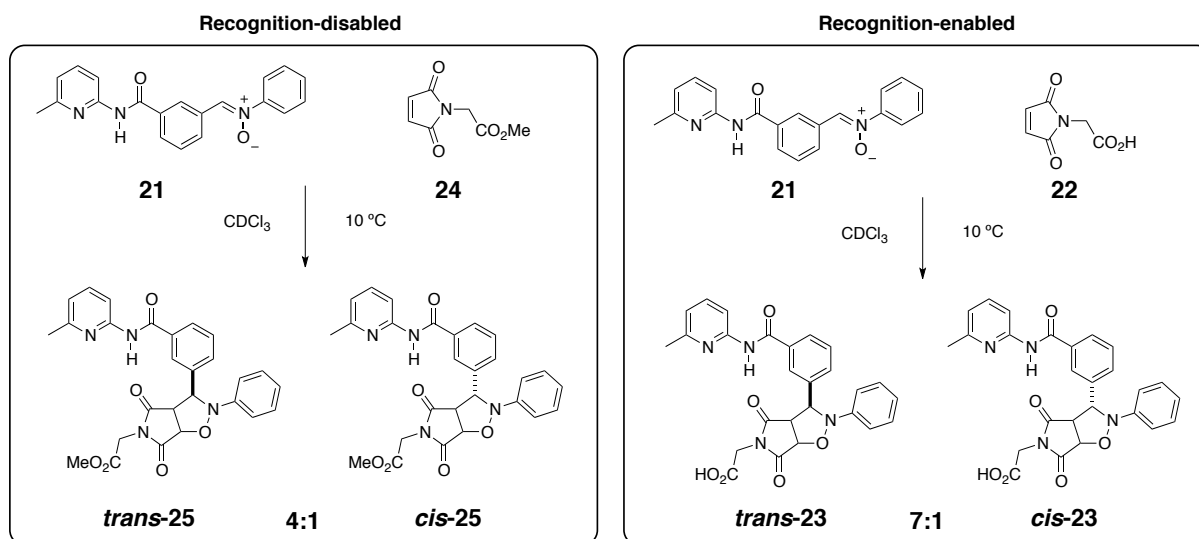


Figure 1.20 Reaction between nitroene **21** and methyl maleimide **24** gives rise to a diastereoisomeric mixture of cycloadducts, *trans*-**25** and *cis*-**25** which vary upon introduction of recognition with maleimide **22** towards self-replication isomer *trans*-**23** as highlighted in **Figure 1.19**. The ratio of diastereoisomers is indicated by the numbers next to the templates.

The deviation in selectivity for the *trans*-isomer of **23** can be assigned to the inherently different geometries of both diastereoisomers. Owing to the relative orientation of the substituents on the bicycle, the *cis*-isomer of **23** possesses a folded geometry in which both recognition units are facing each other making the association of starting reagents sterically unlikely. On the other hand, the *trans*-isomer adopts an open conformation in which both starting materials can be recognised in a ternary complex as shown in **Figure 1.19**. In this geometric arrangement, the reactive sites of **21** and **22** are being put in close proximity and their reaction proceeds with higher rate. Moreover, the diastereoisomeric template truthfully passes on its stereochemical information onto its offspring rendering the formation of the *trans*-isomer autocatalytic. In order to proof the autocatalytic activity of the *trans*-template, presynthesised catalyst was added at the start of the reaction. The rate profile therefore showed the loss of the initial lag period and led to an enhanced formation of the *trans*-isomer, pushing the product ratio to 9:1 after the same time. In the presence of four equivalents of benzoic acid, the rate profile showed a significant decrease for both the rate of the reaction and its selectivity. Benzoic acid acts as a competitive inhibitor that binds to the amidopicoline unit of the nitron compound, thereby confirming that the formation of *trans*-**23** from nitron **21** and maleimide **22** is indeed recognition-mediated. Fitting of the experimental data afforded values for p and ϵ of 0.9 and 5000, respectively.

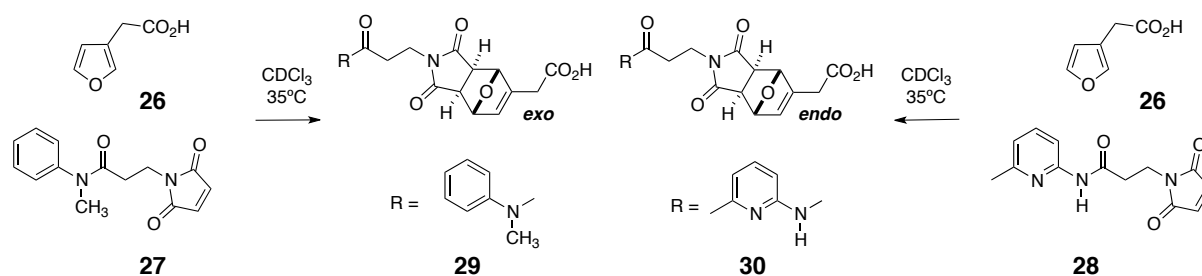


Figure 1.21 Diels-Alder reaction of maleimide **28** with furan **26** gives rise to two diastereoisomeric products, *exo*- and *endo*-**30**, which are both capable of accelerating their own formation in an autocatalytic manner. The two cycloadducts do not have any measurable catalytic effect on the formation of their partner diastereoisomer. Maleimide **27** was used as a control compound to give products *exo*- and *endo*-**29** which highlight the importance of hydrogen bonding since the *N*-methyl anilide is incapable of binding the carboxylic acid recognition site in **26**.

Our group reported on another system in which the Diels-Alder reaction between maleimide **28** and furan **26** generated two diastereoisomeric products of **30** (*endo* and *exo*) which are both capable of catalysing their own formation but show no crosscatalytic effect on the rate of formation of their diastereoisomeric partner (**Figure 1.21**).^[137] Reacting the recognition-disabled derivative **27** with **26** established the background rate for the formation

of the two cycloadducts. The reaction proceeded slow and the *endo:exo* ratio was found to be 1.6:1. Repeating the reaction with recognition-enabled **28** showed a significant increase in the initial rates of formation for *both* diastereoisomers of **30** and a change in diastereoselectivity to a ratio of 1.1:1 in favour of the *endo*-isomer.

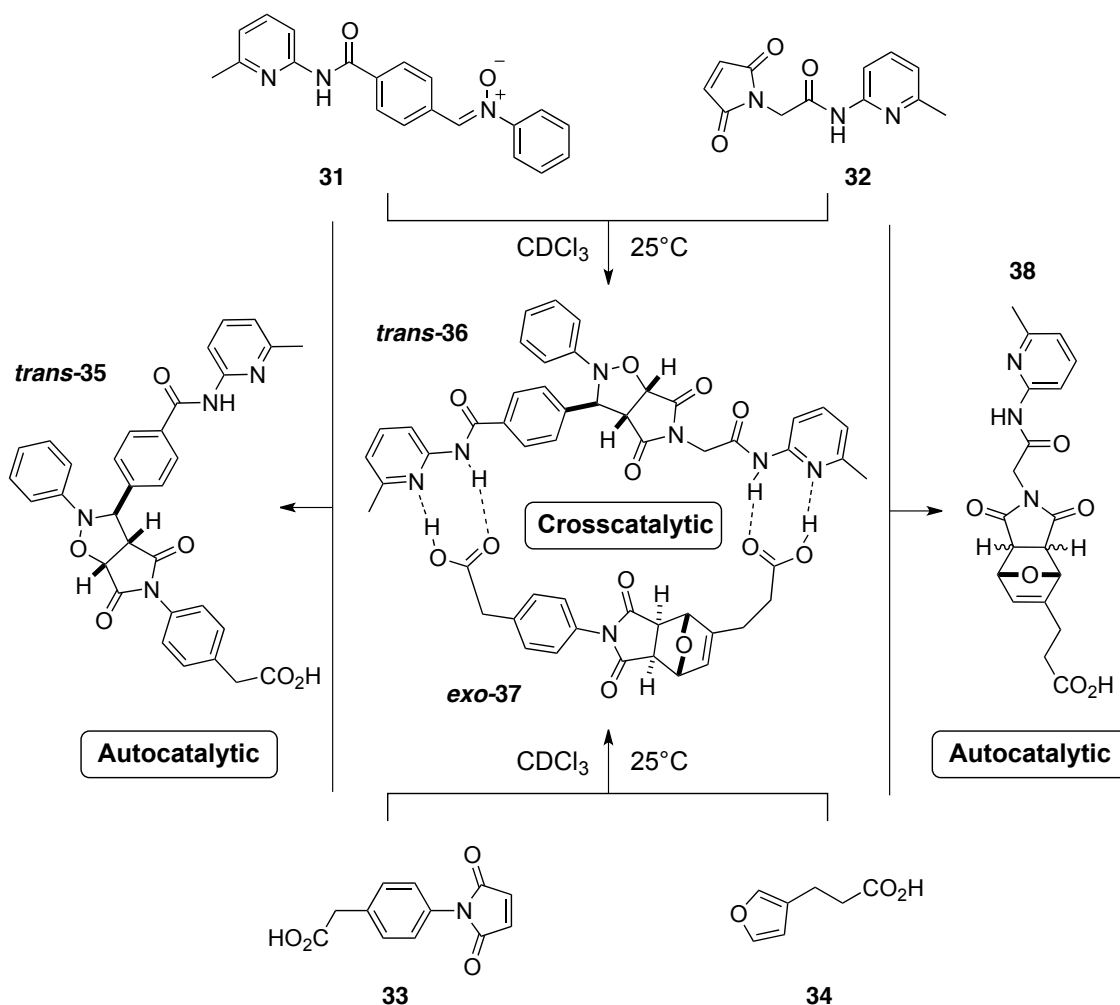


Figure 1.22 Maleimides **32** and **33** together with nitrone **31** and furan **34** form a multicyclic system consisting of two autocatalytic and two reciprocal relationships. *Trans-35* was found to be the template for the autocatalytic reaction of **31** and **33** whereas both isomers of **38** are self-replicating products from the reaction between maleimide **32** and furan **34**. Template *trans-36* can assemble maleimide **33** and furan **34** into a crosscatalytic ternary complex $[33:34:trans-36]$ in which the Diels–Alder reaction between **33** and **34**, forming template *exo-37*, is accelerated. Similarly, template *exo-37* can assemble nitrone **31** and maleimide **32** into a crosscatalytic ternary complex $[31:32:exo-37]$ in which the 1,3-dipolar cycloaddition reaction between **32** and **31**, forming template *trans-36* is accelerated, completing a formal reciprocal replicating cycle. Upon mixing all four components in CDCl_3 at 25°C , template *trans-35* was the dominant product.

Selective doping at the start of the reaction with 10 mol-% of preformed diastereoisomer established selfish autocatalytic enhancement as the only catalytic pathway for both species. Crosscatalysis from one diastereoisomer to the other was not observed. This

finding was rationalised by molecular modelling of both product templates. It could be illustrated that both homodimeric species adopt optimal conformations to align their recognition units and act as a catalyst for the formation of their own isomer whereas the formation of a heterodimer could be ruled out as a consequence of geometric constraints.

Another example of diastereoisomeric heredity in a replicating system using simple organic molecules was demonstrated within a multicyclic set-up for a crosscatalytic system in which two complementary templates were found to stereospecifically catalyse the formation of each other (**Figure 1.22**).^[138] Combining the chemistry based on the Diels-Alder reaction between furan and maleimide, and the 1,3-dipolar cycloaddition between a nitron and a maleimide, a set of four compounds, **31**, **32**, **33** and **34**, were reacted to give rise to four pairs of diastereoisomeric templates. In the absence of complementary recognition units, the native Diels-Alder reaction and the 1,3-dipolar cycloaddition was shown to proceed with poor diastereoselectivity giving an *endo:exo* ratio of only 1:1.3 and a *trans/cis* ratio of 3:1, respectively.

However, the formed templates now contain two identical recognition sites making them potential reciprocal templates. Computational analysis of the template structures suggested an optimal fit for the heterodimer of *trans-36* and *exo-37*. Accordingly, the addition of substoichiometric amounts of presynthesised bisamido template *trans-36* significantly increased the rate of formation for *exo-37* which in turn was shown to possess crosscatalytic activity for the formation of *trans-36*. Kiedrowski *et al.* have demonstrated in their multicyclic system of nucleotide replicators (**Figure 1.5**),^[84] that coexistence between autocatalytic and crosscatalytic species can occur as long as the efficiencies of both catalytic pathways are similar. However, in the present system of reciprocal replicator using simple organic molecules (**Figure 1.22**), this precondition is violated by the use of two different chemical reaction types which differ significantly in rate, with the 1,3-dipolar cycloaddition being the faster one. Moreover, a recombination of starting materials gives rise to two autocatalytic systems. Reacting furan **34** with maleimide **32** leads to a modestly efficient, non-stereoselective replicating system **38**, whereas maleimide **31** and nitron **33** were found to form *trans-35* in an extraordinarily efficient autocatalytic process. This imbalance in reactivity renders the system immune towards instructions by template inputs, an exhaustive kinetic analysis of its features yet provided important insight into the requirements needed for the construction of instructable networks based on simple organic molecules.^[139]

The high autocatalytic efficiency of *trans-35* can be attributed to the optimised geometry of the template (**Figure 1.23**).^[140] The rigid, open-folded structure of *trans-35* shows

a high degree of self-complementarity and the geometry of the reagents in the ternary complex is similar to the one calculated for the bimolecular reaction. In contrast to this, the *cis*-isomer remained catalytically inert with its recognition sites placed in proximity to each other. Reacting nitron 31 with recognition-disabled methyl ester of 33 established the bimolecular rate for the reaction (only 9% conversion at -10 °C) and the native selectivity of 3:1 in favour of the *trans*-isomer. When recognition is introduced by using maleimide 33 with the free acid functionality, the formation of the *trans*-product is enhanced 13-fold. Competitive inhibition experiments with two equivalents of benzoic acid established the pivotal role of hydrogen bonding, whereas adding substoichiometric amounts of preformed *trans*-T_{BC} to the reaction mixture caused a loss of the initial lag period and demonstrated that the *trans*-isomer is indeed a catalyst for its own formation.

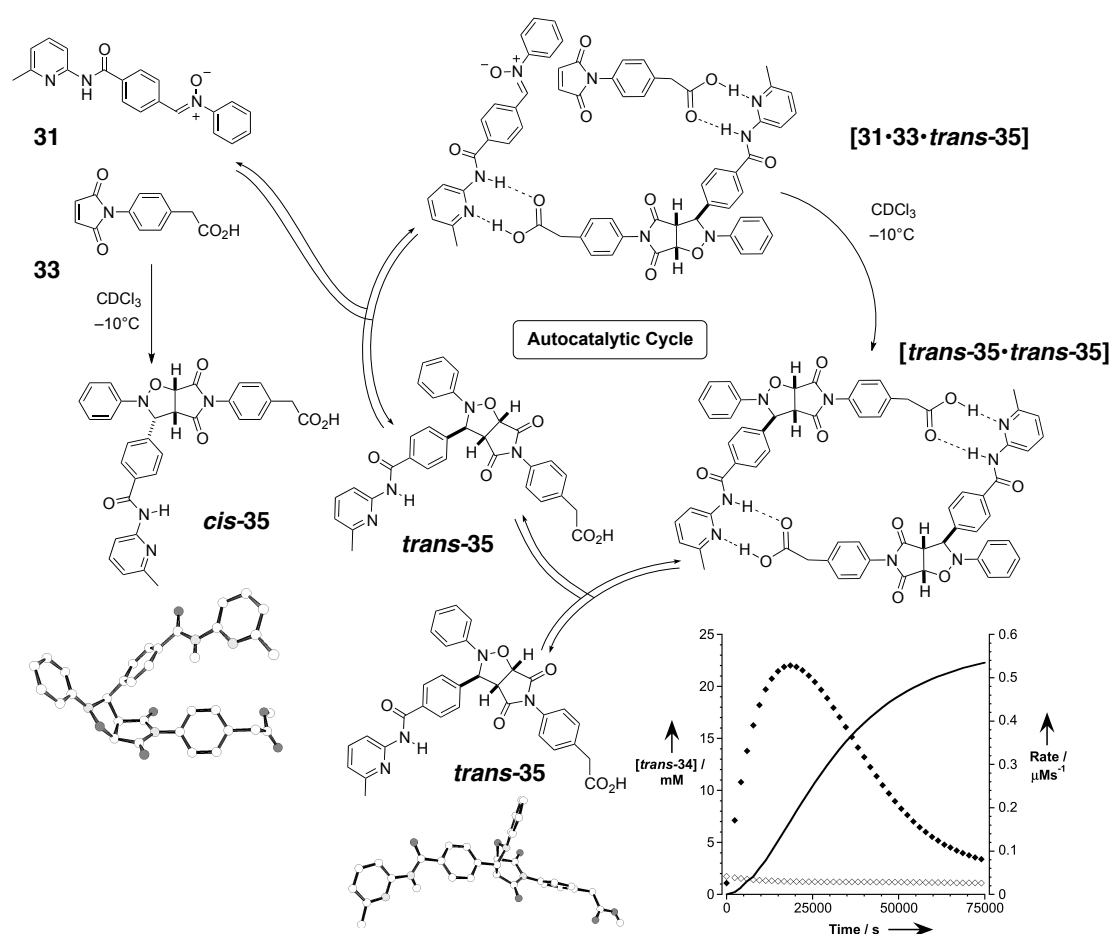


Figure 1.23 Reaction of nitron 31 with maleimide 33 in CDCl₃ at -10 °C can potentially give rise to two diastereomeric cycloadducts – *cis*-35 and *trans*-35. However, the efficient operation of the autocatalytic cycle mediated by the ternary complex [31·33·*trans*-35] in this system ensures that *trans*-35 is formed almost exclusively (solid line in graph, *trans*-35:*cis*-35 100:1, *cis*-35 not shown). The rate *vs* time profile for the reaction at -10 °C in CDCl₃ (filled circles in graph) reveals the classical bell shape characteristic of an autocatalytic process and the rate of reaction is far higher than that observed in the absence of recognition (open circles in graph). Data taken from ref. [113].

The design of the latter minimal self-replicating system marks the culmination of a development in which computational methods were applied to gain a deeper understanding of the requirements to design systematically and optimise efficient self-replicating systems.^[141-143] Calculations of the template structure were conducted to avoid the formation of the undesired binary AB complex, but more importantly, to stabilise the transition state of the bond forming reaction within the ternary complex. In case of the 1,3-dipolar cycloaddition, the transition state is assumed to be late, hence its optimisation automatically led to a fortification of interaction in the product duplex. In replicating systems based on oligonucleotides or peptides, strong association among the template molecules leads to product inhibition hampering the catalytic activity. Dissociation of the duplex becomes rate-limiting leading to sub-exponential growth of the product. Several ways to overcome the issue were presented above. However, in the system depicted in **Figure 1.23**, the 1,3-dipolar cycloaddition was found to be the rate-limiting step. Hence, the key for the development of powerful new replicating systems based on simple organic molecules lies in the optimisation of the transition state to increase the effective molarity of the bond forming reaction.

1.7 Systems Chemistry

With a fundamental understanding of replicating processes at hand, the way is paved for the incorporation of self-replicating systems into more complex scenarios. The last years saw the emergence of the field of Systems Chemistry, a discipline that deals with the elucidation and understanding of the behaviour of complex chemical mixtures.^[144-149] Similar to Systems Biology, research is driven by the desire to understand networks of interacting members as an entity. This holistic approach distinguishes Systems Chemistry from other chemical disciplines in which the main focus lies on dissecting or avoiding mixtures of molecules in order to obtain pure reaction products. The general aspect of this dogma allows for a broad range of research to be combined under the term of Systems Chemistry and besides the focus on autocatalytic phenomena,^[150,151] the development and investigation of molecular logic gates,^[152-155] oscillating reactions,^[156-158] and self-assembly^[159-162] is included.

Dynamic combinatorial chemistry (DCC) has proven extremely useful in creating complex mixtures of interchanging compounds termed dynamic combinatorial libraries (DCL).^[163-165] Key to the formation of such DCLs is a reversible chemical process that allows the library members to interconvert. The formation of imines from aldehydes and amines is a prominent example for the creation of a DCL.^[166] Since the overall distribution of compounds is under thermodynamic control, external stimuli can be used to bias the DCL towards a

specific member of the library. This approach has been exploited successfully in the search of potent receptors for molecules of pharmacological interest,^[167-171] the creation of supramolecular assemblies^[172-175] and ligands for biomacromolecules.^[176-178]

The work group of Nitschke has exploited reversible imine formation to generate libraries that combine multiple, orthogonal exchange processes in one single system. Their original system starts with four simple building blocks, two aldehydes **39** and **40** and two amines **41** and **42**, which can condense to give rise to a library of imines (**Figure 1.24**).^[179] Upon addition of Fe^{2+} and Cu^+ salts, complexes **43** and **44** become the thermodynamically most stable species and the exchange process is directed at the formation of more such complexes in a self-sorting fashion.

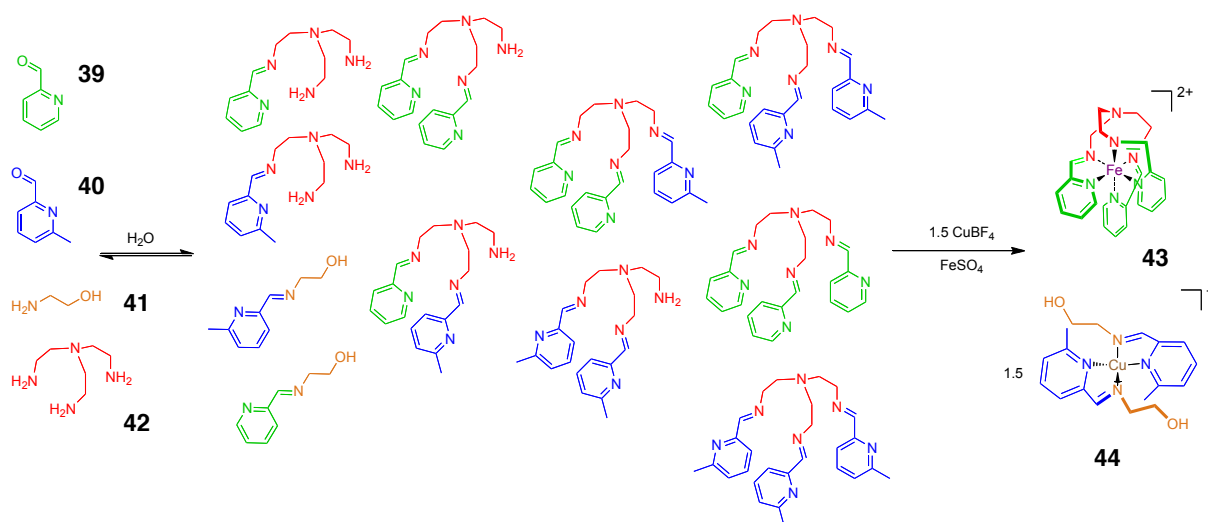


Figure 1.24 Self-sorting of an imine-based DCL upon addition of Fe^{2+} and Cu^+ salts.

In a further example, subcomponent self-assembly of aldehyde **39** with a benzidine derivative in the presence of Fe^{2+} salt and base led to the exclusive formation of a metal-organic cage complex of tetrahedral symmetry which showed the right properties to encapsulate a variety of hydrophobic guests such as cyclohexane or cyclopentane in aqueous solution.^[180] Treatment of this tetrahedral complex with chelating trisamine **42** shifted the equilibrium towards the formation of **43** and resulted in the destruction of the cage under release of the previously incorporated organic molecules. Interestingly, the dimension of the tetrahedral capsule was also found ideal for the binding of white phosphorus and even allowed its storage under air and water since the oxidation process would generate species too large for the capsule.^[181]

Moreover, it has shown possible to manipulate a DCL by equipping some of the library members with complementary recognition units that lead to the formation of a thermodynamically stable duplex structure. Under this aspect, a modification of Rebek's original self-replicating system has been re-investigated on a dynamic platform.^[182] In the original structure, the reaction to form the template proceeds through the irreversible coupling of an activated ester with an amine (**Figure 1.12**). By changing the ester function to an aldehyde, the coupling process between both fragments becomes reversible. Combining both recognition-enabled molecules with two structurally similar but recognition-disabled aldehydes and one recognition-inhibited amine structure created an imine DCL. In this library, the self-complementary structure was indeed found to amplify its own formation under kinetic as well as under thermodynamic control. The recognition-mediated formation of the reactive ternary complex was shown to provide a kinetic advantage whereas strong associations in the final duplex stabilised the product thermodynamically. However, since both interactions in this system, the association by hydrogen bonding and imine formation, are fully reversible, its behaviour will always be governed by the boundaries of thermodynamics.

In order to manipulate such systems beyond their thermodynamic limits, an irreversible chemical reaction can be coupled to the DCL to selectively extract one of the library members.^[183] According to Le Chatelier's principle, withdrawing a member from the DCL through an irreversible process will force the system to constantly readjust its equilibrium position and generate more of the reactive species on the expense of other library members. Ramström *et. al.* exploited crystallisation as secondary selection process to amplify one product from a dynamic nitroaldol library.^[184]

A simple yet instructive example for such behaviour employs amine **45** and aldehyde **46** to generate a self-replicating imine structure **47** (**Figure 1.25**).^[185] The rate profile exhibits the typical sigmoidal shape, control reactions with recognition-disabled species gave much lower conversions and experiments with a competitive inhibitor showed a significant decrease in the rate of reaction. Addition of preformed template at the start of the reaction resulted in disappearance of the lag period and the maximum rate was reached at the beginning of the reaction. However, even though adding template did indeed increase the rate of the recognition-mediated formation of imine **47**, it also decreased the amount of newly formed product. Since the condensation reaction between amine and aldehyde is reversible, adding product to the reaction mixture shifts the equilibrium towards the starting material. Again, the rules of thermodynamic hold in this self-replicating system. In order to breach the limit by the fully dynamic nature of the system, an irreversible reaction is needed

that extracts imine **47** from the equilibrium mixture without influencing the reagents. Using Hantzsch ester to selectively hydrogenate the double bond of the imine **47** to form amine template **48** has proven useful for this purpose.^[186]

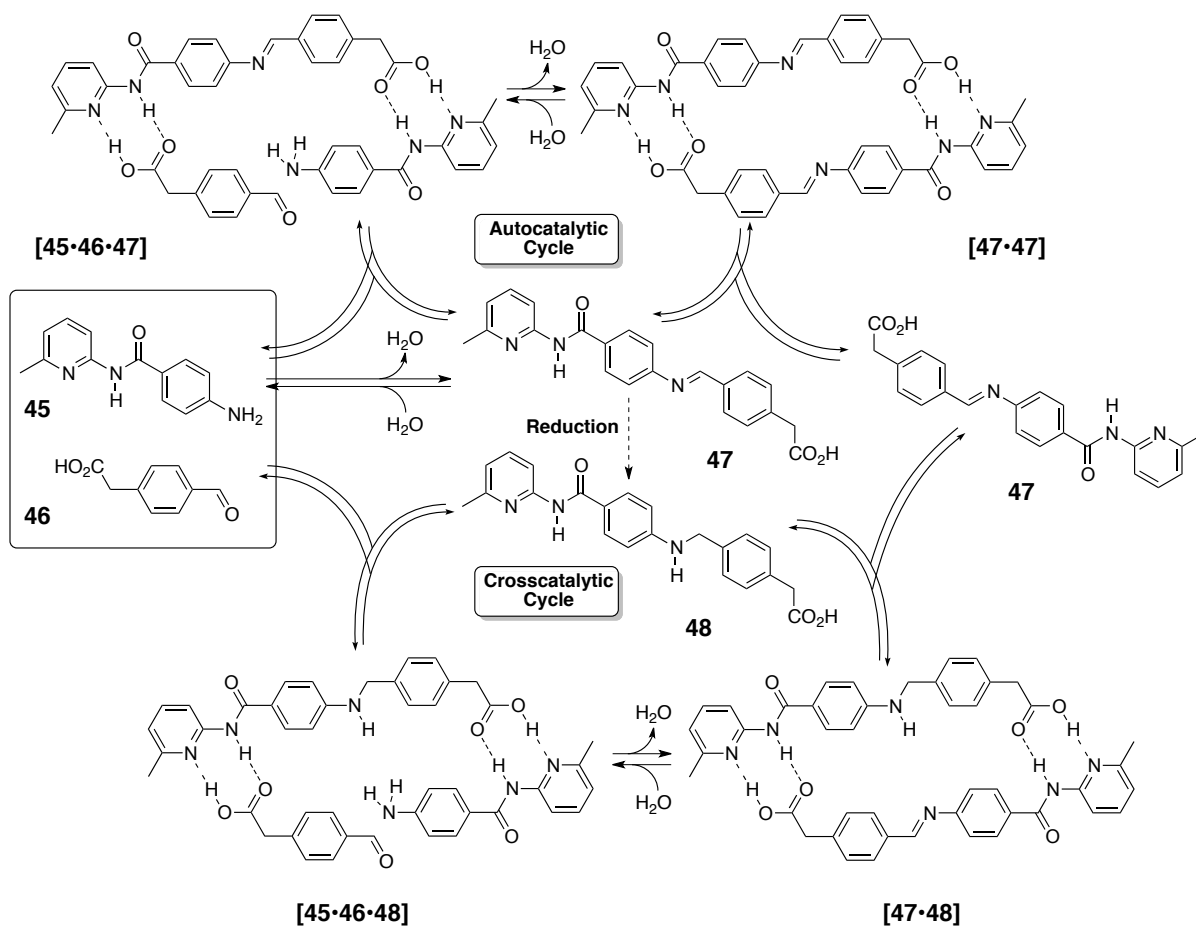


Figure 1.25 Imine **47** can assemble amine **45** and aldehyde **46** in CDCl₃ at 25 °C and accelerate the reaction between them through the autocatalytic cycle mediated by the ternary complex **[45·46·47]**. Reduction of imine **47** affords amine **48** which is also capable of crosscatalytic acceleration of imine **18** through the crosscatalytic cycle mediated by the ternary complex **[45·46·48]**.

Nitrones are structurally very similar to imines. Recently, a protocol to combine both motifs in a DCL has been presented by us.^[187] Reversible hydrolytic cleavage of the double bonds of the initial imines and nitrones leads to the formation of free aldehyde, hydroxylamine and amine, respectively. These building blocks can then either recombine to the original condensation products or reshuffle under exchange of substituents. Over time, an equilibrium point for the concentration of all possible members of the DCL is reached. Having established this principle, our group set out to show how coupling an irreversible self-replication process to a DCL can bias its constituent and selectively extract one of its members. Starting from imine **49** and nitrone **50**, the dynamic exchange process allows for the recombination of substituents forming imine **55** and nitrone **56** (**Figure 1.26**).^[188]

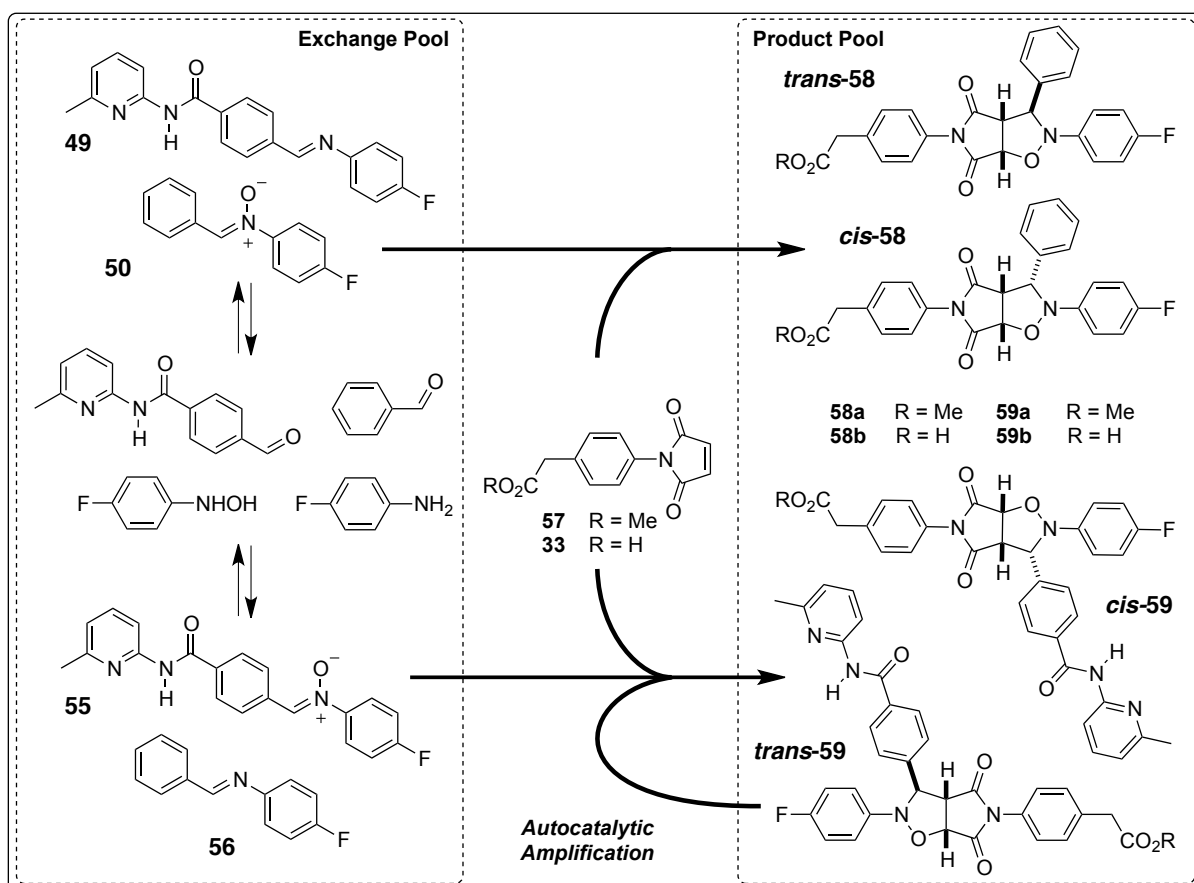


Figure 1.26 A pool of compounds containing imines **49** and **56** and nitrones **50** and **55** can exchange freely in CD_2Cl_2 saturated with *p*-toluenesulfonic acid monohydrate at 273 K *via* simple building blocks. Material can be transferred irreversibly to a pool of products, present in the same solution, that cannot be interconverted or returned to the exchange pool, through reaction of nitrones **50** or **55** with an appropriate maleimide (**57** or **33**). When maleimide **33** is used as the dipolarophile, replicator *trans*-**59b** is formed in the product pool and this species can act as a catalyst for its own formation.

At equilibrium, all four compounds are present in the exchange pool with some slight selectivity for the two nitrones. Addition of any maleimide species irreversibly transferred the nitrone structures from the DCL into the product pool by forming the isoxazolidine cycloadduct. In the case of the recognition-disabled methyl ester **57**, reaction with the nitrone species was slow and unselective. Both nitrones were converted in the same extent and the selectivity between *trans/cis* products was close to 3:1. When using the recognition-enabled free acid maleimide **33**, one of the products, namely *trans*-**59b**, becomes autocatalytic and selectively amplifies its own formation. Since nitrone **55** is the appropriate partner for this self-replicator, it is being used up more rapidly than **50**. This irreversible drain of **55** into the autocatalytic process causes the equilibrium to constantly readjust, forming more **55** on the expense of **50**.

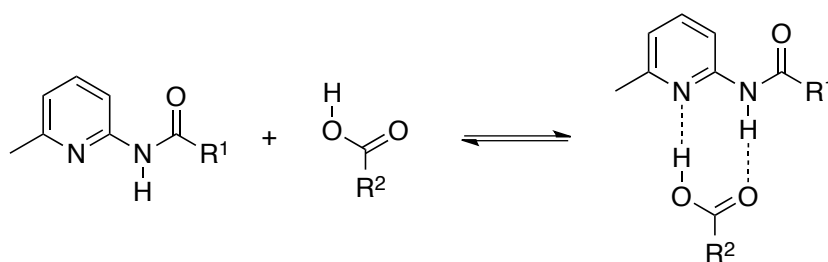
2. Design Principles and Objectives

The main objective of the research described in this thesis is the exploration of replicating systems of increased complexity using three and more building blocks that can be influenced by external stimuli. Ultimately, the design of a multicyclic system consisting of an interconnected network of two minimal and two reciprocal pathways is envisaged. In order to provide the reader a coherent entry into the field, the basic features of the self-replicators used in this thesis are presented and all preceding progress in the creation of a multicyclic system are summed up.

Over the last 10 years, our group has gained expertise in the design and evaluation of highly efficient artificial self-replicating systems. In the course of these investigations, three crucial design criteria have emerged, namely choice of the recognition event, optimisation of the template structure and the chemical reaction employed to form template **T** from building blocks **A** and **B**. In the following sections, these features are explained on the model for minimal replication (**Figure 1.1a**), but also hold for the case of a reciprocal replicator (**Figure 1.1b**).

2.1 The recognition event

The recognition between the two building blocks **A** and **B** has to be strong enough to allow association of the catalytically active ternary duplex $[A \cdot B \cdot T]$ and at the same time be weak enough to enable dissociation of the final product duplex $[T \cdot T]$ to prevent product inhibition. Previous work in our group has demonstrated that the recognition between an amidopyridine and a carboxylic acid can be incorporated into minimal and reciprocal self-replicating systems (**Scheme 2.1**). Association between both moieties takes place through hydrogen bonding of the carboxylic acid hydrogen to the pyridine nitrogen and between the amide proton with the carbonyl group of the acid.



Scheme 2.1 Recognition between amidopyridine and carboxylic acid through hydrogen bonding.

This recognition motif was first described^[189-191] by Hamilton and co-workers in their attempt to develop receptors for biscalboxylic acids. Analysis of the complexed structures by x-ray crystallography showed that the association does not involve proton transfer from the carboxylic acid to the pyridine. Furthermore, the 6-methyl substituent was attached to avoid self-association between the amidopyridine moieties.

Since our group has successfully incorporated this recognition motif into a wide range of replicating structures, no structural variants were synthesised and probed. Only recently, work on the development of self-replicating rotaxane structures led to the replacement of the original 6-methyl substituent with a 4,6-dimethyl moiety for steric reasons.^[192] Preliminary results showed a positive effect of the additional methyl group on the solubility of the investigated compounds. Moreover, controlling the electron density on the pyridine ring by varying the substituent pattern should allow a fine-tuning of the strength of the recognition event. An exhaustive investigation of such variation on the efficiency of self-replicating and AB systems can be found in chapter 4 of this thesis.

The choice of solvent is closely connected with the employed recognition unit. Polar solvents which act as good hydrogen bond donor/acceptor favour the solvation of the recognition sites and disrupt the binding. For this reason, non-polar solvents that do not participate in hydrogen bonding, such as chloroform or dichloromethane, must be chosen.

2.2 Template geometry restraints

Template molecule **T** has to possess the appropriate geometry to align **A** and **B** in a fashion which brings their reactive sites into close proximity. Ideally, template molecules are of rigid and linear structures with their recognition units easily accessible to **A** and **B**. In the case of too much structural flexibility, the peril of forming a catalytically inert [**A**·**B**] complex is increased. However, since rigid structures, e.g. highly conjugated aromatic systems, tend to be less soluble than compounds with more conformational freedom, e.g. alkyl chains, it is often not straightforward to strike a balance between both requirements. Detailed investigations of how small changes in geometry can affect drastically the efficiency of self-replicating systems or how minor changes can turn a self-replicating system into an AB system can be found in chapter 3 of this thesis.

2.3 The chemical reaction suitable for self-replication

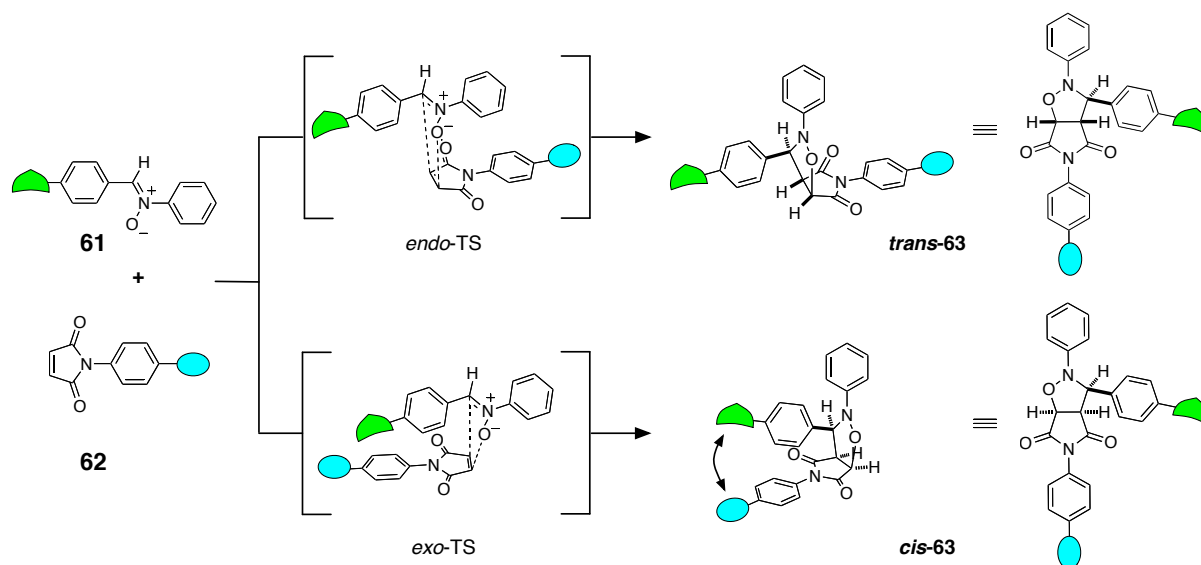
The reaction between **A** and **B** to form template **T** must have certain properties in order to follow conveniently its progression by standard spectroscopic methods such as ¹H NMR

spectroscopy. Ideally, the reaction should not require the addition of a catalyst or working under inert conditions. The formation of the product should furthermore be irreversible to facilitate kinetic analysis. Systems based on a reversible Diels-Alder reaction^[141,193] and the reversible formation of an imine^[185] have been investigated and the increasing complexity arising through the reversibility of the process was verified. Additionally, the chosen reaction should proceed with high (regio-)selectivity without producing any side-products. Moreover, the reactive sites should be fully orthogonal to the chosen recognition sites. The rate of reaction should allow its observation over the course of several hours without having to work at extreme temperatures. Synthetic access to the reagents should be straightforward and for the analysis of the reaction kinetics by ¹H NMR spectroscopy, starting materials and product should produce a defined set of peaks which can be integrated over time.

The 1,3-dipolar cycloaddition between a maleimide and a nitron was found to be a suitable candidate for incorporation in self-replicating structures. The formation of the isoxazolidine product proceeds through a concerted mechanism in which the bonds between the diene and the dienophile are created simultaneously. The rate of the reaction has been found to be virtually insensitive towards addition of acid or base catalysts. As a consequence of the asymmetric geometry of the nitron structure, two racemic diastereoisomeric products can be formed which are distinguished by the relative position of protons on the bicyclic ring system. In case of the *cis*-isomer, all protons are on the same side with respect to the isoxazolidine ring, whereas for the *trans*-isomer, the two hydrogens on the ring junction are opposed to the remaining third proton. In the ¹H NMR spectra, each diastereoisomer therefore shows a characteristic pattern for these protons.

In the absence of any recognition effects, the cycloaddition between an *N*-aryl nitron and a maleimide proceeds through a simple bimolecular pathway with low selectivity, usually leading to a *trans/cis* ratio between 1.4:1 and 3.9:1 depending on the electronic nature of the substituents on the two reagents. This indifference towards electronic modification was also found in a screening of the reaction between an acyclic *N*-phenyl nitron and a set of *N*-aryl maleimides bearing various electronic substituents.^[194] The analysis of the final stereochemistry resulted in modest *trans/cis* ratios in the narrow range of 1.6:1 (for strongly electron donating substituents) to 1:1.8 (for strongly electron withdrawing substituents). Compared to the selectivity found in other [4+2] cycloadditions such as the Diels-Alder reaction, these *trans/cis* ratios are considerably low. This stems from the fact that the frontier orbital orientation of the two reagent does not allow for efficient secondary interactions, thus leaving steric and/or aromatic stacking interactions (π - π interactions) of the substituents as major influences on the stereochemistry.^[195] Energetically, the 1,3 dipolar addition between a

nitron and a maleimide can be steered by both HOMO-LUMO interactions since the frontier molecule orbital (FMO) energies are similar. In this balanced situation, the influence of electron-donating or electron-withdrawing substituents on the reagents can alter the relative FMO energies and tip the scales in favour of one reaction type.

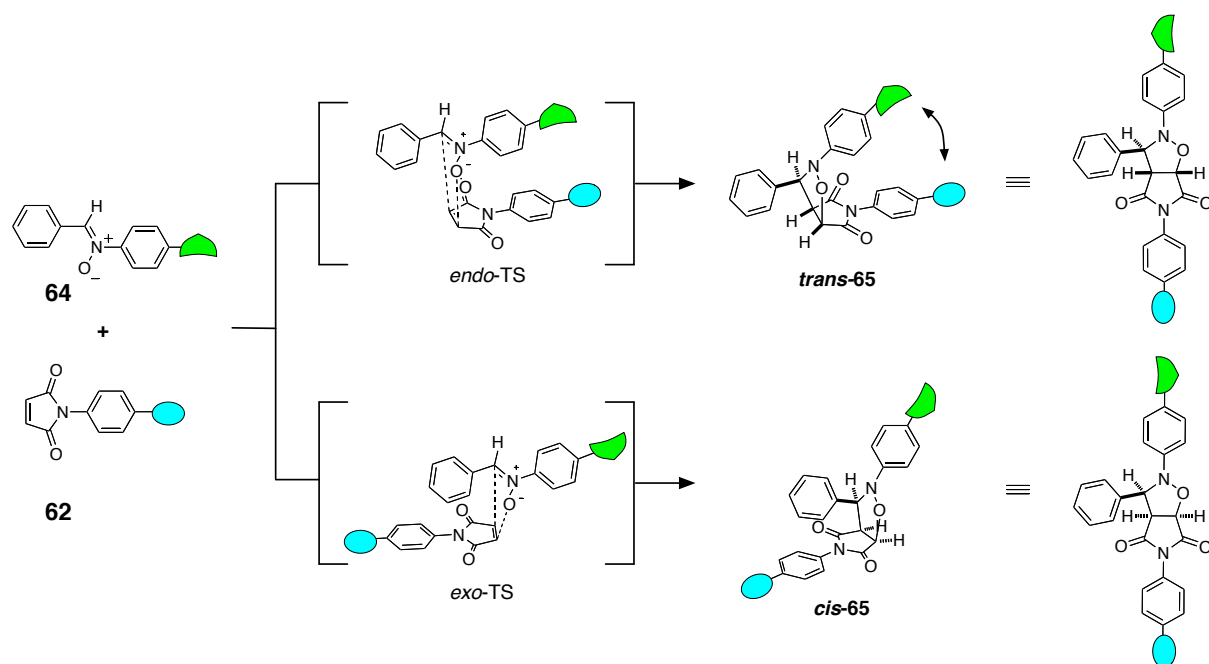


Scheme 2.2 1,3-dipolar cycloaddition reaction between nitron **61** and maleimide **62** proceeding through the *endo*-transition state (TS) to give isoxazolidine **trans-63** and through the *exo*-transition state to give isoxazolidine **cis-63**. Complementary recognition sites are displayed as green and light-blue cartoon images. Favourable internal recognition between the two recognition sites in the AB complex of **cis-63** is highlighted by the arrow.

However, attaching recognition units to the starting materials brings about the possibility of recognition-mediated pathways causing a significant change in reactivity and selectivity of the 1,3 dipolar cycloaddition. **Scheme 2.2** depicts how the orientation of the recognition sites in the transition state governs the stereochemistry of the reaction and consequently the geometry of the product. When the cycloaddition between nitron **61** and maleimide **62** proceeds through the transition state with the recognition units pointing away from each other, the *trans*-diastereoisomer of **63** is formed adopting an open geometry. If the orientation of the maleimide is reversed, attack of the 1,3-dipole occurs *via* the *exo*-side and leads to the generation of **cis-63** which possesses a closed geometry with respect to the recognition units. **Scheme 2.2** also explains why for this given set of reagents rigid *trans*-isomer is expected to function as a template in a self-replicating reaction whereas the *cis*-isomer is the product of an AB system.

However, it should be pointed out that changing the position of the recognition unit on the nitron to the aryl directly connected to the nitrogen reverses the stereochemistry of

the reaction. **Scheme 2.3** shows the reaction between nitrone **64** and maleimide **62**. Nitrone **64** now bears the recognition site on the hydroxylamine part compared to nitrone **61** in **Scheme 2.2**. Maleimide **62** remains unchanged and their reaction leads to the formation of two diastereoisomeric cycloadducts **65**. The *trans*-isomer is formed through the *endo*-transition state in which both recognition sites are in close proximity. Their interaction results in the closed AB complex geometry of the final *trans*-product. On the other hand, the *cis*-isomer is formed through the open *exo*-transition state. In the resulting *cis*-product, both recognition sites are now positioned on the ends of the newly formed rigid molecule and can thereby act as templates for the self-replicating cycle. Overall, altering the position of the recognition site on the nitrone compound indeed reversed the stereochemistry of the reaction.



Scheme 2.3 1,3-dipolar cycloaddition reaction between maleimide **62** and nitrone **64** which now bears the recognition site on the hydroxylamine part compared to nitrone **61** in **Scheme 2.2**. The reaction proceeds through the *endo*-transition state (TS) to give isoxazolidine *trans*-**65** and through the *exo*-transition state to give isoxazolidine *cis*-**65**. Complementary recognition sites are displayed as green and light blue cartoon images. Favourable internal recognition between the two recognition sites in the AB complex of *trans*-**65** is highlighted by the arrow.

2.4 Kinetic investigations of replicating systems

In order to elucidate the nature of the effects that cause a change in reactivity and selectivity of the native cycloaddition between a nitrone and a maleimide, kinetic analysis of the reaction is performed. Deconvolution of the obtained spectroscopic data provides a profile in which the increase of the product concentration is monitored over time. Typical

concentration *vs* time profiles for the formation of the major isomer in a self-replicating reaction, a crosscatalytic system and an AB system are shown in **Figure 2.1**.

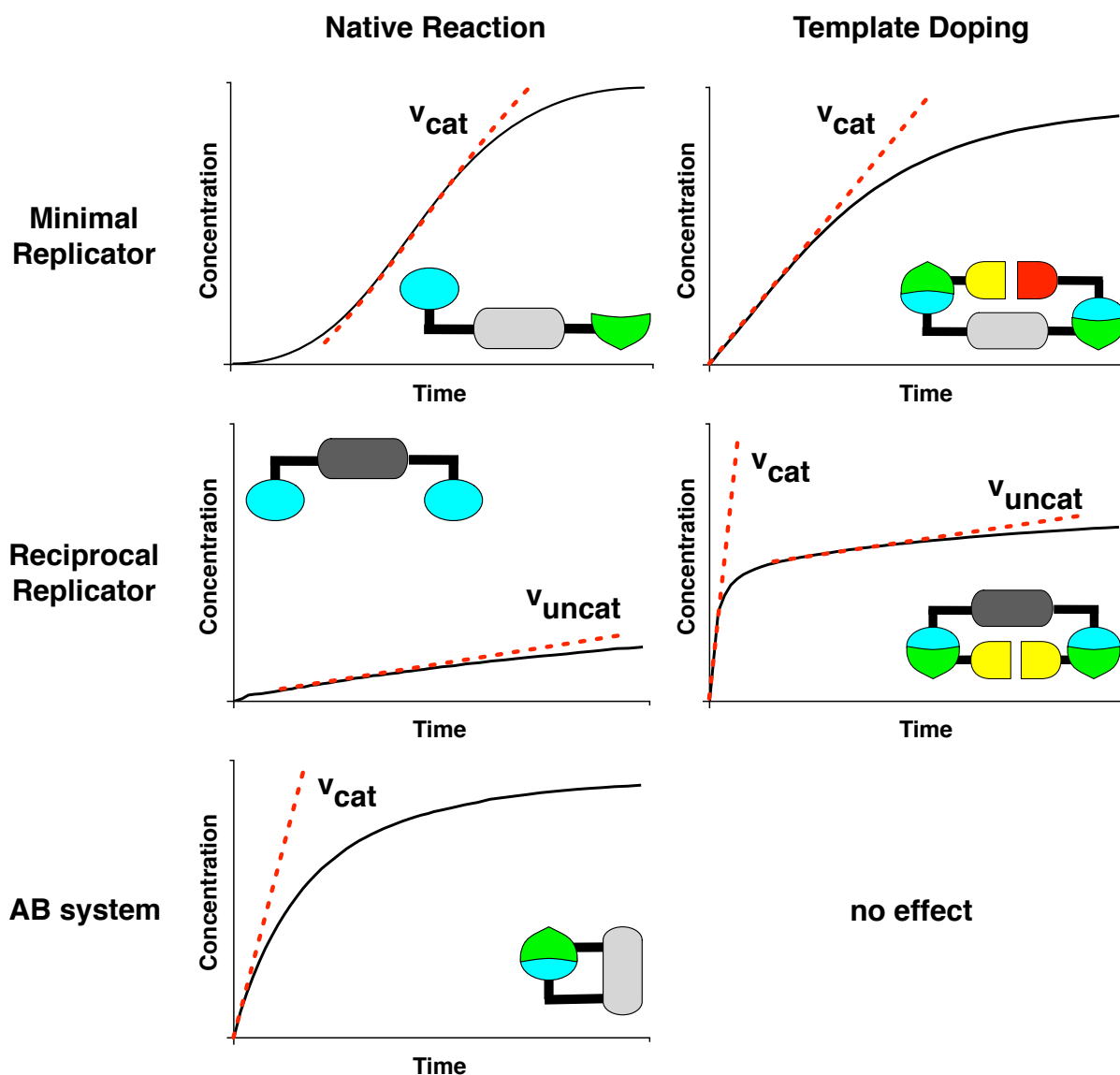


Figure 2.1 Exemplary concentration *vs* time profiles for the comparison of the native and doped 1,3-dipolar cycloaddition reaction of a minimal replicator, reciprocal replicator and an AB system.

The curves for the three native reactions and the doping experiments are intrinsically different. The self-replicating system shows its characteristic sigmoidal shape consisting of a lag phase in the early period of the reaction, since the catalytically active template molecules need to be generated through the slow bimolecular process. As soon as a critical template concentration is reached, the self-replicating cycle can start to operate and the reaction reaches its maximum rate v_{cat} before the concentration of the starting materials becomes too low for further recognition-mediated processes. Doping a fresh batch of reagents with a small amount of presynthesised template verifies the autocatalytic nature of the reaction. The

initial induction period is overcome and the maximum rate of the reaction v_{cat} now occurs at the start of the reaction.

For reciprocal replicating systems, the situation is very different. The native reaction between maleimide and nitron proceeds with a rate v_{uncat} identical to the one found for the bimolecular reaction, since both building blocks bear identical recognition units and are therefore unable to associate with each other. Only addition of presynthesised template with two complementary recognition units allows reciprocal replication to take place. As a consequence, maximum rate v_{cat} is found at the start of the reaction and proved to be dependent on the amount of added template. In the case of strong duplex association, turnover of the catalyst is hampered by product inhibition and the curve shows a defined bend at the initial catalyst concentration and the rate of the reaction drops to the one found in the bimolecular experiment, v_{uncat} .

In the case of an AB system, the reaction proceeds *via* a binary complex of the starting compounds. Since the rate of the reaction is directly proportional to the concentration of this binary complex, its maximum rate v_{cat} can be found at the start of the reaction. The resulting template does not possess any catalytic activity. In its closed structure, the recognition sites are associated through intramolecular hydrogen bonds and are therefore not available for binding reagents. Hence, adding presynthesised AB template at the start of the reaction has no effect on the shape of the curve.

2.5 The design of a multicyclic replicating system

A multicyclic replicating system can be described as a network of at least two interconnected replicating entities in which the connectivity of all building blocks leads to emergent properties. These emergent features are not a property of any single component of the system and cannot be predicted or deduced readily from behaviour of the individual simple components. Key to the development of emergent properties is the number and the type of the interconnections between the simple components of the system. Although the number of interconnections in a system increases combinatorially with the number of components, simply having a large number of interconnections is not enough to guarantee emergent behaviour. The topology of the interconnections is also critical. Therefore, chemical networks that exhibit significant degrees of mutually catalytic relationships between their components and thereby increase the level of feedback within the system, are more likely to develop system-level properties than a large collection of weakly interacting compounds. Replication exhibits a high level of feedback and instructed manipulation of a system of replicating

entities should cause the system to act and respond as a whole. In order to demonstrate such behaviour, **Figure 2.2** provides examples of hypothetical reaction networks consisting of three and four building blocks.

In these examples, the entities are linked together forming arrangements of increasing connectivity. The nature of the linkage between the components is arbitrary; one can imagine a bimolecular reaction between the two connected species **A** and **B** to form product **AB** with a certain rate constant k_{AB} . In the first example, compound **B** reacts with **A** and **C** to form products **AB** and **BC** with rate constants k_{AB} and k_{BC} , respectively (**Figure 2.2a**). As long as both rates remain equal, a reaction between all three entities at 50 mM starting material concentration will form 25 mM of both possible products. If the rate of formation for **AB** is enhanced selectively by a factor of ten, the final product distribution is then in favour of **AB** and the formation of **BC** is consequently down-regulated (**Figure 2.2b**). Final product concentrations were determined by simulating the depicted reaction scenarios using the ISOSIM mode of the SimFit package (chapter 10). Absolute enhancements were calculated as

$$\text{Enhancement \%} = ([XY]_{\text{enhanced rate}} - [XY]_{\text{equal rate}}) \times 100\%$$

with $[XY]_{\text{enhanced rate}}$ being the concentration of a given product after 16 h in the case of a ten-fold increase in rate for k_{AB} and $[XY]_{\text{equal rate}}$ being the concentration of the same product after 16 h for the reaction with equal rate constants.

This trivial situation can be extended by adding a fourth component to form the square arrangement depicted in **Figure 2.2b**. In this case, the four reagents **A** to **D** can react to form a set of four products **AB**, **AC**, **BD** and **CD** with respective rate constants k_{AB} , k_{AC} , k_{BD} and k_{CD} . If all rate constants are set equal and the starting concentrations for the reagents are the same, all four products are formed in the same extent. Increasing rate constant k_{AB} selectively by a factor of ten enhances the formation of product **AB** and correspondingly decreases the production of the two other products that rely on **A** and **B**, **AC** and **BD**. Since **A** and **B** are now being used up more rapidly, building blocks **C** and **D** gradually accumulate in the reaction mixture favouring the formation of product **CD** in the same extent as reflected by the enhancement factors.

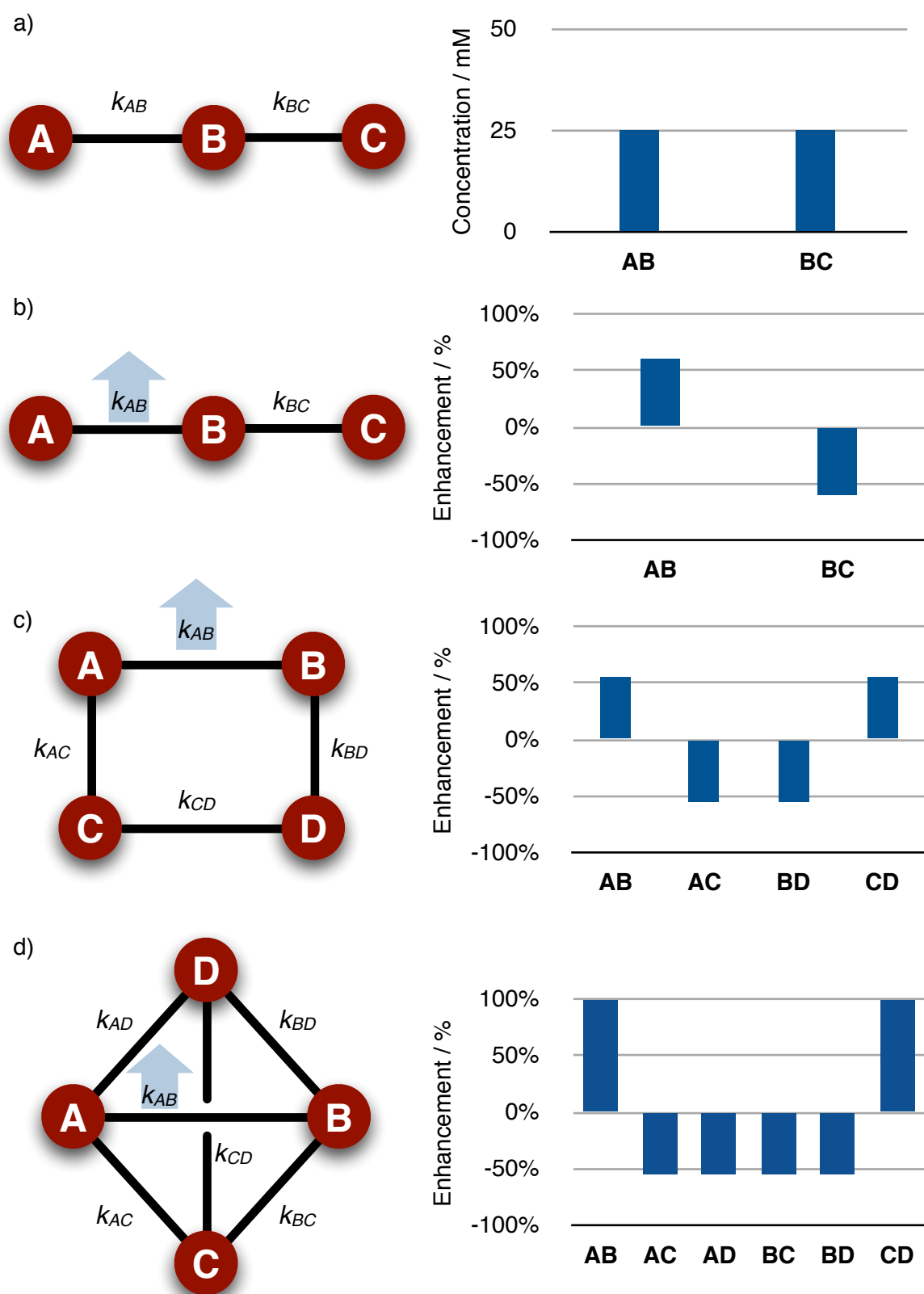


Figure 2.2 Representation of hypothetical reaction networks in which two chemical entities react to form a product molecule. Starting concentrations for all reagents were set to 50 mM. All rate constants were fixed to $1 \times 10^{-3} \text{ M}^{-1} \text{ s}^{-1}$ except for k_{AB} which was increased by a factor of 10 to $1 \times 10^{-2} \text{ M}^{-1} \text{ s}^{-1}$ in b), c) and d) as indicated by the light blue arrow. The calculation of the enhancements is laid out in the text.

However, it should clearly be pointed out that the rate for the formation of **CD**, k_{CD} , remains unchanged in both simulations and that the increase in concentration for **CD** is therefore not directly connected to the enhancement of k_{AB} , but it is solely a result of the interconnectedness of the individual components and can be regarded as an emergent property of the system.

In a second scenario, the four entities are combined to form a tetrahedral arrangement in which every entity can react with the three others to give rise to six products. Again, in the initial simulation with identical rate constants and equal starting material concentrations, all six reaction products are formed in the same extent. Increasing the rate of reaction between **A** and **B** by a factor of ten again increases the formation of **AB**, down-regulates all species that need **A** or **B** and consequently up-regulates the formation of **CD**. However, as a result of the increased interconnectivity in this tetrahedra, the enhancements in product formation are now higher than in the example of the square arrangement. The rate acceleration for **CD** is again not directly encoded in the instruction to the system, but it is a consequence of the interlinkage of the components into a system of higher order in which the alteration of one relationship affects all others.

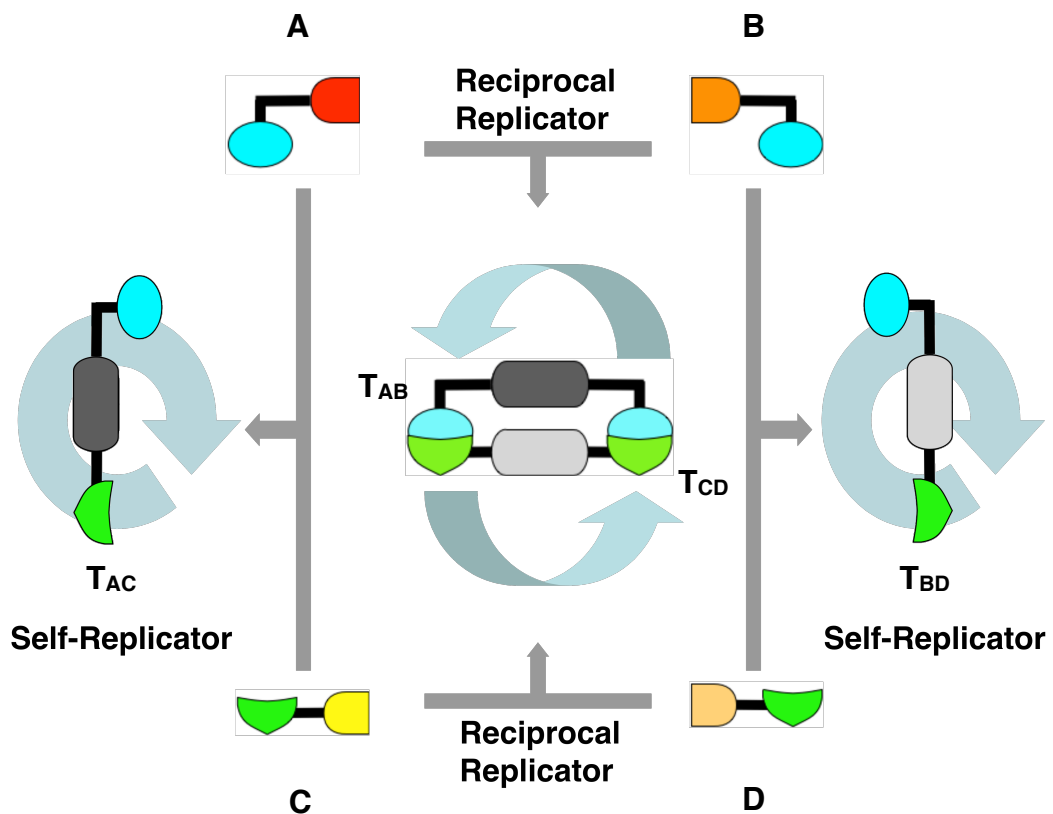


Figure 2.3 Schematic representation of a multicyclic system based on four building blocks, **A-D**, forming two minimal replicators, T_{AC} and T_{BD} , and two reciprocal replicator, T_{AB} and T_{CD} .

The main target of this thesis is to generate a complex chemical system using structurally simple organic replicators that show collective behaviour on a molecular level. The blueprint for the envisaged multicyclic system which is expected to show such behaviour is given in **Figure 2.3**. It consists of four building blocks, **A-D**, that can react *via* four different pathways to form four template structures, **T_{AB}**, **T_{AC}**, **T_{BD}** and **T_{CD}**. Building blocks **A** and **C** are designed to form template **T_{AC}** in an autocatalytic fashion and compounds **B** and **D** are components of a second replicating system leading to template **T_{BD}**. However, if the two replicating templates are formed through reactions of identical chemical nature, the building blocks bearing identical recognition units can react to generate two reciprocal templates, **T_{AB}** and **T_{CD}**, which can potentially enhance each other's formation in a crosscatalytic manner. In total, each of the four building blocks can be part of two replicating systems. Addition of instructional preformed template is expected to allow for selective rate enhancements for one of the replicating reaction and the high degree of interconnectedness between the components will force the system to respond to such external stimuli as a whole.

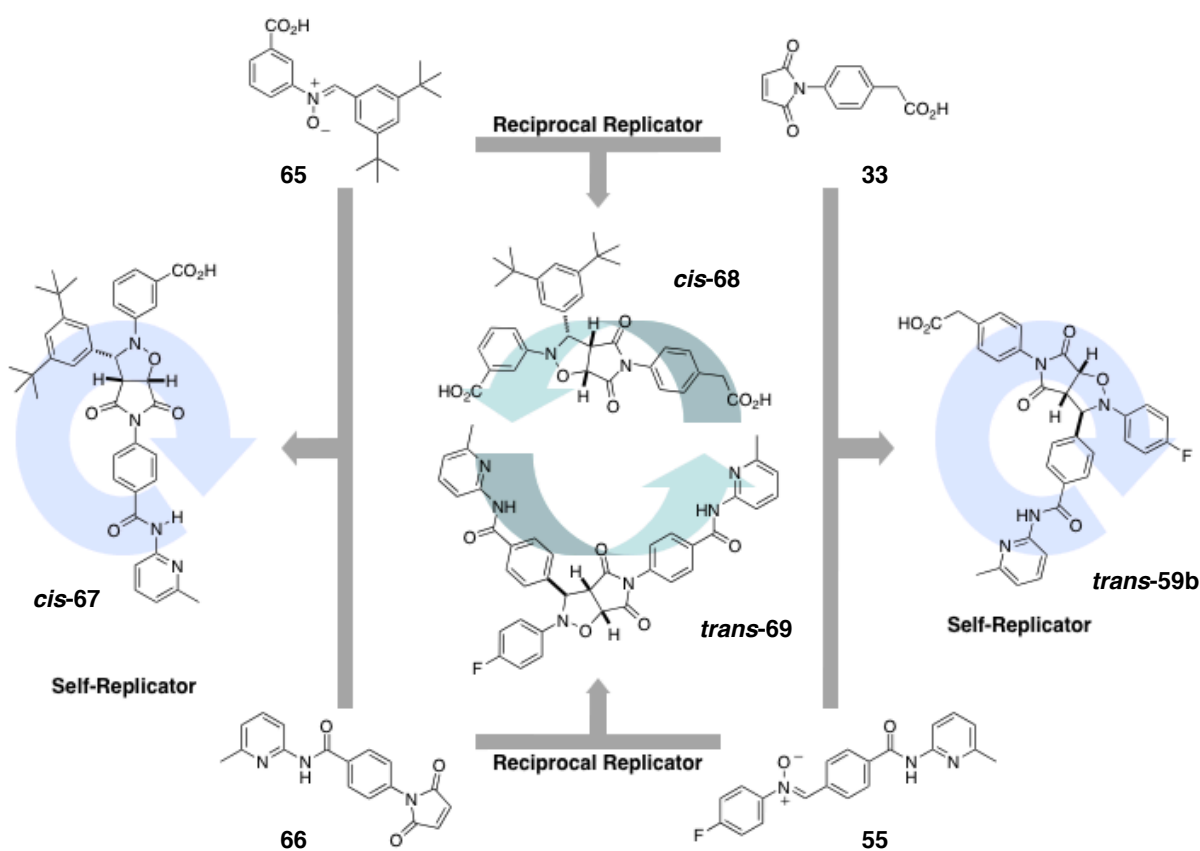


Figure 2.4 Multicyclic system based on the 1,3-dipolar cycloaddition between nitron and maleimide modified from ref. [193]. Two replicating templates, *cis-67* and *trans-59b*, are coupled to generate a crosscatalytic relationship between the two reciprocal templates, *cis-68* and *trans-69*.

Examples of such multicyclic systems in the literature are scarce. On the basis of artificial replicating structures, only one system using oligonucleotides was successfully created and investigated (**Figure 1.5**). The authors state that in order to develop such type of network, the efficiencies of all four replicators should be comparable. In case of our system (**Figure 1.22**), problems arose through the application of two types of chemical reactions with intrinsically different rates, the 1,3-dipolar cycloaddition between a nitron and a maleimide, and the much slower Diels-Alder reaction between a furan and a maleimide.^[139] Thus, replicator *trans*-**35** based on nitron structure **31** proved to be exceptionally fast thereby generating a dramatic imbalance in template efficiency. In addition, different responses to added template exhibited by minimal and reciprocal templates prevented us to instruct the system away from the preferential formation of the nitron based self-replicator.

Taking this initial design as a starting point, recent research has yielded a number of improved systems, the most promising one depicted in **Figure 2.4**.^[193] The weak point of using two different reaction types was eliminated by employing the established replicating system between nitron **55** and maleimide **33** as an anchor, and basing the design of the second replicator on the same chemistry. In order to provide the correct reactivity, the recognition units on the building blocks of this second replicating structure had to be inverted with respect to the existing one. Therefore, the amidopyridine moiety must be incorporated into the maleimide and the acid functionality must be connected with the nitron structure. Compounds **65** and **66** fulfil these criteria and their reaction was found to exhibit features typical for a self-replicating system. It is important to state that, since the recognition unit and the nitrogen of the nitron functionality are now connected to the same aryl group, the diastereoselectivity for the template structure **67** is reversed and the *cis*-isomer becomes self-replicating (**Scheme 2.3**). Separate analysis of the reciprocal replicating system was successful. Doping a mixture of nitron **55** and maleimide **66** with increasing amounts of presynthesised template *cis*-**68** clearly established the crosscatalytic activity between the two reciprocal templates *cis*-**68** and *trans*-**69**.

However, when comparing the efficiencies of the two self-replicators, an imbalance can be seen (**Figure 2.5**). After 16 h at 0 °C and 10 mM concentration of starting compounds, the reaction of maleimide **33** and nitron **55** occurred with 85% conversion and a 50:1 ratio in favour of self-replicating product *trans*-**59b**. On the other hand, the reaction between nitron **65** and maleimide **66** under the same conditions reached only 42% conversion and the ratio of isomers was a mere 2.2:1 for self-replicating template *cis*-**67**. In addition to this imbalance in efficiency, the limited solubility of nitron **65** in chloroform severely hampered the investigation of this system and required a fundamental redesign.

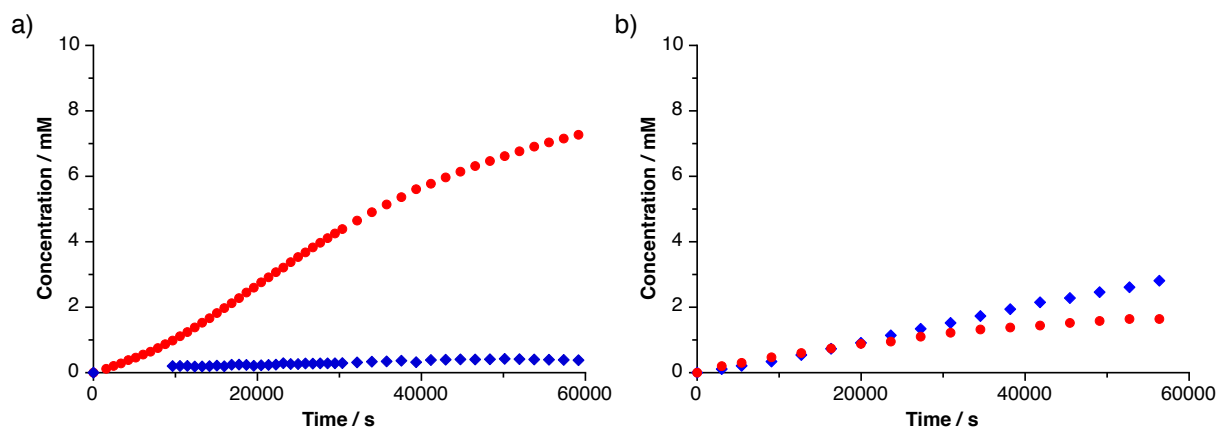


Figure 2.5 Concentration *vs* time profiles for the reactions of a) maleimide 33 and nitrene 55 to form *trans*-59b (●) and *cis*-59b (◆) and b) maleimide 66 and nitrene 65 to form *trans*-67 (●) and *cis*-67 (◆). All reactions were conducted at 0 °C and with 10 mM starting reagent concentration in CDCl₃.

3. Structure-dependent reactivity in a family of self-replicators

3.1 Design of a library of nitrones and maleimides

Valuable contributions towards the understanding of multicyclic systems based on the interactions of four building blocks by two auto- and two crosscatalytic pathways have been made recently.^[139] These investigations have shown that to generate a fully functional network, the participating replicating entities of the system must possess similar catalytic efficiencies. Fair competition between the replicating species will then lead to an almost equal distribution of all four possible product templates in the native reaction. It is only for this scenario that the addition of preformed template is expected to alter significantly the outcome of the competition scenario between the self-replicators and the reciprocal replicators.

Previous experimental investigations failed to create a fully functional multicyclic network. An imbalance in reactivity for the participating self-replicators hampered the performance of the multicyclic system. In the scenario depicted in **Figure 2.4**, self-replicator *trans-59b* was found to be significantly more potent than its self-replicating partner *cis-67* and the resulting crosscatalytic system between *cis-68* and *trans-69*. As a result, this replicator dominated the product pool suppressing the formation of any crosscatalytic species and addition of preformed template at the start of the reaction had very little effect on the final product distribution. At this stage, two possible approaches are imaginable. Lowering the efficiency of self-replicator *trans-59b* to match the one of replicator *cis-67* would eliminate the imbalance. However, reducing the efficiency would also lower the catalytic feedback on the interconnection between the replicators making it more difficult to influence the outcome of the system. Besides, a reduction in reactivity would decrease the selectivity for the replicating diastereoisomers producing a larger amount of unwanted cycloadducts. It is therefore more advantageous to use the efficient replicator *trans-59b* as a benchmark and to focus on the improvement of the efficiency of the partner replicator. Previous attempts yielded structure *cis-67* which can be used as a starting point for further optimisation. It is clear that the novel replicating system must consist of a maleimide compound bearing an amidopyridine recognition site and a matching nitrone compound with an acid functionality. In order to find replicating systems with matching efficiencies, an elaborate approach of adept molecular modeling combined with major synthetic effort is crucial. However, even if a self-replicating system with matching efficiency is found, it

cannot be taken for granted that the combination of all four building blocks will lead to the formation of a reciprocal system with comparable efficiencies.

In this chapter, the synthesis of a set of structurally related self-replicators that meet the criteria mentioned above is reported and the relationship between their structure and replicating activity is established. From this pool of replicators, suitable candidates are chosen and incorporated gradually into systems of higher order to establish some general principles. The most efficient replicators are then coupled with the established replicator *trans-59b* to culminate in the successful construction of fully functional multicyclic systems.

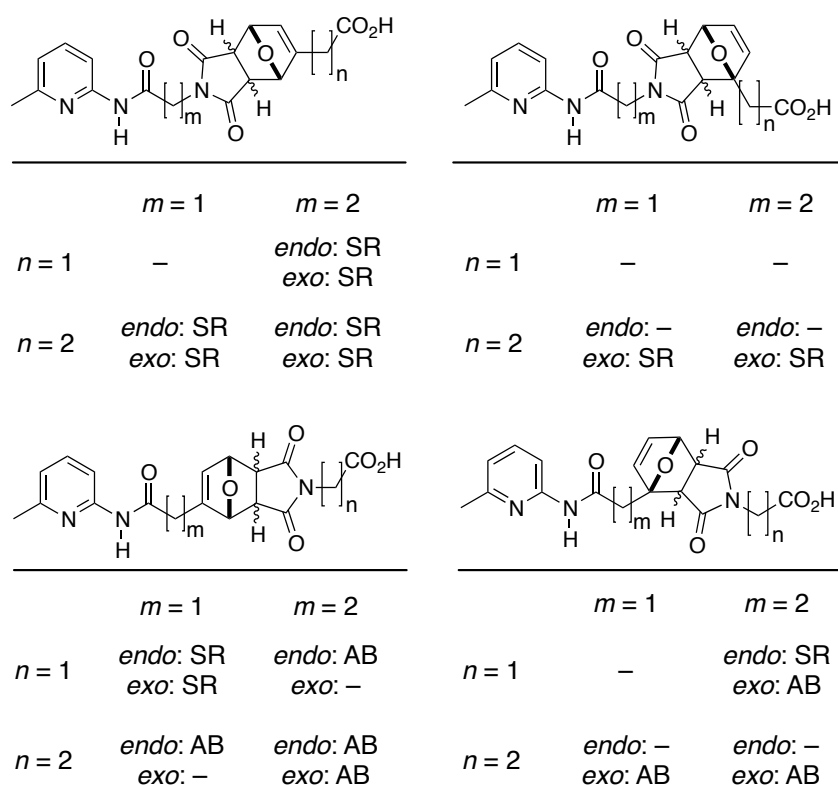


Figure 3.1 Overview over 32 screened templates based on the cycloaddition of maleimide with furan taken from ref. [143]. The kinetic behaviour of each diastereoisomer is labelled as follows: – = no recognition-mediated reactivity observed. AB = Reaction occurs predominantly through a binary reactive complex. SR = Reaction occurs predominantly through an autocatalytic cycle.

Previous screenings for self-replicating activity was performed on the basis of the cycloaddition between maleimide and furan structures (**Figure 3.1**).^[143] Probing a total number of 32 potential candidates with different spacer units on either the maleimide or furan component suggested that there is only a narrow structural window in which replication is observed. The screening yielded only six self-replicating systems with the best one achieving an effective molarity in the range of 2. This low yield was summarised in the clinical statement that ‘our chances of creating an efficient replicating system successfully

even from a rationally designed starting point is only around 1 in 5.' However, the authors observe that the most efficient self-replicating systems are clustered in a certain region in which the right balance between flexibility and rigidity seems to be found.

On the basis of these results, a set of building blocks was designed (**Figure 3.2**). Using *cis*-selective replicator *cis*-67 from **Figure 2.4** as starting point, several modifications led to nitron structure **70**. Attaching a long alkyne chain to the compound showed to have a positive effect on its solubility. Moreover, moving the nitron functionality away from the carboxy acid significantly facilitated the synthesis since the controlled generation of hydroxylamines bearing acid functionalities proved troublesome. In order to further expand the solubility range of the nitron and to generate structural diversity, a second nitron was prepared. The methylene group in **71** breaks the conjugation between the benzene ring and the acid, adds more conformational freedom and renders the structure less rigid.

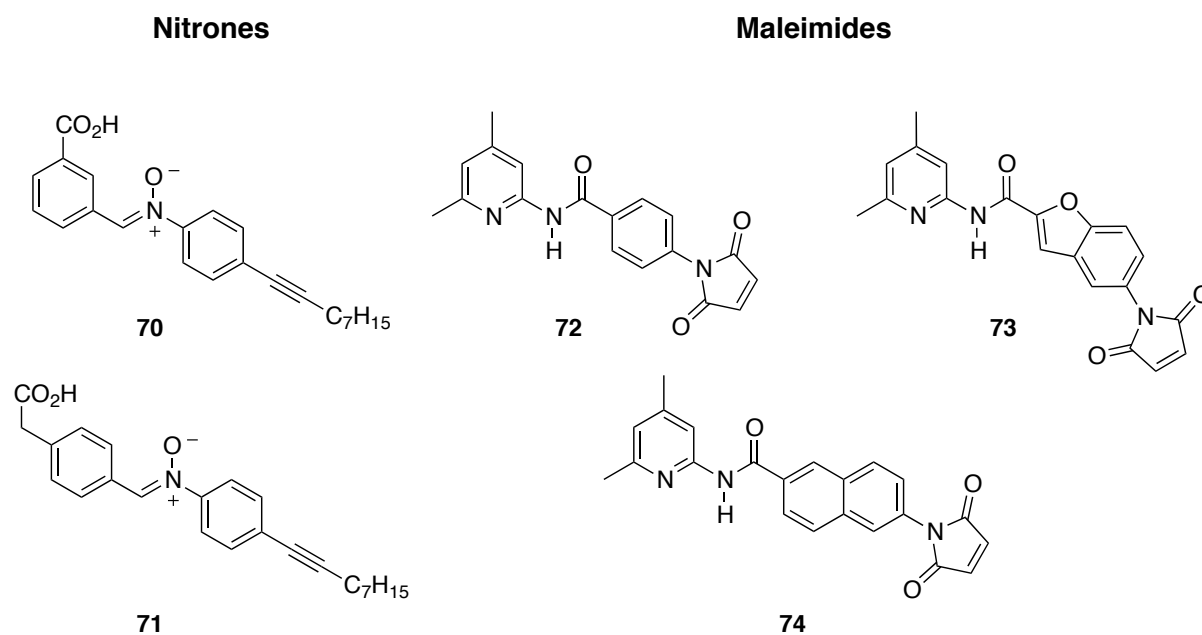


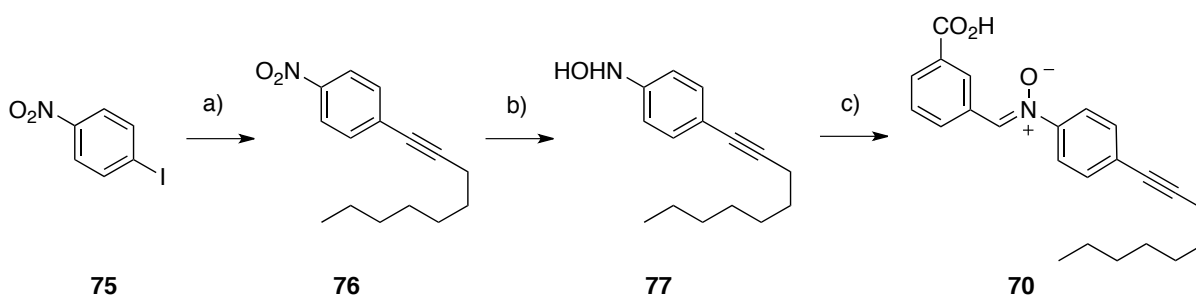
Figure 3.2 Pool of synthesised nitron and maleimide building blocks used in the screening for efficient self-replicating activity.

Three maleimide structures were designed as reactive partners for the two nitron structures. The three compounds **72-74** are structurally similar with an amidopyridine recognition unit and a maleimide functionality. Progressive introduction of flexible alkyl chains was avoided and variation of spacer length was introduced by extension of the aromatic backbone thereby maintaining a certain degree of rigidity in the molecules. The compounds differ in their spacer unit in which the original benzene ring (in structure **72**) was replaced with a benzofuran (in structure **73**) and naphthalene ring (in structure **74**). Problems

caused by the limited solubility of the naphthalene and benzofuran backbone were overcome by changing the original structure of the amidopyridine recognition unit with 6-methyl substitution to the shown 4,6-dimethylamido pyridine moiety. In order to form a coherent set of compounds with identical recognition units, also original maleimide **66** was modified to give **72**.

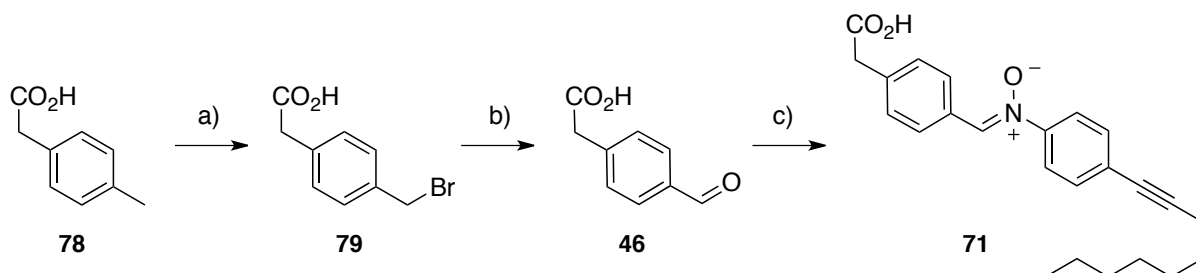
3.2 Synthesis of nitrones **70** and **71**

Key compound for the synthesis of nitrones **1** and **2** was hydroxylamine **77** bearing the alkyne group for improved solubility (**Scheme 3.1**). Sonogashira reaction on 4-iodonitrobenzene **75** furnished **76** in good yield. Partial reduction of the nitro group using rhodium on carbon with hydrazine as hydrogen source yielded the desired hydroxylamine **77**, which was directly reacted with commercially available 3-carboxybenzaldehyde to give acid nitrone **70**.



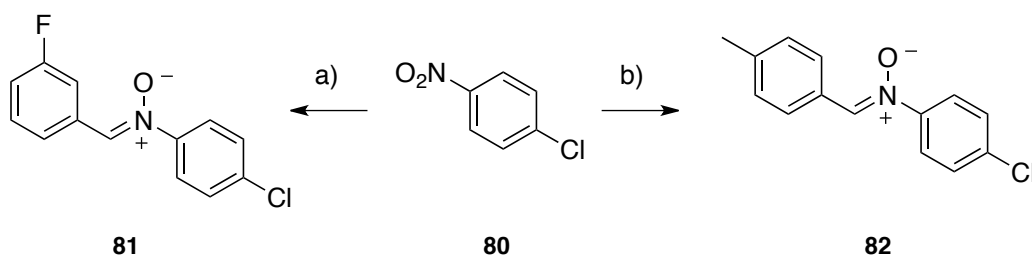
Scheme 3.1 Synthesis of nitrone **70**. Conditions: a) CuI, PPh₃, PdCl₂(PPh₃)₂, 1-nonyne, Et₃N, rt, 86%; b) Rh/C, NH₂NH₂, THF, rt; c) 3-carboxybenzaldehyde, EtOH, rt, 52% over two steps.

In order to synthesis nitrone **71**, aldehyde **46** was prepared in a two step sequence starting from 4-tolylphenylacetic acid **78** (**Scheme 3.2**). Radical bromination gave compound **79** which was treated with HMTA to furnish the desired aldehyde **46**. Condensation of **46** with hydroxylamine **77** gave final nitrone structure **71**.



Scheme 3.2 Synthesis of nitrone **71**. Conditions: a) Br₂, chlorobenzene, 60 W irradiation, rt, 62%; b) HMTA, EtOH/H₂O, 80 °C, 88%; c) **77**, EtOH, -18 °C, 70%.

Two control nitrones without recognition units were synthesised starting from 4-chloronitrobenzene which was converted to the hydroxylamine using rhodium on carbon and hydrazine (**Scheme 3.3**). In order to mimic the electronic environment found in the original carboxy nitrone structures, 3-fluorobenzaldehyde was chosen as the condensation partner for the hydroxylamine of nitro compound **80** to furnish control nitrone **81**. Correspondingly, reaction of the same hydroxylamine with *p*-tolylaldehyde yielded control nitrone **82** with electronic properties similar to phenylacetic acid nitrone **71**.

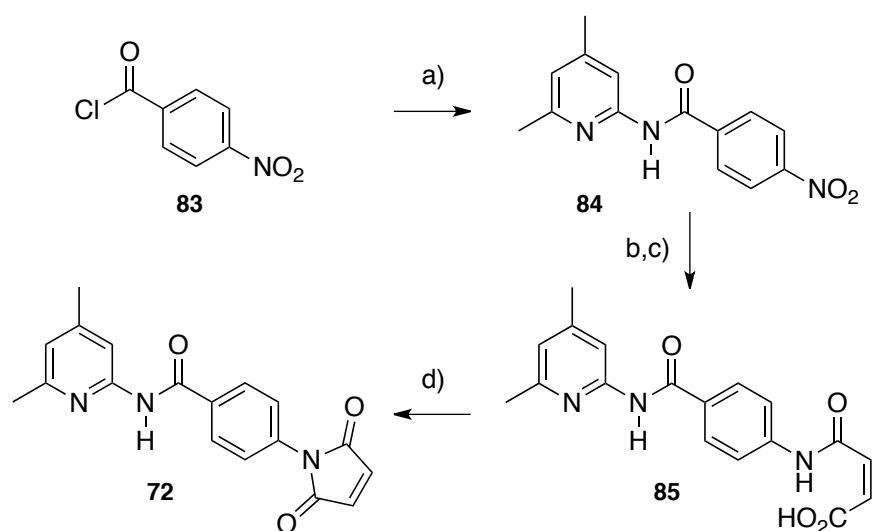


Scheme 3.3 Synthesis of nitrones **81** and **82**. Conditions: a) Rh/C, NH₂NH₂, THF, rt; then 3-fluorobenzaldehyde, EtOH, 63%; b) Rh/C, NH₂NH₂, THF, rt; then 4-methylbenzaldehyde, EtOH, 62%.

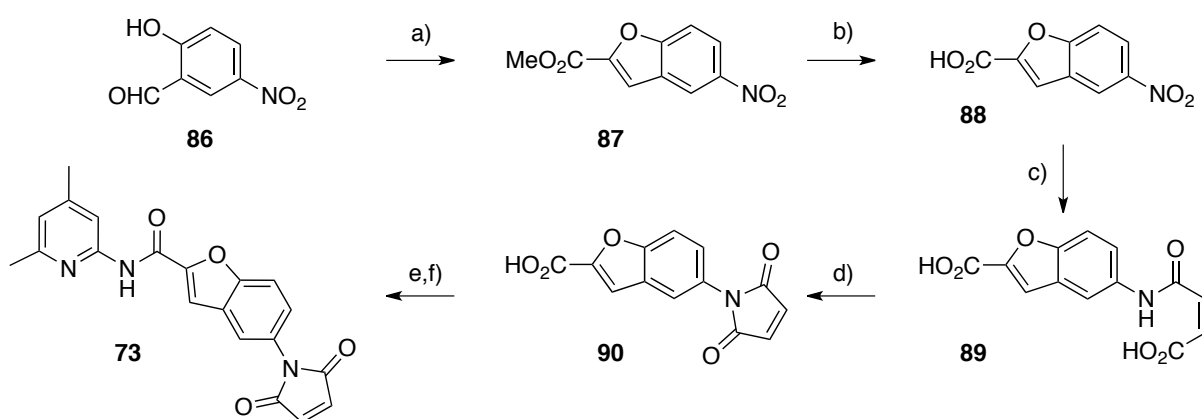
3.3 Synthesis of maleimides **72**, **73** and **74**

The first step for the formation of maleimide structure **72** was the amide coupling between commercially available acid chloride **83** and 4,6-dimethyl-2-amino pyridine to furnish **84** (**Scheme 3.4**). Nitrobenzene derivative **84** was then hydrogenated using palladium on carbon and hydrogen gas. The obtained aniline was directly reacted with maleic anhydride to furnish compound **85** and further treatment with ZnBr₂ and HMDS gave rise to the desired maleimide structure **72**.

Synthesis of maleimide **73** started with the construction of the benzofuran moiety by reacting 2-hydroxy-5-nitrobenzaldehyde **86** with methyl bromoacetate in the presence of K₂CO₃ (**Scheme 3.5**). Resulting methyl ester **87** was deprotected using KOH and free acid **88** was hydrogenated using hydrogen gas and palladium as catalyst. The obtained aniline was consequently reacted with maleic anhydride to give compound **89**. Refluxing in acetic anhydride in the presence of NaOAc furnished acid maleimide **90** which was activated as acid chloride using SOCl₂ and coupled with 4,6-dimethyl-2-amino pyridine to furnish maleimide **73**.

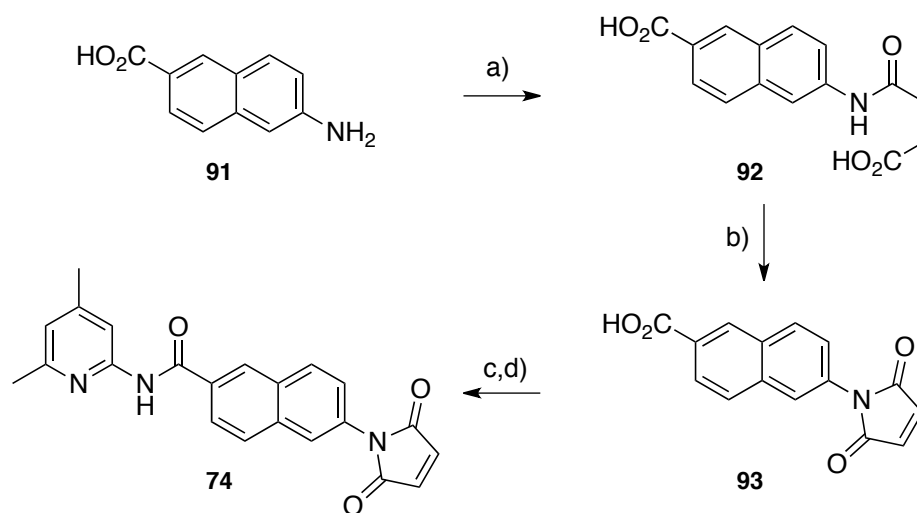


Scheme 3.4 Synthesis of maleimide **72**. Conditions: a) 4,6-dimethyl-2-amino pyridine, DCM, 0 °C, 93%; b) Pd/C, H₂, MeOH/DCM, rt; c) maleic anhydride, AcOH, rt, 93% over two steps. d) ZnBr₂, HMDS, MeCN, 90 °C, 79%.



Scheme 3.5 Synthesis of maleimide **73**. Conditions: a) methyl 2-bromoacetate, K₂CO₃, MeCN, 90 °C, 43%; b) KOH, EtOH/H₂O, 85 °C, 94%; c) Pd/C, H₂, THF, rt, then maleic anhydride, AcOH, 92% over two steps; d) NaOAc, Ac₂O, 100 °C, 80%; e) SOCl₂, toluene, 90 °C; f) 4,6-dimethyl-2-amino pyridine, DCM, 0 °C, 61% over two steps.

Naphthalene maleimide **74** was synthesised in four steps starting from commercially available 6-amino-2-naphthoic acid (**Scheme 3.6**). After treatment with maleic anhydride in acetic acid, amide structure **92** was converted to maleimide **93** in the presence of ZnBr₂ and HMDS. The last reaction step included the activation of **93** with SOCl₂ and consequent coupling of the acid chloride with 4,6-dimethyl-2-amino pyridine furnished the desired maleimide **74**.



Scheme 3.6 Synthesis of maleimide **74**. Conditions: a) maleic anhydride, THF, rt, 97%; b) ZnBr_2 , HMDS, MeCN, 90 °C, 78%; c) SOCl_2 , toluene, 90 °C; d) 4,6-dimethyl-2-amino pyridine, DCM, 0 °C, 63% over two steps.

3.4 Kinetic analysis

Having established the synthesis of all compounds in the library, the reactivity of each pair of nitron and maleimide was investigated next. As every nitron can react with one of the three maleimides to form a pair of diastereoisomeric products, a total of six possible combinations were screened for their potential self-replicating activity. In order to warrant a complete and reliable analysis, a set of four experiments was conducted for each of the six combinations.

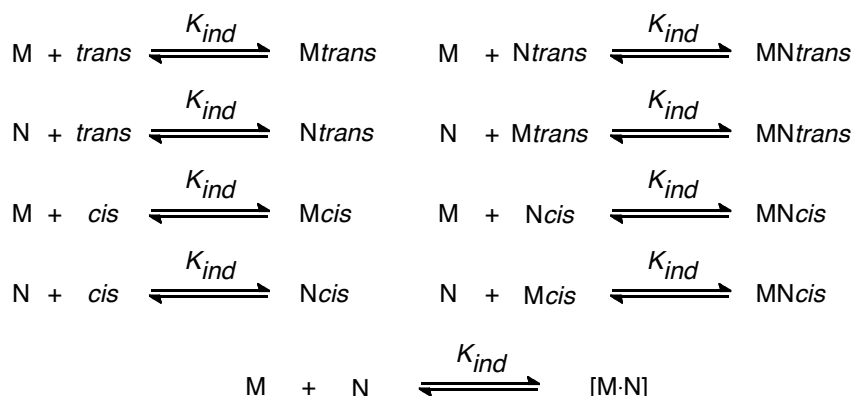
First, the native reaction between nitron and maleimide was performed and a concentration *vs* time profile recorded (see section 10.2.1). A sigmoidal shape for the formation of one of the diastereoisomeric products suggests the presence of self-replicating activity, however, only doping experiments can establish the self-replicating nature of the template. Usually, a fixed amount of presynthesised template was added at the start of the reaction and a concentration *vs* time profile was recorded. If the template is indeed a catalyst for its own formation, the lag period found in the native experiment disappeared and the system had its maximum rate at the start of the reaction.

Repeating the native reaction in the presence of an excess of a competitive inhibitor such as 4-bromobenzoic acid reduced both the conversion and the selectivity of the reaction, thereby verifying the importance of the recognition event in the process. At last, using the appropriate recognition-disabled control nitron provided a baseline for the rates of both diastereoisomers and selectivities for the simple bimolecular reaction. Significant deviation in the native reaction from these baseline values provided further proof for the self-replicating nature of the reaction.

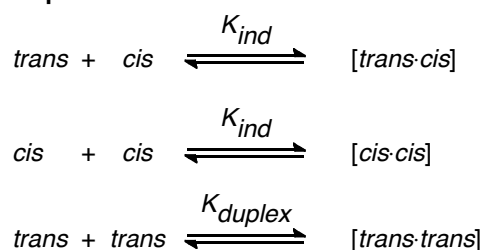
Bimolecular Reactions



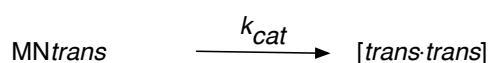
Routes towards formation of binary and ternary complexes



Duplex association



Ternary complex reaction



Bimolecular reactions of complexes

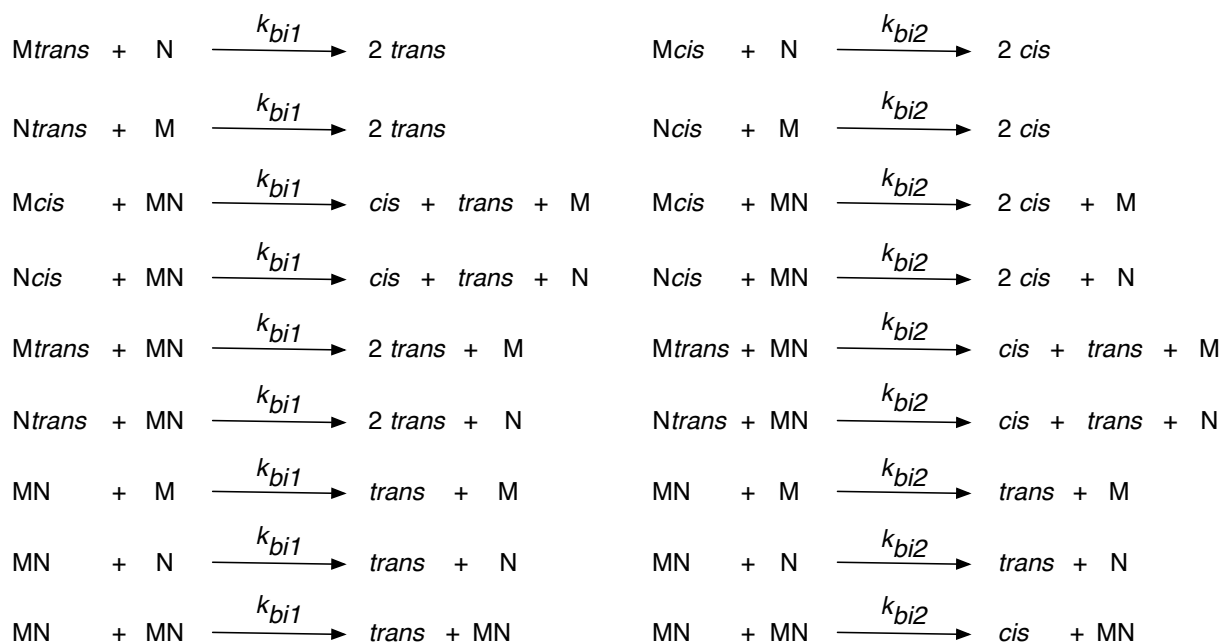


Figure 3.3 Kinetic model used to fit a theoretical curve to experimental data. M and N represent the maleimide and the nitrone, respectively. Their bimolecular reaction leads to products *trans* and *cis* with the corresponding rate constants k_{bi1} and k_{bi2} . Single recognition events between the building blocks are governed by the association constant K_{ind} . Rate-enhanced reaction in the ternary complex is expressed by k_{cat} with a resulting duplex association K_{duplex} .

In the following section, the results for the reaction of each of the three maleimides with both nitrones are presented. Fitting of the experimental data to the kinetic model shown in **Figure 3.3** using the SimFit program provided valuable kinetic parameters which allowed to quantify the observed rate-enhancement and the stability of the catalytically active duplex.

The effective molarity, ϵ or in more recent publications abbreviated as EM, provides a quantitative measure for the acceleration of the reaction in the ternary complex. In the equation

$$EM = \frac{k_{cat}}{k_{bi}}$$

Equation 3.1

k_{cat} is the rate constant for the reaction proceeding through the catalytically active ternary complex. The value for k_{cat} cannot be determined experimentally but is given as a result of the fitting procedure. In the case of self-replicating systems, the EM value can further be understood as the hypothetical concentration at which the intermolecular reaction, that is the bimolecular reactions between the two reagents, proceeds at the same rate as the intramolecular reaction within the ternary complex.

Another key parameter is the free energy of connection, ΔG^s , which gives a direct measure for the quality of the product duplex association. In every self-replicating template duplex binding occurs through two identical recognition motifs. In the case of an optimal fit between both templates, the initial binding event facilitates the second one and the free energy of binding in the complex is more negative than the sum of the free energies for the two individual binding events. This process is called positive cooperativity. On the other hand, a mismatch in template geometry will hamper the second binding event and result in negative cooperativity which implies that the free energy of binding in the complex is more positive than the sum of the free energies for each individual binding interaction. No cooperativity occurs when the free energy of binding equals the sum of the individual binding interactions.

The binding energy of a molecule with two different recognition sites, A-B, to a host consists of three parts, the individual free energies of binding A or B to the host (ΔG_A^i and ΔG_B^i) and the free energy of connection (ΔG^s) which quantifies the cooperativity of the system.

$$\Delta G_{AB}^0 = \Delta G_A^i + \Delta G_B^i - \Delta G^s$$

Equation 3.2

In the special case of the template duplex of a self-replicator, both binding events are identical and the equation can be simplified to

$$\Delta G_{SR}^0 = 2\Delta G_{ind} - \Delta G^s$$

Equation 3.3

with ΔG_{SR}^0 now being the free energy of binding and ΔG_{ind} the free energy of the individual binding event. Subsequent replacement of the terms for the free energies with

$$\Delta G_{SR}^0 = -RT \ln K_{duplex}$$

Equation 3.4

and

$$\Delta G_{ind} = -RT \ln K_{ind}$$

Equation 3.5

leads to an equation which allows to calculate the cooperativity in a template duplex based on the association constants of the individual binding event, K_{ind} , and in the duplex, K_{duplex} .

$$\Delta G^s = RT \ln \left(\frac{K_{duplex}}{K_{ind}^2} \right)$$

Equation 3.6

The association constant K_{ind} can be determined experimentally whereas values for the association in the duplex can be extracted from the experimental data by the fitting procedure. Positive values for ΔG^s represent a favourable positive cooperativity, whereas

negative values indicate negative cooperativity.^[196] In the following sections, the kinetic analysis for the four crucial experiments are discussed in detailed for all possible six systems and, ultimately, a hierarchy of reactivity for the investigated structures is established on the basis of the extracted kinetic parameters.

3.4.1 Reaction of maleimide **72** with nitrone **70**

Kinetic analysis of the reaction between benzene maleimide **72** and nitrone **70** giving rise to template **94** was conducted in CDCl₃ at 0 °C for 16 h with 10 mM concentration of starting materials.

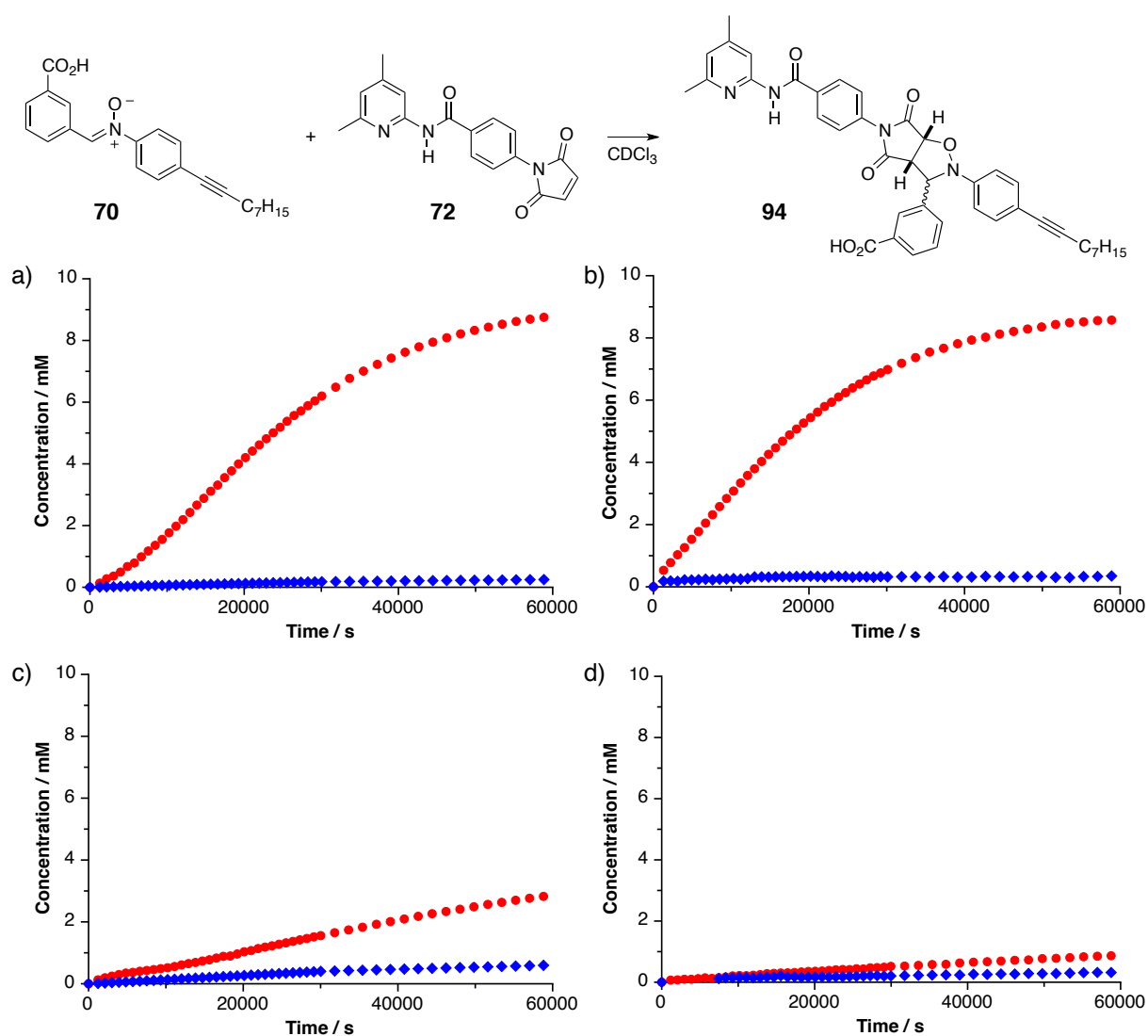


Figure 3.4 Concentration *vs* time profiles for the reaction between a) maleimide **72** and nitrone **70**, b) maleimide **72** and nitrone **70** in the presence of 10 mol-% *trans*-**94**, c) maleimide **72** and nitrone **70** in the presence of 40 mM 3-bromobenzoic acid and d) maleimide **72** and control nitrone **81**. The formation of *trans*-products is shown as red filled circles and the formation of *cis*-products as blue filled diamonds. All reactions were performed at 0 °C in CDCl₃ at 10 mM reagent concentration.

Figure 3.4 shows the concentration *vs* time profiles for the four essential reactions. The native reaction between **70** and **72** shows a sigmoidal shape for the formation of *trans*-**94** hinting at a possible self-replicating nature for the reaction (**Figure 3.4a**). The selectivity was found to be 35:1 in favour of the *trans*-isomer and 90% of the starting material was converted after 16 h. Doping a fresh batch of reagents with 10 mol-% of *trans*-species overcomes the lag period and increased slightly both the selectivity for the *trans*-isomer to 38:1 and the conversion after 16 h to 92 % (**Figure 3.4b**). Further evidence for the presence of a self-replicator is provided by the reaction of **72** and **70** with 4 equivalents of 3-bromobenzoic acid as competitive inhibitor (**Figure 3.4c**). The selectivity for *trans*-**94** now drops to a mere 5:1 and the conversion plunges to 34% establishing the importance of recognition processes in the native reaction. The reaction between maleimide **72** and recognition-disabled control nitrene **81** proceeded slowly. After 16 h, only 12% of the starting materials was converted to products with a ratio of 2.7:1 in favour of the *trans*-isomer (**Figure 3.4d**).

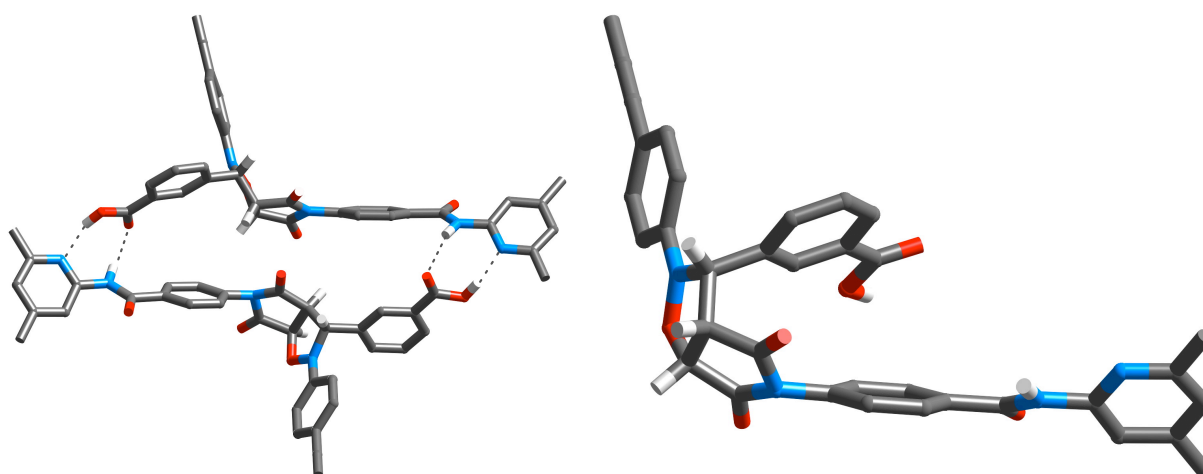


Figure 3.5 Molecular models of the *trans*-**94** duplex (left) and the *cis*-**94** monomer (right). Carbon atoms are shown in dark grey, hydrogen atoms in light grey, nitrogen atoms in blue and oxygen atoms in red. Hydrogen bonds are indicated by dotted lines. Most other hydrogens were omitted for clarity.

Overall, the *trans*-product of the reaction between maleimide **72** and nitrene **70** was found to be an efficient self-replicator, whereas the *cis*-isomer showed no recognition-mediated behaviour. This finding is corroborated by molecular modeling of the template duplex of *trans*-**94** and the structure of *cis*-**94** (**Figure 3.5**). The open geometry of *trans*-**94** allows for the formation of a self-complementary duplex in which hydrogen bonding between the recognition units at both ends of the template molecule can occur without distorting its structure. On the other hand, the *cis*-isomer possesses a folded geometry in which access to the recognition sites is limited. As a consequence of the length mismatch

between the carboxy acid and the benzene spacer, formation of a productive binary complex between nitron and maleimide to form *cis*-**94** by AB pathway can be ruled out. Recognition between the acid and the amidopyridine moiety in the AB complex positions the reactive sites too far away from each other.

Quantitative measures for the efficiency of the self-replicator were extracted from the kinetic data of the native reaction using the SimFit package (**Figure 3.6**). The quality of the fit is reflected by the solid line deriving from the kinetic model compared with the experimental data points. It can clearly be seen that fitting of the experimental data proceeded smoothly.

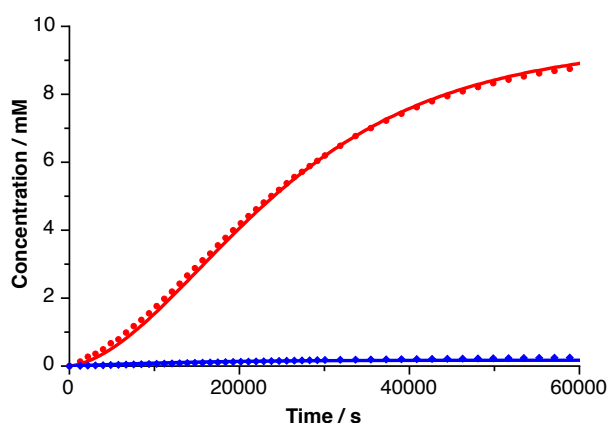


Figure 3.6 Concentration *vs* time profile for the reaction between maleimide **72** and nitron **70** to give template **94**. The formation of *trans*-product is shown as red filled circles and the formation of *cis*-product as blue filled diamonds. Solid lines represent the results for the fitting of the *trans*-(-) and *cis*-(-) product. The reaction was performed at 0 °C in CDCl₃ at 10 mM reagent concentration.

The results of the fit are listed in **Table 3.1**. Bimolecular rates were extracted from the control experiments and used in the fitting protocol. The association constant K_a for the individual interaction between a carboxylic acid and amidopyridine at 10 mM concentration and 0 °C was determined to be 4030 M⁻¹ (see chapter 4, **Table 4.1**). Calculation of the effective molarity and the free energy of connection was conducted as described earlier.

Table 3.1 Kinetic parameters extracted for the self-replicating reaction of maleimide **72** and nitron **70** at 0 °C in CDCl₃ at 10 mM reagent concentration using SimFit. The obtained R-value was 1.6%.

	<i>trans</i> - 94	<i>cis</i> - 94
bimolecular rate constant / M ⁻¹ s ⁻¹	2.23 × 10 ⁻⁴	1.14 × 10 ⁻⁴
recognition-mediated rate constant / s ⁻¹	1.56 × 10 ⁻²	-
effective molarity / M	69.8	-
ΔG^s / kJ mol ⁻¹	11.9	-

The calculated values suggest that *trans-94* is indeed a highly efficient self-replicator with a high effective molarity and strong duplex association. An in-depth discussion about its properties and comparison with the structurally related systems can be found at the end of this chapter.

3.4.2 Reaction of maleimide 72 with nitron 71

The same set of experiments was conducted using phenylacetic acid nitron 71 as reactive partner for maleimide 72 to form template 95. All four crucial experiments were recorded by ¹H NMR spectroscopy in CDCl₃ for 16 h at 0 °C and 10 mM concentration of the starting materials. The native reaction between both compounds gave rise to the concentration *vs* time profile in **Figure 3.7a**. It is instantly evident that the situation is fundamentally different to the one found for the reaction with carboxy nitron 70. After 16 h, *cis-95* was found to be the dominant species over the *trans*-isomer with a ratio of 2.2:1. Conversion of starting material was 85% indicating the presence of a recognition-mediated process. The doping experiment using a mixture of 6.5 mol-% of *cis-95* and 3.5 mol-% of *trans-95* showed that the *trans*-isomer benefited from the added template, whereas the activity of the *cis*-isomer has decreased (**Figure 3.7b**). However, also in this reaction, the *cis*-isomer remains the most abundant species with the ratio of isomers fallen to 1.5:1 and conversion slightly increased to 88% after 16 h. Adding an excess of 4-bromophenylacetic acid as competitive inhibitor brings down the overall conversion to 59%, but shows to have a much higher impact on the formation of the *trans*-species whereas little inhibition occurs for the *cis*-isomer pushing the ratio of isomers to 11:1 for *cis-95* (**Figure 3.7c**). Last, the control reaction with recognition-disabled nitron 82 established the bimolecular background formation of both isomers with a ratio of 1.9:1 in favour of the *trans*-isomer and yielding a mere 15% conversion of the starting materials after 16 h (**Figure 3.7d**).

Altogether, these findings can be rationalised by considering a situation in which *trans-95* acts as a self-replicator, whereas *cis-95* shows rate-enhancement by formation through an AB complex. Strong evidence for the autocatalytic formation of *trans-95* and the AB nature of *cis-95* are found in the doping experiment. The addition of 3.5 mol-% *trans*-template to the reaction indeed strengthened the autocatalytic formation of *trans-95* regarding the *cis*-isomer, which in turn did not show any enhancement even though 6.5 mol-% of its template was added simultaneously to the reaction mixture.

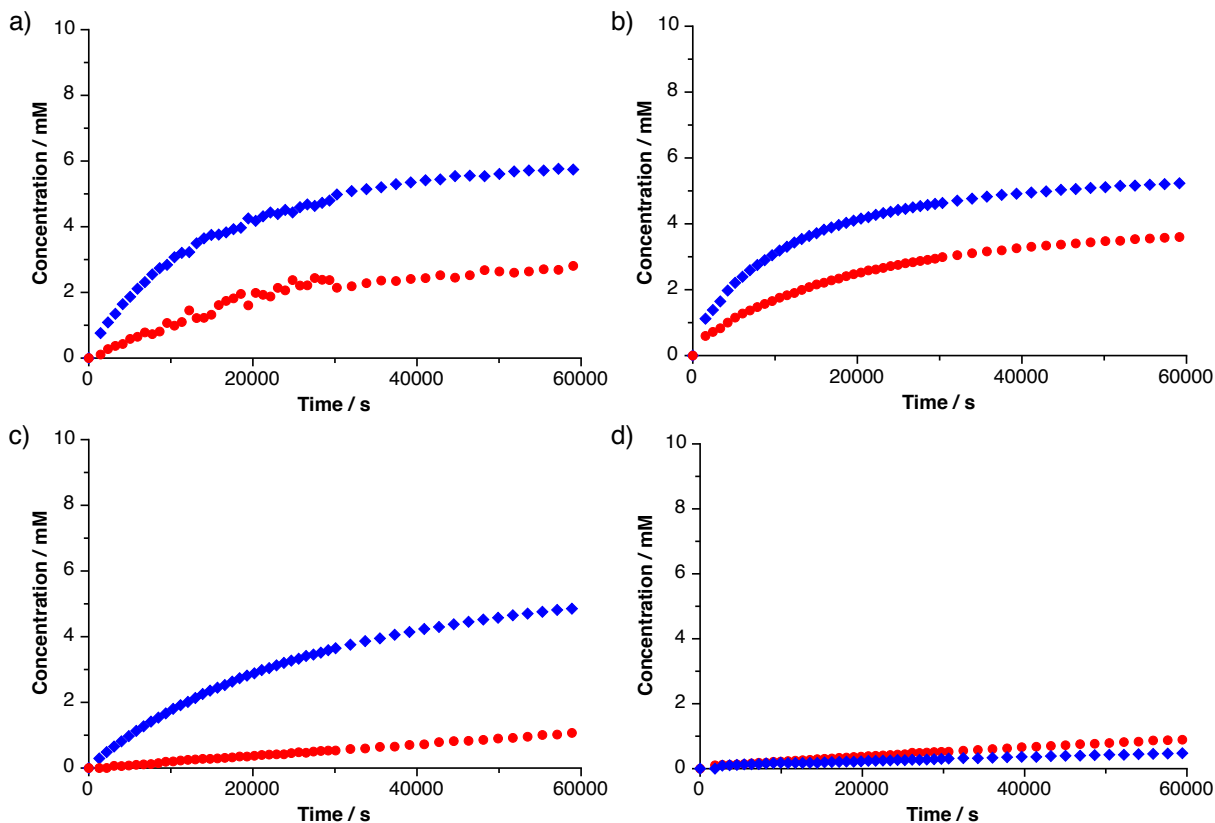
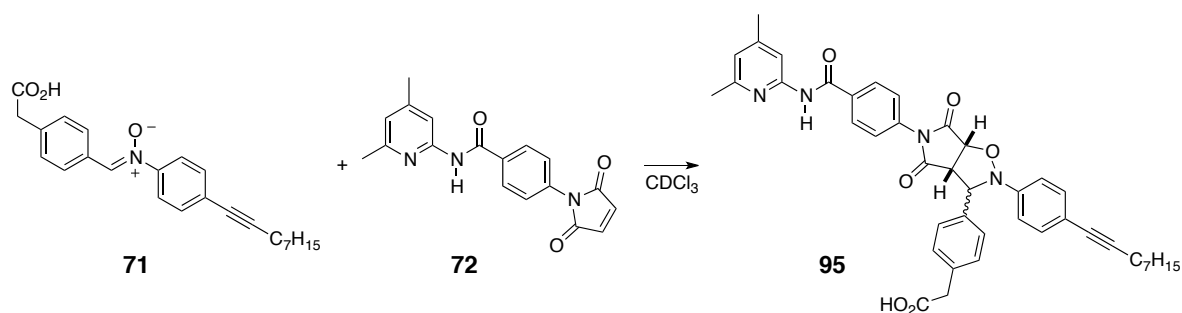


Figure 3.7 Concentration *vs* time profile for the reaction between a) maleimide **72** and nitrone **71**, b) maleimide **72** and nitrone **71** in the presence of 6.5 mol-% *cis*-**95** and 3.5 mol-% *trans*-**95**, c) maleimide **72** and nitrone **71** in the presence of 40 mM 4-bromophenylacetic acid and d) maleimide **72** and control nitrone **82**. The formation of *trans*-product is shown as red filled circles and the formation of *cis*-product as blue filled diamonds. All reactions were performed at 0 °C in CDCl₃ at 10 mM reagent concentration.

The final reaction mixture of this doping experiment was used as a source of templates to dope a fresh batch of reagents and to establish the limiting point of the competition between both isomers for available reagents. Since only the self-replicating *trans*-isomer responds to the addition of its template, taking the end point of a reaction as doping material for a new reaction should gradually accumulate the autocatalytic template on the expense of catalytically inactive *cis*-**95**. This effect already reduced the *cis/trans* ratio from 2.2:1 in the native reaction to 1.5:1 for the first doping experiment. Accordingly, 10 mol-% of the outcome of this first cycle consisting of 6.0 mol-% of the *cis*-isomer and 4.0 mol-% of *trans*-**95** was added to a fresh batch of reagents. Interestingly, this second cycle did not

change the rate for the formation of both isomers, and the selectivity remained at a ratio of 1.5:1 for the *cis*-isomer. Thus, the limit of enhancement for the *trans*-isomer with respect to *cis*-95 is already reached after the first doping experiment.

Further evidence for the simultaneous presence of a self-replicator and AB system was provided by the reaction of maleimide **72** and nitrone **71** with 4 equivalents of 4-bromophenylacetic acid as competitive inhibitor (**Figure 3.7c**). Since the formation of the *cis*-isomer proceeded through a binary complex, the effect of the inhibitor was felt less strongly than in the case of the self-replicating reaction which involved the formation of a ternary complex. Accordingly, the curve for *cis*-95 showed only a small reduction of maximum rate at the start of the reaction while *trans*-95 suffered severely from the presence of the inhibitor. As a result, the ratio increased to 11:1 for the *cis*-isomer.

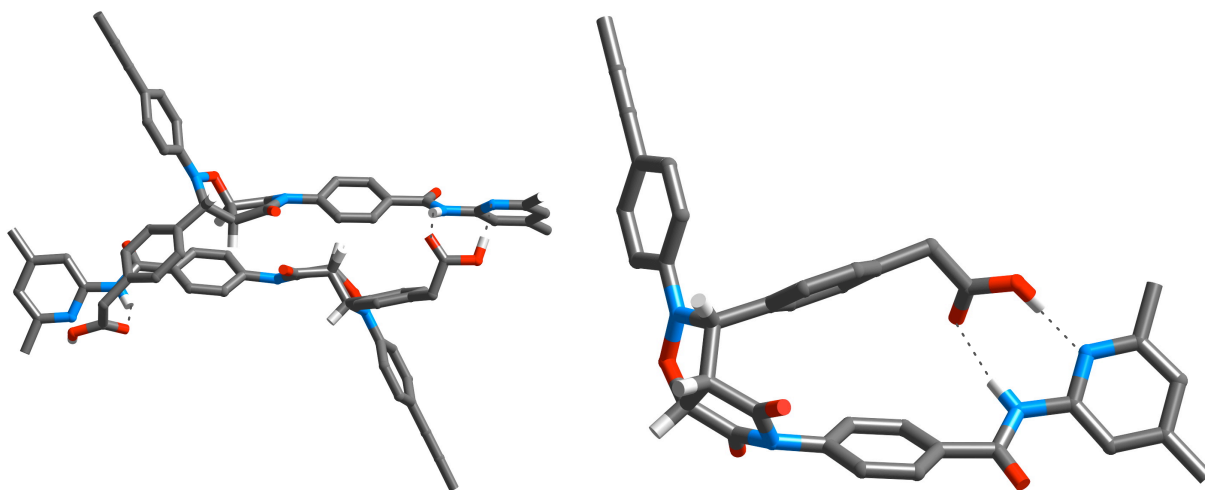


Figure 3.8 Molecular models of the *trans*-95 duplex (left) and the *cis*-95 monomer (right). Carbon atoms are shown in dark grey, hydrogen atoms in light grey, nitrogen atoms in blue and oxygen atoms in red. Hydrogen bonds are indicated by dotted lines. Most other hydrogens were omitted for clarity.

Molecular modeling was performed on both templates and the calculated structures are presented in **Figure 3.8**. Changing from the previous carboxy nitrone **70** to nitrone **71** had some important impact on the structures of the reaction products. Insertion of the methylene group forced the *trans*-templates in the duplex to slightly wrap around each other in order to position the recognition units correctly. However, the self-complementary of the duplex structure is clearly visible and self-replicating activity of *trans*-95 can be assumed. The change in spacer length affected significantly the geometry of *cis*-95. By extending the spacer group of the acid building block, both recognition sites are now in close proximity and internal hydrogen bonding becomes possible without distortion of the geometry. This

arrangement confirms that the rate-enhanced reaction between nitrone **71** and maleimide **72** to form *cis*-**95** proceeds through the AB pathway.

In order to obtain quantitative measures for the rates of the self-replicator and AB system, the kinetic data of the reactions were analysed using SimFit. The quality of fit for the native reaction can be seen in **Figure 3.9**. Broadening peaks in the deconvolution process caused slight scattering in the area around 15000 to 25000 seconds. However, fitting of the experimental data proceeded smoothly and provided sensible kinetic values which are listed in **Table 3.2**. The bimolecular rates used in the fitting protocol were obtained from the control experiment with nitrone **82**. The association constant for the individual interaction between a phenylacetic acid and amidopyridine at 10 mM concentration and 0 °C was found to be 1800 M⁻¹ (see chapter 4, **Table 4.1**). The effective molarity and the free energy of connection were calculated as described previously. The calculated values underpin the finding that both *trans*- and *cis*-**95** engage in recognition-mediated processes.

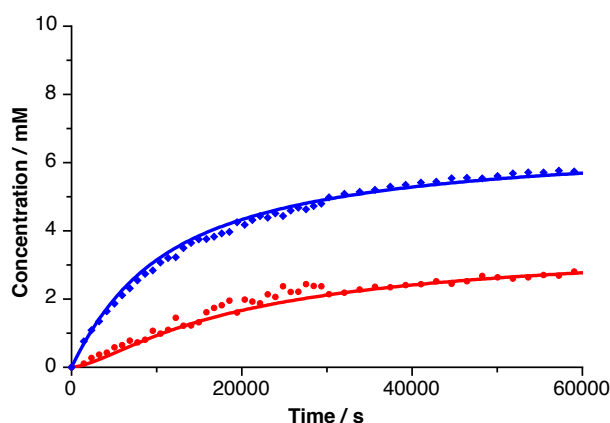


Figure 3.9 Concentration *vs* time profile for the reaction between maleimide **72** and nitrone **71** to give template **95**. The formation of *trans*-product is shown as red filled circles and the formation of *cis*-product as blue filled diamonds. Solid lines represent the results for the fitting of the *trans*-(-) and *cis*-(-) product. The reaction was performed at 0 °C in CDCl₃ at 10 mM reagent concentration.

Table 3.2 Kinetic parameters extracted for the reaction of maleimide **72** and nitrone **71** to give self-replicator *trans*-**95** and AB system *cis*-**95** at 0 °C in CDCl₃ at 10 mM reagent concentration using SimFit. The obtained R-value was 4.6%.

	<i>trans</i> - 95	<i>cis</i> - 95
bimolecular rate constant / M ⁻¹ s ⁻¹	1.84 × 10 ⁻⁴	1.03 × 10 ⁻⁴
recognition-mediated rate constant / s ⁻¹	4.87 × 10 ⁻³	7.03 × 10 ⁻⁵
effective molarity / M	26.5	0.683
Δ <i>G</i> ^s / kJ mol ⁻¹	4.88	-

3.4.3 Reaction of maleimide 73 with nitron 70

Kinetic data for the reaction between maleimide 73 with carboxy nitron 70 to give cycloadduct 96 was recorded for 16 h at 10 °C in CDCl₃ with a starting material concentration of 10 mM. Deconvolution of the obtained ¹H NMR spectra allowed for the construction of the concentration *vs* time profiles depicted in **Figure 3.10**.

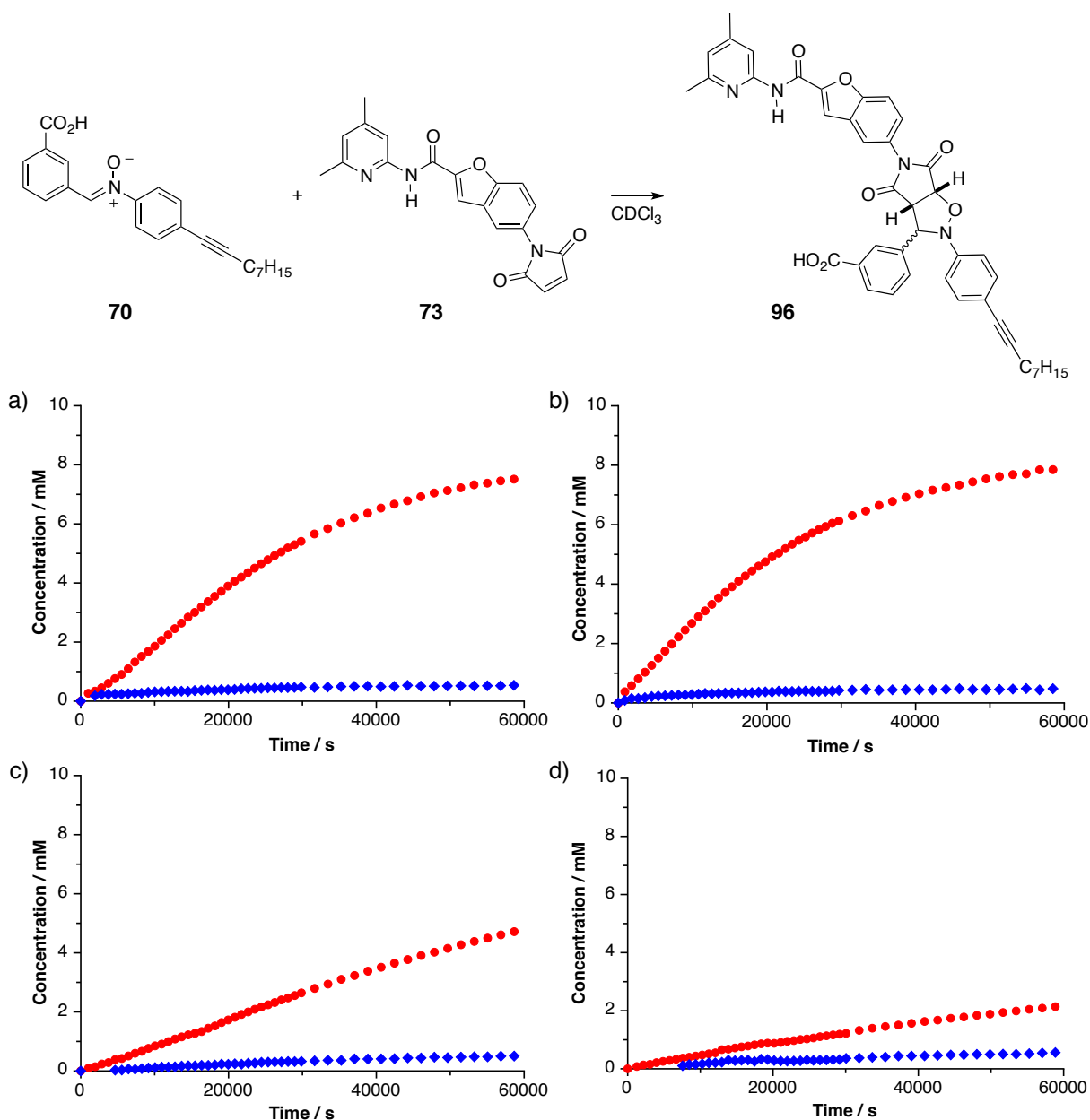


Figure 3.10 Concentration *vs* time profile for the reaction between a) maleimide 73 and nitron 70, b) maleimide 73 and nitron 70 in the presence of 9 mol-% *trans*-96, c) maleimide 73 and nitron 70 in the presence of 40 mM 3-bromobenzoic acid and d) maleimide 73 and control nitron 81. The formation of *trans*-product is shown as red filled circles and the formation of *cis*-product as blue filled diamonds. All reactions were performed at 10 °C in CDCl₃ at 10 mM reagent concentration.

The curve for the native reaction (**Figure 3.10a**) exhibits a gentle sigmoidal shape for the formation of *trans*-96 which was lost in the doping experiment using 9 mol-% of *trans*-template (**Figure 3.10b**). In the native reaction, *trans*-96 was formed in a ratio of 20:1 over *cis*-96 which increased to 23:1 in the doping reaction. Contemporaneously, the conversion increased slightly from 80% to 81%. Addition of 4 equivalents of 3-bromobenzoic acid reduced both the selectivity for the *trans*-isomer and the conversion to 9:1 and 52%, respectively (**Figure 3.10c**). The control reaction between maleimide 73 and control nitrene 81 proceeded with only 27% conversion after 16 h and a ratio of 3.8:1 for *trans*-96 (**Figure 3.10d**). Altogether, kinetic analysis of this reaction provided strong evidence for the self-replicating nature of *trans*-96 and suggested that *cis*-96 is solely formed through the bimolecular reaction.

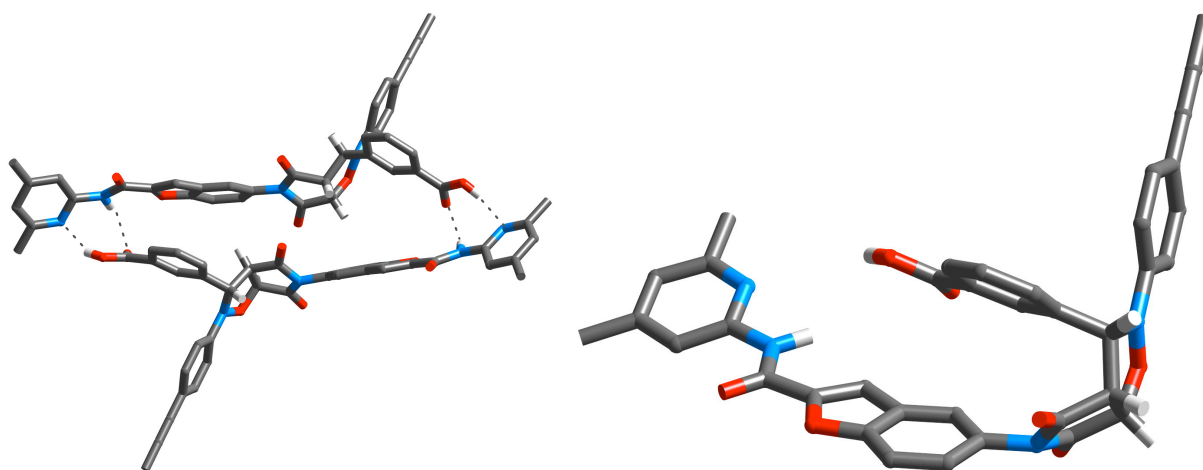


Figure 3.11 Molecular models of the *trans*-96 duplex (left) and the *cis*-96 monomer (right). Carbon atoms are shown in dark grey, hydrogen atoms in light grey, nitrogen atoms in blue and oxygen atoms in red. Hydrogen bonds are indicated by dotted lines. Most other hydrogens were omitted for clarity.

This finding is corroborated by molecular modeling of the template duplex of *trans*-96 (**Figure 3.11**). The open structure of the self-complementary template allowed for the formation of a duplex structure in which the recognition units at both ends can form hydrogen bonding without causing deformation of the backbone. Generation of a catalytically active ternary complex seems plausible. On the other hand, rate-enhanced formation of the *cis*-template through a binary complex can be ruled out as a consequence of the length mismatch between the extended benzofuran spacer of the maleimide and the short carboxy unit.

Fitting of the experimental data with SimFit provided quantitative measures for the efficiency of the self-replicator. The quality of the kinetic model can be seen in the overlay

with the data obtained experimentally in **Figure 3.12**. The results of the fitting are presented in **Table 3.3**. The association between a carboxylic acid and amidopyridine at 10 mM concentration and 10 °C was determined to be 3500 M⁻¹ (see **Table 4.1**) and used for the calculation of the free energy of connection. Bimolecular rates were obtained from the control experiment of maleimide **73** with nitrone **81** and used to calculate the kinetic effective molarity. Altogether, the results suggest the presence of a moderately efficient self-replicator.

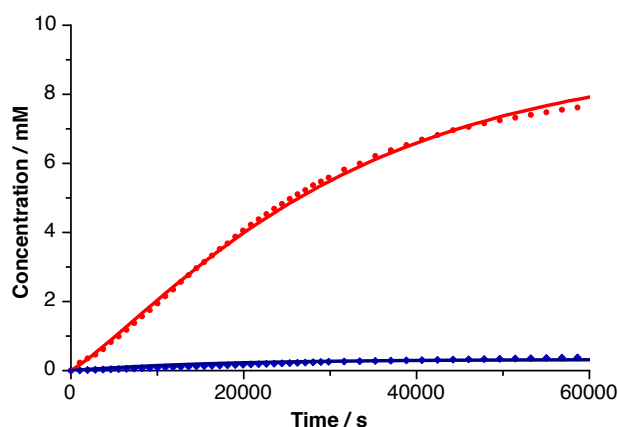


Figure 3.12 Concentration *vs* time profile for the reaction of maleimide **73** and nitrone **70** to give template **96**. The formation of *trans*-product is shown as red filled circles and the formation of *cis*-product as blue filled diamonds. Solid lines represent the results for the fitting of the *trans*-(-) and *cis*-(-) product. The reaction was performed at 10 °C in CDCl₃ at 10 mM reagent concentration.

Table 3.3 Kinetic parameters extracted for the self-replicating reaction of maleimide **73** and nitrone **70** at 10 °C in CDCl₃ at 10 mM reagent concentration using SimFit. The obtained R-value was 3.9%.

	<i>trans</i> -96	<i>cis</i> -96
bimolecular rate constant / M ⁻¹ s ⁻¹	9.03 × 10 ⁻⁴	4.51 × 10 ⁻⁴
recognition-mediated rate constant / s ⁻¹	4.81 × 10 ⁻³	-
effective molarity / M	5.26	-
Δ <i>G</i> ^s / kJ mol ⁻¹	8.08	-

3.4.4 Reaction of maleimide **73** with nitrone **71**

The reaction between maleimide **73** and nitrone **71** in CDCl₃ at 10 mM concentration and 10 °C was followed for 16 h. The kinetic data for the four essential experiments are presented in **Figure 3.13**. The native reaction to give template **97** proceeded with 68% conversion and a selectivity of 8:1 for the *trans*-isomer (**Figure 3.13a**).

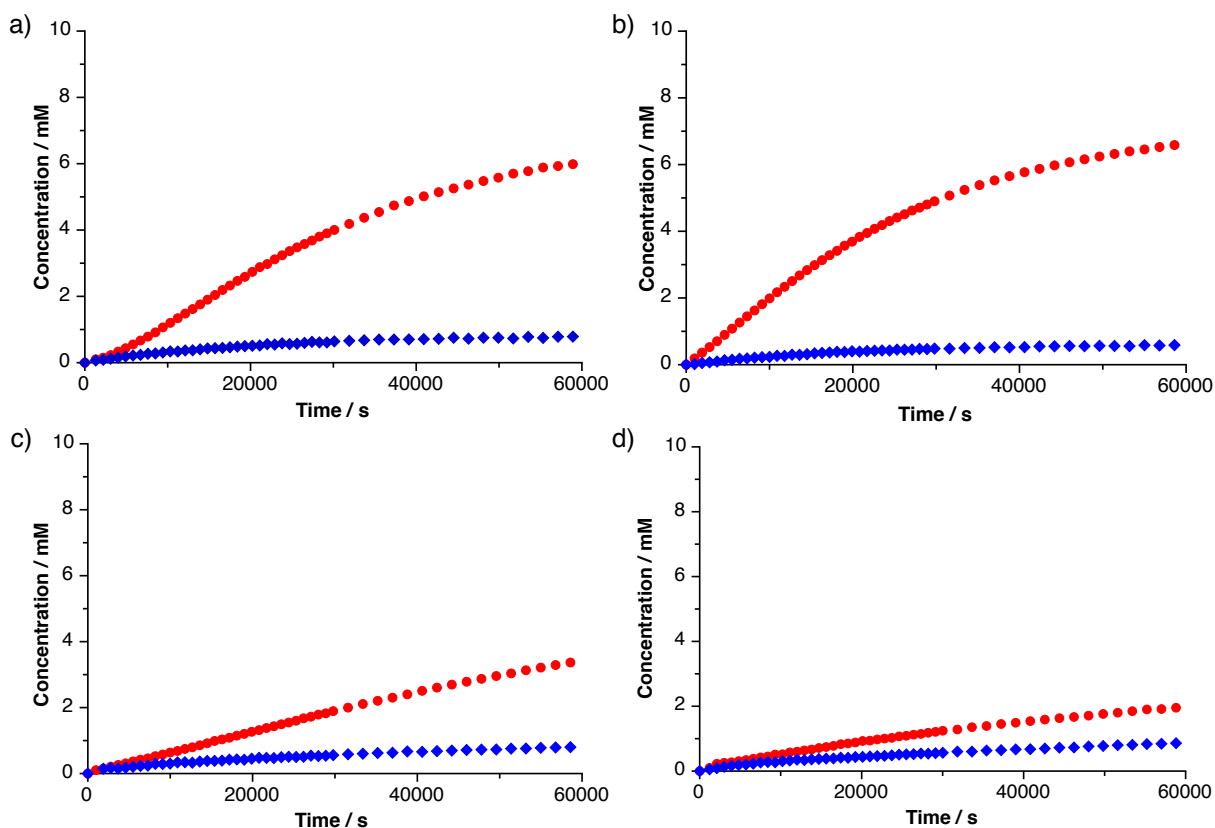
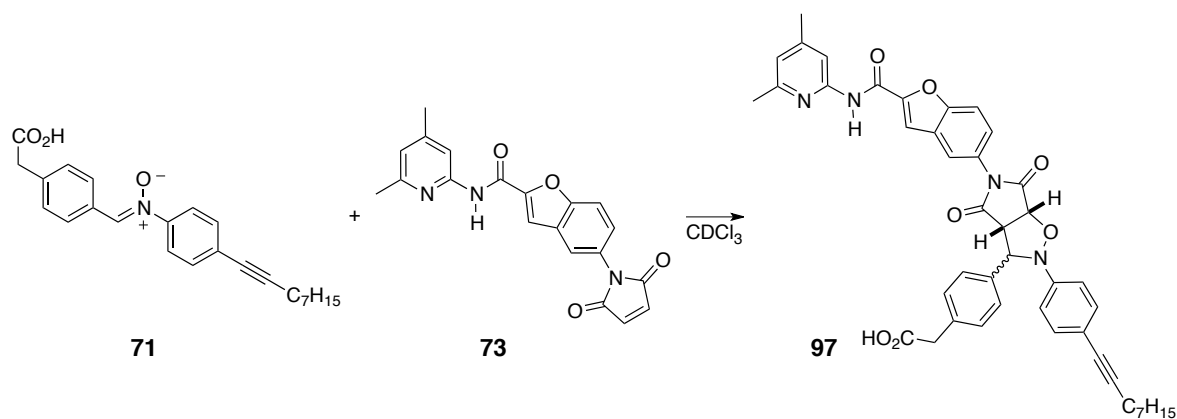


Figure 3.13 Concentration *vs* time profile for the reaction between a) maleimide **73** and nitrone **71**, b) maleimide **73** and nitrone **71** in the presence of 10 mol-% *trans*-**97**, c) maleimide **73** and nitrone **71** in the presence of 40 mM 4-bromophenylacetic acid and d) maleimide **73** and control nitrone **82**. The formation of *trans*-products is shown as red filled circles and the formation of *cis*-products as blue filled diamonds. All reactions were performed at 10 °C in CDCl₃ at 10 mM reagent concentration.

The gentle sigmoidal shape of the formation of *trans*-**97** in the native curve disappeared upon addition of 9 mol-% of presynthesised *trans*-template and the ratio increased to 11:1 yielding 71% of products (**Figure 3.13b**). Addition of 4 equivalents of 4-bromophenylacetic acid at the start of the reaction severely hampered the formation of *trans*-**97** leading to a ratio of only 4:1 in favour of the *trans*-isomer with 42% conversion of starting material (**Figure 3.13c**). The reaction between maleimide **73** and recognition-disabled control nitrone **82** proceeded slowly (**Figure 3.13d**). After 16 h, only 28% of the starting materials was converted to products with a ratio of solely 2.3:1 in favour of the *trans*-isomer.

The kinetic data presented here clearly indicates that *trans*-96 acts as a template for its own formation whereas *cis*-96 exhibits no recognition-mediated activity. This finding is corroborated by molecular modeling of the template duplex of *trans*-97 (Figure 3.14). It can clearly be seen that the rigid backbone separates the recognition units in the template allowing the formation of a stable duplex structure and explaining the self-replicating nature of *trans*-97. The closed shape of *cis*-97 shows a mismatch in length between the phenylacetic acid and the benzofuran spacer that prevents the formation of internal hydrogen bonds. The presence of this mismatch suggests that rate-enhanced reaction through the AB pathway to give *cis*-97 is unlikely and that this isomer is only formed through the bimolecular reaction.

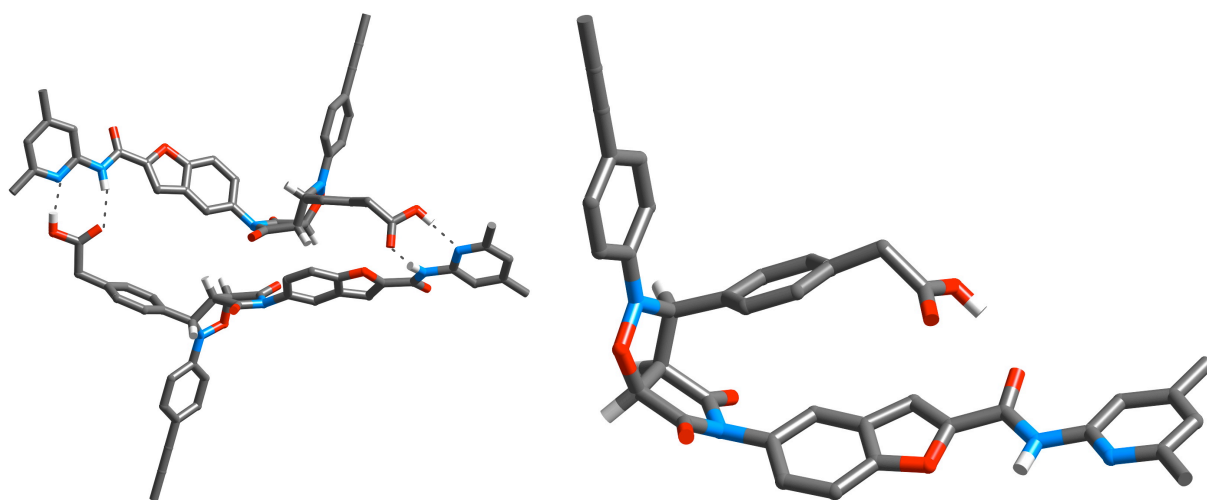


Figure 3.14 Molecular models of the *trans*-97 duplex (left) and the *cis*-97 monomer (right). Carbon atoms are shown in dark grey, hydrogen atoms in light grey, nitrogen atoms in blue and oxygen atoms in red. Hydrogen bonds are indicated by dotted lines. Most other hydrogens were omitted for clarity.

Fitting of the kinetic data for the native reaction using SimFit proceeded smoothly and produced the solid lines seen in Figure 3.15. The corresponding extracted kinetic values are presented in Table 3.4. Bimolecular rates were obtained from the control experiment of maleimide 73 with nitrene 82 and used to calculate the effective molarity. Calculation of the free energy of connection was performed with an association constant of 1600 M^{-1} for the interaction between phenylacetic acid and amidopyridine at 10 mM concentration and 10°C . Altogether, the results suggest the presence of a moderately efficient self-replicator for the *trans*-isomer and no recognition-mediated activity for the *cis*-species. A discussion of the property of this replicator and a comparison with the structurally related systems can be found at the end of this chapter.

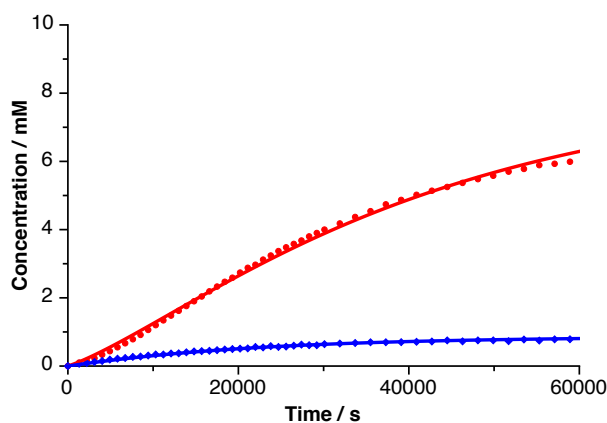


Figure 3.15 Concentration *vs* time profile for the reaction of maleimide **73** and nitron **71** to give template **97**. The formation of *trans*-product is shown as red filled circles and the formation of *cis*-product as blue filled diamonds. Solid lines represent the results for the fitting of the *trans*-(-) and *cis*-(-) product. The reaction was performed at 10 °C in CDCl₃ at 10 mM reagent concentration.

Table 3.4 Kinetic parameters extracted for the self-replicating reaction of maleimide **73** and nitron **71** at 10 °C in CDCl₃ at 10 mM reagent concentration using SimFit. The obtained R-value was 3.8%.

	<i>trans</i> - 97	<i>cis</i> - 97
bimolecular rate constant / M ⁻¹ s ⁻¹	7.29 × 10 ⁻⁴	3.57 × 10 ⁻⁴
recognition-mediated rate constant / s ⁻¹	2.89 × 10 ⁻³	-
effective molarity / M	3.96	-
Δ <i>G</i> ^s / kJ mol ⁻¹	7.43	-

3.4.5 Reaction of maleimide **74** with nitron **70**

The reaction of maleimide **74** with carboxy nitron **70** to give template **98** was recorded for 16 h at 10 °C in CDCl₃ and 10 mM starting concentration. The native reaction exhibits a sigmoidal shape for the formation of *trans*-**98** indicating the presence of a self-replicator (**Figure 3.16**). After 16 h, 78% of the starting material was converted and the *trans/cis* ratio was found to be 11:1 (**Figure 3.16a**). Doping a fresh batch of reagents with 9 mol-% of *trans*-**98** eliminated the initial lag period and the maximum rate was shifted to the start of the reaction (**Figure 3.16b**). Consequently, the ratio increased to 18:1 for the *trans*-isomer and the conversion reached 80%. Repeating the reaction in the presence of 4 equivalents of 3-bromobenzoic acid reduced the selectivity to solely 7:1 for the *trans*-isomer and only 41% of the starting material had reacted after 16 h (**Figure 3.16c**). Using nitron **81** as control compound yielded 26% of product and established the selectivity for the simple bimolecular reaction to be 4.2:1 in favour of the *trans*-isomer (**Figure 3.16d**).

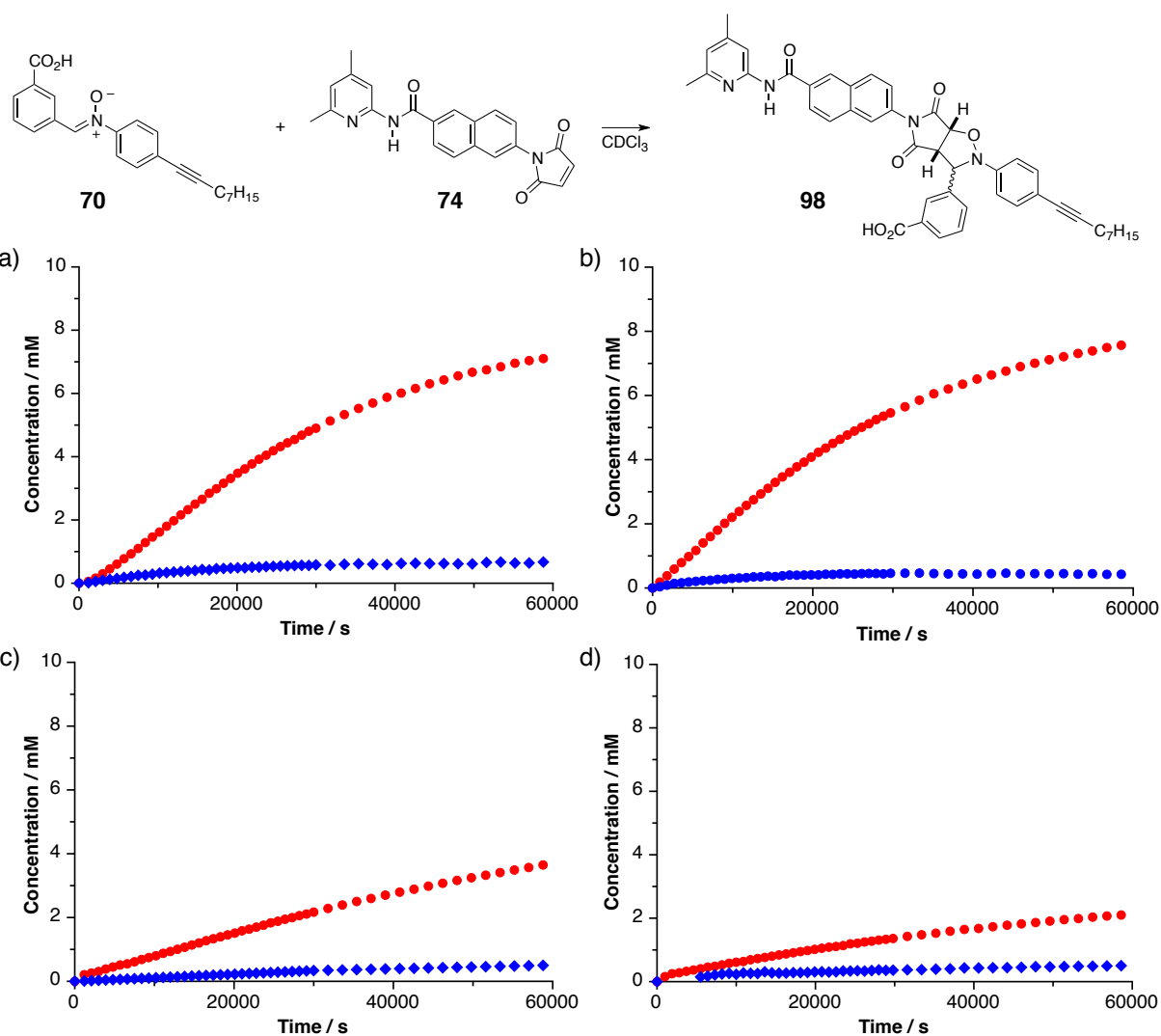


Figure 3.16 Concentration *vs* time profile for the reaction between a) maleimide **74** and nitrone **70**, b) maleimide **74** and nitrone **70** in the presence of 9 mol-% *trans-98*, c) maleimide **74** and nitrone **70** in the presence of 40 mM 3-bromobenzoic acid and d) maleimide **74** and control nitrone **81**. The formation of *trans*-product is shown as red filled circles and the formation of *cis*-product as blue filled diamonds. All reactions were performed at 10 °C in CDCl_3 at 10 mM reagent concentration.

The sigmoidal shape of the native reaction and the behaviour of the system in the doping experiment provide clear evidence for the self-replicating nature of the reaction between maleimide **74** and nitrone **70**. This finding is corroborated by molecular modeling of the template duplex of *trans-98* (Figure 3.17). Its rigid structure allows for the formation of a duplex structure in which the recognition sites on both ends of the template possess the right orientation to associate through hydrogen bonding. As a consequence, template-directed synthesis of *trans-98* through a ternary complex with both reagents seems feasible. Accordingly, the *cis*-isomer shows a folded structure in which the length of the naphthalene spacer prevents the recognition units to come into close proximity rendering a possible reaction through an AB complex highly unlikely.

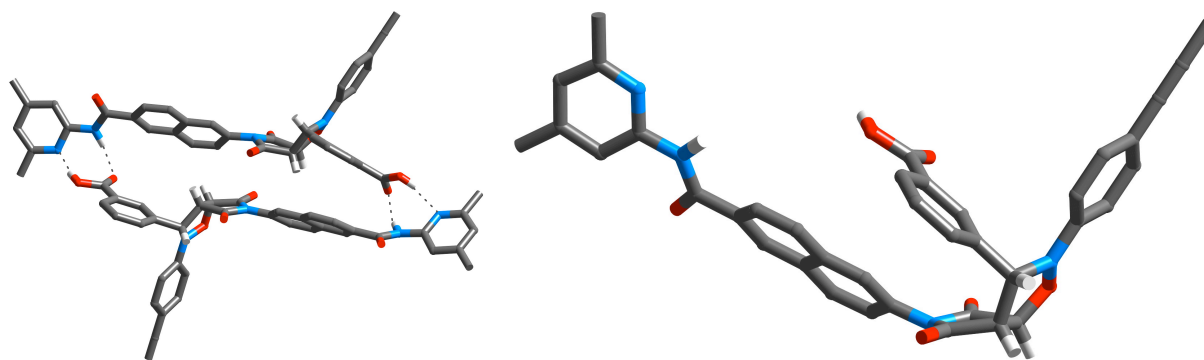


Figure 3.17 Molecular models of the *trans*-98 duplex (left) and the *cis*-98 monomer (right). Carbon atoms are shown in dark grey, hydrogen atoms in light grey, nitrogen atoms in blue and oxygen atoms in red. Hydrogen bonds are indicated by dotted lines. Most other hydrogens were omitted for clarity.

Careful analysis of the obtained data shows two specifics. First, the 4.2:1 ratio for the *trans*-isomer in the native reaction is unusually high. Moreover, careful analysis of the doping experiment shows a rather abnormal behaviour. Adding an increasing amount of template at the start of the reaction gradually enhances its maximum rate (**Figure 3.18**). This phenomena has so far not been observed for artificial self-replicators based on the reaction between nitrones and maleimides. In-depth analysis of the kinetics of previous efficient replicating systems has established that not the duplex dissociation but the cycloaddition reaction is generally the rate-limiting step for the autocatalytic cycle.^[140] Hence, adding more template indeed increases the amount of available free template, but has no influence on the maximum rate of the reaction. In order to identify the reason behind this exceptional behaviour and to extract kinetic parameters, the recorded data was fitted using SimFit.

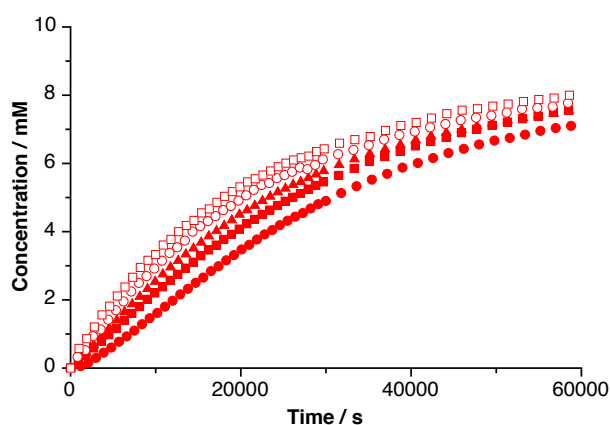


Figure 3.18 Concentration *vs* time profile for the reaction of maleimide **74** with nitrone **70** to give template *trans*-98 in the presence of 0 (●), 9 (■), 18 (▲), 36 (○) and 50 (□) mol-% of *trans*-98. All reactions were performed at 10 °C in CDCl₃ at 10 mM reagent concentration. *Cis*-products were omitted for clarity.

Simultaneous fitting of the native reaction and the five doping experiments established the results presented in **Figure 3.19**. Overlay of the kinetic model with the experimental data for the native reaction demonstrates the quality of the fit. The individual association constant between carboxylic acid and amidopyridine at 10 mM concentration and 10 °C was determined to be 3500 M⁻¹ (see **Table 4.1**). In case of fitting multiple curves, bimolecular rates were optimised in the fitting process which provided values close to the ones obtained from the control experiment. Calculation of the free energy of connection and the effective molarity gave rise to the values depicted in **Table 3.5**. Altogether, the results suggest the presence of a moderately efficient self-replicator for the *trans*-isomer and no recognition-mediated activity for the *cis*-species. Compared with the systems investigated previously, template *trans*-98 has a relatively low free energy of connection. This suggests that the stability of the template duplex is lower leading to a higher concentration of free monomer. This shift in equilibrium might be the reason for its specific doping behaviour.

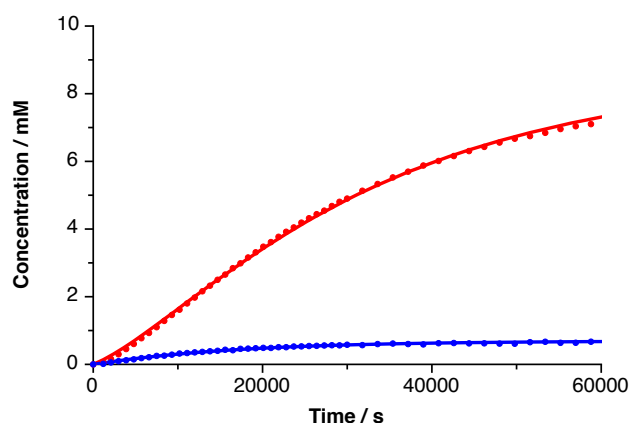


Figure 3.19 Concentration *vs* time profile for the reaction of maleimide **74** and nitrone **70** to give template **98**. The formation of *trans*-product is shown as red filled circles and the formation of *cis*-product as blue filled diamonds. Solid lines represent the results for the fitting of the *trans*-(-) and *cis*-(-) product. The reaction was performed at 10 °C in CDCl₃ at 10 mM reagent concentration.

Table 3.5 Kinetic parameters extracted for the self-replicating reaction of maleimide **74** and nitrone **70** at 10 °C in CDCl₃ at 10 mM reagent concentration using SimFit. The obtained R-value was 2.4%.

	<i>trans</i> -98	<i>cis</i> -98
bimolecular rate constants / M ⁻¹ s ⁻¹	9.72 × 10 ⁻⁴	3.34 × 10 ⁻⁴
recognition-mediated rate constants / s ⁻¹	1.26 × 10 ⁻³	-
effective molarity / M	1.30	-
Δ <i>G</i> ^s / kJ mol ⁻¹	2.67	-

3.4.6 Reaction of maleimide **74** with nitron **71**

The last combination to examine is the reaction between naphthalene maleimide **74** and phenylacetic acid nitron **71** forming cycloadduct **99**. Kinetic data for all four crucial experiments were recorded for 16 h in CDCl₃ at 0 °C and 10 mM concentration of the two reagents (Figure 3.20).

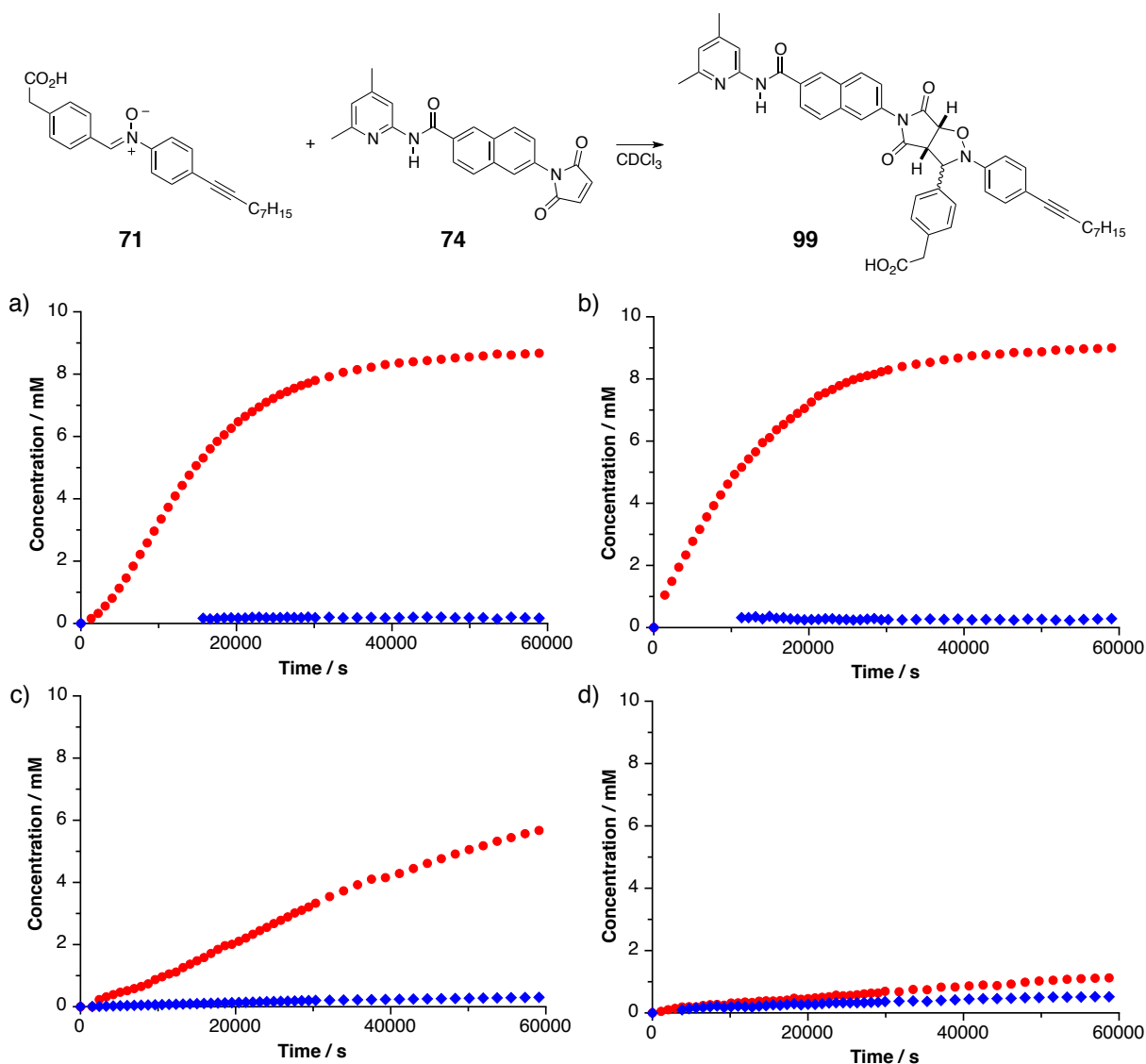


Figure 3.20 Concentration *vs* time profile for the reaction between a) maleimide **74** and nitron **71**, b) maleimide **74** and nitron **71** in the presence of 10 mol-% *trans*-**99**, c) maleimide **74** and nitron **71** in the presence of 40 mM 3-bromobenzoic acid and d) maleimide **74** and control nitron **82**. The formation of *trans*-products is shown as red filled circles and the formation of *cis*-products as blue filled diamonds. All reactions were performed at 0 °C in CDCl₃ at 10 mM reagent concentration.

The native reaction again exhibits the sigmoidal shape typical for a self-replicating system with the *trans*-isomer being formed in a ratio of 43:1 over its isomeric partner and 88% overall conversion (Figure 3.20a). Doping experiments using 10 mol-% of presynthesised *trans*-**99** abolished the initial lag period and pushed the ratio of *trans*- to *cis*-

diastereoisomers to 62:1 with 93% of reagents converted to products (**Figure 3.20b**). Addition of 4 equivalents of 4-bromophenylacetic acid significantly reduced the conversion to 60% and the selectivity dropped to 19:1 with *trans*-**99** still being the most abundant species (**Figure 3.20c**). The reaction of maleimide **74** with control nitrone **82** provided a measure for the efficiency and selectivity for the recognition-disabled process. After 16 h, only 16% of the reagents were converted and the rate for both isomers was found to be a mere 2.2:1 in favour of the *trans*-species (**Figure 3.20d**).

All data presented clearly suggests that the enhanced formation of *trans*-**99** is a result of a highly efficient self-replicating process. The feasibility of the product duplex of *trans*-**99** is highlighted in the calculated structure, in which the flexibility of the phenylacetic acid causes the templates to slightly wrap around each other (**Figure 3.21**). However, the self-complementary of the duplex structure is clearly visible. On the other hand, the *cis*-isomer possesses a folded geometry in which access to the recognition sites is limited. Because of the length mismatch between the phenylacetic acid and the naphthalene spacer, formation of a productive binary complex between nitrone and maleimide to form *cis*-**99** by AB pathway can be ruled out. Recognition between the acid and the amidopyridine moiety would require a drastic deformation of the isoxazolidine core and is therefore disfavoured energetically.

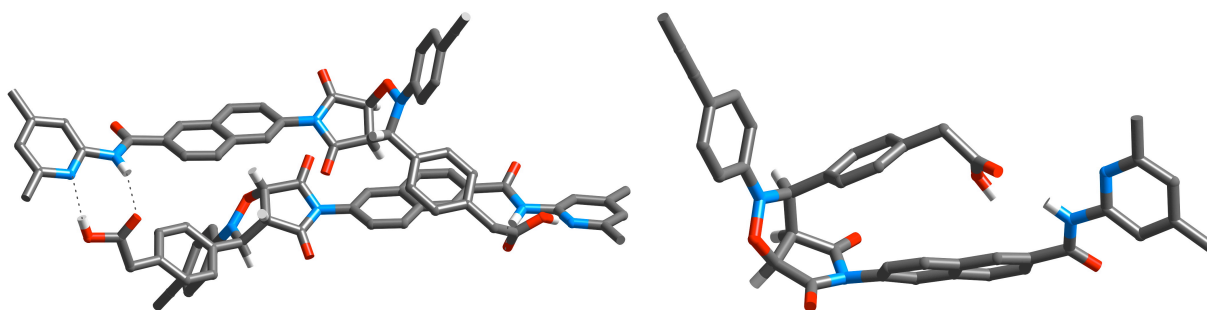


Figure 3.21 Molecular models of the *trans*-**99** duplex (left) and the *cis*-**99** monomer (right). Carbon atoms are shown in dark grey, hydrogen atoms in light grey, nitrogen atoms in blue and oxygen atoms in red. Hydrogen bonds are indicated by dotted lines. Most other hydrogens were omitted for clarity.

Again, the SimFit program was consulted to fit the obtained results and extract valuable kinetic parameters. The results of the investigation are depicted in **Table 3.6** and the quality of the applied kinetic model can be seen in comparison with the experimental data (**Figure 3.22**). Slight deviation of the theoretical curve from the experimental data for high template concentrations can be explained with incipient precipitation of *trans*-**99** from the solution. The association between phenylacetic acid and amidopyridine at 10 mM concentration and 0 °C was determined to be 1800 M⁻¹ (see **Table 4.1**) and used in the

calculation of the free energy of connection as described earlier. Bimolecular rates were obtained from the control experiment with nitrone **82** and used to calculate the effective molarity. Altogether, the results underline the presence of a very efficient self-replicator for the *trans*-isomer and no recognition-mediated activity for the *cis*-species.

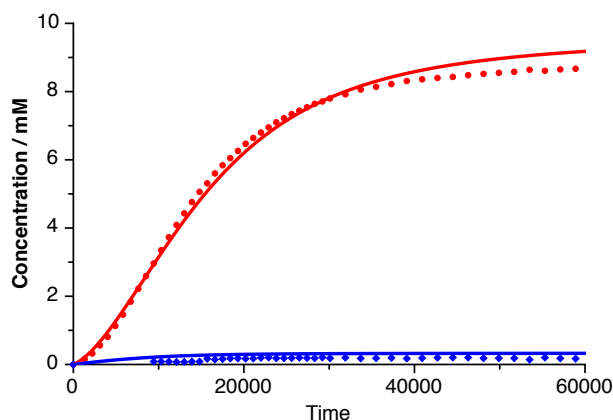


Figure 3.22 Concentration *vs* time profile for the reaction of maleimide **74** and nitrone **71** to give template **99**. The formation of *trans*-product is shown as red filled circles and the formation of *cis*-product as blue filled diamonds. Solid lines represent the results for the fitting of the *trans*-(-) and *cis*-(-) product. The reaction was performed at 0 °C in CDCl₃ at 10 mM reagent concentration.

Table 3.6 Kinetic parameters extracted for the self-replicating reaction of maleimide **74** and nitrone **71** at 0 °C in CDCl₃ at 10 mM reagent concentration using SimFit. The obtained R-value was 5.8%.

	<i>trans</i> -99	<i>cis</i> -99
bimolecular rate constant / M ⁻¹ s ⁻¹	6.99 × 10 ⁻⁴	3.06 × 10 ⁻⁴
recognition-mediated rate constant / s ⁻¹	1.65 × 10 ⁻²	-
effective molarity / M	23.6	-
Δ <i>G</i> ^s / kJ mol ⁻¹	9.43	-

3.5 Comparison of the analysed systems

In the previous sections, thorough analysis of the six possible reactions between nitrone **70** and **71** with each of the three maleimides was conducted. For all combinations, self-replicating activity was found for the *trans*-isomers of each pair of diastereoisomeric products. Additionally, the reaction of nitrone **71** with maleimide **72** gave rise to an AB system for the *cis*-isomer. In order to compare all six systems at the same temperature, the native reactions for the formation of *trans*-**96**, *trans*-**97** and *trans*-**98** were repeated at 0 °C. Concentration *vs* time profiles for the systems using either carboxy nitrone **70** or phenylacetic acid nitrone **71** were created (**Figure 3.23a** and **Figure 3.23c**) and the corresponding rate *vs*

time profiles were deduced (Figure 3.23b and Figure 3.23d) by calculating the first derivative of a polynomial fit to the experimental data.

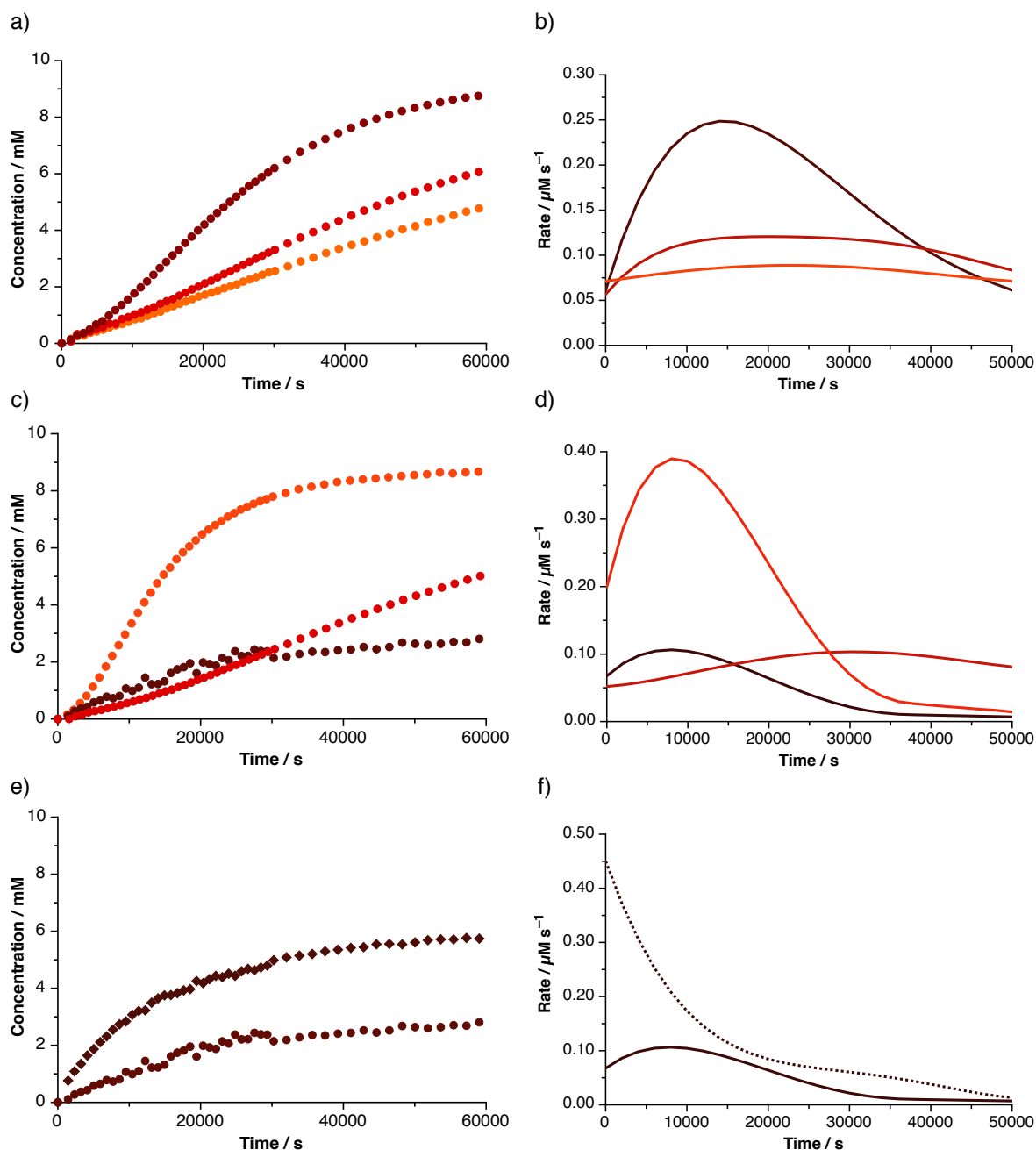


Figure 3.23 a) Arrayed concentration *vs* time profiles for the reaction of maleimide 72, 73 and 74 with carboxylic acid nitrone 70 at 0 °C to give *trans*-94 (●), *trans*-96 (●) and *trans*-98 (●). b) Calculated arrayed rate *vs* time profiles for the reactions described under a) giving *trans*-94 (—), *trans*-96 (—) and *trans*-98 (—). c) Arrayed concentration *vs* time profiles for the reaction of maleimide 72, 73 and 74 with phenylacetic acid nitrone 71 at 0 °C to give *trans*-95 (●), *trans*-97 (●) and *trans*-99 (●). d) Calculated arrayed rate *vs* time profiles for the reactions described under c) giving *trans*-94 (—), *trans*-96 (—) and *trans*-98 (—). e) Concentration *vs* time profile for the reaction of maleimide 72 with phenylacetic acid nitrone 71 at 0 °C to give *trans*-94 (●) and *cis*-94 (◆). f) Calculated arrayed rate *vs* time profiles for the reaction described under c) giving *trans*-94 (—) and *cis*-94 (⋯). All reactions were performed in CDCl₃ and at 10 mM reagent concentration. The formation of all *cis*-isomers except *cis*-94 was omitted for clarity.

In both cases, a distinct hierarchy in reactivity for the formation of the *trans*-products is clearly visible. For the reaction of the maleimides with carboxy nitrene **70**, the efficiency decreases with the spacer length of the maleimide backbone. The reaction of **1** with benzene maleimide **72** leads to the most efficient replicating template *trans*-**94**. Replicators *trans*-**96** and *trans*-**98** possess similar efficiencies with the system based on benzofuran maleimide being slightly stronger than the naphthalene analogue (**Figure 3.23a**). The same conclusion can be drawn from the rate *vs* time profile (**Figure 3.23b**). With $0.25 \mu\text{M s}^{-1}$, the maximum rate for the formation of *trans*-**94** is roughly twice and four times higher than for *trans*-**96** ($0.12 \mu\text{M s}^{-1}$) and *trans*-**98** ($0.08 \mu\text{M s}^{-1}$), respectively. The difference in catalytic efficiency is also reflected in the shape of the curves. As a consequence of the sigmoidal concentration *vs* time profile for *trans*-**94**, the rate profile reveals the classical bell shape characteristic of an efficient autocatalytic process. In the case of *trans*-**96** and *trans*-**98**, the rate *vs* time profiles are broad with a less pronounced maximum indicating autocatalytic processes of minor efficiencies.

A different trend in reactivity is found for the reaction of nitrene **71** with the three available maleimides (**Figure 3.23c** and **3.23d**). It is now the combination of **71** with the naphthalene spacer that provides the strongest system *trans*-**99**. Its dominance can be seen in both plots. The distinct sigmoidal shape of the concentration *vs* time profile translates into the characteristic bell shaped rate *vs* time profile with a maximum rate of $0.39 \mu\text{M s}^{-1}$ after 8000 seconds. This replicator therefore exhibits the highest rate found for all investigated systems. Shortening the spacer to benzofuran maintains the self-replicating nature for the *trans*-isomer of **97** but with significantly reduced efficiency. The rate *vs* time profile is much broader than in the case of *trans*-**99** and the maximum rate of $0.11 \mu\text{M s}^{-1}$ is found after 30000 seconds. Using the even shorter benzene spacer in the maleimide component eventually creates a situation in which the *trans*-isomer possesses the right geometry to function as a self-replicator, but the dominance of AB system *cis*-**95** severely limits its activity.

Separate analysis demonstrates the competition scenario between both diastereoisomers of **95** (**Figure 3.23e** and **3.23f**). A maximum in rate for the formation of *trans*-**95** can be found at the early stage of the reaction ($0.11 \mu\text{M s}^{-1}$ after 8000 seconds) but is superimposed by the formation of *cis*-**95**. Since *cis*-**95** is formed through the AB pathway, the maximum rate of $0.45 \mu\text{M s}^{-1}$ is found at the beginning of the reaction when the concentration of starting material is highest. With this rate profile, *cis*-**95** has a clear advantage over its partner isomer and quickly incorporates a significant amount of available building blocks before *trans*-**95** can unleash its autocatalytic potential. The pronounced bell

shape of the rate *vs* time profile and the early occurrence of the maximum suggest that without its AB partner, *trans*-95 would outperform replicator *trans*-97.

Computational analysis of the systems were performed by fitting appropriate reaction models to the experimentally obtained data. The concentration *vs* time profiles of the individual self-replicating systems provided a clear hierarchy but to further elucidate the origins for the observed trends, the extracted kinetic values for the bimolecular rates, the effective molarities and the free energy of connection need to be dissected.

3.5.1 Comparison of the bimolecular rates

The values of the rate constants for the bimolecular formation of the *trans*-isomers from maleimides **72**, **73** and **74** with control nitrones **81** and **82** at 0 °C are depicted in **Figure 3.24**. Control nitrones **81** and **82** were designed to mimic the electronic environment of carboxy nitrone **70** and phenylacetic acid nitrone **71**, respectively. The results for their bimolecular reaction with the three maleimides show two major trends. Bimolecular rate constants increase with the size of the spacer unit in the maleimide and are in general slightly higher for their reaction with control nitrone **81** than with **82**. The exception to the second observation is the rate constant for the reaction of naphthalene maleimide **74** with **82** which is significantly higher than for the reaction of **74** with **81**.

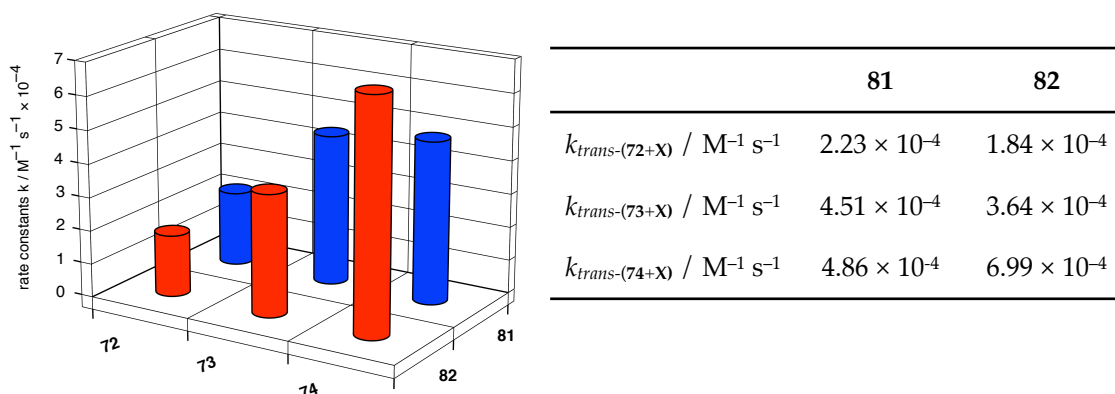


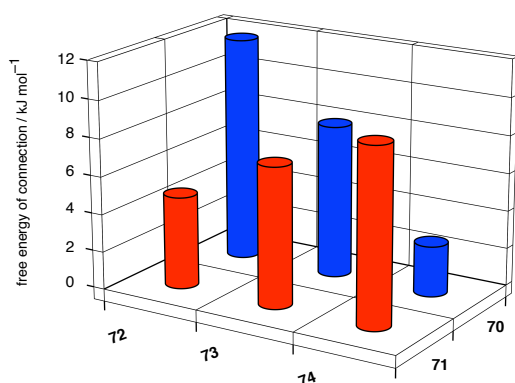
Figure 3.24 Arrayed plot of the bimolecular rate constants k for the formation of the six *trans*-templates between maleimides **72**, **73** and **74** with control nitrones **81** and **82** at 0 °C and 10 mM reagent concentration. Replacing X with either nitrone **81** or **82** identifies the appropriate template.

This finding explains the short lag period observed for the formation of *trans*-99. With the rate constant for the formation of the self-replicating *trans*-template being exceptionally high, the autocatalytic cycle can start to operate much earlier than for low rate constants. On the other hand, the reaction with control nitrone **81** shows that template

trans-94 exhibits a fairly low bimolecular rate suggesting that the source of its autocatalytic efficiency must lay somewhere else. On the basis of the bimolecular control experiments, the lowest rate constant can be found for the formation of *trans-95* with the values for both benzofuran components and *trans-98* midway.

3.5.2 Comparison of the free energies of connection

A comparison of the free energies of connection for all investigated systems is given in **Figure 3.25**. A clear trend for the cooperativity in duplex formation can be seen for the reactions of the maleimides with both nitrones. In the case of nitrone **70**, the strongest stabilisation occurs in the template *trans-94* and decreases with increasing spacer length from benzofuran to naphthalene. A low absolute value indicates lower cooperativity and a less favourable fit for the product duplex. In the case of nitrone **70**, the strongest stabilisation occurs in the template *trans-94* with 11.9 kJ mol⁻¹ and decreases with increasing spacer length to 8.08 kJ mol⁻¹ for benzofuran and only 2.67 kJ mol⁻¹ for *trans-98*.



	70	71
$\Delta G^s_{trans-(72+X)} / \text{kJ mol}^{-1}$	11.9	4.88
$\Delta G^s_{trans-(73+X)} / \text{kJ mol}^{-1}$	8.08	7.43
$\Delta G^s_{trans-(74+X)} / \text{kJ mol}^{-1}$	2.67	9.43

Figure 3.25 Arrayed plot for the free energies of connection ΔG^s for the formation of the *trans*-isomers as extracted from the fitting of the individual experiments between maleimides **72**, **73** and **74** and either nitrone **70** or **71** at 0 °C and 10 mM reagent concentration. Replacing X with nitrone **70** or **71** identifies the appropriate template as **72** + **70** = *trans-94*, **72** + **71** = *trans-95*, **73** + **70** = *trans-96*, **73** + **71** = *trans-97*, **74** + **70** = *trans-98* and **74** + **71** = *trans-99*.

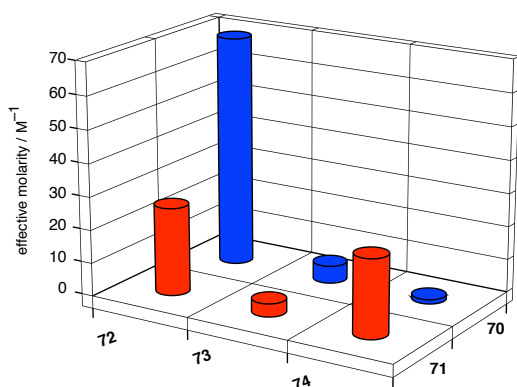
For *trans-98*, this finding may explain the unusual doping behaviour. Adding increasing amounts of preformed *trans-98* to a fresh batch of reagents showed to increase gradually the maximum rate of the reaction. Since the value for the free energy of connection suggests the presence of a relatively weak product duplex, the equilibrium is shifted towards free template molecules which are able to form the catalytically active complex [**70**·**74**·*trans-98*]. Hence, external addition of template molecules at the start of the reaction allows for the formation of a significant amount of such ternary complexes. Increasing the

amount of seeded template further elevates their number and thereby enhances the rate of the reaction.

When looking at the values for nitrone **71**, the opposite trend can be seen. The highest stabilisation is now found for template *trans-99* with 9.43 kJ mol⁻¹ suggesting an optimal fit for the product duplex. The values for *trans-97* (7.43 kJ mol⁻¹) and *trans-95* (4.88 kJ mol⁻¹) indicate that the stability of the template duplex decreases with decreasing size of the spacer unit. This hierarchy is in accordance with the obtained concentration *vs* time profiles and can be directly connected to the different geometries of the templates.

3.5.3 Comparison of the effective molarities

Ultimately, comparison of the effective molarities rounds off the analysis of the six investigated systems (**Figure 3.26**). Again, a clear order can be seen for the reaction of the three maleimides with nitrone **70** depending on the nature of the spacer. By far the highest value was calculated for *trans-94* (69.8 M) compared with *trans-96* (5.26 M) and *trans-98* (1.30 M). This impressive value is a consequence of the low bimolecular rate and the strong duplex association, and reflects the high self-replicating efficiency of *trans-94*. For the templates based on nitrone **71**, the high value of *trans-95* contradicts the expected trend after which template *trans-99* should possess the highest enhancement. One reason for this finding are the differences in bimolecular rate which is exceptionally low for *trans-95*. Accordingly, the value for *trans-97* is lower than the one for *trans-99* which corresponds with the previous observations.



	70	71
EM _{trans-(72+X)} / M	69.8	26.5
EM _{trans-(73+X)} / M	5.26	3.96
EM _{trans-(74+X)} / M	1.30	23.6

Figure 3.26 Arrayed plot for the effective molarities for the formation of the *trans*-isomers between maleimides **72**, **73** and **74** and either nitrone **70** or **71** at 0 °C and 10 mM reagent concentration. Replacing X with nitrone **70** or **71** identifies the appropriate template as **72** + **70** = *trans-94*, **72** + **71** = *trans-95*, **73** + **70** = *trans-96*, **73** + **71** = *trans-97*, **74** + **70** = *trans-98* and **74** + **71** = *trans-99*.

3.6 Summary

In summary, the six investigated systems can be graded according to their efficiencies which are directly connected to their structural properties:

- 1) Templates *trans-94* and *trans-99* are very efficient systems with high EM values and strong duplex associations. The combination of the shorter nitron structure **70** with the short benzene spacer allows for ideal association in the duplex. This matching situation becomes less favourable upon changing one of the components, but when the extended phenylacetic acid nitron **71** is combined with maleimide **74** bearing the naphthalene spacer, the right geometric constellation for the formation of a strong duplex is restored. However, detailed analysis revealed that the functioning of both replicators is slightly different. The source of efficiency for *trans-94* is the pronounced positive cooperativity for the duplex formation which also reflects in the high EM value. Also template *trans-99* exhibits a fairly high duplex association, but it additionally benefits from a very high bimolecular rate constant for the *trans*-isomer, which provides the system with a valuable advantage at the early stage of the reaction by shortening the lag period.
- 2) Both replicators based on the benzofuran maleimide, *trans-96* and *trans-97*, have strikingly similar properties. This corresponds with the fact that they are structurally midway between the two extreme cases of the benzene and naphthalene spacer. It appears that by introducing the benzofuran backbone, the induced geometric change places the molecule midway between the optimal geometry for the reaction with nitron **70** or nitron **71**. As a result, the formation of the *trans*-templates are clearly self-replicating but with reduced efficiency.
- 3) The reaction between short carboxy nitron **70** and extended naphthalene maleimide **74** produces template *trans-98* which is bound to have the strongest mismatch in duplex. Accordingly, the free energy of connection for the duplex is by far the lowest of all six systems and the rate-acceleration is reduced. The interplay of these features and the relatively high bimolecular rate helps to explain the unusual doping behaviour. It appears that in the experiments using increasing amounts of dopant, the template benefits from the low duplex association by creating an increasing amount of catalytic ternary complex [70·74·*trans-98*] which allows to gradually shift the maximum rate of the reaction to higher values.
- 4) The combination of phenylacetic acid nitron **71** with benzene bearing maleimide **72** to give templates **95** favours the formation of an AB system over the replicator. It is now the

combination of the extended length of the nitron with the short benzene spacer which allows for the formation of a catalytic binary complex to form *cis-95* and hinders the performance of the self-replicating *trans-95* template. However, the extracted kinetic values for *trans-95* suggest that duplex is indeed destabilised with respect to most other systems.

4. Fine-tuning the activity by changing the strength of recognition

4.1 Choice of recognition sites

In the previous chapter, a set of structurally similar replicators was investigated and a direct connection was established between the geometry of the template backbone and the efficiency of the autocatalytic cycle. In order to avoid problems regarding the limited solubility of some of the compounds, the original 6-methyl amidopyridine recognition site was replaced with its 4,6-dimethyl analogue. The additional methyl group did indeed increase the solubility of the investigated maleimide starting materials and allowed for a thorough investigation of the replicating systems. Besides having an effect on the solubility of the compounds, the additional methyl group is expected to change the electronic environment on the pyridine ring and to influence the strength of the recognition event with the corresponding acid moiety.

In this chapter, the investigation focuses on the effect that a variation of the association constant has on the performance of self-replicating and AB systems, and whether it is possible to fine-tune their activity by choosing the appropriate substituent pattern on the amidopyridine recognition site. Four substitution motifs were chosen to allow for specific steric and electronic variation of the recognition process (**Figure 4.1**). In addition to the 6-methyl and 4,6-dimethyl moieties discussed previously, an amidopyridine fragment without methyl group ('no-methyl') and one with a methyl substituent in 4-position ('4-methyl') were selected. All four motifs were incorporated into a set of maleimide and nitron compounds and screened in two self-replicating and two AB reactions. The nature of these test reactions, the synthesis of all necessary compounds and the results of the screening experiments are presented in the following sections.

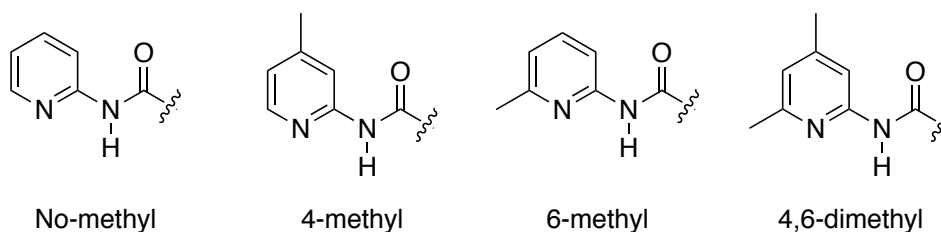


Figure 4.1 Variation of the substituent pattern in the recognition site is expected to alter the reactivity of recognition-mediated processes.

4.2 Choice of test reactions

The test reactions based on the cycloaddition of a nitron with maleimide were chosen according to the following criteria. The reaction between the two components should give rise to an established AB system or self-replicator and reagents should be easily accessible to minimise the synthetic effort when varying the recognition sites. Ideally, systems are chosen that allow such variation on both the maleimide and the nitron. These sets of reagents can then be combined with building blocks bearing complementary reactive and recognition sites to produce a set of kinetic data. In order to allow for the screening of a wide range of association strength, application of more than one kind of acid functionality was envisaged.

4.2.1 Variable substitution pattern on the maleimide building block

The two recognition-mediated processes based on maleimide **72** and nitrones **70** and **71** were chosen as test reactions.

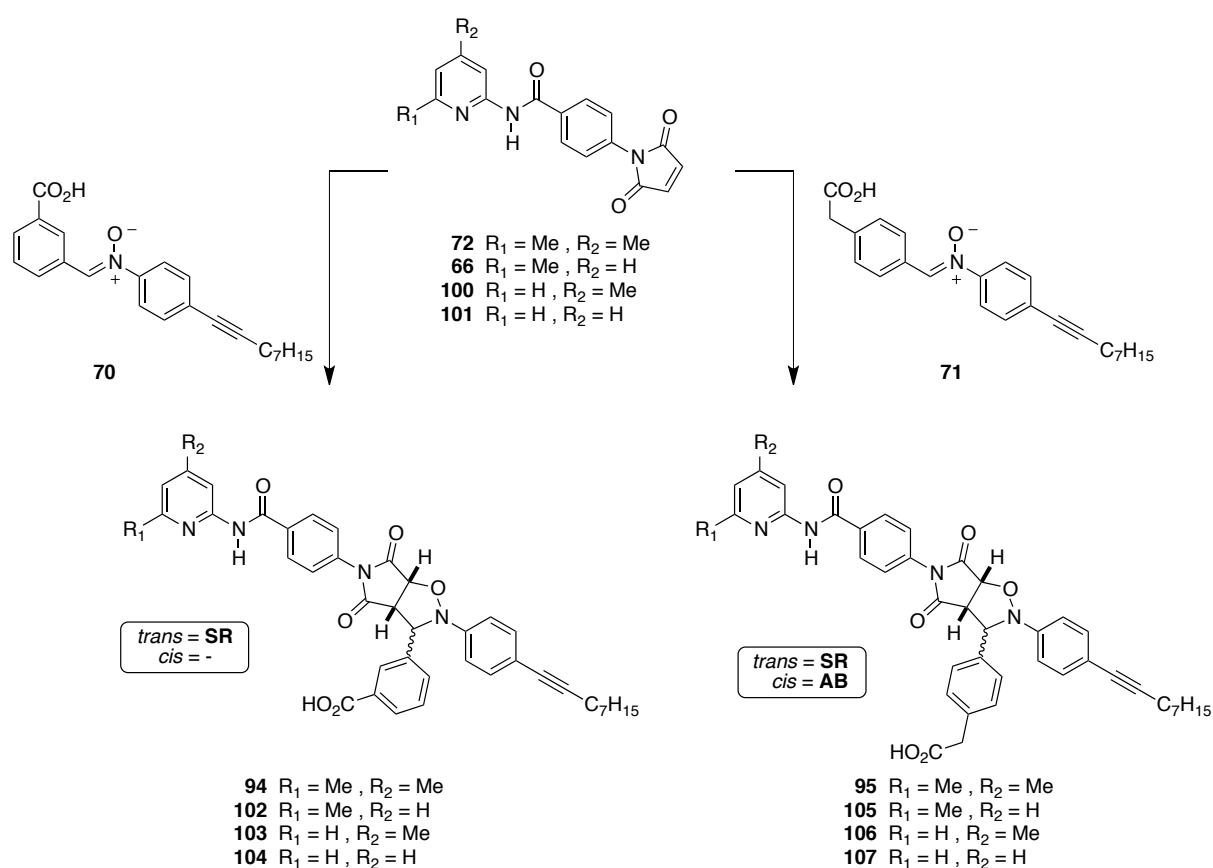
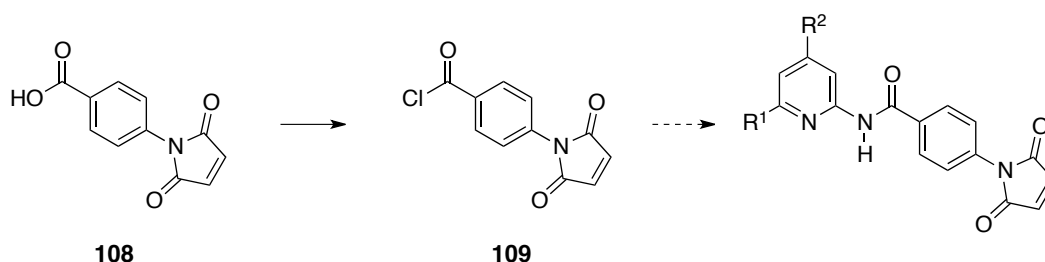


Figure 4.2 Reaction of a set of maleimides with different substituent pattern with nitrones **70** and **71** giving rise to self-replicators **94**, **102**, **103** and **104** and hybrid AB/SR systems **95**, **105**, **106** and **107**, respectively.

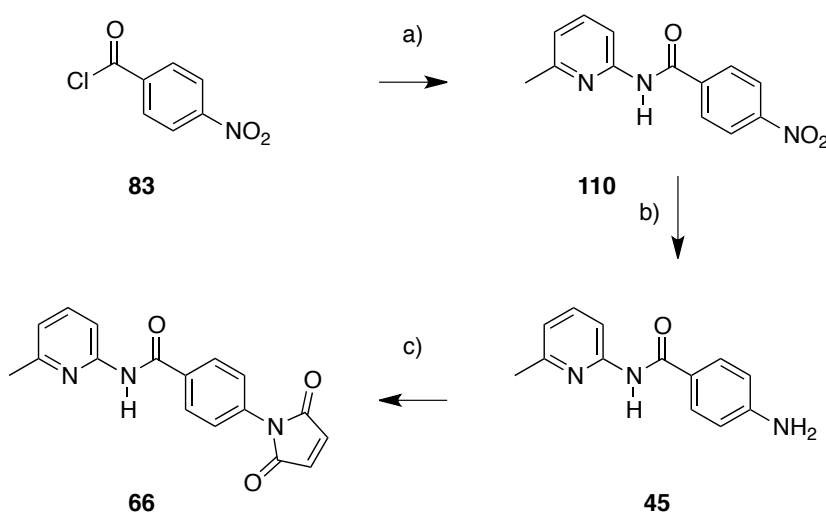
As explained earlier, reaction of maleimide **72** with nitrone **70** gives rise to an efficient self-replicating system *trans*-**94**, whereas using nitrone **71** leads to an AB system for *cis*-**95** with minor self-replicating contribution from the *trans*-diastereoisomer. Variation of the substituent pattern on the recognition site of maleimide **72** generated the set of four maleimide structures which are investigated in this screening (**Figure 4.2**).

Synthesis of 4,6-dimethyl compound **72** was achieved as presented previously. Initial attempts to synthesise the three other maleimide structures through coupling of acid maleimide **109** with the corresponding pyridines failed (**Scheme 4.1**).



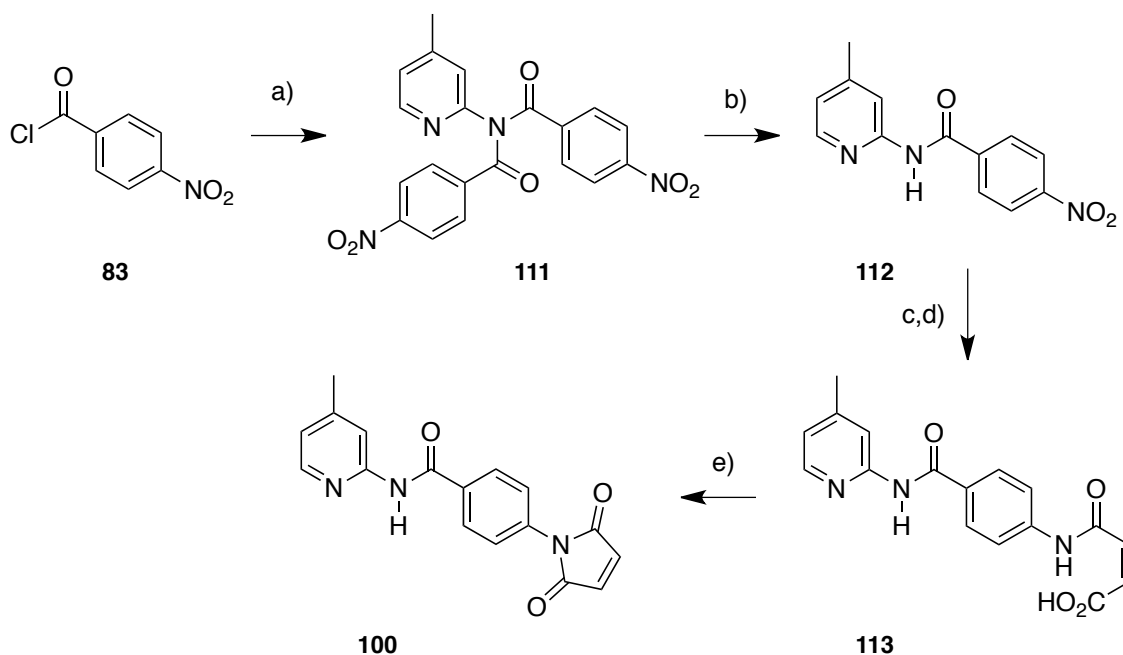
Scheme 4.1 Attempted direct synthesis of the set of maleimides.

However, the three compounds were easily accessible *via* the routes depicted in **Schemes 4.2-4.4**. The second component of the set, maleimide **66**, was synthesised starting from commercially available 4-nitrobenzoyl chloride **83** and 6-methyl-2-aminopyridine to give amide structure **110** in very good yield. Hydrogenation using palladium as catalyst gave rise to the amine derivative **45** which was refluxed with maleic anhydride in acetic acid to furnish the desired maleimide **66** in good yield.

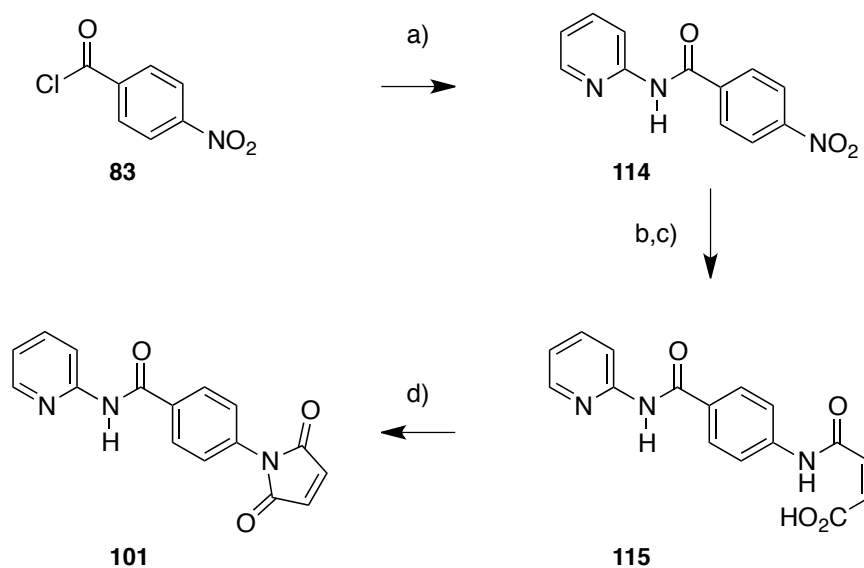


Scheme 4.2 Synthesis of maleimide **66**. Conditions: a) 3 eq. 6-methylpyridin-2-amine, DCM, 0 °C, 97%; b) Pd/C, H₂, THF, rt, 99%; c) maleic anhydride, AcOH, 110 °C, 72%.

For the synthesis of the '4-methyl' species **100**, 4-nitrobenzoyl chloride **83** was reacted with 4-methyl-2-aminopyridine (**Scheme 4.3**). Dibenzamide **111** was cleaved using sodium hydroxide to yield amide **112**. Reduction of the nitro group using palladium on carbon and hydrogen gas gave the amine derivative which was directly converted to **113**. Subsequent cyclisation with ZnBr₂ and HMDS furnished desired maleimide **100**.



Scheme 4.3 Synthesis of maleimide **100**. Conditions: a) 2.5 eq. 4-methylpyridin-2-amine, DCM, 0 °C, 90%; b) NaOH, MeOH/dioxane, rt, 96%; c) Pd/C, H₂, THF, rt; d) maleic anhydride, AcOH, 90% over two steps; e) ZnBr₂, HMDS, MeCN, 90 °C, 81%.



Scheme 4.4 Synthesis of maleimides **101**. Conditions: a) 3 eq. 2-aminopyridine, DCM, 0 °C, 74%; b) Pd/C, H₂, THF, rt; c) maleic anhydride, AcOH, 45% over two steps; d) ZnBr₂, HMDS, MeCN, 90 °C, 83%.

For maleimide **101**, commercially available 4-nitrobenzoyl chloride **83** was reacted with 2-aminopyridine to yield amide structure **114** in good yield (**Scheme 4.4**). Hydrogenation using palladium as catalyst gave rise to the amine derivative which was directly reacted with maleic anhydride. Treatment of **115** with ZnBr₂ and HMDS in MeCN eventually furnished the desired maleimide compound **101**.

It is important to state that the solubility of the four synthesised maleimides in non-polar solvents like chloroform varied significantly with the methyl substitution pattern on the amidopyridine site. Maleimides **101** and **100** showed very limited solubility whereas **66** and **72** proved to be soluble in chloroform at a concentration of 10 mM. The consequences on the performance of the kinetic experiments will be explained later.

4.2.2 Variable substitution pattern on the nitrone building block

In the previous test reactions, variation of recognition site took place on the maleimide building block. In order to screen reactions of reversed reactivity, nitrones **116**, **117**, **118** and **119** were proposed as building blocks for two further test reactions (**Figure 4.3**). Work in the group established that the reaction between a structurally very similar nitrone **55** with maleimide **33** gives rise to a highly efficient self-replicating system *trans*-**59b**,^[140] whereas using *meta*-isomer **120** is known to form a strong AB system.^[197] A long alkyne chain was attached to the original nitrone structure in order to avoid problems with the limited solubility of the nitrone reagents or the resulting templates.

All four nitrone building blocks and both maleimides were easily accessible. The set of nitrones were synthesised in a convergent manner (**Scheme 4.5**). Starting from 4-iodo nitrobenzene **129**, Sonogashira reaction with 1-octyne attached the solubilising group and the nitro group in **130** was subsequently reduced to the hydroxylamine using rhodium on carbon and hydrazine. The aldehyde components **132-135** were formed by activation of acid aldehyde **131** using thionyl chloride and subsequent reaction of the acid chloride with commercially available amino pyridine bearing the correct substituent pattern. Condensation of the hydroxylamine with each of the aldehydes provided the set of four nitrones.

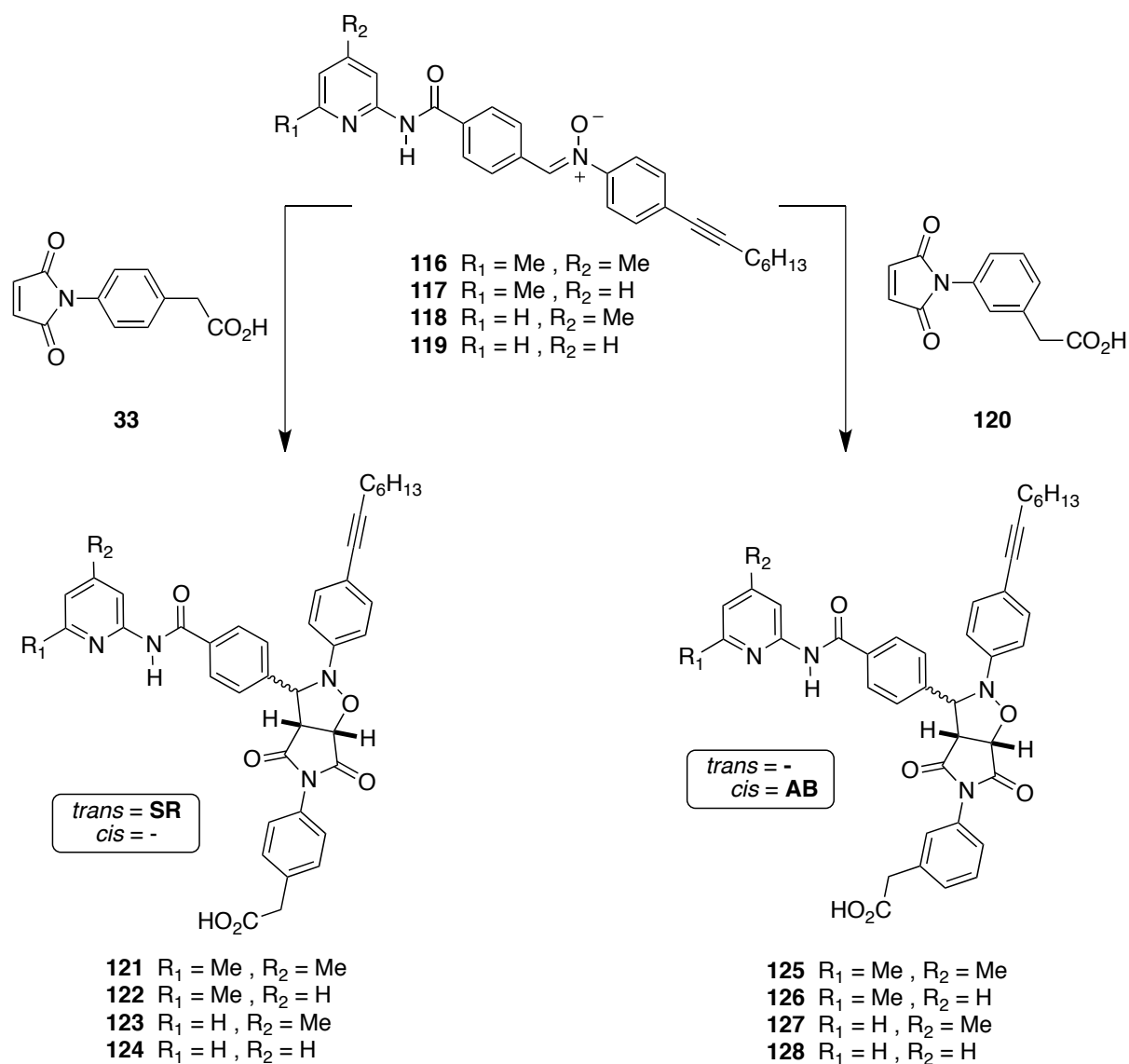
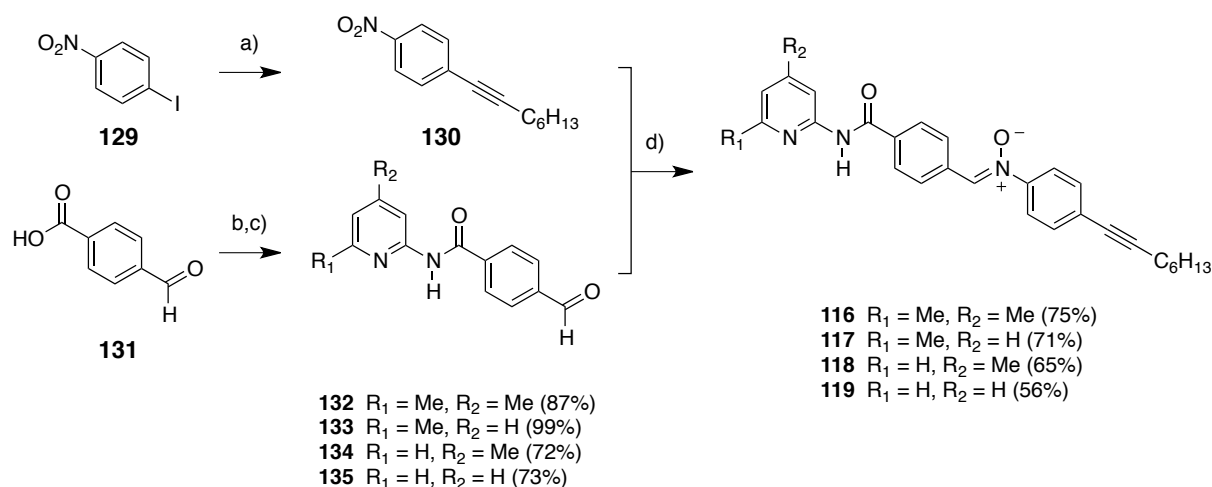
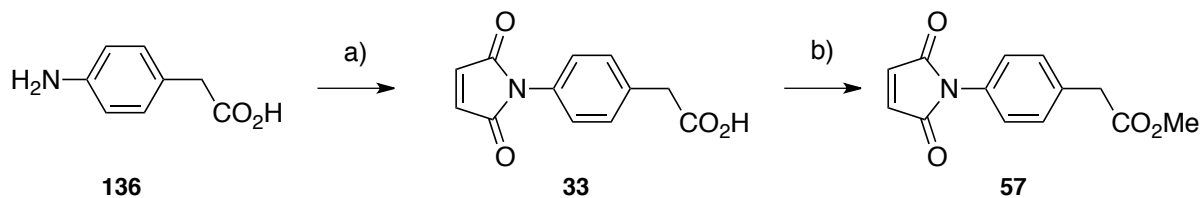


Figure 4.3 Reaction of a set of nitrones **116-119** with different substituent pattern with maleimides **33** and **120** giving rise to self-replicators **120-124** and AB systems **125-128**.

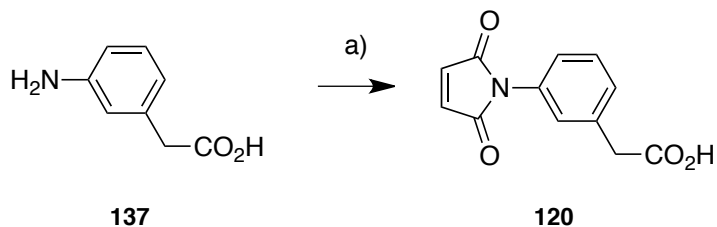


Scheme 4.5 Synthesis of nitrones **116, 117, 118** and **119**. Conditions: a) CuI, PPh₃, PdCl₂(PPh₃)₂, 1-octyne, Et₃N, rt, 83%; b) SOCl₂, toluene, 110 °C, 97%; c) 1.2 eq. aminopyridine, NEt₃, DCM, 0 °C (**132** and **133**) or 1.2 eq. aminopyridine, DMAP, pyridine/DCM, -30 °C (**134** and **135**). d) Rh/C, NH₂NH₂, THF, rt, then **132-135**, EtOH, rt.

Synthesis of maleimides **33** and **120** was achieved by refluxing the corresponding acid aniline in acetic acid together with maleic anhydride (**Scheme 4.6** and **4.7**). A small amount of maleimide **33** was methylated to form recognition-disabled control compound **57**.



Scheme 4.6 Synthesis of maleimides **33** and **57**. Conditions: a) maleic anhydride, AcOH, 110 °C, 70%. b) MeI, Cs₂CO₃, DMF, rt, 56 %.



Scheme 4.7 Synthesis of maleimide **120**. Conditions: a) maleic anhydride, AcOH, 110 °C, 46%.

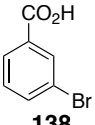
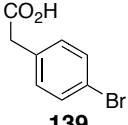
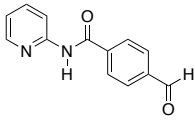
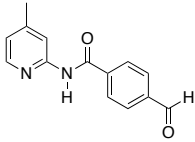
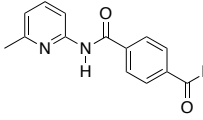
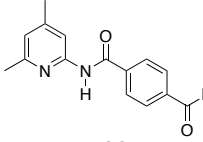
4.3 Determination of association constants

Having established the synthesis of the building blocks, the association constants K_a between the recognition sites were estimated using recognition aldehydes **132-135** and two model acids, 4-bromophenylacetic acid and 3-bromobenzoic acid, which mimic the electronic environment in the applied acid nitrene reagents. The experimental values were determined by the NMR titration method using 499.9 MHz ¹H NMR spectroscopy at 273 and 283 K in CDCl₃. Further details regarding this method can be found in chapter 10 and selected examples are presented in the appendix.

The results of the titration experiments are listed in **Table 4.1** and exhibit some significant trends. As expected for an exothermic process, the association constants measured at 0 °C are in all cases larger than the values for the same interaction at 10 °C. Furthermore, all interactions of the aldehydes with 3-bromobenzoic acid **138** give rise to higher association constants than their interaction with 4-bromophenylacetic **139** acid. This finding is in accordance with the pK_a values found in the literature^[198] for **138** (pK_a = 3.78) and **139** (pK_a = 4.31). For both acid compounds, the effects of the increasing number of methyl groups can be seen. Alkyl groups have a positive inductive effect on the electron density on the aromatic

ring and are therefore expected to increase the association between the two recognition sites. This accounts for the differences in binding strength for both sets of interactions, with the values for **132** being highest, followed by **133** and **134**, and the values for **135** being the lowest. However, the relative impact of increasing the number of methyl groups are different for both acids. For **139**, addition of one methyl group has hardly any effect on the values for the association and it is only the addition of the second methyl group which causes a considerable increase in binding strength. However, in case of **138**, the biggest change is seen for the introduction of the methyl group in 6-position.

Table 4.1 Determination of the association constants between aldehydes **135**, **134**, **133** and **132** at 10 mM concentration and carboxy acid **138** and phenylacetic acid **139** at 273 and 283 K in CDCl₃.

Aldehyde	 138		 139	
	K_a (0 °C / M ⁻¹)	K_a (10 °C / M ⁻¹)	K_a (0 °C / M ⁻¹)	K_a (10 °C / M ⁻¹)
 135	1570	1200	850	620
 134	1810	1520	900	660
 133	3750	2950	1020	680
 132	4030	3470	1770	1620

4.4 Screening the set of maleimides **72**, **66**, **100** and **101**

4.4.1 Reaction of the set of maleimides with nitrone **70**

Each maleimide of the set bearing a different substituent pattern was reacted individually with carboxy nitrone **70** and the progression of the reaction was followed by ¹H NMR spectroscopy. All kinetic measurements performed in this thesis were conducted by mixing identical volumes of the stock solutions of each reagent at 20 mM concentration in CDCl₃ to

obtain a reaction mixture at 10 mM concentration (see section 10.2.1). As mentioned earlier, the solubility of maleimides **101** and **100** did not allow for the generation of stock solutions at such concentrations. In order to overcome this problem, the set-up of the kinetic experiment was altered. A stock solution of nitron **70** at 10 mM concentration in CDCl₃ was prepared and used to dissolve an appropriate amount of neat maleimide to give an equimolar mixture of both reagents. Bringing the maleimides in contact with the nitron bearing complementary recognition site increased their solubility significantly and a clear solution was obtained after sonication for three minutes. The solution was then transferred into an NMR tube and the kinetic measurements were conducted. In order to obtain comparable values for the four maleimide compounds, this procedure was applied to all four reactions. The progression of the reaction was followed by ¹H NMR spectroscopy over 16 h at 0 °C and deconvolution of the obtained spectra gave rise to the arrayed concentration *vs* time profiles depicted in Figure 4.4a.

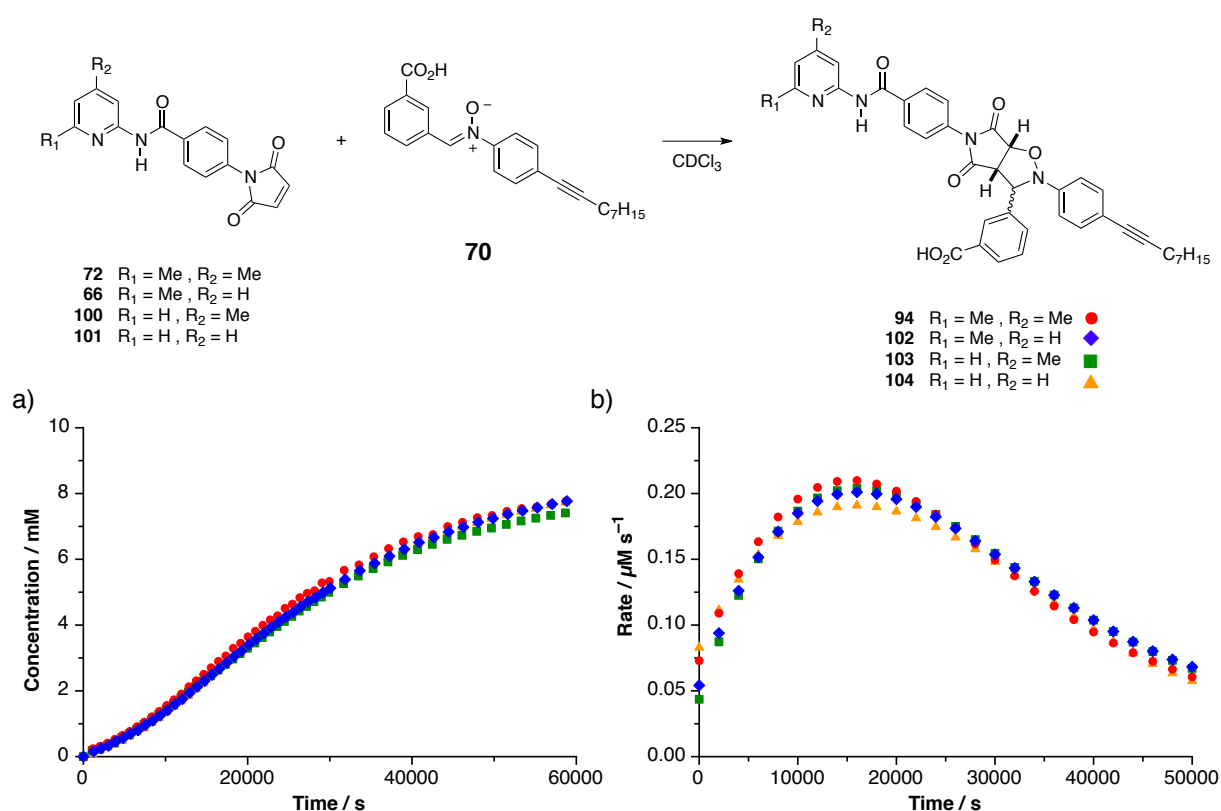


Figure 4.4 a) Arrayed concentration *vs* time profiles for the individual reaction of **72**, **66**, **100** and **101** with nitron **70** at 10 mM reagent concentration in CDCl₃ at 0 °C giving rise to autocatalytic templates *trans*-**94** (●), *trans*-**102** (◆), *trans*-**103** (■) and *trans*-**104** (▲). All *cis*-products were omitted for clarity. b) Rate *vs* time profiles calculated from the profiles in a) with identical colour coding for the reaction products.

As expected, all four reactions proceeded through an autocatalytic pathway for the *trans*-diastereoisomers resulting in the typical sigmoidal shape for the rate profiles. It can also be seen that the differences in activity for the replicators bearing different recognition groups are only marginal. After 16 h, the conversion of starting material was calculated by ¹H NMR spectroscopy to be 80% for **101**, 78% for **100** and 82% for both **66** and **72** with the *trans/cis* ratio to be highest for **104** (24:1) followed by **103** and **94** (both 21:1) and lowest for **102** (19:1).

The effect of altering the set-up of the experiments can be seen for the reaction between **72** and nitrone **70**. Compared to the results presented in chapter 3, a drop in conversion is accompanied by a decrease of the *trans/cis* ratio from a previous 35:1 to 21:1. This finding can be explained with the fact that the concentration of maleimide is less than 10 mM at the start of the reaction reducing the impact of recognition-mediated processes on the expense of the bimolecular reaction which resulted in an increased formation of the *cis*-diastereoisomer.

Fitting a polynomial to the data obtained for the concentration *vs* time profiles and taking the first derivative thereof constructed the corresponding rate *vs* time profiles for the four reactions (**Figure 4.4b**). Again, only a minimal difference can be seen for the set of replicators. The maxima for all four systems can be found after about 15000 seconds and the absolute values vary between 0.191 $\mu\text{M s}^{-1}$ for the system based on **101** and 0.210 $\mu\text{M s}^{-1}$ for **72** with the ones for **100** and **66** calculated as 0.204 and 0.196 $\mu\text{M s}^{-1}$, respectively.

Altogether, it can be stated that the experimental data does not reflect any major trends for the reactivity of the four components. The subtle differences in reactivity seen for the set of replicators are well within the error range of the experiments conducted and it is appropriate to conclude that the variation of the association constant in the range of 1570 - 4030 M^{-1} has no measurable impact on the performance of this type of replicator. In order to establish the source of this indifference, we turned to computational fitting of the experimental results.

4.4.2 Fitting and analysis

The SimFit package was used to fit the experimental data to the kinetic model used in chapter 3 for self-replicating systems. The reaction between control nitrone **81** and maleimide **72** was used to extract a common bimolecular rate constant of $2.23 \times 10^{-4} \text{ M}^{-1} \text{ s}^{-1}$ and the appropriate association constants were taken from **Table 4.1**. Fitting of the four individual reactions proceeded with modest R values and provided values for the recognition-mediated

rate constant and the stability of the duplex which allowed for the calculation of the effective molarity and the free energy of connection (**Table 4.2**). When comparing the kinetic parameters for the individual reactions, no apparent correlation can be seen between the association constants and the efficiency of the replicator. All values for the effective molarities were calculated to be in the range of 12.5 to 25.7 M⁻¹ with **103** showing the highest acceleration followed by **104**, **94** and **102**. Also the duplex stabilities seem to form an arbitrary order with **103** (10.9 kJ mol⁻¹) > **102** (10.5 kJ mol⁻¹) > **94** (10.0 kJ mol⁻¹) > **104** (9.8 kJ mol⁻¹).

Table 4.2 Kinetic parameters extracted for the self-replicating reactions of maleimides **72**, **66**, **100** and **101** with nitrone **70** at 0 °C in CDCl₃ at 10 mM reagent concentration as depicted in **Figure 4.4** using SimFit.

	<i>trans</i> - 94	<i>trans</i> - 102	<i>trans</i> - 103	<i>trans</i> - 104
bimolecular rate constant ‡ / M ⁻¹ s ⁻¹	2.23 × 10 ⁻⁴	2.23 × 10 ⁻⁴	2.23 × 10 ⁻⁴	2.23 × 10 ⁻⁴
recognition-mediated rate constant / s ⁻¹	4.14 × 10 ⁻³	2.79 × 10 ⁻³	5.74 × 10 ⁻³	4.97 × 10 ⁻³
effective molarity / M	18.6 69.8 (<i>cf.</i> 3.4.1)	12.5	25.7	22.3
Δ <i>G</i> ^s / kJ mol ⁻¹	10.0 11.9 (<i>cf.</i> 3.4.1)	10.5	10.9	9.8
R-value / %	6.11	4.04	6.12	3.59

‡ bimolecular rates estimated from the reaction of **72** with **81**

4.4.3 Reaction of the set of maleimides with nitrone **71**

Next, the reactions between the same set of maleimides with phenylacetic acid nitrone **71** were performed following the mixing procedure outlined in section **4.4.1**. Initial experiments were conducted at a reagent concentration of 10 mM in CDCl₃ and 0 °C (**Figure 4.5a**). However, broadening of the signals in the ¹H NMR spectra significantly worsened the quality of the deconvolution at that temperature. Therefore, all four experiments were repeated at 10 °C to produce the array of concentration *vs* time profiles depicted in **Figure 4.5b**.

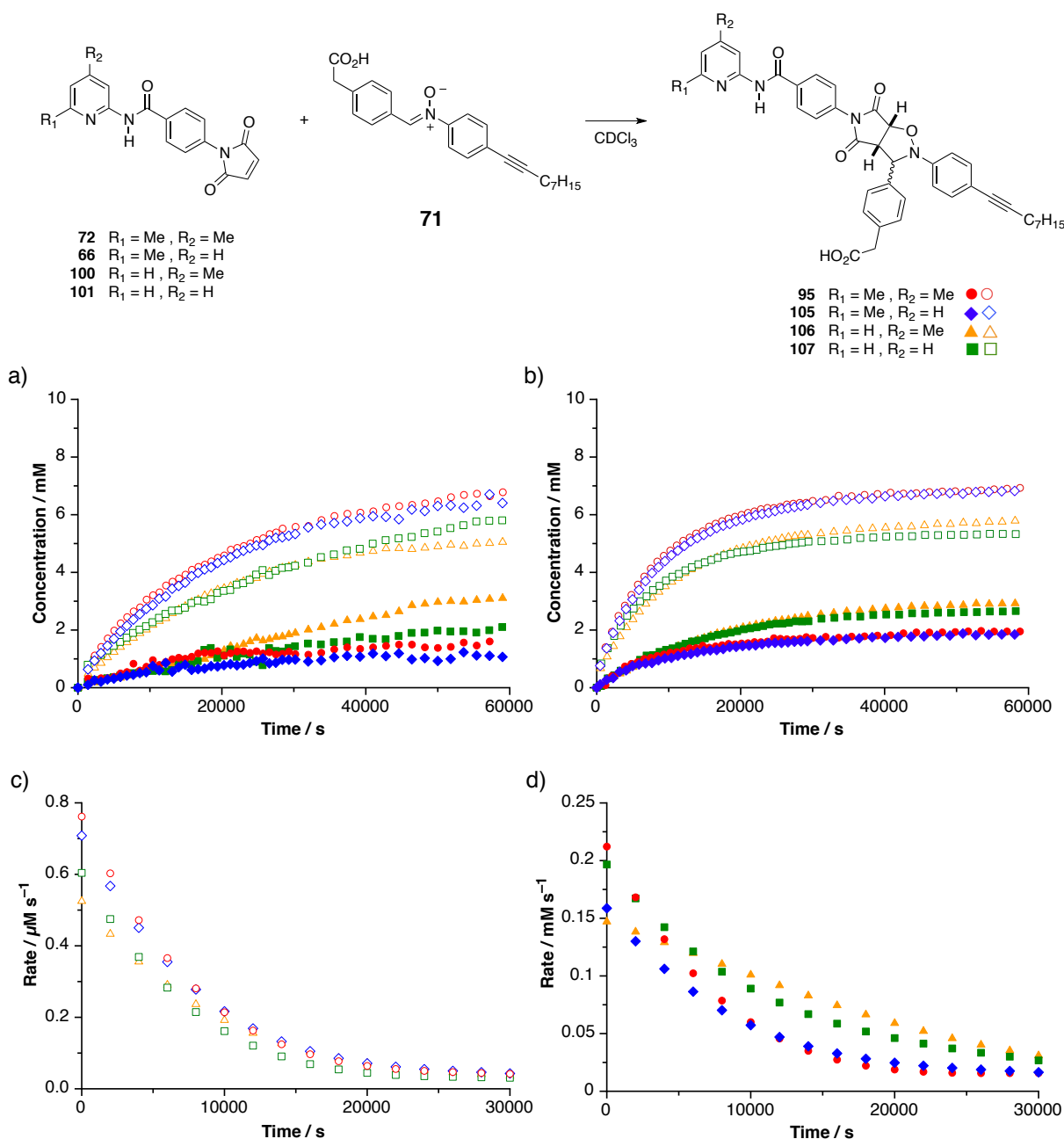


Figure 4.5 Arrayed concentration *vs* time profiles for the individual reaction of **72**, **66**, **100** or **101** with nitrone **71** at 10 mM reagent concentration in CDCl_3 at a) 0 °C and b) 10 °C giving rise to AB systems *cis*-**95** (\circ), *cis*-**105** (\diamond), *cis*-**106** (\square) and *cis*-**107** (\triangle) as well as autocatalytic templates *trans*-**95** (\bullet), *trans*-**105** (\blacklozenge), *trans*-**106** (\blacksquare) and *trans*-**107** (\blacktriangle). Rate *vs* time profiles calculated from the profiles presented in b) for c) the *cis*-isomers of the AB systems and d) the autocatalytic *trans*-isomers with identical colour coding for all reaction products.

Compared to the corresponding reaction between maleimide **72** and nitrone **71** at 0°C as analysed in chapter 3, a very similar progression for the formation of both *trans*- and *cis*-diastereoisomers can be seen. We established that the formation of the *cis*-product proceeded *via* an AB complex whereas the *trans*-product was formed in an autocatalytic manner. The same reactivity is also found for the set of maleimides bearing variable substituent pattern. In all four cases, the *cis*-isomer is the main product and its formation shows the rate profile

typical for an AB system. On the other hand, the rate profiles for the four *trans*-products do not show the usual sigmoidal shape since they are competing against dominant AB systems. Their autocatalytic nature was however established by doping experiments and addition of a competitive inhibitor (see section 3.4.2). The conversion of starting material after 16 h was calculated by ¹H NMR spectroscopy and was found to be highest for **72** (89%) followed by **66** and **101** (both 87%) and **100** (81%). Interestingly, a clear splitting of the rate profiles into two groups can be seen which is reflected by the *cis/trans* ratio of the four diastereoisomeric products. Templates **105** and **95** show a high tendency for the formation of the *cis*-isomer resulting in a ratio of 3.7:1 and 3.6:1, respectively, whereas templates **106** and **107** produced slightly more *trans*-isomers yielding a ratio of 2.0:1 for both.

Additionally, the first derivatives of the concentration *vs* time profiles were determined in order to obtain the corresponding rate *vs* time profiles. The results of the calculations are presented separately for the *cis*-isomers (**Figure 4.5c**) and the *trans*-isomers (**Figure 4.5d**). The order of the initial rates for the formation of the *cis*-isomers was found to be **95** (0.761 μM s⁻¹) > **105** (0.708 μM s⁻¹) > **106** (0.604 μM s⁻¹) > **107** (0.525 μM s⁻¹) which corresponds well with the values for the single point association of the recognition event. No such clear trend was seen for the autocatalytic *trans*-templates with **95** having the highest initial rate of 0.212 μM s⁻¹ followed by **106** (0.197 μM s⁻¹), **105** (0.158 μM s⁻¹) and **107** (0.147 μM s⁻¹).

Overall, it can be stated that despite the complexity caused by the presence of two different recognition-mediated processes, the experimental data suggests a direct relationship between the strength in recognition and the initial rate of formation for the *cis*-products *via* the AB pathway. However, the small differences in initial rate seen for the set of replicators does not provide the basis for drawing similar conclusions. Most importantly, the experimental data provided no explanation for the splitting of the rate profiles into two groups and we therefore once more turned to computational analysis.

4.4.4 Fitting and analysis

The SimFit package was used to fit the experimental data to the kinetic model used in section 3.4.2 for the hybrid system with concomitant formation of an AB system and a self-replicator. The reaction between control nitrone **82** and maleimide **72** was used to extract a bimolecular rate constant of $3.68 \times 10^{-4} \text{ M}^{-1} \text{ s}^{-1}$ for the *trans*-isomer and $2.06 \times 10^{-4} \text{ M}^{-1} \text{ s}^{-1}$ for the *cis*-isomer. The appropriate association constants were taken from **Table 4.1**. In case of the self-replicators, the recognition-mediated rate constants and the stability of the duplexes were

determined which allowed for the calculation of the effective molarities and the free energies of connection (**Table 4.3**). Fitting of the data proceeded smoothly for **95**, **105** and **107** with R values around 2%, whereas the reaction of **106** gave a significantly higher error of 7.87%. As seen for the self-replicating systems, it is not possible to correlate the calculated results with the change in association constant. Also the splitting of the rate profiles is not reflected in the data since the differences for both the effective molarities and the duplex stabilisation are similar for all four reactions. Values for both the effective molarities and the free energy of connection are highest for **105** followed by **95**, **106** and **107**. For the set of AB systems giving rise to the *cis*-species, the fitting procedure provided values for the rate-enhancement which allowed for the calculation of the effective molarities (**Table 4.4**). Other than in the case of the *trans*-isomers, a grouping of the results can be seen. **95** and **105** show significantly higher values, 0.733 and 0.694 M, than **106** and **107** with 0.452 and 0.472 M.

Table 4.3 Kinetic parameters extracted for the self-replicating reactions of maleimides **95**, **105**, **106** and **107** with nitrene **71** at 10 °C in CDCl₃ at 10 mM concentration as depicted in **Figure 4.5** using SimFit.

	<i>trans</i> - 95	<i>trans</i> - 105	<i>trans</i> - 106	<i>trans</i> - 107
bimolecular rate constant † / M ⁻¹ s ⁻¹	3.68 × 10 ⁻⁴	3.68 × 10 ⁻⁴	3.68 × 10 ⁻⁴	3.68 × 10 ⁻⁴
recognition-mediated rate constant / s ⁻¹	7.04 × 10 ⁻³	8.24 × 10 ⁻³	6.17 × 10 ⁻³	5.18 × 10 ⁻³
effective molarity / M	19.1	22.4	16.8	14.1
Δ <i>G</i> ^s / kJ mol ⁻¹	5.20	6.37	4.69	4.15
R-value / %	2.64	2.86	7.87	2.08

† bimolecular rates estimated from the reaction of **72** with **82**

Table 4.4 Kinetic parameters extracted for the AB products between maleimides **72**, **66**, **100** and **101** with nitrene **71** at 10 °C in CDCl₃ at 10 mM concentration as depicted in **Figure 4.5** using SimFit.

	<i>cis</i> - 95	<i>cis</i> - 105	<i>cis</i> - 106	<i>cis</i> - 107
bimolecular rate constant † / M ⁻¹ s ⁻¹	2.06 × 10 ⁻⁴	2.06 × 10 ⁻⁴	2.06 × 10 ⁻⁴	2.06 × 10 ⁻⁴
recognition-mediated rate constant / s ⁻¹	15.1 × 10 ⁻⁵	14.3 × 10 ⁻⁵	9.32 × 10 ⁻⁵	9.74 × 10 ⁻⁵
effective molarity / M	0.733	0.694	0.452	0.472

† bimolecular rates estimated from the reaction of **71** with **82**

4.5 Screening the set of nitrones 116, 117, 118 and 119

4.5.1 Reaction of the set of nitrones with maleimide 33

Having obtained data for two sets of experiments in which the recognition site was altered on the maleimide reagent, we set out to further probe the effect of the same variation on the nitron building block. The set of four nitrones **116**, **117**, **118** and **119** was reacted with maleimide **33** to give rise to four diastereoisomeric products **121**, **122**, **123** and **124**, respectively. Work published by our group established that the reaction between a derivative of nitron **117** bearing a methyl group instead of the solubilising octyne group formed a highly efficient self-replicating system with **33**.^[140]

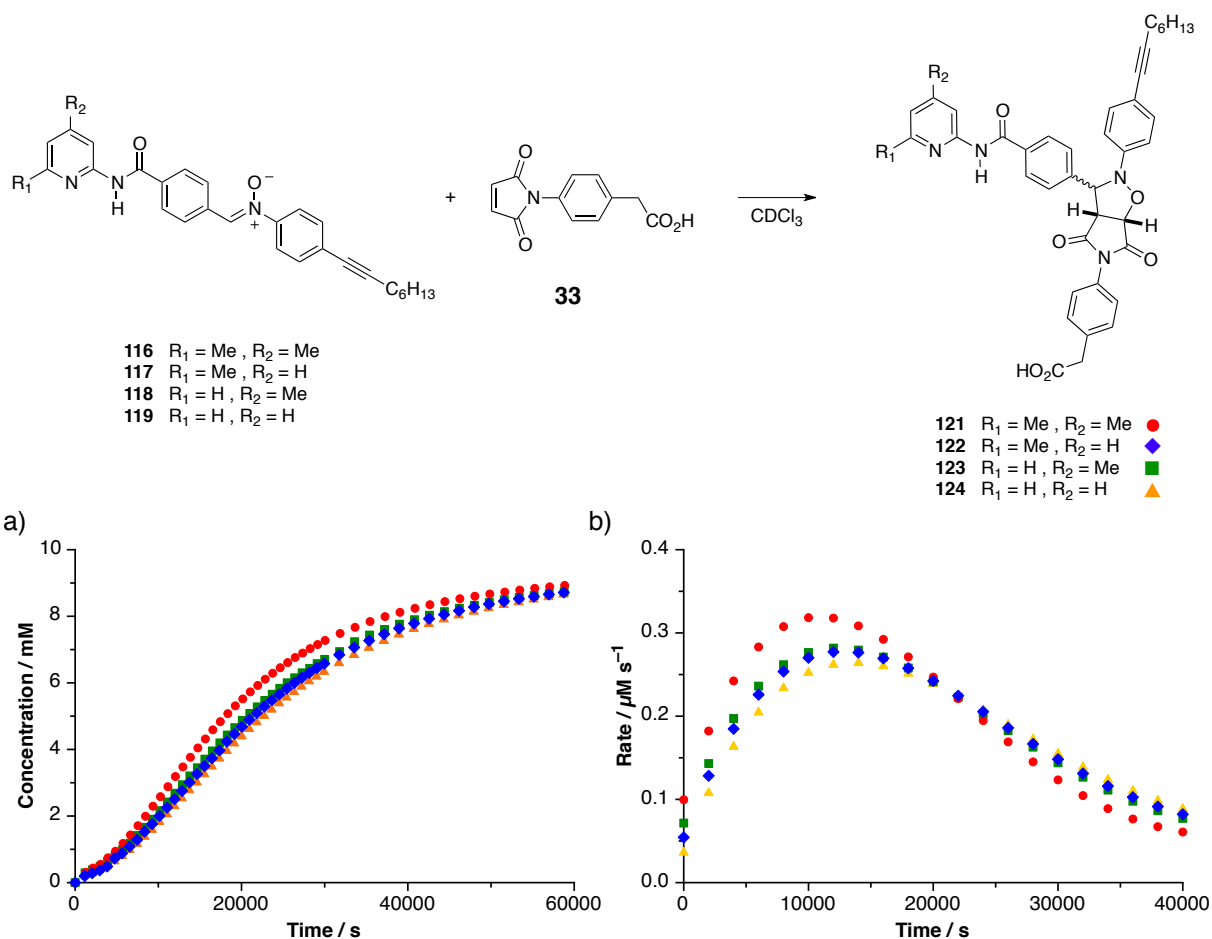


Figure 4.6 a) Arrayed concentration vs time profiles for the individual reaction of **116**, **117**, **118** or **119** with phenylacetic acid **33** at 10 mM reagent concentration in CDCl_3 at 0 °C giving rise to autocatalytic templates *trans*-**121** (●), *trans*-**122** (◆), *trans*-**123** (■) and *trans*-**124** (▲), respectively. All *cis*-products were omitted for clarity. b) Rate vs time profile calculated from the profiles in a) with identical colour coding for all reaction products.

In order to establish the efficiency of the four test reactions, the reagents were mixed at a concentration of 10 mM in CDCl₃ and the solution was incubated at 0 °C. The progression of the reaction was followed by ¹H NMR spectroscopy over 16 h and deconvolution of the obtained spectra gave rise to the arrayed concentration *vs* time profiles depicted in **Figure 4.6a**. As expected, all four reactions proceeded *via* an autocatalytic pathway with the *trans*-diastereoisomers showing the typical sigmoidal shape. It can be seen that the activity for *trans*-**116** is slightly higher than for the other three autocatalytic templates. After 16 h, the conversion of starting material was calculated by ¹H NMR spectroscopy to be 90% for **121** and 88% for the other three templates **122**, **123** and **124** with the *trans/cis* ratio highest for **121** (220:1) followed by **122** (100:1) and **123** (94:1) and lowest for **124** (62:1).

Fitting a polynomial to the obtained concentration *vs* time profiles and taking the first derivative thereof constructed the corresponding rate *vs* time profiles (**Figure 4.6b**). Compared to the analysis of the self-replicating systems based on **72** and **70**, a clear difference can now be seen for the point in time and the magnitude of the maximum rates for the four individual reactions. The maximum rate of 0.318 μM s⁻¹ for *trans*-**121** was found after around 10000 seconds whereas the maximum rates for *trans*-**122** (0.277 μM s⁻¹), *trans*-**123** (0.282 μM s⁻¹) and *trans*-**124** (0.262 μM s⁻¹) occurred after 12000 seconds.

In general, the observed trends are in agreement with the change in association constants as depicted in **Table 4.1**. The interaction between 4-bromophenylacetic acid and the set of four amidopyridine recognition sites showed the highest value for the 4,6-dimethyl substitution (1770 M⁻¹) with the other three substituent pattern giving significantly lower values in the range of 850 - 1020 M⁻¹. The exceptional position of the 4,6-dimethyl substituent is reflected in the concentration *vs* time profile as well as the derived data. The reaction of **116** and **33** had the highest conversion of starting material and resulted in the highest selectivity for the *trans*-product. The maximum rate occurred earlier than for the other three templates and the value was highest. This correlation between *K_a* value and the autocatalytic activity suggests that strengthening the recognition event has a positive impact on the performance of the replicator. However, the relative differences in association constant for the other three templates seem to be too little to have a pronounced effect on their replicating efficiency. In order to further investigate the obtained trends, we again turned to computational fitting of the experimental results.

4.5.2 Fitting and analysis

Fitting of the obtained data was conducted with SimFit using the kinetic model shown in the appendix. The bimolecular rate constant was obtained from the control reaction of **116** with methyl ester **57** as $1.12 \times 10^{-4} \text{ M}^{-1} \text{ s}^{-1}$ for all four reactions and the association constants were taken from **Table 4.1**. In the fitting procedure, the rate constant for the recognition-mediated reaction and the duplex stabilisation were determined and used to calculate the effective molarities and the free energies of connection (**Table 4.5**). Fitting proceeded smoothly with low R-values.

Again, no obvious trends that can be assigned to the increase in association constants can be seen in the data. The order for the effective molarities was found to be **121** > **123** > **122** > **124** with the values for the free energy of connection decreasing in the same order. Interestingly, a splitting for the recognition sites with and without 4-methyl substituent can be seen. The values for the formation of **121** and **123** are similar and significantly higher than the parameters for the formation of **122** and **124**. However, this splitting is not directly visible in the obtained rate profiles suggesting that the increase in effective molarity is neutralised by the increase in free energy of connection.

Table 4.5 Kinetic parameters extracted for the self-replicating reactions of maleimides **116**, **117**, **118** and **119** with phenylacetic acid **33** at 0 °C in CDCl₃ at 10 mM reagent concentration as depicted in **Figure 4.6** using SimFit.

	<i>trans</i> - 121	<i>trans</i> - 122	<i>trans</i> - 123	<i>trans</i> - 124
bimolecular rate constant † / $\text{M}^{-1} \text{s}^{-1}$	1.12×10^{-4}	1.12×10^{-4}	1.12×10^{-4}	1.12×10^{-4}
recognition-mediated rate constant / s^{-1}	7.33×10^{-3}	4.64×10^{-3}	7.21×10^{-3}	3.98×10^{-3}
effective molarity / M	27.5	17.4	27.1	15.0
ΔG^{\ddagger} / kJ mol^{-1}	7.0	5.1	6.6	4.7
R-value / %	3.86	2.46	2.51	1.97

† bimolecular rates estimated from the reaction of **116** with **57**

This irregularity in the performance becomes even more evident when the results for the kinetic parameters for the effective molarity and the free energy of connection for the two self-replicating sets are combined in one graph (**Figure 4.7**). The appropriate values were taken from **Table 4.2** and **Table 4.5**, respectively. In both cases, the distribution of the values

seems arbitrary without any direct connection to the association constants obtained experimentally. In order to gain a clearer insight into the dependence of the performance of a self-replicator on variables such as the effective molarity, the free energy of connection and the association constant, a set of simulations was performed.

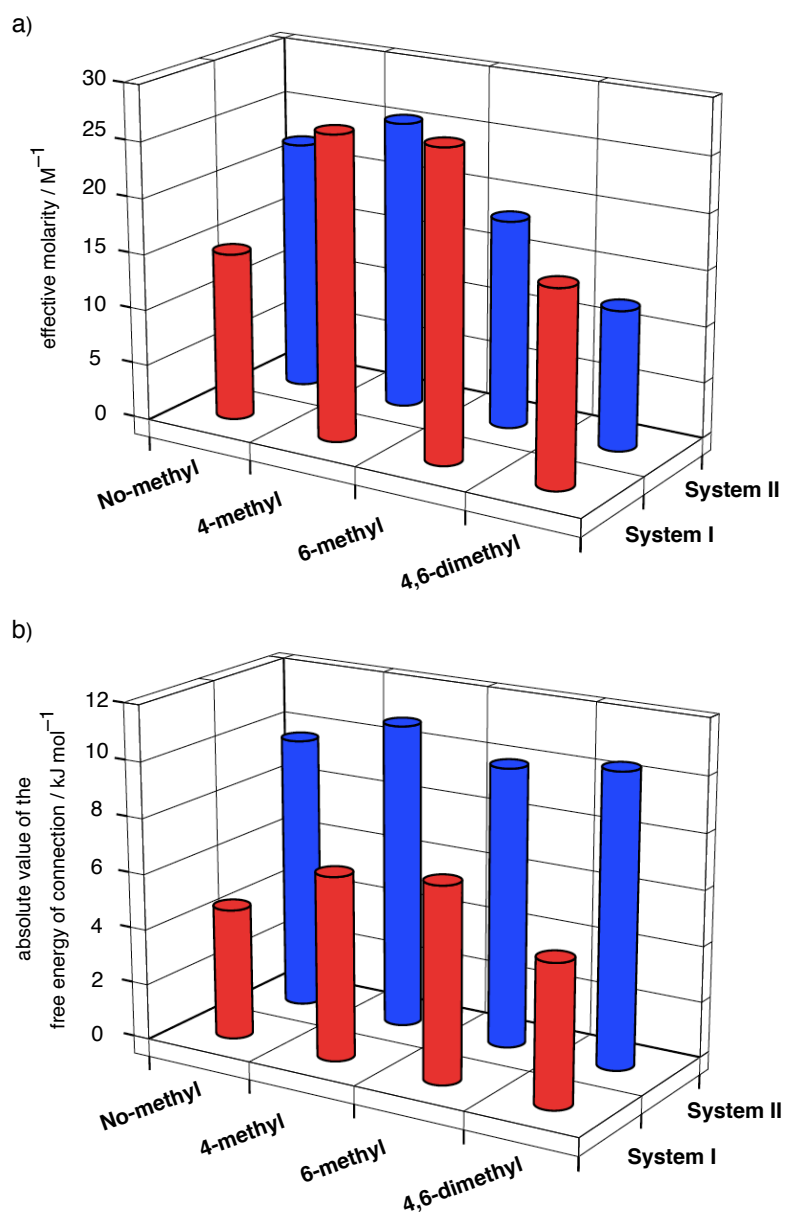


Figure 4.7 Arrayed graph of the calculated values for a) the effective molarity and b) the absolute value of the free energy of connection for the reaction of the set of maleimides with carboxy nitrene **70** (System I, **Figure 4.2**) and the set of nitrenes **116-119** with maleimide **33** (System II, **Figure 4.3**) taken from **Table 4.2** and **Table 4.5**, respectively. The substituent pattern of the reactant is indicated by the y-axis.

4.5.3 General calculations for a self-replicating system

The kinetic model used for the fitting of the experimental data was converted into a simulation script which allowed for the variation of the key kinetic parameters using the ISOSIM mode of the SimFit package. In order to mimic the two regimes of the kinetic parameters obtained by fitting of the experimental data, an effective molarity of 15 M was combined with a free energy of connection of 3.7 kJ mol⁻¹ (**Figure 4.8a**) and an effective molarity of 30 M was used in combination with a free energy of connection of 6.8 kJ mol⁻¹ (**Figure 4.8b**). For both scenarios, values of 500 and 2000 M⁻¹ were chosen for the association constants to allow for a realistic representation of the experimental data. All simulations were performed for 10 mM starting material concentration.

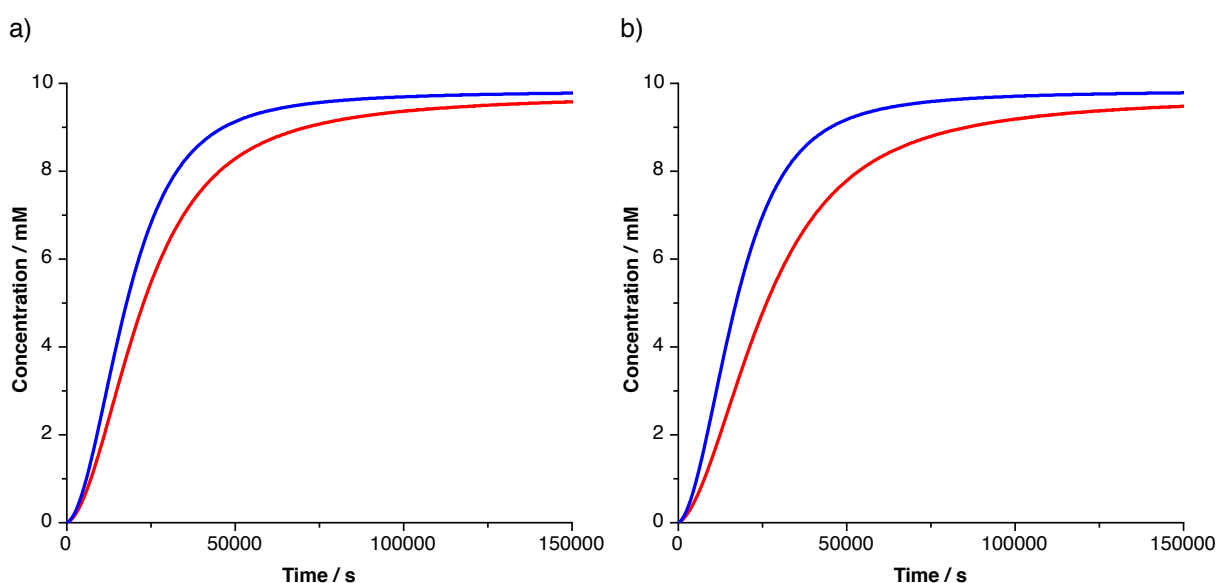


Figure 4.8 Simulated rate profiles on the basis of self-replicating systems **121**, **122**, **123** and **124** at 10 mM starting material concentration. a) The kinetic parameter were set to simulate the situation for the self-replicating formation of **122** and **124** with EM = 15 M and $\Delta G^{\circ} = 3.7$ kJ mol⁻¹ with association constants of 500 M⁻¹ (—) and 2000 M⁻¹ (—). b) The kinetic parameter were set to simulate the situation for the self-replicating formation of **121** and **123** with EM = 30 M and $\Delta G^{\circ} = 6.8$ kJ mol⁻¹ with association constants of 500 M⁻¹ (—) and 2000 M⁻¹ (—).

All four curves exhibit the rate profile of a highly efficient self-replicating system showing the typical sigmoidal shape with a maximum rate after the initial lag period. In both scenarios, the reaction with the higher association constant proceeds with higher efficiency even though the differences between the graphs are rather small. This finding can be explained with the fact that higher binding creates a larger amount of catalytically active ternary complex. With the effective molarity and the stabilisation of the product duplex at a constant level, this increase in concentration leads to the up-regulation of product formation.

Furthermore, a comparison between the rate profiles for the two scenarios implies that, at constant binding strength, the combination of low EM with low ΔG^s gives very similar efficiencies than a combination of high EM and high ΔG^s . This fact can be understood when considering the mechanism of self-replication and the dependences of the reaction rate r on the concentration of the ternary complex $[A \cdot B \cdot T]$ between template **T** and building blocks **A** and **B** as

$$r \sim k_{cat}[A \cdot B \cdot T] + k_{bi}[A][B] = k_{bi}(EM \times [A \cdot B \cdot T] + [A][B])$$

Equation 4.1

A low free energy of stabilisation leads to a larger amount of free product template **T** which is necessary to form the catalytically active ternary complex $[A \cdot B \cdot T]$, however, a low EM means that the reaction within the complex is less enhanced. On the other hand, strong duplex association lowers the amount of available free template but a high EM ensures that once the ternary complex is formed, the reaction proceeds with high rate.

This reasoning again highlights that the concentration of the ternary complex $[A \cdot B \cdot T]$ has a major impact on the performance of the self-replicator. It appears however, that a change in association constant from 500 to 2000 M^{-1} has only very little effect on the overall concentration of the ternary complex since nearly all available product templates are saturated with building blocks. It would therefore be feasible to expand the range of association constants investigated and consider using recognition sites with lower K_d values. Another possibility to weaken the formation of the ternary complex is to work at lower starting material concentration. Reducing the concentration limits the contribution of the recognition-mediated process by weakening the binding event between the recognition sites. The dissociation constant K_d reflects the concentration at which only half of the molecules are bound and can be calculated by taking the inverse of the association constant K_a

$$K_d = \frac{1}{K_a}$$

Equation 4.2

For an association constant of 500 M^{-1} , the K_d is 2 mM and for 2000 M^{-1} the value drops to 0.5 mM. Working at concentrations significantly higher than the K_d ensures that the recognition complex is the dominant species. This is the case for the reactions shown in **Figure 4.8** which were performed at a starting material concentration of 10 mM. As a matter of fact, when the exact same simulations are repeated at a reagent concentration close to the K_d , in this case 1 mM, the rate profiles are of very different shape (**Figure 4.9**).

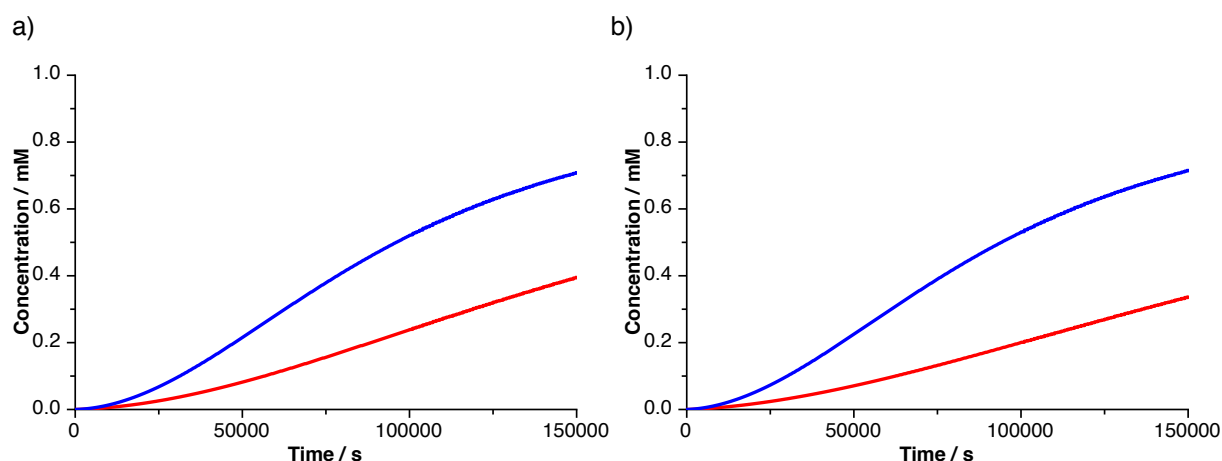


Figure 4.9 Simulated rate profiles on the basis of self-replicating systems **121**, **122**, **123** and **124** at 1 mM starting material concentration. a) The kinetic parameters were set to simulate the situation for the self-replicating formation of **122** and **124** with $EM = 15 \text{ M}$ and $\Delta G^\ddagger = 3.7 \text{ kJ mol}^{-1}$ with association constants of 500 M^{-1} (—) and 2000 M^{-1} (—). b) The kinetic parameters were set to simulate the situation for the self-replicating formation of **121** and **123** with $EM = 30 \text{ M}$ and $\Delta G^\ddagger = 6.8 \text{ kJ mol}^{-1}$ with association constants of 500 M^{-1} (—) and 2000 M^{-1} (—).

It can clearly be seen that the efficiencies of the replicating systems are much lower than for the reactions at 10 mM. The change of association constant is now apparent for both sets of chosen EM and ΔG^\ddagger values with the reaction at 2000 M^{-1} being significantly faster than the reaction at 500 M^{-1} . However, when comparing the reactions between both sets at a fixed association constant of either 500 M^{-1} or 2000 M^{-1} , the differences are still small suggesting that the counterbalancing effect between the effective molarity and the free energy of connection is still valid. It should however be pointed out that working at low starting material concentration close to the K_d results in a relatively high concentration of free building block which can then react in a bimolecular fashion thereby reducing the selectivity of the reaction. This effect was already visible in the *trans/cis* selectivities obtained for the reactions between the set of nitrones **116-119** and maleimide **33**. Further problems might arise with the analysis of reactions run at such low concentrations using ^1H or ^{19}F NMR spectroscopy.

In summary, the theoretical analysis of this type of replicating system has shown that the effect of recognition strength variation is best seen when the reactions are carried out at a concentration close to the value of the dissociation constant of the corresponding binding event. At this point, saturation of the catalytically active ternary complex is avoided without shutting down recognition completely, and changes in the association constants have a higher impact on the performance of the replicator. This finding also explains the failure to detect any change in activity for the self-replicating reaction of the set of maleimides **72**, **66**, **100** and **101** with nitrone **70** since the association constants between carboxylic acid and the amidopyridine moiety were determined to be higher than 2000 M^{-1} . In our simulations based on the set of replicating structures depicted in **Figure 4.6**, lowering the reagent concentration from 10 mM to 1 mM had a major impact on the dependence of the reaction on the association constant. On the other hand, it is also possible to increase the value of the dissociation constant by reducing the association constant of the binding event. This would then allow the test reactions to be performed at higher concentrations, but it would also require a complete re-design of the replicating systems and their recognition sites.

4.5.4 Reaction of the set of nitrones with maleimide **120**

The second test reaction of the set of nitrones **116**, **117**, **118** and **119** was performed with maleimide **120**. Each of the nitrones was reacted with the maleimide at a concentration of 10 mM in CDCl_3 . The two reagents were incubated at 0°C and the progression of the reaction was followed for 16 h by ^1H NMR spectroscopy. Deconvolution of the obtained data allowed for the construction of the concentration *vs* time profiles depicted in **Figure 4.10a**. As established previously, the reaction of a structurally nearly identical nitrone derivative with **120** gave rise to a rate-enhanced formation for the *cis*-product *via* AB pathway.^[197] The same reactivity is also found for the set of nitrones bearing variable substituent pattern.

In all four reactions, the *cis*-isomer is the major product and its formation shows the rate profile typical for an AB system. A splitting for the profiles can be seen with *cis*-**125** showing the most pronounced curvature followed by *cis*-**126**, *cis*-**127** and *cis*-**128**. After 16 h, the conversion of starting material was calculated by ^1H NMR spectroscopy to be in the range of 93-96% for all four reactions with a final *cis/trans* ratio of 74:1 for **116**, 53:1 for **117** and 33:1 for both **119** and **118**.

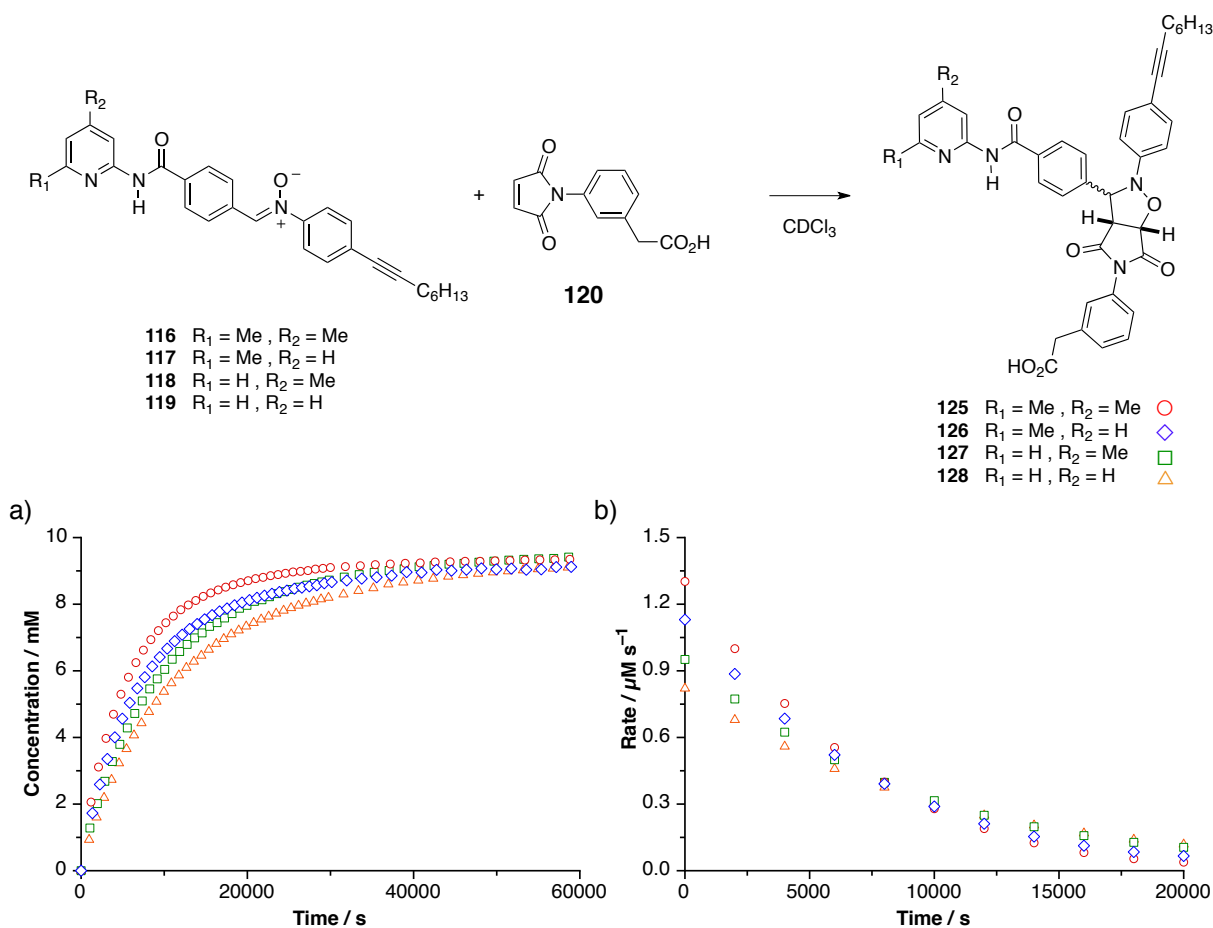


Figure 4.10 a) Arrayed concentration *vs* time profiles for the individual reaction of **116**, **117**, **118** or **119** with phenylacetic acid **120** at 10 mM reagent concentration in CDCl₃ at 0 °C giving rise to AB systems *cis*-**125** (○), *cis*-**126** (◇), *cis*-**127** (□) and *cis*-**128** (△), respectively. All *trans*-products were omitted for clarity. b) Rate *vs* time profile calculated from the profiles in a) with identical colour coding for all reaction products.

Taking the derivative of the polynomial fitted to the obtained concentration *vs* time profiles resulted in the corresponding rate *vs* time profiles (**Figure 4.10b**). A clear trend can be seen for the differences in maximum rate for the four reactions all of which were found at the start of the reaction. The highest rate was calculated for *cis*-**125** (1.30 μM s⁻¹) followed by *cis*-**126** (1.13 μM s⁻¹), *cis*-**127** (0.95 μM s⁻¹) and *cis*-**128** (0.82 μM s⁻¹).

Overall, analysis of the experimental data suggests that the efficiencies of the screened AB systems correspond with the values for the single point association of the recognition event. Strong association results in a high initial rate for the formation of the *cis*-isomers. In order to rationalise this trend, we once more turned to calculations to extract kinetic parameters for the set of four experiments.

4.5.5 Fitting and analysis

A kinetic model was developed for all plausible interactions between the building blocks within the AB system (see appendix). For the fitting procedure, this script was used to extract values for the recognition-mediated rate constant which allowed for the calculation of the effective molarities. The corresponding association constants were taken from **Table 4.1** and the same bimolecular rates as in **4.5.2** were employed for all four compounds. Fitting of the experimental data proceeded smoothly with good to modest R values (**Table 4.6**). Satisfyingly, the trend observed for the rate profiles is reflected in the results of the calculation. The highest rate-acceleration of $1.97 \times 10^{-4} \text{ s}^{-1}$ was found for the reaction of **116** followed by **117** ($1.58 \times 10^{-4} \text{ s}^{-1}$), **118** ($1.44 \times 10^{-4} \text{ s}^{-1}$) and **119** ($1.14 \times 10^{-4} \text{ s}^{-1}$). The calculations of the effective molarities are based on the assumption that a variation of the substituent pattern on the amidopyridine site has no influence on the bimolecular rate constants of the reactions between the maleimide and the four nitrones. Using the same rate constants for all four reactions maintains the same order for the effective molarities with the highest value of 1.76 M^{-1} for **125** followed by 1.42 M^{-1} for **126**, 1.29 M^{-1} for **4EA** and 1.02 M^{-1} for **NoEA**.

Table 4.6 Kinetic parameters extracted for the AB products of the reaction between maleimides **116**, **117**, **118** and **119** with maleimide **120** at 0°C in CDCl_3 at 10 mM reagent concentration using SimFit.

	<i>cis</i> - 125	<i>cis</i> - 126	<i>cis</i> - 127	<i>cis</i> - 128
bimolecular rate constant † / $\text{M}^{-1} \text{ s}^{-1}$	1.12×10^{-4}	1.12×10^{-4}	1.12×10^{-4}	1.12×10^{-4}
recognition-mediated rate constant / s^{-1}	1.97×10^{-4}	1.58×10^{-4}	1.44×10^{-4}	1.14×10^{-4}
effective molarity / M	1.76	1.42	1.29	1.02
R-value / %	4.60	5.12	1.18	2.21

† bimolecular rates estimated from the reaction of **116** with **57**

It is evident from the calculated data that the effective molarities increase with the association constant. Stronger binding between the two reactive partners favours their reaction *via* the AB pathway. In order to interpret these results, some basic principles of the AB system are highlighted in the energy profile depicted in **Figure 4.11**.

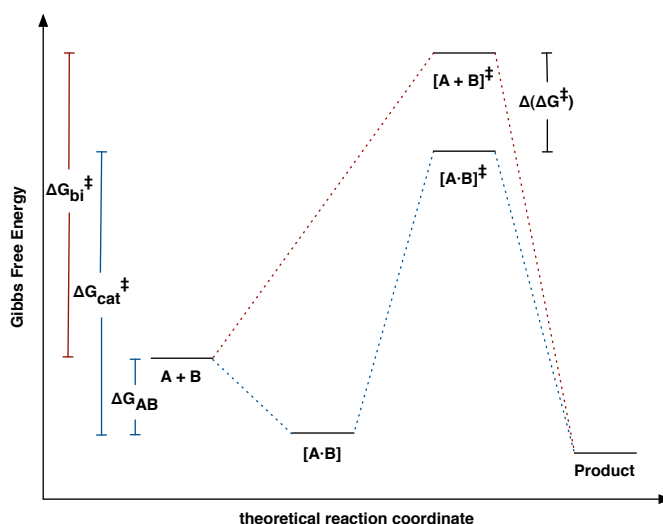


Figure 4.11 Energy profile for the reaction between A and B *via* bimolecular (red) and AB (blue) pathway.

Depending on whether association can take place between both starting materials, two different energy profiles can be created. In the absence of recognition, two hypothetical reagents **A** and **B** react to give a product *via* transition state $[A+B]^\ddagger$ with the corresponding free energy of activation ΔG_{bi}^\ddagger . If recognition takes place, the ground state between **A** and **B** is stabilised by the free energy ΔG_{AB} and the reaction proceeds *via* transition state $[A \cdot B]^\ddagger$ which differs from the previous transition state by $\Delta(\Delta G^\ddagger)$. Overall, the difference $\Delta(\Delta G^\ddagger)$ between the activation free energies ΔG_{bi}^\ddagger and ΔG_{cat}^\ddagger can be derived as

$$\Delta(\Delta G^\ddagger) = \Delta G_{bi}^\ddagger + \Delta G_{AB} - \Delta G_{cat}^\ddagger$$

Equation 4.3

Furthermore, the Eyring equation allows for the calculation of reaction constant k from the free energy of activation ΔG^\ddagger

$$k = \frac{k_B T}{h} e^{-\frac{\Delta G^\ddagger}{RT}}$$

Equation 4.4

with k_B as the Boltzmann constant, h the Planck constant, R the gas constant and T the temperature. Combining this equation with the definition for the effective molarity EM provides a direct relationship between the activation free energies for the bimolecular

reaction ΔG_{bi}^\ddagger and the recognition-mediated reaction ΔG_{cat}^\ddagger , and the rate acceleration in the binary complex

$$E_M = \frac{k_{cat}}{k_{bi}} = e^{\frac{1}{RT}(\Delta G_{bi}^\ddagger - \Delta G_{cat}^\ddagger)} = e^{\frac{1}{RT}(\Delta(\Delta G^\ddagger) - \Delta G_{AB})}$$

Equation 4.5

In the last transformation, the relationship from **Equation 4.3** was employed, providing a clear picture of the dependences of the effective molarity. High EM values are achieved when the absolute value of the transition state stabilisation $\Delta(\Delta G^\ddagger)$ is large compared to the absolute value of the ground state stabilisation ΔG_{AB} . With the value for ΔG_{AB}

$$\Delta G_{AB} = RT \ln K_a$$

Equation 4.6

Equation 4.5 can be altered to give

$$RT \ln(E_M \times K_a) = \Delta(\Delta G^\ddagger)$$

Equation 4.7

For an effective molarity of 1 M, the equation simplifies to

$$RT \ln K_a = \Delta(\Delta G^\ddagger) = \Delta G_{AB}$$

Equation 4.8

in which the ground state stabilisation caused by the recognition event is identical to the transition state stabilisation $\Delta(\Delta G^\ddagger)$. Even though the rate constants are the same for the bimolecular reaction and the recognition-mediated reaction, the recognition process creates a larger concentration of reactive complex and the reaction therefore proceeds with higher rate. The rate of the reaction can be estimated as

$$r \approx k_{cat} \times [A \cdot B] + k_{bi} \times [A] \times [B] = k_{bi}(E_M \times [A \cdot B] + [A] \times [B])$$

Equation 4.9

For reactions at starting material concentrations significantly larger than the dissociation constant K_d , nearly all of the reagents are bound as binary complex and the contribution of the bimolecular reaction can be neglected to give

$$r \approx k_{bi} \times E_M \times [A \cdot B]$$

Equation 4.10

which, unlike for self-replicating system, points at a direct relationship between the rate of the reaction, the effective molarity and the concentration of the binary complex.

Using the obtained values for the association constants K_a and the EM allowed for the calculation of the absolute values for both the free energy of the transition state $\Delta(\Delta G^\ddagger)$ and the ground state stabilisation ΔG_{AB} (**Table 4.7**). It is evident that the stabilisation of the ground state ΔG_{AB} increases with increasing association constant. This trend is compensated by $\Delta(\Delta G^\ddagger)$ which is in all four cases larger than ΔG_{AB} . However, the absolute difference between both free energies diminishes with decreasing association constants from 1.3 kJ mol⁻¹ for **125** to only 0.1 kJ mol⁻¹ for **128**.

Table 4.7 Calculation of absolute values of the free energies ΔG_{AB} and $\Delta(\Delta G^\ddagger)$ for the AB products of the reaction between maleimides **116**, **117**, **118** and **119** with maleimide **120** at 0 °C in CDCl₃ at 10 mM reagent concentration as depicted in **Figure 4.11** using **Equations 4.5** and **4.6**.

	<i>cis</i> -125	<i>cis</i> -126	<i>cis</i> -127	<i>cis</i> -128
$\Delta G_{AB} / \text{kJ mol}^{-1}$	17.0	15.7	15.4	15.3
EM / M	1.76	1.42	1.29	1.02
$\Delta(\Delta G^\ddagger) / \text{kJ mol}^{-1}$	18.3	16.5	16.0	15.4
$\Delta(\Delta G^\ddagger) - \Delta G_{AB} / \text{kJ mol}^{-1}$	1.3	0.8	0.6	0.1

These calculations verify that stabilisation of the transition state occurs for all four systems and, in addition, that a direct relationship between the recognition strength and the absolute value of $\Delta(\Delta G^\ddagger)$ is evident. This fact suggests that stronger binding between the two

building blocks lowers the transition state by positioning the two reactive partner in a more favourable orientation.

With these results at hand, we next envisaged to simulate scenarios on the basis of this set of AB systems to gain deeper insight into the principles of this type of recognition-mediated reaction.

4.5.6 General calculations for an AB system

Initially, we simulated the AB systems by converting the kinetic model used by SimFit in the fitting procedure to the corresponding ISOSIM file. Values for the bimolecular rates remained unaltered, but the effective molarities were varied to 0.6, 1.2, 1.8 and 2.4 M to give rise to four sets of simulations (**Figure 4.12**). For each set, five different association constants ranging from $1 \times 10^2 \text{ M}^{-1}$ to $1 \times 10^6 \text{ M}^{-1}$ were employed.

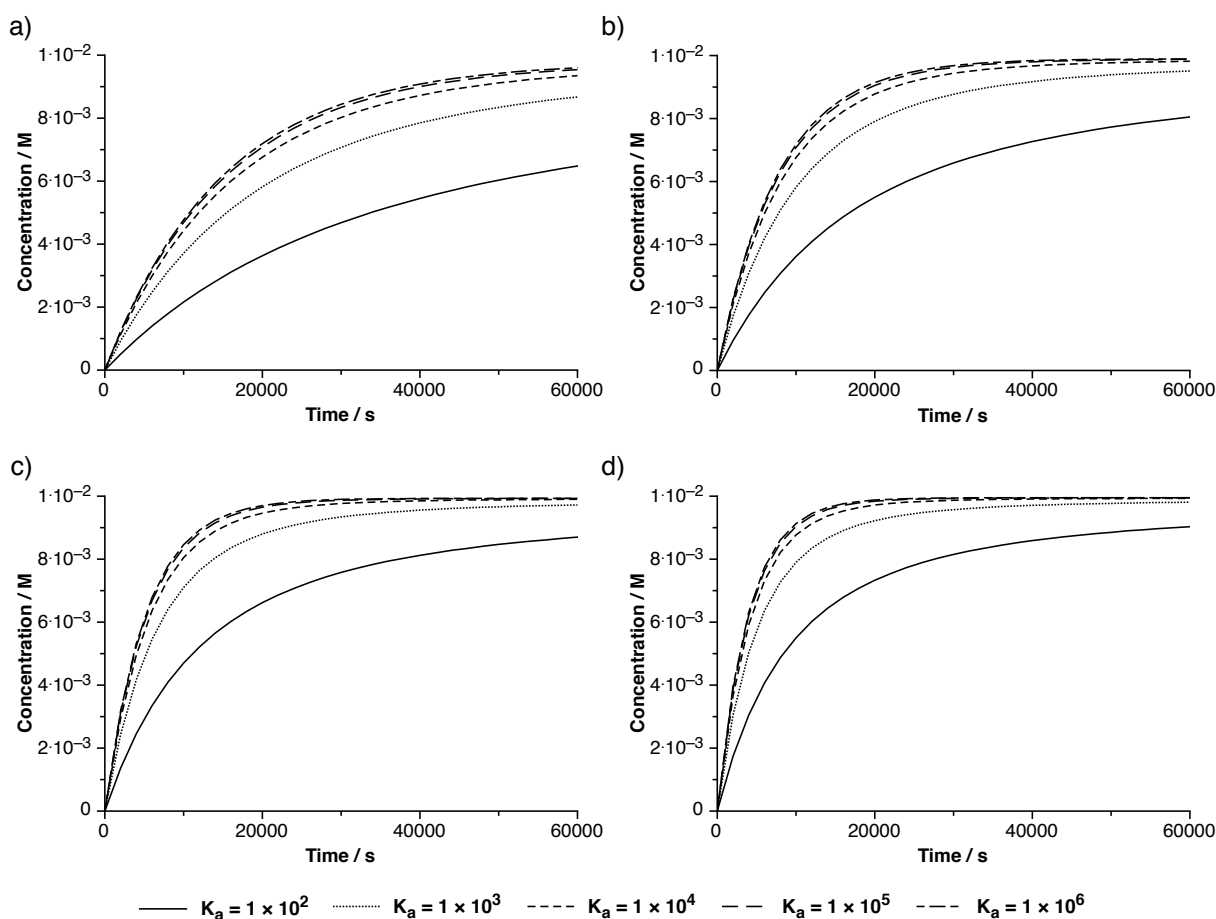


Figure 4.12 Simulation of the concentration *vs* time profiles for an AB system on the basis of the reaction of maleimide **116** and nitrone **120** with bimolecular rate constants of $2.66 \times 10^{-4} \text{ M}^{-1} \text{ s}^{-1}$ and $1.12 \times 10^{-4} \text{ M}^{-1} \text{ s}^{-1}$ for the formation of the *trans*- and *cis*-isomers, respectively. The unimolecular rate constants were set to give effective molarities of a) 0.6 M, b) 1.2 M, c) 1.8 M and d) 2.4 M. The value of the association constant in M^{-1} is indicated by the legend below the graphs.

In all four sets of simulation, some fundamental principles can be seen. The efficiency of the AB system increases with increasing association constant at a given effective molarity. Effective molarities lower than 1 M suggest ground state stabilisation with $\Delta G_{AB} > \Delta(\Delta G^\ddagger)$ whereas effective molarities larger than 1 M indicate some stabilisation of the transition state and $\Delta(\Delta G^\ddagger) > \Delta G_{AB}$. In this case, the observed enhancement for a constant effective molarity is solely a consequence of the increase in concentration of the reactive binary complex since a fixed EM value results in a constant value for the difference between $\Delta(\Delta G^\ddagger)$ and ΔG_{AB} according to **Equation 4.5**. This finding explains the saturation seen for high association constants at which an increase has only very little effect on the concentration of the catalytically active binary complex. When working at 10 mM starting material concentration, an increase in K_a from $1 \times 10^2 \text{ M}^{-1}$ to $1 \times 10^3 \text{ M}^{-1}$ implies a change in concentration for the binary complex from 9.69 mM to 9.90 mM while a further increase to $1 \times 10^4 \text{ M}^{-1}$ contributes only another 0.07 mM to 9.97 mM.

An up-regulation of the EM value leads to an increased stabilisation of the transition state resulting in a greater value for $\Delta(\Delta G^\ddagger)$ and can be seen in the shape of the rate profiles which show higher initial rates and a stronger curvature. However, the relative change in efficiency again remains equal for all five association constants.

The most realistic situation reflecting the experimental data can be seen in **Figure 4.12b** with an association constant of $1 \times 10^3 \text{ M}^{-1}$. It becomes evident that the system acts close to saturation and that further strengthening of the association constant or an increase in effective molarity has little impact on the efficiency of the AB system.

In order to elucidate the boundaries of this type of system, we performed additional calculations using the Gepasi program (version 3.30)^[199] which allowed for the simultaneous variation of two parameters and the construction of the response surfaces depicted in **Figure 4.13**. Four sets of simulations were conducted with increasing starting material concentration ranging from 1 mM to 20 mM. Variation of the effective molarity EM was performed in the range of 0.1 to 10 M and assigned to the x-axis on a logarithmic scale. The y-axis constitutes the variation of the association constant K_a from 0 to 2000 M^{-1} which encompasses the range of the experimental data. The initial rate was identified as an appropriate measure for the efficiency of the AB system and was set as z-axis in the graphs. In order to allow for facile interpretation of the graphs, the surface was furthermore coloured using a code in which dark blue tones indicate low initial rates while high initial rates are shown in light colours. For better comparison of the four scenarios, all graphs are shown on the same scale for the initial rate. It should be noted that also the simulation for the concentration of 1 mM shows a profile identical to the other three graphs only less pronounced.

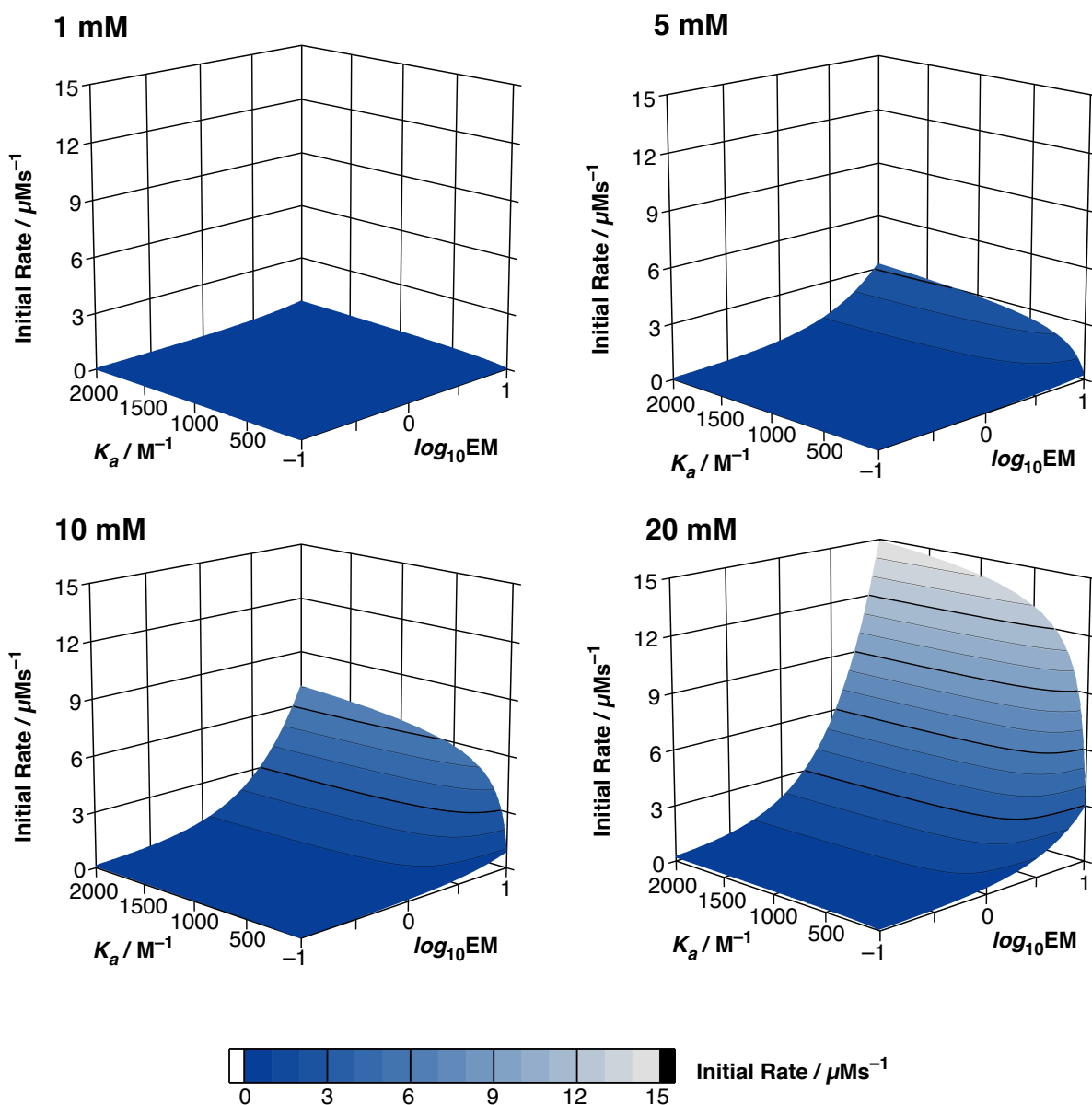


Figure 4.13 Simulated response surfaces for the AB reaction between A and B on the basis of the set of reactions listed in **Table 4.6** using Gepasi. The bimolecular rate was set to $1.12 \times 10^{-4} \text{ M}^{-1} \text{ s}^{-1}$. The surface shows the change of initial rate upon variation of the association constant and the effective molarity. The initial concentration of starting material is indicated as header. The shading of the response surface reflects the initial rate according to the legend below the graphs and is meant for visual guidance.

For all four concentrations, clear trends are visible. The general **Equation 4.10** can be modified to provide an expression for the initial rate of the reaction $r_{initial}$

$$r_{initial} \approx k_{bi} \times E_M \times [A \cdot B]_{initial}$$

Equation 4.11

with $[A\cdot B]_{initial}$ as concentration of the binary complex at the start of the reaction. From this modified equation, the shape of the response surfaces can be explained. The initial rates are proportional to the magnitude of the effective molarity and the concentration of the binary complex which again is a direct function of the association constant and the reagent concentration. The equation further explains the linear relationship between the effective molarity and the initial rate of the reaction at constant K_d . It also highlights why the increase of association constant at a given effective molarity leads to a saturation of the response curve. As mentioned earlier, increasing the association constant beyond a certain value has only little impact on the concentration of the binary complex. For an association constant of 1000 M^{-1} , the K_d is 1 mM and when working at that concentration, only half of the molecules are bound and the contribution of the recognition-mediated reaction is limited. When working at a concentration greater than the K_d , nearly all starting material is bound in the $[A\cdot B]$ complex.

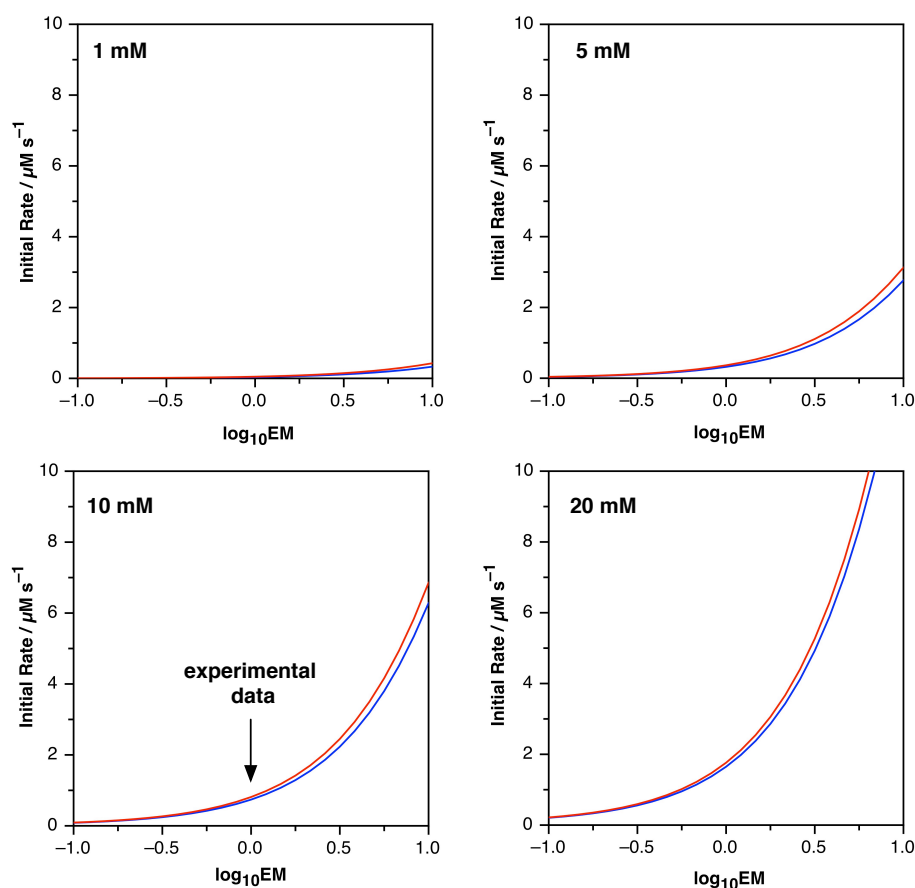


Figure 4.14 Cross sections of the response surfaces from **Figure 4.13** at 850 M^{-1} (—) and 1770 M^{-1} (—) at 1, 5, 10 and 20 mM starting material concentration.

This indifference towards variation of the association constant can be seen in the cross sections for the lowest and highest association constant used in the experiment, 850 M^{-1} and 1770 M^{-1} , respectively (**Figure 4.14**). Again, four different concentrations ranging from 1 mM to 20 mM were analysed. It can clearly be seen that the differences for the two curves are minimal in all four cases. The situation which is closest to the experimental data recorded at 10 mM concentration is indicated by an arrow and also at that particular point, very little difference can be seen for the initial rates of the two association constants.

4.6 Summary and conclusion

In this chapter, the effect of varying the recognition strength on the performance of self-replicating and AB systems was investigated. Four different amidopyridine recognition moieties were combined with two kinds of acids to give rise to a set of association constants in the range of 620 and 4030 M^{-1} . Experimental data for the autocatalytic and AB systems were obtained and the results were further analysed by computational methods. It was evident that both recognition-mediated processes have a different mode of functioning which reflected on their differing dependences on the association constant.

For both investigated self-replicating systems, no distinct relationship between the increase in association constant and the autocatalytic efficiency was determined within the investigated range of K_a . As a matter of fact, the efficiency of a self-replicating system relies on the interplay of many interconnected parameters. As shown in **Equation 4.1**, the rate of the reaction increases with the effective molarity and the concentration of the ternary complex $[\mathbf{A}\cdot\mathbf{B}\cdot\mathbf{T}]$, which itself depends on the strength of the single point association between the recognition sites and the concentration of free template \mathbf{T} . In turn, the concentration of \mathbf{T} is a function of the free energy of connection and furthermore related to the association constant of the template duplex. Strong positive cooperativity in the product duplex therefore limits the amount of free template and reduces the concentration of the ternary complex. An ideal fit of the template duplex was shown to increase the rate enhancement leading to a high effective molarity.

This situation of counteracting forces is most pronounced when working at relatively high concentrations causing near saturation of all available product template with reagents. As mentioned earlier, one possibility to circumvent this rigid scenario is to reduce the concentration of the starting material. This would induce larger changes for the concentration of the ternary complex upon variation of the strength of recognition. On the

other hand, limiting the importance of the recognition-mediated process will increase the impact of the bimolecular reaction and reduce the selectivity of the reaction.

For the AB system between the set of nitrones **116-119** and maleimide **120**, a relationship between the increase in association constant and efficiency of the reaction was seen. According to **Equation 4.10**, the rate of the reaction is a direct function of the effective molarity and the concentration of the binary complex $[A \cdot B]$. The calculations have proven that an increase in K_a indeed generated higher values for the effective molarity and increased the concentration of $[A \cdot B]$. However, when working at 10 mM starting materials concentration, association constants in the range of 1000 to 2000 M^{-1} induce only small changes in the concentration of the binary complex. Accordingly, the simulations have shown that the biggest impact on the initial rate of the AB system upon variation of the association constant is seen for high effective molarities and when working with low association constants.

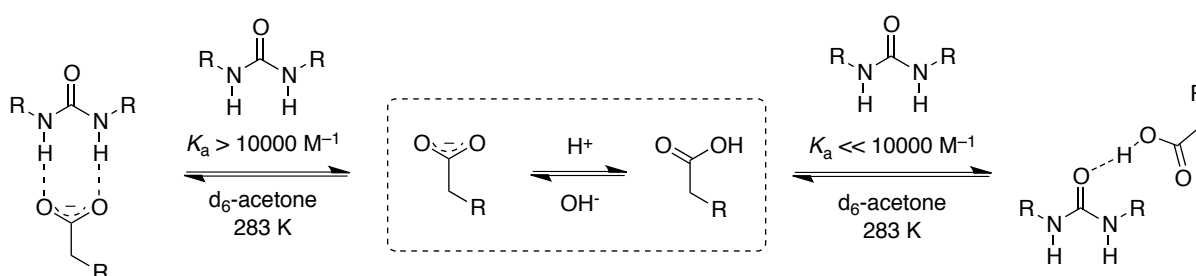
It would therefore be insightful to repeat the reactions at concentrations close to the value of the K_d or to consider a complete re-design of the test reaction. A variation of the association constant using substituents other than methyl groups offers the possibility to weaken the recognition event below the value of the 'no-methyl' substituted amidopyridine. Electronegative functional groups like nitrile, nitro or acetylene are suitable candidates.

5. Controlling replicating activity with a reversible proton switch

5.1 Using changes in pH to reversibly block recognition

In the previous two chapters, it was shown how changes in the geometry of the spacer unit can have a significant impact on the efficiency of a self-replicating process and how these differences can further be fine-tuned by variation of the strength of the association between the recognition units.

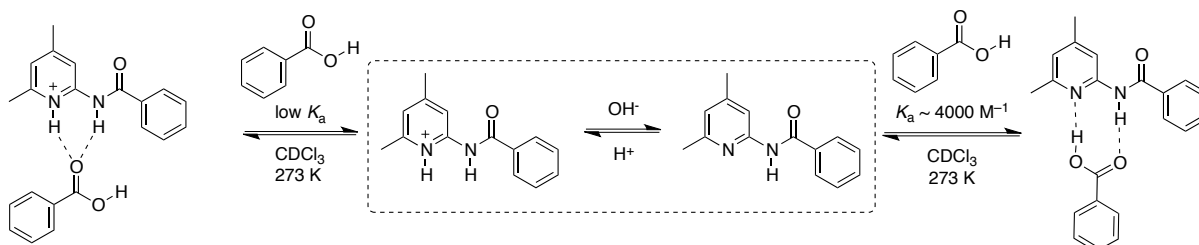
In order to execute full control over the self-replicating process, it would be highly advantageous to design a protocol in which the recognition event can be reversibly influenced by external stimuli. Ideally, finding a way to selectively block and activate one or both of the recognition moieties without influencing the reactive sites would provide a remote control for switching the replicating process on and off. Previous attempts in this group to construct such kind of switch have focused on an AB system mediated by a binary complex between a maleimide bearing an acid functionality and a nitron with a complementary urea recognition site (**Scheme 5.1**).^[200] Addition of triethylamine was found to deprotonate the acid group on the maleimide, thereby strengthening significantly the recognition event between both compounds and enhancing their reaction through the AB pathway under preferential formation of one of two possible diastereoisomers. Addition of trifluoroacetic acid shut down all recognition by protonating the acid and reducing both the rate and selectivity of the reaction.



Scheme 5.1 Reversible proton switch based on the recognition between an urea and a phenylacetic acid in acetone modified from ref. ^[200]. Under neutral conditions, association between the two entities is limited to one hydrogen bond in resulting in a low K_a value (right side). Deprotonation allows for the formation of a binary complex through a two hydrogen bonding pattern (left side).

With regard to the development of a switchable self-replicating reaction, it is important to note that the stability of both reagents was unaffected by the addition of the base and acid, and that the cycloaddition reaction proceeded smoothly independent of the

pH. **Scheme 5.2** shows how the acid-base chemistry from the original urea recognition site can be translated to the recognition motif between a carboxylic acid and an amidopyridine which was used extensively in the preceding chapters for the design of a set of self-replicating systems.

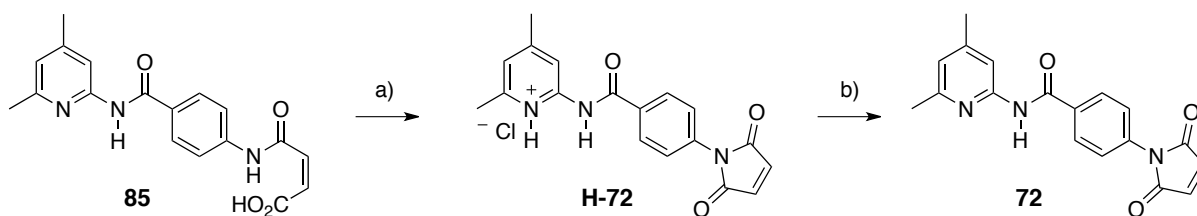


Scheme 5.2 Reversible proton switch using the recognition between an amidopyridine and a carboxylic acid in CDCl_3 . Under neutral conditions, strong association between the two entities occurs through the hydrogen bond pattern (right side). Protonation of the recognition site limits the association by blocking the pyridine nitrogen and lowers the K_a value (left side).

Association of a protonated pyridine species with a carboxylic acid was expected to occur with a very low association value whereas removal of the proton with a base should release the strong recognition between amidopyridine and acid to allow for association. As a consequence of the reversibility of all involved steps, it was deemed possible to enter this pH dependent equilibrium from both sides, by deprotonating the protonated pyridine species or protonating the unprotonated amidopyridine. In order to assure complete analysis of the operational mode of such system, the synthesis of the protonated amidopyridine analogue of maleimide **72** was first envisaged.

5.2 Synthesis of maleimide H-72

The final step for the formation of maleimide **72** is the closure of the maleic acid amide **85**. Refluxing **85** in acetonitrile in the presence of 1 equivalent of ZnBr_2 and an excess of HMDS gave rise to the desired maleimide in good yield and excellent purity. During the work-up, treatment of the reaction mixture with 1M HCl was followed by consecutive base wash of the organic fraction. Without the final basic wash, the hydrochloride salt **H-72** of the native compound **72** could be isolated (**Scheme 5.3**).



Scheme 5.3 Synthesis of maleimide **H-72** as intermediate on the route to recognition maleimide **72**. Conditions: a) ZnBr_2 , HMDS, MeCN, 80 °C, 65%, then 1M aq. HCl; b) 1M aq. EDTA, DCM, rt, 97%.

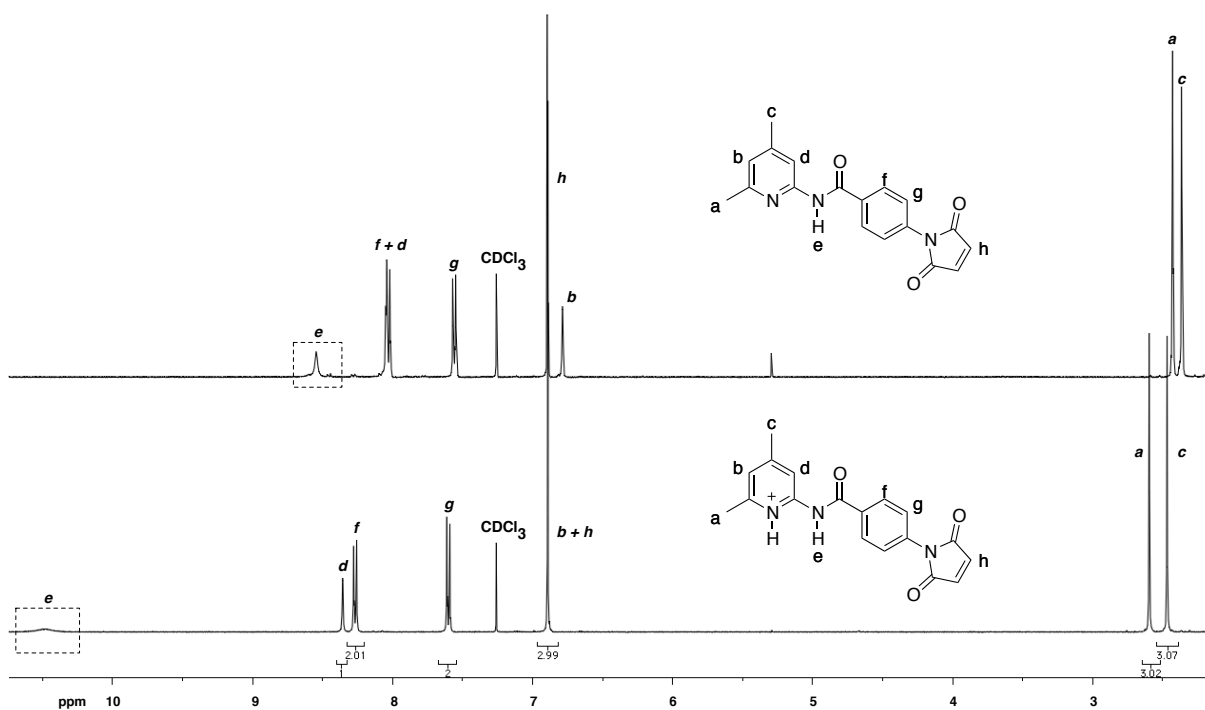


Figure 5.1 Partial 500.1 MHz ¹H NMR spectra of **72** (top) and its protonated derivative **H-72** (below).

Compared to **72**, most noticeable in the ¹H NMR spectrum of **H-72** (**Figure 5.1**) is a drastic downfield shift of more than 2 ppm for the resonance arising from the amide proton as a consequence of the protonated pyridine ring (signal *e*). Simultaneously, other resonances from protons close to the positive charge were equally shifted although to a much lower degree. The signals for pyridine ring protons *b* and *d* show a change in ppm value of 0.31 and 0.11 ppm, respectively, and the signals for methyl groups *a* and *c* are being moved by 0.17 and 0.10 ppm, respectively. Changes in resonance arising from the aryl protons on the benzene ring decreased from 0.23 ppm for *f* to 0.04 ppm for *g* with increasing distance to the pyridine ring. Farthest from the charged ring, signals for the maleimide protons are least affected and only vary by less than 0.005 ppm. Addition of one equivalent of benzoic acid to a 10 mM solution **H-72** in CDCl₃ did not have a measurable influence on the amide proton resonance suggesting that the single-point interaction between the protonated pyridine ring and the acid functionality is much lower than for the neutral pyridine derivative **72**.

5.2.1 Reactivity of maleimide H-72

The structure of recognition-disabled maleimide **H-72** was further proven by reacting it with carboxy nitron **70**. The reaction between maleimide **72** and carboxy nitron **70** was found to be a highly efficient self-replicating system for the *trans*-isomer (see chapter 3). However, blocking the recognition site in the maleimide by protonation prevents a strong hydrogen bonding pattern between both moieties and is expected to shut down all recognition-mediated processes. Kinetic data was recorded in CDCl₃ at 0 °C with 10 mM reagent concentration for **H-72** and **70** and the concentration *vs* time profile for the reaction is depicted in **Figure 5.2**. After 16 h, only 12% of starting materials were converted to cycloadducts with a selectivity of 1.3:1 in favour of *cis*-**H-94**. The low conversion suggests that the protonated recognition site in the hydrochloride compound is unable to promote recognition-mediated processes like the autocatalytic formation of *trans*-**H-94** and both diastereoisomers are being formed through simple bimolecular reactions only.

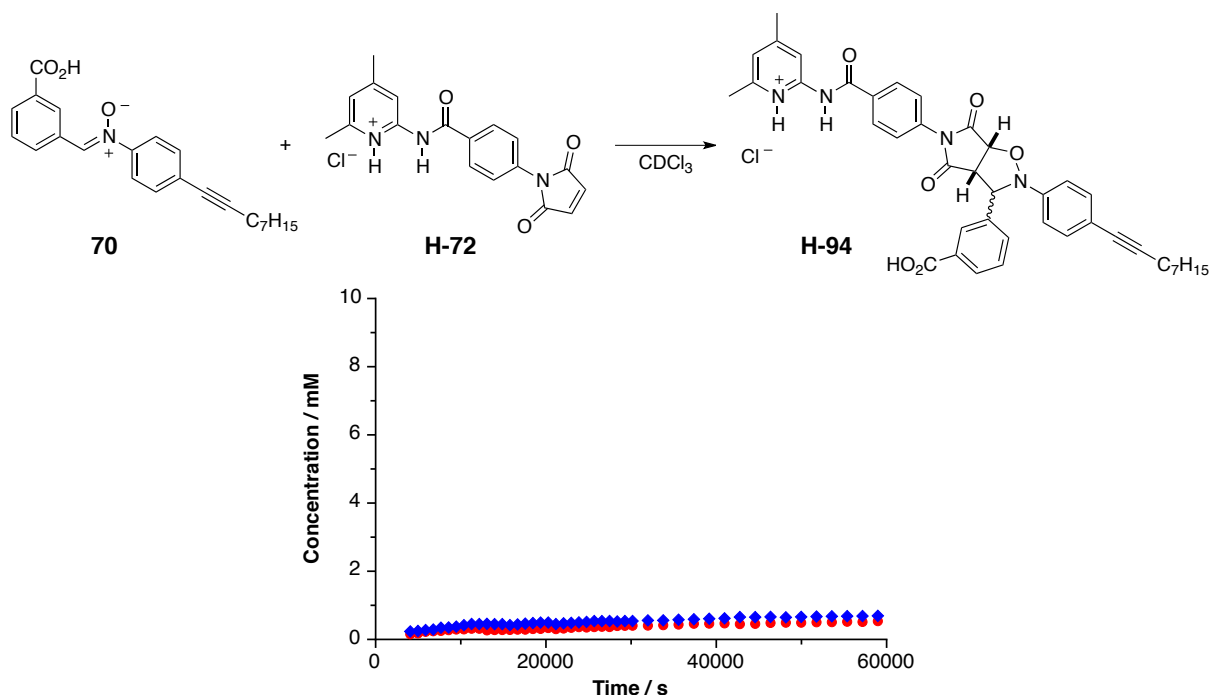


Figure 5.2 Concentration *vs* time profile for the reaction between maleimide **H-72** and carboxy nitron **70** to give cycloadduct **H-94**. The reaction was performed at 0 °C in CDCl₃ at 10 mM reagent concentration. The formation of *trans*-product is shown as red filled circles and the formation of *cis*-product as blue filled diamonds.

However, in all previous bimolecular reactions, e.g. between a maleimide and control nitron **81** or **82**, the final ratio of diastereoisomers was roughly 3:1 in favour of the *trans*-isomer. In order to investigate the cause for the slight preference of *cis*-**H-94** in the reaction

between maleimide **H-72** and nitrone **70**, a reaction between maleimide **H-72** and control nitrone **81** was conducted for comparison. A 10 mM solution of each reagent was incubated at 0 °C for 16 h and the progression of the reaction was followed by ¹H NMR spectroscopy. From the obtained data, the concentration *vs* time profile in **Figure 5.3** could be constructed. At the end of the measurement, 11% of starting materials were converted to a diastereoisomeric mixture of products **H-140** with a *trans/cis* ratio of 3.1:1 suggesting the bimolecular pathway to be the only contribution.

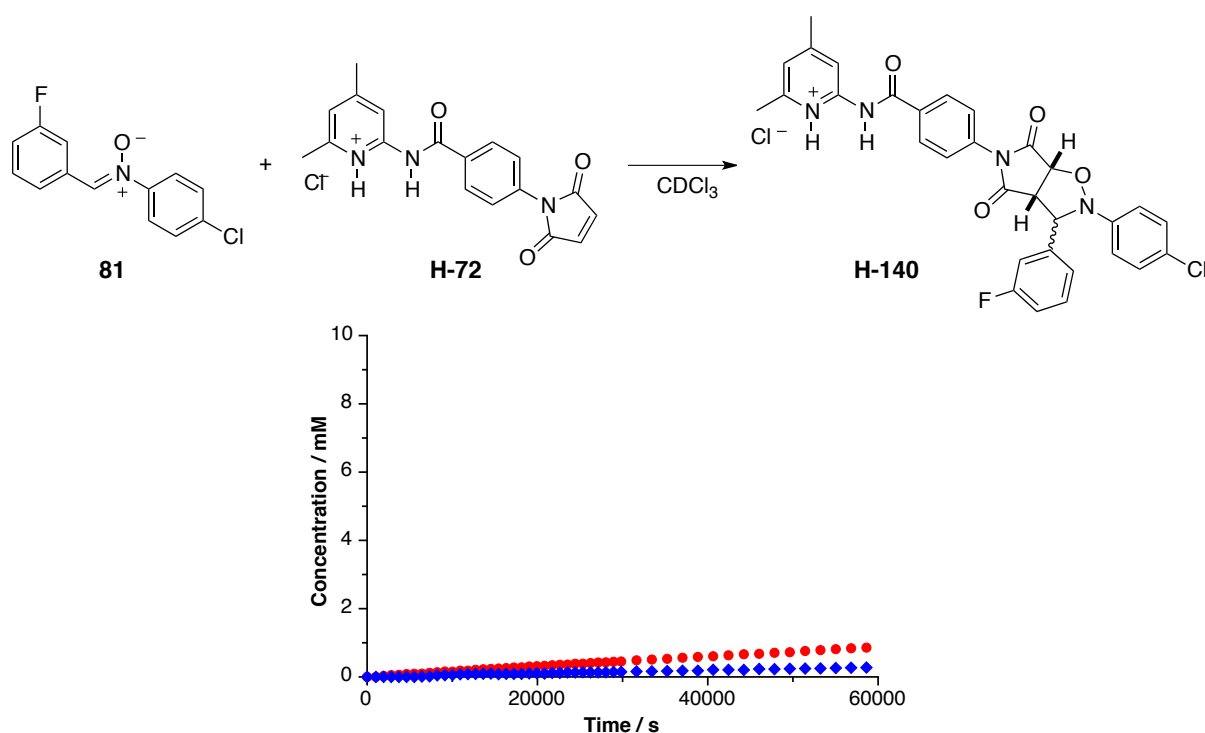


Figure 5.3 Concentration *vs* time profile for the reaction between maleimide **H-72** and control nitrone **81** to give cycloadduct **H-140**. The reaction was performed at 0 °C in CDCl₃ at 10 mM reagent concentration. The formation of *trans*-product is shown as red filled circles and the formation of *cis*-product as blue filled diamonds.

When comparing the reactions of maleimide **H-72** with acid nitrone **70** and control nitrone **81**, a difference in selectivity becomes apparent. In the latter case, the obtained ratio of 3:1 in favour of the *trans*-diastereoisomer corresponds with the selectivity usually found for the bimolecular cycloaddition of a nitrone with a maleimide. The low conversion of 11% after 16 h further indicates the absence of any recognition-mediated reaction pathways. When using acid nitrone **70** as reactive partner, the ratio changes to 1.3:1 in favour of the *cis*-isomer with the conversion remaining low at 12%. This low conversion again suggests that the reaction proceeds predominantly through the bimolecular pathway. As mentioned before, the association constant between the protonated amidopyridine recognition site and

the carboxylic acid was found to be too low to be determined by standard methods. However, the change in selectivity indicates the presence of some kind of minor interaction between the acid functionality and the protonated amidopyridine site. Since the *cis*-isomer is being up-regulated in the process, its rate-enhanced formation through the binary AB shown in **Scheme 5.2** seems plausible. Hydrogen bonds between the carbonyl of the acid and the protons of the amidopyridinium moiety ensure some degree of association between the two components. In this complex, the reactive sites are being brought into close proximity, thereby increasing the rate of the reaction that leads to the formation of the *cis*-isomer. However, this enhancement in reactivity is rather small suggesting that the positioning of the reactive sites in the anticipated transition state is not optimal. Additionally, the existence of a binary complex between maleimide **H-72** and acid nitron **70** implies that less unbound building blocks are available in the solution which reduces the bimolecular rate of the formation of *trans*-**H-94** and maintains the overall conversion at a level similar to the one found for a simple bimolecular reaction. Altogether, the presence of an AB type complex between maleimide **H-72** and acid nitron **70** inverts the selectivity of the two possible diastereoisomers by enhancing the formation of the *cis*-isomer while simultaneously decreasing the bimolecular rate for the formation of *trans*-**H-94**. It should be pointed out that the presence of weak single point interactions between **H-72** and **70** corresponds with the absence of an effective autocatalytic pathway for the formation of *trans*-**H-94**. Key for the performance of a self-replicator is the formation of the active ternary complex between the template and the building blocks through *two* recognition events. With the individual association between the amidopyridinium and the acid moiety already being weak, the total concentration of this ternary complex is too low to promote any self-replicating activity.

Overall, it was successfully demonstrated that the presence of the proton in maleimide **H-72** inhibits its autocatalytic performance with carboxy nitron **70** by reducing significantly the association between the two recognition sites. With the self-replicating pathway being shut down, the presence of a binary AB type complex between the two reagents leading to a minor enhancement of the *cis*-isomer was revealed.

5.3 Kinetic analysis of a pH triggered self-replicating system

Deprotonation of maleimide **H-72** was probed under conditions compatible with the performance of kinetic experiments. Treatment of a 10 mM solution of **H-72** in CDCl₃ with 1 equivalent of NEt₃ at 0 °C was followed by ¹H NMR spectroscopy and was found to give rise smoothly to **72** in a period of about one hour without generating any side-products. Initial broadening of the signals in the ¹H NMR spectra visualised the proceeding

deprotonation. Ultimately, the base completely converted the protonated species into the neutral pyridine compound and the affected peaks sharpen to give rise to a spectra that entirely matches the one of maleimide **72**.

Next, the *in-situ* deprotonation of **H-72** to **72** in the presence of carboxy nitron **70** as reactive partner was probed. An equimolar mixture of both reagents and NEt_3 at 10 mM concentration was dissolved in CDCl_3 and incubated at 0°C for 16 h. The progression of the reaction was followed by ^1H NMR spectroscopy and a concentration *vs* time profile could be constructed from the obtained data (**Figure 5.4a**). It can be seen that the presence of the base has a dramatic effect on the shape of the concentration *vs* rate profile as it now exhibits the characteristic sigmoidal shape. Mixing both reagents with NEt_3 at the start of the reaction seems to instantly activate the recognition unit releasing the original self-replicating process for the formation of *trans*-**94**. The ratio of diastereoisomers for **94** after 16 h was determined to be 29:1 in favour of the *trans*-species and the conversion increased to 87%. Both values are only slightly lower than the ones found for the original system presented in chapter 3 (*trans/cis* ratio of 38:1 and 92% total conversion) underlining the efficiency of the deprotonation.

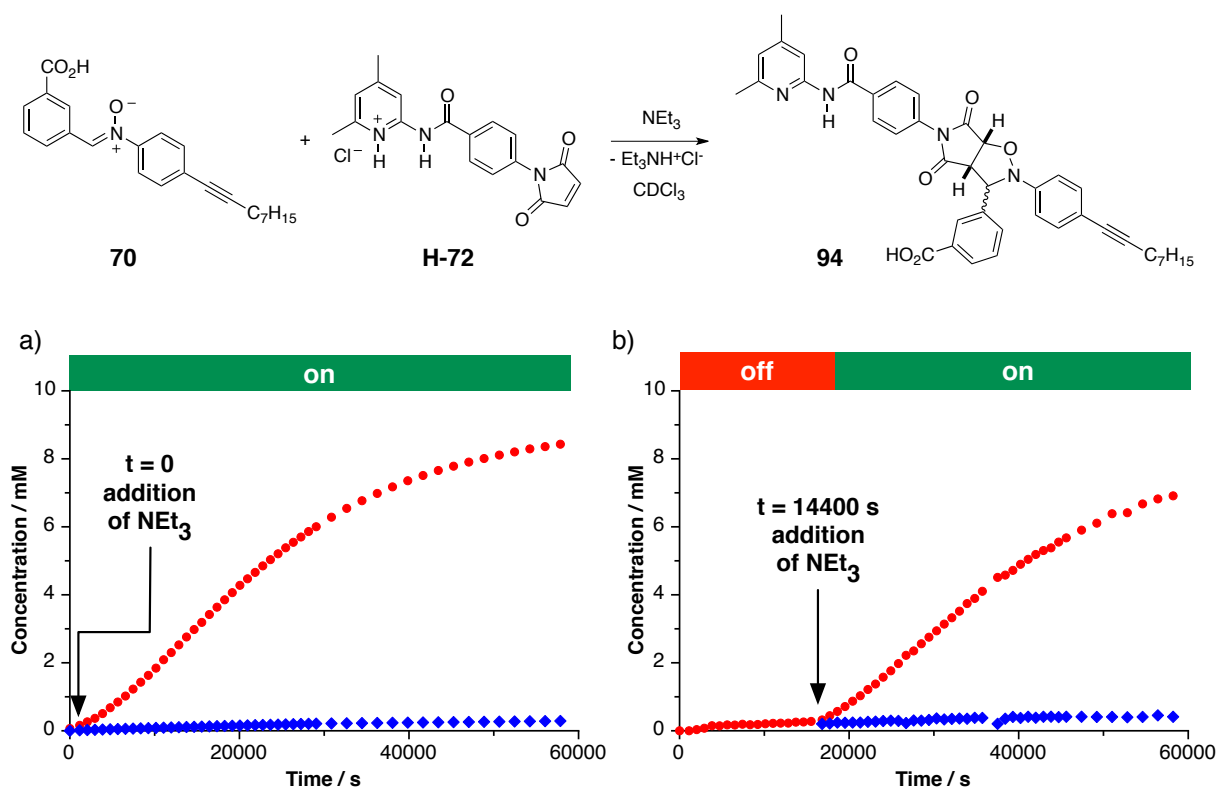


Figure 5.4 Concentration *vs* time profile for the reaction between maleimide **H-72** and carboxy nitron **70** to give template **94** in the presence of 1.0 equivalent of NEt_3 added at a) $t = 0$ s and b) $t = 14400$ s. The formation of *trans*-product is shown as red filled circles and the formation of *cis*-product as blue filled diamonds. All reactions were performed at 0°C in CDCl_3 at 10 mM reagent concentration. The horizontal bar above the graph indicates the presence ('on' with green background) and absence ('off' with red background) of NEt_3 .

On the basis of this first result, another experiment was conducted to probe whether release of the recognition site can be done at any stage of the reaction. In this case, one equivalent of NEt_3 was injected to the native reaction mixture of maleimide **H-72** and nitrone **70** after 4 h (**Figure 5.4b**). The concentration *vs* time profile clearly shows that the self-replicating mode kicks in instantly after addition of the base. The characteristic sigmoidal rate profile can be seen and after 16 h, the ratio of isomers was clearly in favour of *trans*-**94** (24:1). It is important to state at this point that working with a two-fold excess of NEt_3 significantly hampered the performance of the self-replicator mainly because of deprotonation of carboxy nitrone **70**.

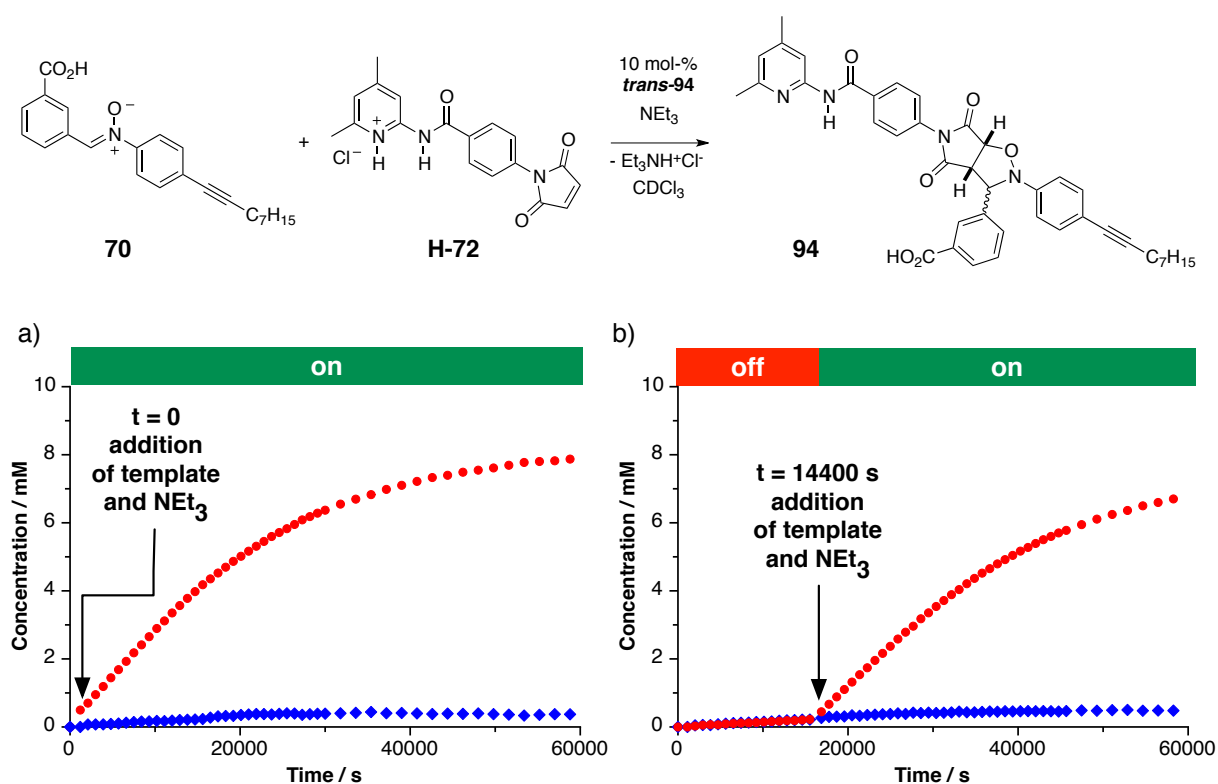


Figure 5.5 Concentration *vs* time profile for the reaction between maleimide **H-72** and carboxy nitrone **70** to give template **94** in the presence of 1.0 equivalent of NEt_3 and 10 mol-% *trans*-**94** added a) at the start of the reaction and b) at t = 14400 s. The formation of *trans*-product is shown as red filled circles and the formation of *cis*-product as blue filled diamonds. All reactions were performed at 0 °C in CDCl_3 at 10 mM reagent concentration. The horizontal bar above the graph indicates the presence ('on' with green background) and absence ('off' with red background) of NEt_3 .

In order to ascertain the presence of a self-replicating pathway, doping experiments were conducted in which one equivalent of NEt_3 was added to the reaction mixture together with 10 mol-% of presynthesised *trans*-**94** template (**Figure 5.5**). The additives were injected to a reaction mixture containing a 10 mM solution of maleimide **H-72** and carboxy nitrone **70** in CDCl_3 at 0 °C at two different stages of the reaction. Both experiments demonstrated

successfully the interplay between the base and the template independent of whether the addition occurs at the start of the reaction (**Figure 5.5a**) or at a later stage (**Figure 5.5b**). Activating the recognition site with the base released the active maleimide compound **72** which instantly underwent template directed synthesis to form self-replicating template *trans*-**94**. The presence of preformed template removes the initial lag period of the released self-replicator and shifts the maximum rate of the process to the start of the reaction.

In order to rule out base catalysis for the enhancement in this system, protonated maleimide **H-72** was reacted with recognition disabled control nitrene **81** in the presence of 1 equivalent of NEt_3 (**Figure 5.6**). Both reagents and base were incubated in CDCl_3 for 16 h at 0°C and 10 mM reagent concentration. The corresponding concentration *vs* time profile is depicted in **Figure 5.6**. Compared with the base free reaction (**Figure 5.3**), addition of the base did not alter the shape of the curve and resulted in comparable values for the selectivity (*trans/cis* 3.1:1) and conversion (11 % after 16 h) for both reactions.

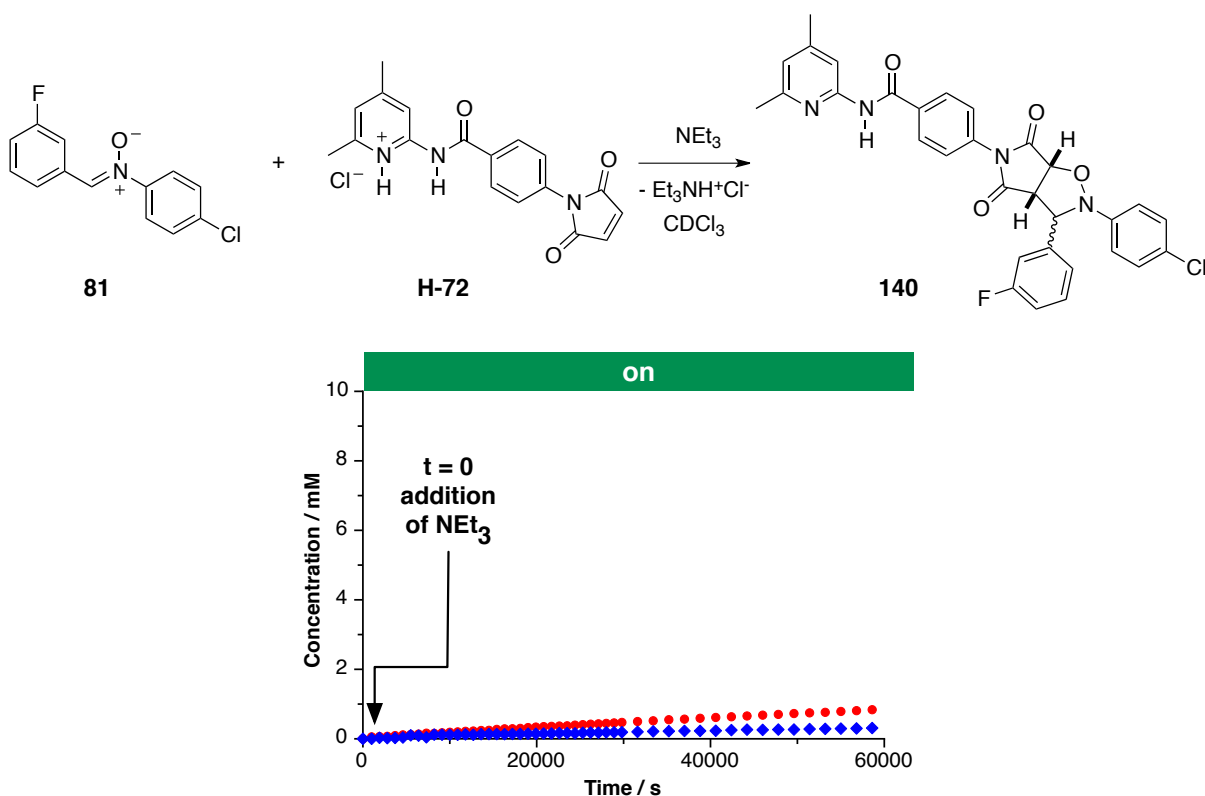


Figure 5.6 Concentration *vs* time profile for the reaction between maleimide **H-72** and control nitrene **81** to give product **140** in the presence of 1.0 equivalent of NEt_3 . The formation of *trans*-product is shown as red filled circles and the formation of *cis*-product as blue filled diamonds. The reactions were performed at 0°C in CDCl_3 at 10 mM reagent concentration. The horizontal bar above the graph indicates the presence of NEt_3 ('on' with green background).

5.4 Controlling a self-replicating reaction with a reversible pH switch

In the previous section, the pH controlled release of an efficient self-replicating system by activating the recognition-unit was successfully demonstrated. As the next step, the reversibility of the activating process was investigated in order to generate a switch protocol in which the reactivity of the self-replicator can be manipulated reversibly. Trifluoroacetic acid (TFA) was chosen to disrupt the hydrogen bonding between the recognition units by protonating the amidopyridine moiety. The low pK_a value, its solubility in chloroform and the absence of any interfering signal peaks in the ^1H NMR spectra make TFA a suitable proton source.

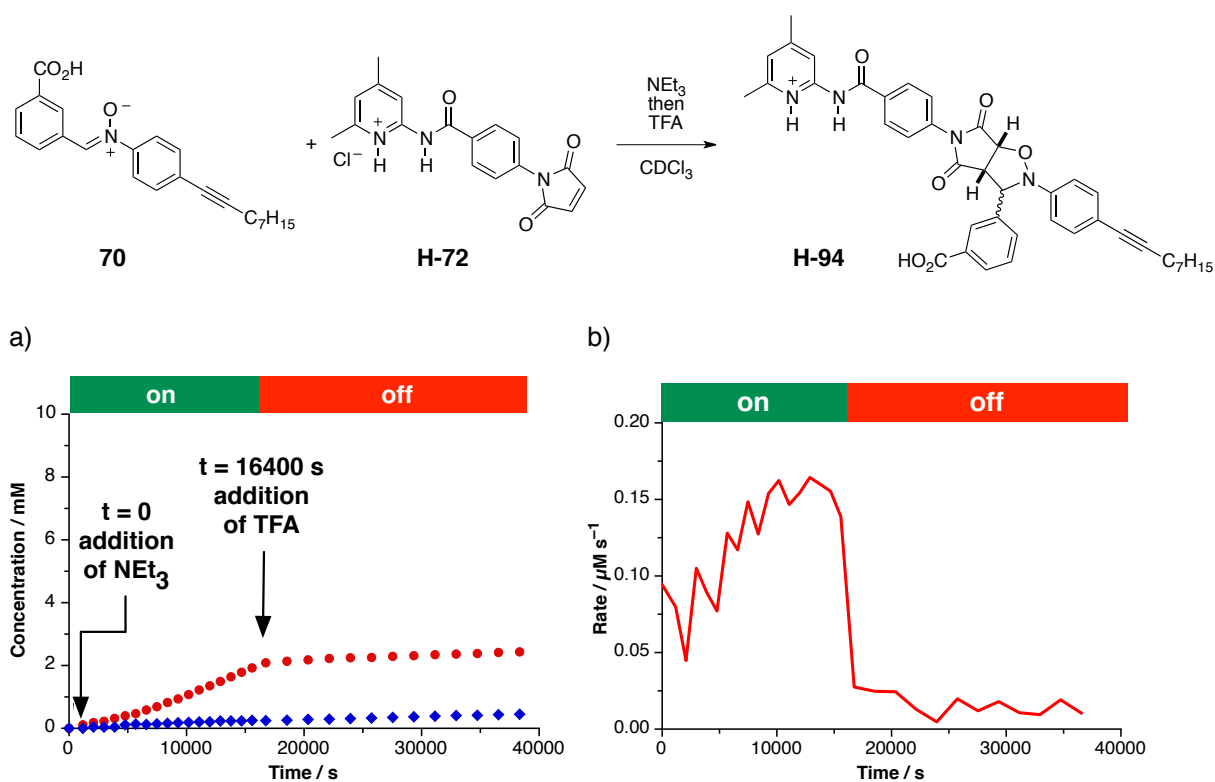


Figure 5.7 a) Concentration *vs* time profile for the reaction between maleimide H-72 and carboxy nitrone 70 to give template H-94 in the presence of 1 equivalent of NEt_3 with addition of 1 equivalent of TFA at $t = 16400$ s. The formation of *trans*-product is shown as red filled circles and the formation of *cis*-product as blue filled diamonds. b) Computed rate profile for the progression of the *trans*-product (–) of the reaction depicted in a). All reactions were performed at 0°C in CDCl_3 at 10 mM reagent concentration. The horizontal bar above the graph indicates the state of the recognition.

To test the usability of TFA in combination with the established activating protocol, the following experiment was conducted. Blocked maleimide H-72 and nitrone 70 were reacted in the presence of one equivalent NEt_3 for 16400 seconds after which one equivalent TFA was injected. The progression of product formation was followed by ^1H NMR spectroscopy and is depicted in Figure 5.7a. The effect of TFA on the shape of the curve is

instantly visible. In the early phase of the experiment, the activated maleimide starts to produce *trans*-94 template *via* the autocatalytic pathway until addition of the acid abruptly shuts down recognition. This effect is also seen clearly in the rate *vs* time profile in **Figure 5.7b**. Protonation of the amidopyridine site prevents the formation of hydrogen bonds with the carboxylic acid, abolishes any further self-replicating activity and reduces the rate to the one found in the bimolecular control reaction. Analysis by ^1H NMR spectroscopy proceeded smoothly showing the absence of any side-products or decomposition. This result suggests that the interplay of NEt_3 and TFA can indeed be exploited to reversibly tune self-replicating processes.

In order to explore the robustness of this reversible protocol, an experiment was conducted in which five alternating injections of NEt_3 and TFA generated the step-like concentration *vs* time profile shown in **Figure 5.8a**. Starting with a mixture of maleimide **H-72** and nitron 70 at 10 mM concentration in CDCl_3 at 10 °C, the presence of the blocked maleimide compound generated the low gradient at the very start of the reaction until NEt_3 was added after 7200 seconds inducing the first self-replicating phase. Addition of TFA after 14400 seconds shut down all recognition-mediated processes and a first plateau was reached. From there, further injection of NEt_3 and TFA at 21600 and 28800 seconds completed a second cycle until the reaction was finally allowed to phase out after final addition of NEt_3 at 36000 seconds.

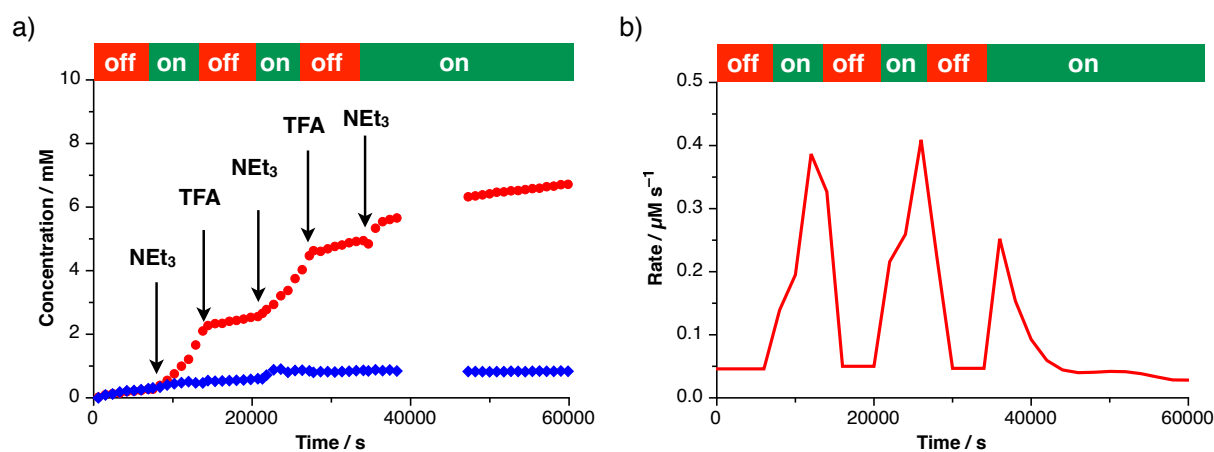


Figure 5.8 a) Concentration *vs* time profile for the reaction between maleimide **H-72** and carboxy nitron 70 with consecutive addition of 1 equivalent NEt_3 at $t = 7200$, 21600 and 36000 s and 1 equivalent of TFA at $t = 14400$ and 28800 s at 10 °C. The formation of *trans*-product is shown as red filled circles and the formation of *cis*-product as blue filled diamonds. b) Computed rate profile for the progression of the *trans*-product (–) of the reaction depicted in a). The reaction was performed at 10 °C in CDCl_3 at 10 mM reagent concentration. The horizontal bar above the graph indicates the state of the recognition.

Calculating the first derivative of the fits to the individual reaction segments gives rise to the rate *vs* time profile depicted in **Figure 5.8b**. A linear fit was applied for all data points taken in the recognition-disabled region whereas all self-replicating phases were fitted by a polynomial curve. The effect of pH variation on the efficiency of the self-replicating process can clearly be seen. Initially, the replicating process is switched off and the reaction proceeds at a constant rate in the order of magnitude typical for a bimolecular reaction ($0.05 \mu\text{M s}^{-1}$). Addition of NEt_3 releases the native self-replicating system and a maximum in rate can be observed. Two cycles of consequent addition of TFA first deactivates the replicating process with the rate dropping to a bimolecular level until injection of another equivalent of NEt_3 generates a second and third maximum. The magnitude and shape of the maxima is affected by the concentration of starting material and available *trans*-isomer acting as dopant. The first activation was done at an early stage of the reaction at which a large amount of reagent but a small amount of preformed *trans*-product was present in the solution. The second activation occurred at a point at which less starting material but more *trans*-template molecules were available. In this case, both effects seem to counterbalance each other and the resulting rate profiles are of similar shapes with similar values for the maximum rates (0.38 and $0.40 \mu\text{M s}^{-1}$ for the first and second maximum, respectively). It is only at the third addition of NEt_3 that the reduction in available starting material cannot be compensated by the presence of the template and the amplitude of the maximum rate ($0.25 \mu\text{M s}^{-1}$) is significantly lowered.

With these results at hand, fully reversible control over the activity of a self-replicator by means of a pH trigger process has convincingly been demonstrated. The effect of the proton switch on the performance of an AB system in competition with a self-replicator will be investigated in the next chapter.

5.5 pH controlled competition between an AB and a self-replicating system

In the previous section, reversible activation of a replicating process was demonstrated for the reaction of maleimide **H-72** and nitron **70** in the presence of proton donors and acceptors. Working at low pH was expected to eliminate all recognition processes between the amidopyridine and the carboxylic acid. However, analysis of the native reaction between maleimide **H-72** and carboxy nitron **70** revealed the presence of subtle interactions between the two components leading to a minor increase in concentration of *cis*-template *via* the AB pathway. If the postulated transition state with association between the carbonyl group of the acid and the protons of the amidopyridinium moiety proved feasible, it should be

possible to improve the efficiency of this AB system by replacing carboxy nitron **70** with phenylacetic acid nitron **71**. In chapter 3, the screening of maleimide **72** with both nitrones **70** and **71** indeed revealed a significant difference in reactivity depending on their structural properties. The reaction of maleimide **72** with carboxy nitron **70** gave rise to an efficient self-replicating system for *trans*-**94** whereas the presence of the longer phenylacetic acid group in nitron **71** allowed for the enhanced formation of *cis*-**95** via AB complex with reduced self-replicating activity of the *trans*-template.

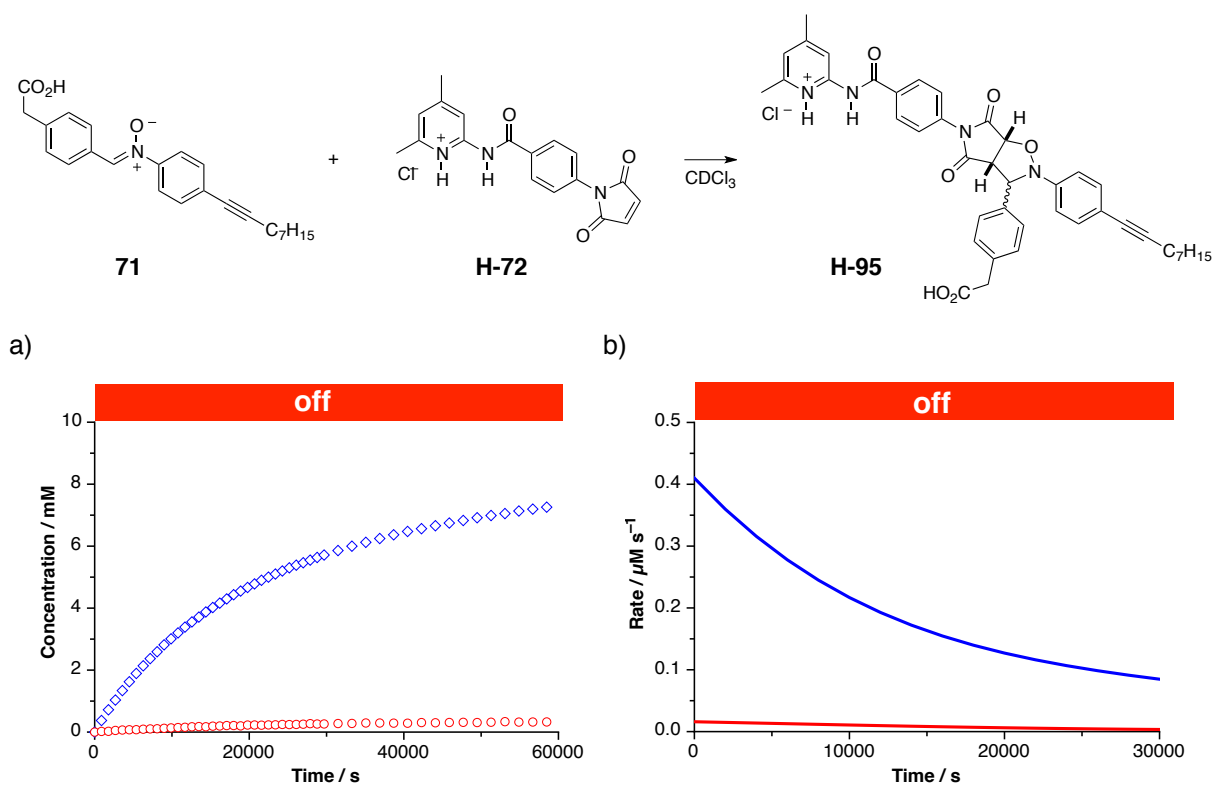


Figure 5.9 a) Concentration *vs* time profile for the reaction between maleimide **H-72** and phenylacetic acid nitron **71** to give **H-95** in the absence of any additives. The formation of *trans*-product is shown as red hollow circles and the formation of *cis*-product as blue hollow diamonds. b) Computed rate profile for the progression of the *trans*-(-) and *cis*-(-)product of the reaction depicted in a). The reaction was performed at 0 °C in CDCl₃ at 10 mM reagent concentration. The horizontal bar above the graph indicates the absence of NEt₃ ('off' with red background).

In order to probe whether this change in reactivity can be translated into the current proton switch scenario, a 10 mM solution of maleimide **H-72** in CDCl₃ was reacted with nitron **71** at 0 °C for 16 h and followed by ¹H NMR spectroscopy (**Figure 5.9**). Deconvolution of the obtained kinetic data gives rise to the concentration *vs* time profile depicted in **Figure 5.9a**. It can clearly be seen that even in the absence of NEt₃, maleimide **H-72** engages in a recognition-mediated reaction. The dominance of the *cis*-isomer suggests the presence of the anticipated binary complex between the two building blocks which enhances eventually the

reaction in an AB fashion. Unlike in the reaction of nitron 71 and maleimide 72 as presented in chapter 3, autocatalytic formation of the *trans*-template of 95 is now completely suppressed. Calculation of the rate *vs* time profile underlines this observation (Figure 5.9b). The characteristic curve for the AB system exhibits its highest rate of $0.41 \mu\text{M s}^{-1}$ at the start of the reaction whereas the shape of the linear curve for the *trans*-isomer suggests the absence of any contribution other than through the bimolecular pathway. It is to be pointed out that the maximum rate for *cis*-H-95 is only marginally lower than the one found for the reaction of nitron 71 with activated maleimide 72 ($0.45 \mu\text{M s}^{-1}$, see chapter 3), even though the association between the protonated amidopyridine and the carboxylic acid was determined to be much lower than for the original interaction. This impediment seems to be counterbalanced by the absence of any competing self-replicating activity for the formation of *trans*-H-95. With the *trans*-isomer only being formed in a bimolecular fashion, a larger amount of building blocks remains in solution thereby increasing the concentration of AB complex.

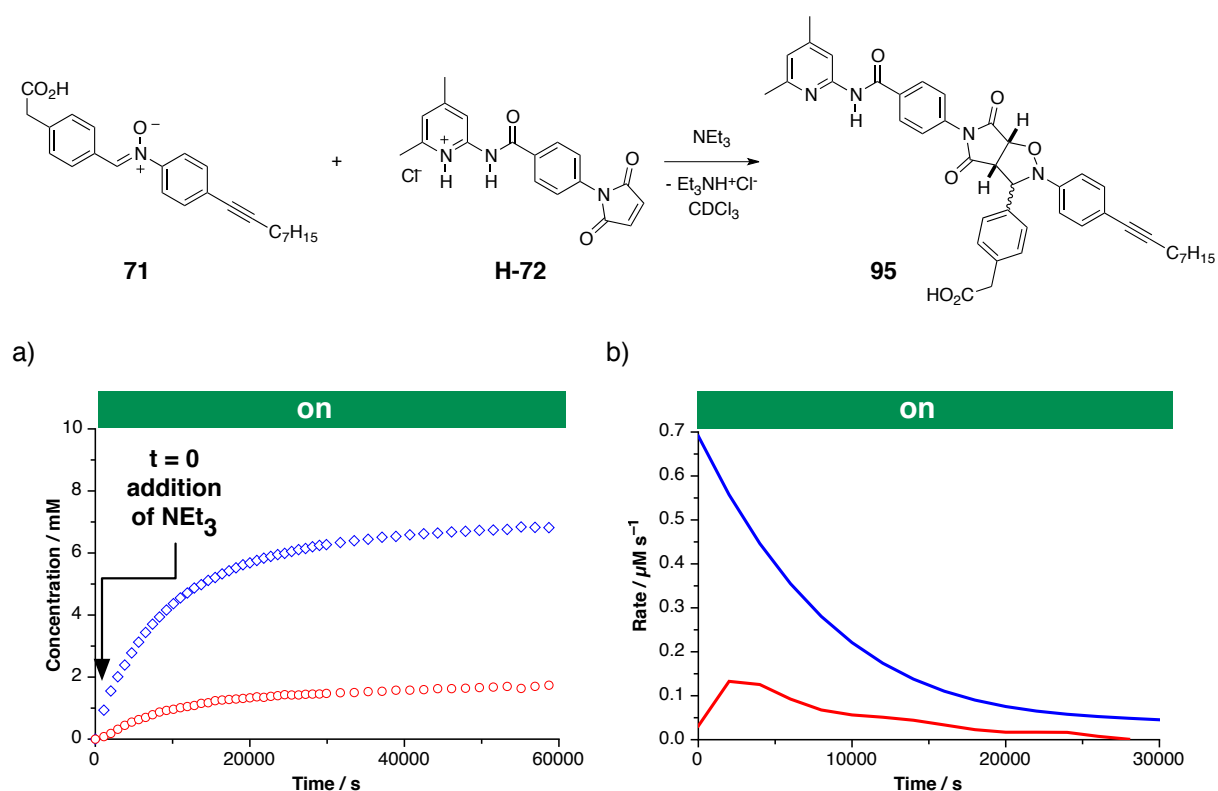


Figure 5.10 a) Concentration *vs* time for the reaction between maleimide H-72 and phenylacetic acid nitron 71 to give 95 in the presence of 1 equivalent NEt₃. The formation of *trans*-product is shown as red hollow circles and the formation of *cis*-product as blue hollow diamonds. b) Computed rate profile for the progression of the *trans*-(-) and *cis*-(-)product of the reaction depicted in a). The reaction was performed at 0 °C in CDCl₃ at 10 mM reagent concentration. The horizontal bar above the graph indicates the presence of NEt₃ ('on' with green background).

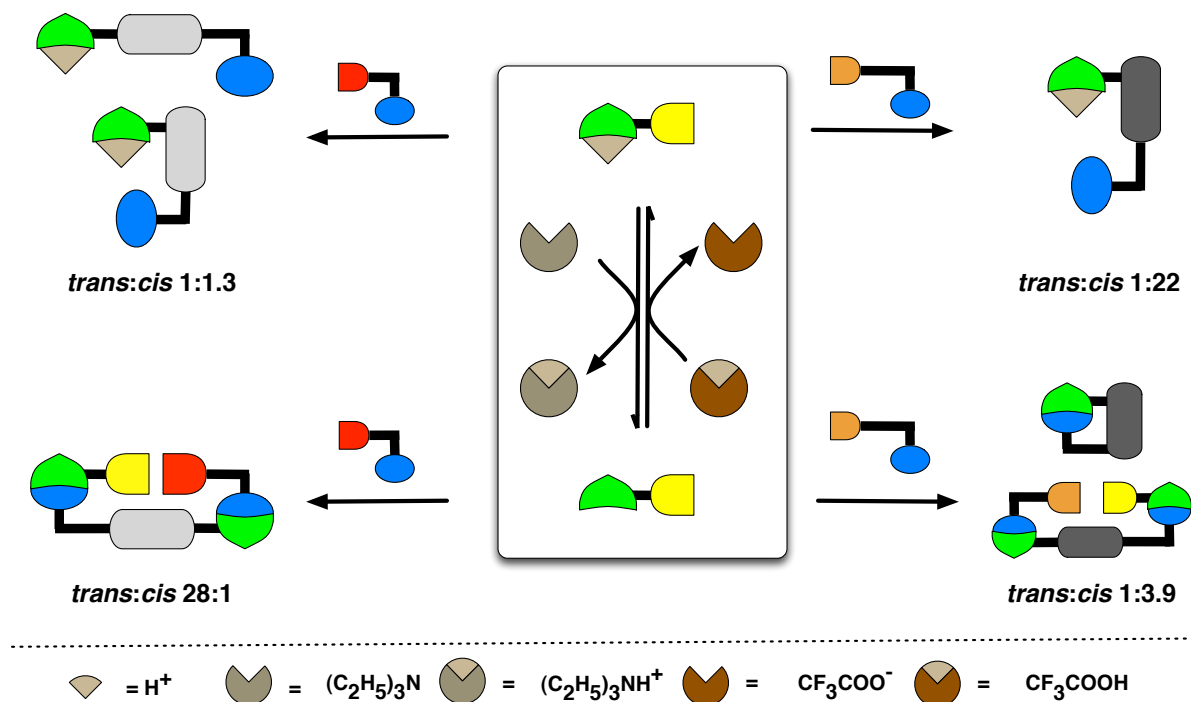
In summary, replacing carboxy nitrone **70** with nitrone **71** bearing the more flexible phenylacetic acid spacer led to a significant up-regulation of the *cis*-product. Even though association between the blocked recognition site and the acid remains weak, the additional methylene group now allows for better positioning of the reactive sites in the AB complex and significantly enhances the rate of recognition-enhanced formation of *cis*-**H-95**.

Next, the reaction between maleimide **H-72** with nitrone **71** was repeated in the presence of 1 equivalent of NEt₃ (**Figure 5.10**). The base is expected to deprotonate **H-72** to set free maleimide **72** which reacts with the nitrone to give rise to a diastereoisomeric mixture of AB product *cis*-**95** and self-replicator *trans*-**95**. In order to verify the predicted reactivity, a 10 mM solution of maleimide **H-72** in CDCl₃ was reacted with nitrone **71** at 0 °C for 16 h together with 1 equivalent NEt₃ and followed by ¹H NMR spectroscopy. Subsequent deconvolution of the obtained kinetic data gives rise to the concentration *vs* time profile depicted in **Figure 5.10a**. It can clearly be seen that both isomers now exhibit rate-enhanced formation. Addition of the base to the reaction mixture restores the situation known from the original experiment in which formation of the *cis*-isomer proceeds *via* AB pathway whereas the *trans*-partner acts as autocatalyst. The final ratio of isomers is 3.9:1 in favour of *cis*-**95** compared to 2.1:1 for the reaction of maleimide **72** with nitrone **71** under the same conditions. This difference can be explained with the concentrations of reactive building blocks available at the start of the two reactions. In the original reaction, both reagents are readily available at the start of the reaction and can directly be incorporated into both AB system and replicator. When using maleimide **H-72**, addition of base is necessary to convert the maleimide into its reactive form. Even though deprotonation is quick, it still takes a certain amount of time to completely activate all present maleimide. This delay may only have a minor impact on the performance of an individual replicator, but when in competition with an AB system, this short delay can have important implications on the initial rates of the reaction. It was shown previously that self-replicating systems are more sensitive to the blocking of recognition sites than AB systems, a reduction of the amount of active starting material would therefore explain the enhanced formation of *cis*-**95**. This reasoning is underlined by the rate *vs* time profile depicted in **Figure 5.10b**. The maximum rate for the AB system is higher than in the original reaction (0.69 μM s⁻¹ compared to 0.45 μM s⁻¹) with the rate for the self-replicator nearly staying the same (0.13 μM s⁻¹ compared to 0.11 μM s⁻¹).

In summary, we have demonstrated that blocking the recognition site has a lesser impact on the performance of the AB system than on the self-replicator. In the competition scenario between the two diastereoisomers of **95**, the ratio of final products can, to a certain degree, be tuned by addition of base to the start of reaction.

5.6 pH controlled temporal separation of a SR from a coexisting AB system

A concise summary of the pH controlled reactions between maleimide **H-72** and nitrones **70** and **71** is given in **Scheme 5.4**. The reversible protonation of the maleimide building block with NEt_3/TFA is highlighted in the centre of the diagram. In the upper section, the reactions of blocked maleimide **H-72** with the two nitrones is depicted. The performance of the potentially self-replicating reaction with carboxy nitrone **70** was found to be suppressed giving a mixture of diastereoisomers in a slow and unselective manner (**Figure 5.2**). On the other hand, the reaction with phenylacetic acid nitrone **71** was found to be highly selective for AB system *cis*-**H-95** (**Figure 5.9a**). After deprotonation of maleimide **H-72** to **72**, the selectivities for the two reactions change; the activated maleimide can now engage in a very efficient self-replicating system with carboxy nitrone **70** giving rise to autocatalyst *trans*-**94** (**Figure 5.4a**). At the same time, the AB system loses some of its supremacy in the reaction with phenylacetic acid nitrone **71** (**Figure 5.10a**).



Scheme 5.4 Schematic summary of the possible reactions between maleimide **72** (yellow building block) and nitrones **70** (red) and **71** (orange) to give templates **94** (light grey) and **95** (dark grey) as presented in the previous sections. Selectivities lower than 5:1 are represented by both diastereoisomers, selectivities greater than 5:1 by the dominant cycloadduct species only.

Altogether, two combinations give rise to high selectivity for one of the two diastereoisomers, reaction of blocked maleimide **H-72** with phenylacetic acid nitrone **71** in favour of the *cis*-product and activated maleimide **72** with carboxy nitrone **70** leading to

trans-94. In order to create a scenario in which the reactivity of these two systems are played off against each other, a pair of experiments were constructed. First, one equivalent of each nitrone **70** and **71** at 10 mM concentration in CDCl₃ was reacted with two equivalents NEt₃ and two equivalents of maleimide **H-72**. The reaction was kept at 0 °C for 16 h and was followed by ¹H NMR spectroscopy. Deconvolution of the obtained kinetic data shows the concomitant formation of both major isomers, *cis*-95 and *trans*-94 (Figure 5.11a).

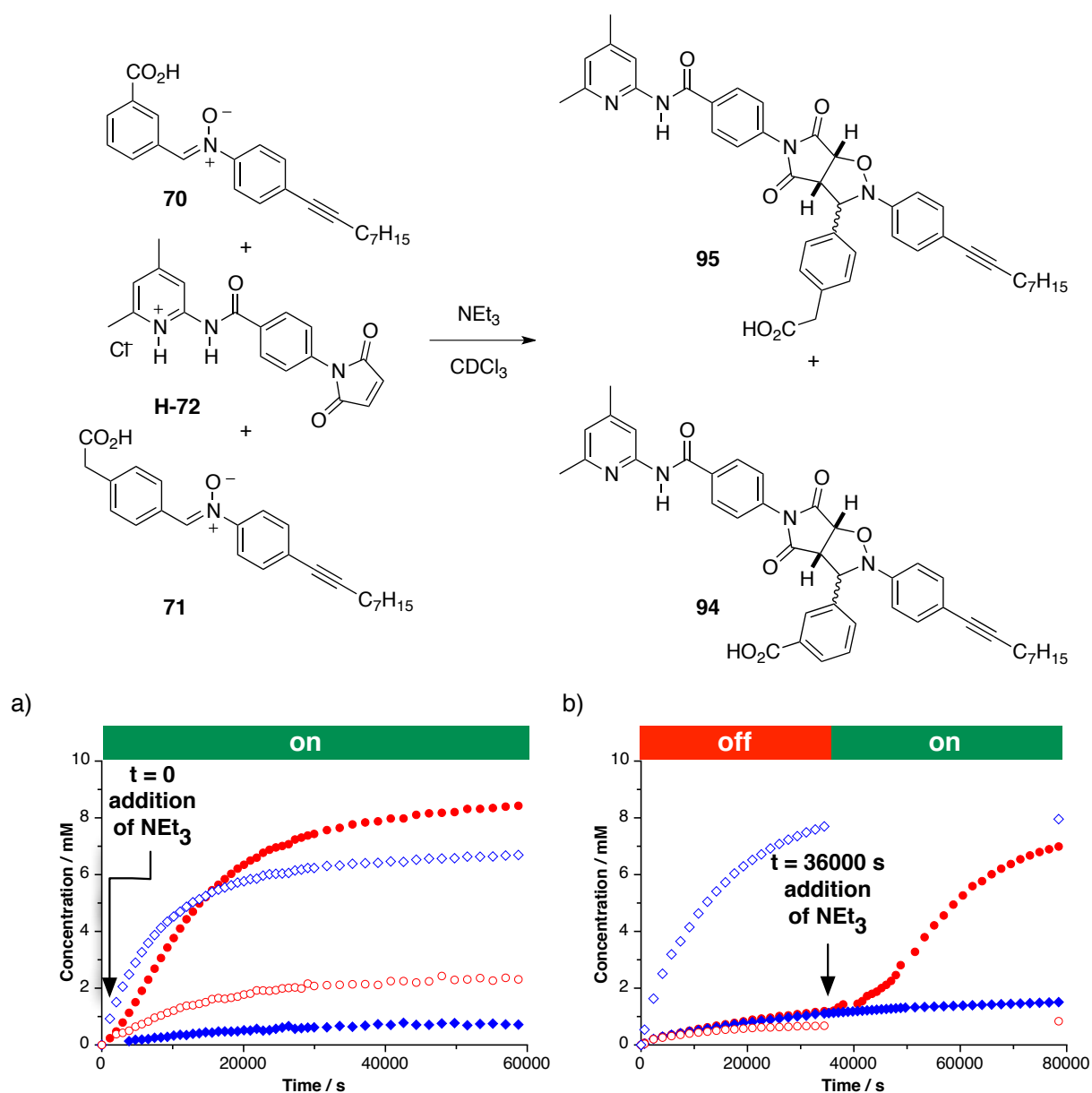


Figure 5.11 Concentration *vs* time profile for the reaction of maleimide **H-72** with carboxy nitrone **70** and phenylacetic acid nitrone **71** to concomitantly form templates *trans*-94 (●), *cis*-94 (○), *trans*-95 (◆) and *cis*-95 (◇) in the presence of 2.0 equivalent of NEt₃ added a) at the start of the reaction and b) at t = 36000 s. All reactions were performed at 0 °C in CDCl₃ at 20 mM reagent concentration for **H-72** and 10 mM reagent concentration for **70** and **71**.

In the early stage of the reaction, the product of the AB pathway is the most abundant species, however, the superior selectivity of the self-replicating process renders *trans*-**94** to be in slight excess at the end of the reaction. Since the reagent pool contains a balanced ratio of maleimide to nitrones, the reactivity of the system can be seen as a superimposition of the isolated processes shown in the lower section of **Scheme 5.4**. However, changing the timing of the NEt₃ addition significantly alters the shape of the concentration *vs* time profiles for all present species. **Figure 5.11b** depicts the scenario in which two equivalents of NEt₃ were only added after 10 h (36000 seconds) to a mixture containing two equivalents of maleimide **H-72** and one equivalent of each nitron **70** and **71**. Analysis of the kinetic data provides instantly a clear picture of the process. Before addition of NEt₃, a major amount of *cis*-**95** was formed *via* the binary AB complex whereas all self-replicating pathways were considerably suppressed. Since the maleimide was not consumed in the self-replicating process, the probability of forming a catalytically active AB complex is higher than in the previous experiment. The maximum rate of the AB reaction is therefore increased even though the recognition site on the maleimide is blocked. Addition of NEt₃ restores the recognition site necessary for the self-replicating reactions. In case of replicator *trans*-**94**, the AB species has already consumed most of the necessary nitron and no efficient autocatalytic production can take place. However, a sigmoidal shape for the formation of *trans*-**94** can be observed right after injection of the base. At this stage of the reaction, a considerable amount of maleimide has already been used up for the formation of both isomers of **94** as well as *cis*-**95** which could accumulate undisturbed by the self-replicator. For this reason, self-replicating template *trans*-**94** does not exceed the concentration of *cis*-**95** as in the previous experiments, but easily outperforms its diastereoisomeric partner.

Altogether, the experiments presented here show how the switch protocol can be used to temporally delay the appearance of the self-replicator with respect to a coexisting AB system. The timing of the NEt₃ addition allows to control the ratio of products for the pair of reactions. Early addition favours the *trans*-species of **95** and **94** on the expense of their isomeric partners, whereas addition at a later stage reduces the amounts of final *trans*-products.

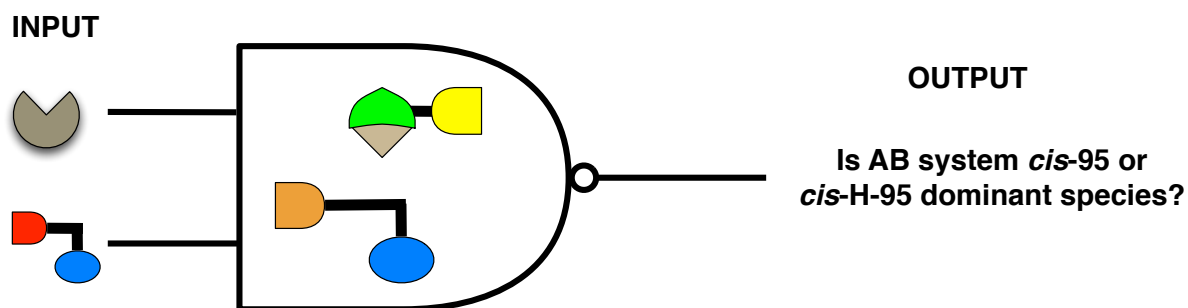
5.7 Interpretation of the pH switch reactions as NAND logic gate

In the last years, a large number of examples have appeared in the literature in which chemical entities perform binary logic operations.^[201-203] Most commonly, the synthetic targets are molecular switches which translate input stimuli into output signals. This

behaviour mimics the Boolean operations of traditional logic gates used in electronics which can be described in the binary code by using zeros and ones. A zero is used to indicate no input or no change in output of the system, a one describes a certain input and change of output of the system. Assembling the zeros and ones into a truth table specifies every Boolean function.

Our group has recently developed two examples of small synthetic networks of synthetic replicators that are capable of performing the logical OR operation.^[155,197] They respond to instructional input such that its output is an excess of one of the replicator whenever the input contains either or both of the minimal replicators. Presynthesised template was applied as input and selective response of the network was stimulated by intrinsically different geometric properties of the autocatalytic and crosscatalytic ternary complexes.

Blocked maleimide **H-72** and phenylacetic acid **71** can be taken as the centerpiece of a reaction network that can be interpreted on the basis of molecular logic. Using carboxy nitrene **70** and NEt₃ as input to the system allows for the construction of a NAND logic gate (**Scheme 5.5**).



Scheme 5.5 Design of a NAND logic gate with the AB reaction between maleimide **H-72** (yellow) and nitrene **71** (orange) as core interaction. NEt₃ (grey symbol) and carboxy nitrene **70** (red) function as input that generate a certain responds of the system stated as output.

For all four possible input combinations - none, both or one of the two inputs - the output of the system is monitored. In the case of this logic gate, the output is screened for whether AB systems *cis-95* or *cis-H-95* are the dominant species in the reaction mixture after 35000 seconds. Dominance *D* of the AB system in the product pool is therefore defined as

$$\text{Dominance } D = \frac{[AB]}{([AB] + [Y])} \times 100\%$$

with $[AB]$ as concentration of the AB product between maleimide **H-72** and nitron **71** and $[Y]$ as concentration of the second most abundant species. Only outputs for dominance D larger than 50% are taken as true 'one' values of the system. The individual experiments crucial for this logic gate are summarised in **Figure 5.12**.

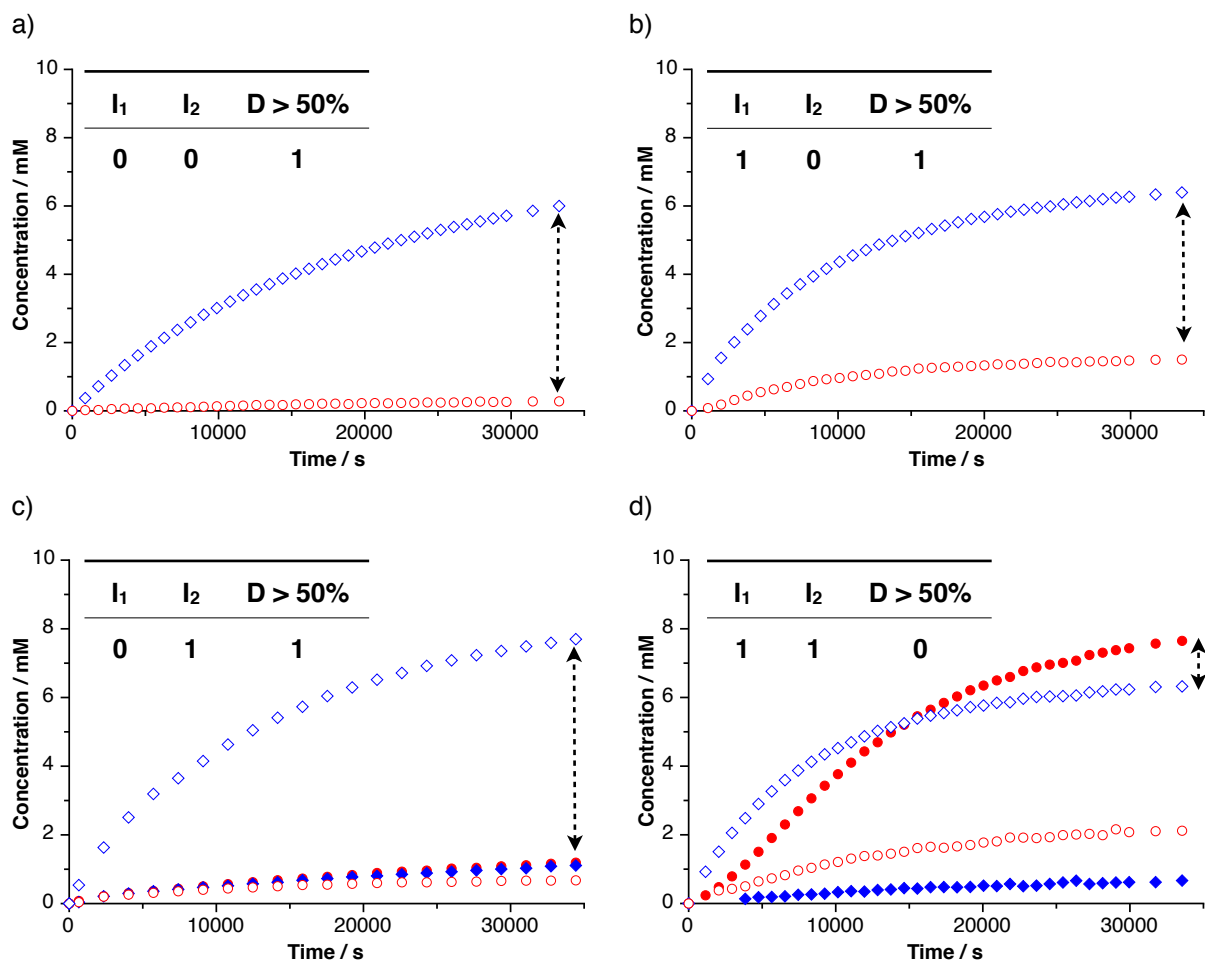


Figure 5.12 Individual analyses of the components of the NAND logic gate depicted in **Scheme 5.5**. Core reaction between maleimide **H-72** and phenylacetic acid nitron **71** a) without addition of any inputs (cf. **Figure 5.9a**), b) addition of NEt_3 as input I_1 (cf. **Figure 5.10a**), c) addition of carboxy nitron **70** as input I_2 (cf. **Figure 5.11b**) and d) addition of both NEt_3 and carboxy nitron **70** (cf. **Figure 5.11a**). Dashed arrows indicate the concentration difference of the two most abundant species used for the read-out of the system. The tables reflect the corresponding rows for the final truth table depicted in **Figure 5.13**.

The graph in **Figure 5.12a** shows the first 35000 seconds of the reaction between maleimide **H-72** and phenylacetic acid **71** in the absence of any inputs ($I_1=I_2=0$). Since *cis*-**H-95** is indeed the major product, a '1' is assigned to the output column. The addition of NEt_3 to the system ($I_1=1, I_2=0$) does not change the outcome of the reaction with *cis*-**H-95** still being the most abundant species (**Figure 5.12b**). Also the addition of nitron **70** ($I_1=0, I_2=1$) at the start of the reaction does not prevent *cis*-**H-95** to be the dominant product (**Figure 5.12c**). However, when both inputs, carboxy nitron **70** and NEt_3 , are present ($I_1=1, I_2=1$), the

dominance of *cis*-95 in the product pool is overcome by *trans*-94 and the output is marked as '0' (Figure 5.12d). It should be pointed out that for all experiments two equivalents of maleimide H-72 should be used with respect to all other components. This is not the case for the reactions depicted in the upper row of Figure 5.12, but it is obvious that doubling the amount of maleimide will not prevent *cis*-A to be the most abundant species.

The exact values for dominance D were calculated and combined to form the response diagram in Figure 5.13. The threshold value for D of 50% indicated by the dashed line is only under-run when both inputs are present. Furthermore, a truth table could be constructed from the individual experiments and confirmed that this set of building blocks is capable of acting in concert to perform the logical NAND operation in which the dominance of the AB system, *cis*-95 or *cis*-H-95, is only denied in the presence of both inputs.

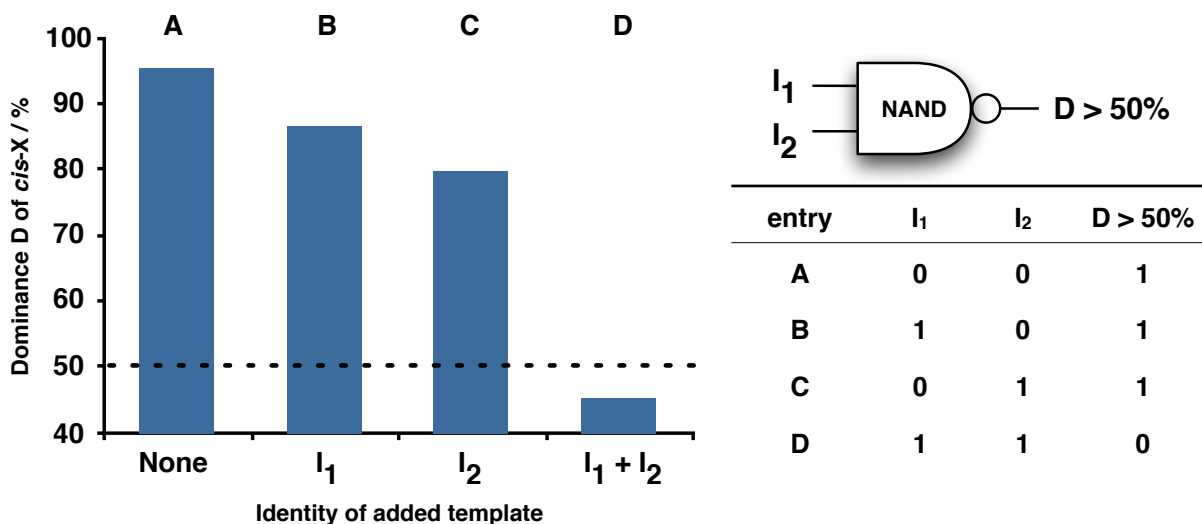


Figure 5.13 Overview of the individual reactions of the logical NAND operation. Dominance D is only above the threshold when both inputs I₁ and I₂ are present (lane D) otherwise the AB system is dominant (lanes A-C). The states of lanes A-D are indicated in the truth table. I₁ stands for input NEt₃ and I₂ stands for input nitrene 70.

This novel system is a further step to the development of more complex recognition-mediated reaction networks since it does not simply rely on the template-directed manipulation of a set of structurally similar self-replicators but incorporates a complex competition scenario between an AB system and a replicating system whose outcome proved highly susceptible to variation in the environmental pH. A combination of both approaches can potentially create and express even more complex programmed responses to various chemical inputs.

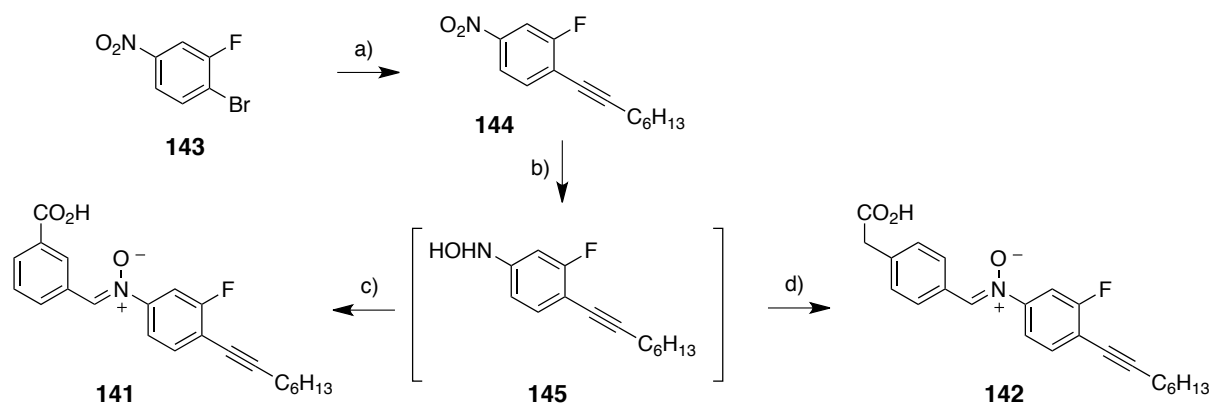
6. Replicating networks of three and more building blocks

6.1 Designing systems of increased complexity

In the last chapters, a set of structurally similar self-replicators were characterised and the effects of geometric changes in their backbone structure on their efficiency was established. Overall, five self-replicating systems of various strength have been analysed whereas one system was found to produce both, an AB system and a self-replicator. The target of this chapter is to develop situations in which two of these systems compete for a limited amount of common building blocks. Analysis of such experiments provides insight into how far a replicator's ability to compete with another system can be deduced directly from their efficiency in isolation or whether the interaction between both systems gives rise to unforeseen behaviour. Furthermore, the possibility of influencing the product distribution by adding informational template at the start of the reaction will be probed. Addition of preformed template to a reaction mixture of several components should enhance selectively the autocatalytic formation of more original template. This implies that the generation of other templates that rely on the same building blocks will be suppressed on the expense of the instructed template. In order to rationalise the obtained results, computational fitting of the experimental data will be conducted and the resulting kinetic model will be used to explore situations beyond practical feasibility.

6.2 Analytical requirements

All systems so far have been analysed using ^1H NMR spectroscopy. With increasing complexity of the mixtures, this proved to be insufficient as many of the system components have similar structural motifs. Spectra of such mixtures showed significant overlap for the characteristic ^1H NMR signals, especially in the region of the peaks for the three isoxazolidine protons between 4.1-6.3 ppm that was exploited extensively in the two component systems to follow the formation of product (section 10.2.1). In order to reduce the analytical effort, both original nitrene compounds **70** and **71** were equipped with a fluorine tag. With a wider ppm range and a higher resolution, ^{19}F NMR spectroscopy allows for the clear monitoring of the evolution of the product molecules not only in the case of the competition experiments but also with respect to the envisaged design of a multicyclic system.



Scheme 6.1 Synthesis of fluorine-tagged nitrones **141** and **142**. Conditions: a) 1-nonyne, Pd(PPh₃)₂Cl₂, CuI, PPh₃, 85 °C, 94%; b) Rh/C, NH₂NH₂, THF; c) 3-carboxybenzaldehyde, EtOH, -18 °C, 44% over two steps; d) **46**, EtOH, -18 °C, 48% over two steps.

Scheme 6.1 shows the synthesis of the new fluorine-tagged nitrones **141** and **142**. Starting from commercially available 1-bromo-2-fluoro-4-nitrobenzene **143**, Sonogashira reaction led to coupling product **144**. Partial reduction of **144** using rhodium as catalyst and hydrazine as hydrogen source yielded hydroxylamine **145** which was directly reacted with the appropriate aldehydes to form nitrones **141** and **142**.

Several other substituent pattern have been investigated, but the present design has proven to be a good compromise between minimising the electronic effect of the fluorine, maintaining the necessary degree of solubility and improving the analytical accuracy of the measurement. Putting the fluorine tag in *meta*-position to the nitrone functionality reduced its impact on the reactivity of the cycloaddition while keeping the acetylene group in *para*-position was found to prevent unfavourable steric interaction. For example, reversing both substituents created a situation in which the long chain of the acetylene group in *meta*-position caused some steric hindrance with respect to the reactive site and significantly reduced the efficiency of the self-replicators, whereas simply replacing the alkyl chain in the original nitrones **70** and **71** with a fluorine molecule caused severe problems with template solubility.

6.3 The reagent pool

Having eliminated eventual problems with the analysis of multicomponent replicating systems, the scope of the investigation was limited to a selected set of reagents. As laid out in chapter 3, combination of the two nitrones with three maleimides gave rise to the formation of six systems with recognition-mediated activity. Excluding benzofuran maleimide **73** for its central position in reactivity, a pool of two maleimides (**72** and **74**) and two nitrones (**141** and **142**) was defined as the source for the envisaged competition scenarios (**Figure 6.1**). Within

this pool, two highly efficient self-replicators (*trans*-146 and *trans*-149), one significantly weaker replicating system (*trans*-147) and an AB system (*cis*-148) with minor self-replicating contribution from its *trans*-isomer can be found allowing for a number of interesting competition combinations.

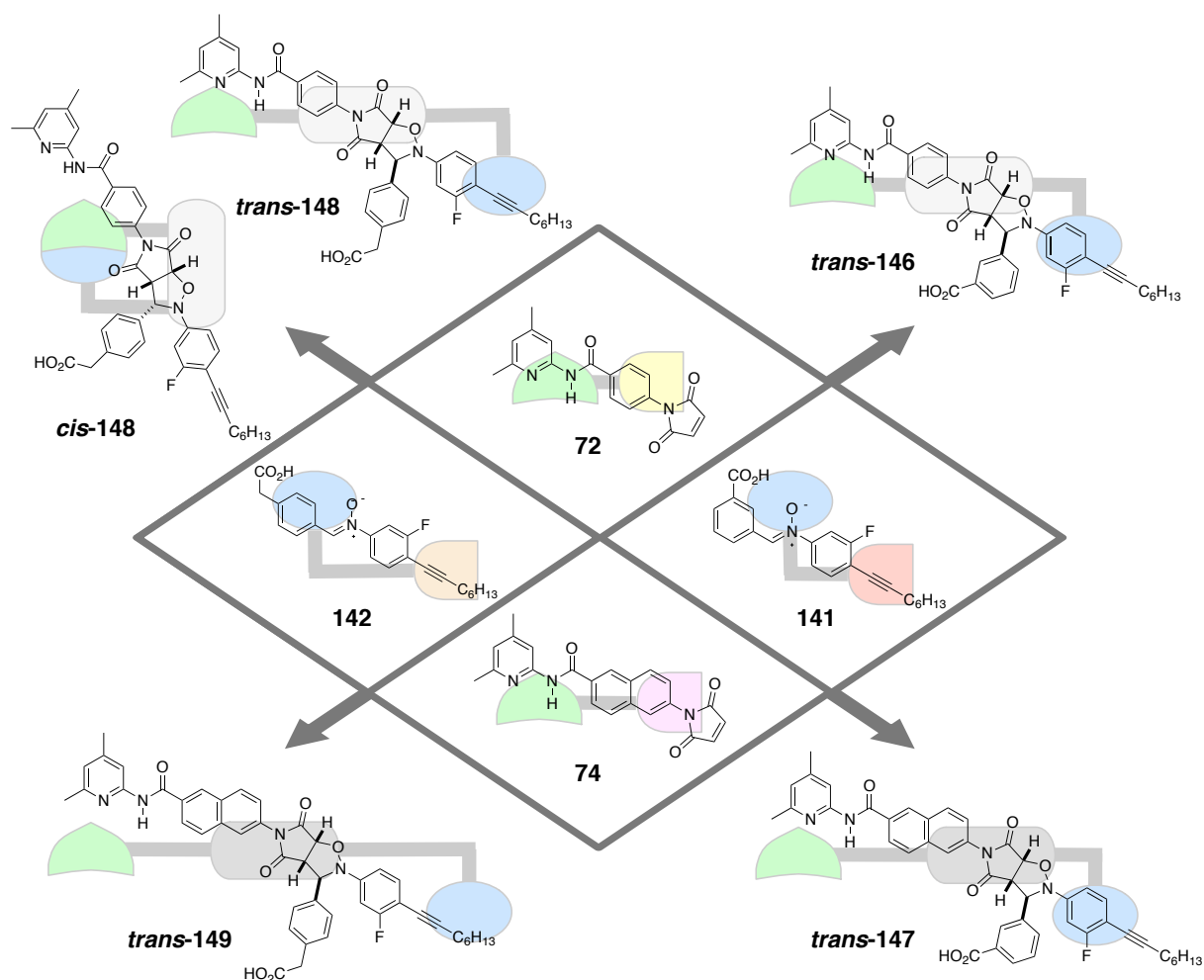


Figure 6.1 Reagent pool for the development of competition scenarios between recognition-mediated systems. From the set of four components (72, 74, 141 and 142) a set of five products can be generated by four replicating (*trans*-146, *trans*-147, *trans*-148 and *trans*-149) and one AB pathway (*cis*-148). In the cartoon structures, recognition sites are blue (acid) and green (amidopyridine). Cycloadducts deriving from maleimide 72 are depicted as light grey whereas products of maleimide 74 are depicted dark grey.

Alternatively leaving out one of the components from the pool leads to four sets of three component systems. Using an equimolar amount of the three remaining building blocks generates a two-fold excess for either the nitrones or the maleimides, and renders the other species as the limiting building block. For example, leaving out maleimide 74 creates a scenario in which both nitrones compete for a limited amount of benzene maleimide 72. In order to allow for a comparable analysis of all four systems, a common procedure was

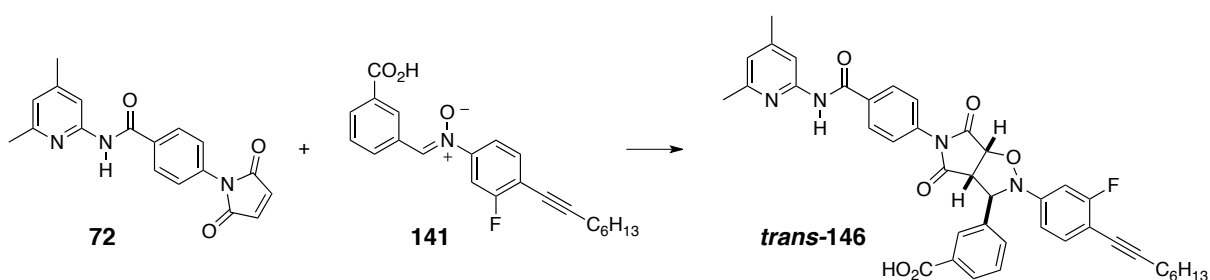
established. First, the outcome of the native competition experiment is monitored to establish a base value for the final product distribution. Addition of presynthesised template is then conducted to favour the formation of the instructed template. Comparison of the outcome of the instructed reactions with the native values should establish whether template addition has the expected impact on the efficiencies of the participating systems.

6.4 Individual analysis of the replicators with fluorine tags

Computational fitting of the experimental data presented in chapter 3 allowed to extract valuable kinetic parameters for each system and helped to establish a clear hierarchy in replicating efficiency. Since the insertion of the fluorine into **141** and **142** changed the electronic nature of the nitron compounds, their native reactions with both maleimides was repeated and the experimental data was fitted using SimFit.

6.4.1 Reaction of maleimide **72** with nitron **141**

Maleimide **72** and nitron **141** giving self-replicating template *trans*-**146** were reacted for 16 h at 0 °C with a starting concentration of 10 mM (**Scheme 6.2**). Deconvolution of the recorded ¹H NMR spectra allowed for the construction of the concentration *vs* time profile depicted in **Figure 6.2**.



Scheme 6.2 Reaction of maleimide **72** with nitron **141** to give self-replicator *trans*-**146**.

The obtained data was fitted using SimFit (solid line in **Figure 6.2**) and the extracted kinetic values are presented in **Table 6.1**. It can clearly be seen that introduction of the fluorine tag has only very little effect on the efficiency of the replicator. The effective molarity decreased slightly to 58.8 M from 69.8 M for non-fluorinated *trans*-**94** and the free energy of connection increased from a previous 11.9 kJ mol⁻¹ by 1.4 kJ mol⁻¹ to 13.3 kJ mol⁻¹ indicating a slightly more stable product duplex.

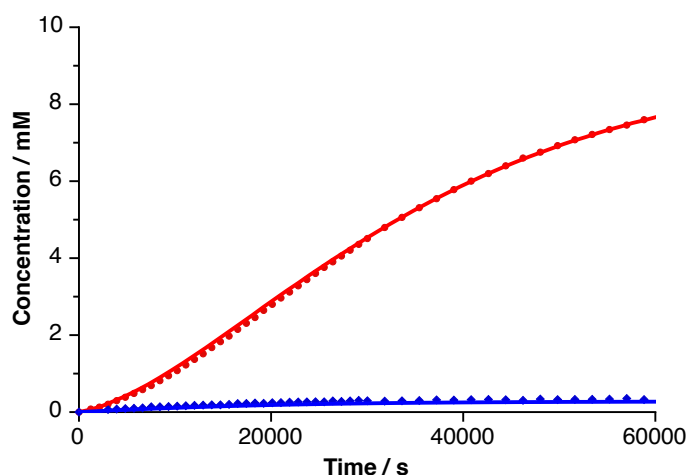


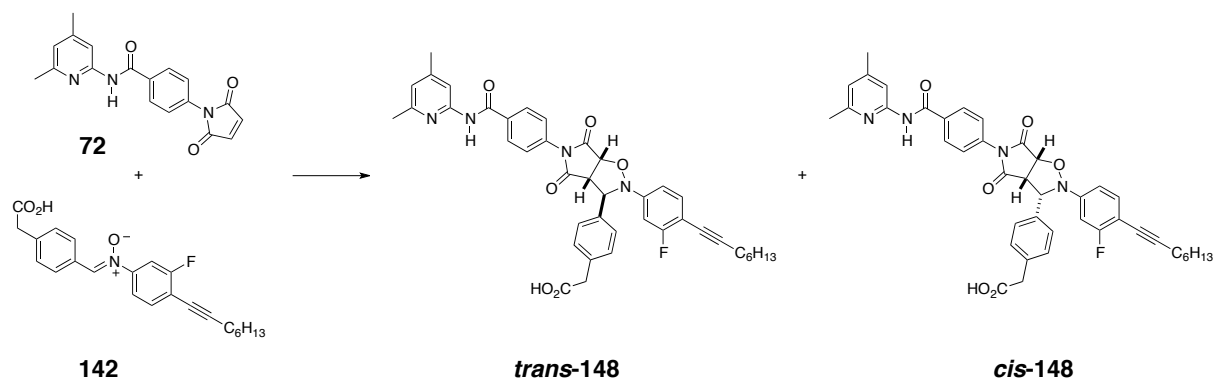
Figure 6.2 Concentration *vs* time profile for the reaction of maleimide **72** and nitrone **141** to give template **146**. The formation of *trans*-product is shown as red filled circles and the formation of *cis*-product as blue filled diamonds. Straight lines represent the results for the fitting of the *trans*-(-) and *cis*-(-) product. The reaction was performed at 0 °C in CDCl₃ at 10 mM reagent concentration.

Table 6.1 Kinetic parameters extracted for the self-replicating reaction of maleimide **72** and nitrone **141** at 0 °C in CDCl₃ at 10 mM reagent concentration using SimFit. The obtained R-value was 2.7%.

	<i>trans</i> - 146	<i>cis</i> - 146
bimolecular rate constant / M ⁻¹ s ⁻¹	2.45 × 10 ⁻⁴	1.25 × 10 ⁻⁴
recognition-mediated rate constant / s ⁻¹	1.44 × 10 ⁻²	-
effective molarity / M	58.8 (<i>cf.</i> 69.8 for <i>trans</i> - 94)	-
Δ <i>G</i> [‡] / kJ mol ⁻¹	13.3 (<i>cf.</i> 11.9 for <i>trans</i> - 94)	-

6.4.2 Reaction of maleimide **72** with nitrone **142**

Consequently, the reaction between maleimide **72** and nitrone **142** was investigated at 0 °C and 10 mM concentration of starting material (**Scheme 6.3**). The progress of the reaction was followed for 16 h and the recorded ¹⁹F NMR spectra was deconvoluted to construct the concentration *vs* time profile shown in **Figure 6.3**. Comparing this rate profile with the one for template **95** from **Figure 3.7** shows that introduction of the fluorine alters the outcome of the reaction. In the previous experiment, 2.77 mM *trans*-**95** and 5.69 mM *cis*-**95** were formed after 16 h giving a *cis/trans* ratio of 2.1:1. Using fluorine tagged nitrone **142** yielded 2.16 mM *trans*-**148** and 6.25 *cis*-**148** increasing the ratio to 2.9:1 after the same time. For both reactions the conversion was 84%.



Scheme 6.3 Reaction of maleimide **72** with nitron **142** to give self-replicating template *trans*-**148** and AB system *cis*-**148**.

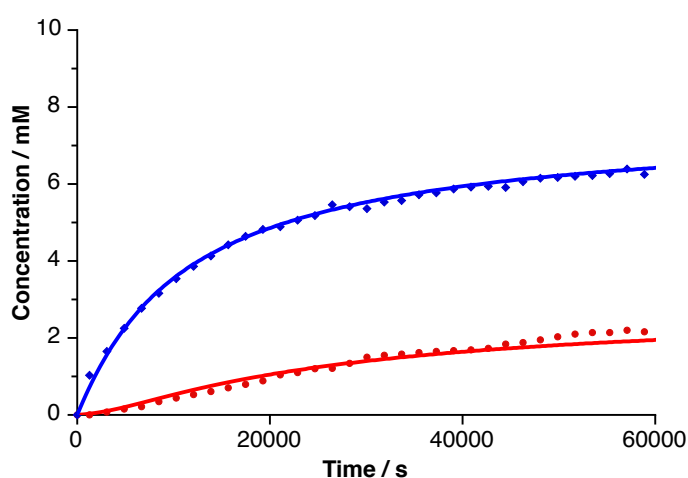


Figure 6.3 Concentration *vs* time profile for the reaction of maleimide **72** and nitron **142** to give template **148**. The formation of *trans*-product is shown as red filled circles and the formation of *cis*-product as blue filled diamonds. Straight lines represent the results for the fitting of the *trans*-(-) and *cis*-(-) product. The reaction was performed at 0 °C in CDCl₃ at 10 mM reagent concentration.

The solid lines in **Figure 6.3** reflect the best fit to the experimental data using SimFit. The corresponding kinetic values are listed in **Table 6.2**.

Table 6.2 Kinetic parameters extracted for the self-replicating reaction of maleimide **72** and nitron **142** at 0 °C in CDCl₃ at 10 mM reagent concentration using SimFit. The obtained R-value was 2.1%.

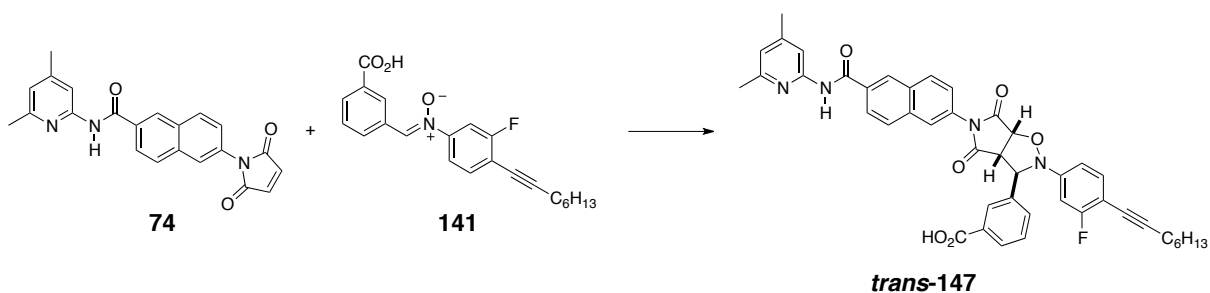
	<i>trans</i> - 148	<i>cis</i> - 148
bimolecular rate constant / M ⁻¹ s ⁻¹	1.84 × 10 ⁻⁴	1.03 × 10 ⁻⁴
recognition-mediated rate constant / s ⁻¹	4.27 × 10 ⁻⁴	7.65 × 10 ⁻⁵
effective molarity / M	2.32 (<i>cf.</i> 26.5 for <i>trans</i> - 95)	0.743 (<i>cf.</i> 0.683 for <i>cis</i> - 95)
Δ <i>G</i> ^s / kJ mol ⁻¹	-8.99 (<i>cf.</i> 4.88 for <i>trans</i> - 95)	-

Introduction of the fluorine group induces only minor changes in the efficiency of the AB system. The effective molarity has increased slightly to 0.743 M from 0.683 M for *cis*-95 (Table 3.2). On the other hand, values for the self-replicating template *trans*-148 are dramatically different than for *trans*-95. The effective molarity has dropped from 26.5 M for non-fluorinated *trans*-95 to 2.32 M and the free energy of connection has decreased by almost 14 kJ mol⁻¹ to a negative value of -8.99 kJ mol⁻¹ indicating negative cooperativity for the product duplex.

It should be pointed out that the effective molarity of the AB system is indeed lower than for the self-replicator even though its enhancement is higher. This counterintuitive observation can be explained by the relative differences in reactive complex that leads to the products. The concentration of the binary AB complex is naturally higher than for the ternary complex necessary for the formation of the autocatalyst. With the rate of the reaction being proportional to the rate constant and the concentration of the reactive complex, the high concentrations of binary complex counterbalance the low effective molarity and renders the AB system the dominant species over its self-replicating partner.

6.4.3 Reaction of maleimide 74 with nitron 141

Next, the reaction between maleimide 74 and nitron 141 at 10 mM concentration was monitored for 40 h at 0 °C (Scheme 6.4). Deconvolution of the recorded ¹⁹F NMR spectra gave rise to the concentration *vs* time profile shown in Figure 6.4. The longer reaction time is a result of the low reactivity of self-replicator *trans*-147.



Scheme 6.4 Reaction of maleimide 74 with nitron 141 to give self-replicating template *trans*-147.

The solid lines in Figure 6.4 reflect the best fit to the experimental data using SimFit. Table 6.3 gives the extracted kinetic values for the formation of 147. The value for the effective molarity has slightly dropped to 0.25 M from a previous 1.30 M for non-fluorinated *trans*-98 (Table 3.5). The negative value of -1.36 kJ mol⁻¹ for the free energy of connection

now suggests a somewhat negative cooperativity for the template duplex. These findings indicate that the addition of the fluorine slightly reduces the self-replicating activity of *trans*-147 with respect to non-tagged template *trans*-98.

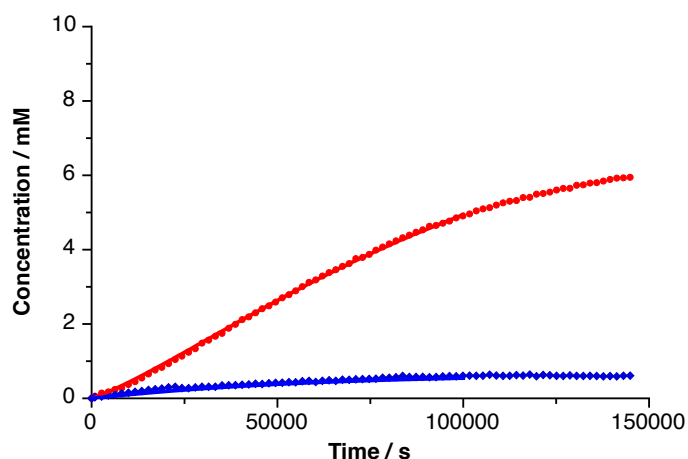


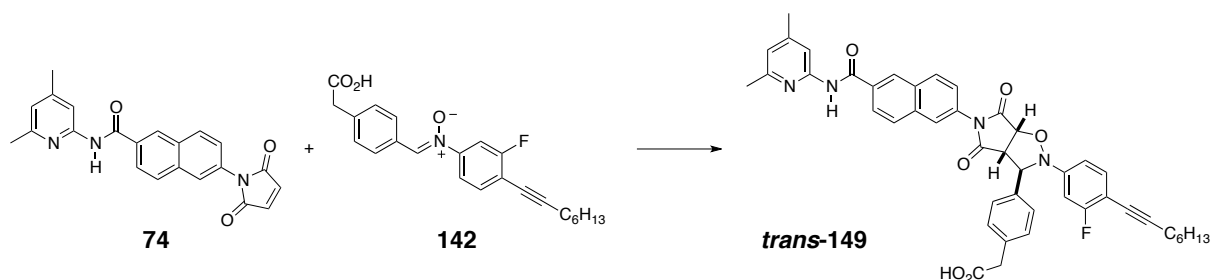
Figure 6.4 Concentration *vs* time profile for the reaction of maleimide **74** and nitrone **141** to give template **147**. The formation of *trans*-product is shown as red filled circles and the formation of *cis*-product as blue filled diamonds. Straight lines represent the results for the fitting of the *trans*-(-) and *cis*-(-) product. The reaction was performed at 0 °C in CDCl₃ at 10 mM reagent concentration.

Table 6.3 Kinetic parameters extracted for the self-replicating reaction of maleimide **74** and nitrone **141** at 0 °C in CDCl₃ at 10 mM reagent concentration using SimFit. The obtained R-value was 1.9%.

	<i>trans</i> -147	<i>cis</i> -147
bimolecular rate constant / M ⁻¹ s ⁻¹	3.47 × 10 ⁻⁴	1.19 × 10 ⁻⁴
recognition-mediated rate constant / s ⁻¹	8.68 × 10 ⁻⁵	-
effective molarity / M	0.25 (<i>cf.</i> 1.30 for <i>trans</i> -98)	-
Δ <i>G</i> ^s / kJ mol ⁻¹	-1.36 (<i>cf.</i> 2.67 for <i>trans</i> -98)	-

6.4.4. Reaction of maleimide **74** with nitrone **142**

The last combination from the pool of four compounds is self-replicating system *trans*-149 based on the cycloaddition between maleimide **74** and nitrone **142** (Scheme 6.5). Their reaction at 10 mM reagent concentration was followed by ¹⁹F NMR spectroscopy for 16 h at 0 °C. Deconvolution of the obtained spectra resulted in the concentration *vs* time profile depicted in Figure 6.5.



Scheme 6.5 Reaction of maleimide **74** with nitron **142** to give self-replicating template *trans*-**149**.

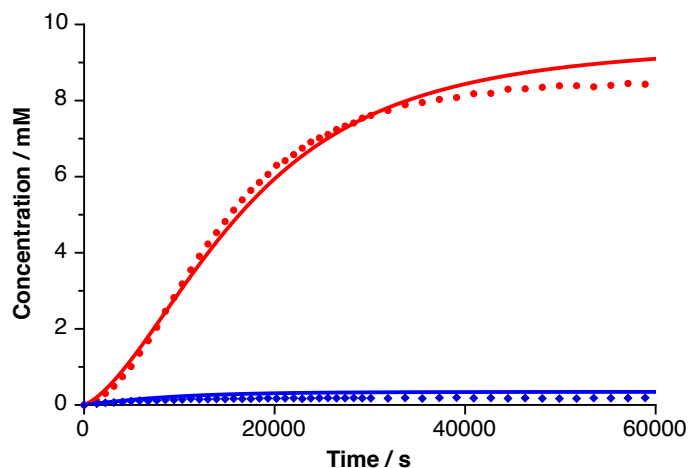


Figure 6.5 Concentration *vs* time profile for the reaction of maleimide **74** and nitron **142** to give template **149**. The formation of *trans*-product is shown as red filled circles and the formation of *cis*-product as blue filled diamonds. Straight lines represent the results for the fitting of the *trans*-(-) and *cis*-(-) product. The reaction was performed at 0 °C in CDCl₃ at 10 mM reagent concentration.

Table 6.4 Kinetic parameters extracted for the self-replicating reaction of maleimide **74** and nitron **142** at 0 °C in CDCl₃ at 10 mM reagent concentration using SimFit. The obtained R-value was 5.2%.

	<i>trans</i> - 149	<i>cis</i> - 149
bimolecular rate constant / M ⁻¹ s ⁻¹	6.99 × 10 ⁻⁴	3.06 × 10 ⁻⁴
recognition-mediated rate constant / s ⁻¹	1.57 × 10 ⁻²	-
effective molarity / M	22.5 (<i>cf.</i> 23.6 for <i>trans</i> - 99)	-
Δ <i>G</i> [‡] / kJ mol ⁻¹	9.46 (<i>cf.</i> 9.43 for <i>trans</i> - 99)	-

The obtained data was fitted using SimFit (solid line in **Figure 6.5**) and the extracted kinetic values are presented in **Table 6.4**. The poor fit towards the end of the measurement is a consequence of beginning precipitation of the template. It can however be seen that

introduction of the fluorine tag has only very little effect on the efficiency of the replicator. The effective molarity of the reaction and the value of the free energy of connection remain nearly the same when compared with the formation of *trans*-99 (Figure 3.20 and Table 3.6).

6.4.5 Comparison of the fluorinated systems and influence of the tag

Analysis of the individual systems shows a certain pattern for the influence of the fluorine tag on the efficiencies of the recognition-mediated processes. The impact on the strong replicators *trans*-146 and *trans*-149 was relatively small whereas the kinetic values for *trans*-147 were altered to some extent. The biggest differences occurred for the hybrid system of 148 giving rise to a mixture of both diastereoisomers.

Overall, it can be seen that the matching combinations between 'short' benzene maleimide 72 with carboxy nitrone 141 and 'long' naphthalene maleimide 74 with phenylacetic acid nitrone 142 that give rise to very efficient replicating systems are least effected by the introduction of the fluorine tag. The 'mismatch' situation between maleimide 74 and nitrone 141 leading to replicator *trans*-147 responds more strongly to the electronic shift induced by the tag than the other two self-replicators. The biggest differences are found for the internal competition between replicator *trans*-148 and AB system *cis*-148. It was shown before that the efficiencies of the two competing systems are more sensitive to variations than in systems that show recognition-mediated activity for only one of the isomers. Since the formations of both isomers are directly connected, a change in reactivity for the AB system also has an impact on the performance of the self-replicator and *vice versa*.

6.5 Competition scenarios

Choosing three out of the four reagents from the pool shown in Figure 6.1 opens up the possibility to generate situations in which two building blocks compete for a limited amount of a third species. In the following sections, a systematic investigation of all four possible systems was performed to elucidate the major principles of such competition scenarios and the possibility to influence the outcome with instructional template.

6.5.1 System I: benzene maleimide 72 with nitrones 141 and 142

Excluding maleimide 74 leads to the system depicted in Figure 6.6. Maleimide 72 is the common building block for the formation of AB system *cis*-148 with nitrone 142 and self-replicating system *trans*-146 using nitrone 141.

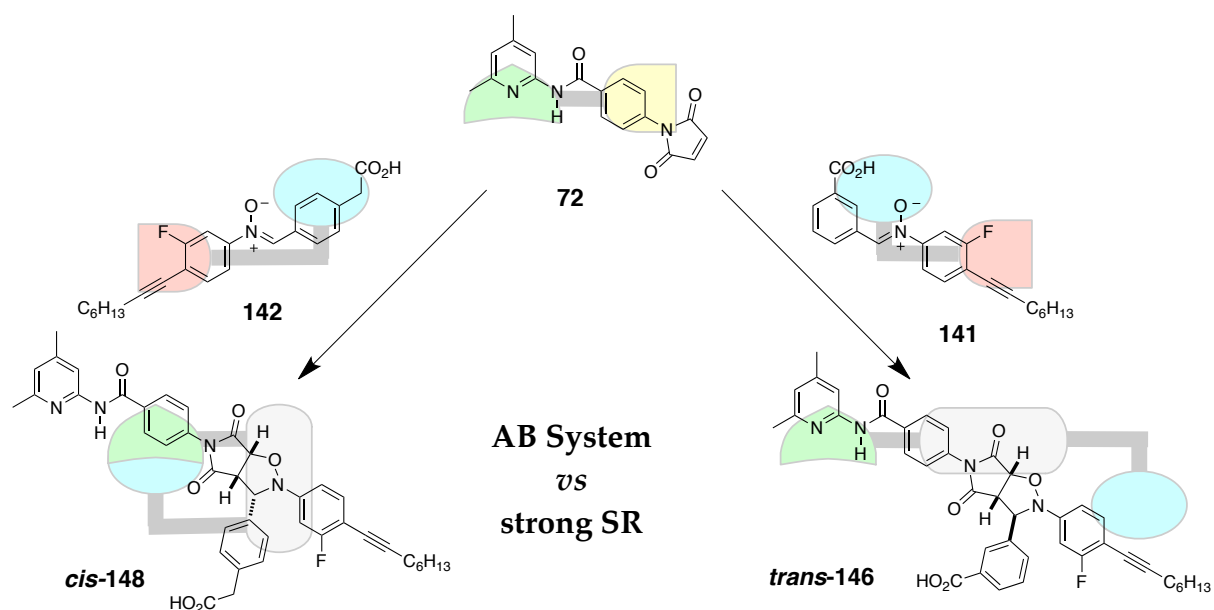


Figure 6.6 Competition scenario with maleimide **72** as limiting building block. Its reaction with phenylacetic acid **142** and carboxy nitron **141** gives rise to AB system *cis*-**148** and self-replicator *trans*-**146**, respectively. Self-replicating isomer *cis*-**148** which is usually formed in minor extent was omitted for clarity.

The reaction between an equimolar amount of all three components provides an excess of nitrones and renders the maleimide to be the limiting building block. Having established the differences in behaviour for an AB system and a self-replicator, dominance of *cis*-**148** in the product pool was expected. The maximum rate for the formation of *cis*-**148** via the binary AB complex is at the start of the reaction. On the other hand, the self-replicator reaches its maximum rate only after a lag period and is therefore disadvantaged in the quest for resources. The same holds for *trans*-**148** that acts as a weak self-replicator and is expected to be formed to minor degree as third product.

Kinetics of the native reaction were recorded at 0 °C for 12 hours in CDCl₃ with 10 mM concentration for all three reagents and deconvoluted using ¹⁹F NMR spectroscopy (Figure 6.7a). At the end of the measurement, 80% of maleimide was converted into products. The progression of each of the three major products exhibits the characteristic curve. *Cis*-**148** was found to be the most abundant species and its formation showed a line shape typical for an AB system. The rate of formation was highest at the start of the reaction when the concentrations of both required building blocks was highest. As soon as maleimide **72** became less available, the concentrations of reactive binary complex decreased and the curve flattened significantly.

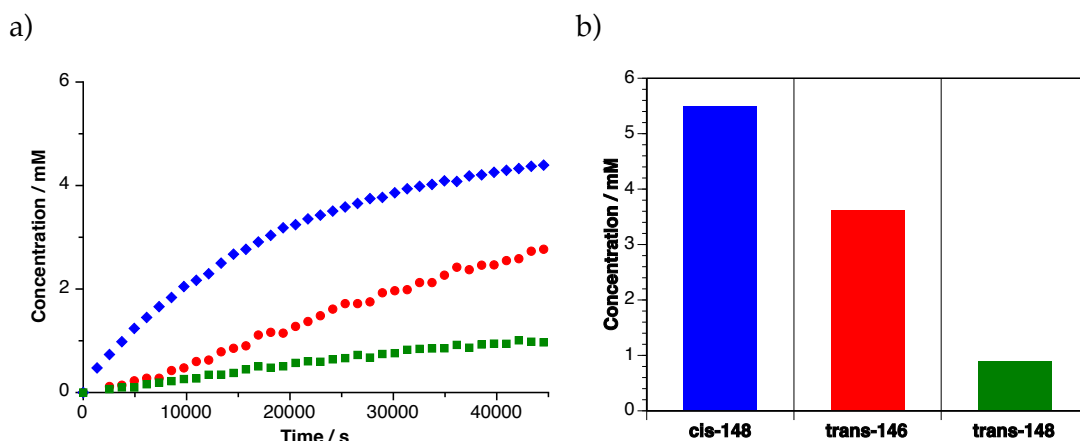


Figure 6.7 a) Concentration *vs* time profile for the reaction between maleimide **72** with nitrone **141** and **142** to give *cis*-**148** (◆), *trans*-**146** (●) and *trans*-**148** (■) monitored by ^{19}F NMR spectroscopy. The reaction was performed in CDCl_3 at 0°C and with 10 mM reagent concentration. b) Detection of the final product distribution after full conversion of maleimide **72**.

The differences in progression for self-replicating template *trans*-**146** are apparent. At the early stage of the reaction, the characteristic lag period is visible and it is only after sufficient amount of template has been formed in the bimolecular reaction that the self-replicating mechanism starts to drive the reaction. In the meantime, the AB system has availed itself of maleimide **72** which hampered significantly the growth of the self-replicator.

Self-replicator *trans*-**148** was identified as the third product in this competition experiment. As expected, it shows to be inferior to its two rivals and was only formed in minor amount since it has to compete for both of its building blocks. Despite the low concentration, a sigmoidal shape for the formation of *trans*-**148** is visible. Altogether, a clear ranking in reactivity can be seen for the three competing systems with the AB system being the strongest. Monitoring the product distribution after full conversion of maleimide using ^{19}F NMR spectroscopy established the product distribution as 5.49 mM *cis*-**148**, 3.61 mM *trans*-**146** and 0.90 mM *trans*-**148** (Figure 6.7b). Compared with the reaction of maleimide **72** and phenylacetic acid **142** in isolation that yields the AB system in 2.9-fold excess, the ratio of isomers for **148** is now 4:1 in favour for the *cis*-species since the self-replicator has not only to compete for the maleimide building block but also for the nitrone.

As established in chapter 2, it should be possible to influence the product distribution by adding preformed self-replicating template at the start of the reaction which shifts the maximum rate of the doped species, eliminates the unprofitable lag period and strengthens the performance of the seeded template. In order to verify the possibility of giving the self-replicator a head start, a set of additional experiments were conducted. An equimolar amount of maleimide **72** with both nitrones at 10 mM concentration were incubated in 800 μL CDCl_3 at 0°C together with 9, 18 and 36 mol-% of preformed *trans*-**146** and kept until

full conversion of the maleimide (**Figure 6.8**). Analysis of the ^{19}F NMR spectra established the product ratio which was compared with the one of the native experiment (**Figure 6.7b**). In this case, ^1H NMR spectroscopy could additionally be used to calculate the final concentrations and satisfyingly provided nearly identical values.

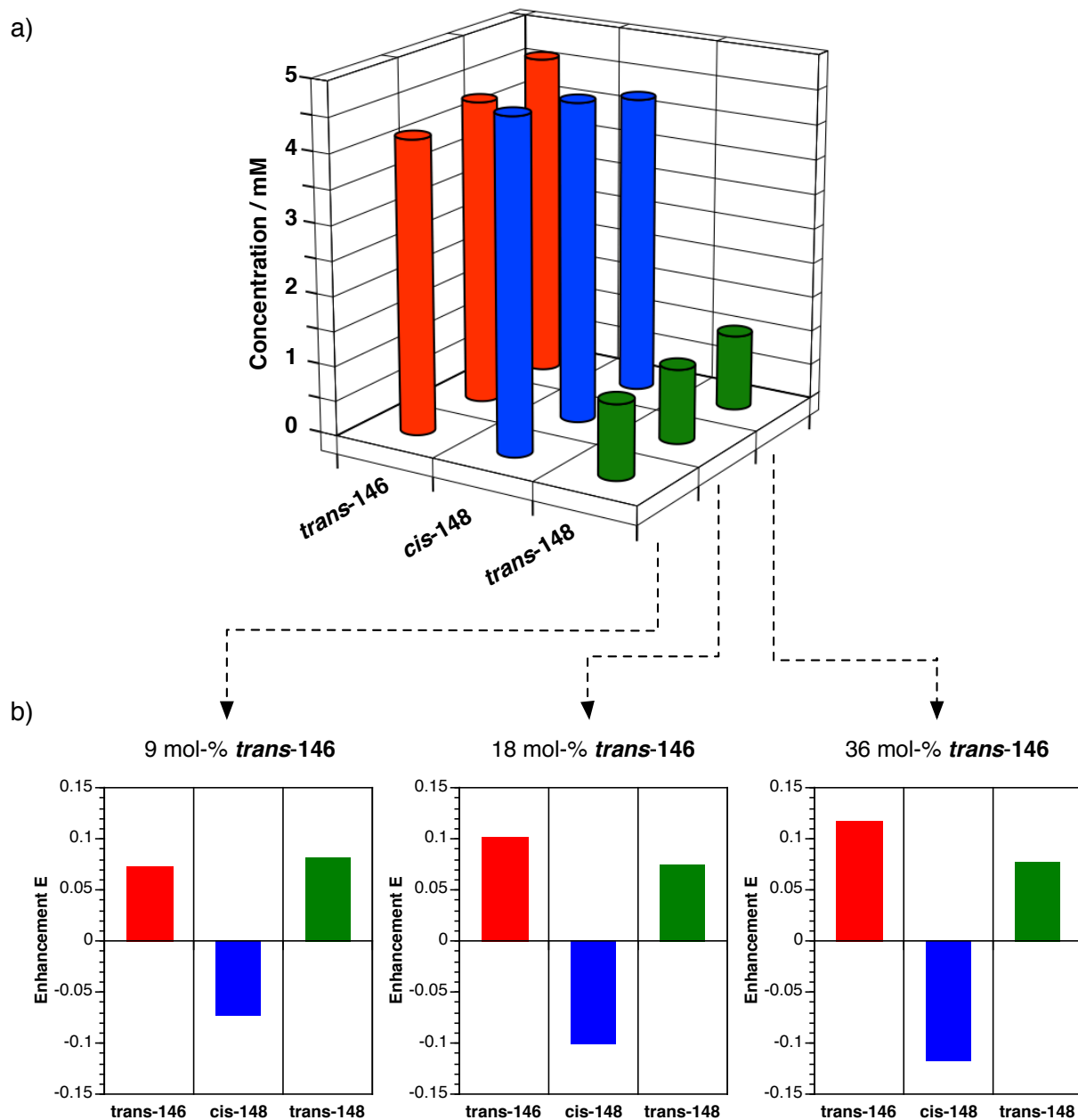


Figure 6.8 Product distributions for the reaction between maleimide **72** with nitrone **141** and **142** to give *cis*-**148**, *trans*-**146** and *trans*-**148** in the presence of 9 mol-%, 18 mol-% and 36 mol-% *trans*-**146** template monitored by ^{19}F NMR spectroscopy. In a) the final product concentration after full conversion of maleimide **72** is depicted. Section b) shows the enhancements with respect to the native reaction from **Figure 6.7**. All reactions were performed at 0 °C in CDCl_3 at 10 mM reagent concentration.

In order to highlight the effect of the doping process, values for the enhancement E were calculated as

$$E = \log_{10} \left(\frac{c_{doping}}{c_{native}} \right)$$

with c_{doping} and c_{native} being the final concentration of one of the three products in the doping and native experiment, respectively.

From the diagrams in **Figure 6.8**, it can instantly be seen that addition of preformed template indeed changed the product distribution towards self-replicator *trans*-146. With 9 mol-% template at the start of the reaction, the final ratio of *cis*-148 to *trans*-146 had nearly equalled. When adding more template, *trans*-146 eventually became the dominant species. This finding is further clarified in the graphs showing the relative enhancement for each template. Addition of 9 mol-% significantly decreased the formation of *cis*-148 and elevated the proportion for both self-replicators. The increase in concentration of *trans*-148 is a direct consequence of the suppression of *cis*-148. With the AB system being less strong, more nitrene building block is available to the self-replicator. As a consequence of the logarithmic term for the calculation of the enhancement factor and since it is formed only in minor amounts in the native reaction, the small increase in concentration for *trans*-148 in the doping experiments caused a relatively high value for the enhancement.

In the presence of more *trans*-146 template, the initial trends are even more pronounced. However, increasing the amount of template from 18 to 36 mol-% had a somewhat smaller impact on the product distribution indicating the presence of a saturation point at which addition of more template does not alter the outcome of the reaction. It is nevertheless important to note that in this multicomponent system, adding template at the start of the reaction did indeed increase the formation of the self-replicating species. In the isolated experiment, only small amounts of template were necessary to overcome the lag period and move the maximum rate of the reaction to its start. Addition of an increasing amount of template generally had no effect on the position and absolute value of the maximum rate (an exception is discussed in 3.4.5). This finding can be rationalised by considering the concentrations of all productive ternary complexes in the reaction mixture for the native two component replicators. In the absence of any competing third component, the maximum rate for a self-replicator corresponds with the maximum in concentration for the catalytically active ternary complex which is directly proportional to the amount of free

template. Addition of template thus shifts this maximum to the start of the reaction by instantly creating a high concentration of the ternary complex. However, increasing the amount of dopant does indeed increase the amount of reactive complex, but it is now the cycloaddition reaction that becomes rate-limiting. In the presence of a third recognition-enabled component, an equilibrium between all possible ternary complexes is established. In this scenario, the added template does not only favour the formation of the instructed ternary complex but it also decreases the concentration of undesired or unproductive complexes. Increasing continuously the amount of dopant shifts the equilibrium towards the desired ternary complex, thereby favouring the formation of the intended template.

6.5.2 Fitting and simulation

The experimental results presented in **Figure 6.8** clearly prove that the competition reaction between AB system *cis-148* and the two self-replicators, *trans-148* and *trans-146*, can be influenced by the addition of instructional template. Seeding the reaction mixture with increasing amounts of preformed *trans-146* stimulated the autocatalytic formation of more template on the expense of the other systems. With these experimental results at hand, turning to simulation should provide an insight into how far the behaviour of the system can be predicted from the behaviour of the simple individual components.

Fitting of the individual systems provided the kinetic parameters necessary for the simulation of the scenario using the ISOSIM mode of the SimFit package. The scripts used for the fitting of the experimental data for replicator *trans-146* and AB/SR hybrid system **148** were combined under consideration of all combinatorial interactions between the three building blocks and their template products (see appendix). Using this script, the native competition reaction between maleimide **72** and nitrones **141** and **142** and four situations with added *trans-146* (9, 18, 36 and 100 mol-%) were simulated.

The results of the calculation are depicted in **Figure 6.9** together with the experimental data. In addition to the three products observed in the reaction, the calculations provided values for the *cis*-diastereoisomer of **146** which was formed to minor extent (around 0.2 mM). It can be seen that the calculation matches quite well the experimental results for the reaction without template addition (0 mol-% *trans-146*). The concentrations for both diastereoisomers of **148** diverge less than 0.1 mM from their experimental values whereas the calculated concentration for *trans-146* was 0.46 mM short of the one found in the experiment. This difference can be explained partially by the fact, that the contribution of *cis-146* is neglected in the experiment. Altogether, the developed script allows for a reliable

simulation of the native competition scenario reproducing the correct ranking order of products. However, the features of the doping experiments using increasing amounts of *trans*-146 are only captured to some extent by the simulation. Data was simulated with 9, 18, 36 and 100 mol-% of added *trans*-146 to generate the solid lines in **Figure 6.9**. In the competition scenario, addition of *trans*-146 resulted in an autocatalytic increase of the seeded template whereas the concentration of the main competitor, *cis*-148, was gradually reduced. Even though the progression for *trans*-146 and *cis*-148 is reflected correctly in the simulation, the gradients for the curves clearly underestimate the influence of the template on the outcome of the competition scenario. In the simulation, the crossing point at which the concentrations of *trans*-146 and *cis*-148 are equal occurs for the addition of around 50 mol-% *trans*-146 whereas the same point is reached in the experiment for the addition of less than 18 mol-% *trans*-146 template. This shortcoming can largely be attributed to the low gradient for the progression of *trans*-146 and the systematic error for the values of self-replicator *trans*-146 for the simulation.

Moreover, the simulated formation for *trans*-148 does not correspond with the experimental data. With the concentration of *cis*-148 gradually decreasing in the competition reactions, more phenylacetic acid nitrone **142** becomes available and the formation of *trans*-148 should be slightly up-regulated. In the simulation, the final concentration of *trans*-148 decreases with increasing amounts of added template.

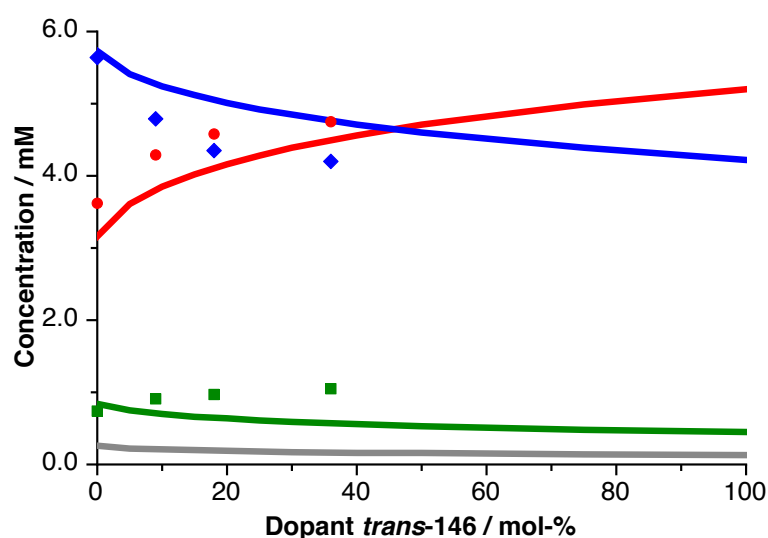


Figure 6.9 Simulation of the competition scenario between maleimide **72** and nitrones **141** and **142** to give templates *trans*-146 (–), *cis*-146 (–), *trans*-148 (–) and *cis*-148 (–) with increasing amounts of *trans*-146 template added at the start of the reaction. Experimental values for *trans*-146 (●), *trans*-148 (■) and *cis*-148 (◆) as in **Figure 6.8**.

Altogether, simulation of the competition scenario could reproduce the experimental results to some extent. The gross behaviour of the two major products, *trans*-146 and *cis*-148, was interpreted correctly even though the absolute concentration values diverge from the experiment, whereas the progression of *trans*-148 is not reproduced correctly in the simulation. The reason for these shortcomings can be found in the kinetic model which is based on the assumption that all reaction constants k and association constants K are equal to the ones found for the individual interactions. If the topology of the novel reaction network was a mere superimposition of the individual systems, this approach would be successful. Best results are indeed obtained for the native competition scenario in which the reaction was performed without addition of template and conditions seem to be coherent with the individual systems. However, in the presence of preformed template, unpredictable system-level behaviour gives rise to more complex interconnections between the components. As a consequence of this emergence, the reaction network appears to be more susceptible to the addition of preformed template producing larger amounts of *trans*-146.

The results presented here imply that even relatively simple systems with only three components become increasingly difficult to comprehend if the interconnections between the entities give rise to behaviour that cannot be deduced readily from the behaviour of the individual simple components. Even though all kinetic parameters for the individual systems were at hand, it was not possible to foresee the implication of the emergent properties and to include this knowledge into the development of a kinetic model that allowed for the successful simulation of the experimental results.

Since the kinetic model applied in the simulation of the experimental results reflected the gross behaviour of the system, it can be used as a basis to explore scenarios that are not directly accessible in the laboratory. Reacting maleimide 72 with nitrene 142 gave rise to a diastereoisomeric mixture of 148. Since the isomers could not be separated by column chromatography to furnish a clean sample of *trans*-148, it was not possible to investigate experimentally the influence of this autocatalytic template on the outcome of the competition reaction. Turning to simulation furnished the graph depicted in **Figure 6.10** in which the response of the system to increasing amounts of *trans*-148 is highlighted. It can clearly be seen that the autocatalytic enhancement of *trans*-148 is very pronounced. Addition of 5 mol-% preformed template nearly tripled the concentration for *trans*-148 from a previous 0.8 mM in the native reaction to 2.1 mM. At dopant concentrations larger than 40 mol-%, *trans*-148 becomes the most abundant species reaching a total concentration of around 4.8 mM for the addition of 100 mol-% template. Concomitantly, after addition of one equivalent of template, the concentrations for *cis*-148 and *trans*-146 were reduced by 2.6 mM and 1.3 mM,

respectively. Bearing in mind that the influence of the seeded template was underestimated in the simulations of the scenario discussed above, the response of the real system might be even higher.

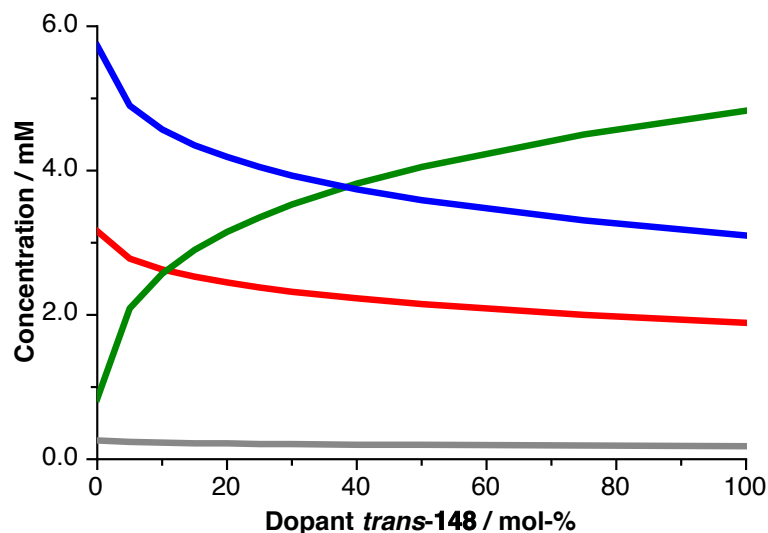


Figure 6.10 Simulation of the competition scenario between maleimide **72** and nitrones **141** and **142** to give templates *trans*-**146** (–), *cis*-**146** (–), *trans*-**148** (–) and *cis*-**148** (–) with increasing amounts of *trans*-**148** template added at the start of the reaction.

An explanation for this strong enhancement can be found in the negative cooperativity of the product duplex for *trans*-**148** ($\Delta G^s = -8.99$ kJ mol⁻¹). With the formation of the duplex severely disfavoured, the addition of preformed template generates a larger amount of free template in solution than for templates with strong positive cooperativity. Every free template can then bind the appropriate building blocks to form the catalytically active ternary complex that leads to the autocatalytic production of another template molecule. The same phenomena was observed in the unusual doping behaviour of *trans*-**98** in chapter 3 in which addition of increasing amounts of dopant shifted the maximum rate and the overall concentration of the self-replicating isomer to higher values.

6.5.3 Coupling the competition scenario to a DCL

In the previous section, the possibility of influencing the outcome of the competition reaction between an AB system and a self-replicator by addition of autocatalytic template at the start of the reaction was verified. Even though there was a clear trend for the increased formation of the self-replicator, the enhancements were rather modest and the system quickly reached a point of saturation at which addition of more template had hardly any effect on the product

distribution. This rather rigid behaviour is observed because the competition process is solely governed by the kinetics of the two individual systems. Since all three building blocks are present at the start of the reaction at maximum concentration, the rates of the AB system as well as the bimolecular reactions to form the self-replicating templates were also highest at that point. This means that addition of substoichiometric amounts of template to this reaction mixture had only limited possibility to bridle the efficiency of the AB system.

Higher enhancements can be expected by mimicking nature's dynamic approach in which necessary reagents are created only when they are really needed. If it were possible to devise a process in which one or all of the building blocks are slowly generated from a precursor during the course of the reaction, the initial concentrations of the building blocks would be low and the rates of the reactions would be severely limited. Addition of the same amount of template would now have a higher impact on the product distribution than in the rigid, kinetically controlled competition scenario and greater enhancements for the formation of self-replicator *trans*-**146** can be expected.

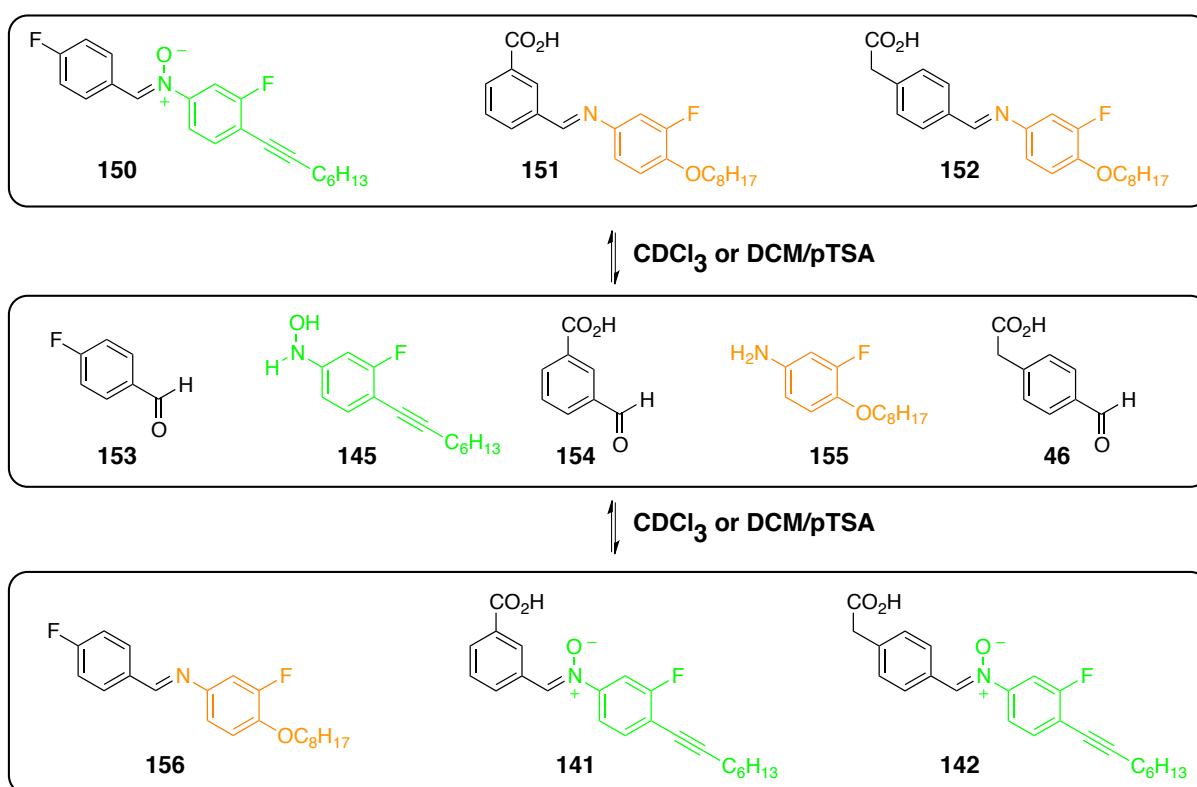
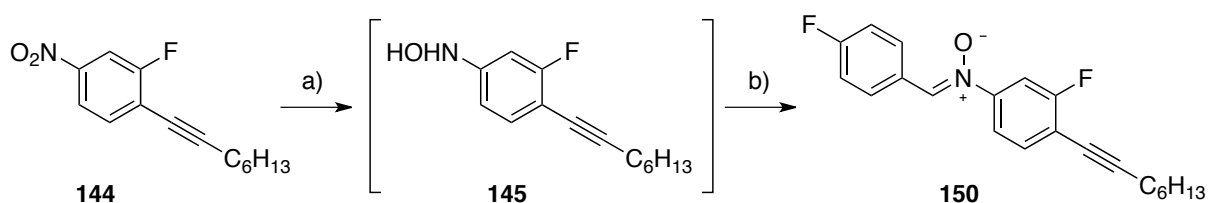


Figure 6.11 Dynamic combinatorial library of nitron and imine compounds.

Figure 6.11 shows the dynamic exchange protocol that was used to generate the two reactive acid nitrones **141** and **142** from a pool of two acid imines **151** and **152** bearing a

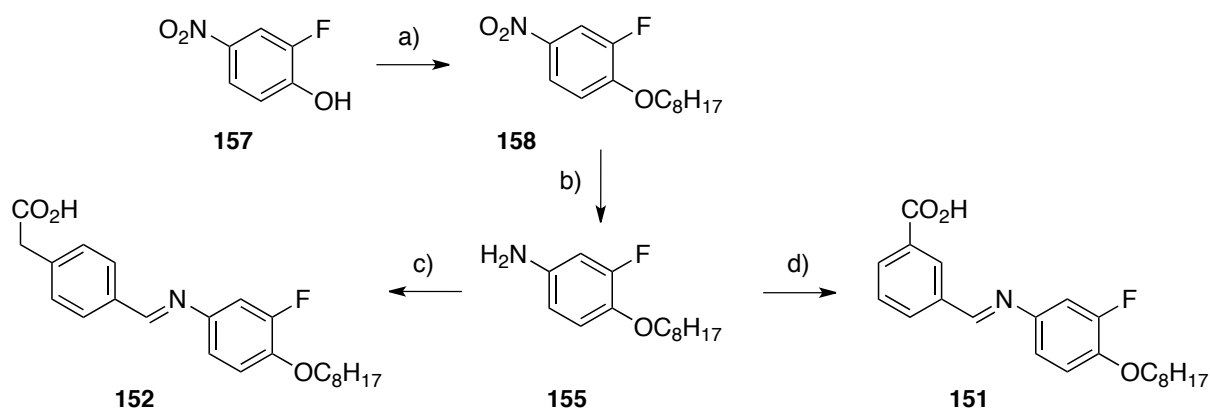
fluorine tag and solubilising alkoxy group, and a feed nitrone **150** bearing two fluorine tags but no recognition site. An exchange protocol exploiting the reversible hydrolysis of nitrones and imines was already investigated successfully in the group and presented previously.^[188] In order to maintain the right stoichiometry in this newly devised exchange process, two equivalents of feed nitrone **150** were dissolved in dry CDCl_3 together with one equivalent of each of the acid imines **151** and **152** to form the dynamic library. Traces of water cause partial hydrolysis of the three initial reagents leading to a mixture of aldehydes **153**, **154** and **46**, hydroxylamine **145** and amine **155**. Since this hydrolytic step is fully reversible, the smaller building blocks can recondensate to form the original three starting reagents. However, recombination of the aldehydes with the hydroxylamine and amine leads to the formation of imine **156** and the two acid nitrones **141** and **142**, the necessary reagents for the reaction with maleimide **72** in the competition scenario. It should be pointed out that also feed nitrone **150** can react with maleimide **72**, but since **150** does not possess any recognition sites, its reaction is expected to be slow and unselective for both of its two possible diastereoisomers.

Synthesis of the three starting building blocks was straightforward. Feed nitrone **150** was available through partial reduction of nitro compound **144** to hydroxylamine **145** and further condensation with commercially available 4-fluorobenzaldehyde (Scheme 6.6).



Scheme 6.6 Synthesis of nitrone **150**. Conditions: a) Rh/C, NH_2NH_2 , THF, rt; b) 4-fluorobenzaldehyde, EtOH, $-18\text{ }^\circ\text{C}$, 61% over two steps.

Both imines were synthesised on the basis of amine structure **155** which was formed by alkylation of the free phenol group in **157** using K_2CO_3 and bromooctane in acetone and subsequent hydrogenation of the nitro functionality of **158** in ethanol with palladium on carbon as catalyst and hydrogen gas (Scheme 6.7).



Scheme 6.7 Synthesis of imines **151** and **152**. Conditions: a) K_2CO_3 , bromooctane, acetone, 60°C , 82%; b) Pd/C, H_2 , EtOH; c) **46**, EtOH, rt, 53% over two steps; d) 3-carboxy benzaldehyde, EtOH, rt, 61% over two steps.

Once all necessary components were synthesised, the exchange process was followed in isolation using ^{19}F NMR spectroscopy. A solution mixture of 20 mM **150**, 10 mM **151** and 10 mM **152** in 800 μL CDCl_3 was incubated at 0°C and the progression was monitored for 8 hours. Deconvolution of the obtained spectra allowed for the construction of the concentration *vs* time profile in **Figure 6.12a**. It can clearly be seen that the equilibrium point of the DCL is on the side of the condensed compounds with an equal distribution between them (**Figure 6.12b**).

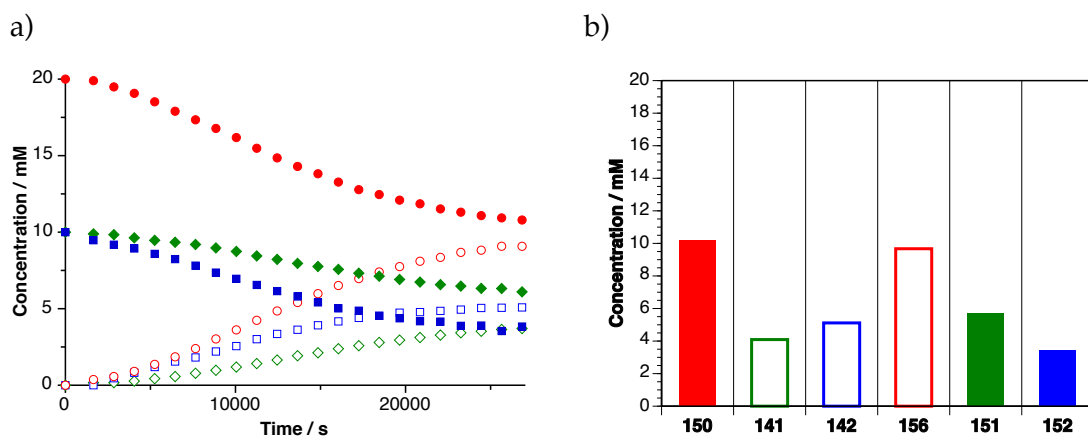


Figure 6.12 a) Exchange dynamics over 8 hours and b) final equilibrium concentration after 8 hours of the DCL at 0°C in CDCl_3 starting from nitrone **150** (●), imine **151** (◆) and imine **152** (■) to follow the formation of imine **156** (○), nitrone **141** (◇) and nitrone **142** (□). Starting concentrations were 10 mM for imines **151** and **152**, and 20 mM for feed nitrone **150**. The exchange process was monitored by ^{19}F NMR spectroscopy.

Having established the efficiency of the exchange process, the competition scenario including the three doping experiments were repeated within this dynamic framework. In order to establish the native reactivity, a 10 mM solution of maleimide **72** in 800 μL was incubated at 0°C together with two equivalents of feed nitrone **150** and one equivalent of

each imine **151** and **152** in the absence of any added self-replicating template. After complete conversion of the maleimide, the final product distribution was analysed by ^1H NMR spectroscopy which happened to show clean resolution for the characteristic singlet signals for all three *trans*-cycloadducts and the doublet for the *cis*-cycloadduct. This procedure was repeated under addition of 9, 18 and 36 mol-% of *trans*-**146**. The results of these four experiments are summarised in **Figure 6.13a**.

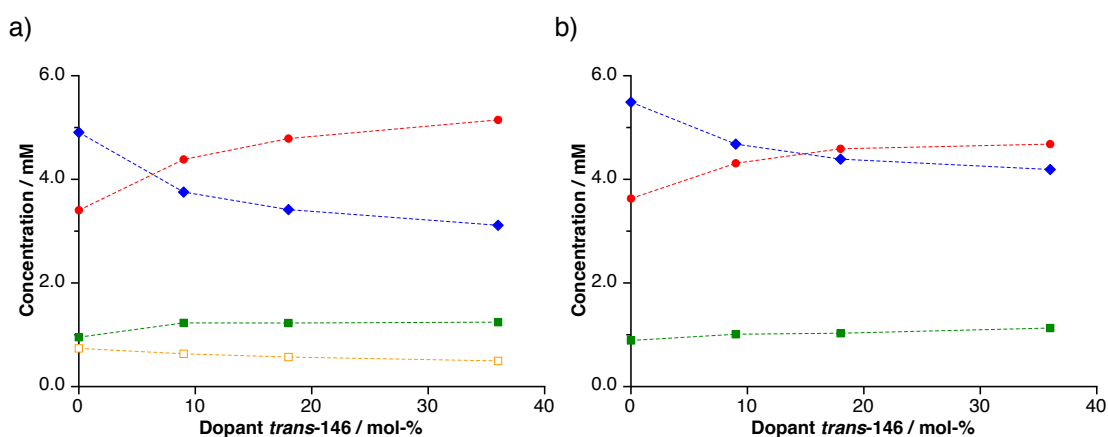


Figure 6.13 a) Product distribution for the reaction between maleimide **72** with the DCL of nitrone **150** (2.0 equiv.), imine **151** and **152** as starting material in the presence of 9, 18 and 36 mol-% *trans*-**146** template to give products *trans*-**146** (●), *trans*-**148** (■), *cis*-**148** (◆) and *trans*-**159** (□). b) Product distribution for the reaction between maleimide **72** and nitrones **141** and **142** to give products *trans*-**146** (●), *trans*-**148** (■) and *cis*-**148** (◆). All reactions were performed at 0 °C in CDCl_3 at 10 mM reagent concentration and analysed by ^1H NMR spectroscopy.

The effect of working in a dynamic environment can already be seen in the product distribution of the native reaction. The final concentration of the product of the AB system, *cis*-**148**, was determined to be 5.0 mM. Second most abundant species was *trans*-**146** with a concentration of around 3.3 mM followed by the *trans*-isomer of the AB system with 0.9 mM. As expected, the major isomer of the reaction between feed nitrone **150** and maleimide **72**, *trans*-**159**, was detected as fourth product from the reaction of maleimide **72** with feed nitrone **150** with a concentration of 0.8 mM. The amount of corresponding *cis*-isomer proved too little for detection by NMR and was neglected in the calculations. The concentration can however be estimated to be around 0.2 mM since the ratio of *trans*- to *cis*-isomer is roughly 3:1 for non-recognition mediated bimolecular reactions. With this fourth reaction product present in the solution, the amounts of AB product and self-replicating templates were slightly reduced. However, the ratio for the three recognition-mediated products was very similar to the one found in the previous native experiment even though the concentration of available reactive nitrone compounds during the reaction was coupled to the dynamic exchange process.

With the initial position for the competition between *trans*-146 and *cis*-148 nearly the same as in the kinetic variant, the drastic effect of instructing the system with preformed *trans*-146 template can clearly be seen. Addition of 9 mol-% of *trans*-146 template enhanced its autocatalytic formation and rendered the very self-replicating template to be the most abundant species in the product pool. This trend was further amplified upon addition of 18 and 36 mol-% of *trans*-146 which resulted in a final difference in concentration between both competing systems of more than 2 mM in favour of the self-replicator. But also in this case, the system seemed to reach a point of saturation at which addition of increasing amounts of *trans*-146 had only very little effect on the final product distribution. Consequently, small changes in concentration for *trans*-148 and *trans*-159 were detected. The formation of *trans*-148 was slightly up-regulated with increasing amounts of seeded *trans*-146. Since the partner AB system struggled to compete for essential maleimide, more nitron 142 was available for the formation of *trans*-148. On the other hand, less *trans*-159 was produced in the presence of increasing amounts of added *trans*-146 template. This finding suggests that the amount of added template had a direct influence on the exchange process which created the reactive nitron compounds. With increasing amounts of *trans*-146, nitron 150 was more rapidly incorporated into the final template product causing the equilibrium between all components of the dynamic library to readjust more quickly in favour of nitrones 141 and 142 than in the native experiment. As a consequence, feed nitron 150 was converted into the two reactive species at higher rate thereby reducing its concentration and availability to react with maleimide 72 to form *trans*-159.

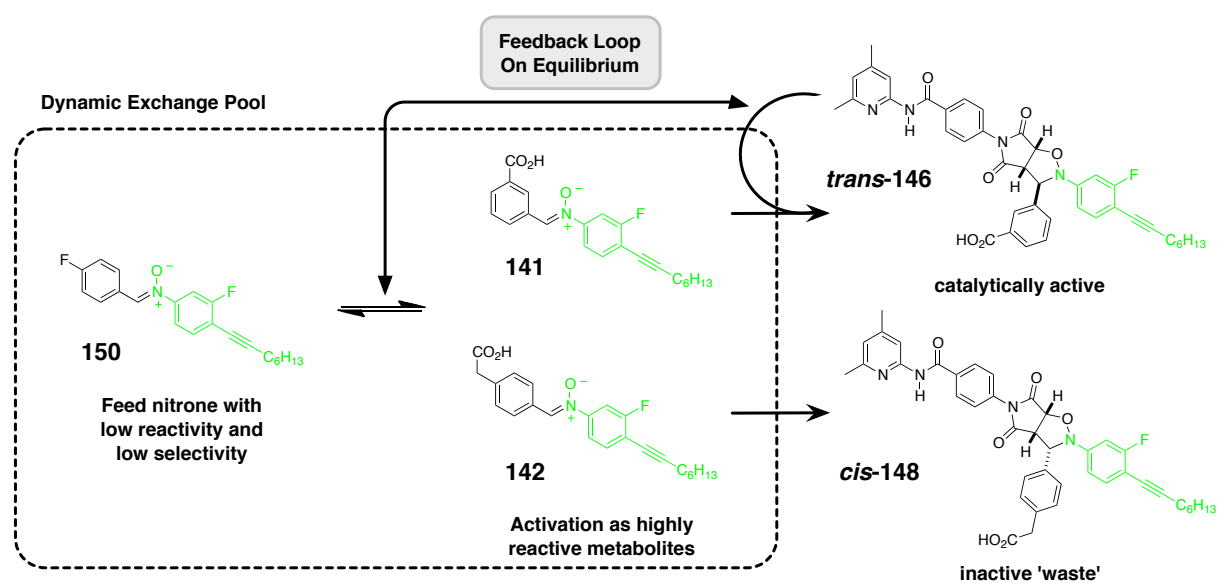


Figure 6.14 Interpretation of the dynamic competition scenario as feedback loop.

With this knowledge at hand, the autocatalytic effect of template *trans*-146 on the product distribution of the competition scenario can be interpreted as a feedback loop similar to the ones known from biological systems (Figure 6.14). In the exchange process that generates the dynamic combinatorial library, recognition-disabled feed nitrone 150 possesses only low reactivity towards maleimide 72 before it is reversibly converted into nitrones 141 and 142. This process can be regarded as the activation of a precursor of limited reactivity to form a species of higher reactivity. Both nitrones can then react with maleimide *via* their recognition-mediated pathways to form AB template *cis*-148 and self-replicating template *trans*-146. Template *cis*-148 was shown to be inert catalytically and can be seen as an undesired waste product. On the other hand, template *trans*-146 does possess the ability to catalyse its own formation. So working in an environment rich in *trans*-146 creates a situation in which the template not only supports its own formation but also influences the activation step that generates the necessary nitrone building block in a feedback loop manner.

Overall, the outcome of the competition reaction between maleimide 72 and nitrones 141 and 142 was manipulated successfully by addition of instructional templates. Seeding the reaction mixture with *trans*-146 ensured enhanced autocatalytic production of more self-replicating template and reduced the efficiency of the AB system. However, in case of the purely kinetic scenario, the stimulated changes in product distribution were only modest. Better enhancements were achieved by coupling the irreversible competition reactions to a dynamic library. Starting from a feed nitrone without recognition site and two acid imine structures, reversible condensation reactions created a library which contained the two reactive nitrone structures in equilibrium with its precursors. Addition of presynthesised *trans*-146 template at the start of the reaction of maleimide 72 with an interchanging mixture of components 150, 151 and 152, caused much higher changes on the final product distribution of the competition reaction than in the kinetic scenario. Since the reactive nitrones were only generated through the exchange process, their concentration especially at the start of the reaction was significantly lower than in the kinetic variant of the experiment and the impact of the autocatalytic template to direct the selfish production of increasing amounts of *trans*-146 was much more pronounced. In both cases, autocatalytic enhancement of *trans*-146 reached a point of saturation after which increasing the amount of added template has only very little impact on the outcome of the competition reaction.

6.5.4 Scenario II: Maleimides 72 and 74 with nitrone 142

In the last section, the possibility of strengthening a self-replicating system in its quest for a building block shared with an AB system was elucidated. It was shown that addition of presynthesised template enhanced the autocatalytic pathway generating an increased amount of self-replicating product. In order to establish whether this is a general finding, a second competition scenario was developed. Phenylacetic acid nitrone **142** was shown to react with maleimide **74** to form highly efficient self-replicator *trans*-**149**, whereas the reaction with maleimide **72** leads to *cis*-**148**, the product of the well established AB system.

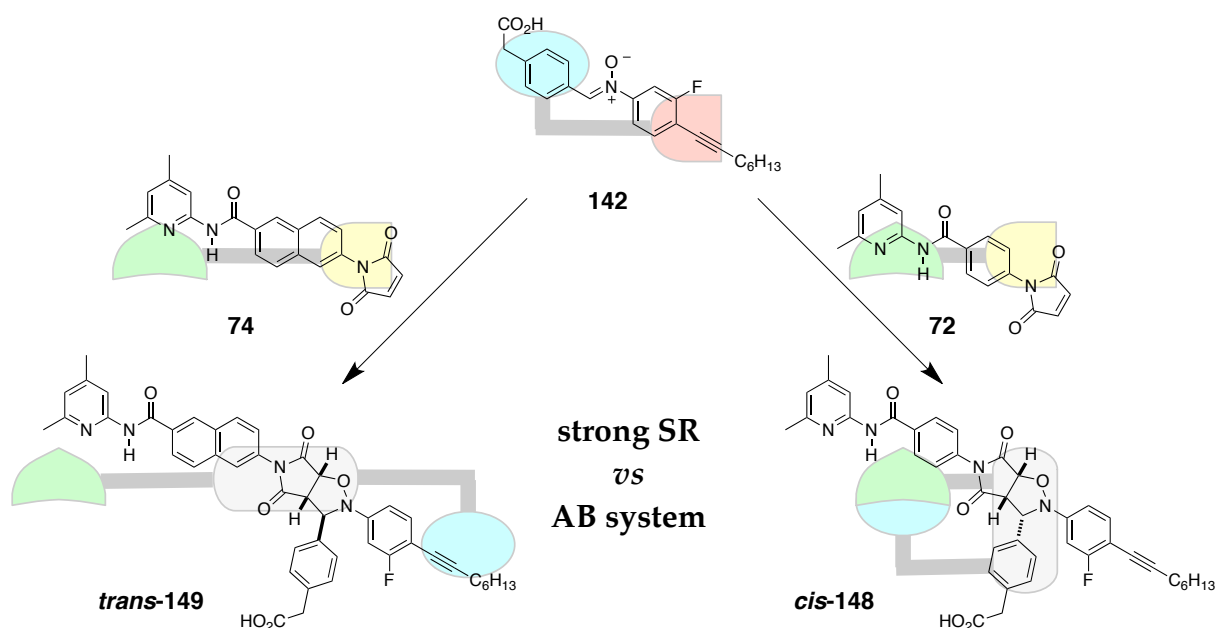


Figure 6.15 Competition scenario with phenylacetic acid nitrone **142** as limiting building block. Its reaction with naphthalene maleimide **74** and benzene maleimide **72** gives rise to self-replicator *trans*-**149** and AB system *cis*-**148**, respectively. Self-replicating isomer *cis*-**148** which is usually formed in minor extent was omitted for clarity.

Using nitrone **142** as the limiting building block creates a competition experiment between a strong self-replicator and an AB system (**Figure 6.15**). The isolated analysis of the set of self-replicating structures suggested that template *trans*-**149** is an exceptionally efficient self-replicator. Its maximum rate was higher than for *trans*-**146** and as a consequence of its high bimolecular rate, this maximum appeared at an earlier stage of the reaction hinting at the possibility that this replicator can better hold its ground against the AB system in the struggle for limited building block.

Unfortunately, working at 0 °C caused the product peaks in the ¹⁹F NMR spectra to broaden and resulted in their overlap making it impossible to construct a concentration *vs*

time profile for the native reaction of this system. However, the product distribution after full conversion of nitrene **142** using ^{19}F NMR spectroscopy established the exact values for the native three component reaction (**Figure 6.16**). It can clearly be seen that self-replicating system *trans-149* is competing successfully with the AB system for the limiting nitrene compound. At the end of the reaction, *trans-149* was found to be the most abundant species with a concentration of roughly 5.4 mM followed by *cis-148* with 3.2 mM. Also the autocatalytic *trans*-isomer of the AB system can be detected in the reaction mixture reaching a concentration of 1.4 mM.

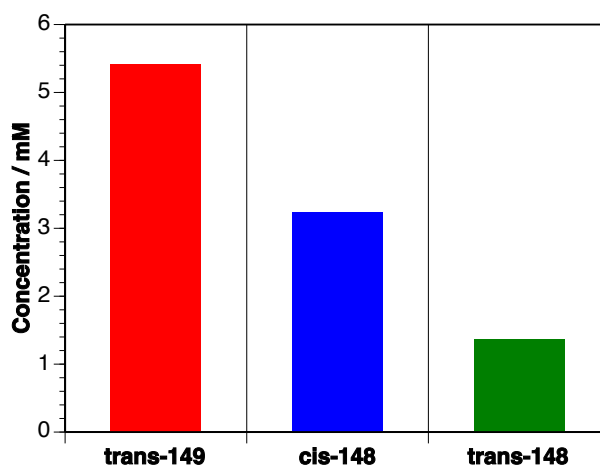


Figure 6.16 Product distribution for the native reaction between maleimide **72** and maleimide **74** with nitrene **142** to give templates *trans-149*, *trans-148* and *cis-148*. The reaction was performed in CDCl_3 at 0°C with 10 mM reagent concentration and analysed by ^{19}F NMR spectroscopy.

This trend is in complete agreement with the performances of the individual systems. Self-replicating template *trans-149* was expected to compete more successfully with *cis-148* than self-replicator *trans-146*. Since the performance of the AB system was limited by the strong self-replicating system, its partner *trans-148* was taking advantage of the slight increase in available maleimide and is marginally up-regulated.

Next, a series of doping experiments were conducted to establish the possibility of further pushing the autocatalytic formation of *trans-149* by adding presynthesised self-replicating template at the start of the reaction. The results are listed in **Figure 6.17** with the graph on top showing the absolute concentration of all three reaction products for the doping reaction with 10, 20 and 40 mol-% *trans-149*, respectively. Underneath, the corresponding enhancements with respect to the native reaction are presented. Altogether, the diagrams clearly show the effect of template addition. Increasing the amount of dopant shifted the product distribution towards the self-replicating species thereby suppressing the

formation of AB product *cis*-148. Since *trans*-149 is already the dominant species in the native reaction, the relative enhancement is smaller than in the case of *trans*-146, however, the negative trend for *cis*-148 is well reflected. Just as in the case of the first scenario, the self-replicating by-product of the AB system, *trans*-148, is slightly up-regulated, a direct consequence of the suppression of *cis*-148.

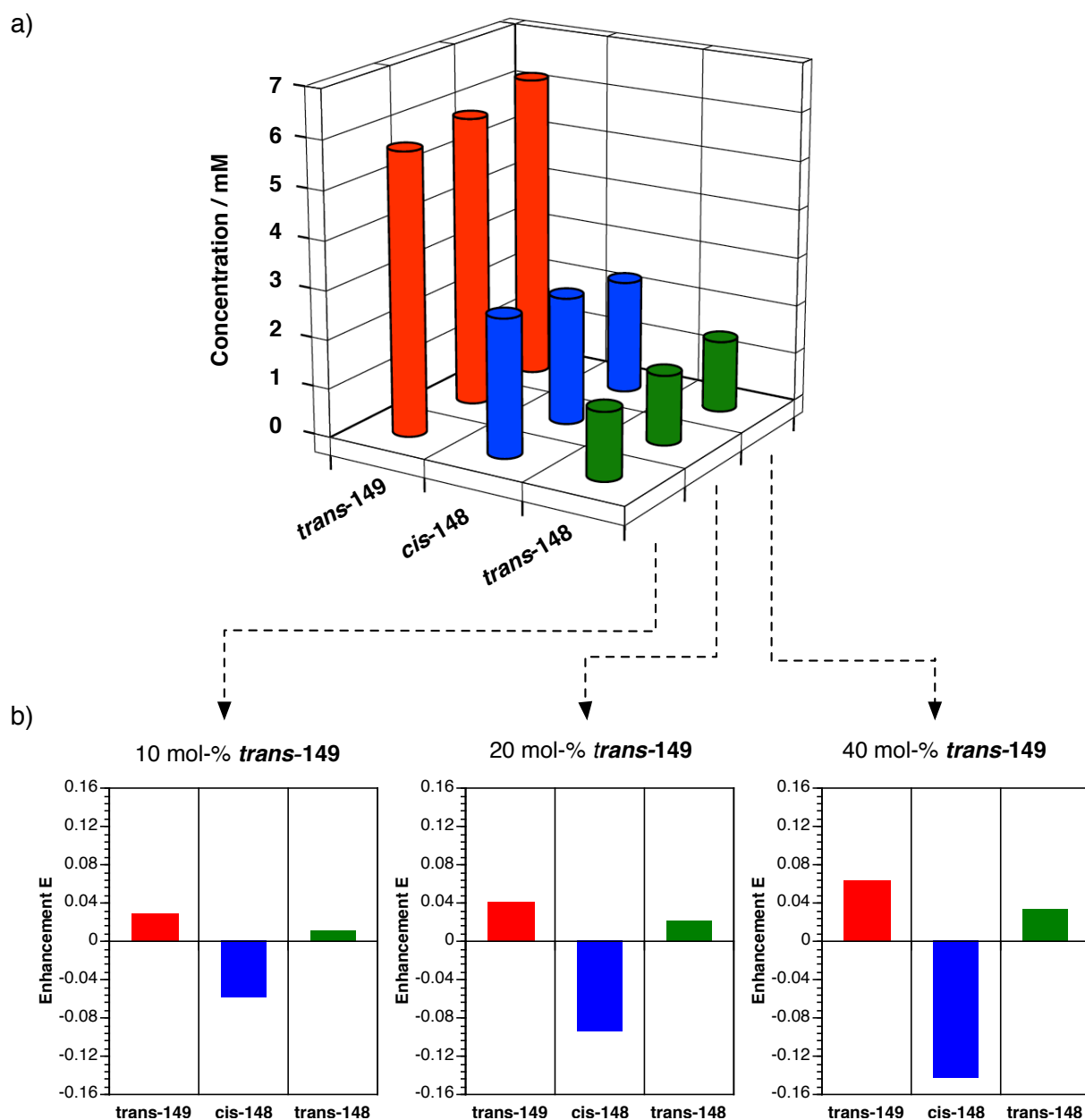


Figure 6.17 Product distributions for the reaction between maleimide 72 and maleimide 74 with nitron 142 to give *trans*-149, *cis*-148 and *trans*-148 in the presence of 10 mol-%, 20 mol-% and 40 mol-% *trans*-149 template. In a) the final product concentration after full conversion of maleimide 72 is depicted. Section b) shows the enhancements with respect to the native reaction from **Figure 6.16**. All reactions were performed at 0 °C in CDCl₃ at 10 mM reagent concentration and analysed by ¹⁹F NMR spectroscopy.

Also the second competition scenario between an AB system and a self-replicator proved to be prone to the addition of instructional template. In the native experiment, autocatalytic template *trans*-149 was detected to be the most abundant species and this dominance was further enhanced by seeding fresh batches of reagents with increasing amounts of preformed self-replicating template. Since *trans*-149 was already present at high concentrations in the native experiment, the effect of template addition is less pronounced than in the system presented in **Figure 6.8**.

6.5.5 Scenario III: maleimide 74 with nitrones 141 and 142

Having established the possibility of strengthening the performance of a self-replicator in its quest for a limited building block shared with an AB system by addition of instructional template in two different cases, the next envisaged scenario was constructed to create a competition between two self-replicating systems. Removing maleimide 72 from the pool of reagents leaves maleimide 74 as common building block to react with nitrones 141 and 142 to form the two self-replicating systems *trans*-147 and *trans*-149, respectively (**Figure 6.18**). Template *trans*-149 was already shown to be an extraordinarily efficient self-replicator both in isolation and in a competition situation with the AB system *cis*-148 as presented in the previous section.

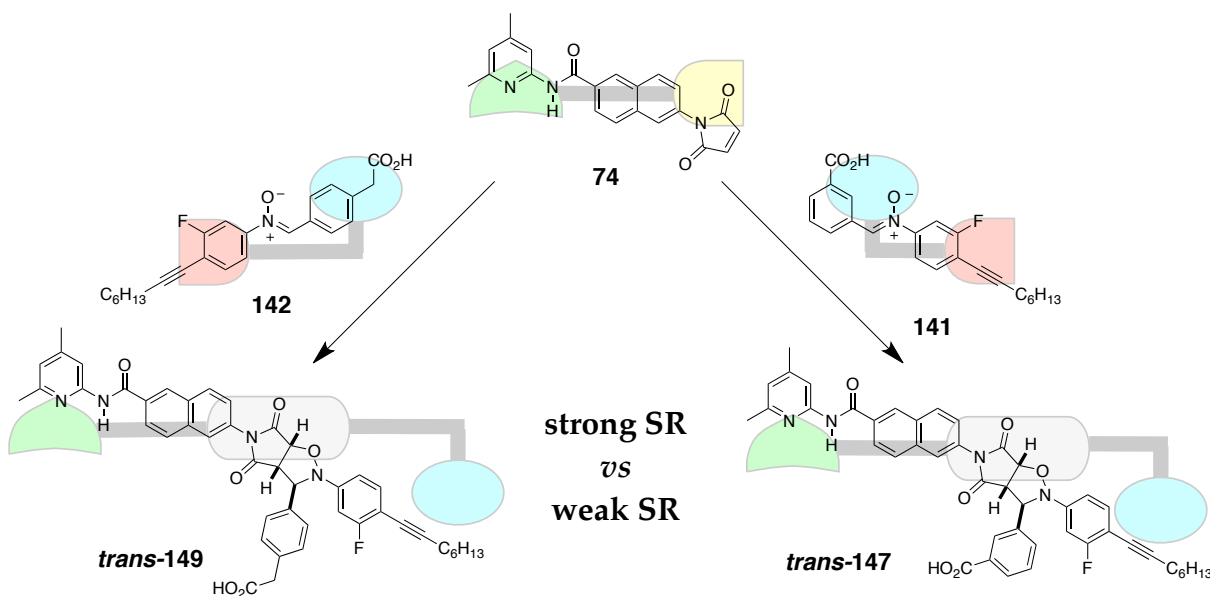


Figure 6.18 Competition scenario with naphthalene maleimide 74 as limiting building block. Its reaction with phenylacetic acid nitron 142 and carboxy acid nitron 141 gives rise to replicators *trans*-149 and *trans*-147, respectively.

On the other hand, the reaction between maleimide 74 and carboxy nitron 141 gave rise a self-replicating system of moderate efficiency. The formation of *trans*-147 was found to

be the least efficient of all investigated replicating systems. With the knowledge about the performance of the isolated systems at hand, *trans*-149 was expected to outcompete *trans*-147 in the quest for a limited amount of maleimide building blocks. Once the native distribution of products was established, the possibility of influencing the outcome of the competition reaction by addition of autocatalytic templates was probed. It seemed plausible that the presence of one of the two self-replicating templates at the start of the reaction influences the final product distribution by autocatalytic enhancement of the doped species.

In order to test this hypothesis, a native experiment and two sets of template doped reactions were performed. For the native experiment, a 10 mM solution of an equimolar mixture of maleimide **74** with both nitrones **141** and **142** in 800 μL CDCl_3 were incubated at 0 $^\circ\text{C}$ and the progression of the reaction was followed by ^{19}F NMR spectroscopy. Deconvolution of the obtained spectra allowed for the construction of the concentration *vs* time profile shown in **Figure 6.19**. Working at low temperature caused broadening of the ^{19}F NMR signals for both templates *trans*-149 and *trans*-147, and resulted in significant overlapping which reduced the quality of the deconvolution. However, the formation of both templates can be seen with *trans*-149 being the main product.

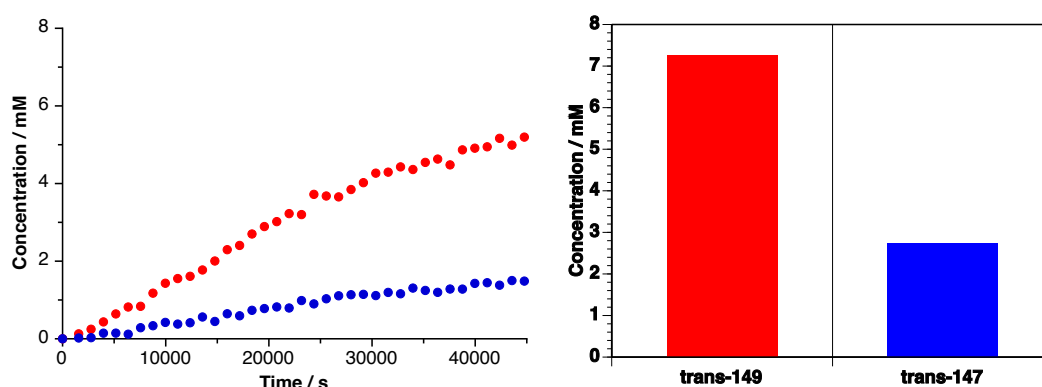


Figure 6.19 Concentration *vs* time profile for the reaction between maleimide **74** with nitrone **141** and **142** to give *trans*-149 (●) and *trans*-147 (●). The reaction was performed in CDCl_3 at 0 $^\circ\text{C}$ with 10 mM reagent concentration and analysed by ^{19}F NMR spectroscopy.

At the end of the kinetic measurement, the solution mixture was kept at 0 $^\circ\text{C}$ until full conversion of maleimide was stated and the final product distribution was extracted by ^{19}F NMR spectroscopy. In addition, the same set-up was repeated with three different amounts of one of the two self-replicating templates present at the start of the reaction and the final product distributions were subsequently determined.

In the case of using *trans*-147 as dopant, 8, 16 and 32 mol-% of template were added at the start of the reaction. The effect of the dopant on the outcome of the competition

reaction can be seen in **Figure 6.20a**. Addition of the autocatalytic template was indeed found to enhance selfishly the formation of *trans*-**147** while the formation of *trans*-**149** was consequently down-regulated. However, the overall influence of the instructional template on the product distribution is only marginal and merely improves the final concentration of *trans*-**147** from 2.7 mM in the native experiment to 3.2 mM in the experiment with 32 mol-% dopant. Once more, the system exhibits a saturation limit at which addition of increasing amounts of *trans*-**147** has no further impact on the final product distribution.

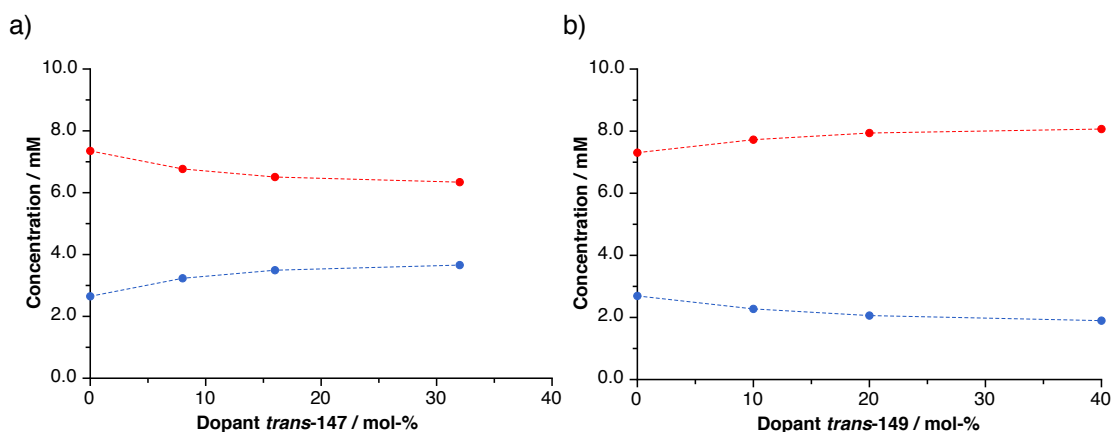


Figure 6.20 Product distribution for the reaction between maleimide **74** with nitrones **141** and **142** a) in the presence of 8, 16 and 32 mol-% *trans*-**147** and b) in the presence of 10, 20 and 40 mol-% *trans*-**149** to give *trans*-**149** (●) and *trans*-**147** (●). All reactions were performed at 0 °C in CDCl₃ at 10 mM reagent concentration and analysed by ¹⁹F NMR spectroscopy.

Correspondingly, doping experiments with 10, 20 and 40 mol-% of *trans*-**149** was performed using the same procedure as described previously. Starting from the same product distribution for the native reaction, the analysis of the doping experiments by ¹⁹F NMR spectroscopy gave rise to **Figure 6.20b**. It can clearly be seen that addition of increasing amounts of *trans*-**149** indeed showed an increase in autocatalytic formation of this very template with respect to the competing species. However, the level of enhancements were again modest and the system exhibits a saturation limit at which addition of increasing amounts of *trans*-**149** has no further impact on the final product distribution.

Overall, the experiments have shown that the outcome of the competition reaction between two self-replicators can be manipulated by addition of preformed replicating template. Each template proved to possess the ability to selectively enhance its own formation and shifted the product distribution in its own favour. The level of enhancements for both of the templates were however rather small, even for relatively large amounts of added template.

6.5.6 Scenario IV: maleimides **72** and **74** with nitrone **141**

The last competition scenario unfolds when phenylacetic acid nitrone **142** is excluded from the reagent pool. The three remaining components create a scenario in which the two self-replicators *trans*-**146** and *trans*-**147** compete for a limited amount of carboxy nitrone **141** (Figure 6.21). Self-replicating template *trans*-**147** is formed by reacting the nitrone with maleimide **74** and *trans*-**146** is the product of the reaction between nitrone **141** and maleimide **72**. In isolation, *trans*-**146** has shown to be the more efficient replicating system, however, it does not quite match the strength of replicator *trans*-**149** which was the competitor of *trans*-**147** in the previous section.

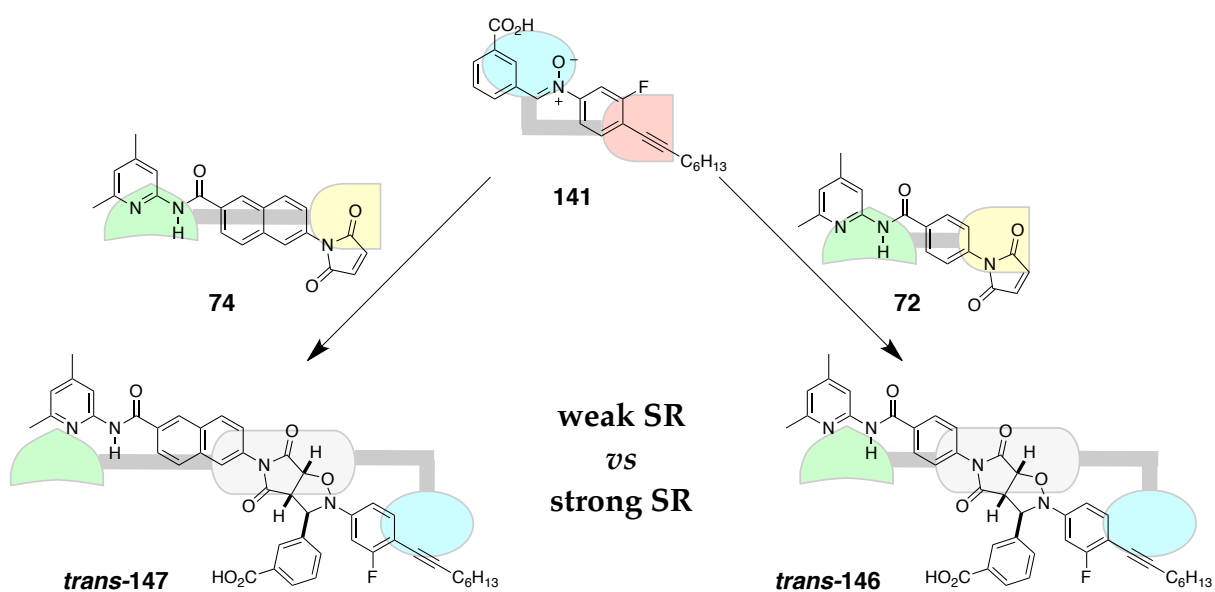


Figure 6.21 Competition scenario with carboxy nitrone **141** as limiting building block. Its reaction with naphthalene maleimide **74** and benzene maleimide **72** gives rise to replicators *trans*-**147** and *trans*-**146**, respectively.

Once more, the possibility of influencing the outcome of this competition reaction by adding preformed template was probed. First, the kinetics of the native experiment were recorded. A 10 mM solution of an equimolar mixture of carboxy nitrone **141** and both maleimides **72** and **74** in 800 μ L CDCl₃ were incubated at 0 °C and the progression of the reaction was followed by ¹⁹F NMR spectroscopy. Working at low temperature caused broadening of the ¹⁹F NMR signals for both templates *trans*-**147** and *trans*-**146** and resulted in significant overlapping which reduced the quality of the deconvolution. However, the formation of both templates can be seen with *trans*-**146** being the main product (Figure 6.22).

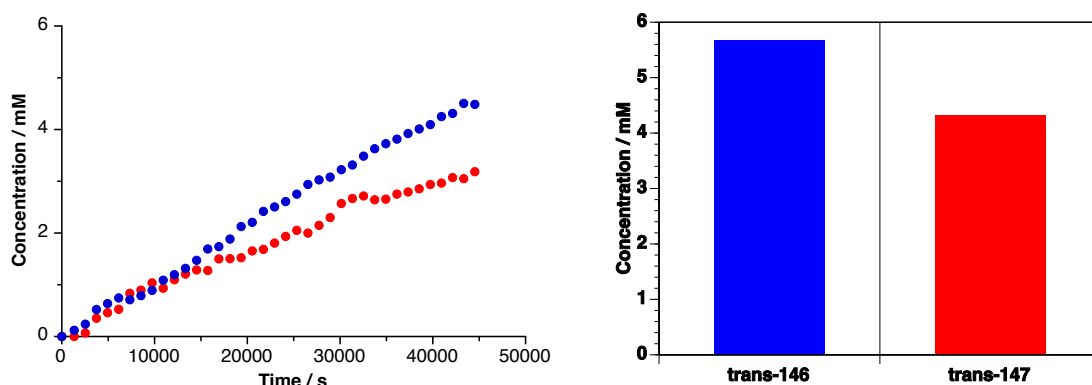


Figure 6.22 Concentration *vs* time profile for the reaction between carboxy nitrone **141** with maleimides **72** and **74** to give *trans*-**147** (●) and *trans*-**146** (●). The reaction was performed in CDCl_3 at 0°C and with 10 mM reagent concentration and analysed by ^{19}F NMR spectroscopy.

At the end of the kinetic measurement, the solution mixture was kept at 0°C until full conversion of nitrone **141** was stated and the final product distribution was extracted by ^{19}F NMR spectroscopy. In addition, the same set-up was repeated with three different amounts of one of the two self-replicating templates present at the start of the reaction and the final product distributions were subsequently determined (**Figure 6.23**).

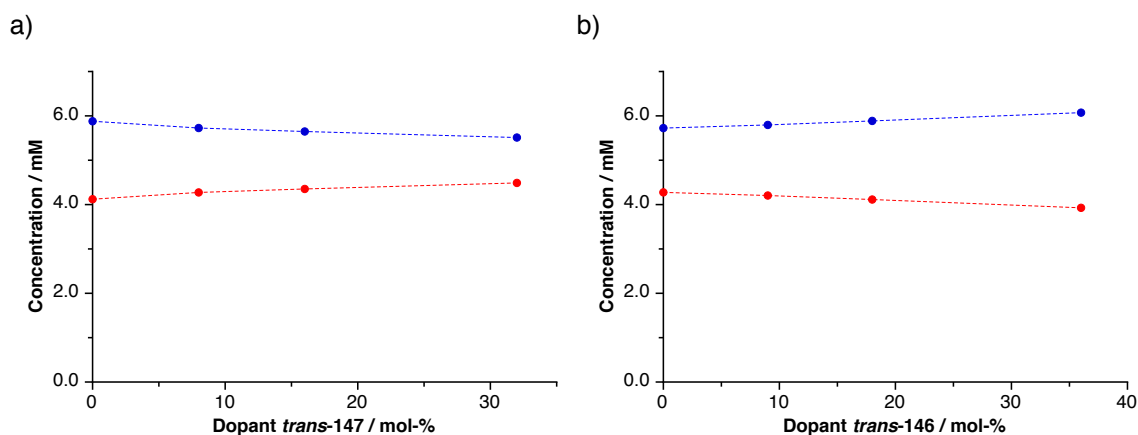


Figure 6.23 Product distribution for the reaction between carboxy nitrone **141** with maleimides **72** and **74** a) in the presence of 8, 16 and 32 mol-% *trans*-**147** and b) in the presence of 9, 18 and 36 mol-% *trans*-**146** to give *trans*-**147** (●) and *trans*-**146** (●). All reactions were performed at 0°C in CDCl_3 at 10 mM reagent concentration and analysed by ^{19}F NMR spectroscopy.

When using *trans*-**147** as dopant, 8, 16 and 32 mol-% of replicating template were added at the start of the reaction. The effect of the dopant on the outcome of the competition reaction can be seen in **Figure 6.23a**. Addition of the autocatalytic template was indeed found to selfishly enhance the formation of *trans*-**147** whereas the formation of *trans*-**146** was consequently down-regulated. Just like in the example shown in the previous section, the overall influence of the instructional template on the product distribution was only marginal and merely improved the final concentration of *trans*-**147** from 4.1 mM in the native experiment to 4.4 mM in the experiment with 32 mol-% dopant. Also in this case, the system

exhibits a saturation limit at which addition of increasing amounts of *trans*-147 has no further impact on the final product distribution.

Correspondingly, doping experiments with 9, 18 and 36 mol-% of template *trans*-146 was performed using the same procedure as described previously. Analysis of the doped experiments by ¹⁹F NMR spectroscopy gave rise to **Figure 6.23b** which clearly shows that addition of increasing amounts of *trans*-146 did indeed increase the autocatalytic formation of this very template with respect to the competing species. However, the level of enhancements were again modest and the system exhibits a saturation limit at which addition of increasing amounts of *trans*-146 has no further impact on the final product distribution.

6.5.7 A four component network

Having established the relationships between the competing systems in the three-component experiments, the combination of the two maleimides **72** and **74**, and nitrones **141** and **142** ultimately creates a scenario in which the four reagents can give rise to a mixture of eight diastereoisomeric products of which four exploit recognition to enhance their own formation in a self-replicating fashion. Additionally, the formation of AB system *cis*-148 needs to be taken into account. An overview of the five major products is given in **Figure 6.24**.

A reaction between all four building blocks will yield the native mixture of products. It was shown previously that the behaviour of the components in the competition scenario can be deduced to some extent from their individual performance. For example, the result of the outcome of the competition between two replicating systems could be deduced from the performances of the individual systems. In both cases, the more efficient replicator dominated its weaker rival. If this four component system was to follow the same principle, a clear hierarchy in reactivity could be expected for the reaction of an equimolar mixture of all four building blocks. Replicators *trans*-149 and *trans*-146 have proven to be exceptionally efficient and are bound to be the major products in this experiment. Moreover, their formation can proceed independently since both replicators do not have to compete for any common building blocks. On the other hand, based on their individual performances, the chances for *trans*-147 and hybrid system **148** to enforce themselves against the stronger systems seems to be small. Each of the three diastereoisomers has to compete against at least two other more efficient systems. *Trans*-147 is expected to struggle with *trans*-149 for its maleimide building block and with *trans*-146 for nitrone reagent. In addition to the rivalry with *trans*-149 and *trans*-146, the two diastereoisomers for **148** rely on the same building

blocks which will further reduce their chance of prosperity. Overall, the reaction between two maleimides and two nitrones as depicted in **Figure 6.24** is expected to give rise to two dominant self-replicators, *trans*-146 and *trans*-149, and three less efficient systems, *trans*-147, *cis*-148 and *trans*-148.

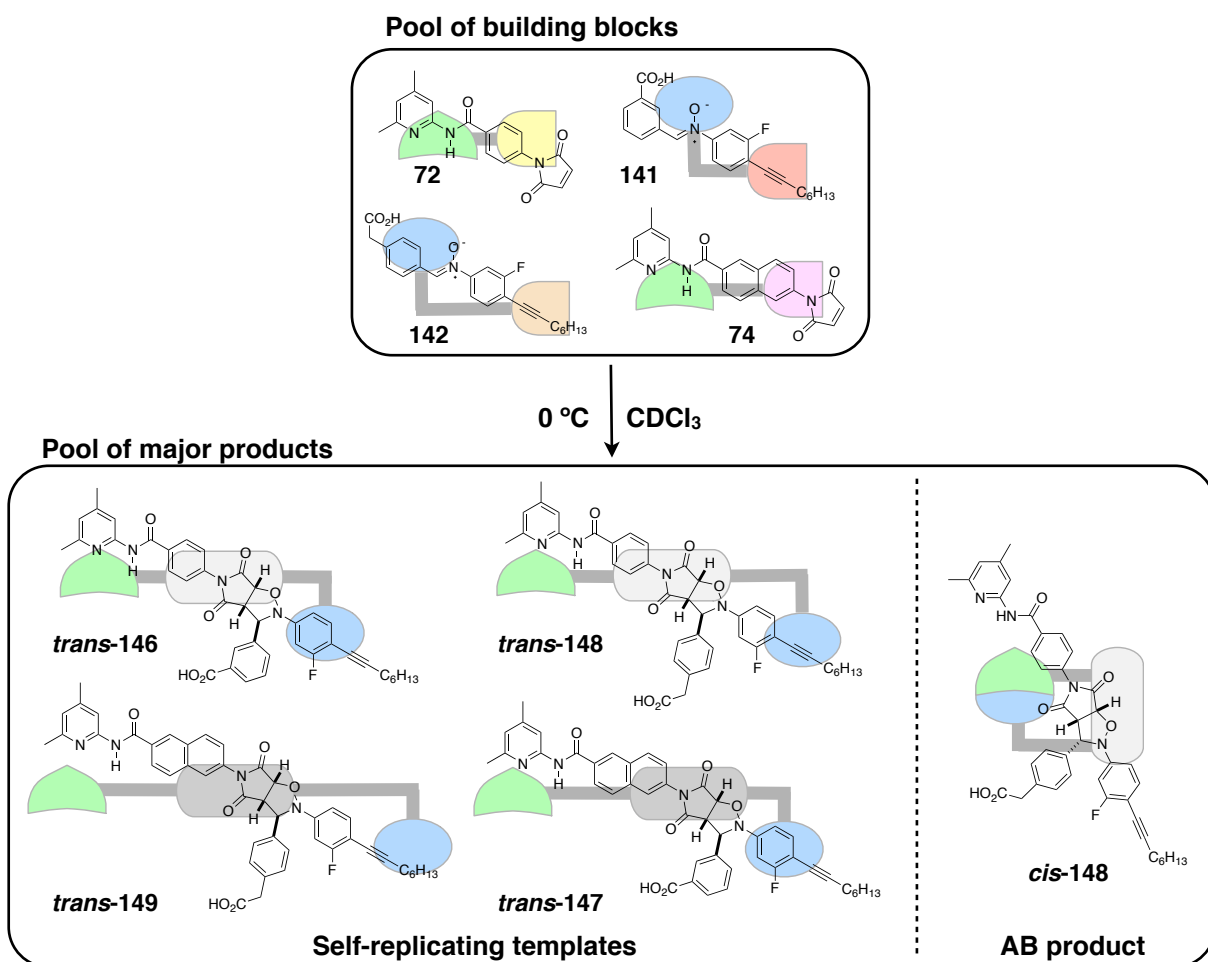


Figure 6.24 Four-component reaction of building blocks nitron 141 and 142, and maleimide 72 and 74 leading to the formation of four self-replicating products *trans*-146, *trans*-148, *trans*-149 and *trans*-147 as well as AB system *cis*-148. The reaction was carried out at 0 °C in CDCl₃ with 10 mM starting material concentration. All *cis*-isomers formed only through bimolecular pathways were omitted.

In order to verify this assumption, the native experiment using a 10 mM concentration of maleimides 72 and 74, and nitrones 141 and 142 in CDCl₃ was conducted. The solution mixture was incubated at 0 °C until all reagents were converted after 72 h. Addition of a fixed amount of d₆-DMSO resulted in separation of the signals for the five products and allowed for their deconvolution by ¹⁹F NMR spectroscopy. The final product concentration for this native reaction can be seen in **Figure 6.25a**. Despite all rational expectations, *trans*-147 was found to be the most abundant species with a concentration of 6.4 mM followed by *cis*-148 (3.7 mM), *trans*-146 (3.6 mM), *trans*-149 (3.4 mM) and *trans*-148 (2.8

mM). This rather unexpected result demonstrates once more that the behaviour of a complex network based on mutually catalytic relationships between their components can not easily be deduced from the properties of the individual components.

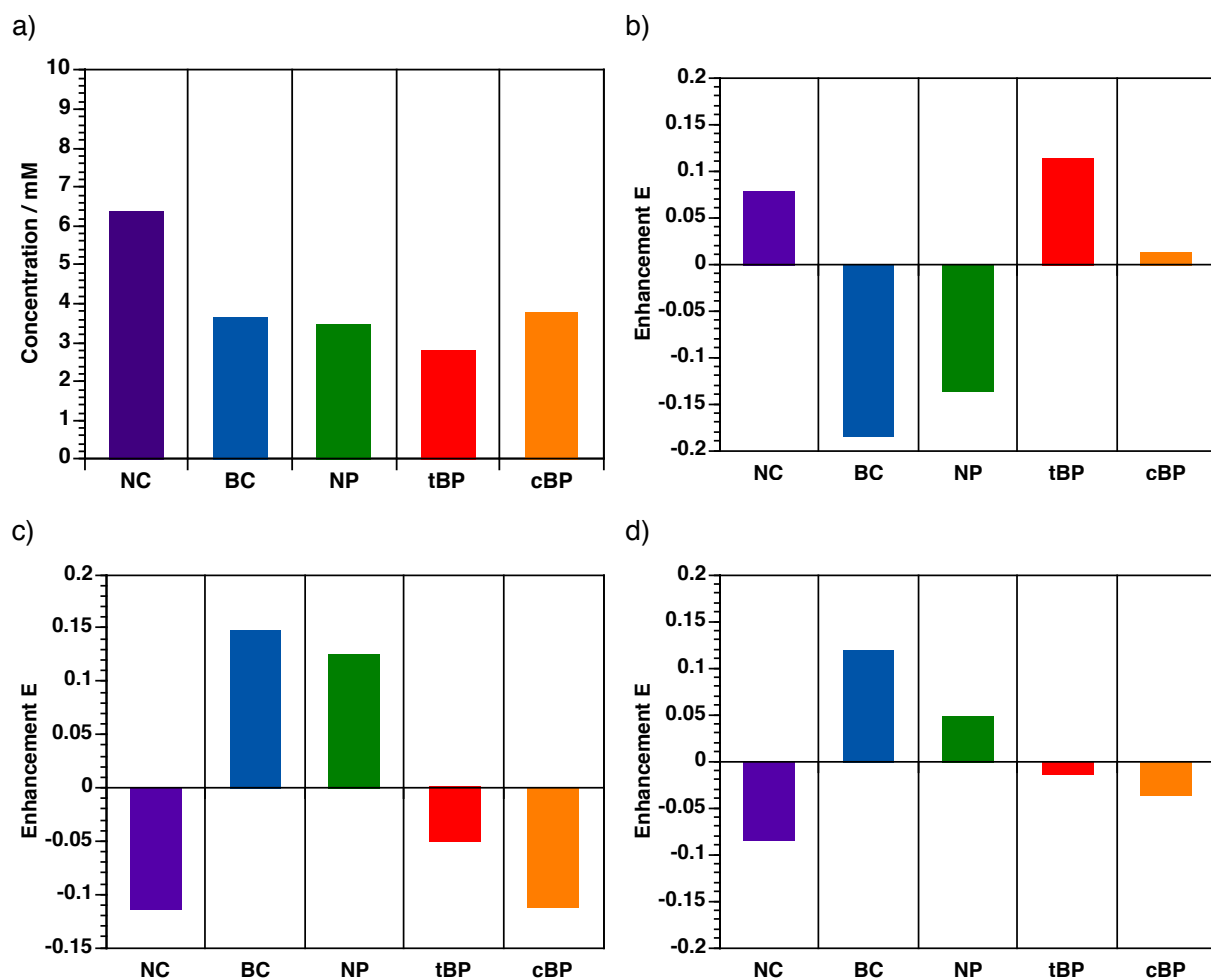


Figure 6.25 a) Product distribution for the four component experiment of maleimide **72** and **74** with nitrones **141** and **142** to give templates *trans*-**147** (NC), *trans*-**146** (BC), *trans*-**149** (NP), *trans*-**148** (tBP) and *cis*-**148** (cBP). Enhancements for the addition of b) 35 mol-% *trans*-**147**, c) 50 mol-% *trans*-**149** and d) 45 mol-% *trans*-**146** at the start of the reaction. All reactions were performed at 0 °C in CDCl₃ at 10 mM reagent concentration.

In the present discussion, it is the unusual dominance of *trans*-**147** accompanied by the suppression of *trans*-**146** and *trans*-**149** which demands a closer look at the emergent features of this system. The individual analysis of non-fluorinated *trans*-**98** revealed an uncommon behaviour for the doping experiments in which the maximum rate increased with the amount of added template. It was reasoned that the negative cooperativity of the template duplex leads to a larger amount of free template and increases correspondingly the number of catalytically active ternary complexes. The same principle seems to be responsible for the astounding performance of *trans*-**147** in this competition scenario. A negative value

for the free energy ($-1.36 \text{ kJ mol}^{-1}$) indicates negative cooperativity. With the duplex formation disfavoured energetically, more free template will be available in solution and can recognise the building blocks to form the ternary complex *via* two independent recognition events. In the two and three component scenarios, the actual cycloaddition reaction remains the rate-limiting step, but with more interacting components present in solution, the concentration of catalytic complexes becomes more crucial. In this 'crowded' four component system, it looks as *trans-147* has a clear advantage over the other systems simply by not having most of its template molecules locked up in the duplex.

According to this logic, *trans-148* should also perform much better than anticipated since it possesses the lowest value for the free energy of connection ($-8.99 \text{ kJ mol}^{-1}$). In fact, the isomer is being formed to nearly the same extent as the two replicators that were expected to be strongest, *trans-146* and *trans-149*. It also performs much better in the competition with its rivalling AB system, *cis-148*, with the final *cis/trans* ratio of diastereoisomers dropping to 1.4:1 from a previous 2.9:1. Overall, a total of 6.5 mM for both diastereoisomers of **148** were formed, a value nearly identical to the amount of *trans-147*. This symmetry in product formation stems from the connectivity of the four components. Every maleimide can react with one of the two nitrones, and *vice versa*. If one of the reactions is strengthened, the two building blocks become more scarce and all reactions depending on them are being down-regulated. Correspondingly, the reaction that does not rely on any of the two building blocks is enhanced even though its general reactivity remains unaffected. This beneficial relationship stimulates the concomitant formation of *trans-147* and both diastereoisomers of **148**. With *trans-147* and *trans-148* having the advantage of a low duplex stability and *cis-148* working as an AB system, all four building blocks are being depleted more rapidly. As a result, the formation of *trans-146* and *trans-149* is down-regulated. It is however not certain which of the two favoured autocatalytic systems in the network exerts the strongest pull, but their interconnectivity assures that any enhancement for one of the systems affects the other. If *trans-147* is indeed the most efficient system, maleimide **74** and nitrone **141** are being used up more rapidly and are missing for the formation of *trans-146* and *trans-149*. This in turn leaves a larger amount of maleimide **72** and nitrone **142** to react to **148**. The same logic applies when *trans-148* is seen as the dominant species.

Having established the main principles of this competition scenario, three doping experiments were performed. First, 35 mol-% of preformed *trans-147* template was added to the four reagents at the start of the reaction. The reaction was incubated at 0 °C and the product distribution was determined after complete conversion of all starting material. An increase in formation for *trans-147* can be seen from the calculation of the enhancements

and this up-regulation can be reasoned with the autocatalytic ability of the template (**Figure 6.25b**). Strengthening the formation of *trans*-147 corresponds with an increase in concentration for *trans*- and *cis*-148 in which the self-replicator was found to be more up-regulated than the AB system. The ratio between *cis* and *trans* has further dropped to 1.1:1 indicating that a surplus in building blocks favours the formation of the self-replicator. Since addition of *trans*-147 template enhances the autocatalytic formation of more template under depletion of maleimide 72 and carboxy nitron 141, the reactions for *trans*-146 and *trans*-149 are being down-regulated.

Next, the same experiment was repeated for the addition of 50 mol-% *trans*-149 and the enhancements for the five products relative to the native reaction were calculated (**Figure 6.25c**). It can clearly be seen that the presence of the template enhances the autocatalytic formation of more *trans*-149. With building blocks maleimide 74 and nitron 142 being less available, the formation of *trans*-147 and both diastereoisomers of 148 is down-regulated. As a result of the interconnectivity of the system, more maleimide 72 and nitron 141 becomes available and the concentration of *trans*-146 is increased to nearly the same extent as for *trans*-147.

The same principle holds for the addition of 45 mol-% *trans*-146 (**Figure 6.25d**). Autocatalytic enhancement of the added template is accompanied by an increase for self-replicator *trans*-149 with which it does not share any of the building blocks. Simultaneously, the concentrations for all competing species, *trans*-147 and 148, is lowered. The results presented in the last sections prove that even though the topology of the reaction network now exhibits emergent features, it can still be addressed with instructional template to alter the outcome of the competition scenario.

6.6 General conclusions

Using the results for the screening performed in chapter 3, four simple building blocks were combined successively in this chapter to form four three-component and one four-component set in which recognition-mediated templates are generated while engaging in competition for a limited amount of resources. The concerted introduction of fluorine tags into the building blocks allowed for direct and facile analysis of the progression and the outcome of the competition scenarios. The initial rivalry between AB system *cis*-148 and self-replicator *trans*-146 highlighted some fundamental principles. Having established the performance of the individual systems, the outcome of the competition reaction can be rationalised qualitatively, and the kinetic observation of the reaction progress corresponds

with what is expected: the AB system dominates the early phase of the reaction and depletes the common building block thereby suppressing the formation of *trans*-146. However, as a consequence of the self-replicating nature of *trans*-146, addition of increasing amounts of presynthesised replicating template fabricated more *trans*-146 on the expense of the AB system. Unfortunately, the relative impact of this manipulation decreases with increasing amount of added template, thus the system tends towards a saturation point at which the addition of more template does not alter the reaction outcome. This effect is a direct consequence of the fact that the template associates in solution to form a duplex structure. With a high association constant, the relative amount of free template decreases with template concentration. Hence, even when a significantly large amount of template is added to the reaction mixture, most of the template is trapped as duplex. The same response was seen for the second AB *vs* SR competition and the two scenarios between two replicators. Also in these cases, the outcome of the native reaction corresponded well with the performance of the individual systems and all three systems reacted rather rigidly to the manipulation with presynthesised template showing the presence of such saturation point.

For the initial competition between an AB system and a replicator, we were indeed able to rationalise qualitatively our findings and the behaviour of the system upon template addition, but we have failed to generate a reliable kinetic protocol that simulates the outcome of the competition and the formation of the major products quantitatively (**Figure 6.8**). Even though we have collected all necessary data for the individual reactions, merging the parameters into one script resulted in small but noticeable deviations. The prediction for the native reaction is rather satisfactory, but the simulation underestimates the effect of the doping experiments giving rise to lower amounts of replicator *trans*-146 than found in the experiment. Also the increase for side-product *trans*-148 is interpreted wrongly by the simulation. With these findings at hand, we can conclude that even for a relatively straightforward situation like the competition of an AB system with a self-replicator, a mere superimposition of the two individual reactions does not reflect the native situation and the directed manipulation with instructive template.

Using the established exchange procedure to generate the reactive nitron from an imine and a feed nitron limited the kinetic regime of the reaction network and resulted in greater enhancements upon addition of instructive template. With one of the building blocks formed only during the reactions, the relative concentration of the added template and its impact on the final product distribution is higher. It can be expected that this effect would also be seen for all other systems.

A rather unexpected result - when considering the performance of the individual systems - was found for the four component reaction. In this reaction network of increased complexity, the priority for a successful system shifted away from the catalytic prowess of the reaction in the ternary complex in favour of templates that possess the ability to generate a high concentration of free template. This finding again highlights that networks of higher order do not necessarily perform as a simple superimposition of their individual parts would suggest, but that their ability to interact and the connectedness of all entities result in emergent properties of the system. It is therefore to conclude that an analysis of single replicating systems and the extraction of kinetic data provides us with a qualitative understanding and allows for a comparison of reactivity, but in the context of networks with increasing complexity, the importance of these features has to be reclassified.

7. Multicyclic replicating systems

In the last chapter, several competition scenarios based on a set of four interacting compounds, two maleimides and two nitrones, were created and investigated. We showed that the equilibrium concentrations in the three component systems depended merely on the ratio of the catalytic efficiencies of the competing species. For the four component system, autocatalysts with low duplex association and high concentration of catalytic ternary complex were found to dominate the product pool. This change in mode of operation can be regarded as system-level behaviour caused by the increased interconnectedness of the individual entities. Despite this more complex behaviour, the system remained instructable by informational templates.

The four building blocks used for this complex network form two sets of reagents bearing the same reactive and recognition sites, amidopyridine maleimides and acid nitrones, giving rise to autocatalytic and AB products (**Figure 1.1a**). In order to further increase the interconnectedness of the building blocks in the network, we wish to incorporate reciprocal replication into our design. A reciprocal template bears two identical recognition sites and is dependent on a second template with complementary recognition units (**Figure 1.1b**). The formation of such templates therefore requires the presence of compounds that possess orthogonal reactive and recognition sites. In **Figure 2.3**, the design of a multicyclic system was presented in which two minimal replicators are interlinked to form two additional reciprocal catalytic cycles by pairwise combination of four starting reagents. Given the failure of designing such instructable multicyclic system in the laboratory, kinetic simulations were conducted to elucidate the network features essential for the generation of such complex system and the possibility to instruct them with informational template.

7.1 Computational analysis of a multicyclic system^[139]

A simple kinetic model (**Figure 7.1**) was constructed with the intention of creating a balanced situation between two self-replicators, **R1** and **R2**, which are formed by reacting building block **A** with **B** and **C** with **D**, respectively, and two reciprocal species, **T1** and **T2**, which are the products of the reaction of building block **A** with **D** and **B** with **C**, respectively. The rate constants for the bimolecular formation of all four templates were therefore set to a common value ($k_I = 5 \times 10^{-5} \text{ M}^{-1}\text{s}^{-1}$) and the rate constants for the formation of products through the template directed pathways were adjusted to give the same effective molarity for all replicators ($k_A = k_C = 1 \times 10^{-4} \text{ s}^{-1}$). The association for the individual recognition was set to $K_a = 1000 \text{ M}^{-1}$ with the association for the auto- and crosscatalytic duplex both being $1 \times 10^6 \text{ M}^{-1}$.

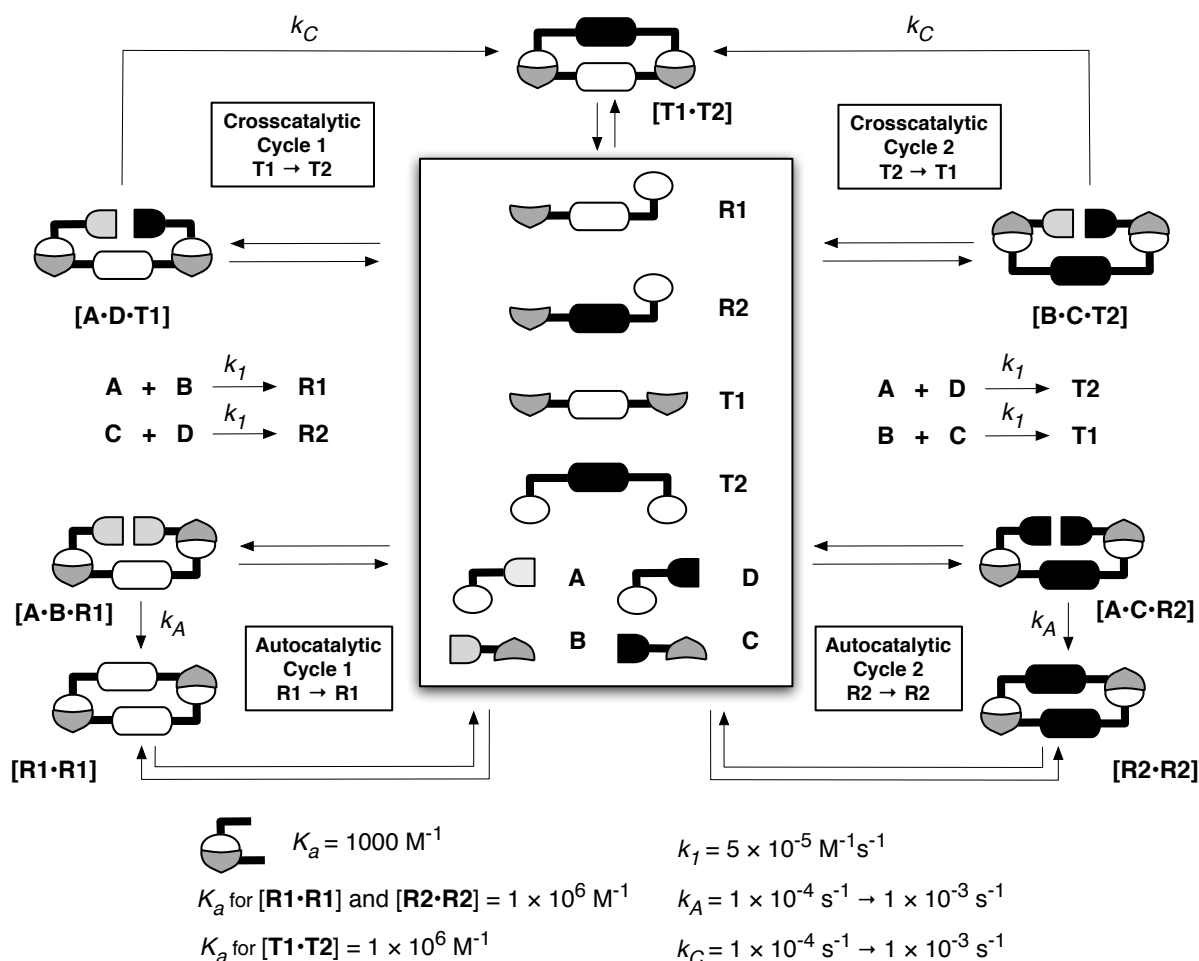


Figure 7.1 Replicator network constructed from two minimal replicators, **R1** and **R2**, and two reciprocal replicators, **T1** and **T2**. The network contains two autocatalytic cycles, mediated by the complexes **[R1·R1]** and **[R2·R2]**, and two linked crosscatalytic cycles, mediated by the complex **[T1·T2]**. The four templates are formed by pairwise combinations of the four starting reagents, **A** through **D**.

Accordingly, simulations were performed in which the initial concentrations of **R1**, **R2**, **T1** and **T2** were all set to zero and the initial concentrations of the reagents were set to 25 mM (**Figure 7.2**). In this situation, the two minimal replicators and two reciprocal replicators were indeed found to co-exist and after 16 h their concentrations were almost equal (lane marked **Native** in **Figure 7.2**). Taking this scenario as the initial starting point, the possibility of influencing the outcome of the multicyclic system by addition of preformed template at the start of the reaction was probed. For example, addition of template **R1** is expected to instruct the system to autocatalytically enhance the formation of more **R1**. However, as a consequence of the interconnected nature of the reaction network, an up-regulation of both self-replicating templates was observed on the addition of only one template or the other. Initial addition of 50 mol-% of minimal replicator **R1** resulted in an increase of the amount of **R1** from around 12 mM to around 18 mM (lane marked **+R1** in **Figure 7.2**). Concomitantly, there was also an enhancement for the formation of **R2** (to

around 17 mM) and a decrease in the amounts of the reciprocal templates **T1** and **T2** (to around 7 mM from 12 mM). Thus, the introduction of a substoichiometric amount of minimal template **R1** resulted in the output of the network being biased towards the formation of both **R1** and **R2**. The addition of the **R2** minimal replicator at the start of the reaction resulted in the same pattern of outputs (lane marked **+R2** in **Figure 7.2**). The amount of newly formed **R2** increased to around 18 mM, the amount of **R1** to around 17 mM and a decrease in the formation of **T1** and **T2** to around 7 mM was stated.

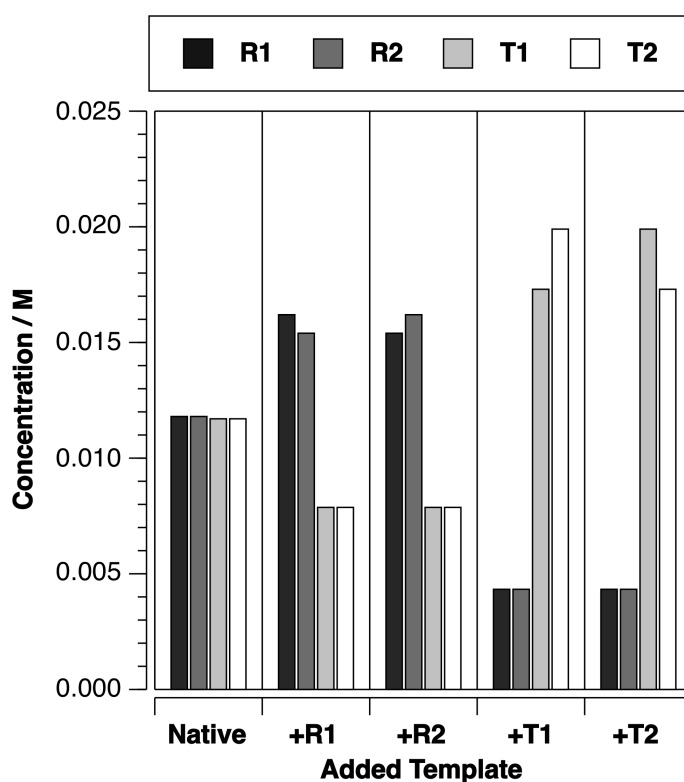


Figure 7.2 Simulation of a multicyclic system as depicted schematically in **Figure 7.1** with **R1** and **R2** as self-replicating templates, and **T1** and **T2** as reciprocal templates taken from ref. ^[139]. Bimolecular rate constants, effective molarities, association constants for the individual recognition and for the product duplex were chosen to be equal for all four replicating species. The concentration of reagents **A-D** was adjusted to 25 mM. In all lanes, the bars indicate the concentration of each template after 16 h and the bars are shaded to identify the individual templates according to the legend. The lane marked **Native** reflects the selectivity of the system without added template. In the other lanes, the identity of the added template is indicated by the label at the bottom of the lane.

The observed output pattern can be explained easily. The addition of preformed autocatalytic template **R1** at the start of the reaction ensures that the formation of this species is enhanced and building blocks **A** and **B** are being used up rapidly. Since both reciprocal templates **T1** and **T2** require either building block **A** or **B**, these two templates have a competitive disadvantage compared with **R1** and are being formed in lesser extent. On the

other hand, replicator **R2** does not share any building blocks with **R1** and, thus, it is free to exploit an increasing amount of building blocks **C** and **D** for its own construction.

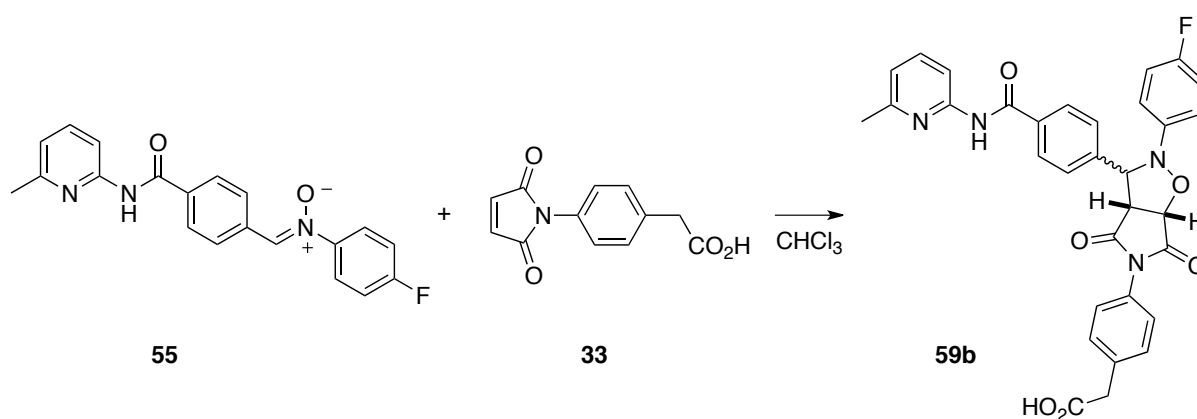
The reaction outcome is reversed upon addition of 50 mol-% of template **T1** at the start of the reaction (lane marked +**T1** in **Figure 7.2**). It is now the crosscatalytic partner **T2** which benefits the most with an enhancement from around 12 mM to around 20 mM after 16 h. Concomitantly, there is also an increase in the amount of **T1** to around 17 mM and a decrease in the amounts of the minimal template **R1** and **R2** to a mere 4 mM. The addition of 50 mol-% of the corresponding reciprocal replicator **T2** stimulates a very similar outcome (lane marked +**T2** in **Figure 7.2**). The same logic outlined for the addition of minimal template can be applied to explain the behaviour induced by addition of reciprocal template. Initial addition of **T1** crosscatalyses the formation of **T2**. Since **T2** needs building blocks **B** and **C** for its formation, a component required for the formation of each of the minimal replicators is removed rapidly from the reagent pool. With the enhanced formation of **T2**, it can then start to act as a catalyst for the formation of **T1** and this process begins to consume building blocks **B** and **C** which further limits the generation of both minimal replicators **R1** and **R2**. Since the crosscatalytic relationship connects both reciprocal templates **T1** and **T2**, their joint operation consumes all four building blocks creating a positive feedback loop which results in higher selectivities than in the case of the independently proceeding autocatalysts **R1** and **R2**. Addition of one of the self-replicating templates instructs the directed removal of only two of the available building blocks from the system whereas the enhancement of the other minimal template is an indirect and non-instructed feature of the process and an example of emergent system-level behaviour.

These theoretical results confirm that it is possible to construct a multicyclic network on the basis of a pair of reciprocal and two minimal replicators, and to influence the outcome of the system by addition of instructional template. However, the calculations discussed above assumed that the efficiencies of all four recognition-mediated processes were identical. It is highly unlikely that such an ideal situation can be reproduced in practice, but a scenario in which all efficiencies are of similar magnitude should suffice to verify the theoretical results.

7.2 Using *trans*-59b as preset replicator in the design of a multicyclic system

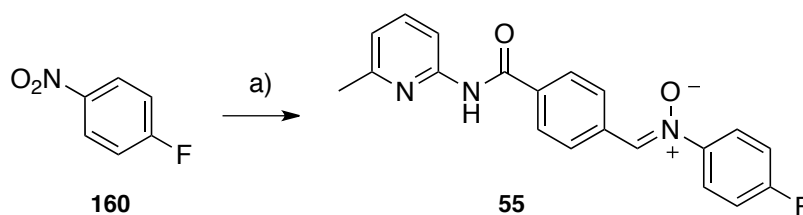
Each multicyclic system consists of four recognition-mediated interactions, two autocatalytic and two reciprocal (**Figure 7.1**). In the previous chapters, the reaction of two recognition-enabled maleimides with two acid nitrones leading to three self-replicating templates and

one hybrid system was investigated. Each of these systems can potentially be used as a fragment to build a multicyclic system, but they cannot be combined to form reciprocal templates, since the second self-replicating system must consist of two building blocks with reversed recognition and reactive sites in order to generate templates with two identical recognition sites. The reaction between amidopyridine nitrone **55** and acid maleimide **33** leads to the well-established replicator *trans*-**59b** and fulfills the criteria of orthogonal reactive and recognition sites (**Scheme 7.1**).^[140,188]



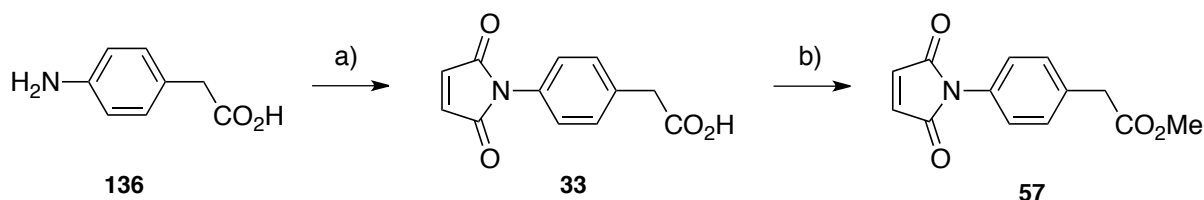
Scheme 7.1 Formation of template **59b** from nitrone **55** and maleimide **33** shows strong self-replicating activity for *trans*-**59b** and is used as a benchmark reaction for the design of a multicyclic system.

Both components of this self-replicating system were easily accessible from commercially available compounds. Nitrone **55** was synthesised in good yield from nitro compound **160** through partial reduction using bismuth trichloride and potassium borohydride as hydrogen source, and consequent condensation of the obtained hydroxylamine with aldehyde **134** presented previously (**Scheme 7.2**). The presence of the fluorine allows for the analysis of the autocatalytic and reciprocal products by ¹⁹F NMR spectroscopy.



Scheme 7.2 Synthesis of nitrone **55**. Conditions: a) BiCl₃, KBH₄, EtOH/H₂O, then **134**, EtOH, 46%.

Synthesis of maleimide **33** was achieved in acceptable yield by heating commercially available 4-amino-phenylacetic acid **136** in the presence of maleic anhydride in acetic acid. A small portion of the obtained acid maleimide **33** was further converted with methyl iodide and cesium carbonate in DMF to methyl ester **57** which was used as a recognition-disabled control compound (Scheme 7.3).



Scheme 7.3 Synthesis of maleimide **33** and control compound **57**. Conditions: a) maleic anhydride, AcOH, 80 °C, 70%; b) MeI, Cs₂CO₃, DMF, rt, 56%.

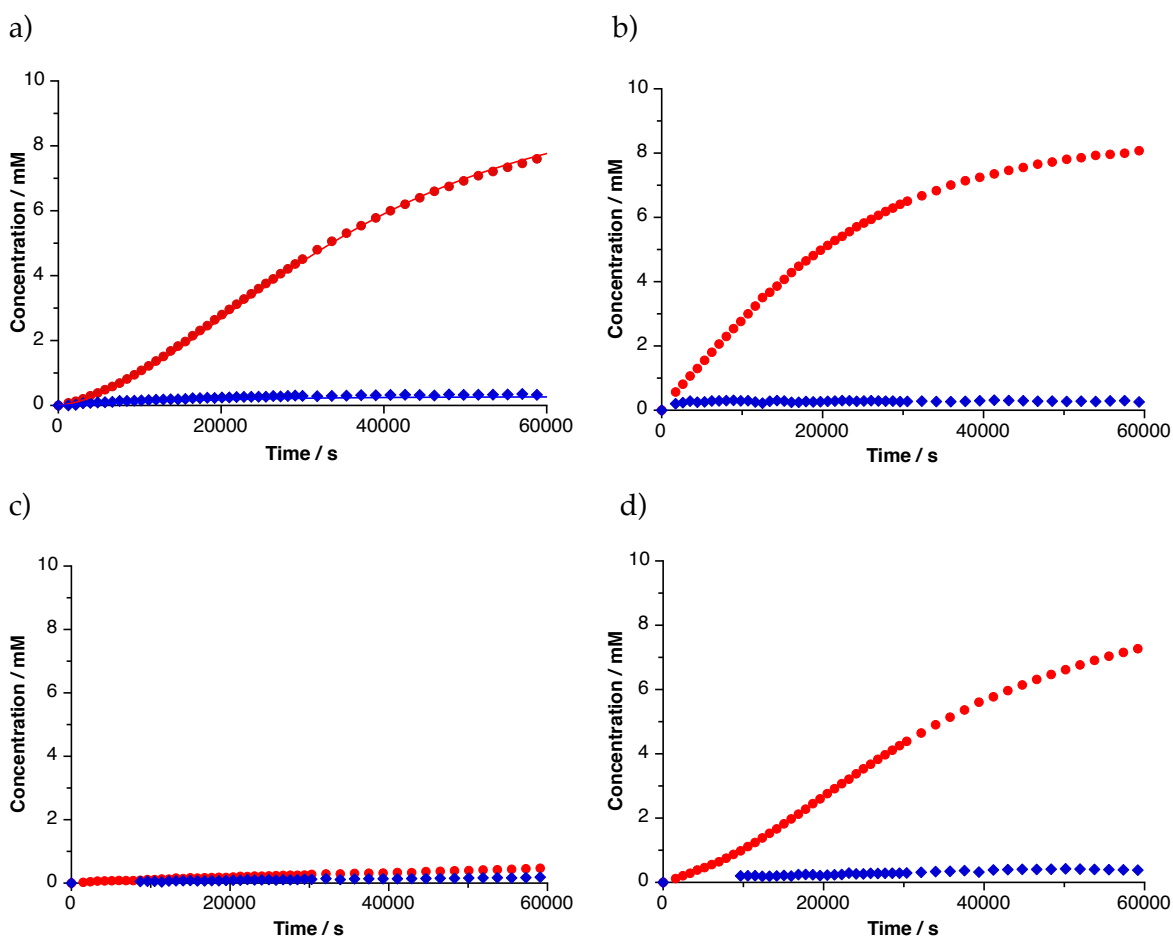


Figure 7.3 Concentration *vs* time profile for the reaction between a) maleimide **33** and nitrene **55** with straight lines representing the result for the fitting of the *trans*-(-) and *cis*-(-) product using SimFit, b) maleimide **33** and nitrene **55** in the presence of 10 mol-% *trans*-**59b**, c) maleimide **33** and nitrene **55** and d) maleimide **33** and nitrene **55** in the presence of 9 mol-% *trans*-**146**. The formation of *trans*-product is shown as red filled circles and the formation of *cis*-product as blue filled diamonds. All reactions were performed at 0 °C in CDCl₃ at 10 mM reagent concentration.

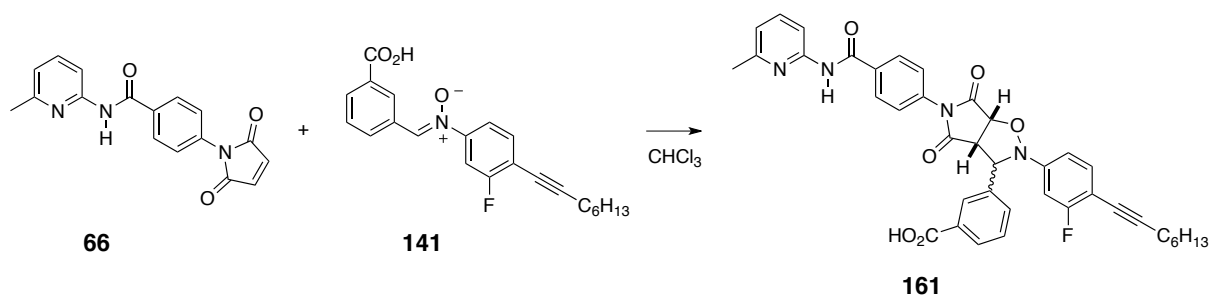
Following the reaction of **55** and **33** for 16 h in CDCl₃ at 0 °C with 10 mM concentration of starting materials clearly showed the characteristic sigmoidal shape for the formation of *trans*-**59b** (Figure 7.3a). Addition of 10 mol-% presynthesised *trans*-template verified the autocatalytic nature by overcoming the initial lag period (Figure 7.3b), whereas reaction of nitrone **55** with control maleimide **57** established the bimolecular rate of the reaction (Figure 7.3c). With respect to its application in the multicyclic system, it was crucial to demonstrate that there is no crosscatalytic relationship between this self-replicator and any of the other systems introduced in chapter 6. Hence, 9 mol-% of *trans*-**146** was added at the start of the reaction between nitrone **55** and maleimide **33**. It is obvious from the concentration *vs* time profile that the presence of the other template failed to catalyse the formation of *trans*-**59b** (Figure 7.3d). Identical profiles were obtained upon addition of *trans*-**149** (10 mol-%), *trans*-**147** (8 mol-%) and a mixture of *cis*- and *trans*-**148** (6.5 and 3.5 mol-%, respectively). Fitting of the native experiment with SimFit went smoothly (Figure 7.3a) and provided the kinetic parameter listed in Table 7.1 suggesting that *trans*-**59b** is a fairly strong self-replicating system.

Table 7.1 Kinetic parameters extracted for the self-replicating reaction of maleimide **33** and nitrone **55** at 0 °C in CDCl₃ at 10 mM reagent concentration using SimFit.

	<i>trans</i> - 59b	<i>cis</i> - 59b
bimolecular rate constant / M ⁻¹ s ⁻¹	2.66 x 10 ⁻⁴	1.12 x 10 ⁻⁴
recognition-mediated rate constant / s ⁻¹	1.32 x 10 ⁻³	-
effective molarity / M	4.96	-
ΔG^s / kJ mol ⁻¹	12.5	-

7.3 Using *trans*-**161** as replicator in the design of a multicyclic system

Having established the efficiency of replicator *trans*-**59b**, this autocatalyst can now be combined with any of the four replicating systems discussed in the previous chapters. We chose *trans*-**161** to be the first candidate. In order to facilitate later computational analysis of the envisaged multicyclic system, maleimide **72** bearing the 4,6-dimethyl pyridine recognition unit was replaced by maleimide **66** (Scheme 7.4). Separate kinetic analysis of this novel system allowed for the fitting of the experimental data (Figure 7.4 and Table 7.2).



Scheme 7.4 Formation of template **161** from maleimide **66** and nitron **141** shows strong self-replicating activity for *trans*-**161**.

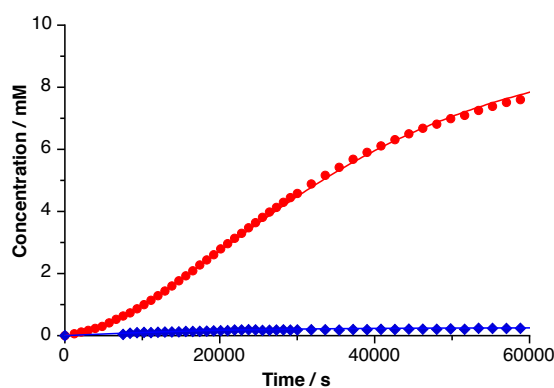


Figure 7.4 Concentration *vs* time profile for the reaction between maleimide **66** and nitron **141** to give template **161**. The formation of *trans*-product is shown as red filled circles and the formation of *cis*-product as blue filled diamonds. Straight lines represent the results for the fitting of the *trans*-(-) and *cis*-(-) product. The reaction was performed at 0 °C in CDCl₃ at 10 mM reagent concentration.

It can be seen that the removal of the second methyl group has very little effect on the performance of the self-replicator. Compared with the original replicator *trans*-**146** (in 6.4.1), the effective molarity is increased slightly and the duplex association remains the same. Even though *trans*-**161** has a significantly higher EM than *trans*-**59b**, the construction of a fully functional multicycle is first attempted by coupling these two self-replicators.

Table 7.2 Kinetic parameters extracted for the self-replicating reaction of maleimide **66** and nitron **141** at 0 °C in CDCl₃ at 10 mM reagent concentration using SimFit.

	<i>trans</i> - 161	<i>cis</i> - 161
bimolecular rate constant / M ⁻¹ s ⁻¹	2.23 x 10 ⁻⁴	1.14 x 10 ⁻⁴
recognition-mediated rate constant / s ⁻¹	1.59 x 10 ⁻²	-
effective molarity / M	71.3 (<i>cf.</i> 58.8 for <i>trans</i> - 146)	-
ΔG^s / kJ mol ⁻¹	13.4 (<i>cf.</i> 13.3 for <i>trans</i> - 146)	-

However, not only the efficiencies of the two self-replicating systems play a crucial role, but in order to allow for clean analysis of the final four component systems, the crosscatalytic activities between the reciprocal templates were tested before the original set of four compounds was ultimately combined to form the multicyclic system. Once the functioning of a multicyclic system has been established, the instruction of the reaction by addition of preformed template was probed.

7.4 A Multicyclic system based on *trans*-59b and *trans*-161

The envisaged network of maleimides **66** and **33** and nitrones **141** and **55** is depicted in **Figure 7.5**. In this scenario, maleimide building block **33** can perform as a self-replicator with nitron **55** to give rise to template *trans*-59b, but it can also react with nitron **141** to form template **162**. The second replicating system is established by reacting maleimide **66** with nitron **55**, whereas combining maleimide **66** with nitron **55** leads to bisamido template **69**.

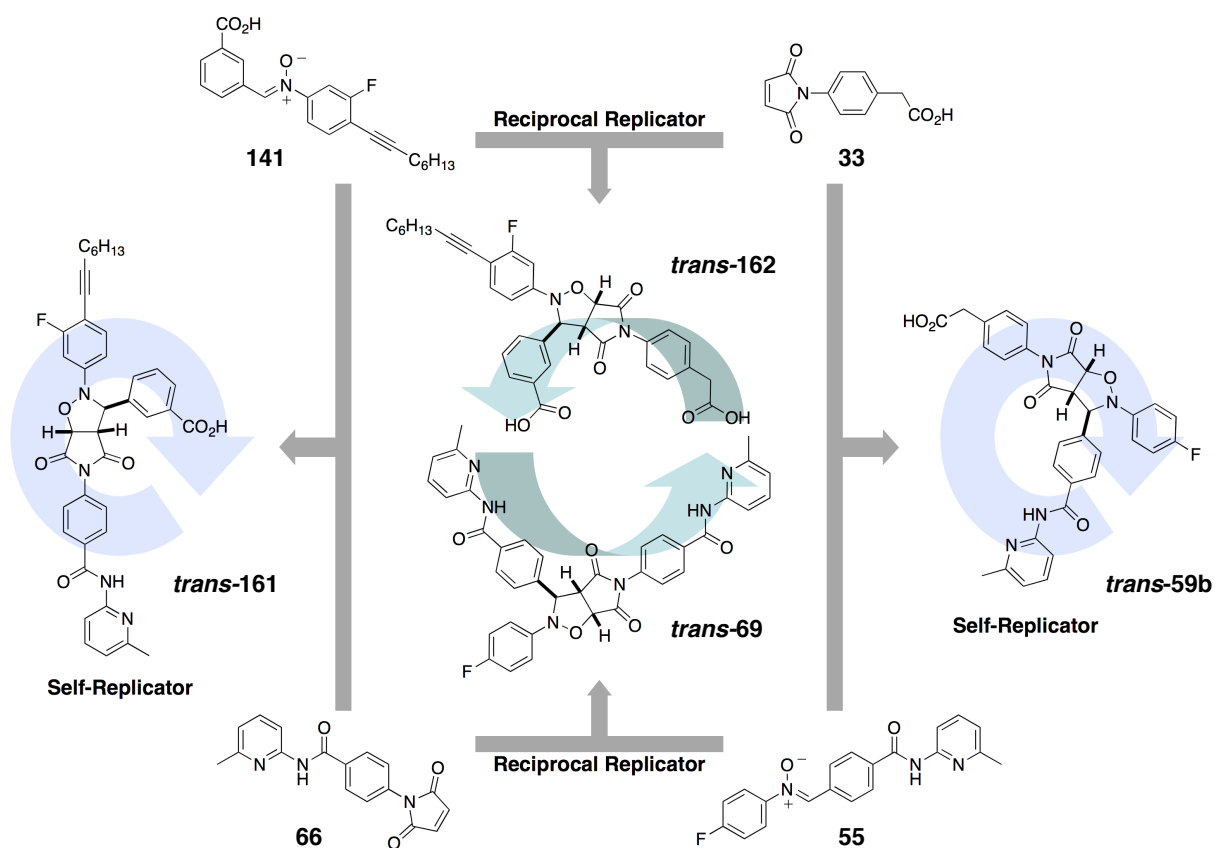


Figure 7.5 Multicyclic network combining the self-replicating systems *trans*-161 (from maleimide **66** and nitron **141**) and *trans*-59b (from maleimide **33** and nitron **55**) to form two additional reciprocal templates *trans*-162 and *trans*-69.

Besides the well-established self-replicating nature of the building blocks, the functionality of this system relies heavily on the presence of a crosscatalytic relationship between the reciprocal templates. Computational modeling of the template structures suggests that the main reciprocal interaction is bound to occur between the *trans*-isomers of the diacid and the bisamido template (**Figure 7.6**), since they possess a linear structure in which the recognition sites are available for association. The length of the templates appears to be suitable for formation of the product duplex [*trans*-**69**·*trans*-**162**]. Template *trans*-**162** bears two acid moieties that recognise amido pyridine with different single-point association constants. However, application of 6-methyl maleimide **66** instead of 4,6-dimethyl maleimide **72** rendered the bisamido template symmetrical in terms of recognition and it is difficult to rationalise the precise respective orientation of the two reciprocal templates. It can be speculated whether the carboxylic acid or phenylacetic acid has any preference for one side of the bisamido template or whether geometric factors favour one orientation over the other.

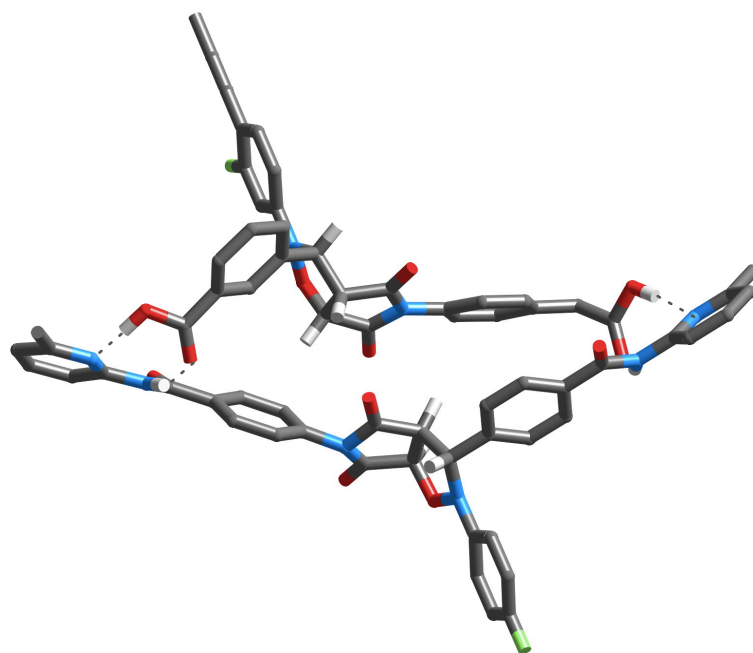
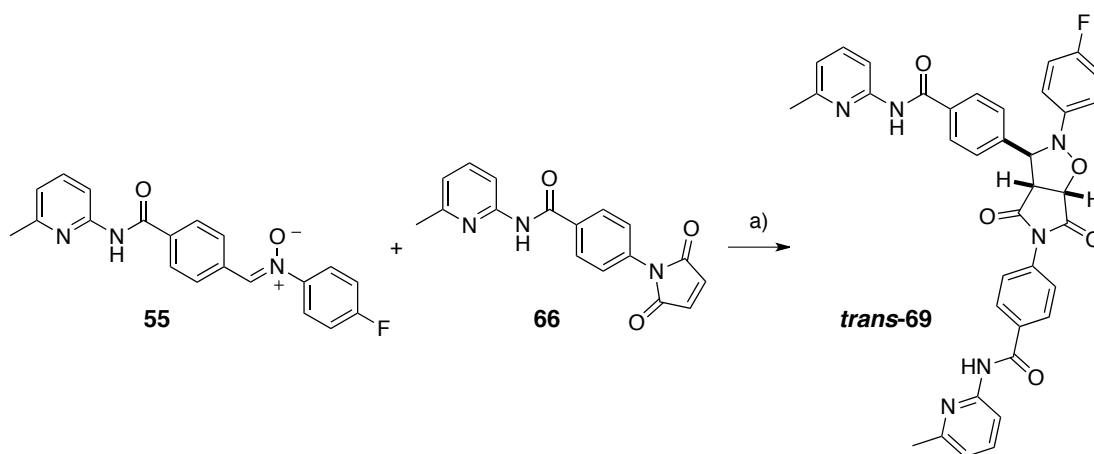


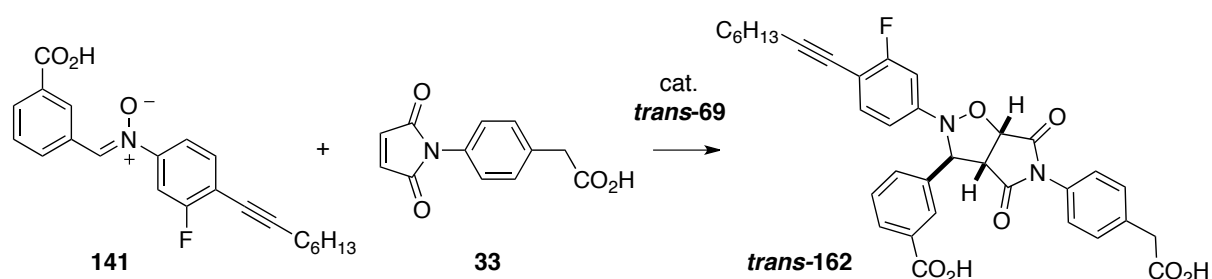
Figure 7.6 Molecular model of the reciprocal duplex of *trans*-**162** and *trans*-**69**. Carbon atoms are shown in dark grey, hydrogen atoms in light grey, nitrogen atoms in blue and oxygen atoms in red. Hydrogen bonds are indicated by the dotted lines. Most other hydrogens were omitted for clarity.

In order to probe the efficiency of the reciprocal interaction, bisamido template *trans*-**69** was synthesised by reacting nitrone **55** and maleimide **66** in chloroform at room temperature and separating the diastereoisomers by column chromatography (**Scheme 7.5**).



Scheme 7.5 Synthesis of template *trans*-69. Conditions: a) CHCl₃, rt, 50%.

Next, purified template *trans*-69 was used as reciprocal catalyst for the reaction of maleimide **33** and nitron **141** (**Scheme 7.6**). In absence of any added template, the reaction between both acids was found to be slow and unselective. Kinetic analysis at 0 °C for 16 h at 10 mM concentration showed a ratio of 1.7:1 for the *trans*-isomer of **162** with only 12% of the starting material converted (**Figure 7.7a**). Addition of various amounts of presynthesised *trans*-69 at the start of the reaction confirmed instantly the crosscatalytic relationship between both *trans*-templates (**Figure 7.7b**). Injecting 16 mol-% *trans*-69 to a fresh batch of reagents increased the selectivity to 18:1 in favour of the *trans*-product with 31% of the starting material converted. After the same time, doping the mixture with 55 mol-% *trans*-69 further pushed the ratio to 110:1 with 63% conversion of starting material. Addition of a stoichiometric amount of template (98 mol-% *trans*-69) gave almost complete conversion of all starting material and only the *trans*-product was detected by ¹H NMR spectroscopy.



Scheme 7.6 Formation of *trans*-162 in the absence or presence of reciprocal template *trans*-69. Kinetics for the native reaction and doping experiments using various amounts of *trans*-69 are depicted in **Figure 7.7**.

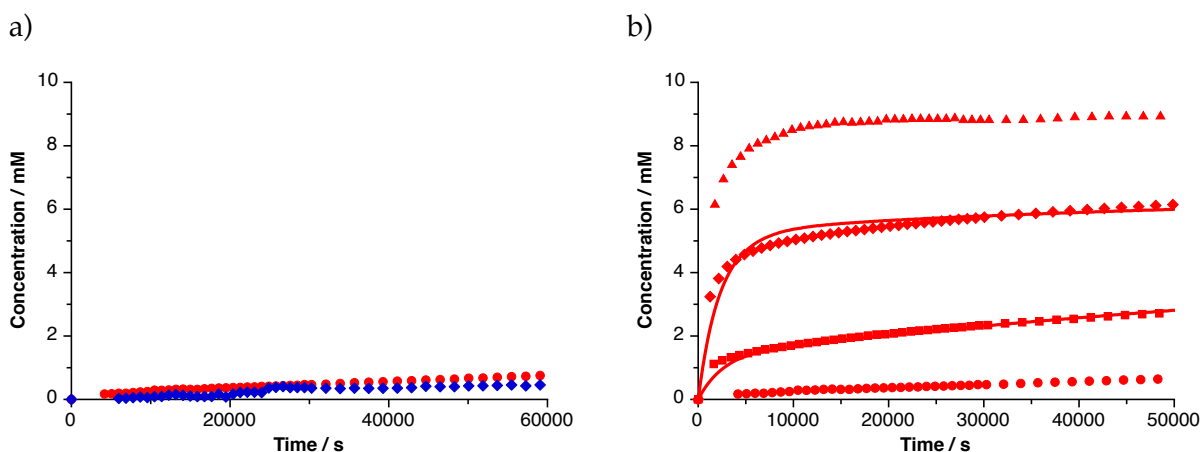


Figure 7.7 Concentration *vs* time profiles for the reaction of nitrone **141** and maleimide **33** to give *trans*-(●) and *cis*-(◆) **162** a) in the absence of any added template b) in the presence of 0 (●), 16 (■), 55 (◆) and 98 (▲) mol-% added *trans*-**69**. In b) straight lines (–) represent the results for the fitting of the *trans*-product with all *cis*-isomers omitted for clarity.

In all cases, the initial increase in rate for the formation of *trans*-**162** was found to be proportional to the amount of added reciprocal template *trans*-**69**. However, once the concentration of the product matched the amount of added template, the rate of the reaction decreased significantly suggesting strong product inhibition between the reciprocal templates and therefore limiting the catalytic turnover. When all *trans*-**69** template added initially is saturated with product molecules, the main contribution for formation of further product stems only from the bimolecular reaction.

In order to establish the effectiveness of the corresponding diacid template *trans*-**162**, attempts were made to synthesis, purify and separate the catalytically active *trans*-template from starting materials **141** and **33**. However, in the presence of an excess of acid, nitrone **141** showed only limited stability and decomposed over the course of the reaction, thereby diminishing significantly the yield of the reaction and making the purification by column chromatography very difficult. Crystallisation from acetone provided a clean sample of a mixture of both isomers, but all attempts to redissolve the diastereoisomeric template mixture in CDCl₃ to study its catalytic property failed, most probably as a consequence of the presence of the two acid functionalities. Despite the limited solubility of purified **162** template, no precipitate was observed for the reciprocal experiments depicted in **Figure 7.7b** or during the investigation of the multicyclic system owing to the hydrogen bonds between the acid moieties and the amidopyridine units.

In order to extract kinetic parameters for this reciprocal system, the experimental data from **Figure 7.7** were fitted to a kinetic model using SimFit (see appendix). The bimolecular rates for the formation of both diastereoisomers of **162** were extracted from the native experiment. Mutual fitting of the experimental results for the doping with 16 and 55 mol-%

trans-**69** proceeded smoothly and provided the results listed in **Table 7.3**. The free energy of connection was calculated using

$$\Delta G^s = RT \ln \left(\frac{K_{duplex}}{K_{ind,1} \times K_{ind,2}} \right)$$

with gas constant R and temperature T. The single-point associations $K_{ind,1}$ and $K_{ind,2}$ between 6-methyl amido pyridine and both acids were taken from **Table 4.1** ($K_{ind,1} = 1020 \text{ M}^{-1}$ for phenylacetic acid and $K_{ind,1} = 3750 \text{ M}^{-1}$ for carboxylic acid). The value for K_{duplex} was provided by the fitting procedure.

Table 7.3 Kinetic parameters for the reaction of maleimide **33** and nitrone **141** to give cycloadduct **162** at 0 °C in CDCl₃ at 10 mM reagent concentration. The kinetic parameters for the crosscatalytic relationship between *trans*-**162** and *trans*-**69** were determined by fitting the experimental data depicted in **Figure 7.7b** using SimFit. Values for replicators *trans*-**161** and *trans*-**59b** are listed for comparison.

	<i>trans</i> - 162	<i>cis</i> - 162	<i>trans</i> - 161	<i>trans</i> - 59b
bimolecular rate constant / $\text{M}^{-1} \text{s}^{-1}$	1.51×10^{-4}	9.39×10^{-5}	2.23×10^{-4}	2.66×10^{-4}
recognition-mediated rate constant / s^{-1}	1.53×10^{-3}	-	1.59×10^{-2}	1.32×10^{-3}
effective molarity / M	10.1	-	71.3	4.96
ΔG^s / kJ mol^{-1}	10.6	-	13.4	12.5

Computational analysis confirmed the experimental findings that *trans*-**69** is a selective catalyst for the enhanced formation of *trans*-**162** and that both *trans*-templates can associate to form a well-matched duplex. When bound to the bisamido catalyst, the rate constant for the cycloaddition of building blocks **141** and **33** is ten times higher than in the bimolecular reaction (EM = 10.1 M) and the emerging product duplex shows major positive cooperativity. The values are similar to the ones found for the analysis of the reciprocal system in the multicyclic design depicted in **Figure 1.22** (EM = 27.0 M and $\Delta G = 5.2 \text{ kJ mol}^{-1}$).^[138] But more importantly, the EM and the duplex stabilisation are in the same magnitude as for the two self-replicators *trans*-**59b** and *trans*-**161** with which they will compete in the final multicycle. Comparison of the kinetic parameters obtained for all participating systems in isolation reveals that *trans*-**161** possesses by far the highest effective molarity and might be expected to be the dominant species in the multicyclic network.

7.5 Analysis of the multicyclic system based on *trans*-59b and *trans*-161

Having established the efficiencies of the autocatalysts as well as the reciprocal relationships between templates *trans*-69 and *trans*-162, the functionality of the multicycle as a whole could now be investigated. All four compounds, 33, 55, 141 and 66 were mixed in CDCl₃ at 10 mM starting concentration and the progression of the reaction was followed by ¹⁹F NMR spectroscopy. Initially, kinetic data was recorded at 0 °C, but overlap of the broadening product peaks from template *trans*-162 and template *trans*-161 at higher concentrations hampered the deconvolution of the obtained spectra. Increasing the temperature to 10 °C gave a better resolution of the particular peaks and facilitated the analysis of the recorded data. The resulting concentration *vs* rate profiles for both temperatures are presented in **Figure 7.8**. The shapes of the curves for the formation of the four possible template products are very similar in both experiments. The only major difference between both profiles is the increase in rate and shortening of the time frame of observation. In both experiments, no noticeable formation of *cis*-products was detected.

Overall, both reciprocal templates *trans*-69 and *trans*-162 are formed in greater abundance than the two self-replicating templates *trans*-161 and *trans*-59b. More intriguingly, their formation shows a sigmoidal rate profile with almost identical gradient for both templates. This simultaneous progression is a result of the crosscatalytic nature which links inseparably both reciprocal templates and forces them to work in a symbiotic manner. At the start of the reaction, all templates need to be formed through the slow and unselective bimolecular reaction. As soon as a reciprocal template is formed, it can start to crosscatalyse its partner template which in turn can catalyse the reaction to form another molecule of the initial template. It is interesting to state that in the multicyclic system, the performance of the reciprocal pathway is not hampered by product inhibition. Efficient catalytic turnover of the formed cycloadduct templates leads to the formation of the sigmoidal curve usually found for self-replicating systems.

With the reciprocal system being the dominant species in this network, both self-replicators are only formed to smaller amounts. Despite their independent catalytic cycles, both replicators are also being formed isochronously. As a consequence, a clear splitting can be seen in the rate profile for both types of replication with the reciprocal version being the more efficient one. A different pattern can be seen when combining the formation of products deriving from the same nitrene, *trans*-162 with *trans*-161 and *trans*-69 with *trans*-59b (**Figure 7.8c**). Both nitrenes are being incorporated into the product templates at nearly identical rate with the profiles showing the characteristic sigmoidal shape.

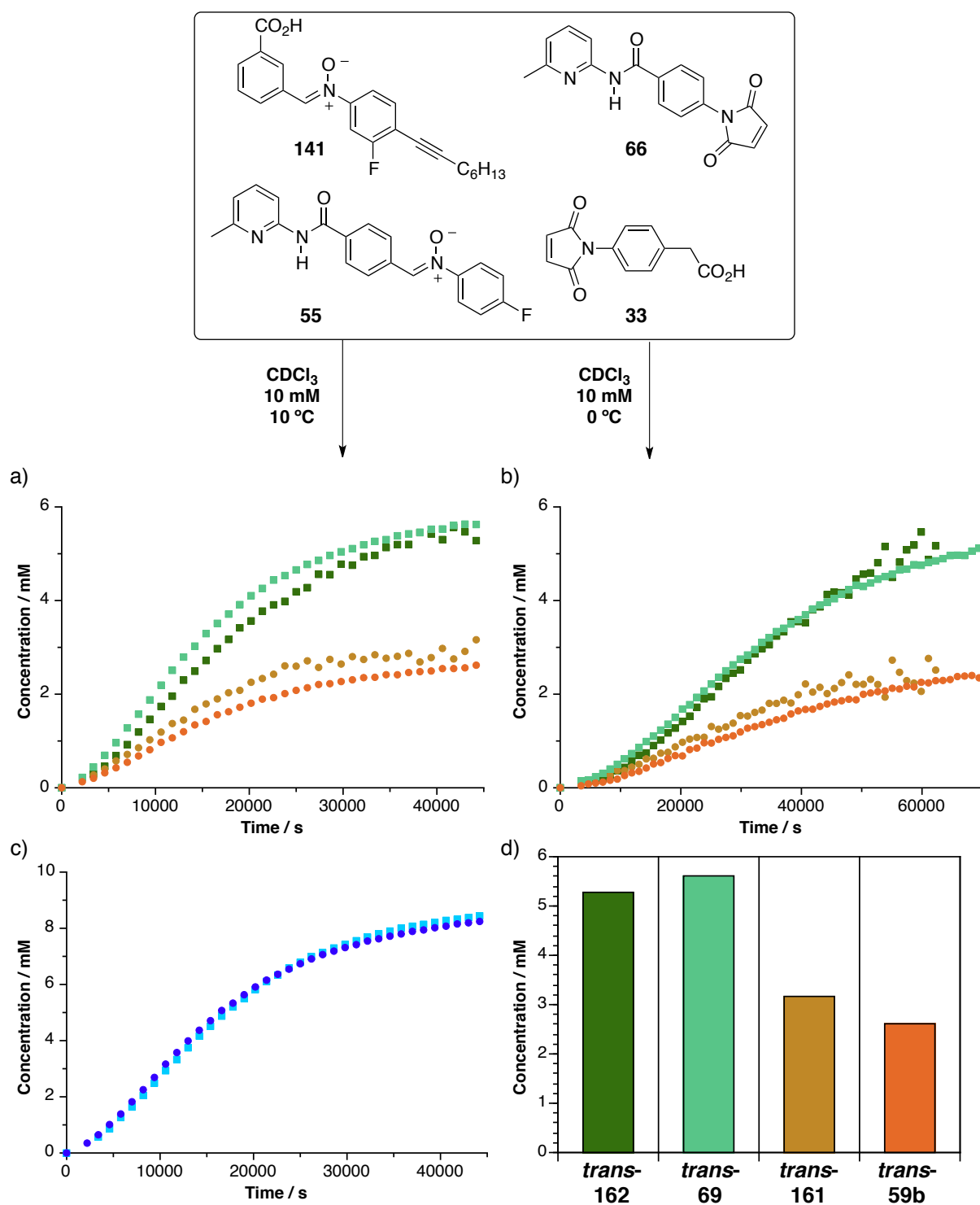


Figure 7.8 Concentration *vs* time profiles of the multicyclic system depicted in **Figure 7.5** at a) 0°C and b) 10°C followed by ^{19}F NMR spectroscopy. The reaction of maleimides **33** and **66** with nitrones **141** and **55** gives rise to self-replicating templates *trans*-**161** (●) and *trans*-**59b** (●) and reciprocal templates *trans*-**162** (■) and *trans*-**69** (■). c) Overlay of all template products deriving from nitrone **141** (■) and **55** (●) are depicted for the reaction at 10°C . d) Product distribution for the templates after 12 h at 10°C .

After 12 h at 10°C , the conversions of nitrones **141** and **55** were determined to be 84% and 83%, respectively, with similar concentrations for *trans*-**162** (5.28 mM) and *trans*-**69** (5.62 mM). The concentration of self-replicator *trans*-**161** (3.16 mM) was slightly higher than

trans-59b (2.61 mM). The reaction solution was further monitored until complete conversion of all starting material was detected. The final ratio of reciprocal replicators to self-replicators was calculated to be 2.1 which reflects an absolute concentration of 6.87 mM *trans*-162 and *trans*-69, and only 3.13 mM self-replicators *trans*-161 and *trans*-59b.

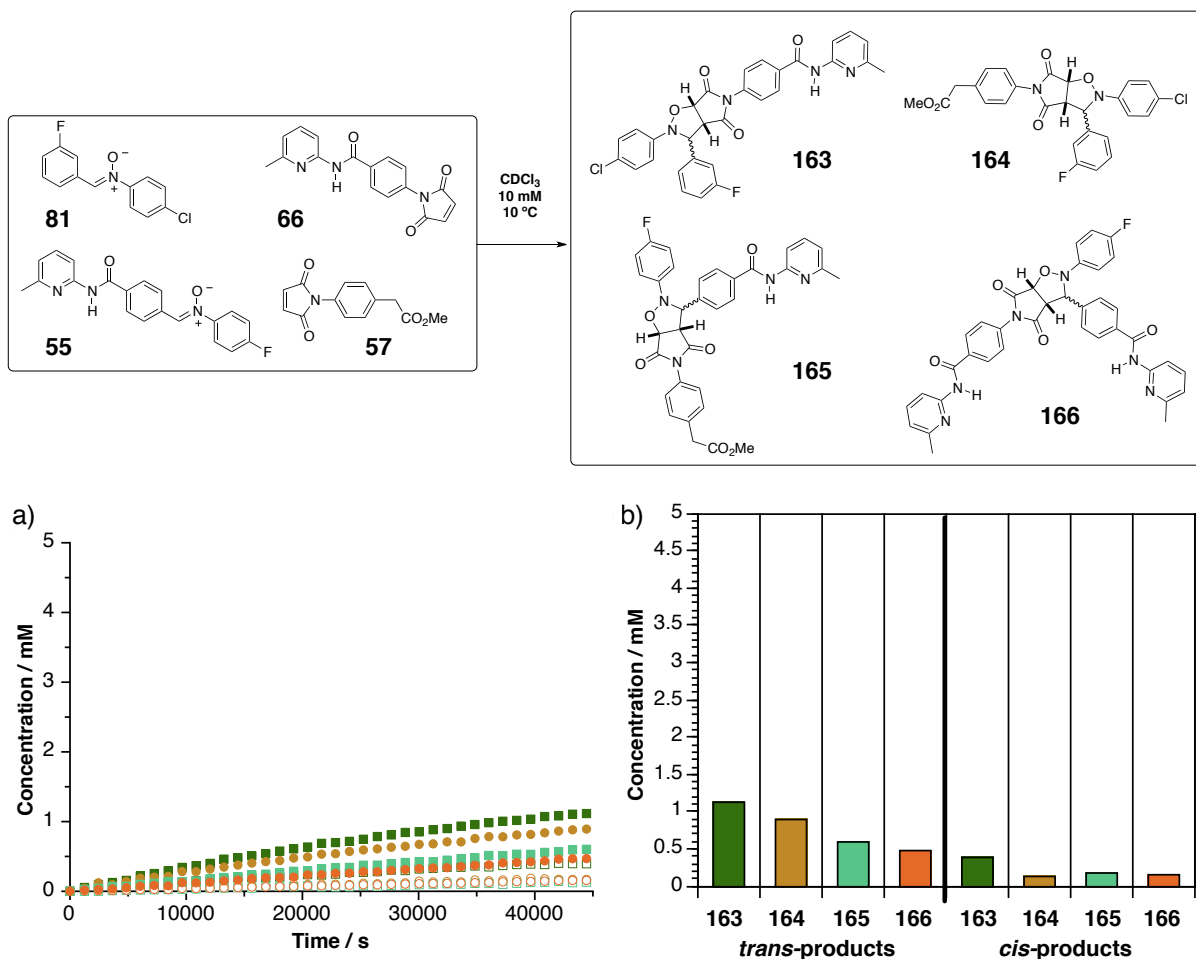


Figure 7.9 Concentration *vs* time profile of the control reaction of the multicyclic system between nitrones **81** and **55**, and maleimides **57** and **66** at 10 °C and 10 mM starting material concentration followed by ^{19}F NMR spectroscopy to form four sets of diastereoisomeric templates with a) *trans*-templates shown as filled circles and squares, and *cis*-templates as hollow circles and squares. b) Product distribution for the reaction at 10 °C after 12 h.

In order to rule out any non-recognition mediated processes as source of the reactivity found in the multicycle, a control reaction was conducted in which acid maleimide **33** was replaced with its methyl ester **57** and acid nitrone **141** was substituted with its control compound **81**. In this system, the lack of productive hydrogen bonding prevented the rate-enhanced formation for any of the possible diastereoisomers (**Figure 7.9**). Accordingly, the reaction between the building blocks proceeded with low selectivity giving rise to a mixture of four sets of diastereoisomeric products, none of which was formed to more than 1.2 mM after 12 h.

7.6 Instructing the multicyclic system

As shown in the previous section, a fully functional multicyclic network was established in which two self-replicating systems were coupled to give rise to an additional reciprocal relationship. Next, we set out to probe whether the interconnectedness of the system can be exploited to generate responses to external stimuli. In the theoretical discussion presented previously (**Figure 7.1 and 7.2**), addition of preformed template at the start of the reaction was shown to alter the network topology by strengthening selectively one of the catalytic relationships. In chapter 6, this instruction method was used to manipulate the outcome of various competition scenarios in favour of the added autocatalyst. Replicator systems with up to four building blocks were investigated and all proved to be instructable. Up to this point, no experimental work has dealt with the directed instruction of a network of increased complexity such as the multicycle presented in the previous section. In **Figure 2.2**, we presented simple calculations on hypothetical reaction networks which suggested that the response of the network to the addition of instructional template is proportional to the degree of interconnection among the building blocks. In the multicycle, each starting compound can react *via* two catalytic modes, two independent autocatalytic cycles and one crosscatalytic relationship. It is especially for the presence of the reciprocal replicators that the entities in this reaction network are tightly linked, rendering the network susceptible to manipulation with instructional template.

Taken the results of the theoretical discussion as a lead, we can speculate about the behaviour of this multicycle upon addition of instructional template. The presence of reciprocal template in the reaction mixture is expected to shift the product distribution towards the crosscatalytic products whereas addition of self-replicating template should influence the outcome in a selfish manner by up-regulating the formation of more autocatalyst. In order to elucidate this hypothesis, a set of experiments were conducted in which a fixed amount of bisamido template *trans*-**69** or one of the autocatalytic templates *trans*-**161** or *trans*-**59b** was added to the four components of the multicycle at the start of the reaction.

7.6.1 Addition of 20 mol-% reciprocal template *trans*-**69**

The first experiment was conducted by adding 20 mol-% *trans*-**69** to an equimolar mixture of compounds **141**, **33**, **66** and **55** at 10 mM concentration in CDCl₃. The reaction mixture was incubated at 10 °C and its progression was followed by ¹⁹F NMR spectroscopy. Deconvolution of the obtained spectra gave rise to the rate profile depicted in **Figure 7.10**.

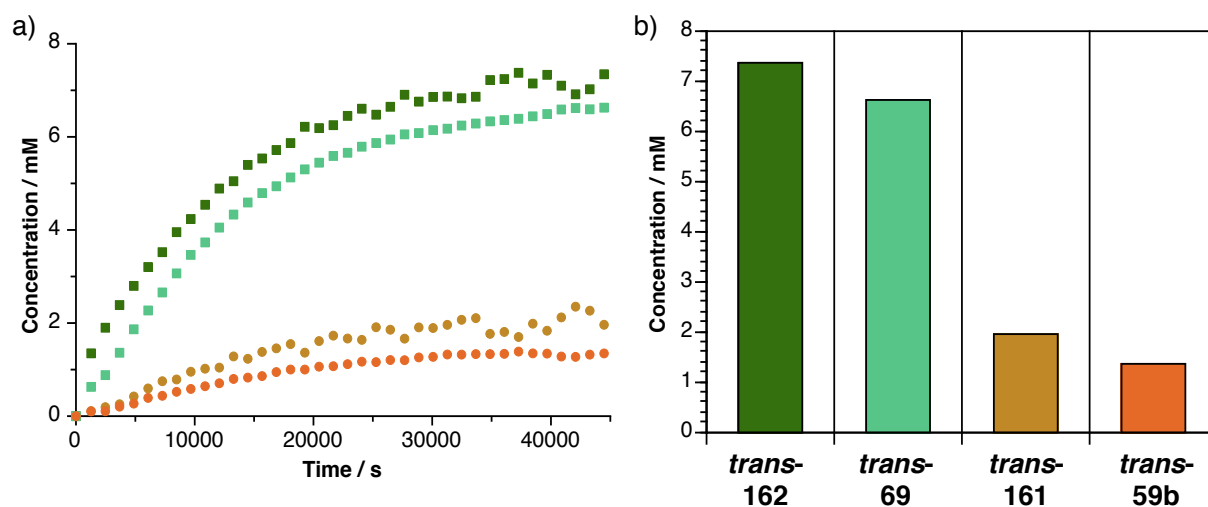
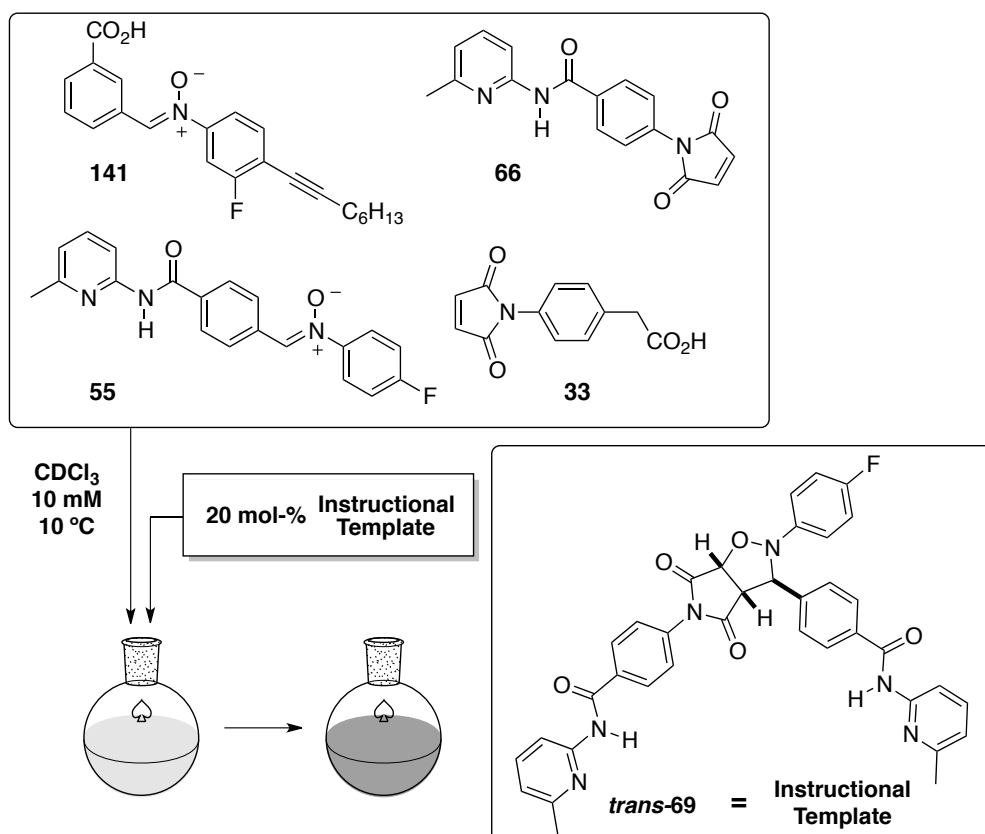


Figure 7.10 Concentration *vs* time profile of the multicyclic system depicted in **Figure 7.5**. a) The reaction of maleimides **33** and **66** with nitrones **141** and **55** in the presence of 20 mol-% *trans*-**69** gives rise to self-replicating templates *trans*-**161** (●) and *trans*-**59b** (●) and reciprocal templates *trans*-**162** (■) and *trans*-**69** (▣). The reaction was performed at 10°C in CDCl_3 at 10 mM reagent concentration and followed by ^{19}F NMR spectroscopy. b) Product distribution for the templates after 12 h.

Satisfyingly, the expected response of the multicyclic system to the addition of preformed reciprocal template can clearly be seen. Both reciprocal templates were formed in larger extent than in the initial experiment and, accordingly, the formation of the self-replicating templates *trans*-**161** and *trans*-**59b** was down-regulated. Right from the start, diacid template *trans*-**162** is the most abundant species in the reaction mixture owing to the direct catalytic relationship with seeded template *trans*-**69** whose overall concentration was

corrected by subtracting the amount of added template to only account for the newly formed molecules. This correction is reflected in the difference of concentration between both reciprocal replicators which is roughly 1 mM throughout the reaction. Since the *trans-69* template added initially was readily available at the start of the reaction, formation of corresponding *trans-162* template did not show any lag period but a relatively steep incline similar to the case of isolated reciprocal doping experiments. At the start of the reaction, a significant amount of *trans-162* was present which in turn catalysed the formation of more *trans-69* template thereby completing the crosscatalytic relationship between both templates. As a consequence of the rapid initial formation of diacid template, the lag period for the formation of *trans-69* is less pronounced than in the native experiment. After 12 h, *trans-162* was found to be the dominant species with a concentration of 7.34 mM followed by *trans-69* with 6.63 mM.

Both self-replicating systems perform significantly weaker than in the native experiment because all four necessary building blocks are used up more rapidly by the crosscatalytic system. With a smaller concentration of reagents present at the early stage of the reaction, the bimolecular reaction to form the autocatalytic templates was suppressed and once a certain amount was produced, most of the reagents have already been incorporated into one of the reciprocal templates. As a consequence, the curves for both self-replicating templates do not show a pronounced sigmoidal shape. Since the amplified reciprocal system is using all four of the available building blocks, both self-replicating templates are being down-regulated in the same extent. After 12 h, their concentration was established to be 1.96 mM for *trans-161* and 1.34 mM for *trans-59b*. The conversion of nitrene **141** into products increased from 84% in the native reaction to 93% as a result of the induced rate-enhancements.

In order to compare the results of the doping reaction with the native multicycle, the reaction was kept at 10 °C until all starting material was converted into products. As a consequence of the symmetry of the closed network, equal concentrations for the two self-replicating and the two reciprocal species were obtained. In the native experiment, the final ratio between the reciprocal and the autocatalytic replicators was found to be roughly 2.1 with a final concentration of 3.13 mM for both self-replicators and 6.87 mM for the reciprocal templates. In the doping experiment, the final RR/SR ratio for the two replicator species increased to 3.6 with the final concentration for both self-replicating species dropping to 2.16 mM and increasing to 7.84 mM for the reciprocal templates (**Figure 7.11a**). The change in product formation with respect to the native reaction is highlighted as enhancement E according to

$$\text{Enhancement } E = \log_{10} \frac{C_{\text{dopant}}}{C_{\text{native}}}$$

Equation 7.1

with C_{dopant} and C_{native} as concentration of a particular species in the doped and native experiment, respectively. A clear enhancement for the formation of reciprocal replicators can be seen (**Figure 7.11b**). Since they were already the dominant species in the native experiment, the relative enhancement is smaller than the decrease for the self-replicators. The change in template concentration is reflected in the pie chart depicted in **Figure 7.11c**.

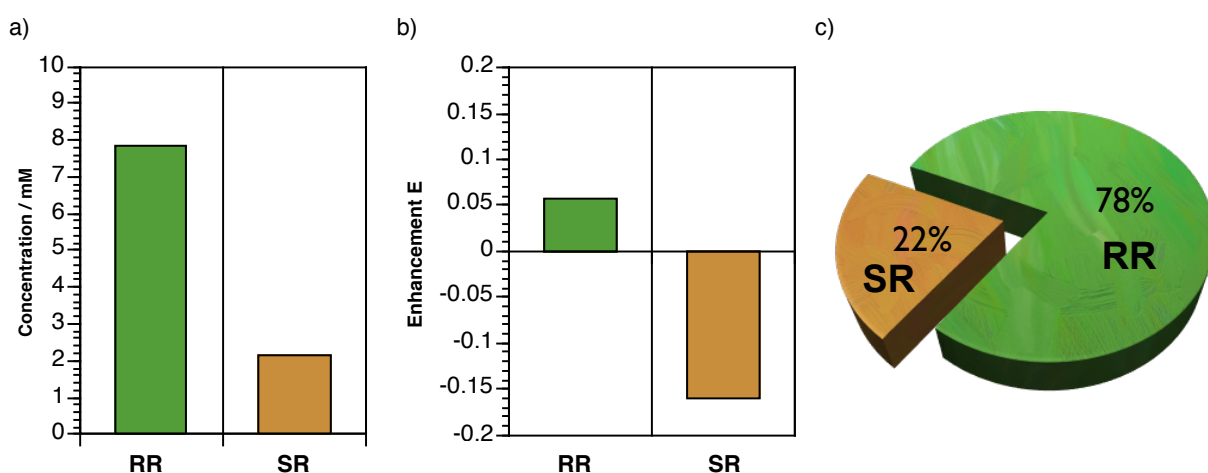


Figure 7.11 a) Concentration for each reciprocal (RR) and self-replicator (SR) product in the reaction of maleimides **33** and **66** with nitrones **141** and **55** in the presence of 20 mol-% *trans*-**69** after full conversion of starting materials determined by ^{19}F NMR spectroscopy. b) Enhancements in product formation with respect to the native reaction calculated according to **Equation 7.1**. c) Pie chart reflecting the product distribution of reciprocal replicators (RR) and self-replicators (SR).

In summary, this experiment demonstrates that the multicyclic system can be instructed by the addition of reciprocal template. Injection of a substoichiometric amount of *trans*-**69** at the start of the reaction resulted in strengthening its crosscatalytic relationship with *trans*-**162**. Unfortunately, *trans*-**162** could not be employed as a dopant for reasons described above, but we can assume that a very similar results would be obtained.

7.6.2 Addition of 20 mol-% autocatalytic template *trans*-**161**

Having established how the multicyclic system responds to addition of reciprocal template, the next task was to elucidate the impact of seeding preformed autocatalytic template to the reaction mixture. The first investigated template was *trans*-**161** of which 20 mol-% was

added at the start of the reaction between equimolar amounts of reagents **141**, **33**, **66** and **55** at 10 mM concentration. The reaction mixture was incubated at 10 °C and its progression was followed by ^{19}F NMR spectroscopy. Deconvolution of the recorded spectra gave rise to the concentration *vs* time profile depicted in **Figure 7.12**.

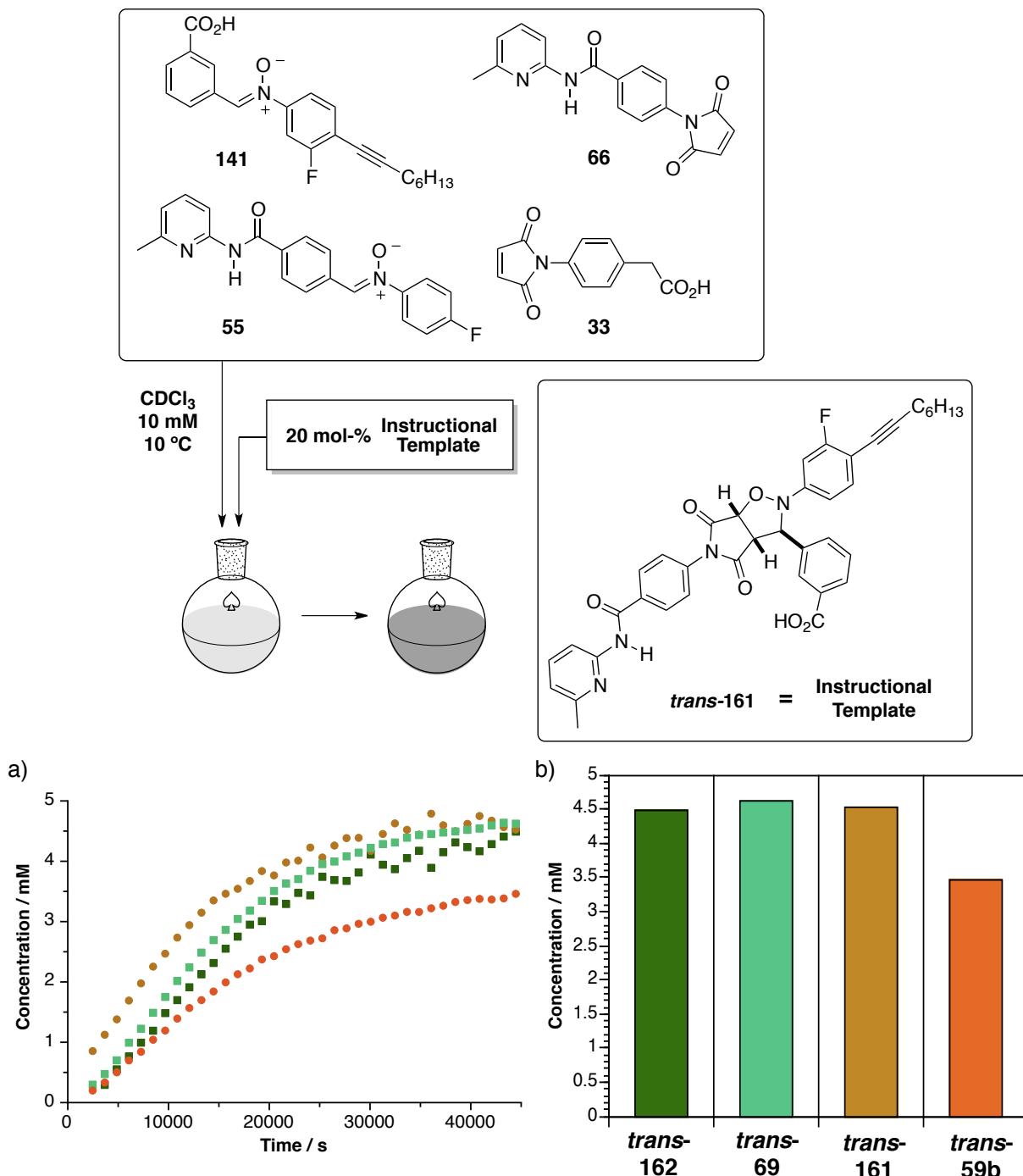


Figure 7.12 Concentration *vs* time profile of the multicyclic system depicted in **Figure 7.5** a) The reaction of maleimides **33** and **66** with nitrones **141** and **55** in the presence of 20 mol-% *trans*-**161** gives rise to self-replicating templates *trans*-**161** (●) and *trans*-**59b** (●) and reciprocal templates *trans*-**162** (■) and *trans*-**69** (■). The reaction was performed at 10 °C in CDCl_3 at 10 mM reagent concentration and followed by ^{19}F NMR spectroscopy. b) Product distribution for the templates at after 12 h.

It can be seen that the distribution between both types of replication has changed at the expense of the reciprocal templates. Since there is no concomitant formation for the self-replicating templates, the previous splitting pattern between the two groups of products is lost. The initial lag period for *trans*-161 has disappeared and the maximum rate for the formation of *trans*-161 can now be found at the start of the reaction. Since the self-replicator did not have to rely on template to be formed *via* the bimolecular reaction, it was instantly able to perform at the start of the reaction when a high concentration of building blocks was present in solution. By rapid incorporation of the necessary reagents 141 and 66 into the self-replicating template *trans*-161, the reciprocal systems *trans*-69 and *trans*-162 severely felt the shortage of the two building blocks and were not able to perform as well as they did in the native reaction. Although the formation of the reciprocal templates was suppressed, its main feature, the concomitant formation of both templates through the crosscatalytic cycle can still be seen and both profiles exhibit a nearly identical, characteristic sigmoidal shape.

With the activity of the reciprocal replicating system down-regulated, the second self-replicator *trans*-59b also benefited from the increased rate of the instructed self-replicator. Since the solution contained an equimolar mixture of all four reagents, the formation of every template molecule *trans*-161 using maleimide 141 and nitrone 66 implies that there is one molecule of maleimide 33 and nitrone 55 left which can react to form a molecule of *trans*-59b. However, unlike in the scenario discussed above during which a fixed amount of reciprocal template stimulated the concomitant formation of an increasing amount of the seeded template and its partner, doping the system with self-replicating template *trans*-161 does only instruct the system to enhance autocatalytically the formation of more *trans*-161. The resulting increase in partner template *trans*-59b can be regarded as an emergent property of the multicyclic network and is a direct consequence of the fact that the experiments are performed in a closed system. This independent relationship between the two self-replicators can be seen in the rate profile in which the formation of *trans*-59b is significantly slower than for *trans*-161. After 12 h, *trans*-59b was the least abundant species with a concentration of 3.46 mM, whereas the two reciprocal replicators, *trans*-162 (4.49 mM) and *trans*-69 (4.62 mM), and *trans*-161 (4.52 mM) were formed to nearly equal amounts. The conversion of nitrone 141 into products increased from 84% in the native reaction to 90% as a result of the induced rate-enhancements.

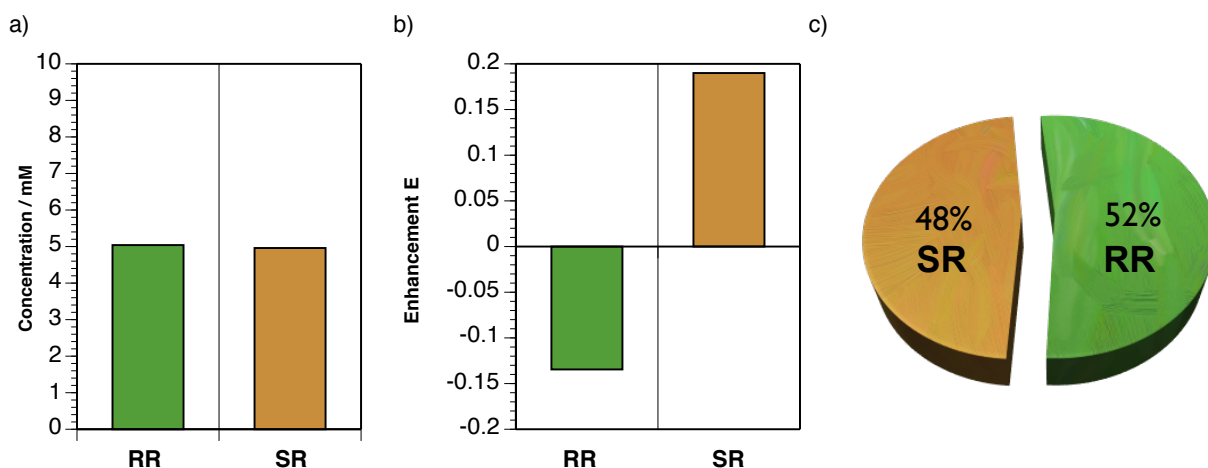


Figure 7.13 a) Concentration for each reciprocal (RR) and self-replicator (SR) product in the reaction of maleimides **33** and **66** with nitrones **141** and **55** in the presence of 20 mol-% *trans*-**161** after full conversion of starting materials determined by ^{19}F NMR spectroscopy. b) Enhancements in product formation with respect to the native reaction calculated according to **Equation 7.1**. c) Pie chart reflecting the product distribution of reciprocal replicators (RR) and self-replicators (SR).

After full conversion of starting material, the concentration for each reciprocal template was 5.04 mM and 4.96 mM for the self-replicators (**Figure 7.13a**). The final RR/SR ratio was therefore calculated as 1.1 compared to the value of 2.1 found in the native reaction. The change in concentration is also highlighted in the calculation of the relative enhancements E (**Figure 7.13b**) and the pie chart (**Figure 7.13c**).

7.6.3 Addition of 20 mol-% autocatalytic template *trans*-**59b**

Having established the influence of *trans*-**161** on the outcome of the experiment, another experiment was performed in which 20 mol-% of template *trans*-**59b** was added at the start of the reaction. The experiment was conducted under the same conditions as the native and both previous doping experiments. The reaction mixture containing equimolar amounts of reagents **141**, **33**, **66** and **55** at 10 mM concentration including the dopant was incubated at 10 °C and its progression was followed by ^{19}F NMR spectroscopy. Deconvolution of the recorded spectra allowed for the generation of the concentration *vs* time profile as shown in **Figure 7.14**.

Satisfyingly, also this system responded to the addition of *trans*-**59b** template in the expected manner. The formation of both self-replicating templates was enhanced whereas the amount of final reciprocal templates was decreased. Addition of preformed *trans*-**59b** had the expected autocatalytic effect by abolishing the lag period for the formation of this template and moving the maximum rate of formation at the start of the reaction.

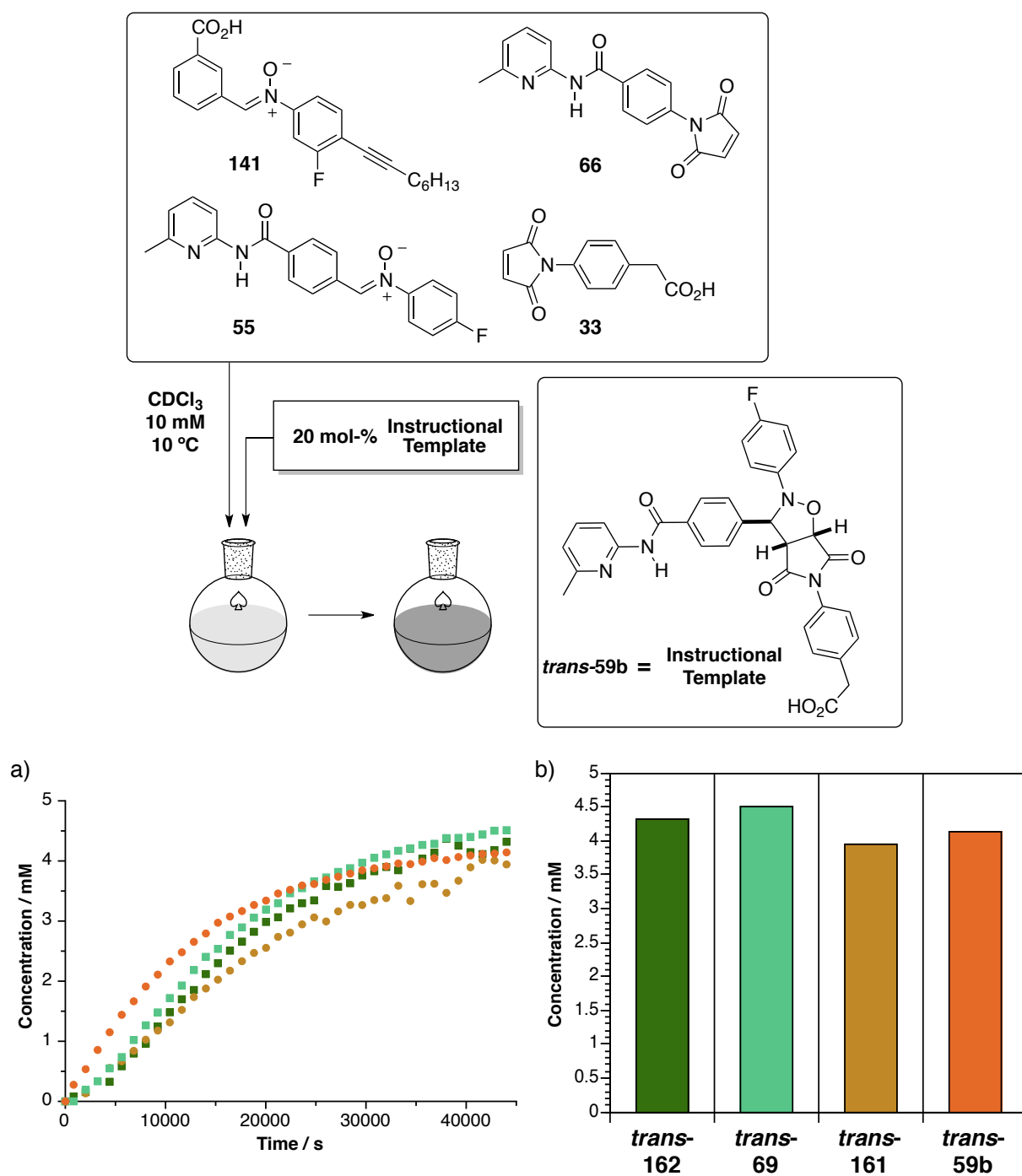


Figure 7.14 Concentration *vs* time profile of the multicyclic system depicted in Figure 7.5 a) The reaction of maleimides **33** and **66** with nitrones **141** and **55** in the presence of 20 mol-% *trans-59b* gives rise to self-replicating templates *trans-161* (●) and *trans-59b* (●) and reciprocal templates *trans-162* (■) and *trans-69* (■). The reaction was performed at 10°C in CDCl_3 at 10 mM reagent concentration and followed by ^{19}F NMR spectroscopy. b) Product distribution for the templates after 12 h.

As a result of this increased reactivity, nitron **55** and maleimide **33** were consumed rapidly and incorporated into *trans-59b*, depriving the crosscatalytic system of necessary reagents. This reagent pull caused by *trans-59b* left a relatively large amount of nitron **141** and maleimide **66** available for the formation of the second self-replicating template *trans-161*. As a consequence, also the synthesis of *trans-161* was up-regulated even though

there is no direct connection between both self-replicators. When comparing the formation of the self-replicator other than the dopant, that is *trans*-161 in the present and *trans*-59b in the previous experiment, a fundamental difference can be seen. When using 20 mol-% *trans*-161 as dopant, the progression of *trans*-59b lags behind the formation of the instructed autocatalyst (Figure 7.12a). In the case of 20 mol-% *trans*-59b, however, the difference in shape for the rate profiles of the self-replicators is less pronounced (Figure 7.14a). This finding corresponds with the respective effective molarities of the two replicators. Self-replicator *trans*-161 was established to be the stronger system, hence, it is more capable of taking advantage of the excess of its building blocks in the presence of doped *trans*-59b. In the reversed scenario, *trans*-59b does not possess the prowess to keep up with the enhanced partner. This difference also reflects in the change in final concentration. The increase for the self-replicators was calculated as 1.83 mM for doping with *trans*-161 and slightly less, only 1.71 mM, for doping with *trans*-59b (Figure 7.14c).

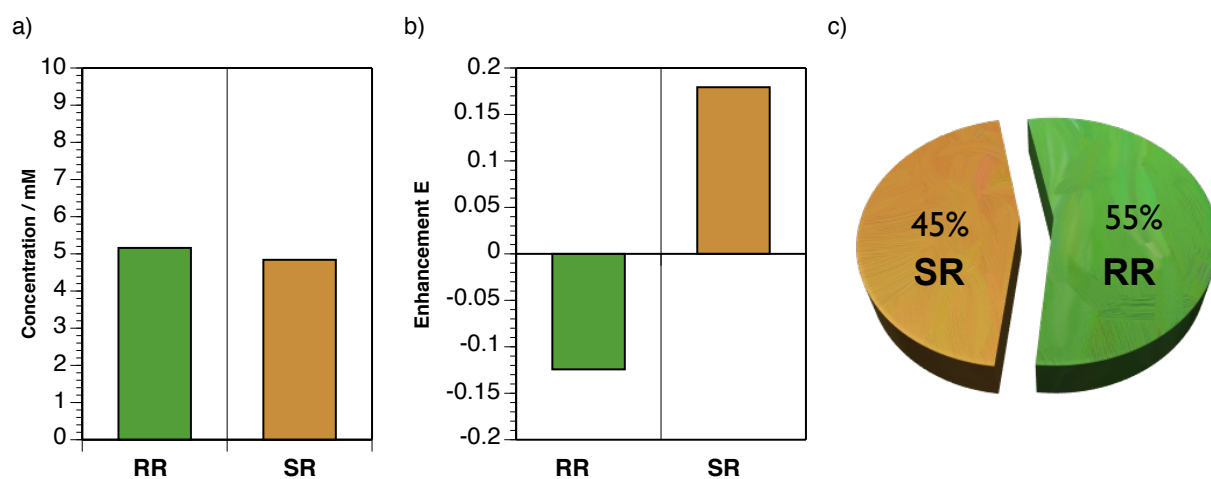


Figure 7.15 a) Concentration for each reciprocal (RR) and self-replicator (SR) product in the reaction of maleimides **33** and **66** with nitrones **141** and **55** in the presence of 20 mol-% *trans*-59b after full conversion of starting materials determined by ^{19}F NMR spectroscopy. b) Enhancements in product formation with respect to the native reaction calculated according to Equation 7.1. c) Pie chart reflecting the product distribution of reciprocal replicators (RR) and self-replicators (SR).

The absolute concentration for both self-replicators and reciprocal replicators were determined to be 4.84 mM and 5.16 mM, respectively, leading to a final RR/SR ratio of 1.2 (Figure 7.15a). A clear increase for self-replicating templates is also reflected in the calculation of the relative enhancements E for both types of replication (Figure 7.15b) and in the presentation as pie chart (Figure 7.15c).

7.6.4 Summary of the doping experiments

The results of the previous sections are summarised to highlight the behaviour of the multicyclic system upon addition of instructional template. The concentrations of the reciprocal and self-replicators after 12 h at 10 °C for the native experiment are depicted next to the three doping scenarios (Figure 7.16). Overall, it can be seen that the behaviour of the system matches the theoretical predictions from Figure 7.2 and that it is indeed possible to instruct this multicyclic network in a programmable manner using informational template.

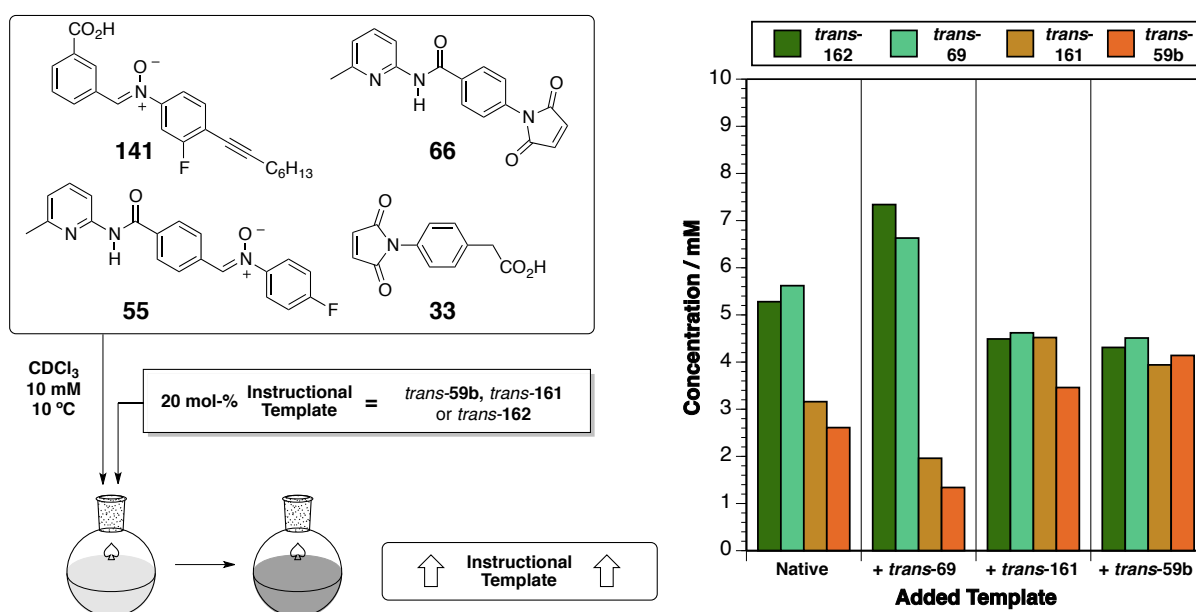


Figure 7.16 Summary of the responses of the multicyclic system of maleimides **33** and **66** with nitrones **141** and **55** in the presence of 20 mol-% added template at 10 °C in CDCl₃. In all lanes, the four bars indicate the concentration of the respective replicator after 12 h and the bars are shaded to identify the individual templates according to the legend. The lane marked **Native** depicts the selectivity of the system without added template. In other lanes, the identity of the added template is indicated by the label at the bottom of the lane.

The initial four component reaction established the ratio of the four products in the absence of any added template (lane +**Native**). Both reciprocal replicators were formed in greater extent than their autocatalytic competitors with the concentration for bisamido template *trans-69* marginally higher than for its partner template *trans-162*. In isolation, the kinetic parameters for the reciprocal system did not suggest such a clear dominance since the effective molarity was much smaller than for *trans-161* (10.1 M compared to 71.3 M) and only slightly higher than for *trans-59b* (4.96 M). Once more, the explanation for this behaviour may be attributed to the differences in duplex stability. Of all three product duplexes, the reciprocal complex [*trans-BAT*·*trans-162*] shows the lowest stabilisation (10.6

kJ mol^{-1}) with regard to *trans-161* (13.4 kJ mol^{-1}) or *trans-59b* (12.5 kJ mol^{-1}). In the set-up of the multicycle, this difference in association may provide an important advantage since a decrease in duplex concentration results in an increase in concentration of ternary catalytic complex. The difference in efficiency between *trans-161* (EM = 71.3 M) and *trans-59b* (EM = 4.96 M) reflects in a concentration difference of 0.55 M after 12 h in favour of *trans-161*. It can be speculated that this difference would be higher if the efficiencies of the reciprocal replicators was down-regulated. An example of such situation will be presented shortly.

Addition of 20 mol-% *trans-69* to the reaction altered the outcome of the competition in favour of the crosscatalytic templates (lane + *trans-69*). Both templates are now being formed in greater extent than in the native experiment with *trans-162* being the dominant species with a concentration of 7.34 mM. The gap to its partner replicator *trans-69* is caused by the fact that the value is corrected by the amount of added template so that only newly formed template is considered in the calculation of the concentrations. Once more, a difference in activity for both self-replicators is visible resulting in a concentration gap of 0.62 mM in favour of *trans-161*.

The presence of *trans-161* template at the start of the reaction favours the autocatalytic production of more template and limits the activity of the reciprocal replicators (lane + *trans-161*). After 12 h, *trans-161* and both reciprocal replicators were formed to nearly equal amounts. Simultaneously, also the production of *trans-59b* was up-regulated even though to a minor degree. As a consequence of the tight interconnectedness of the four building blocks, system-level behaviour stimulates an up-regulation for one of the self-replicators upon addition of the partner replicator even though there is no direct connection between the two systems. This independence in formation is reflected by the gap in concentration of 1.06 mM between the two replicators after 12 h. Being the weaker replicator, *trans-59b* does not possess the prowess to instantly capitalise on the excess of its building blocks provided by the presence of enhanced *trans-161*. On the other hand, being the stronger replicator, *trans-161* can respond more effectively to such favourable situation and the difference in concentration is less pronounced when adding *trans-59b* to the reaction mixture (lane + *trans-59b*). After 12 h, all four templates are being formed to nearly the same extent with *trans-161* only slightly less abundant than seeded template *trans-59b*.

In summary, the crosscatalytic relationship between *trans-69* and *trans-162* was found to be the major pathway in this multicyclic system. This dominance may be a consequence of the slightly less favourable reciprocal product duplex compared to the two self-complementary duplexes of the autocatalysts. Upon addition of instructional template, the interconnectedness of the crosscatalytic pathways led to a concomitant increase of both

reciprocal templates upon addition of the reciprocal template (lane + *trans*-162). Seeding the reaction with self-replicating template primarily enhanced the formation of the very template whereas an increase in concentration of the partner self-replicator was found to be a consequence of the topology of the multicyclic system and can be regarded as emergent property of the multicyclic network (lanes + *trans*-161 and + *trans*-59b).

7.7 Recycling experiments

Having established the directed manipulation of the multicyclic network, we next envisaged an experiment in which the behaviour of this system was probed under conditions that simulated evolution in a closed environment (**Figure 7.17a**). In this set-up, an equimolar amount of maleimides **33** and **66** and nitrones **141** and **55** were reacted in the absence of any additives (**Cycle 0**). Sub-stoichiometric amounts of the outcome of this reaction were then used as dopant for a fresh batch of reagents (**Cycle 1**). This procedure was repeated a second and third time while the product distribution was monitored for each cycle (**Cycle 2 and 3**).

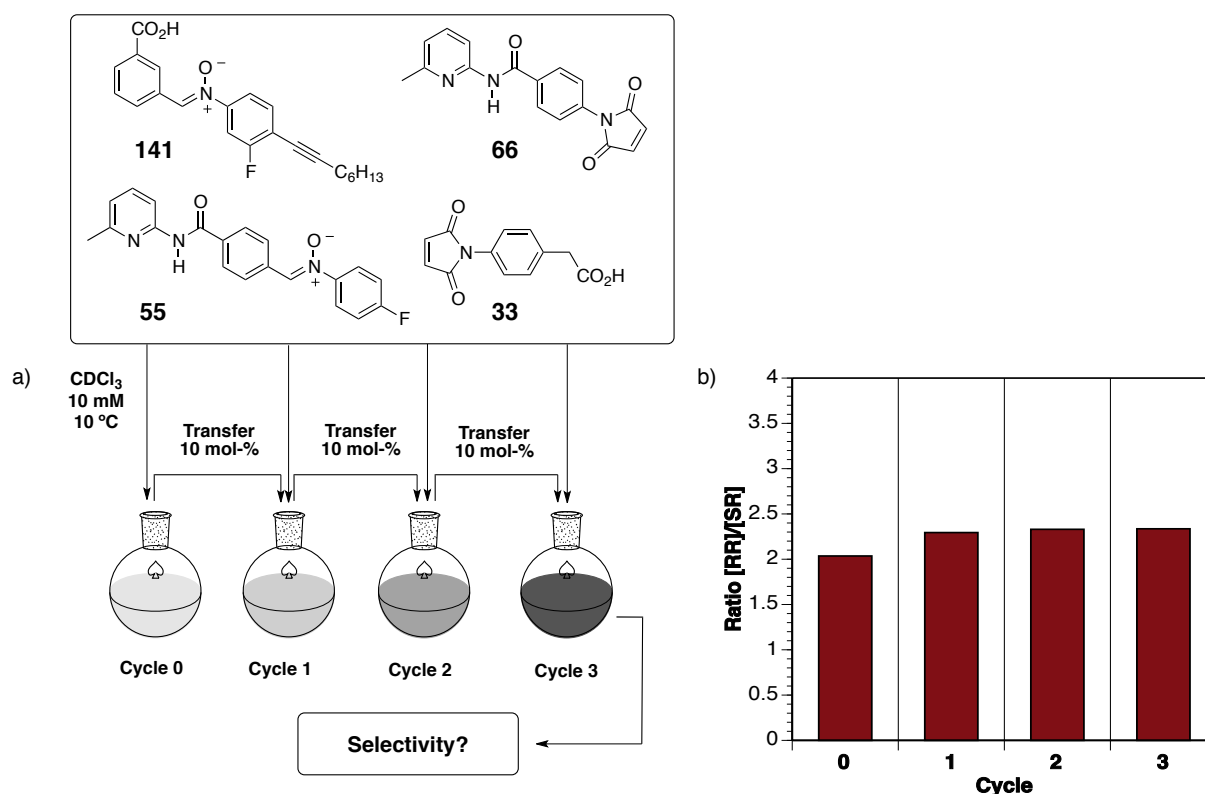


Figure 7.17 a) Design of a recycling experiment on the basis of the multicyclic system depicted in **Figure 7.5** in which the outcome of the native reaction (**Cycle 0**) is used as input for further reaction cycles. b) The outcome of each reaction cycle was monitored by ^{19}F NMR spectroscopy and the concentration of the reciprocal replicator (RR) was divided by the concentration of the self-replicating products.

In the previous sections, we showed that addition of instructional template manipulated the outcome of the multicyclic system in a foreseeable manner. In all cases, the seeded template was purified template of either a self-replicator or reciprocal replicator ensuring that the system ‘understands’ unambiguously the input. In the present experiment, we use mixtures of all four templates as dopants and focus our main attention on whether this repetitive doping procedure will cause one of the two replicating species to start to dominate the product pool under extinction of the inferior species. A first indication for such behaviour can be found in the previous sections, in which addition of a relatively small amount of template showed to have a major impact on the final product distribution for the benefit of the seeded template. Knowing about the prowess of the reciprocal replicators in the native reaction and their response to addition of template *trans-69*, we considered that repetitive cycling might result in a steady strengthening of the crosscatalytic pathway leading to the eventual extermination of all autocatalytic pathways.

Besides this ‘survival of the fittest’ scenario, it is also possible that repetitive cycling leads to co-existence with the concentrations for all four template products approaching a constant value. Szathmary *et al.* have established^[204-206] that competition between a set of sub-exponential replicators will always lead to co-existence and never cause the extinction of the weaker species. However, the present multicyclic system is more complex than the simple combination of individual replicators and the tight linking of the building blocks causing system-level behaviour was highlighted previously.

With these theoretical considerations at hand, the native reaction of the multicyclic system between maleimides **33** and **66** with nitrones **141** and **55** was repeated and the ratio of reciprocal replicators, *trans-69* and *trans-162*, to self-replicators, *trans-161* and *trans-59b*, was determined as 2.1 by ¹⁹F NMR spectroscopy after full conversion of all starting materials (**Cycle 0** in **Figure 7.17b**). Next, 10 mol-% of the product mixture containing 344 μM of each reciprocal template and 156 μM of each self-replicating template was added to a fresh batch of reagents at 10 mM concentration in CDCl₃ and the outcome was analysed after full conversion of starting materials. The ratio between reciprocal replicators and self-replicators changed marginally to around 2.2 (**Cycle 1**). This recycling procedure was repeated twice and the values for the RR/SR ratio were recorded to be 2.3 in both cases (**Cycle 2** and **3**). It can clearly be seen that after a slight increase in ratio in the first recycling step, further cycles of doping had no impact on the final product distribution. In order to find a coherent explanation for this behaviour, two additional experiments were conducted in which the recycling experiments were performed after the equilibrium concentration of the native experiment was biased by the addition of either reciprocal or autocatalytic template.

7.8 Imbalance reaction

In the previous section, repetitive cycling of the outcome of the multicyclic network led to coexistence of both species of replication at a fixed ratio. In two additional experiments, the initial reaction was performed in the presence of either 20 mol-% reciprocal template *trans*-69 or 20 mol-% of self-replicating template *trans*-161 (Figure 7.18a). The outcome of this reaction was then again used as dopant in a fresh batch of reagents and so forth. We reasoned that by doping the original solution, an imbalance in product distribution is created and the reaction network is moved away from its equilibrium point. Repetitive cycling might then lead to an amplification of this initial imbalance causing a lasting change in product distribution generating selectivity for one of the two replicating species.

Reciprocal replicator *trans*-69 was chosen to be the first dopant and 20 mol-% were added to an equimolar mixture of maleimides 33 and 66 with nitrones 141 and 55 at 10 mM concentration in CDCl₃. Analysis of the reaction by ¹⁹F NMR spectroscopy verified the up-regulation of both reciprocal replicators pushing the RR/SR ratio to 3.7:1 (Cycle 0 in Figure 7.18b). However, subsequent addition of 20 mol-% of this mixture to a fresh batch of reagents failed to further enhance the selectivity for the reciprocal templates and the ratio dropped to 3.3:1 (Cycle 1). Three further recycling experiments were performed resulting in a continuous reduction of fabricated reciprocal replicator and a decrease in RR/SR ratio from 2.7:1 (Cycle 2) over 2.6:1 (Cycle 3) to 2.5:1 (Cycle 4). The progression for the calculated values again suggests an equilibrium ratio for both replicating species similar to the one found in Figure 7.17b. The slight deviation for the ratios might be explained by the increase in dopant from 10 mol-% in the previous experiment to 20 mol-% for the recent set-up.

Since the reciprocal replicators failed to establish their supremacy, we repeated the experiments using 20 mol-% of autocatalytic template *trans*-161 as initial dopant. Self-replicators operate in a less cooperative way than reciprocal replicators and might therefore be able to take advantage of any favourable initial disturbance of the equilibrium point of the multicyclic network. As expected, the formation of autocatalyst was favoured in the doping reaction lowering the RR/SR ratio to around 1.1 (Cycle 0 in Figure 7.18b). However, using 20 mol-% of the product mixture as dopant for the next cycle did not result in a propagation of the induced imbalance. Instead, the ratio for both types of replicating first increased to 1.8 in favour of the reciprocal replicators (Cycle 1) before continuously approaching the exact same equilibrium ratio of 2.5 found in the previous experiment (Cycle 2-4).

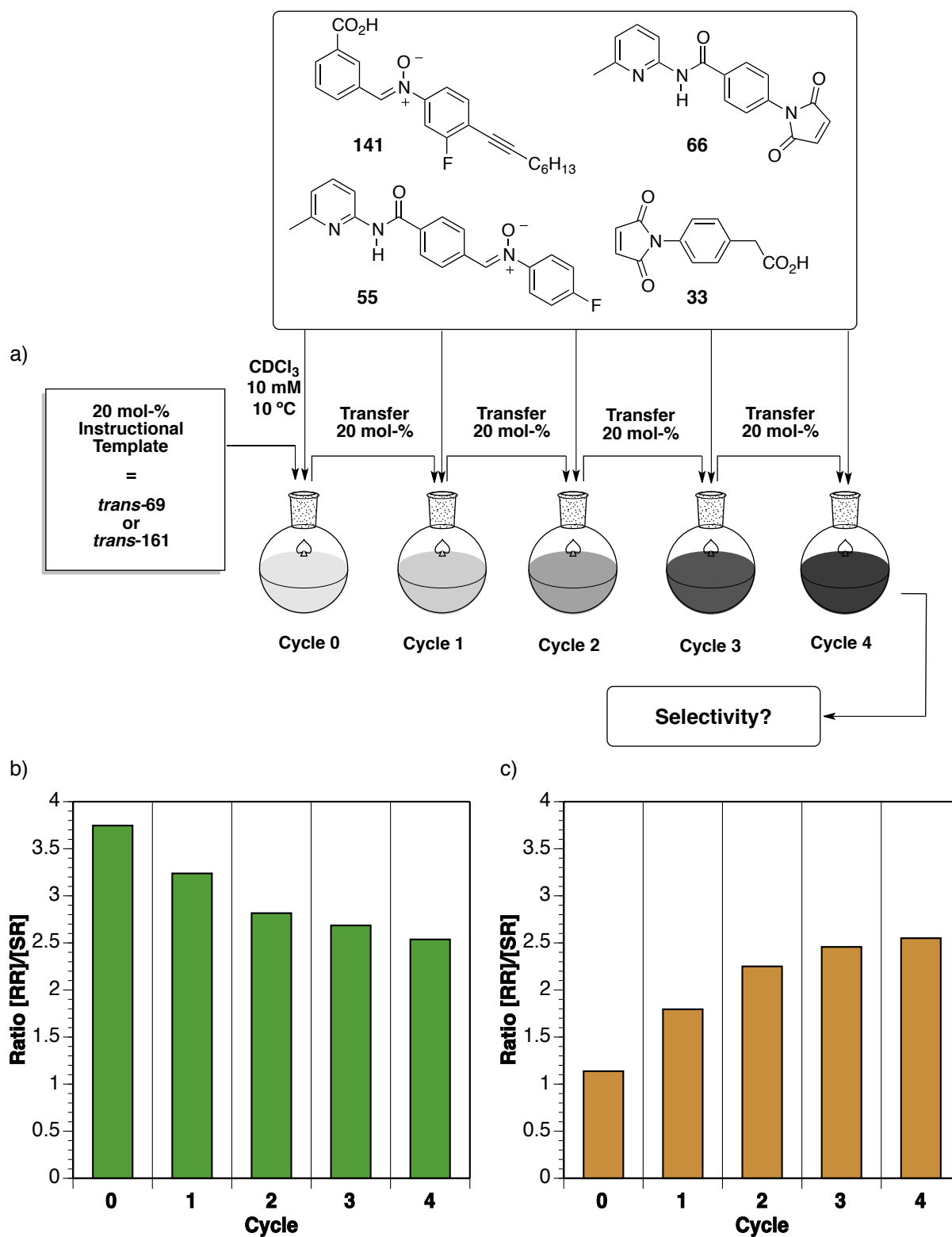


Figure 7.18 a) Experimental set-up to investigate the behaviour of the multicyclic system depicted in **Figure 7.5** after initial addition of 20 mol-% of instructional template followed by repetitive doping of 20 mol-% of the outcome of the previous cycle in a fresh batch of reagents. After full conversion of starting materials, the product distribution was determined by ¹⁹F NMR spectroscopy and the concentration of the reciprocal replicators (RR) was divided by the concentration of the self-replicator (SR) to provide values for the RR/SR ratio obtained upon initial addition of b) reciprocal template *trans*-69 or c) autocatalytic template *trans*-161.

In the last two sections, attempts were made to induce selection into a complex reaction network composed of four interlinked replicating competitors by subjecting it to a repetitive sequence in which the outcome of each cycle was used as an instruction for the next generation. However, the multicyclic system presented in this chapter did not show a specific selectivity for any of its two possible replicating species. Instead, an 'equilibrium position' for the ratio in concentrations of reciprocal and self-replicators was established. Depending on the extent of the imbalance created in the initial reaction, this ratio was reached sooner or later. Without any bias, this equilibrium in ratio was already established after the first cycle (**Figure 7.17b**), whereas injection of 20 mol-% of preformed template created a greater imbalance and the equilibrium was found after four cycles only (**Figure 7.18a** and **Figure 7.18b**).

These results are summarised in **Figure 7.19a** and compared with simulations based on the kinetic model with two minimal ($A + B \rightarrow R1$ and $C + D \rightarrow R2$) and two reciprocal replicators ($B + C \rightarrow T1$ and $A + D \rightarrow T2$) depicted in **Figure 7.1**. In order to mimic the reactivity found for the multicyclic system established experimentally, the parameters for the enhanced rate constants were altered from their original common value. The rate constants for formation of the two reciprocal replicators **T1** and **T2** through their ternary complexes were set to $1.35 \times 10^{-3} \text{ s}^{-1}$ and $1.55 \times 10^{-3} \text{ s}^{-1}$, respectively. The value for the minimal replicator **R1** was adjusted to $0.85 \times 10^{-3} \text{ s}^{-1}$ whereas the rate for **R2** was fixed at $1.00 \times 10^{-3} \text{ s}^{-1}$. Values for the bimolecular reactions ($5 \times 10^{-5} \text{ M}^{-1} \text{ s}^{-1}$), single point associations (1000 M^{-1}) and association in the auto- and crosscatalytic duplexes ($1 \times 10^6 \text{ M}^{-1}$) were not changed. All calculations were performed with a starting concentration of 10 mM for all reagents. The kinetic model used for the native experiment without any additives can be found in the appendix. **Figure 7.19b** shows the outcome of the theoretical analysis of the recycling experiments. In all calculations, the final concentration of reciprocal replicators was divided by the concentration of minimal replicators to provide the ratio of both species, $[RR]/[SR]$. Again, three different scenarios were considered. First, all four reagents were allowed to react until completion without any added template in a native reaction. 10 mol-% of the outcome was then used as dopant for the next cycle which in turn was applied as dopant to the next cycle (red data points). The same calculation was repeated using either 20 mol-% of **T1** (green data points) or 20 mol-% of **R2** (orange data points) as dopant in the initial reaction. Even though the kinetic models is rather idealised ignoring many of the subtleties of the real system such as different association constants between the individual building blocks, the calculated results correspond well with the ones found in the experiment, and the

trend towards a common equilibrium ratio for all three experiments can be seen clearly. After three cycles, the ratio for all three scenarios was found to be close to a ratio of 2.9 (compared to 2.5 in the experiment). The only outlier occurs for the native reaction when doping with T1, but its behaviour is corrected instantly in the following cycles. Overall, the calculations underline the conclusion drawn from the experimental results, that an unperturbed recycling system will always approach a predetermined ratio between the replicator species. This rigid behaviour was explained with a saturation of reactive ternary complexes at the early stage of the reaction and was also seen in chapter 6 when trying to perturb the outcome of several competition scenarios.

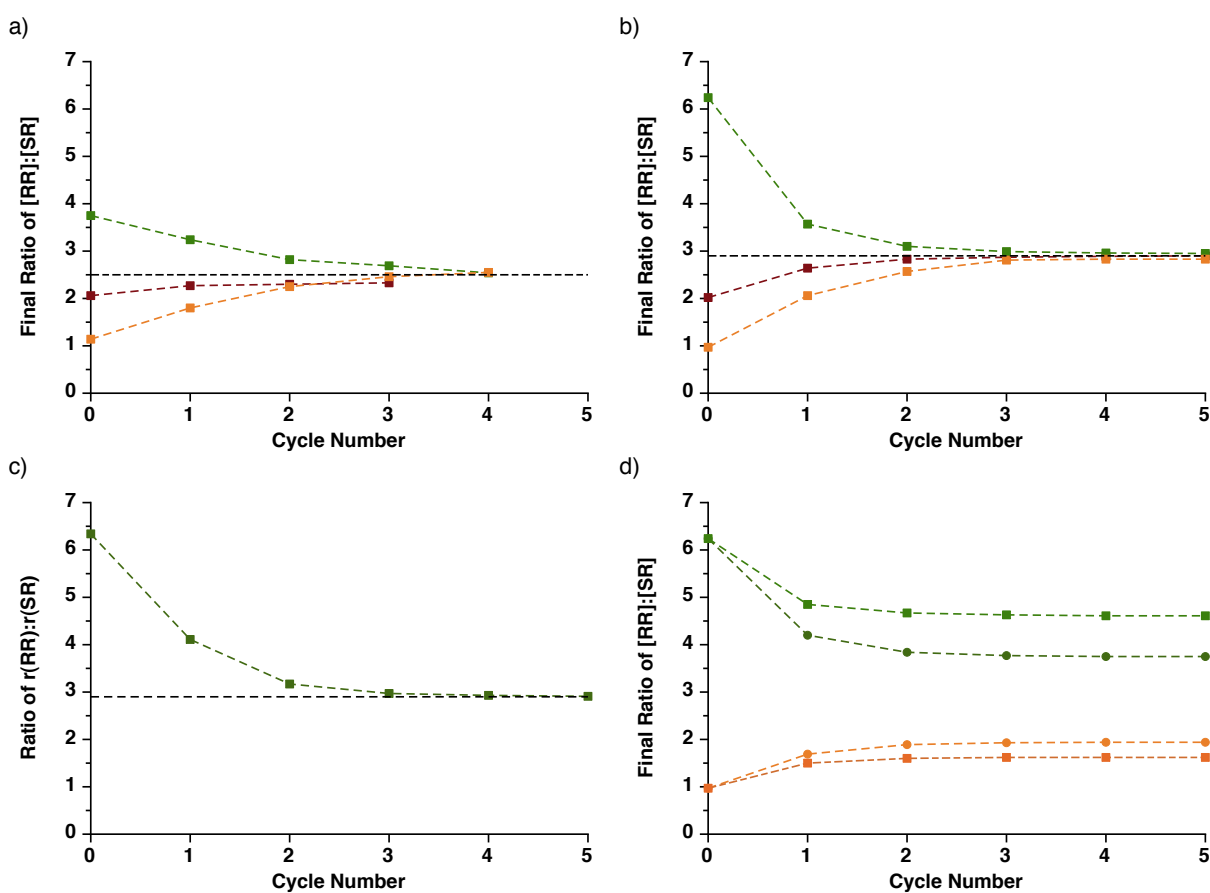


Figure 7.19 a) Overview over the results for the recycling experiments in **Figure 7.18** using no template (---■---), 20 mol-% *trans*-69 (---■---) and *trans*-161 (---■---). b) Results for the calculation of the scenarios shown in **Figure 7.18** based on a variation of the kinetic model from **Figure 7.1** using no template (---■---), 20 mol-% T1 (---■---) and R2 (---■---). c) Computed ratios of reaction rates for the formation of reciprocal (RR) and minimal (SR) templates after 500 s based on the results for the calculations using 20 mol-% *trans*-69 as initial dopant in **Figure 7.19b**. d) Calculation of a recycling experiment in which the initial reaction was biased by addition of 20 mol-% T1 or R2 and every further cycle was doped with 10 mol-% of the reaction outcome and a further 10 mol-% T1 (---●---), 20 mol-% T1 (---■---), 10 mol-% R2 (---○---) or 20 mol-% R2 (---■---). Equilibrium ratios between reciprocal and minimal replicators in a), b) and c) are highlighted by the dashed black line.

With a reliable kinetic model at hand, it was now possible to extract the concentrations of all four reactive ternary complexes, $[A \cdot B \cdot R1]$, $[A \cdot B \cdot R2]$, $[A \cdot D \cdot T1]$ and $[B \cdot C \cdot T2]$, and to calculate the reaction rates for the formation of each template after 500 s. **Figure 7.19c** shows the ratio of the averaged rate of formation for reciprocal to minimal replicators over five cycles for the case of initial doping with 20 mol-% **T1** (**Figure 7.19b**, green data points). A direct correlation between the ratio of the reaction rates and the ratio of the final product concentration can be seen. Again, the highest ratio of 6.4 is seen for the native experiment (**Cycle 0**) which gradually decreases towards the equilibrium ratio of about 2.9 (from **Cycle 3** onwards). This match between the two graphs confirm the assumption made earlier that the final ratio in concentration between both replicating species is governed by the speciation of their active ternary complexes and their reaction rates at the start of the experiment. Addition of presynthesised template therefore has a major impact on the product distribution by changing the concentrations of ternary complexes, however, this advantage is lost in the course of the recycling procedure as the concentration of original dopant decreases in every following cycle on the expense of all other templates until it reaches the predetermined ratio in concentrations.

Having said this, it would be interesting to simulate a scenario in which the system is forced out of equilibrium not only in the initial reaction but in all following reaction cycles. A protocol was therefore established in which not only the initial reaction was doped with various amounts of purified **T1** or **R2** but also every following cycle. In addition to the application of presynthesised template, 10 mol-% of the reaction outcome was also injected continuously to new batches of reagents. Since the final mixture of templates always contains a large amount of the initial dopant, one would expect an increased dominance of this very template with progressing recycling. However, the simulations once more show a degradation rather than dominance for the amplified template over the course of the experiment (**Figure 7.19d**). For all four investigated scenarios, the impact of the template addition decreases with every cycle until the system reaches the fixed ratio in concentration between both product types. This ratio is now dependent on the amount of purified template which is continuously added to the reaction mixture. Larger amounts of template create a more pronounced deviation from the natural ratio of the system. It is important to point out that, since every reaction outcome consists of all four templates, the net amount of the original dopant increases from **Cycle 0** to **Cycle 1** by the amount present in the previous reaction mixture. However, since this mixture also contains molecules of the competing templates, it is again the ratio of active ternary complexes formed at the start of the reaction that governs the performance of the multicyclic system and results in a decrease of the

concentration of the original template. With this set of experiments, it was shown that it is only possible to steer systems away from their equilibrium under continuous input of presynthesised template. It can be assumed that a continuation of this recycling protocol without any added pure template input will very soon reach the established equilibrium RR/SR ratio of 2.9.

Altogether, these findings further highlight that working in a closed system limits drastically the possibility of performing evolutionary selection. In a static environment, initial advantages for the formation of a preferred species cannot be fully passed on to the next generation but inevitably result in an equilibrium concentration for both the dominant and the inferior species. Previous investigations on the behaviour of the multicyclic system depicted in **Figure 7.2** in a similar recycling scenario also failed to induce selectivity despite using equimolar amounts of dopants. This shortcoming was explained with the fact that reciprocal and self-replicating templates exhibit different responses to the addition of template.^[139] With the current results at hand, a more general explanation can be formulated. Instructing the network with template strengthens the catalytic efficiency for one type of replicator and this allows to selectively increase the formation of either the auto- or crosscatalyst. Amplification in this doping process is proportional to the influence that the added template has on the concentrations of active ternary complexes at the start of the reaction. Since all ternary complexes are in equilibrium, an infinite excess of dopant is required to eliminate all unwanted complexes, a situation that cannot be reached in practice. Accordingly, all competition scenarios from chapter 6 showed saturation points at which the addition of increasing amounts of template had only little effect on the outcome of the reaction. Since we are not able to completely erase the weaker species through addition of large amounts of strong template, using the outcome of the reaction as the sole source for the next doping experiment ensures that the amount of template for the stronger species will at best be constant (when doping stoichiometric amounts) or gradually diminish (with sub-stoichiometric amounts) until the ratio for both competing species are again governed by their intrinsic catalytic efficiencies.

The reasoning outlined above explains that when dealing with replicating networks in a closed environment, work has to be preformed in order to move the system away from its equilibrium point. In the case of the multicyclic system, this work is done by addition of preformed template which manipulates the system in a defined way. However, the impulse does not persist over time and the system eventually falls back to its equilibrium state. Moving away from a closed environment to open systems might allow for the envisaged

selection process to take place. A basic discussion of the advantages of open systems can be found in section 8.4.

7.9 Creating an imbalance by changing the recognition site

In the design of the multicycle depicted in **Figure 7.5**, we purposely employed maleimide **66** bearing the 6-methyl substituent instead of 4,6-dimethyl derivative **72** to avoid the presence of two amidopyridine moieties with different substitution patterns. In chapter 4, we have established that the additional methyl group on the recognition site increases its single point association with both carboxylic and phenylacetic acid. This increase was shown to only have a minor impact on the functioning of self-replicating and AB systems studied. We therefore wish to investigate whether replacing maleimide **66** with **72** as building block in the multicycle has an effect on the performance of the network. Since the maleimide will be incorporated into both autocatalytic template *trans*-**146** and reciprocal template *trans*-**167** now bearing two different amidopicoline sites, we can only speculate about its impact on the overall ratio of the two replicating types, however, the change in association strength is expected to create a slight imbalance in reactivity for the two self-replicating systems by further favouring the formation of template *trans*-**161** over replicator *trans*-**59b**.

In this experiment, an equimolar amount of maleimide **33** and **72**, and nitrones **141** and **55** at 10 mM concentration in CDCl₃ were incubated at 10 °C and the progression of the reaction was followed by ¹⁹F NMR spectroscopy. Deconvolution of the obtained spectra allowed for the construction of the rate profile depicted in **Figure 7.20a**, but overlay of the peaks for the products arising from nitrone **141** in the ¹⁹F NMR spectra again limited significantly the quality of the deconvoluted rate profile. However, it can clearly be seen that the formation of all four products is very similar to the original scenario. The two reciprocal replicators dominated the product pool with the two autocatalysts being formed to minor extent (**Figure 7.5a**). Comparison of the two graphs confirms that variation of the recognition site has only a negligible impact on the final product distribution and is within the accuracy given by the deconvolution of the obtained ¹⁹F NMR spectra. From the individual concentrations of the four products, 84% conversion of nitrone **141** and 82% conversion of nitrone **55** into products was established (compared to 84% and 83% in the previous experiment). After full conversion of building blocks, the RR/SR ratio was calculated as 2.0 with a concentration of 6.7 mM for the reciprocal templates and 3.3 mM for the autocatalysts (compared to 2.1:1).

These results suggest that a subtle variation of substituent pattern on the amidopyridine site to increase selectively the association constant of one building block has no measurable impact on the overall performance of the multicyclic system.

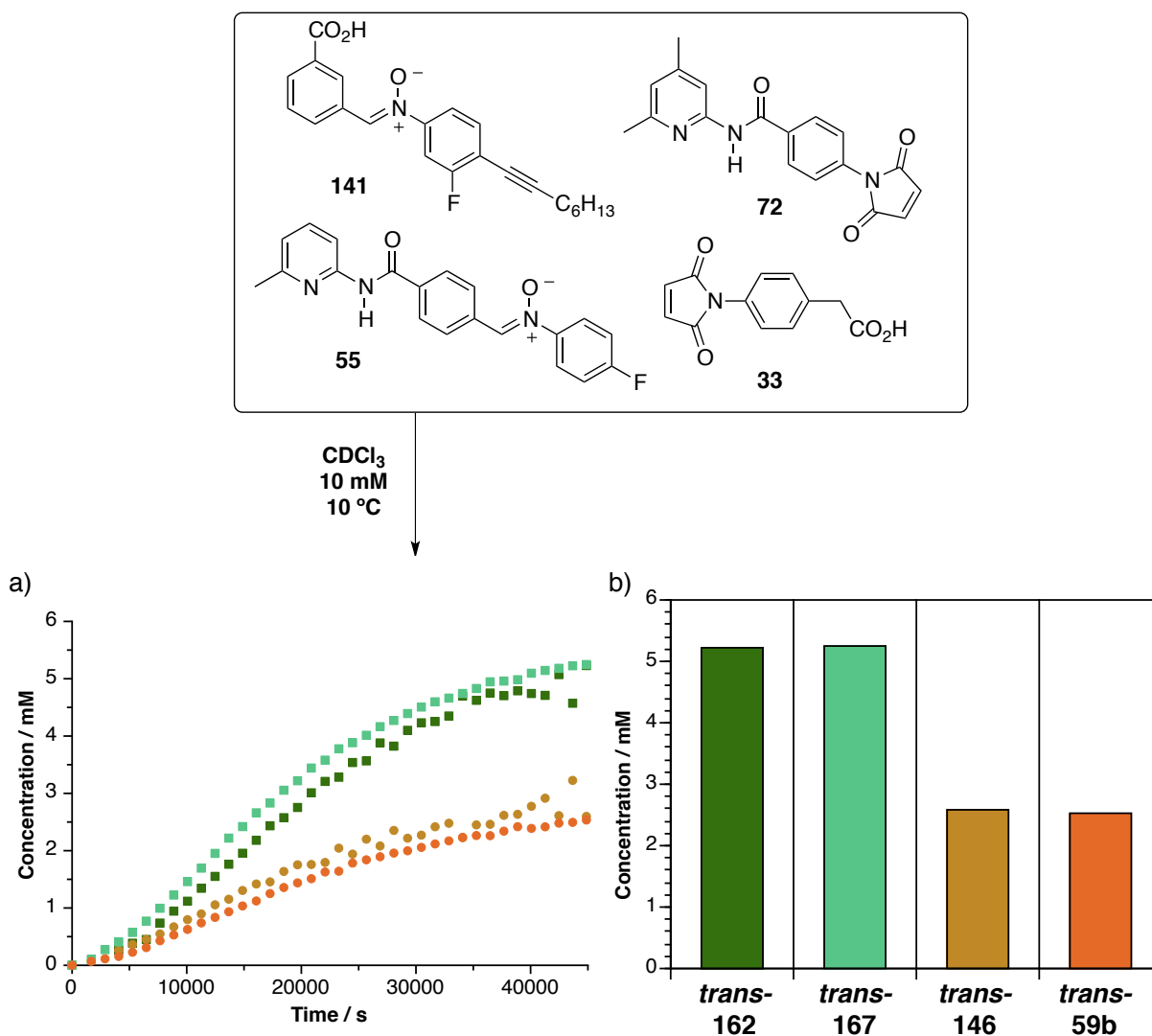


Figure 7.20 a) Concentration *vs* time profiles for reaction of maleimides **33** and **72** with nitrones **141** and **55** gives rise to self-replicating templates *trans*-**146** (●) and *trans*-**59b** (●) and reciprocal templates *trans*-**162** (■) and *trans*-**167** (■). b) Product distribution for the templates after 12 h. All reactions were performed at 10 °C in CDCl₃ at 10 mM reagent concentration and monitored by ¹⁹F NMR spectroscopy.

7.10 Using *trans*-**149** as autocatalyst in the multicyclic system

In the previous chapters, a set of replicating systems based on three maleimides and two nitrones was presented (chapter 3) and some selected replicators were used as building blocks for various competition scenarios (chapter 6). In the course of these investigations, a clear hierarchy was established for the efficiency of these systems. In the following sections, the two self-replicating systems *trans*-**149** and *trans*-**147** as well as an analogue of hybrid system **148** will be coupled to replicator *trans*-**59b** to give rise to three multicyclic networks

with different topology. For each system, the reciprocal relationship was first investigated before the functionality of the multicycle was probed and analysed.

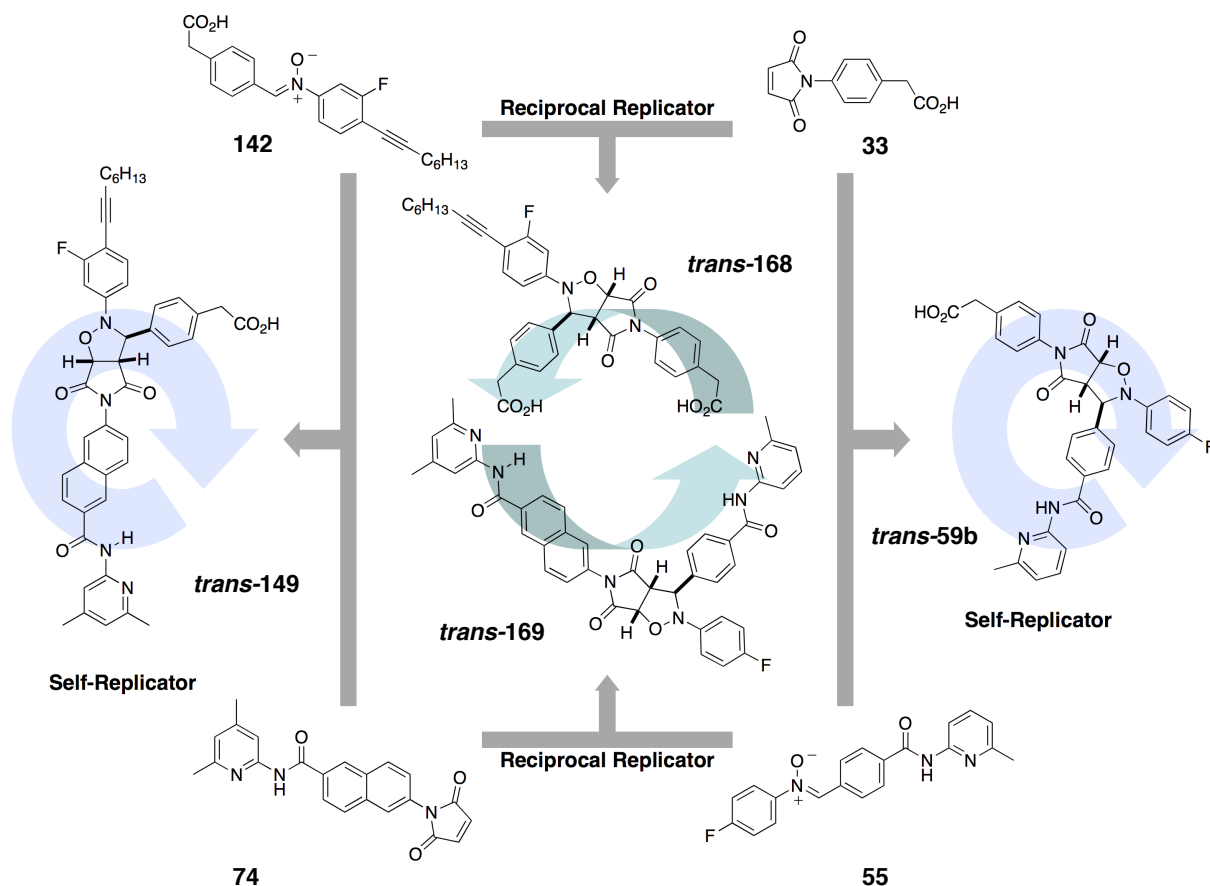
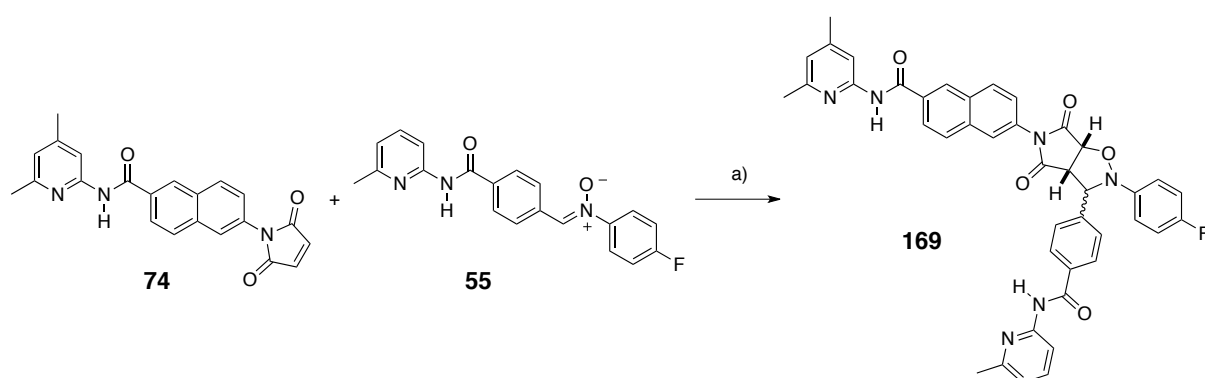


Figure 7.21 Multicyclic network combining the self-replicating systems *trans*-149 (from maleimide **74** and nitronium **142**) and *trans*-59b (from maleimide **33** and nitronium **55**) to form two additional reciprocal templates *trans*-168 and *trans*-169.

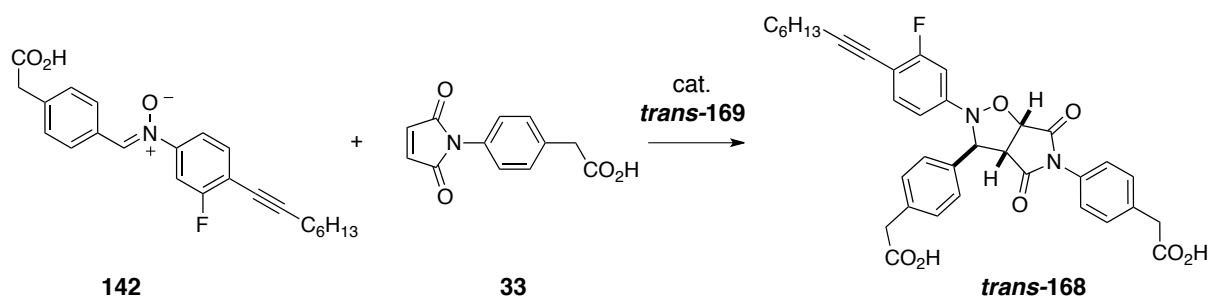
Replacing maleimide **66** with maleimide **74**, and nitronium **141** with nitronium **74** leads to the design depicted in **Figure 7.21**. In order to warrant sufficient solubility of self-replicating template *trans*-149 in non-polar solvents, maleimide **74** maintained its 4,6-dimethyl recognition site. It was demonstrated in the previous section that small changes in strength of recognition have only a minor impact on the performance of the individual systems in the network.

As shown in **6.4.4**, the autocatalytic formation of template *trans*-149 proceeds with exceptionally high efficiency. As a consequence of the relatively high bimolecular rate for *trans*-149, its effective molarity is however lower than the one for *trans*-161 (23.6 compared to 58.8). Additionally, a relatively low duplex stabilisation is observed for the product duplex and the replicator was found to perform better in the competition scenario against AB system *cis*-148. Introduction of *trans*-149 is therefore expected to strengthen the autocatalytic contribution within the network.

Substitution of the two building blocks does not only influence the self-replicating system but it also creates a geometric change for the crosscatalytic system. In order to investigate the influence of the novel building blocks on the efficiency of the reciprocal system, a diastereoisomeric mixture of template **trans-169** bearing two amidopyridine moieties was synthesised by reacting an equimolar amount of maleimide **74** with nitron **55** in CDCl₃ at room temperature for five days (**Scheme 7.7**). The *trans/cis* ratio was determined as 2.0:1. Separation of the mixture by crystallisation or column chromatography was unsuccessful but showed to be only a minor handicap for the investigation of the reciprocal system.



Scheme 7.7 Synthesis of template **169**. Conditions: a) CHCl₃, 5 d, rt, 98% for both diastereoisomers with a *trans/cis* of 2.0:1.



Scheme 7.8 Formation of *trans-168* in the absence and presence of reciprocal template *trans-169*. Kinetics for this reaction are depicted in **Figure 7.22**.

The influence of template **169** on the reaction between acid maleimide **33** and acid nitron **142** was investigated (**Scheme 7.8**). First, the reaction between the acids was performed in the absence of template **169** by reacting an equimolar amount of both reagents at 10 mM concentration in CDCl₃ for 16 h at 0 °C. The progression was followed by ¹H NMR spectroscopy and the obtained data were deconvoluted to give the corresponding rate profile (**Figure 7.22a**).

It can clearly be seen that the reaction is slow and unselective, only 17 % of starting material were converted into products after 16 h. Interestingly, the *cis*-product was found to be the major diastereoisomer in the product pool resulting in a *cis/trans* ratio of 1.9:1. This rather surprising selectivity can be explained with the presence of an AB-like complex in which weak hydrogen bonds between both phenylacetic acid moieties position the reactive sites in close proximity to form the *cis*-isomer in a rate-enhanced fashion. The potential of this recognition-mediated process is currently under investigation in the group.

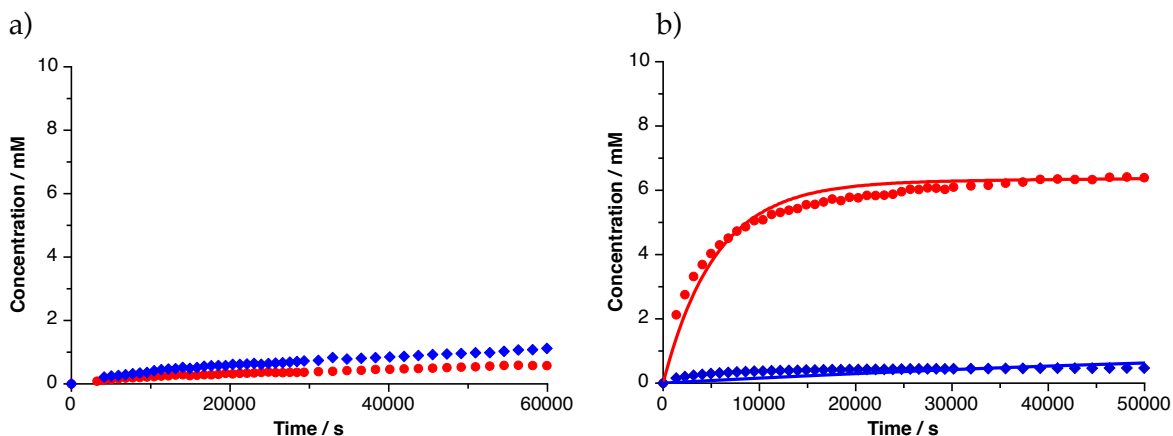


Figure 7.22 Concentration *vs* time profiles for the reaction of nitrone **142** and maleimide **33** to give *trans*- and *cis*-**168** a) in the absence of any added template b) in the presence of 67 mol-% *trans*-**169** and 33 mol-% *cis*-**169**. The formation of *trans*-product is shown as red filled circles and the formation of *cis*-product as blue filled diamonds. Straight lines in b) represent the results for the fitting of the *trans*-(-) and *cis*-(-) product. All reactions were performed at 0 °C in CDCl₃ at 10 mM reagent concentration and monitored by ¹H NMR spectroscopy.

Next, the reaction was repeated in the presence of 100 mol-% of a diastereoisomeric mixture of **169** consisting of 67% *trans*- and 33% *cis*-template. The dopant was added to a fresh batch of reagents, **142** and **33**, and the progression of the reaction gave rise to the concentration *vs* time profile in **Figure 7.22b**. After 16 h, 70% of starting material were converted into products and the selectivity was calculated to be 14:1 in favour of the *trans*-isomer. Clearly, addition of a diastereoisomeric mixture of template had no impact on the formation of *cis*-**168** which is in accordance with its predicted folded structure. The rate profile for *trans*-**168** however exhibits the characteristic progression for the reaction of a reciprocal template in the presence of its crosscatalytic partner. The maximum rate of the reaction is found at the start with a gradient that is slightly smaller than for the crosscatalytic system between *trans*-**69** and *trans*-**162** (**Figure 7.7**). As soon as nearly all of the added template is saturated, product inhibition causes the curve to flatten and the bimolecular pathway becomes the main contribution to the formation of *trans*-**168**. This saturation is reached at a concentration of roughly 6 mM and the proportional relationship between the

amount of added template and newly formed template further suggests that the catalytic duplex in this reciprocal system exists between *trans*-169 and *trans*-168.

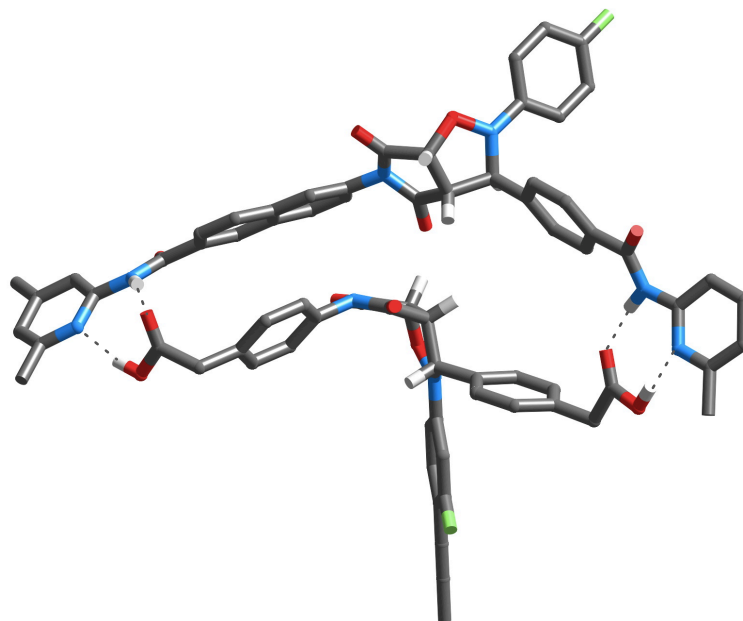


Figure 7.23 Molecular model of the reciprocal duplex of *trans*-168 and *trans*-169 monomer. Carbon atoms are shown in dark grey, hydrogen atoms in light grey, nitrogen atoms in blue and oxygen atoms in red. Hydrogen bonds are indicated by the dotted lines. Most other hydrogens were omitted for clarity.

The model for the two reciprocal templates *trans*-168 and *trans*-169 further support this finding as they show a reasonably well-matched duplex in which the bisamido template encloses its partner template (**Figure 7.23**). Once more, we can only speculate about the respective orientation of the two templates and this ambiguity needs to be considered in the computational analysis of the system.

In order to extract kinetic parameters for this reciprocal relationship, we conducted fitting of the experimental data using SimFit. The results of the fitting are listed in **Table 7.3** and the quality of the fit can be seen in **Figure 7.22b**. The association constant between two phenylacetic acids at 10 mM concentration in CDCl_3 and 0 °C was determined as 50 M^{-1} and attempts were made to include the AB mediated formation of *cis*-168 into the kinetic model. However, an additional term ultimately generated a situation for the native reaction in which three parameters, the rate-enhanced formation of *cis*-168 and the bimolecular rates for both isomers, had to be determined by only two data sets, formation of the *trans*- and *cis*-isomers. Since *cis*-168 does not engage in any crosscatalytic processes, the contribution of this weak AB system to the overall performance of the template doped scenario was considered to be minimal and was therefore neglected in the kinetic model (see appendix). As a result, the

bimolecular rate for *cis*-168 includes the contribution of the AB system and was found to be higher than the rate for *trans*-168.

Table 7.3 Kinetic parameters for the reaction of maleimide **33** and nitrone **142** to give cycloadduct **168** at 0 °C in CDCl₃ at 10 mM reagent concentration. The kinetic parameters for the crosscatalytic relationship between *trans*-168 and *trans*-169 were determined by fitting the experimental data depicted in **Figure 7.22** using SimFit. Values for the replicators *cis*-149 and *trans*-59b are listed for comparison.

	<i>trans</i> -168	<i>cis</i> -168	<i>trans</i> -149	<i>trans</i> -59b
bimolecular rate constant / M ⁻¹ s ⁻¹	1.37 x 10 ⁻⁴	2.51 x 10 ⁻⁴	6.99 x 10 ⁻⁴	2.66 x 10 ⁻⁴
recognition-mediated rate constant / s ⁻¹	6.42 x 10 ⁻⁴	-	1.57 x 10 ⁻²	1.32 x 10 ⁻³
effective molarity / M	4.69	-	22.5	4.96
ΔG ^s / kJ mol ⁻¹	12.9	-	9.46	12.5

Fitting of the doped reaction provided the values for the effective molarity and the free energy of connection. Compared to the crosscatalytic relationship between *trans*-162 and *trans*-69 (**Table 7.2**), the effective molarity was lower (4.96 M compared to 10.1 M) and the templates in the product duplex were found to be more tightly bound (12.9 kJ mol⁻¹ compared to 10.6 kJ mol⁻¹). This difference in reactivity is also reflected in the rate profile which exhibits a lower gradient and a slightly less pronounced curvature at the start of the reaction. In general, the replacement of the benzene spacer with a naphthalene group in the bisamido building block was compensated by the introduction of the phenylacetic acid to give rise to a second reciprocal system. However, comparison of the kinetic parameters for the reciprocal and the self-replicating systems clearly suggest that replicator *trans*-149 will be a strong competitor in this multicyclic reaction. Its low template association guarantees for high concentrations of catalytically active ternary complexes and the high effective molarity will ensure for rapid reaction of the building blocks.

Having established the crosscatalytic relationship between the two reciprocal templates, the native experiment using all four components **142**, **74**, **33** and **55** at a starting concentration of 10 mM were conducted at 10 °C. The progression of the reaction was monitored by ¹⁹F NMR spectroscopy and the deconvolution of the spectra allowed for the construction of the concentration *vs* time profile shown in **Figure 7.24**. Broadening of the signals for products *trans*-59b and *trans*-169 caused them to overlap and reduced slightly

the quality of the deconvolution. However, the main trends of the formation of all four products are clearly visible.

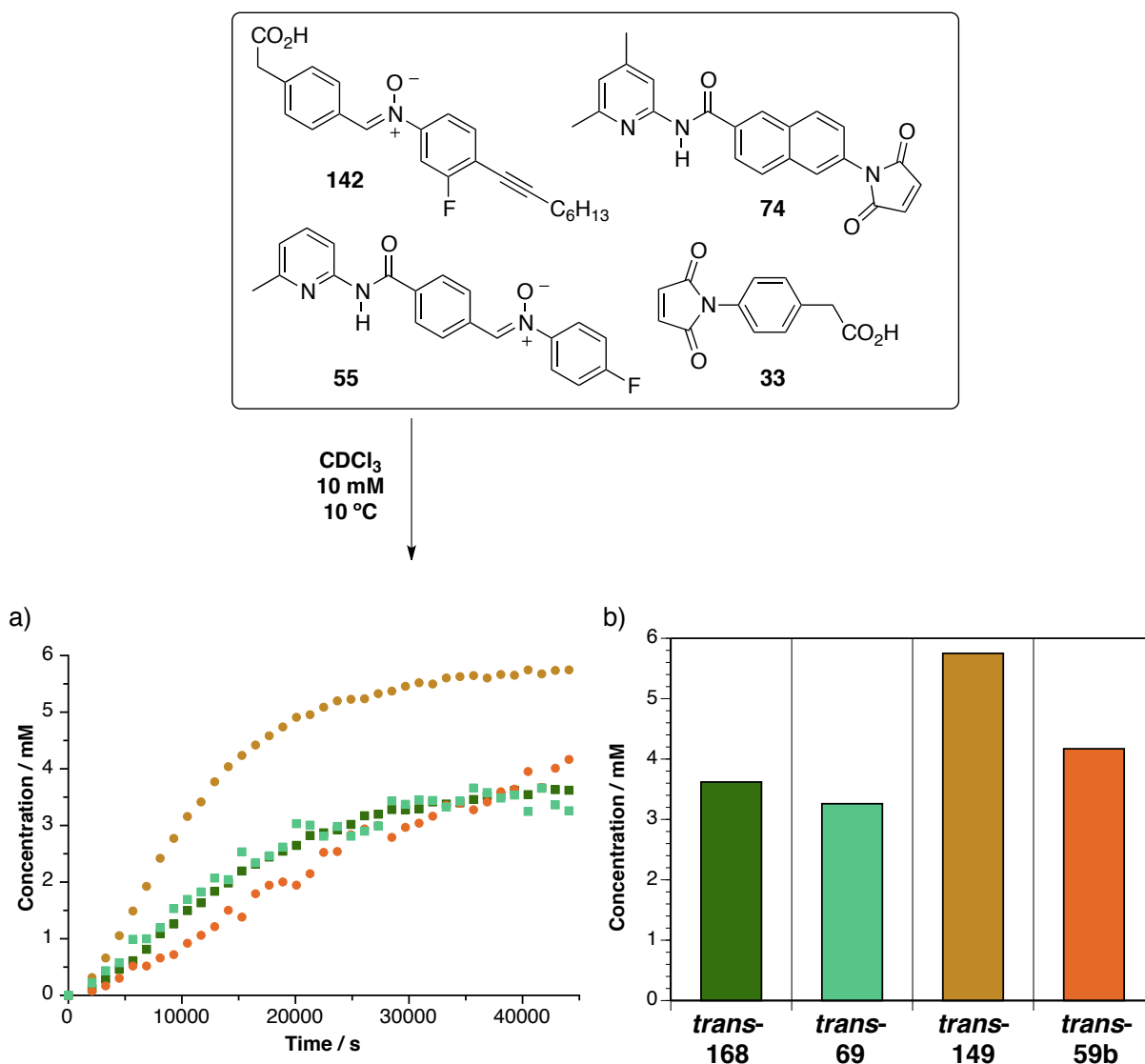


Figure 7.24 a) Concentration *vs* time profile of the multicyclic system depicted in **Figure 7.21**. The reactions of maleimides **33** and **74** with nitrones **142** and **55** gives rise to self-replicating templates *trans*-**149** (●) and *trans*-**59b** (●) and reciprocal templates *trans*-**168** (■) and *trans*-**169** (■). b) Product distribution for the templates after 12 h. All reactions were performed at 10 °C in CDCl₃ at 10 mM reagent concentration and monitored by ¹⁹F NMR spectroscopy.

It can instantly be seen that replacing original replicator *trans*-**161** with *trans*-**149** has a dramatic effect on the functioning of the multicyclic network. As a consequence of its intrinsic efficiency, it is newly introduced self-replicator *trans*-**149** that drives the reaction becoming the most dominant species in the product pool with a concentration of 5.75 mM after 12 h (**Figure 7.24b**). The formation of *trans*-**149** starts with a short lag period which is followed by a relatively steep gradient for the maximum rate of the reaction. Identical to the doping scenarios in which self-replicating template is added to the multicyclic system, the

enhanced efficiency of one of the autocatalysts causes a drain in reagents which correspondingly down-regulates the formation of the two interconnected reciprocal templates. Since maleimide **74** and nitron **142** are now preferably incorporated into *trans*-**149**, a larger amount of the other two building blocks are available for the construction of *trans*-**59b**. However, the autocatalytic production of *trans*-**59b** cannot quite keep up with its partner template and after 12 h, its concentration was 4.17 mM. After full conversion of starting material, the self-replicating species were determined to be in 1.4-fold excess over the reciprocal templates.

Even though the reciprocal templates *trans*-**162** and *trans*-**69** were outperformed by the self-replicators, both cycloadducts were still being formed to a reasonable amount after 12 h (3.62 mM and 3.26 mM, respectively). As a consequence of their crosscatalytic relationship, the formation of the two reciprocal templates proceeded simultaneously. Both curves again exhibited a sigmoidal rate profile with an initial lag period as seen for the original multicyclic network.

Overall, replacing self-replicating system **trans**-**161** with more efficient replicator *trans*-**149** has proven to change drastically the outcome of the multicyclic system in favour of the self-replicators. The induced geometric changes furthermore resulted in a less effective reciprocal system between *trans*-**168** and *trans*-**169** with lower EM and more stable duplex. Both factors lead to a weakening of the crosscatalytic pathway since both the amount of active ternary complex and the rate-enhanced formation of the cycloadduct are decreased.

The analysis of this multicyclic network demonstrated once more that strengthening one of the relationships between the building blocks has a severe impact on the performance of all other present interactions. In this case, increasing the efficiency of one of the two self-replicating fragments in the network simultaneously stimulated the enhanced production of the second autocatalytic system in a non-directed manner and at the same time, down-regulated the formation of the reciprocal templates.

7.11 Using *trans*-**147** as autocatalyst in the multicyclic system

Another replicating system that was thoroughly investigated in the previous chapters is based on the reaction between naphthalene maleimide **74** and carboxy nitron **141** to give template *trans*-**147**. Even though it was shown to be the least efficient replicator when studied in isolation, this system has proven to be surprisingly robust in complex competition scenarios (section 6.5.7). With this knowledge at hand, it would be interesting to see how this self-replicator performs within a multicyclic system. **Figure 7.25** shows the design in with the

original benzene maleimide **66** was replaced with maleimide **74** bearing the naphthalene spacer.

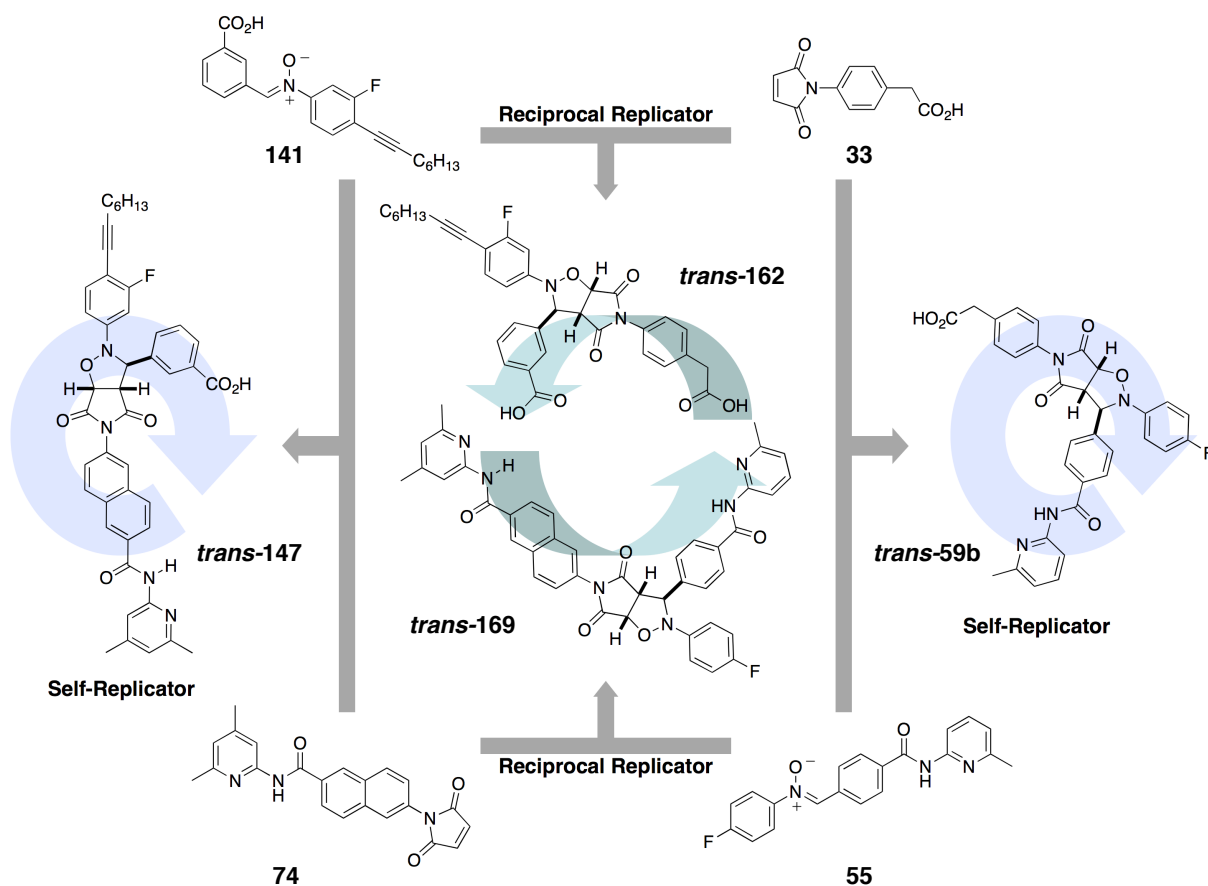


Figure 7.25 Multicyclic network combining self-replicating systems *trans*-147 (from maleimide **74** and nitron **141**) and *trans*-59b (from maleimide **33** and nitron **55**) to form two additional reciprocal templates *trans*-162 and *trans*-169.

As a consequence of the interconnectedness of the network, changing one of the self-replicating systems has an impact on the performance of the reciprocal system between templates *trans*-162 and *trans*-169. In order to elucidate the crosscatalytic relationship between both templates, two crucial experiments were conducted. The reaction between acid maleimide **33** and nitron **141** has been shown to be slow and unselective in the absence of any added template yielding a diastereoisomeric mixture of **162** (**Figure 7.7**). In the presence of 92 mol-% diastereoisomeric mixture of **169**, consisting of 58 mol-% of *trans*-isomer and 34 mol-% of *cis*-isomer, a catalytic effect is clearly visible (**Figure 7.26**). The formation of *trans*-**162** is enhanced significantly pointing at a crosscatalytic relationship between the two *trans*-isomers. The amount of *cis*-isomer is unaltered with respect to its bimolecular reaction confirming that this isomer has no catalytic relationship with either of the two isomers of **169**. However, compared with the two reciprocal systems discussed above, the catalytic efficiency of *trans*-**169** for the formation of *trans*-**162** is relatively low. The initial rate of

product formation is slower and after 16 h, only 48% of starting material was converted into products with a *trans/cis* ratio of 16:1. This reduced reactivity is a result of the geometric change induced when replacing benzene maleimide **66** with naphthalene maleimide **74**.

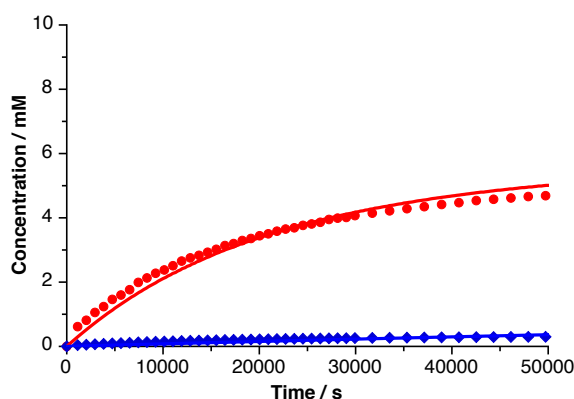


Figure 7.26 Concentration *vs* time profile for the reaction of nitrone **141** and maleimide **33** to give *trans*- and *cis*-**162** in the presence of 58 mol-% *trans*-**169** and 34 mol-% *cis*-**169**. The formation of *trans*-product is shown as red filled circles and the formation of *cis*-product as blue filled diamonds. Straight lines in represent the results for the fitting of the *trans*-(-) and *cis*-(-) product. The reaction was performed at 0 °C in CDCl₃ at 10 mM reagent concentration and monitored by ¹H NMR spectroscopy.

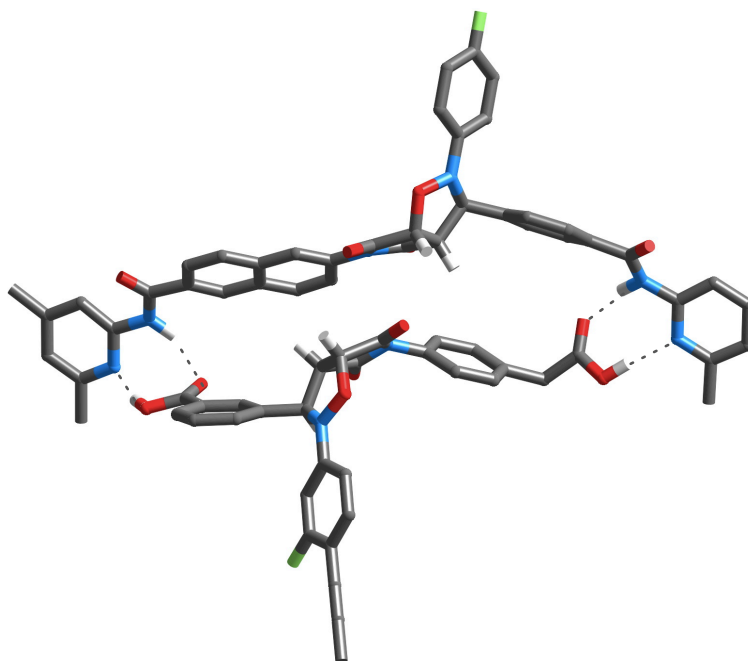


Figure 7.27 Molecular model of the reciprocal duplex of *trans*-**162** and *trans*-**169** monomer. Carbon atoms are shown in dark grey, hydrogen atoms in light grey, nitrogen atoms in blue and oxygen atoms in red. Hydrogen bonds are indicated by the dotted lines. Most other hydrogens were omitted for clarity.

In the scenario discussed in the previous section, the additional distance between the recognition and reactive site in the naphthalene maleimide **74** was compensated by employing phenylacetic acid nitrone **142** instead of shorter carboxy nitrone **141**. However,

the calculated structure of the reciprocal duplex does not show any apparent mismatch for both reciprocal templates (**Figure 7.27**). In this duplex, the orientation of the two templates was fixed to allow for the strong interaction between the carboxylic acid and the 4,6-dimethyl amido pyridine moiety.

In order to elucidate the origin of the reduced activity for this reciprocal system, we fitted the experimental data using SimFit (**Table 7.4**). The bimolecular rates were established previously and the procedure yielded the parameters for the effective molarity and the free energy of connection. The quality of the fit can be seen in **Figure 7.26**. Interestingly, this reciprocal system shows very strong duplex stabilisation which corresponds with the good match for the calculated structures of both templates. However, the effective molarity of this system is much lower than for the two previous systems which explains the limited efficiency of the reciprocal relationship.

Table 7.4 Kinetic parameters for the reaction of maleimide **33** and nitron **141** to give cycloadduct **162** at 0 °C in CDCl₃ at 10 mM reagent concentration. The kinetic parameters for the crosscatalytic relationship between *trans*-**162** and *trans*-**169** were determined by fitting the experimental data depicted in **Figure 7.26** using SimFit. Values for the replicators *cis*-**147** and *trans*-**59b** are listed for comparison.

	<i>trans</i> - 162	<i>cis</i> - 162	<i>trans</i> - 147	<i>trans</i> - 59b
bimolecular rate constant / M ⁻¹ s ⁻¹	1.51 × 10 ⁻⁴	9.39 × 10 ⁻⁵	3.47 × 10 ⁻⁴	2.66 × 10 ⁻⁴
recognition-mediated rate constant / s ⁻¹	1.62 × 10 ⁻⁴	-	8.68 × 10 ⁻⁵	1.32 × 10 ⁻³
effective molarity / M	1.07	-	0.25	4.96
Δ <i>G</i> ^s / kJ mol ⁻¹	22.6	-	-1.36	12.5

Comparison of the kinetic parameters for all four participating replicating systems reveals that *trans*-**59b** possesses the highest effective molarity. However, the exceptionally low value for the free energy of connection for *trans*-**147** was already shown to provide the replicator with an advantage in complex reaction networks. Low duplex stabilisation leads to an increasing concentration of free template which further increases the concentration of ternary complexes.

In order to investigate whether *trans*-**147** can exploit this advantage in the scenario of a multicyclic system, the native experiment using all four components **141**, **33**, **55** and **74** at a starting concentration of 10 mM were conducted at 10 °C. The progression of the reaction

was monitored by ^{19}F NMR spectroscopy and the deconvolution of the spectra allowed for the construction of the concentration *vs* time profile shown in **Figure 7.28a**.

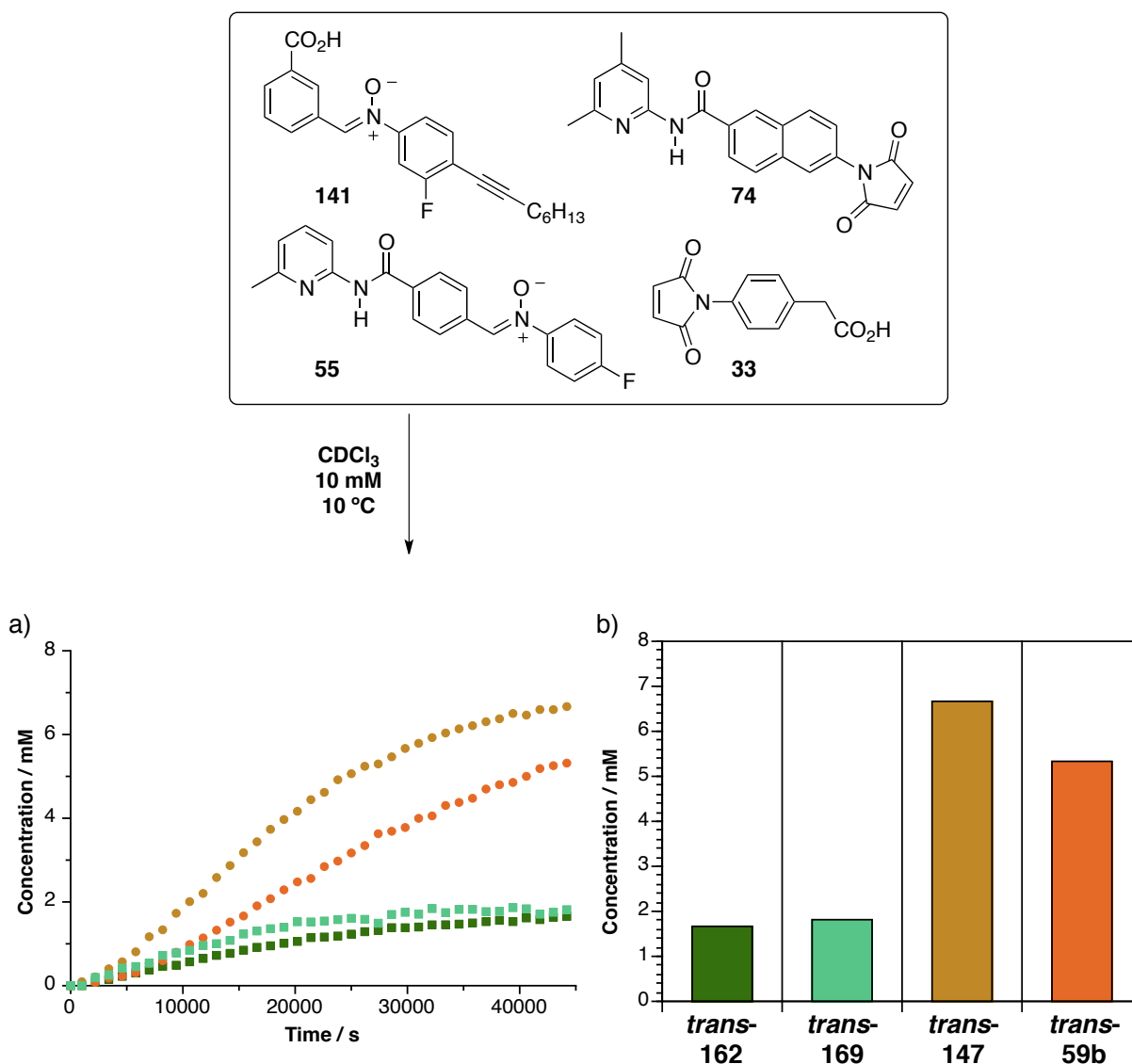


Figure 7.28 a) Concentration *vs* time profile of the multicyclic system depicted in **Figure 7.25**. The reactions of maleimides **33** and **74** with nitrones **141** and **55** gives rise to self-replicating templates *trans*-**147** (●) and *trans*-**59b** (●) and reciprocal templates *trans*-**162** (■) and *trans*-**169** (■). b) Product distribution for the templates after 12 h. The reaction was performed at 10 °C in CDCl_3 at 10 mM reagent concentration and monitored by ^{19}F NMR spectroscopy.

When compared with the original multicyclic system, it instantly becomes apparent that replacing maleimide **66** with its naphthalene counterpart **74** has a major impact on the product distribution. All four curves show the characteristic sigmoidal shape but it is now the self-replicating systems *trans*-**147** and *trans*-**59b** that clearly dominate over their reciprocal counterpart (**Figure 7.28b**). As expected, replicator *trans*-**147** is the most abundant species with a concentration of 6.67 mM after 12 h followed by *trans*-**59b** with 5.32 mM. Both reciprocal templates were formed to a concentration of only 1.65 mM (*trans*-**162**) and 1.82

mM (*trans*-69). After full conversion of all starting material, the self-replicating species were determined to be in 3.3-fold excess over the reciprocal templates. The driving force in this network is template *trans*-147 whose stamina in competition scenarios has already been shown. Even though their reactivity in isolation would suggest otherwise, replicator *trans*-147 is performing better than its self-replicating partner *trans*-59b. It is however not only for the efficiency of the self-replicators that they are doing well in the competition for building blocks, but the weakness of the reciprocal templates reduces drastically their ability to compete for reagents. Despite their reduced activity, both reciprocal template are still formed simultaneously proving the presence of the crosscatalytic cycle to be the major reaction pathway.

Once more, the sensitivity of the multicyclic system with respect to geometric changes has been demonstrated by replacing benzene maleimide 66 with maleimide 74. This extension in spacer group reduced significantly the efficiency of the reciprocal system and simultaneously introduced a self-replicator with proven assertiveness in competition situation. As a result, the production of autocatalytic templates was enhanced drastically on expense of the reciprocal replicators.

7.12 Using AB system *cis*-170 in the multicyclic system

In the examples discussed so far, the variations of compounds in the multicyclic system were designed to replace one autocatalytic system with another system of different efficiency. In this section, replacing carboxy acid nitron 141 from the original multicyclic design with phenylacetic acid 142 converted the efficient self-replicating template *trans*-161 into hybrid system 170 giving rise to AB system *cis*-170 with replicator *trans*-170 being formed in minor extend (Figure 7.29).

As pointed out in the previous chapters for the non-fluorinated system *cis*-105 and 4,6-dimethyl analogue *cis*-148, the rate-enhanced formation of *cis*-170 proceeds through a binary complex which results in an intrinsically different rate profile as found for self-replicators. The maximum rate of the AB reaction is found at its start when the concentration of the reagents is highest providing a clear advantage over all other replicators who reach their maximum rate only after overcoming the initial lag period. Hence, in the context of a multicyclic system, the AB system is expected to be the driving force. Withdrawing the necessary reagents for *cis*-170 from the crosscatalytic system leaves a larger amount of building blocks *trans*-59b which is therefore expected to perform better than in the original experiment.

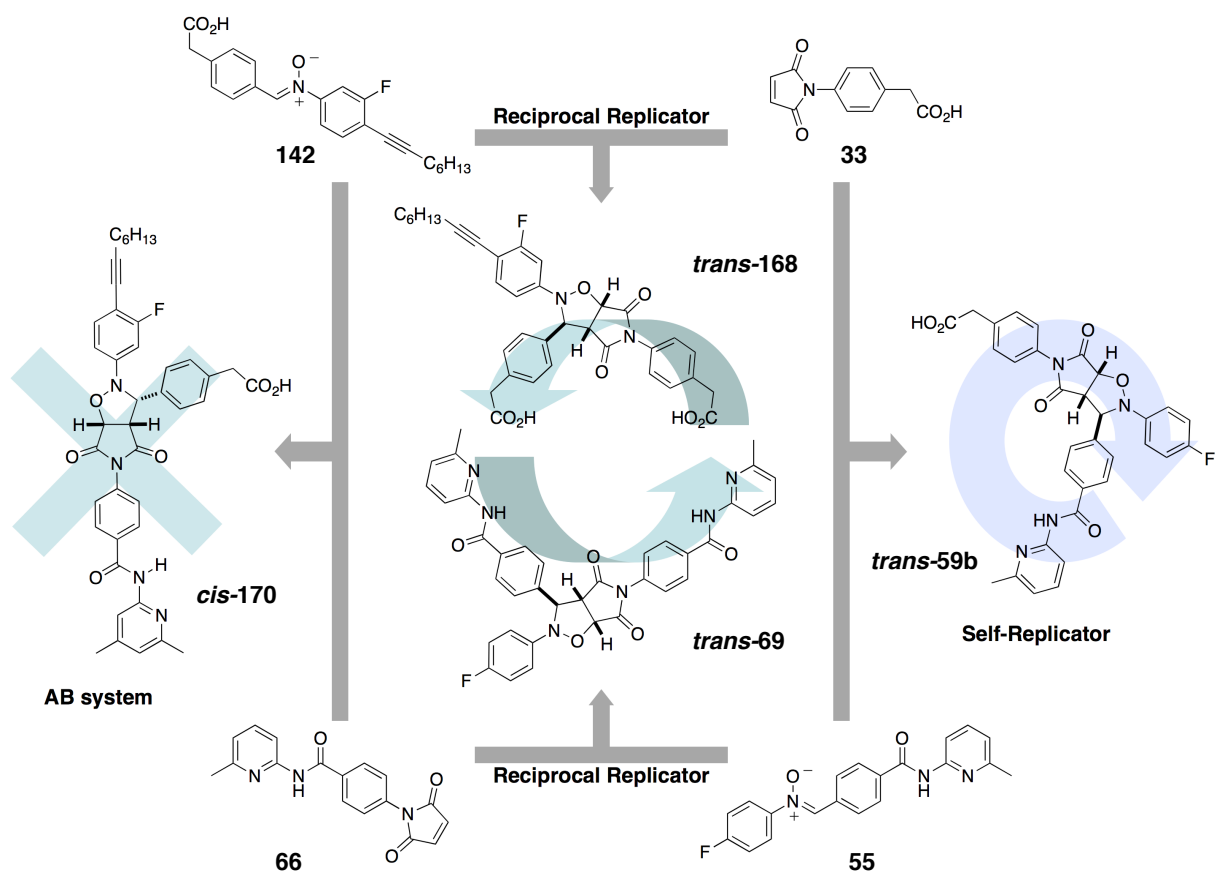


Figure 7.29 Multicyclic network combining AB system *trans*-170 (from maleimide **66** and nitronium **142**) and self-replicator *trans*-59b (from maleimide **33** and nitronium **55**) to form two additional reciprocal templates *trans*-168 and *trans*-69.

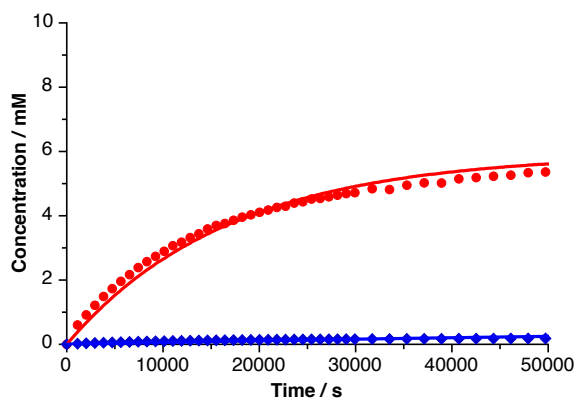


Figure 7.30 Concentration *vs* time profile for the reaction of nitronium **142** and maleimide **33** to give *trans*- and *cis*-168 in the presence of 59 mol-% *trans*-69. The formation of *trans*-product is shown as red filled circles and the formation of *cis*-product as blue filled diamonds. Straight lines in represent the results for the fitting of the *trans*-(-) and *cis*-(-) product. The reaction was performed at 0 °C in CDCl₃ at 10 mM reagent concentration and monitored by ¹H NMR spectroscopy.

Before the native experiment can be conducted, the efficiency of the reciprocal replicating system needs to be investigated in isolation. The reaction between both phenylacetic acid compounds has already been shown to be slow and unselective even

though a small contribution of a binary AB complex between both acids leads to a slight increase for the *cis*-isomer (**Figure 7.22**). In order to probe for crosscatalytic activity between the two reciprocal templates, the reaction between nitron 142 and maleimide 33 was repeated in the presence of presynthesised 59 mol-% *trans*-69.

Deconvolution of the obtained ¹H NMR spectra allowed for the construction of the concentration *vs* rate profile depicted in **Figure 7.30**. It instantly becomes visible that addition of *trans*-69 has a catalytic effect on the formation of *trans*-168. As seen for other crosscatalytic systems, the maximum rate of the reaction is at the start when the concentration of free *trans*-69 is highest. As the reaction progresses, *trans*-168 binds to the reciprocal template thereby reducing the amount of available catalyst. This product inhibition limits drastically the rate of formation of *trans*-168 and the rate of reaction is gradually reduced in the course of the reaction. After 16 h, 75% of starting material was converted into products with a ratio of diastereoisomers 29:1 in favour of *trans*-168. Once more, addition of *trans*-69 has no effect on the formation of the *cis*-isomer since the closed structure of this isomer does not allow for the formation of a catalytically active ternary complex.

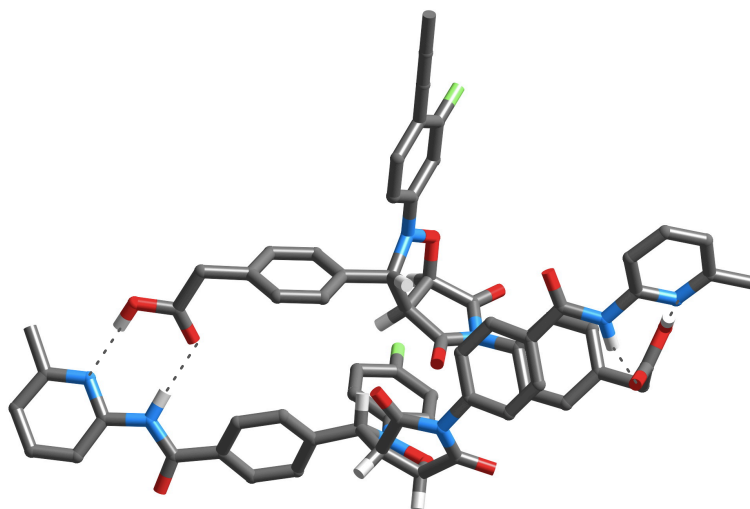


Figure 7.31 Molecular model of the reciprocal duplex of *trans*-168 and *trans*-169 monomer. Carbon atoms are shown in dark grey, hydrogen atoms in light grey, nitrogen atoms in blue and oxygen atoms in red. Hydrogen bonds are indicated by the dotted lines. Most other hydrogens were omitted for clarity.

The computational simulation of the product duplex [*trans*-168·*trans*-69] is depicted in **Figure 7.31**. A significant mismatch can be seen which forces the two templates to wrap around each other. Using the extended phenylacetic acid for the diacid template while maintaining the benzene spacer in the corresponding bisamido template created an imbalance in length between the two templates. Even though bisamido template *trans*-69 is

still able to recognise both acid building blocks, the additional methylene group in nitron **142** seems to induce too much flexibility and it is more difficult to bring both reactive sites into the correct position to ensure highly efficient rate-enhanced template formation.

Kinetic fitting of the doping reaction using SimFit confirm these observations by providing a low EM value, however, the stability of the template duplex is surprisingly high (Table 7.5). The kinetic parameters for analogue AB system *cis-148* bearing a 4,6-dimethylpyridine substituent and replicator *trans-59b* are listed for comparison. Since the mechanism for the recognition-mediated process *via* AB pathway is intrinsically different from the ones for the replicator, it is not instructive to compare the values for the individual reactions. We can however assume that *cis-170* will use its bimolecular mode of formation to its advantage providing a pull for the second replicator *trans-59b*. It will furthermore be interesting to see how *trans-170*, the replicating isomer of the AB system, will behave in this multicyclic set-up.

Table 7.5 Kinetic parameters for the reaction of maleimide **33** and nitron **142** to give cycloadduct **168** at 0 °C in CDCl₃ at 10 mM reagent concentration. The kinetic parameters for the crosscatalytic relationship between *trans-168* and *trans-69* were determined by fitting the experimental data depicted in Figure 7.30 using SimFit. Values for the replicators *cis-148* and *trans-59b* are listed for comparison.

	<i>trans-168</i>	<i>cis-168</i>	<i>cis-148</i>	<i>trans-59b</i>
bimolecular rate constant / M ⁻¹ s ⁻¹	1.37 × 10 ⁻⁴	2.51 × 10 ⁻⁵	1.03 × 10 ⁻⁴	2.66 × 10 ⁻⁴
recognition-mediated rate constant / s ⁻¹	2.07 × 10 ⁻⁴	-	7.65 × 10 ⁻⁵	1.32 × 10 ⁻³
effective molarity / M	1.51	-	0.743	4.96
Δ <i>G</i> ^s / kJ mol ⁻¹	25.7	-	-	12.5

Having established the crosscatalytic relationship between both reciprocal templates, the native experiment using all four building blocks **142**, **33**, **66** and **55** was conducted at 10 °C and with 10 mM reagent concentration. ¹⁹F NMR spectroscopy was employed to record the kinetics of the reaction. Deconvolution of the obtained spectra allowed for the construction of the concentration *vs* time profile shown in Figure 7.32a.

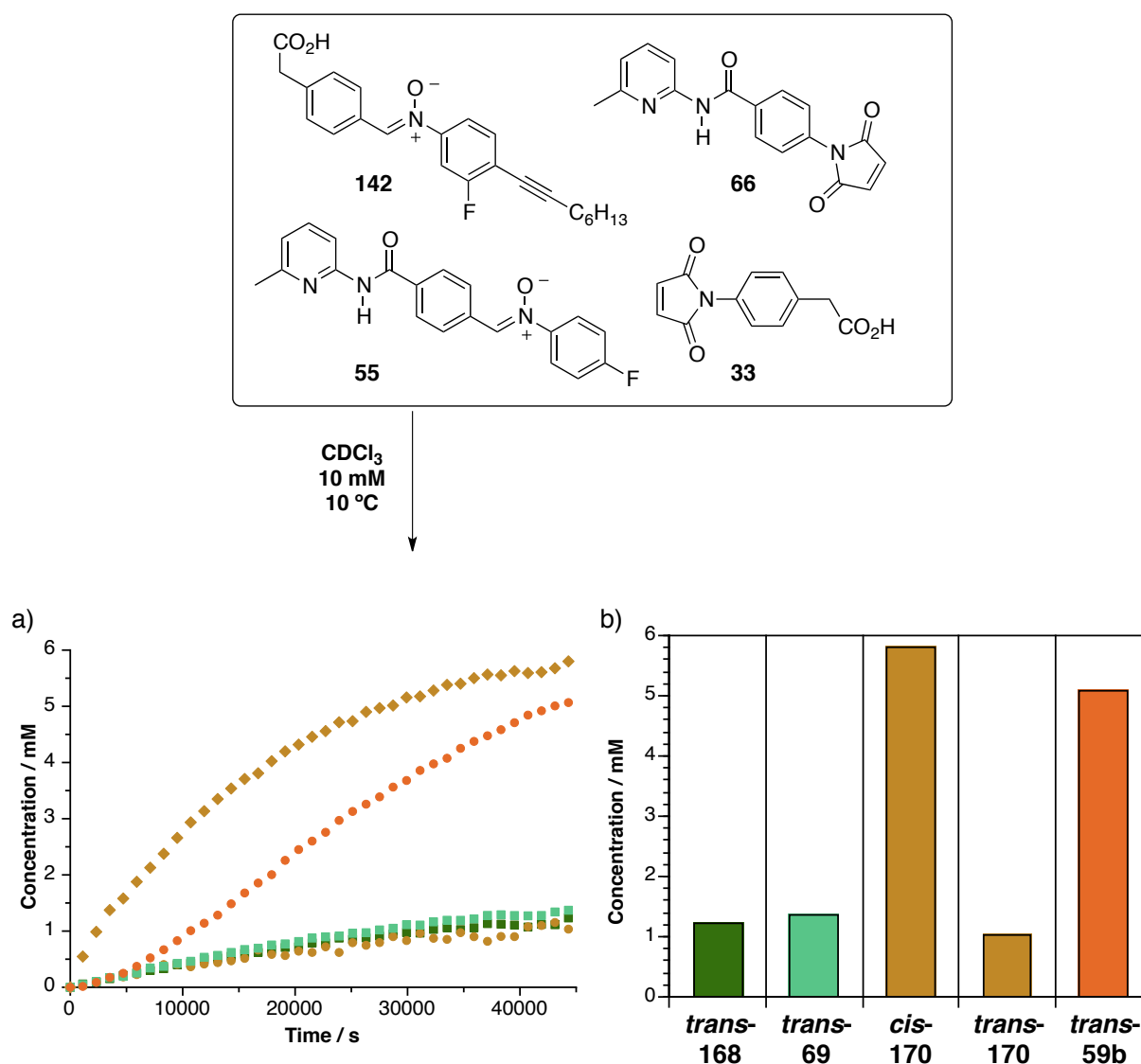


Figure 7.32 a) Concentration *vs* time profile of the multicyclic system depicted in Figure 7.29. The reactions of maleimides 33 and 74 with nitrones 142 and 55 gives rise to AB system *cis*-170 (♦), self-replicating templates *trans*-170 (●) and *trans*-59b (●) and reciprocal templates *trans*-168 (■) and *trans*-69 (▲). b) Product distribution for the templates after 12 h. The reaction was performed at 10 °C in CDCl₃ at 10 mM reagent concentration and monitored by ¹⁹F NMR spectroscopy.

It can clearly be seen, that throughout the reaction, the AB system *cis*-170 is performing better than all other systems. As a result of the bimolecular reaction mechanism, the maximum rate of formation for *cis*-170 is at the start of the reaction when the amount of building blocks is highest. As the reaction progresses, the amount of available reagents is reduced and the rate of the recognition-mediated formation decreases. The high efficiency of the AB system consequently allows self-replicator *trans*-59b to perform better than in the original experiment by providing it with a larger amount of building block. After 12 h, the concentration for *cis*-170 and *trans*-59b was 5.80 mM and 5.07 mM, respectively (Figure 7.32b). Both reciprocal replicators *trans*-162 and *trans*-69 were formed to a concentration of 1.23 mM and 1.37 mM, respectively. Despite their failure to compete successfully for building

blocks, the simultaneous progression for both crosscatalysts again proves the interconnectedness of both templates. Additionally, the concentration of the self-replicating partner of the AB system, *trans*-170, was determined as 1.03 mM. The dominance of *cis*-170 could even be more pronounced if its *trans*-isomer did not function as direct competitor for the same two building blocks. After complete conversion of all starting material, the RR/SR ratio between reciprocal replicator *trans*-69 and self-replicator *trans*-59b, which both competed for a limited amount of nitron 55, was calculated to be 0.25 compared to the ratio of 2.1 found in the original network.

Introduction of an AB system into the multicyclic framework suppressed significantly the formation of reciprocal templates. From the start of the reaction, the AB system drives the reaction resulting in a concomitant increase for its partner replicator *trans*-59b. But their ascendancy is also a consequence of the poor crosscatalytic performance of the two reciprocal templates.

7.13 Summary of results

The combination of replicators *trans*-161 and *trans*-59b was shown to form a fully functional multicyclic system (Figure 7.5). Replacing either or both of the building blocks for *trans*-161 by structurally similar compounds did not only alter the nature of this replicating fragment in the multicycle but the functioning of the whole network. The effect of these substitutions on the outcome of the multicyclic reaction are summarised in Figure 7.33. It can clearly be seen that every variation of the original multicycle (lane I) leads to an increased production of self-replicating species with concomitant down-regulation of both reciprocal replicators (lanes II, III and IV). In every case, it is the newly introduced system which turns out to be the dominating force in the networks. However, the cause for this inversion in reactivity is different for each of the investigated systems.

The most conservative replacement from a structural point of view was made by using *trans*-149 instead of *trans*-161 (lane II). The increase in spacer length from benzene to naphthalene was compensated by using phenylacetic acid nitron 142 instead of the shorter carboxy nitron 141. In isolation, this compensation guarantees that both replicating systems are especially efficient. As a matter of fact, *trans*-149 has shown to be the stronger replicator which also reflected in the context of the multicyclic system. Separate analysis of the reciprocal replicators revealed only a small reduction in activity compared to the original system. Hence, it is mainly the efficiency of replicator *trans*-149 which boosted the formation of autocatalysts on expense of the reciprocal replicators.

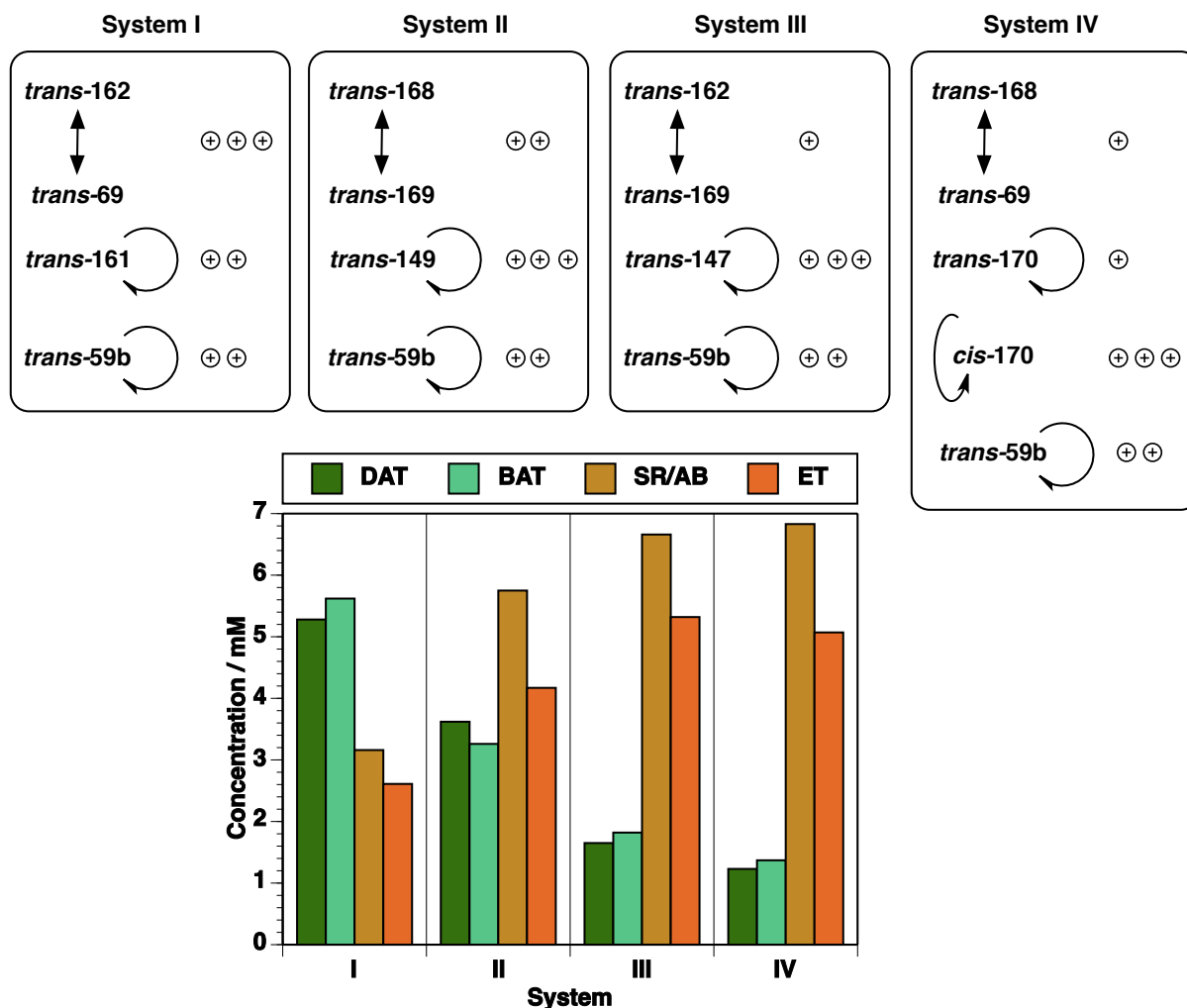


Figure 7.33 Overview over the multicyclic systems investigated in this chapter depicted in **Figure 7.5** (System I), **Figure 7.21** (System II), **Figure 7.25** (System III) and **Figure 7.29** (System IV). The efficiency of each individual autocatalytic (circular arrow on the right side of template name), crosscatalytic (double-headed arrow between two template names) and AB (circular arrow on the left side of template name) system is classified on basis of their kinetic values as either low (⊕), medium (⊕ ⊕) or high (⊕ ⊕ ⊕). Reaction products are summarised to form four groups: diacid templates (**DAT** = *trans*-162 or *trans*-168), templates bearing bisamidopyridine moieties (**BAT** = *trans*-69 or *trans*-169), self-replicator (**SR** = *trans*-147, *trans*-149 or *trans*-161) a variable self-replicator or AB system 170 (**SR** = *trans*-170 and **AB** = *cis*-170) and reference replicator 59b (**ET**).

The situation is fundamentally different for the substitution of only one of the building blocks. Replacing benzene maleimide **66** with naphthalene maleimide **74** altered the geometry of the product duplex for the two complementary reciprocal templates (lane **III**). Calculations have revealed that even though the stability of the duplex is increased, the effective molarity for the reaction of the two acid building blocks catalysed by the bisamido template was reduced. Simultaneously, the change in maleimide building block generated replicator *trans*-147 who benefits from its low duplex stabilisation in competition scenarios. Both factors, weakening of the reciprocal system and installation of a highly competitive

replicator, led in a drastic increase in production for the autocatalysts on the expense of the replicating systems.

In the third scenario, carboxy nitrone **141** was replaced by phenylacetic acid **142** (lane **IV**). Combination of this acid with benzene maleimide **66** resulted in the construction of AB system *cis-170*. AB systems proceed through a bimolecular pathway exhibiting their maximum rate at the start of the reaction. They are therefore able to compete very effectively for available building blocks at the start of the reaction and hamper the formation of both reciprocal species. Concomitantly, also *trans-59b* benefits from the presence of the AB system.

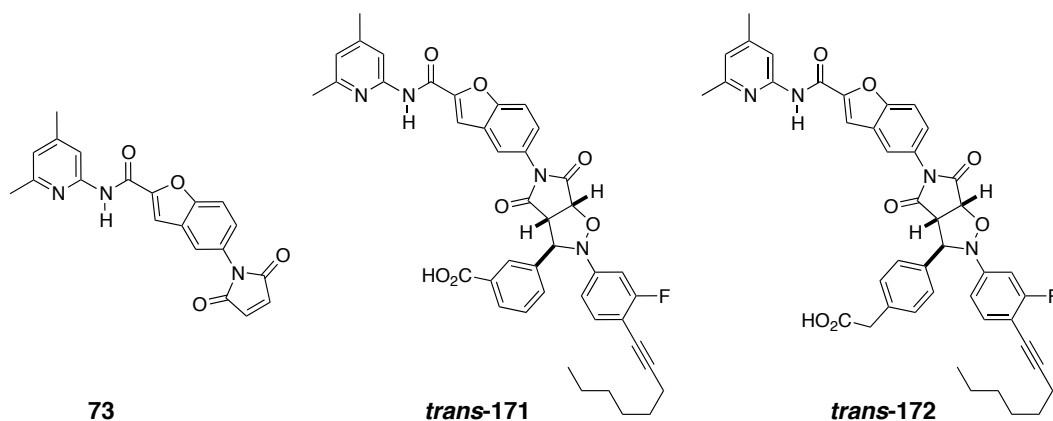
Especially the last example demonstrates that very subtle changes can cause a drastic change in the topology of the network. The only difference between system **I** and **IV** is one additional methyl group in the nitrone building block and yet, the behaviour of the system is entirely different. In the design of single replicating structures (chapter 3), we showed that it is crucial to limit the flexibility of the building blocks in order to avoid reactive bimolecular complexes while maintaining the possibility to form self-complementary template duplexes. The same recipe should be used for the design of more complex systems. However, when working with networks consisting of several building blocks such as this multicycle, modification of one particular building block will have consequences on more than one replicating pathway. In order to learn more about the principles, it would be highly instructive to investigate further variations of this type of multicycle. Several example can be found in the next chapter.

8. Future work

The results presented in this thesis shed some light on the collective behaviour of interacting replicating species. A wide array of future experiments can potentially tie in with these recent achievements to deepen the understanding of emergent behaviour in such complex networks. These future experiments may include the expansion of the established procedure of competing self-replicators, coupling the reaction network with a reversible exchange process or choosing an entirely thermodynamic platform for the design of a multicyclic system. An example for each of these potential research targets is highlighted briefly in this chapter. Ultimately, the feasibility of moving away from working in closed systems is probed and some encouraging initial results are discussed.

8.1 Systems including maleimide 73

In chapter 3, six self-replicating and one AB system were established by combining three maleimides with two nitrones. For the individual systems, a clear hierarchy was found and the two most and the least efficient system as well as the hybrid system producing both the AB and autocatalytic system were used as building blocks for the investigation of competition scenarios and complex networks.

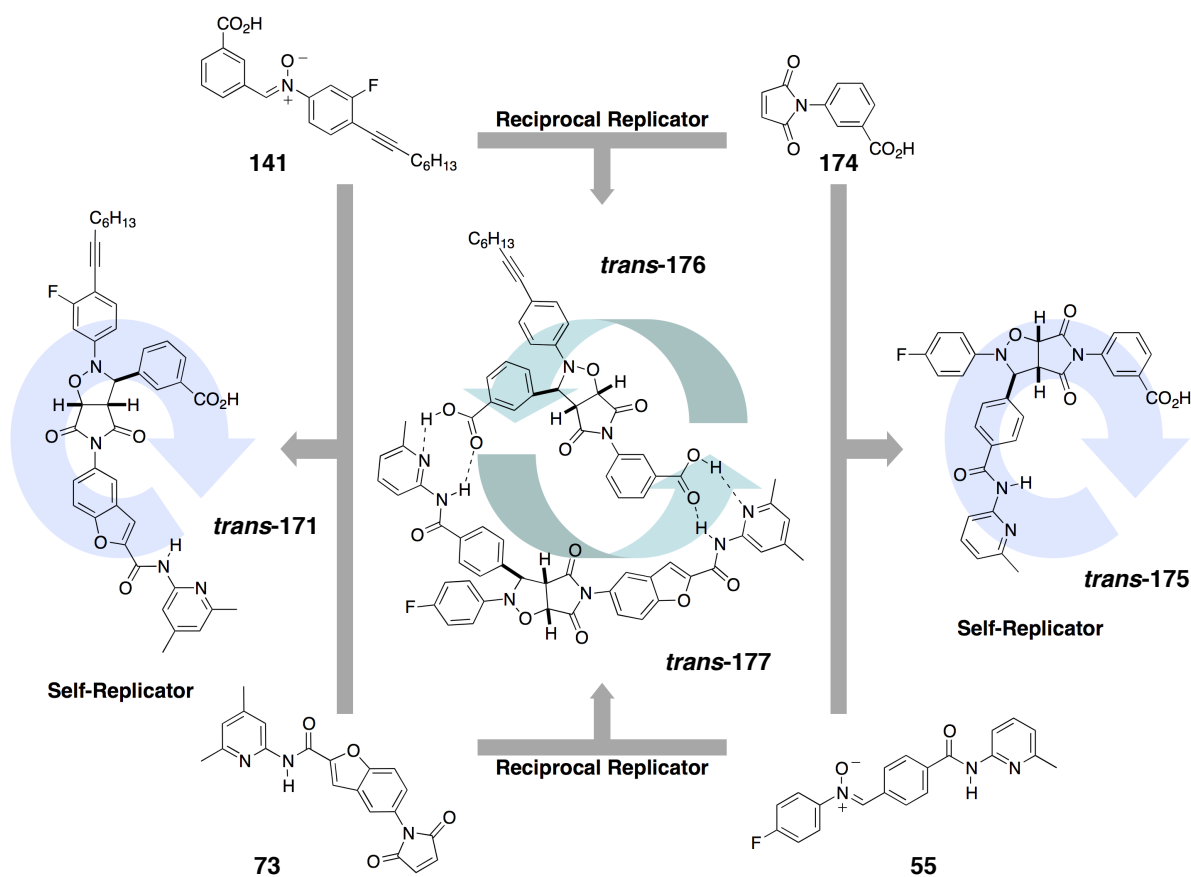


Scheme 8.1 Structure of benzofuran maleimide 73 and the potential autocatalytic templates of its reaction with carboxylic acid 141 (*trans*-171) and phenylacetic acid 142 (*trans*-172).

Since the efficiencies of the two replicating systems based on the reaction of maleimide 73 were found to be rather moderate, they were thought to make less interesting building blocks and were disregarded in the following experiments. However, with the results of this thesis at hand, we should have understood that the efficiency of a replicator in isolation does not necessarily reflect their behaviour within multi-component networks of

higher order. It would therefore be of great interest to incorporate templates *trans*-171 and *trans*-172 into multicomponent networks similar to the competition scenarios in chapter 6 (Scheme 8.1).

Many possible combinations of building blocks can be imagined to produce scenarios of increasing complexity. The relatively simple three component reaction between maleimide **73** and nitrones **141** and **142** would induce a competition between *trans*-171 and *trans*-172. Compared to the previous rivalry between two autocatalysts, such as *trans*-147 and *trans*-149, both replicators now show similar replicating efficiencies. The outcome of the native three component reaction can therefore be expected to be more balanced and the influence of template addition may be greater. A combination of all three maleimides with carboxy nitronone will lead to the formation of three different self-replicating products of distinctively different efficiencies. Emergent behaviour can be revealed by comparing the experimentally obtained order of product formation with the individual activities of the systems. Exchanging carboxy nitronone with phenylacetic acid nitronone creates a scenario in which two self-replicators compete with an AB system. Provided that clean analysis can be guaranteed, a system including all five building blocks can be set up.



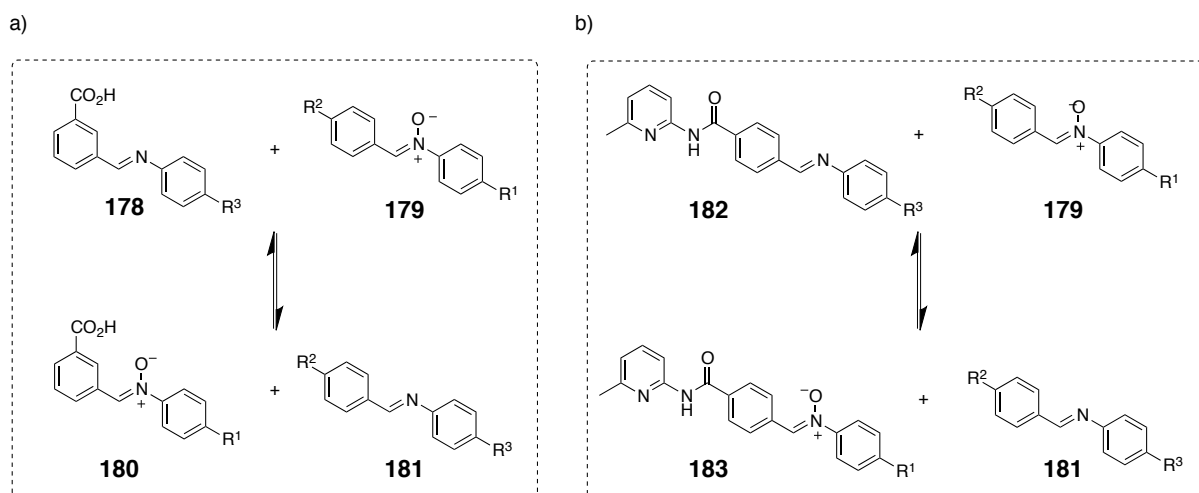
Scheme 8.2 Proposed design of a multicycle using benzofuran maleimide **73** with carboxy nitronone **141** and maleimide **174** with nitronone **55**.

Ultimately, *trans*-172 or *trans*-171 can be combined with *trans*-59b to form two further sets of multicycle. In this respect, it would also be interesting to investigate the possibility of substituting the benchmark replicator *trans*-59b with a less efficient autocatalytic system but similar geometry such as *trans*-175 from nitrone 55 and maleimide 174 (Scheme 8.2). By weakening the self-replicating contributions in the multicycle without causing a dramatic change in the geometry of the building blocks, it might be possible to generate a network in which the dominance of the reciprocal systems in the product pool is strengthened.

8.2 Developing a dynamic multicyclic system

In this thesis, the design and characterisation of a set of self-replicating structures is presented. Ultimately, some of these replicators were successfully incorporated in the design of fully functional multicyclic systems. In these constructs, the hierarchy of interactions among the replicating entities was dissected and the feasibility of influencing the outcome of the experiments by adding informational templates was established. However, since the cycloaddition that leads to the template is relatively fast and irreversible, the limits of enhancing selectively one species is fixed within certain kinetic boundaries. One possibility of reducing the kinetic drive would be to feed in slowly some of the reagents during the reaction as shown in chapter 6 for the competition scenario between a self-replicator and an AB system. By doing this, the concentrations of reactive components would be low, thereby reducing the contributions of the bimolecular pathways and emphasising the template directed formation of products. In the case of doping a reaction mixture with presynthesised template, the formation of the unwanted template would therefore be suppressed and enhancements for the instructed template would be much greater. At the same time, undesired bimolecular background reactions which unselectively form all templates in nearly equal amounts are suppressed.

Instead of slow addition of one reagent to the reaction mixture, the exchange protocol established previously in which a reactive nitrone bearing a recognition unit is formed from a pool of imines and nitrones under hydrolytic cleavage and recombination of the fragments can be exploited (Scheme 8.3). Starting from recognition-disabled nitrone 179 and imine 178 bearing an acid recognition site, recombination of the aldehyde fragments generates carboxy nitrone 180, a member of the original multicyclic system (Scheme 8.3a). The process can be modified for the formation of amidopyridine nitrone 183 from feed nitrone 179 and recognition imine 182 (Scheme 8.3b).



Scheme 8.3 Proposed imine-nitron exchange protocol to form a) carboxy nitron **180** from feed nitron **179** and acid imine **178**, and b) amidopyridine nitron **183** from the same feed nitron **179** and imine **182**. In both cases, the stoichiometry also leads to the formation of feed imine **181**. Details for the mechanism and conditions of the exchange reaction can be found in chapter 6. Substituents R₁, R₂ and R₃ ideally increase the solubility of the components and facilitate the analysis of this system.

Thus, substitution of both nitrones in the original multicycle from **Figure 7.5** with the corresponding imine structures produces a system that can only perform upon addition of feed nitron **179** (**Figure 8.1**). Both nitrones needed for the multicyclic system are now only formed through the exchange processes. Since the concentration of active compounds is kept low, this approach is bound to generate higher selectivities for the doping experiments using preformed template. However, incorporation of the dynamic exchange pools leads to two further products. Feed nitron **179** can react with both maleimides **33** and **66** to form two sets of diastereoisomeric products, **184** and **185**. With feed nitron **179** being needed for both exchange pools, its concentration is twice as high as for the other building blocks and its bimolecular reaction at the start of the reaction will be rather high. The investigation of this dynamic multicyclic system therefore requires a well thought-out concept regarding the analysis of such complex network and its mixture of products. Also other important factors such as the solubility and stability of all participating species have to be considered.

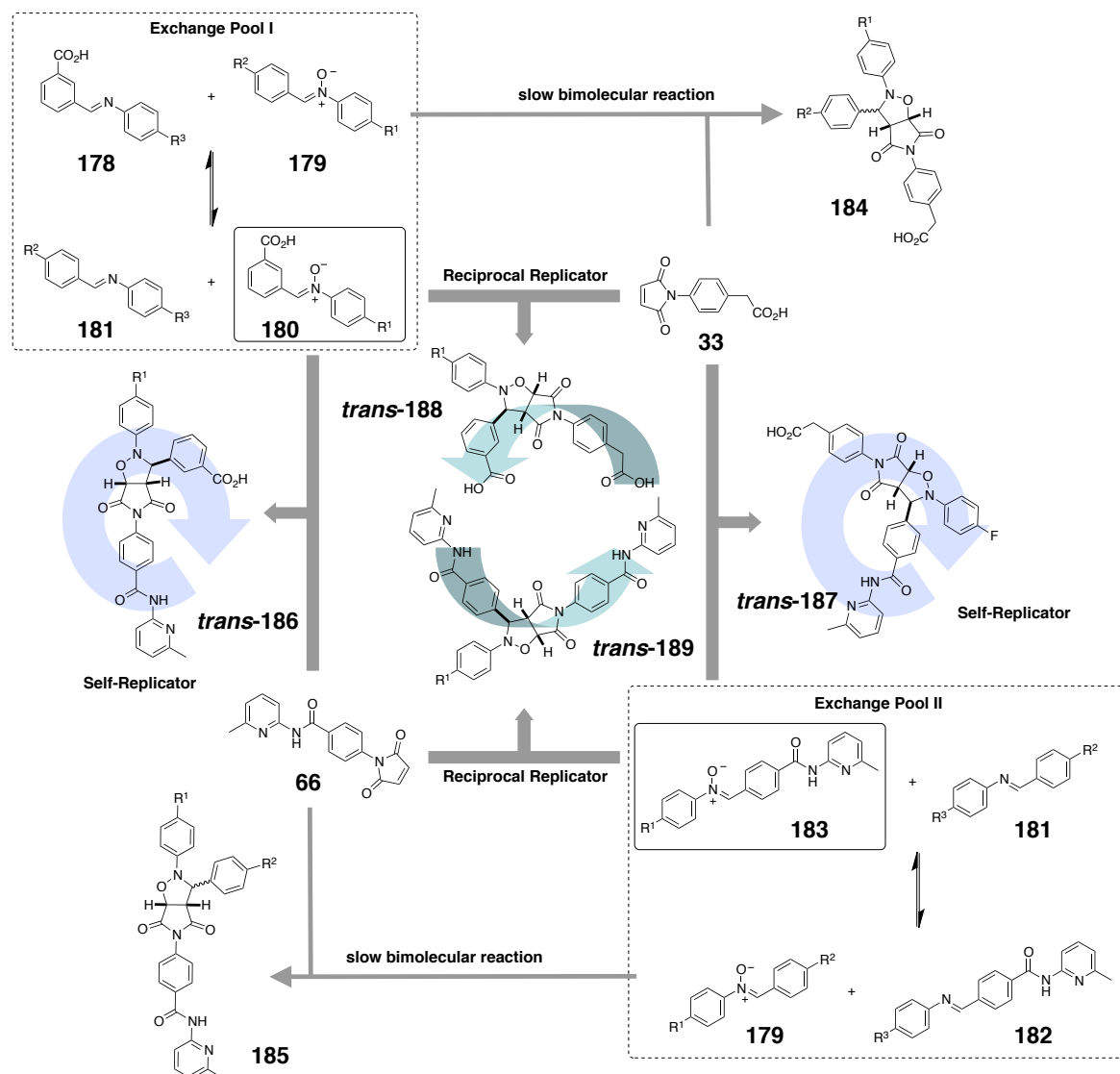


Figure 8.1 Proposed dynamic multicyclic network based on the system presented in **Figure 7.5** and the exchange processes in **Scheme 8.3**. The nitrones required, **180** and **183** (highlighted as solid boxed building blocks), are formed through exchange pool I and II, respectively, and highlighted as members of the multicycle. The reaction of feed nitrone **179** with maleimide **33** and **66** leads to the formation of diastereoisomeric sets of **184** and **185** as side-products.

8.3. Developing a multicyclic imine system

The design of a multicyclic system on an entirely dynamic basis is another interesting research target. Recent work has established^[185] the self-replicating nature of the condensation reaction between amine **45** and aldehyde **46** to form imine **47** (left side of **Figure 8.2**). When doping preformed template **47** into a fresh batch of reagents, the reaction was indeed found to be enhanced at the early stage of the reaction. However, the amount of newly formed **47** actually decreased with increasing amount of dopant. Since the formation of the product is under thermodynamic control, adding imine to the reaction mixture shifts the equilibrium towards the reagents. This behaviour is in contrast to the kinetic scenario in which addition of template strengthens the native template.

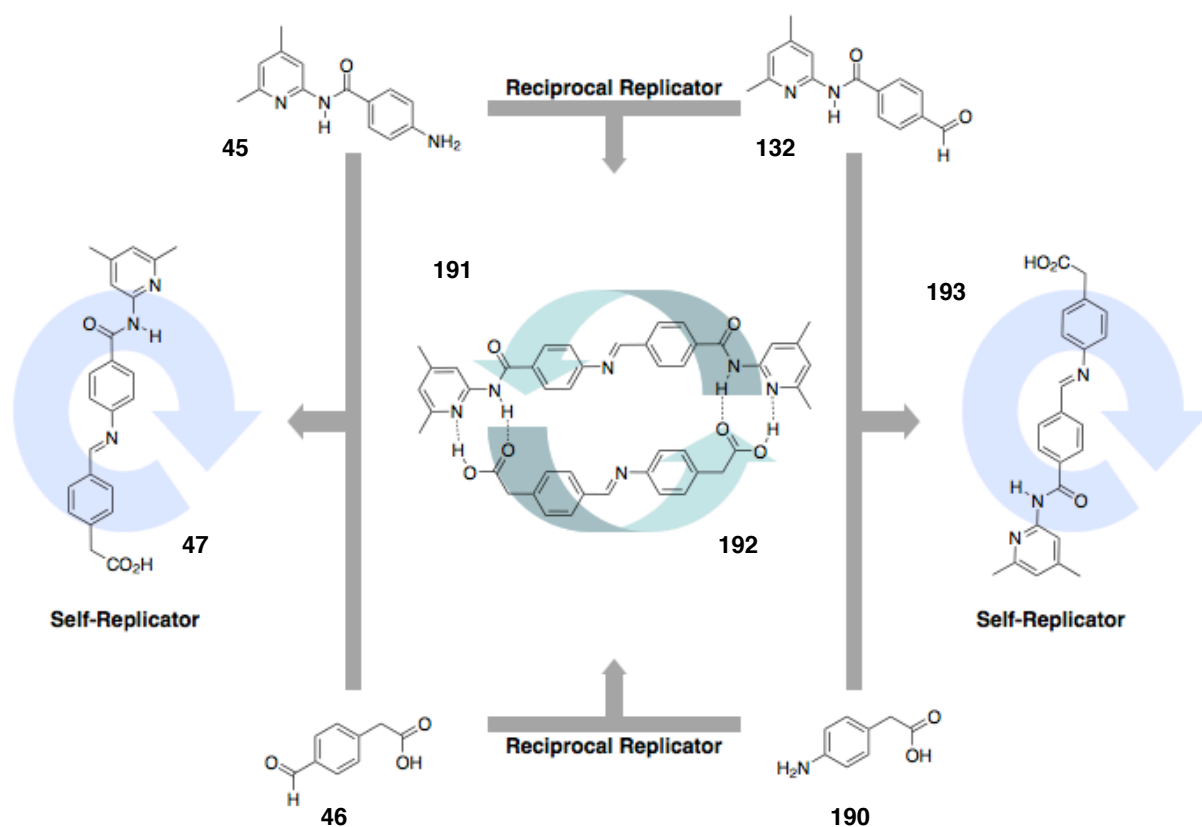


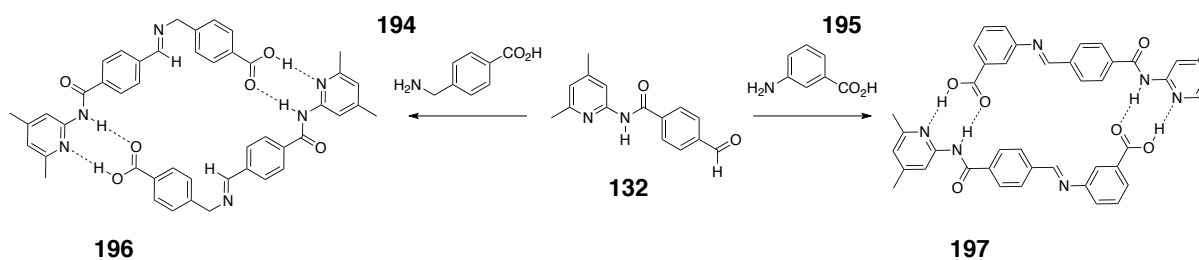
Figure 8.2 Proposed design of a multicyclic system based on the condensation reaction between aldehyde and aniline to reversibly form an imine template. Two self-replicating templates **47** and **193** can be combined to open up the crosscatalytic pathway between the reciprocal templates **191** and **192**. The self-replicating system **47** has previously been established.^[185] Formation of template **193** from aldehyde **132** and **190** has not yet been achieved because of the limited solubility of **190** in chloroform and dichloromethane.

In this context, the development of a multicyclic replicating system based entirely on reversible interactions could shed light on the connectivity and the interplay of the individual components. One possible scenario is depicted in **Figure 8.2**, in which the existing imine replicator **47** is coupled with a second system based on acid amine **190** and recognition aldehyde **132**. The self-replicating efficiency of **193** has not yet been investigated since **190** showed very limited solubility in CDCl_3 . However, attaching solubilising groups to the benzene core in **190** should allow to overcome this problem and permit to investigate the interplay between both imine replicators. Just as in the case of the nitron replicators, merging both autocatalytic systems could open the formation of a reciprocal relationship between template **191** and **192**. As a consequence of the interconnectedness of the system, addition of one template will cause the system to respond as a whole. For example, addition of a fixed amount of minimal template **193** is expected to shift the equilibrium towards its building blocks, amine **132** and aldehyde **190**. Since both compounds are also part of the crosscatalytic system, an increase in their concentration will favour the formation of the reciprocal templates, **191** and **192**. Both templates also require aldehyde **132** and amine **190** as

building blocks who in turn will be subducted from the second minimal replicator **193**. In effect, addition of template **191** or **192** is expected to cause a reduction in template concentration for both minimal templates while strengthening the equilibrium position of the reciprocal templates.

Additionally, experimental investigation of such system could also provide important information about how the equilibrium position of the condensation reaction varies under different conditions. A fully equilibrated system responds to stimuli like changes in temperature, progressive dilution or gradual modification of the polarity of the solvent, and the changes could be monitored conveniently by ^1H or ^{19}F NMR spectroscopy.

The situation presented in **Figure 8.2** is only one possibility to couple the existing replicator **47** with a suitable second system based on simple building blocks. As previously mentioned, initial attempts to investigate the depicted system failed because of the limited solubility of amine **190** in non-polar solvents. Two further candidates for the design of a self-replicating imine that can potentially be coupled with **47** are presented in **Scheme 8.4**. Variation of the substituents on the benzene ring gives rise to another pair of self-complementary imines structures **196** and **197**. However, also the two additional amine structures **194** and **195** will surely need to be modified to increase their solubility and to facilitate the analysis of the final multicyclic system.



Scheme 8.4 Two potential self-replicating imine templates for the incorporation into the dynamic multicyclic system depicted in **Figure 8.2**. Aldehyde **132** could react with **194** or **195** to form replicating templates **196** and **197**, respectively.

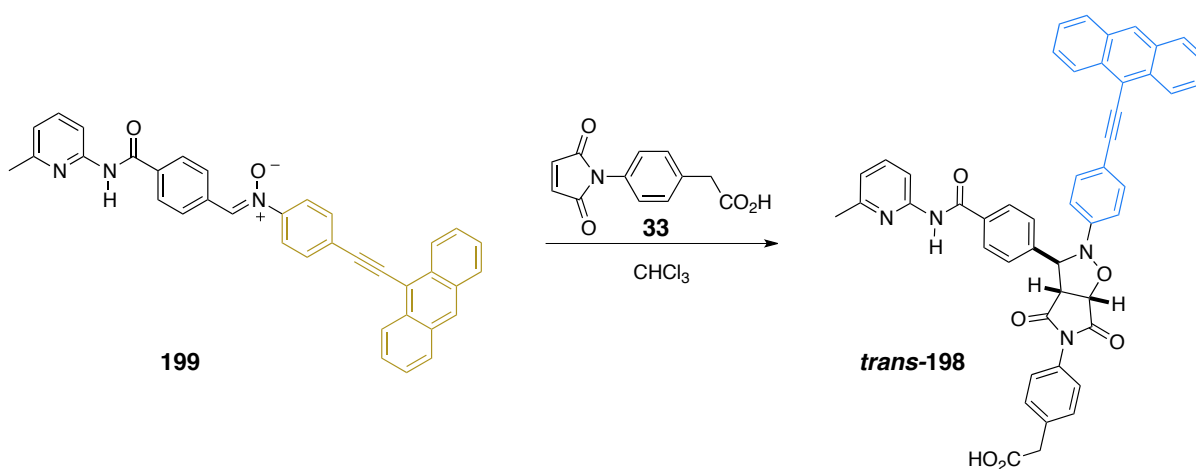
8.4 Chemical waves

The experiments presented in this thesis including the hypothetical ones in this chapter are carried out in a closed system. In general, all reagents are dissolved in an NMR tube or flask using a suitable solvent and this solution is then incubated at a certain temperature while the progression of the reaction is followed by NMR spectroscopy. Except for the pH controlled reactions in chapter 5 which required specific addition of acid or base, no exchange of matter

takes place with the environment and the reaction set-up follows the model of the static well-stirred batch reactor (WSBR). We have established that working in a closed system places fundamental limits on the ability of replication networks to express complex outcomes since the amount of reagent is limited. Most intriguingly, the envisaged selection for one of the two replicating types within the multicyclic framework by repetitive recycling failed and led to cooperation of all species rather than extinction of the weaker one.

As a future direction of research, our well-characterised replicating systems may be moved from closed reaction systems into two different kinds of open systems. Firstly, the design of reaction diffusion systems can be envisaged in which a chemical process is initiated at one point in a reactor and a reaction wave propagates from this origin through the reactor. For example, traveling waves of short self-replicating RNA variants along thin capillary tubes have been reported.^[207,208] Secondly, the use of a continuous stirred tank reactor (CSTR) would provide the possibility to introduce one or more fluid reagents into a tank reactor to generate a continuous flow of reagents. Adjusting the steady state condition of the CSTR, it is possible to manipulate the system such that an autocatalyst present can operate under its optimum conditions at all times.

In order to permit real-time monitoring of the reaction mixture, alternative methods of analysis must be sought. Attaching a fluorescent tag to one of the building blocks allows for optical sensing by fluorescent spectroscopy and by naked eye (**Scheme 8.5**). Replicator *trans*-**198** is based on system *trans*-**59b** but bears an anthracene group which exhibits a shift in emission from yellow for nitron **199** to blue for cycloadduct *trans*-**198**. Despite the bulky tag, the efficiency of the self-replicator remains nearly as high as for the original system.



Scheme 8.5 Autocatalytic formation of *trans*-**198** from nitron **199** and maleimide **33**. The presence of the anthracene group leads to a yellow emission for **199** and blue emission for *trans*-**198**.

With this system at hand, a propagating reaction-diffusion front could be created by transferring an equimolar mixture of reagents into a syringe and seeding at one end with a fixed amount of preformed template.^[209] Encouraged by these initial results, we are currently investigating a set of variants of nitron **199** bearing slightly different fluorescent tags. Ultimately, we wish to study more complex phenomena such as the behaviour of a system comprising two competitive autocatalytic processes in an open system. In a WSBR, the equilibrium composition will always correspond to a mixture of the two products, with their respective equilibrium concentrations depending on the ratio of the rate constants and their initial concentrations. When the same reaction is carried out in a reaction diffusion system, exclusive product selectivity might occur since both replicator waves propagate differentially. One of the autocatalysts will propagate more efficiently thereby depleting the common building block more rapidly leading to a level of selectivity which is unattainable in closed systems.

9. Conclusion

The emerging field of Systems Chemistry aims at gaining insight into the construction, the analysis and the understanding of complex molecular networks. Autocatalytic processes feature prominently in the discussion of such networks. The feedback caused by the non-linear amplification of a self-replicator allows for its directed selection over other molecules. This principle not only provides a means to control the composition and evolution of mixtures of small molecules, but it may further provide answers to fundamental questions regarding the Origin of Life or the homochirality of natural building blocks.

Early research on the topic of self-replication focused on the mathematical explanation of experimental observations. This approach led to a thorough understanding of some of the major principles and within a short time period, a large amount of replicators based on nucleotides, peptides and small organic molecules appeared in literature. Besides looking at the performance of individual replicators, systems appeared in which the main focus was on the study of the interaction between replicators. Especially systems of peptide replicators reached a high degree of sophistication, whereas only few examples of networks based on organic replicators are known.

The main objective of the thesis presented here was therefore to explore if structurally simple organic molecules can be used as building blocks for the construction of complex replicator networks. Once such networks were established, the next step was to probe to what degree external stimuli can influence their behaviour and whether their networks' topology can be deduced directly from the properties of the individual building blocks.

The initial task of establishing a set of replicators to construct these networks was achieved using computational methods and insight gained from previous screenings for replicating systems. Kinetic parameters could be extracted showing non-exponential growth for all systems and a clear hierarchy in efficiency could be explained by the geometric variations of the incorporated backbone. Two of these systems together with two systems established previously in the group were used to test how subtle variations in recognition strength change the outcome of recognition-mediated reactions. It was shown that such variation had very little effect on the performance of the self-replicators. Strong single point interaction indeed created a high concentration of active ternary complex but for the tested systems this favourable interaction lived on in the product duplex leading to product inhibition. On the other hand, changes in recognition strength effected the performance of the AB system in a more direct way. Strong interaction between the building blocks created a high concentration of binary complex, a higher initial rate and, therefore, more product.

The same AB and self-replicating system were then used as the first example of a scenario in which two recognition-mediated processes competed for a limited amount of building block. It was shown that in these three-component systems, the outcome of the competition could be predicted by the properties of the individual systems. For instance, replicators that proved efficient in isolation would always dominate weaker systems. Moreover, the outcome of the competition could be influenced by the addition of autocatalytic template at the start of the reaction. This manipulation did, however, achieve only small shifts in the product distribution and with increasing amounts of added template, a saturation point was reached. Moving away from a purely kinetic environment into a scenario in which some of the building blocks were formed in a dynamic exchange process pushed the degree of enhancement beyond the original point of saturation.

A combination of four building blocks from the original set of replicators gave rise to five major products *via* four autocatalytic and one AB pathway. As a consequence of the increased interconnectedness between the building blocks, the outcome of the competition scenario could not be deduced from the kinetic and thermodynamic parameters determined for the individual systems. It was found that in this scenario, replicators with low duplex stability, leading to an increased amount of free template, had an advantage over systems with strong duplex association. This change in mode of functioning can be regarded as a case of emergence, since the behaviour of the four-component network could not be readily predicted from the behaviour of any of its subsystems.

A multicyclic network was constructed by combination of one of the replicators presented in this thesis with a previously established system bearing reversed recognition and reactive sites. In this network, the four building blocks could interact *via* four interlinked replicating pathways, two autocatalytic and two crosscatalytic. Conceptually, this network bears some resemblance to Ghadiri's hypercycle based on peptides (**Figure 1.9**). Our multicyclic system however differs not only by the number and chemical nature of its constituents, but also from the degree of interaction between the building blocks. By definition, a hypercycle consists of autocatalysts that organise to form a cyclic network in which each member is closely connected to another member in a crosscatalytic fashion. By doing this, the hypercycle can compete more efficiently for existing resources than any member on its own. Accordingly, the peptide hypercycle gives rise to two autocatalytic products which catalyse the formation of each other in a symbiotic manner.

In the multicyclic system presented in this thesis, every building block can react *via* two different reaction modes to form an auto- or crosscatalytic template giving rise to four reaction products. This high degree of connectivity between the building blocks creates a

situation of competition between the two modes of replication reducing the activity for every replicator compared to its individual performance. Our network is therefore more closely related to the system presented by von Kiedrowski using four oligonucleotides (**Figure 1.5**).

In both cases, the interconnectedness between the building blocks rendered the systems intractable to the addition of informational template. Addition of reciprocal template up-regulated the formation of both reciprocal templates in a symbiotic manner, whereas addition of minimal template instructs only the autocatalytic enhancement of one of the two templates. The enhancement of the partner autocatalyst occurs without explicit instruction and can be seen as another example of system-level behaviour. Subsequent replacement of one of the autocatalysts with a close structural variant modified the product distribution by changing the efficiency of **both** replicating modes.

With a functioning multicyclic system at hand, experiments were carried out in which the outcome of a reaction was used as template for a fresh batch of reagents. This repetitive doping procedure was thought to lead ultimately to the dominance of one of the two replicating modes, auto- or crosscatalytic, but the envisaged selection failed and co-operation of all species was instead observed. The intrinsic ratio between the two competing species was governed by the initial concentrations of their active ternary complexes. Addition of pre-synthesised template altered this ratio but the perturbation did not propagate over the doping cycles with the ratio always degrading to the original value. In the context of the Origin of Life, this finding gives experimental evidence that for sub-exponential replicators Darwinian evolution in a closed environment is improbable leading to a scenario in which 'everybody lives'.^[205,206]

The repetitive doping experiments have clearly shown that working in closed systems places artificial boundaries on the selectivities of replicators, since they function outside their optimum concentration range for much of the reaction time course. Theoretical discussions of replicating networks in open systems suggest that scenarios exhibiting temporal and spatial separation are capable of displaying much more diverse behaviour. It is therefore time to take the next step forward and to incorporate the well-established replicators developed in our group into the context of open reaction systems.

10. Experimental

10.1 General procedures

Chemicals were purchased from ABCR GmbH & Co, Alfa Aesar, Apollo Scientific Ltd., Fisher Scientific UK Ltd., TCI UK Ltd., Sigma–Aldrich Company Ltd. or VWR International Ltd. and purified by standard techniques where necessary.^[210] Where appropriate and if not otherwise stated, all non-aqueous reactions were carried out under an inert nitrogen or argon atmosphere with the inert gas passing through a bed of 4 Å molecular sieves and self-indicating silica gel. Brine refers to a saturated aqueous solution of sodium chloride. Anhydrous solvents were obtained under the following conditions: dry THF was distilled from sodium in a recycling still using benzophenone ketyl as indicator; dry acetonitrile was distilled from calcium hydride in a recycling still; dry CH₂Cl₂ was obtained using a MBRAUN GmbH MB SPS–800 solvent purification system, where solvent was dried by passage through filter columns and dispensed under an atmosphere of N₂ or Ar gas; CDCl₃ was neutralised by filtering through CaCl₂ and then stored over 4 Å activated molecular sieves. Analytical Thin Layer Chromatography (TLC) analysis was performed on MACHEREY–NAGEL GmbH & Co. POLYGRAM SIL G/UV₂₅₄ plates, plastic backed 0.2 mm silica gel plates with fluorescent indicator. Developed plates were air-dried and visualised under a UV lamp (λ_{max} 254 or 366 nm) or after incubating with iodine on sand. Where necessary, thermal development after dipping in: methanolic DNP and sulfuric acid solution, ninhydrin in *n*-butanol or a solution of aqueous potassium permanganate, potassium carbonate and sodium hydroxide, was used to aid visualisation. Flash Column chromatography and silica plugs were carried out on Apollo Scientific Ltd. silica gel 40–63 micron or Silicycle SiliaFash P60 silica gel (230–400 mesh) eluting with solvents as supplied under a positive pressure of compressed air. Melting points were determined using an Electrothermal 9200 melting point apparatus and are uncorrected. Mass spectra were recorded on a Micromass GCT spectrometer for electron impact ionisation (EI) operating at 70 eV or chemical ionisation (CI) using isobutane as the ionising gas. Electrospray ionisation spectra (ES) were performed on a Micromass LCT spectrometer operating in positive or negative mode from solutions of methanol, acetonitrile or water. *m/z* values are reported in Daltons and followed by their percentage abundance in parentheses.

10.2 NMR spectroscopy

^1H NMR spectra were recorded on a Bruker Avance 500 (500.1 MHz), a Varian UNITYplus 500 (500.1 MHz), a Bruker Avance II 400 (400.1 MHz) or a Bruker Avance 300 (300.1 MHz) spectrometer using the deuterated solvent as the lock and the residual solvent as the internal reference in all cases. In the assignment of ^1H NMR spectra the chemical shift information (δ_{H}) for each resonance signal is given in units of parts per million (ppm) relative to trimethylsilane (TMS) where $\delta_{\text{H}} \text{ TMS} = 0.00$ ppm. The number of protons (n) for a reported resonance signal are indicated as $n\text{H}$ from their integral value and their multiplicity by the symbols s, d, t, q, m and br which denote singlet, doublet, triplet, quartet, multiplet and broad singlet respectively. Their coupling constants (J) are determined by analysis using the iNMR software (Version 3.4.6, Mestrelab Research, 2007) quoted to the nearest 0.1 Hz. Identical coupling constants are averaged in each spectrum and are reported to the nearest 0.1 Hz. ^{13}C NMR spectra were recorded on a Bruker Avance 500 (125.7 MHz), a Bruker Avance II 400 (100.6 MHz) or a Bruker Avance 300 (75.5 MHz) spectrometer using the CPD or DEPTQ pulse sequences with broadband proton decoupling using the deuterated solvent as the lock and the residual solvent as the internal reference in all cases. The chemical shift informations (δ_{C}) for each resonance signal are given in units of parts per million (ppm) relative to trimethylsilane (TMS) where $\delta_{\text{C}} \text{ TMS} = 0.00$ ppm. All signals are singlets unless stated, in which case their multiplicity is represented by the symbol d for doublet. ^{19}F NMR spectra were recorded using a Bruker Avance 500 (470.3 MHz), a Bruker Avance II 400 (376.5 MHz) or a Bruker Avance 300 (282.4 MHz) spectrometer using a broadband proton decoupling pulse sequence with the deuterated solvent as the internal lock. The chemical shift informations (δ_{F}) for each resonance signal are given in units of parts per million (ppm) relative to CCl_3F where $\delta_{\text{F}} \text{ CCl}_3\text{F} = 0.00$ ppm. All ^1H , ^{13}C and ^{19}F spectra were analysed using iNMR software (Version 3.4.6, Mestrelab Research, 2007).

10.2.1 Kinetic measurements using ^1H NMR spectroscopy

500.1 MHz ^1H NMR spectroscopy was used for kinetic analysis of the systems described in chapters 3, 4 and 5. Masses of reagents were measured using a Sartorius BP 211D balance (± 0.01 mg). Stock solutions of the appropriate starting materials were made using a fresh batch of CDCl_3 stored over 4 Å molecular sieves and equilibrated in a thermostatically controlled water bath at reaction temperature.

In a typical experiment, an NMR sample was prepared in a 5 mm NMR tube (Wilmad 528PP) by mixing appropriate volumes of stock solutions such that the total volume was 800

μL and the concentration of each component was 10 mM. A polyethylene pressure cap was then applied to the top of the tube to prevent solvent evaporation. The NMR tube was transferred to an NMR spectrometer (Varian UNITYplus) regulated at the desired temperature, and 500.1 MHz ^1H NMR spectra were acquired automatically at a given time interval over a period of 8-40 hours. Analysis and deconvolution of the arrayed set of ^1H NMR spectra recorded during this time was performed using iNMR software (Version 3.4.6, Mestrelab Research, 2007).

The chemical reaction monitored in the described systems was a 1,3-dipolar cycloaddition between a maleimide and a nitrene, giving rise to two cycloadduct products. The percentage completion of the reaction was monitored through the disappearance of the maleimide protons signal and the appearance of the cycloadduct proton signals. The two diastereoisomeric products of the reaction between a nitrene and a maleimide are easily distinguishable in the ^1H NMR spectrum, since the signals of the isoxazolidine protons give a different splitting pattern for the two cycloadducts (**Figure 9.1**).

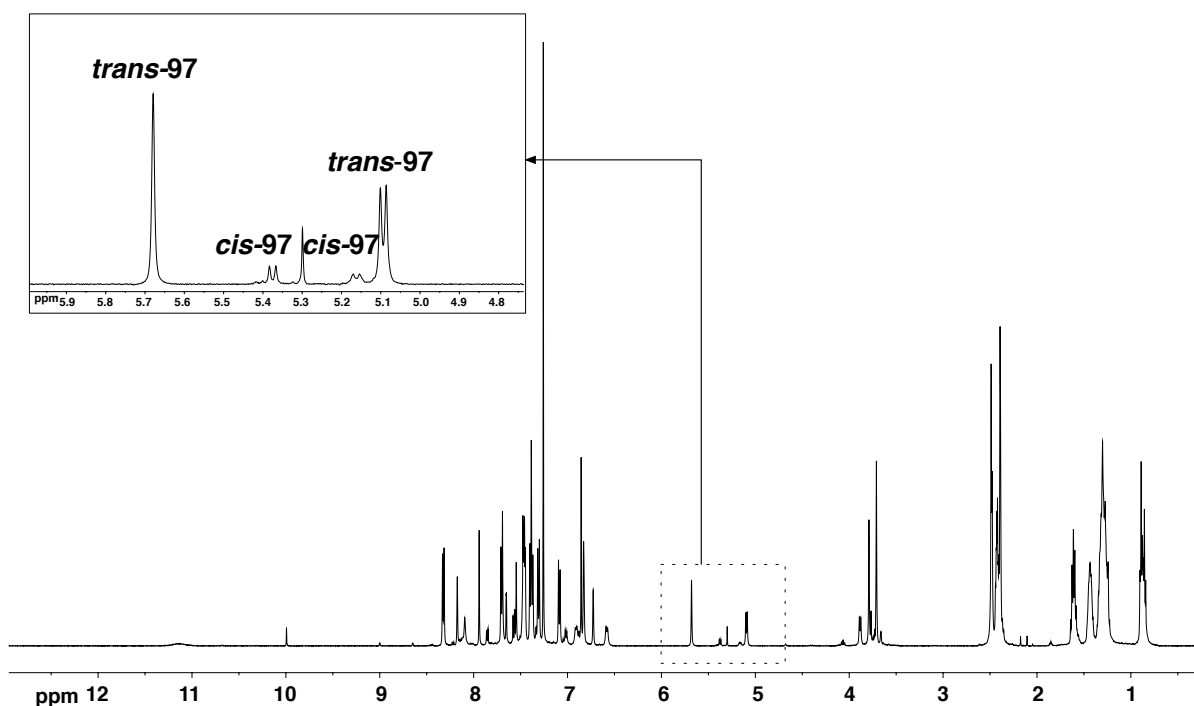


Figure 9.1 500.1 MHz ^1H NMR spectra for the reaction between benzofuran maleimide **73** and phenylacetic acid nitrene **71** at 10 mM concentration recorded at 10 $^\circ\text{C}$ after 32000 s. The inset shows the signals used to identify the products of the reaction.

In order to extract product concentrations from the ^1H NMR spectrum the area of the maleimide proton signals and one of the signals of the corresponding cycloadduct proton were calculated through deconvolution of the spectrum. The area of the maleimide protons

signal was divided by two and added to the area of the cycloadduct proton signal. The obtained number signifies the area of a proton signal of a species at a concentration of 10 mM and was used as a reference to calculate the concentration of all species detectable in the spectrum. This procedure was repeated for all spectra recorded at different time points. The time at which each spectrum was recorded was extracted from the log file, which accompanies the NMR spectroscopy data. Knowing the concentration of the products at each time point, it was possible to plot a reaction profile for each reaction using the ProFit program (version 6.1.12, Quantum Soft, Switzerland).

10.2.2 Kinetic measurements using ^{19}F NMR spectroscopy

470.4 MHz ^{19}F NMR spectroscopy was used for kinetic analysis of the systems described in chapters 6 and 7. Masses of reagents were measured using a Sartorius BP 211D balance (± 0.01 mg). Stock solutions of the appropriate starting materials were made using a fresh batch of CDCl_3 stored over 4 Å molecular sieves and equilibrated in a thermostatically controlled water bath at reaction temperature. In a typical experiment, an NMR sample was prepared in a 5 mm NMR tube (Wilmad 528PP) by mixing appropriate volumes of stock solutions such that the total volume was 800 μL and the concentration of each component was 10 mM. A polyethylene pressure cap was then applied to the top of the tube to prevent solvent evaporation. The NMR tube was transferred to an NMR spectrometer Bruker Avance 500 regulated at reaction temperature, and 470.4 MHz $^{19}\text{F}\{^1\text{H}\}$ NMR were acquired automatically at a given time interval for 8-40 hours. Analysis and deconvolution of each of the ^{19}F NMR spectra recorded during this time was performed using iNMR software (Version 3.4.6, Mestrelab Research, 2007). The percentage completion of the reaction was monitored through the disappearance of the nitron fluorine signals and the appearance of the cycloadduct fluorine signals (three examples of increasing complexity in **Figure 9.2**, **9.3** and **9.4**). In order to extract product concentrations from the ^{19}F NMR spectrum, the areas of all fluorine signals were calculated through deconvolution of the spectrum. The area of the nitron fluorine signals and the area of all cycloadduct fluorine signals were summed up. The obtained number was used as a reference to calculate the concentration of other species detectable in the spectrum. This procedure was repeated for all spectra recorded at different time points. The time at which each spectrum was recorded was extracted from the log file, which accompanies the NMR spectroscopy data. Knowing the concentration of the products at each time point it was possible to plot a reaction profile for each reaction using graphing the ProFit program (version 6.1.12, Quantum Soft, Switzerland).

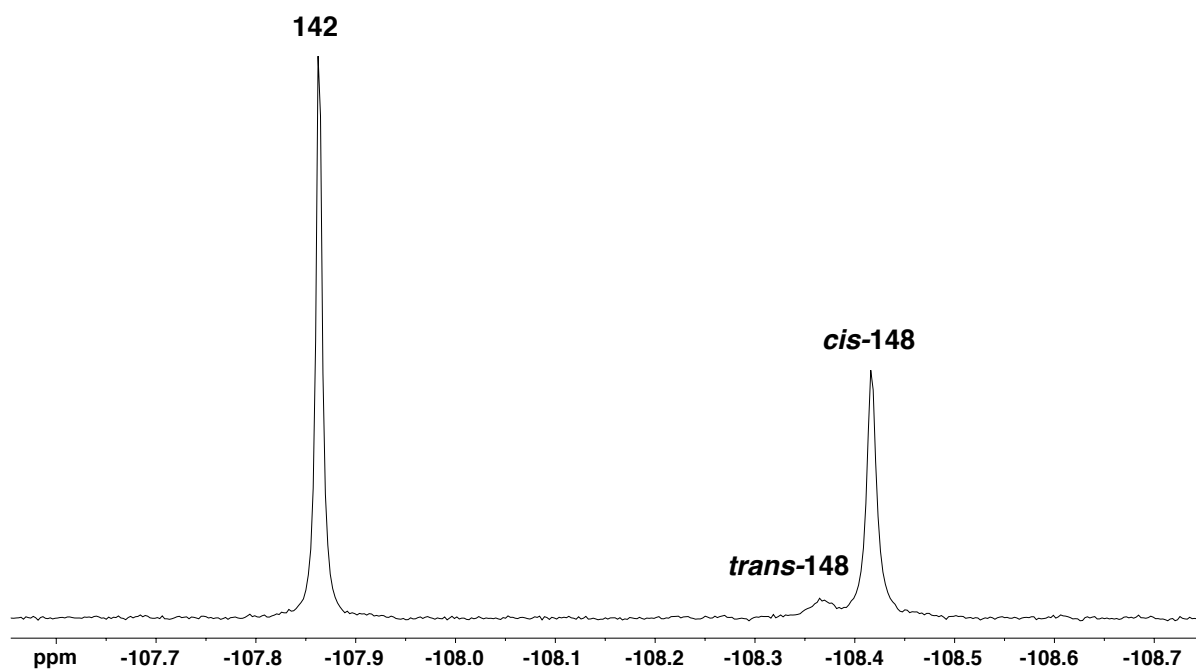


Figure 9.2 Partial 470.4 MHz ¹⁹F NMR spectra for the reaction between benzene maleimide **72** and phenylacetic acid nitrene **142** at 10 mM concentration recorded at 0 °C after 10000 s.

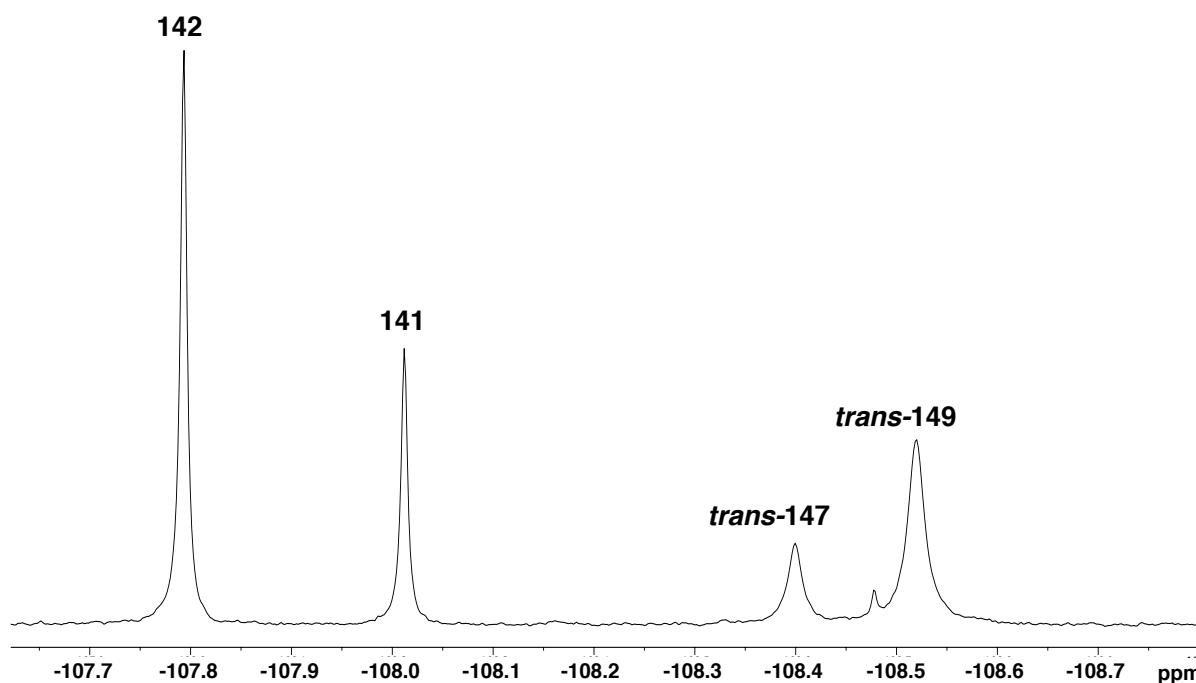


Figure 9.3 Partial 470.4 MHz ¹⁹F NMR spectra for the competition reaction between naphthalene maleimide **72**, phenylacetic acid nitrene **142** and carboxylic nitrene **141** at 10 mM concentration recorded at 25 °C after 58000 s.

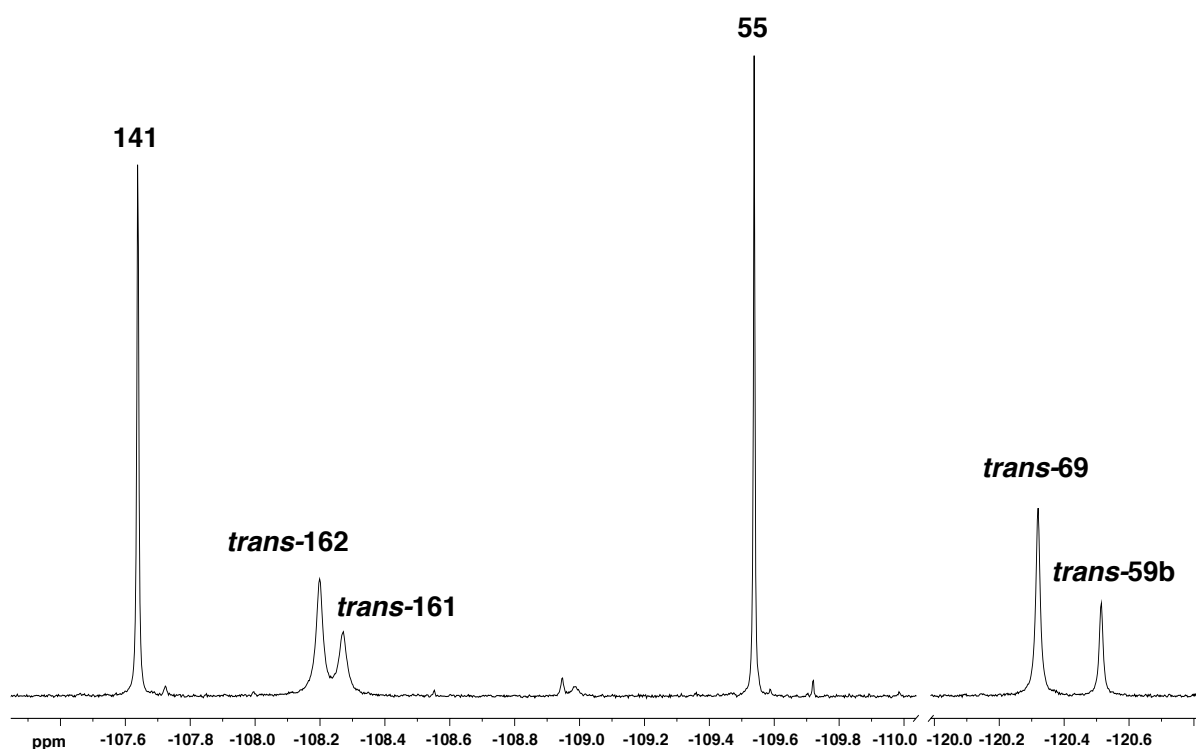


Figure 9.3 Partial 470.4 MHz ^{19}F NMR spectra for the multicyclic network between nitrones **55** and **141**, and maleimides **66** and **33** 10 mM concentration recorded at 10 °C after 17800 s.

10.3 Determination of binding constants^[211,212]

Experimental values for the association constants K_a were determined by the NMR titration method using ^1H NMR spectroscopy at 273 or 283 K. All stock solutions and samples were made up in CDCl_3 using volumetric flasks (accuracy ± 0.02 mL). In a typical NMR titration experiment, small aliquots of guest are added to a solution of host of known concentration and the NMR spectrum of the sample monitored as a function of guest concentration. Commonly, changes in chemical shift are noted for various atomic nuclei. The binding constant is extracted from the titration curve (plot of changes in chemical shift against added guest concentration) by fitting the curve using a non-linear curve-fitting program. Selected examples of titration curves can be found in the appendix.

10.4 Kinetic simulation and fitting

All kinetic fitting and simulations were performed using the software package SimFit (Version 32, Günther von Kiedrowski, 2003) and the ISOSIM package incorporated within the SimFit package. A detailed kinetic model of all possible interactions involved in the studied systems was constructed. This model was converted into a series of rate equations

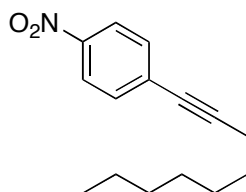
whose solution determine the concentration of reactant and product species as a function of time. The program varies experimentally inaccessible kinetic values until the calculation matches the experimental data. The ISOSIM mode of SimFit allowed the usage of data obtained from the fitting to simulate scenarios under a range of different conditions some of which were not directly experimentally available. Selected examples of kinetic models and simulation scripts can be found in the appendix.

10.5 Molecular modelling

Molecular modelling calculations were performed on a Linux workstation using Macromodel (Version 9.5, Schrödinger Inc., 2008) as part of the Maestro program. Each model was initially energy minimised using the MMFFs forcefield with the Polak-Riierre Conjugate Gradient (PRCG) method and under the GB/SA solvation model for chloroform. The energy minimised structures were then further investigated by running a Monte-Carlo Multiple Minimum (MCMM) conformational search method to minimise 1000 iterations using the AMBER* forcefield and GB/SA solvation model for chloroform. Transition states were successfully located by semi-empirical calculations using the RM1 method as implemented in MOPAC2009 (version 10.014L) running on a Linux cluster.

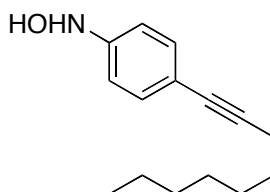
10.6 Synthetic Procedures

1-nitro-4-(non-1-ynyl)benzene **76**



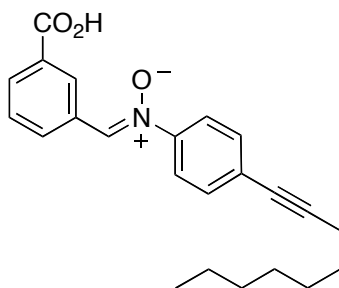
1-iodo-4-nitrobenzene **75** (3.74 g, 15.0 mmol) was suspended in Et₃N (100 mL). Triphenylphosphine (421 mg, 1.61 mmol), copper iodide (245 mg, 1.29 mmol) and dichlorobis(triphenylphosphine) palladium (563 mg, 800 μmol) were added and the mixture was degassed with argon for 30 min. 1-nonyne (2.48 g, 20.0 mmol) was added *via* syringe under a protective argon atmosphere and the mixture was stirred overnight. The occurring brown solution was filtered through celite, concentrated and purified by column chromatography over silica using hexane as eluent to obtain the desired product as a dark yellow liquid (4.22 g, 86%). ¹H NMR (400.1 MHz, CDCl₃): δ_H 8.15 (d, *J* = 8.9 Hz, 2H, Ar CH), 7.51 (d, *J* = 8.9 Hz, 2H, Ar CH), 2.44 (t, *J* = 7.1 Hz, 2H, CH₂), 1.60-1.64 (m, 2H, CH₂), 1.51-1.39 (m, 2H, CH₂), 1.39-1.24 (m, 6H, 3 × CH₂), 0.93-0.86 (m, 3H, CH₃). ¹³C NMR (100.6 MHz, CDCl₃): δ_C 146.7 (quat. C), 132.4 (CH), 131.4 (quat. C), 123.6 (CH), 97.0 (quat. C), 79.4 (quat. C), 31.9 (CH₂), 29.1 (CH₂), 28.9 (CH₂), 28.6 (CH₂), 22.8 (CH₂), 19.7 (CH₂), 14.2 (CH₃). MS (ES⁺) *m/z* 268 (100%, [M + Na]⁺), 300 (28%). HRMS (ES⁺) calc. for C₁₅H₁₉NO₂Na 268.131, found 268.1310.

N-(4-(non-1-ynyl)phenyl)hydroxylamine **77**



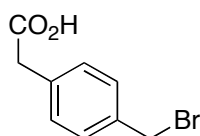
1-nitro-4-(non-1-ynyl)benzene **76** (613 mg, 2.50 mmol) was dissolved in THF (20 mL). Rhodium (125 mg, 5 wt.-% on carbon, wet) and hydrazine monohydrate (129 mg, 2.58 mmol) were added and the reaction was followed by tlc (Hex:EtOAc, 1:1). After completion, the solution was filtered through celite and concentrated *in vacuo* to obtain the desired intermediate product as a dark brown liquid which was directly used in the next step without further purification. ¹H NMR (300.1 MHz, CDCl₃): δ_H 7.31 (d, *J* = 8.7 Hz, 2H, Ar CH), 6.90 (d, *J* = 8.7 Hz, 2H, Ar CH), 2.38 (t, *J* = 7.1 Hz, 2H, CH₂), 1.61-1.57 (m, 2H, CH₂), 1.48-1.37 (m, 2H, CH₂), 1.38-1.24 (m, 6H, 3 × CH₂), 0.91-0.85 (m, 3H, CH₃).

(Z)-N-(3-carboxybenzylidene)-4-(non-1-ynyl)aniline oxide 70



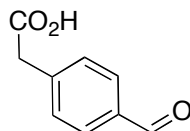
Crude (4-(non-1-ynyl)phenyl)hydroxylamine **77** (2.50 mmol) was dissolved in EtOH (15 mL) and 3-carboxybenzaldehyde (375 mg, 2.50 mmol) was added neat. The solution was left to stir overnight in the dark at room temperature. After removal of EtOH, the crude solid was recrystallised using DCM and petroleum ether to yield the desired product as a white solid (476 mg, 52% over two steps). M.p.: 175.2 - 175.5 °C. ^1H NMR (400.1 MHz, CDCl_3): δ_{H} 9.00 (d, $J = 8.0$ Hz, 1H, Ar CH), 8.77 (s, 1H, Ar CH), 8.18 (d, $J = 7.8$ Hz, 1H, Ar CH), 8.03 (s, 1H, CH), 7.74 (d, $J = 8.6$ Hz, 2H, Ar CH), 7.61 (dd, $J = 8.0, 7.8$ Hz, 1H, Ar CH), 7.50 (d, $J = 8.6$ Hz, 2H, Ar CH), 2.43 (t, $J = 7.1$ Hz, 2H, CH_2), 1.67-1.56 (m, 2H, CH_2), 1.49-1.40 (m, 2H, CH_2), 1.38-1.25 (m, 6H, 3 \times CH_2), 0.93-0.86 (m, 3H, CH_3). ^{13}C NMR (100.6 MHz, CDCl_3): δ_{C} 170.6 (quat. C), 147.3 (quat. C), 134.3 (CH), 133.4 (CH), 132.5 (CH), 132.5 (CH), 131.5 (CH), 130.9 (quat. C), 130.2 (quat. C), 129.3 (CH), 126.7 (quat. C), 121.7 (CH), 93.6 (quat. C), 79.6 (quat. C), 31.9 (CH_2), 29.1 (CH_2), 29.0 (CH_2), 28.7 (CH_2), 22.8 (CH_2), 19.6 (CH_2), 14.2 (CH_3). MS (ES+) m/z 386 (100%, $[\text{M} + \text{Na}]^+$). HRMS (ES+) calc. for $\text{C}_{23}\text{H}_{25}\text{NO}_3\text{Na}$ 386.1732, found 386.1731.

2-(4-(bromomethyl)phenyl)acetic acid 79



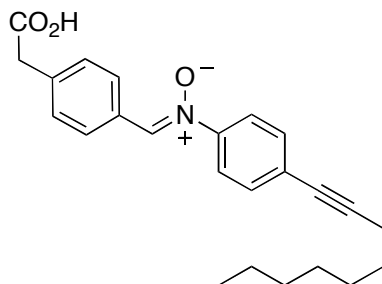
A solution of p-tolylacetic acid **78** (6.30 g, 42.0 mmol) and bromine (7.35 g, 46.0 mmol) in chlorobenzene (50 mL) was stirred for 2 hours under irradiation of a 60 watt tungsten lamp. The occurring precipitate was filtered, washed with copious amounts of hexanes and dried to yield the desired product as a white solid (6.03 g, 62%). M.p.: 177.6 - 178.5 °C (lit.^[213]: 180 °C). ^1H NMR (400.1 MHz, d_6 -DMSO): δ_{H} 7.38 (d, $J = 8.2$ Hz, 2H, Ar CH), 7.24 (d, $J = 8.2$ Hz, 2H, Ar CH), 4.69 (s, 2H, CH_2), 3.57 (s, 2H, CH_2). ^{13}C NMR (75.5 MHz, d_6 -DMSO): δ_{C} 172.5 (quat. C), 136.3 (quat. C), 135.2 (quat. C), 129.7 (CH), 129.2 (CH), 40.3 (CH_2), 34.4 (CH_2).

2-(4-formylphenyl)acetic acid **46**



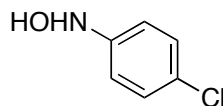
2-(4-(Bromomethyl)phenyl)acetic acid **79** (5.70 g, 24.9 mmol) was suspended in a mixture of EtOH (20 mL) and H₂O (20 mL). Hexamethylenetetramine (10.4 g, 79.5 mmol) was added and the mixture was refluxed at 80 °C for 4 hours. After addition of conc. HCl (10 mL), the solution was refluxed for another 30 minutes. The mixture was then allowed to cool to room temperature and extracted into DCM (2 x 40 mL). The combined organic layers were dried over MgSO₄, filtered and concentrated. The crude product was recrystallised from DCM/hexanes to yield the desired product as a white solid (3.63 g, 88%). M.p.: 125.5 - 126.6 °C (lit.^[214]: 131 °C). ¹H NMR (400.1 MHz, CDCl₃): δ_H 10.00 (s, 1H, C(O)H), 7.86 (d, *J* = 8.0 Hz, 2H, Ar CH), 7.46 (d, *J* = 8.0 Hz, 2H, Ar CH), 3.74 (s, 2H, CH₂). ¹³C NMR (100.6 MHz, CDCl₃): δ_C 192.1 (CH), 176.5 (quat. C), 140.3 (quat. C), 135.6 (quat. C), 130.29 (CH), 130.18 (CH), 41.2 (CH₂).

(*Z*)-*N*-(4-(carboxymethyl)benzylidene)-4-(non-1-ynyl)aniline oxide **71**



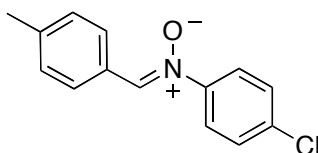
Crude (4-(non-1-ynyl)phenyl)hydroxylamine (1.75 mmol) was dissolved in EtOH (15 mL) and 2-(4-formylphenyl)acetic acid **46** (287 mg, 1.75 mmol) was added neat. The solution was left to stir overnight in the dark at room temperature and placed in the fridge. The precipitate was filtered, washed with hexanes and dried to furnish the desired product as a white solid (460 mg, 70%). M.p.: 138.2 - 138.5 °C. ¹H NMR (300.1 MHz, CDCl₃): δ_H 8.28 (d, *J* = 8.4 Hz, 2H, Ar CH), 7.93 (s, 1H, CH), 7.71 (d, *J* = 8.8 Hz, 2H, Ar CH), 7.48 (d, *J* = 8.8, 2H, Ar CH), 7.35 (d, *J* = 8.4 Hz, 2H, Ar CH), 3.64 (s, 2H, CH₂), 2.43 (t, *J* = 7.1 Hz, 2H, CH₂), 1.57-1.65 (m, 2H, CH₂), 1.50-1.38 (m, 2H, CH₂), 1.39-1.27 (m, 6H, 3 x CH₂), 0.92-0.87 (m, 3H, CH₃). ¹³C NMR (100.6 MHz, CDCl₃): δ_C 174.2 (quat. C), 147.3 (quat. C), 137.7 (quat. C), 136.2 (CH), 132.4 (CH), 129.9 (CH), 129.8 (CH), 129.2 (quat. C), 126.5 (quat. C), 121.8 (CH), 93.5 (quat. C), 79.6 (quat. C), 41.5 (CH₂), 31.9 (CH₂), 29.07 (CH₂), 28.97 (CH₂), 28.7 (CH₂), 22.8 (CH₂), 19.6 (CH₂), 14.3 (CH₃). MS (ES⁺) *m/z* 755 (23%), 400 (48%, [M+Na]⁺), 378 (100%, [M+H]⁺). HRMS (ES⁺) calc. for C₂₄H₂₈NO₃ 378.2078, found 378.2069.

***N*-(4-chlorophenyl)hydroxylamine**^[215]



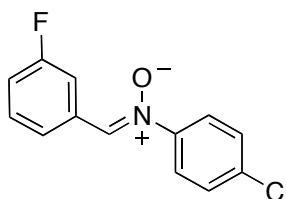
1-chloro-4-nitrobenzene **80** (1.58 g, 10.0 mmol) was dissolved in THF (25 mL). Rhodium (500 mg, 5 wt.-% on carbon, wet) and hydrazine monohydrate (516 mg, 10.3 mmol) were added and the reaction was followed by tlc (Hex:EtOAc, 1:1). After completion, the solution was filtered through celite and concentrated *in vacuo* to obtain the desired intermediate product as a light yellow solid which was directly used in the next step without further purification. The obtained spectra is in accordance with the literature. ¹H NMR (400.1 MHz, CDCl₃): δ_H 7.24 (d, *J* = 8.9 Hz, 2H, Ar CH), 6.93 (d, *J* = 8.9 Hz, 2H, Ar CH), 6.77 (s, 1H, NH), 5.69 (s, 1H, OH). ¹³C NMR (75.5 MHz, CDCl₃): δ_C 148.3 (quat. C), 129.1 (CH), 127.3 (quat. C), 115.9 (CH).

(*Z*)-4-chloro-*N*-(4-methylbenzylidene)aniline oxide **82**



Crude *N*-(4-chlorophenyl)hydroxylamine (574 mg, 4.00 mmol) was dissolved in EtOH (10 mL) and 4-methylbenzaldehyde (421 mg, 3.50 mmol) was added neat. The mixture was kept overnight in the dark at room temperature. The following day, the precipitate was filtered, washed with a copious amount of petroleum ether and dried to yield the desired product as a white solid (611 mg, 62%). M.p.: 179.7 - 180.2 °C. ¹H NMR (300.1 MHz, CDCl₃): δ_H 8.28 (d, *J* = 8.4 Hz, 2H, Ar CH), 7.86 (s, 1H, CH), 7.73 (d, *J* = 9.0 Hz, 2H, Ar CH), 7.44 (d, *J* = 9.0 Hz, 2H, Ar CH), 7.29 (d, *J* = 8.1 Hz, 2H, Ar CH), 2.42 (s, 3H, CH₃). ¹³C NMR (100.6 MHz, CDCl₃): δ 147.4 (quat. C), 142.0 (quat. C), 135.6 (quat. C), 134.7 (CH), 129.5 (CH), 129.3 (CH), 129.2 (CH), 127.8 (quat. C), 123.0 (CH), 21.9 (CH₃). MS (ES⁺) *m/z* 300 (15%), 270 (30%), 268 (100%, [M + Na]⁺). HRMS (ES⁺) calc. for C₁₄H₁₂NONaCl 268.0512, found 268.0505.

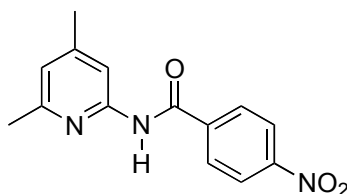
(*Z*)-4-chloro-*N*-(3-fluorobenzylidene)aniline oxide **81**



Crude *N*-(4-chlorophenyl)hydroxylamine (574 mg, 4.00 mmol) was dissolved in EtOH (10 mL) and 3-fluorobenzaldehyde (434 mg, 3.50 mmol) was added neat. The mixture was kept

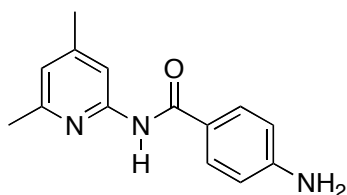
overnight in the dark at room temperature. The following day, the precipitate was filtered, washed with a copious amount of petroleum ether and dried to yield the desired product as a white solid (629 mg, 63%). M.p.: 128.9 - 129.3 °C. ¹H NMR (400.1 MHz, CDCl₃): δ_H 8.42 (d, *J* = 10.6 Hz, 1H, Ar CH), 7.91 (s, 1H, CH), 7.88 (d, *J* = 7.8 Hz, 1H, Ar CH), 7.73 (d, *J* = 8.9 Hz, 2H, Ar CH), 7.46 (d, *J* = 8.9 Hz, 2H, Ar CH), 7.42 (d, *J* = 8.0 Hz, 1H, Ar CH), 7.18 (t, *J* = 8.3 Hz, 1H, Ar CH). ¹⁹F NMR (282 MHz, CDCl₃): δ_F -112.0. MS (ES⁺) *m/z* 304 (40%), 274 (15%), 272 (100%, [M+Na]⁺). HRMS (ES⁺) calc. for C₁₃H₉NONaFCl 272.0254, found 272.0254.

***N*-(4,6-dimethylpyridin-2-yl)-4-nitrobenzamide 84**



4-nitrobenzoyl chloride (2.13 g, 11.5 mmol) was suspended in dry DCM (25 mL) and cooled to 0 °C. A solution of 4,6-dimethylpyridin-2-amine (3.05 g, 25.0 mmol) in dry DCM (25 mL) was slowly added dropwise. The addition resulted in the formation of a clear solution, which was stirred overnight while warming to room temperature. Work-up included extraction of excess amine from the organic layer with 1M HCl solution (2 x 30 mL), re-extracting the aqueous layer with DCM (2 x 30 mL), washing the combined organic layers with sat. aqueous NaHCO₃ solution (30 mL), drying over MgSO₄, filtration and concentration *in vacuo* to furnish the desired product as a white powder (2.89 g, 93%). M.p.: 205.7 - 206.9 °C (lit.^[216]: 163 °C). ¹H NMR (300.1 MHz, CDCl₃): δ_H 8.83 (s, 1H, NH), 8.30 (d, *J* = 9.0 Hz, 2H, Ar CH), 8.06 (d, *J* = 9.0 Hz, 2H, Ar CH), 8.00 (s, 1H, Ar CH), 6.79 (s, 1H, Ar CH), 2.36 (s, 3H, CH₃), 2.36 (s, 3H, CH₃). ¹³C NMR (75.5 MHz, CDCl₃): δ_C 163.8 (quat. C), 156.7 (quat. C), 150.6 (quat. C), 150.4 (quat. C), 150.0 (quat. C), 140.1 (quat. C), 128.5 (CH), 124.1 (CH), 121.4 (CH), 112.1 (CH), 23.8 (CH₃), 21.5 (CH₃). MS (ES⁺) *m/z* 272 (100%, [M+H]⁺). HRMS (ES⁺) calc. for C₁₄H₁₄N₃O₃ 272.1035, found 272.1037.

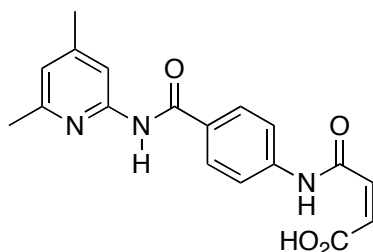
4-amino-*N*-(4,6-dimethylpyridin-2-yl)benzamide^[216]



N-(4,6-dimethylpyridin-2-yl)-4-nitrobenzamide (1.20 g, 4.98 mmol) was dissolved in a 9:1 MeOH/DCM mixture (50 mL). Palladium (120 mg, 10 wt.-% on carbon, dry) was added

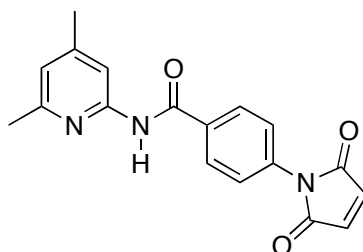
carefully. The solution was purged with hydrogen and kept under a hydrogen atmosphere overnight using hydrogen filled balloons. The following day, the solution was filtered through celite and concentrated *in vacuo* to yield the desired product in sufficient quality for further conversion. The obtained spectra is in accordance with the literature. ^1H NMR (400.1 MHz, CDCl_3): δ_{H} 8.49 (s, 1H, NH), 8.04 (s, 1H, Ar CH), 7.77 (d, $J = 8.7$ Hz, 2H, Ar CH), 6.74 (s, 1H, Ar CH), 6.69 (d, $J = 8.6$ Hz, 2H, Ar CH), 2.42 (s, 3H, CH_3), 2.34 (s, 3H, CH_3).

(Z)-4-(4-(4,6-dimethylpyridin-2-ylcarbamoyl)phenylamino)-4-oxobut-2-enoic acid 85



Crude 4-amino-*N*-(4,6-dimethylpyridin-2-yl)benzamide was dissolved in acetic acid (30 mL) and maleic anhydride (586 mg, 5.98 mmol) was added neat. The reaction was left to stir overnight at room temperature before the precipitate was filtered and thoroughly washed with Et_2O (60 mL) to yield the desired product as a light yellow solid (1.57 g, 93% over two steps). M.p.: 198.0 - 199.0 °C. ^1H NMR (400.1 MHz, d_6 -DMSO): δ_{H} 10.58 (s, 1H, NH), 10.52 (s, 1H, NH), 8.02 (d, $J = 8.8$ Hz, 2H, Ar CH), 7.86 (s, 1H, Ar CH), 7.73 (d, $J = 8.8$ Hz, 2H, Ar CH), 6.87 (s, 1H, Ar CH), 6.50 (d, $J = 12.0$ Hz, 1H, CH), 6.34 (d, $J = 12.0$ Hz, 1H, CH), 2.40 (s, 3H, CH_3), 2.31 (s, 3H, CH_3). ^{13}C NMR (100.6 MHz, d_6 -DMSO): δ_{C} 166.9 (quat. C), 165.1 (quat. C), 163.6 (quat. C), 155.9 (quat. C), 151.5 (quat. C), 149.2 (quat. C), 141.9 (quat. C), 131.7 (CH), 130.2 (CH), 129.02 (CH), 128.86 (quat. C), 120.0 (CH), 118.5 (CH), 112.2 (CH), 23.3 (CH_3), 20.9 (CH_3). MS (ES $^-$) m/z 338 (100%, $[\text{M}-\text{H}]^-$). HRMS (ES $^+$) calc. for $\text{C}_{18}\text{H}_{18}\text{N}_3\text{O}_4$ 340.1295, found 340.1297.

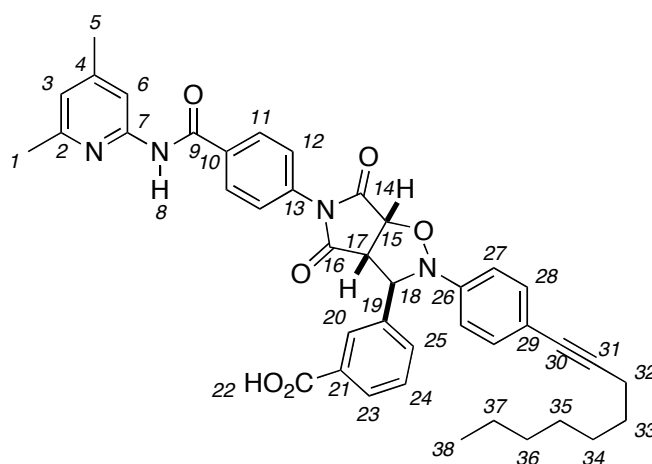
***N*-(4,6-dimethylpyridin-2-yl)-4-(2,5-dioxo-2,5-dihydro-1H-pyrrol-1-yl)benzamide 72**



(*Z*)-4-(4-(4,6-dimethylpyridin-2-ylcarbamoyl)phenylamino)-4-oxobut-2-enoic acid **85** (1.19 g, 3.50 mmol) was suspended in dry MeCN (30 mL). ZnBr_2 (791 mg, 3.50 mmol) and

hexamethyldisilazane (2.82 g, 17.5 mmol) were added at room temperature. The reaction was refluxed at 90 °C for 1 h. After cooling to room temperature, the precipitate was filtered and the filtrate was reduced to roughly 10% of its original volume. Water (25 mL) was added and a pH of 1 was adjusted using 1M HCl. The solution was extracted with DCM (3 x 50 mL). The combined organic layers were subsequently treated with an aqueous 0.1M EDTA solution (2 x 50 mL), H₂O (2 x 50 mL) and brine (50 mL), dried over MgSO₄, filtered and concentrated to yield the desired product as a light yellow solid (890 mg, 79%). M.p.: 226.1 - 226.9 °C. ¹H NMR (400.1 MHz, CDCl₃): δ_H 8.55 (s, 1H, NH), 8.05 (s, 1H, Ar CH), 8.03 (d, *J* = 8.8 Hz, 2H, Ar CH), 7.56 (d, *J* = 8.8 Hz, 2H, Ar CH), 6.90 (s, 2H, 2 × CH), 6.79 (s, 1H, Ar CH), 2.43 (s, 3H, CH₃), 2.37 (s, 3H, CH₃). ¹³C NMR (100.6 MHz, CDCl₃): δ_C 169.1 (quat. C), 164.7 (quat. C), 156.4 (quat. C), 150.7 (quat. C), 141.1 (quat. C), 134.9 (quat. C), 134.6 (CH), 133.4 (quat. C), 128.3 (CH), 125.7 (CH), 121.0 (CH), 111.8 (CH), 23.9 (CH₃), 21.5 (CH₃). MS (ES⁺) *m/z* 322 (100%, [M+H]⁺). HRMS (ES⁺) calc. for C₁₈H₁₆N₃O₃ 322.1180, found 322.1192.

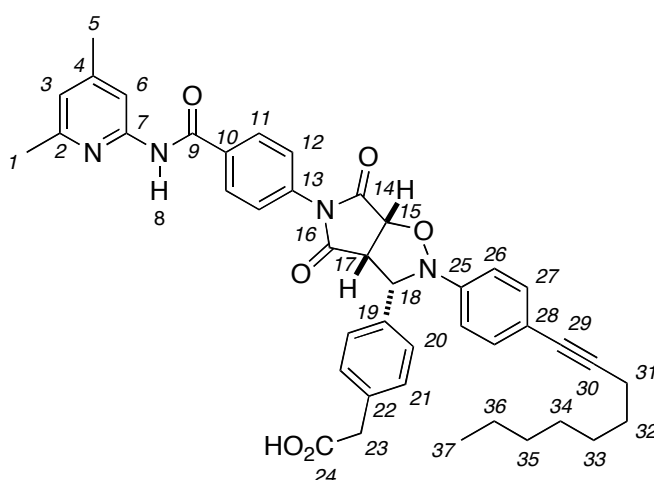
Template *trans*-94



In an NMR tube, maleimide **72** (5.14 mg, 16.0 μmol) in CDCl₃ (400 μL) was combined with a solution of nitrone **70** (5.81 mg, 16.0 μmol) in CDCl₃ (400 μmol). After 48 hours at 0 °C, the reaction showed complete conversion of the starting materials and proved sufficiently pure for characterisation (*trans/cis* > 15:1). ¹H NMR (400.1 MHz, CDCl₃): δ_H 11.86 (s, 1H, H₈), 8.24 (s, 1H, H₆), 8.18 (s, 1H, H₂₀), 8.14 (d, *J* = 8.9 Hz, 2H, H₁₁), 8.07 (d, *J* = 7.7 Hz, 1H, H₂₃), 7.63 (d, *J* = 7.4 Hz, 1H, H₂₅), 7.44 (t, *J* = 7.7 Hz, 1H, H₂₄), 7.27 (d, *J* = 8.9 Hz, 2H, H₂₇), 7.04 (d, *J* = 8.8 Hz, 2H, H₂₈), 7.01 (d, *J* = 8.8 Hz, 2H, H₁₂), 6.84 (s, 1H, H₃), 5.76 (s, 1H, H₁₈), 5.19 (d, *J* = 7.4 Hz, 1H, H₁₅), 4.21 (d, *J* = 7.2 Hz, 1H, H₁₇), 2.56 (s, 3H, H₁), 2.42 (s, 3H, H₅), 2.36 (t, *J* = 7.2 Hz, 2H, H₃₂), 1.61-1.53 (m, 2H, H₃₃), 1.43-1.38 (m, 2H, H₃₄), 1.32-1.24 (m, 8H, H₃₅₋₃₇), 0.88-0.84 (m, 3H, H₃₈). ¹³C NMR (75.5 MHz, CDCl₃): δ 174.2 (quat. C, C₁₆), 173.2 (quat. C, C₁₄), 171.4 (quat. C, C₂₂), 166.5 (quat. C, C₉), 155.1 (quat. C₂), 152.8 (quat. C, C₄), 151.5 (quat. C, C₇), 147.2 (quat. C₂₆),

137.9 (quat. C, C₁₉), 135.2 (quat. C, C₁₃), 134.2 (quat. C, C₁₀), 132.7 (CH, C₂₃), 132.7 (CH, C₂₇), 131.9 (quat. C, C₂₁), 129.8 (CH, C₂₅), 129.7 (CH, C₁₁), 128.9 (CH, C₂₄), 128.4 (CH, C₂₀), 126.0 (CH, C₁₂), 121.2 (CH, C₃), 119.3 (quat. C, C₂₉), 115.0 (CH, C₂₈), 113.9 (CH, C₆), 90.3 (quat. C, C₃₀), 79.9 (quat. C, C₃₁), 77.5 (CH, C₁₅), 69.5 (CH, C₁₈), 56.1 (CH, C₁₇), 31.9 (CH₂, C₃₅), 29.9 (CH₂, C₃₆), 29.1 (CH₂, C₃₄), 29.0 (CH₂, C₃₃), 22.8 (CH₂, C₃₇), 21.9 (CH₃, C₁), 21.8 (CH₃, C₅), 19.6 (CH₂, C₃₂), 14.2 (CH₃, C₃₈). MS (ES⁺) *m/z* 685 (100%, [M+H]⁺), 495 (10%). HRMS (ES⁺) calc. for C₄₁H₄₁N₄O₆ 685.3026, found 685.3036.

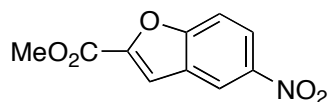
Template *cis*-95



In an NMR tube, maleimide **72** (5.14 mg, 16.0 μ mol) in CDCl₃ (400 μ L) was combined with a solution of nitrone **71** (6.03 mg, 16.0 μ mol) in CDCl₃ (400 μ mol). After 48 hours at 0 °C, the reaction showed complete conversion of the starting materials and proved sufficiently pure for characterisation of the *cis*-isomer (*cis/trans* = 3:1). ¹H NMR (499.9 MHz, CDCl₃): δ _H 8.10 (s, 1H, H₆), 7.91 (d, *J* = 8.3 Hz, 2H, H₁₁), 7.39 (d, *J* = 8.1 Hz, 2H, H₂₁), 7.28 (d, *J* = 8.7 Hz, 2H, H₂₆), 7.21 (d, *J* = 8.1 Hz, 2H, H₂₀), 7.10 (d, *J* = 8.3 Hz, 2H, H₁₂), 6.99 (d, *J* = 8.6 Hz, 2H, H₂₇), 6.79 (s, 1H, H₃), 5.08 (d, *J* = 8.6 Hz, 1H, H₁₅), 5.01 (d, *J* = 8.7 Hz, 1H, H₁₈), 4.13 (t, *J* = 8.6 Hz, 1H, H₁₇), 3.65 (d, *J* = 16.3 Hz, 1H, H₂₃), 3.62 (d, *J* = 16.3 Hz, 1H, H_{23'}), 2.42 (s, 3H, H₁), 2.38 (s, 3H, H₅), 2.36 (t, *J* = 7.2 Hz, 2H, H₃₁), 1.61-1.54 (m, 2H, H₃₂), 1.45-1.37 (m, 2H, H₃₃), 1.35-1.27 (m, 6H, H₃₄₋₃₆), 0.91-0.85 (m, 3H, H₃₇). ¹³C NMR (125.7 MHz, CDCl₃): δ _C 176.4 (quat. C, C₂₄), 172.4 (quat. C, C₁₄), 170.8 (quat. C, C₁₆), 166.3 (quat. C, C₉), 155.0 (quat. C, C₄), 152.9 (quat. C, C₂), 151.0 (quat. C, C₇), 147.5 (quat. C, C₂₅), 135.2 (quat. C, C₁₉), 134.2 (quat. C, C₁₀), 134.1 (quat. C, C₁₃), 133.1 (quat. C, C₂₂), 132.4 (CH, C₂₇), 130.5 (CH, C₂₀), 129.0 (CH, C₁₁), 127.9 (CH, C₂₁), 125.8 (CH, C₁₂), 121.2 (CH, C₃), 120.4 (quat. C, C₂₈), 116.9 (CH, C₂₆), 113.7 (CH, C₆), 90.7 (quat. C, C₂₉), 79.9 (quat. C, C₃₀), 77.4 (CH, C₁₅), 72.2 (CH, C₁₈), 54.5 (CH, C₁₇), 40.6 (CH₂, C₂₃), 31.9 (CH₂, C₃₄), 29.9 (CH₂, C₃₅), 29.1 (CH₂, C₃₃), 28.9 (CH₂, C₃₂), 22.8 (CH₂, C₃₆), 21.9 (CH₃, C₁), 21.7

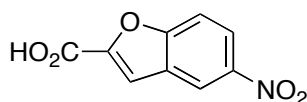
(CH₃, C₅), 19.6 (CH₂, C₃₁), 14.3 (CH₃, C₃₇). MS (ES+) *m/z* 699 (100%, [M+H]⁺). HRMS (ES+) calc. for C₄₂H₄₃N₄O₆ 699.3170, found 699.3183.

Methyl 5-nitrobenzofuran-2-carboxylate **87**



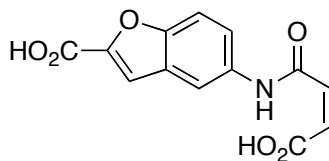
2-Hydroxy-5-nitrobenzaldehyde (500 mg, 3.00 mmol) was dissolved in dry MeCN (15 mL). Methyl 2-bromoacetate (459 mg, 3.00 mmol) and K₂CO₃ (1.24 g, 9.00 mmol) were added and the yellow solution was stirred for 4 hours at room temperature before being refluxed at 90 °C overnight. Cooling to room temperature and addition of H₂O (60 mL) resulted in the formation of a precipitate, which was filtered, washed intensively with H₂O and dissolved in DCM (75 mL). The organic solution was then dried over MgSO₄, filtered and concentrated *in vacuo* to furnish the desired product as a light brown solid (264 mg, 43%). M.p.: 164.6 - 165.1 °C (lit.^[217]: 163.5 - 164.5 °C). ¹H NMR (400.1 MHz, CDCl₃): δ_H 8.65 (dd, *J* = 2.3, 0.5 Hz, 1H, Ar CH), 8.38 (dd, *J* = 9.2, 2.3 Hz, 1H, Ar CH), 7.70 (ddd, *J* = 9.2, 0.9, 0.5 Hz, 1H, Ar CH), 7.65 (d, *J* = 0.9 Hz, 1H, Ar CH), 4.02 (s, 3H, CH₃). ¹³C NMR (75.5 MHz, CDCl₃): δ_C 159.0 (quat. C), 158.0 (quat. C), 148.4 (quat. C), 144.8 (quat. C), 127.2 (quat. C), 123.1 (CH), 119.6 (CH), 114.2 (CH), 113.0 (CH), 52.9 (CH₃). MS (CI+) *m/z* 222 (100%, [M+H]⁺). HRMS (CI+) calc. for C₁₀H₈NO₅ 222.0400, found 222.0402.

5-nitrobenzofuran-2-carboxylic acid **88**



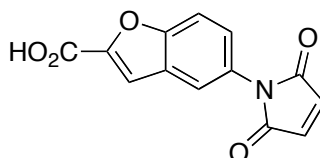
Methyl 5-nitrobenzofuran-2-carboxylate **87** (1.90 g, 8.59 mmol) was suspended in a mixture of EtOH (95 mL) and H₂O (5 mL). KOH powder (964 mg, 17.2 mmol) was added and the mixture was refluxed overnight at 85 °C. After cooling to room temperature, the solution was poured into H₂O (50 mL) and acidified to pH 1 using 1M HCl. The occurring precipitate was filtered and redissolved in EtOAc (100 mL). The filtrate was extracted thoroughly with EtOAc (3 x 75 mL). The combined organic layers were dried over MgSO₄, filtered and concentrated *in vacuo* to yield the desired product as a light brown solid (1.66 g, 94%). M.p.: 236.1 - 238.4 °C (lit.^[218]: 274 - 275 °C). ¹H NMR (300.1 MHz, d₆-DMSO): δ_H 8.73 (d, *J* = 2.4 Hz, 1H, Ar CH), 8.33 (dd, *J* = 9.2, 2.4 Hz, 1H, Ar CH), 7.94 (d, *J* = 9.2 Hz, 1H, Ar CH), 7.82 (s, 1H, Ar CH). ¹³C NMR (75.5 MHz, d₆-DMSO): δ_C 159.4 (quat. C), 157.5 (quat. C), 149.0 (quat. C), 144.2 (quat. C), 127.4 (quat. C), 122.7 (CH), 119.8 (CH), 114.1 (CH), 113.2 (CH). MS (CI+) *m/z* 208 (100%, [M+H]⁺). HRMS (CI+) calc. for C₉H₆NO₅ 208.0249, found 208.0246.

(Z)-5-(3-carboxyacrylamido)benzofuran-2-carboxylic acid 89



5-nitrobenzofuran-2-carboxylic acid **88** (300 mg, 1.45 mmol) was dissolved in THF (15 mL). Palladium (30 mg, 10 wt.-% on carbon, dry) was added at room temperature. The flask was purged with hydrogen and kept under a hydrogen atmosphere overnight using hydrogen filled balloons. The following day, the solution was filtered through celite to remove the catalyst and maleic anhydride (147 mg, 1.50 mmol) was added neat. After stirring at room temperature for 3 hours, the precipitate was filtered, washed with a copious amount of THF and dried to give the desired product as a light brown solid (366 mg, 92% over two steps). M.p.: 208.0 - 208.8 °C. ¹H NMR (300.1 MHz, d₆-DMSO): δ_H 10.53 (s, 1H, NH), 8.23 (d, *J* = 1.9 Hz, 1H, Ar CH), 7.69 (s, 1H, Ar CH), 7.66 (s, 1H, Ar CH), 7.56 (dd, *J* = 8.8, 2.2 Hz, 1H, Ar CH), 6.51 (d, *J* = 12.0 Hz, 1H, CH), 6.32 (d, *J* = 12.0 Hz, 1H, CH). ¹³C NMR (75.5 MHz, d₆-DMSO): δ_C 166.8 (quat. C), 163.3 (quat. C), 160.0 (quat. C), 151.7 (quat. C), 146.8 (quat. C), 134.7 (quat. C), 131.8 (CH), 130.4 (CH), 127.1 (quat. C), 120.5 (CH), 113.8 (CH), 113.1 (CH), 112.3 (CH). MS (ES⁻) *m/z* 549 (45%), 274 (100%, [M-H]⁻), 230 (9%). HRMS (ES⁻) calc. for C₁₃H₈NO₆ 274.0352, found 274.0347.

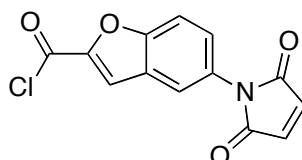
5-(2,5-dioxo-2,5-dihydro-1H-pyrrol-1-yl)benzofuran-2-carboxylic acid 90



(Z)-5-(3-carboxyacrylamido)benzofuran-2-carboxylic acid **89** (311 mg, 1.13 mmol) was suspended in acetic anhydride (10 mL). Sodium acetate (9.27 mg, 113 μmol) was added and the reaction was refluxed overnight at 100 °C. After cooling to room temperature, water (20 mL) was added and the biphasic solution was stirred vigorously for 2 hours while being cooled over an ice bath. The solution was then extracted with EtOAc (3 x 50 mL), the organic layer dried over MgSO₄, filtered and concentrated. After being redissolved in DCM (25 mL), an excess of trifluoroacetic acid (2 mL) was added and the mixture was stirred for 2 hours. Water was added (25 mL) and the mixture was left to stir for an additional 2 hours. The solution was then extracted with EtOAc (3 x 50 mL), the organic layer dried over MgSO₄, filtered and concentrated to yield the desired product (231 mg, 80%). M.p.: 283.5 - 285.8 °C. ¹H NMR (300.1 MHz, d₆-DMSO): δ_H 7.81 (d, *J* = 8.8 Hz, 1H, Ar CH), 7.75 (d, *J* = 1.9 Hz, 1H,

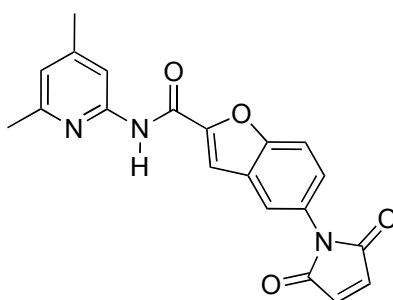
Ar CH), 7.73 (s, 1H, Ar CH), 7.44 (dd, $J = 8.8, 2.1$ Hz, 1H, Ar CH), 7.20 (s, 2H, 2 × CH). ^{13}C NMR (75.5 MHz, $\text{d}_6\text{-DMSO}$): δ_{C} 170.1 (quat. C), 160.0 (quat. C), 153.9 (quat. C), 147.6 (quat. C), 134.7 (CH), 127.4 (quat. C), 127.2 (quat. C), 126.7 (CH), 121.8 (CH), 113.4 (CH), 112.5 (CH). MS (ES⁻) m/z 256 (100%, [M-H]⁻), 212 (40%). HRMS (ES⁻) calc. for $\text{C}_{13}\text{H}_6\text{NO}_5$ 256.0244, found 256.0246.

5-(2,5-dioxo-2,5-dihydro-1H-pyrrol-1-yl)benzofuran-2-carbonyl chloride



5-(2,5-dioxo-2,5-dihydro-1H-pyrrol-1-yl) benzofuran-2-carboxylic acid **90** (257 mg, 1.00 mmol) was suspended in toluene (25 mL). An excess of thionyl chloride (15 mL) was added and the mixture was refluxed overnight at 90 °C. The next day, all solvent was removed *in vacuo*, the resulting solid was dried thoroughly and proved to be sufficiently pure for further conversion. ^1H NMR (400.1 MHz, CDCl_3): δ_{H} 7.87 (d, $J = 0.9$ Hz, 1H, Ar CH), 7.76 (d, $J = 1.6$ Hz, 1H, Ar CH), 7.70 (d, $J = 9.0$ Hz, 1H, Ar CH), 7.54 (dd, $J = 9.0$ Hz, 2.1, 1H, Ar CH), 6.91 (s, 2H, 2 × CH). ^{13}C NMR (100.6 MHz, CDCl_3): δ_{C} 169.5 (quat. C), 157.3 (quat. C), 155.7 (quat. C), 147.8 (quat. C), 134.5 (CH), 128.07 (CH), 128.03 (quat. C), 127.0 (quat. C), 121.5 (CH), 120.3 (CH), 113.6 (CH).

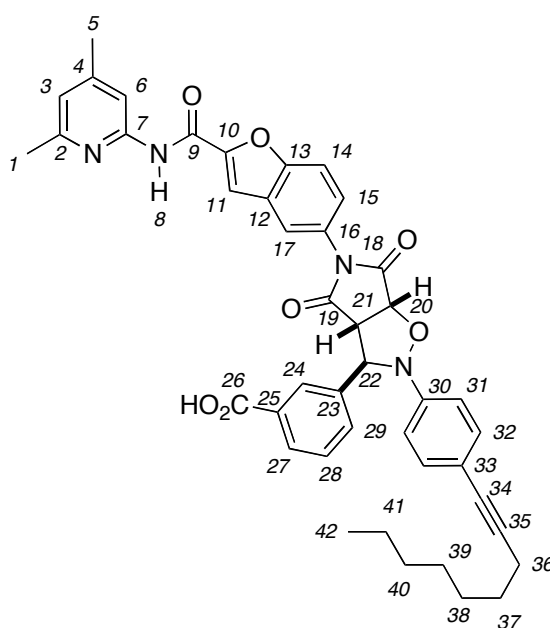
N-(4,6-dimethylpyridin-2-yl)-5-(2,5-dioxo-2,5-dihydro-1H-pyrrol-1-yl)benzofuran-2-carboxamide **73**



Crude 5-(2,5-dioxo-2,5-dihydro-1H-pyrrol-1-yl)benzofuran-2-carbonyl chloride (276 mg, 1.00 mmol) was suspended in dry DCM (10 mL) and 2-amino-4,6-dimethyl pyridine (269 mg, 2.20 mmol) in dry DCM (10 mL) was added dropwise at 0 °C. The solution was left to stir overnight while warming to room temperature. In order to precipitate the product, the solution was kept in the fridge overnight. The filtered solid was redissolved in DCM (20 mL) and washed with 1M HCl (2 × 20 mL). The organic layer was dried over MgSO_4 , filtered and

concentrated to give directly the desired product as a light brown solid (222 mg, 61% over two steps). M.p.: 157.5 - 158.8 °C. ¹H NMR (400.1 MHz, CDCl₃): δ_H 8.96 (s, 1H, NH), 8.03 (s, 1H, Ar CH), 7.69-7.63 (m, 3H, Ar CH), 7.42 (dd, *J* = 8.9, 2.1 Hz, 1H, Ar CH), 6.90 (s, 2H, 2 × CH), 6.82 (s, 1H, Ar CH), 2.47 (s, 3H, CH₃), 2.38 (s, 3H, CH₃). ¹³C NMR (100.6 MHz, CDCl₃): δ_C 169.6 (quat. C), 156.6 (quat. C), 156.3 (quat. C), 153.8 (quat. C), 150.5 (quat. C), 149.9 (quat. C), 149.4 (quat. C), 134.3 (CH), 128.2 (quat. C), 127.2 (quat. C), 125.7 (CH), 121.1 (CH), 120.9 (CH), 112.7 (CH), 111.90 (CH), 111.72 (CH), 23.8 (CH₃), 21.4 (CH₃). MS (ES⁺) *m/z* 384 (80%, [M + Na]⁺), 362 (100%, [M + H]⁺). HRMS (ES⁺) calc. for C₂₀H₁₆N₃O₄ 362.1146, found 362.1141.

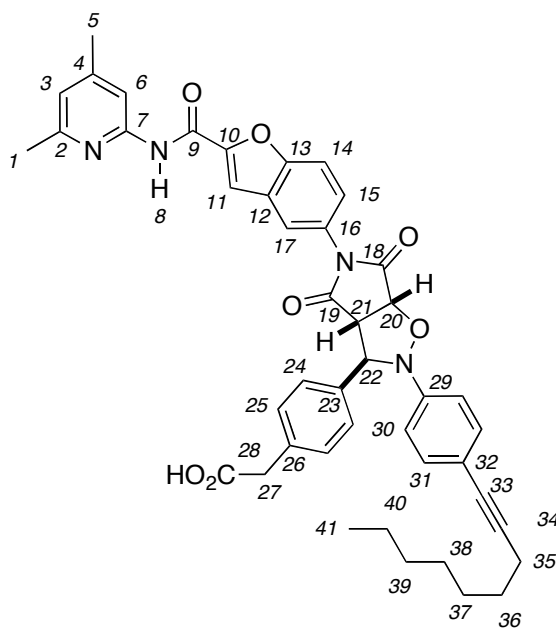
Template *trans*-96



In an NMR tube, maleimide **73** (5.78 mg, 16.0 μmol) in CDCl₃ (400 μL) was combined with a solution of nitrone **70** (5.81 mg, 16.0 μmol) in CDCl₃ (400 μL). After 48 hours at 0 °C, the reaction showed complete conversion of the starting materials and proved sufficiently pure for characterisation (*trans/cis* > 15:1). ¹H NMR (300.1 MHz, CDCl₃): δ_H 11.44 (s, 1H, H₈), 8.28 (s, 1H, H₂₄), 8.18 (s, 1H, H₆), 8.13 (d, *J* = 7.8 Hz, 1H, H₂₇), 7.93 (s, 1H, H₁₁), 7.74 (d, *J* = 7.9 Hz, 1H, H₂₉), 7.51 (t, *J* = 7.4 Hz, 1H, H₂₈), 7.48 (d, *J* = 8.8 Hz, 1H, H₁₄), 7.29 (d, *J* = 8.8 Hz, 2H, H₃₁), 7.16 (s, 1H, H₁₇), 7.07 (d, *J* = 8.8 Hz, 2H, H₃₂), 6.84 (s, 1H, H₃), 6.64 (d, *J* = 8.4 Hz, 1H, H₁₅), 5.78 (s, 1H, H₂₂), 4.99 (d, *J* = 7.4 Hz, 1H, H₂₀), 4.00 (d, *J* = 7.4 Hz, 1H, H₂₁), 2.55 (s, 3H, H₁), 2.42 (s, 3H, H₅), 2.39 (t, *J* = 7.2 Hz, 2H, H₃₆), 1.65-1.55 (m, 2H, H₃₇), 1.48-1.38 (m, 2H, H₄₁), 1.37-1.19 (m, 6H, H₃₈₋₄₀), 0.92-0.82 (m, 3H, H₄₂). ¹³C NMR (75.5 MHz, CDCl₃): δ_C 174.4 (quat. C, C₁₉), 173.2 (quat. C, C₁₈), 171.0 (quat. C, C₂₆), 157.7 (quat. C, C₇), 155.3 (quat. C, C₂), 154.8 (quat. C, C₁₃), 152.6 (quat. C, C₄), 150.8 (quat. C, C₁₀), 149.5 (quat. C, C₉), 147.6 (quat. C, C₃₀), 138.7 (quat. C, C₂₅), 132.8 (CH, C₃₁), 132.1 (CH, C₂₉), 131.8 (quat. C, C₂₃), 129.9 (CH, C₂₇), 129.1 (CH,

C₂₈), 128.3 (quat. C, C₁₂), 128.1 (CH, C₂₄), 126.9 (quat. C, C₁₆), 125.6 (CH, C₁₅), 121.4 (CH, C₃), 121.2 (CH, C₁₇), 119.2 (quat. C, C₃₃), 114.7 (CH, C₃₂), 113.8 (CH, C₆), 113.0 (CH, C₁₄), 111.6 (CH, C₁₁), 90.5 (quat. C, C₃₅), 79.8 (quat. C, C₃₄), 77.5 (CH, C₂₀), 69.5 (CH, C₂₂), 56.9 (CH, C₂₁), 31.9 (CH₂, C₃₉), 29.9 (CH₂, C₄₀), 29.1 (CH₂, C₃₈), 29.0 (CH₂, C₃₇), 22.8 (CH₂, C₄₁), 22.1 (CH₃, C₁), 21.8 (CH₃, C₅), 19.6 (CH₂, C₃₆), 14.2 (CH₃, C₄₂). MS (ES⁺) *m/z* 725 (100%, [M+H]⁺). HRMS (ES⁺) calc. for C₄₃H₄₁N₄O₇ 725.2970, found 725.2965.

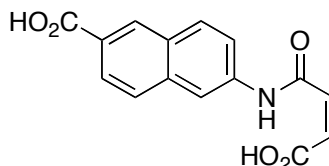
Template *trans*-97



In an NMR tube, maleimide **73** (5.78 mg, 16.0 μ mol) in CDCl₃ (400 μ L) was combined with a solution of nitrone **71** (6.03 mg, 16.0 μ mol) in CDCl₃ (400 μ L). After 48 hours at 0 °C, the reaction showed complete conversion of the starting materials and proved sufficiently pure for characterisation (*trans/cis* > 15:1). ¹H NMR (300.1 MHz, CDCl₃): δ _H 11.16 (s, 1H, H₈), 8.18 (s, 1H, H₆), 7.54 (s, 1H, H₁₁), 7.45 (d, *J* = 8.2 Hz, 2H, H₂₅), 7.38 (d, *J* = 8.2 Hz, 2H, H₂₄), 7.31 (d, *J* = 8.9 Hz, 2H, H₃₀), 7.09 (d, *J* = 8.9 Hz, 2H, H₃₁), 6.92 (d, *J* = 8.7 Hz, 1H, H₁₄), 6.83 (s, 1H, H₃), 6.74 (d, *J* = 1.9 Hz, 1H, H₁₇), 6.61 (dd, *J* = 8.8, 2.0 Hz, 1H, H₁₅), 5.68 (s, 1H, H₂₂), 5.10 (d, *J* = 7.4 Hz, 1H, H₂₀), 3.89 (d, *J* = 7.6 Hz, 1H, H₂₁), 3.79 (s, 2H, H₂₇), 2.49 (s, 3H, H₁), 2.43 (t, *J* = 7.2 Hz, 2H, H₃₅), 2.39 (s, 3H, H₅), 1.68-1.56 (m, 2H, H₃₆), 1.51-1.38 (m, 2H, H₄₀), 1.39-1.15 (m, 6H, H₃₇₋₃₉), 0.94-0.78 (m, 3H, H₄₁). ¹³C NMR (75.5 MHz, CDCl₃): δ _C 176.7 (quat. C, C₂₈), 175.3 (quat. C, C₁₉), 173.2 (quat. C, C₁₈), 157.5 (quat. C, C₇), 155.5 (quat. C, C₂), 154.4 (quat. C, C₁₃), 152.3 (quat. C, C₄), 150.8 (quat. C, C₁₀), 149.5 (quat. C, C₉), 148.0 (quat. C, C₂₉), 137.1 (quat. C, C₂₃), 135.1 (quat. C, C₂₆), 132.8 (CH, C₃₀), 130.7 (CH, C₂₄), 128.3 (quat. C, C₁₂), 127.1 (CH, C₂₅), 126.7 (quat. C, C₁₆), 125.0 (CH, C₁₅), 121.5 (CH, C₃), 121.2 (CH, C₁₇), 119.0 (quat. C, C₃₂), 114.7 (CH, C₃₁), 113.8 (CH, C₆), 113.1 (CH, C₁₄), 111.5 (CH, C₁₁), 90.4 (quat. C, C₃₄), 79.9 (quat. C,

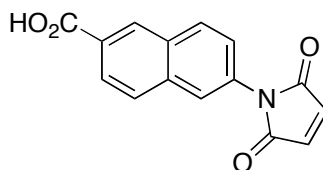
C₃₃), 77.6 (CH, C₂₀), 70.0 (CH, C₂₂), 56.8 (CH, C₂₁), 40.5 (CH₂, C₂₇), 31.9 (CH₂, C₃₈), 29.9 (CH₂, C₃₉), 29.1 (CH₂, C₃₇), 29.0 (CH₂, C₃₆), 22.8 (CH₂, C₄₀), 22.1 (CH₃, C₁), 21.7 (CH₃, C₅), 19.6 (CH₂, C₃₅), 14.2 (CH₃, C₄₁). MS (ES⁺) *m/z* 739 (100%, [M+H]⁺). HRMS (ES⁺) calc. for C₄₄H₄₃N₄O₇ 739.3132, found 739.3134.

(Z)-6-(3-carboxyacrylamido)-2-naphthoic acid 92



6-amino-2-naphthoic acid (449 mg, 2.40 mmol) was dissolved in THF (10 mL). Maleic anhydride (236 mg, 2.40 mmol) was added and the solution was stirred overnight. The occurring precipitate was filtered, washed with Et₂O and dried under high vacuum to furnish the desired product as a pale yellow solid (664 mg, 97%). M.p.: 241.7 - 242.0 °C. ¹H NMR (400.1 MHz, d₆-DMSO): δ_H 10.68 (s, 1H, NH), 8.53 (s, 1H, Ar CH), 8.45 (s, 1H, Ar CH), 8.08 (d, *J* = 8.9 Hz, 1H, Ar CH), 7.96-7.91 (m, 2H, Ar CH), 7.67 (dd, *J* = 8.9, 1.9 Hz, 1H, Ar CH), 6.54 (d, *J* = 12.0 Hz, 1H, CH), 6.37 (d, *J* = 12.0 Hz, 1H, CH). ¹³C NMR (100.6 MHz, d₆-DMSO): δ_C 167.5 (quat. C), 167.0 (quat. C), 163.7 (quat. C), 138.4 (quat. C), 135.7 (quat. C), 131.4 (CH), 130.6 (CH), 130.3 (CH), 130.2 (CH), 129.0 (quat. C), 127.7 (CH), 126.8 (quat. C), 125.8 (CH), 120.6 (CH), 115.2 (CH). MS (ES⁻) *m/z* 567 (20%), 284 (100%, [M-H]⁻), 240 (20%), 186 (18%). HRMS (ES⁻) calc. for C₁₅H₁₀NO₅ 284.0559, found 284.0562.

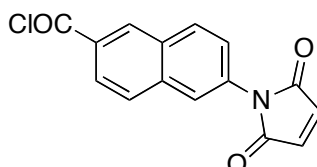
6-(2,5-dioxo-2,5-dihydro-1H-pyrrol-1-yl)-2-naphthoic acid 93



(Z)-6-(3-carboxyacrylamido)-2-naphthoic acid 92 (571 mg, 2.00 mmol) was suspended in dry MeCN (40 mL). ZnBr₂ (450 mg, 2.00 mmol) and HMDS (1.61 g, 10.0 mmol) were added and the mixture was refluxed at 90 °C for 1 hour. After cooling to room temperature, the solution was filtered and reduced to roughly 10% of its original volume. Water (25 mL) was added and the pH was adjusted to 1 using 1M HCl. The solution was washed intensively with EtOAc (10 x 50 mL). All combined organic fractions were dried over MgSO₄, filtered and reduced to yield the desired product as a brown solid (417 mg, 78%). M.p.: 341.2 - 342.0 °C. ¹H NMR (400.1 MHz, d₆-DMSO): δ_H 8.66 (s, 1H, Ar CH), 8.23 (d, *J* = 8.8 Hz, 1H, Ar CH),

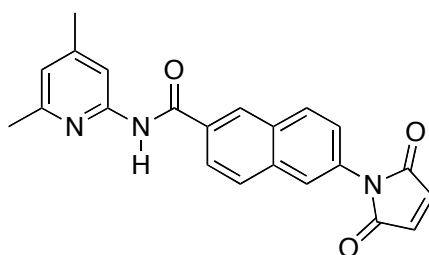
8.08-7.99 (m, 3H, Ar CH), 7.58 (dd, $J = 8.8, 1.8$ Hz, Ar CH, 1H), 7.26 (s, 2H, 2 \times CH). ^{13}C NMR (100.6 MHz, d_6 -DMSO): δ_{C} 169.9 (quat. C), 167.3 (quat. C), 134.9 (CH), 134.7 (quat. C), 131.2 (quat. C), 131.0 (quat. C), 130.3 (CH), 130.1 (CH), 128.8 (quat. C), 128.3 (CH), 125.9 (CH), 125.5 (CH), 124.9 (CH). MS (ES $^-$) m/z 266 (100%, [M-H] $^-$). HRMS (ES $^-$) calc. for $\text{C}_{15}\text{H}_8\text{NO}_4$ 266.0456, found 266.0453.

6-(2,5-dioxo-2,5-dihydro-1H-pyrrol-1-yl)-2-naphthoyl chloride



6-(2,5-dioxo-2,5-dihydro-1H-pyrrol-1-yl)-2-naphthoic acid **93** (350 mg, 1.31 mmol) was suspended in a mixture of thionyl chloride (50 mL) and toluene (50 mL). The mixture was refluxed at 90 °C overnight. A clear solution was obtained which was concentrated *in vacuo* to yield the desired product as a brown solid in sufficient purity for direct further conversion. ^1H NMR (400.1 MHz, CDCl_3): δ_{H} 8.76 (s, 1H, Ar CH), 8.10 (m, 2H, Ar CH), 7.97-7.94 (m, 2H, Ar CH), 7.67 (dd, $J = 8.8, 2.0$ Hz, 1H, Ar CH), 6.94 (s, 2H, 2 \times CH).

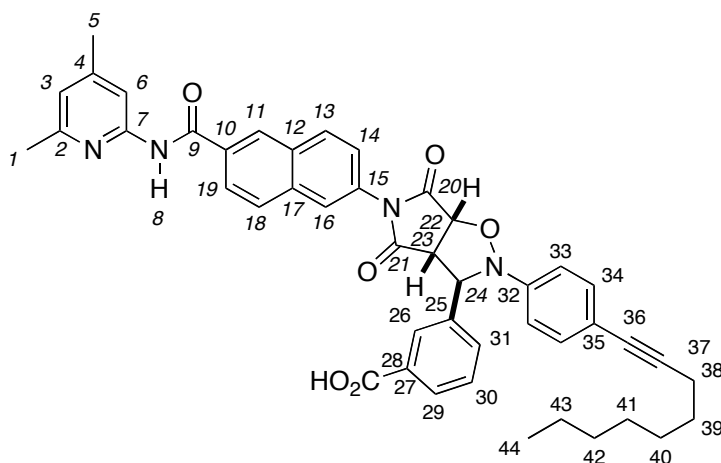
N-(4,6-dimethylpyridin-2-yl)-6-(2,5-dioxo-2,5-dihydro-1H-pyrrol-1-yl)-2-naphthamide **74**



6-(2,5-dioxo-2,5-dihydro-1H-pyrrol-1-yl)-2-naphthoyl chloride (350 mg, 1.28 mmol) was dissolved in dry DCM (20 mL). 4,6-dimethylpyridin-2-amine (345 mg, 2.82 mmol) in dry DCM (10 mL) was slowly added to the acid chloride at 0 °C. The solution was stirred overnight while warming to room temperature. The occurring precipitate was filtered and washed with cold DCM (10 mL) to yield the desired product as a pale grey solid (305 mg, 63% over two steps). M.p.: 264.8 - 265.0 °C. ^1H NMR (400.1 MHz, d_6 -DMSO): δ_{H} 10.80 (s, 1H, NH), 8.74 (s, 1H, Ar CH), 8.17 (d, $J = 8.9$ Hz, 1H, Ar CH), 8.10 (dd, $J = 8.6, 1.6$ Hz, 1H, Ar CH), 8.07 (d, $J = 8.7$ Hz, 1H, Ar CH), 7.99 (d, $J = 1.8$ Hz, 1H, Ar CH), 7.94 (s, 1H, Ar CH), 7.59 (dd, $J = 8.7, 2.0$ Hz, 1H, Ar CH), 7.26 (s, 2H, 2 \times CH), 6.89 (s, 1H, Ar CH), 2.42 (s, 3H, CH_3), 2.33 (s, 3H, CH_3). ^{13}C NMR (100.6 MHz, d_6 -DMSO): δ_{C} 169.9 (quat. C), 165.7 (quat. C), 156.2 (quat. C), 151.6 (quat. C), 149.0 (quat. C), 134.8 (CH), 134.1 (quat. C), 131.9 (quat. C), 130.82 (quat.

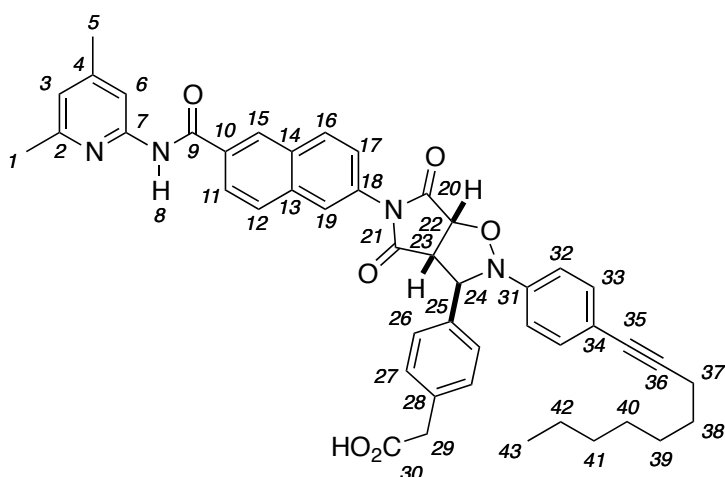
C), 130.8 (quat. C), 129.8 (CH), 128.4 (CH), 127.9 (CH), 125.4 (CH), 125.2 (CH), 124.8 (CH), 120.1 (CH), 112.1 (CH), 23.4 (CH₃), 20.9 (CH₃). MS (ES⁺) *m/z* 394 (100%, [M+Na]⁺), 123 (12%). HRMS (ES⁺) calc. for C₂₂H₁₈N₃O₃ 372.1347, found 372.1348.

Template *trans*-98



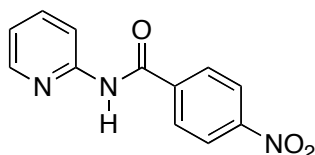
In an NMR tube, maleimide **74** (5.94 mg, 16.0 μ mol) in CDCl₃ (400 μ L) was combined with a solution of nitrone **70** (5.81 mg, 16.0 μ mol) in CDCl₃ (400 μ L). After 48 hours at 0 °C, the reaction showed complete conversion. Removal of the solvent provided sufficiently pure material (*trans/cis* > 25:1). M.p.: 198.2 - 198.8 °C. ¹H NMR (300.1 MHz, d₆-DMSO): δ_{H} 10.87 (s, 1H, H₈), 8.72 (s, 1H, H₁₁), 8.16 (s, 1H, H₂₆), 8.09 (d, *J* = 8.6 Hz, 2H, H₁₃), 8.08 (d, *J* = 8.5 Hz, 2H, H₂₉), 7.96-7.90 (m, 3H, H_{6,18,19}), 7.82 (d, *J* = 8.0 Hz, 1H, H₃₁), 7.58 (t, *J* = 7.7 Hz, 1H, H₃₀), 7.33 (d, *J* = 9.0 Hz, 2H, H₃₃), 7.28 (d, *J* = 9.1 Hz, 2H, H₃₄), 7.05 (dd, *J* = 8.7, 2.0 Hz, 1H, H₁₄), 6.92 (s, 1H, H₃), 6.86 (d, *J* = 1.7 Hz, 1H, H₁₆), 6.13 (s, 1H, H₂₄), 5.46 (d, *J* = 7.3 Hz, 1H, H₂₂), 4.24 (d, *J* = 7.4 Hz, 1H, H₂₃), 2.43 (s, 3H, H₁), 2.43 (t, *J* = 6.8 Hz, 2H, H₃₈), 2.34 (s, 3H, H₅), 1.60-1.51 (m, 2H, H₃₉), 1.46-1.36 (m, 2H, H₄₀), 1.32-1.19 (m, 6H, H₄₁₋₄₃), 0.82-0.77 (m, 3H, H₄₄). ¹³C NMR (75.5 MHz, d₆-DMSO): δ_{C} 174.3 (quat. C, C₂₁), 173.0 (quat. C, C₂₀), 167.1 (quat. C, C₂₈), 165.6 (quat. C, C₉), 155.9 (quat. C, C₂), 151.4 (quat. C, C₇), 149.4 (quat. C, C₄), 148.4 (quat. C, C₃₂), 139.5 (quat. C, C₂₇), 133.8 (quat. C, C₁₇), 132.4 (quat. C, C₁₀), 132.2 (CH, C₃₃), 131.4 (quat. C, C₂₅), 131.4 (CH, C₃₁), 131.1 (quat. C, C₁₂), 130.6 (quat. C, C₁₅), 130.0 (CH, C₁₃), 129.0 (CH, C₃₀), 128.7 (CH, C₁₈), 128.5 (CH, C₁₁), 127.9 (CH, C₁₉), 127.9 (CH, C₂₆), 125.3 (CH, C₂₉), 125.1 (CH, C₁₆), 124.8 (CH, C₁₄), 120.2 (CH, C₃), 117.4 (quat. C, C₃₅), 114.6 (CH, C₃₄), 112.2 (CH, C₆), 89.9 (quat. C, C₃₆), 80.1 (quat. C, C₃₇), 78.1 (CH, C₂₂), 67.9 (CH, C₂₄), 56.6 (CH, C₂₃), 31.2 (CH₂, C₄₃), 28.36 (CH₂, C₄₂), 28.33 (CH₂, C₄₁), 28.27 (CH₂, C₄₀), 23.2 (CH₃, C₁), 22.0 (CH₂, C₃₉), 20.9 (CH₃, C₅), 18.7 (CH₂, C₃₈), 13.9 (CH₃, C₄₄). MS (ES⁻) *m/z* 733 (100%, [M-H]⁻). HRMS (ES⁺) calc. for C₄₅H₄₁N₄O₆ 733.3026, found 733.3026.

Template *trans*-99



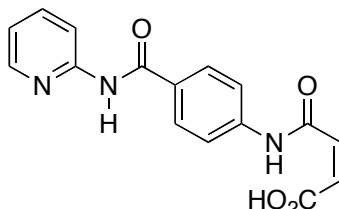
In an NMR tube, maleimide **74** (5.94 mg, 16.0 μmol) in CDCl_3 (400 μL) was combined with a solution of nitrone **71** (6.03 mg, 16.0 μmol) in CDCl_3 (400 μL). After 48 hours at 0 $^\circ\text{C}$, the reaction showed complete conversion of the starting materials and proved sufficiently pure for characterisation (*trans/cis* > 15:1). M.p.: 218.0 - 218.6 $^\circ\text{C}$. ^1H NMR (400.1 MHz, CDCl_3): δ_{H} 11.29 (s, 1H, H₈), 8.57 (s, 1H, H₁₅), 8.30 (s, 1H, H₆), 8.10 (d, J = 9.7 Hz, 1H, H₁₁), 7.85 (d, J = 8.6 Hz, 1H, H₁₂), 7.40 (d, J = 7.9 Hz, 1H, H₁₇), 7.36 (d, J = 8.7 Hz, 2H, H₃₃), 7.29 (d, J = 7.5 Hz, 2H, H₂₇), 7.21 (d, J = 7.8 Hz, 2H, H₂₆), 7.13 (d, J = 8.7 Hz, 2H, H₃₂), 6.90 (d, J = 5.0 Hz, 1H, H₁₆), 6.81 (s, 1H, H₃), 6.70 (s, 1H, H₁₉), 5.71 (s, 1H, H₂₄), 5.00 (d, J = 7.0 Hz, 1H, H₂₂), 3.89 (d, J = 7.0 Hz, 1H, H₂₃), 3.75 (s, 2H, H₂₉), 2.48 (s, 3H, H₁), 2.44 (t, J = 7.3 Hz, 2H, H₃₇), 2.41 (s, 3H, H₅), 1.67-1.60 (m, 2H, H₃₈), 1.50-1.43 (m, 2H, H₄₂), 1.38-1.18 (m, 6H, H₃₉₋₄₁), 0.91-0.82 (m, 3H, H₄₃). ^{13}C NMR (100.6 MHz, CDCl_3): δ_{C} 177.2 (quat. C, C₃₀), 175.3 (quat. C, C₂₀), 173.1 (quat. C, C₂₁), 166.6 (quat. C, C₉), 152.5 (quat. C, C₄), 155.1 (quat. C, C₂), 151.6 (quat. C, C₇), 148.2 (quat. C, C₃₁), 136.6 (quat. C, C₂₅), 134.9 (quat. C, C₁₀), 134.7 (quat. C₁₈), 132.9 (CH, C₃₃), 132.3 (quat. C, C₁₄), 132.2 (quat. C, C₁₃), 131.0 (CH, C₁₆), 130.6 (CH, C₂₆), 130.2 (quat. C, C₂₈), 128.9 (CH, C₁₂), 128.4 (CH, C₁₅), 126.8 (CH, C₂₇), 126.2 (CH, C₁₁), 125.9 (CH, C₁₉), 123.8 (CH, C₁₇), 121.2 (CH, C₃), 118.9 (quat. C, C₃₄), 114.6 (CH, C₃₂), 113.9 (CH, C₆), 90.5 (quat. C, C₃₆), 80.1 (quat. C, C₃₅), 77.9 (CH, C₂₂), 69.5 (CH, C₂₄), 56.6 (CH, C₂₃), 40.4 (CH₂, C₂₉), 31.9 (CH₂, C₄₂), 29.9 (CH₂, C₄₁), 29.2 (CH₂, C₄₀), 29.1 (CH₂, C₃₉), 29.0 (CH₂, C₃₈), 21.9 (CH₃, C₁), 21.8 (CH₃, C₅), 19.6 (CH₂, C₃₇), 14.2 (CH₃, C₄₃). MS (ES⁺) m/z 749 (20%, [M+H]⁺), 372 (70%), 123 (100%). HRMS (ES⁺) calc. for C₄₆H₄₅N₄O₆ 749.3339, found 749.3347.

4-nitro-*N*-(pyridin-2-yl)benzamide **114**



4-nitrobenzoyl chloride (928 mg, 5.00 mmol) was suspended in dry DCM (20 mL) and cooled to 0 °C. A solution of 2-aminopyridine (113 mg, 12.5 mmol) in dry DCM (20 mL) was slowly added dropwise. The addition resulted in the formation of a clear solution, which was stirred overnight while warming to room temperature. Work-up included extraction of excess amine from the organic layer with 1M HCl solution (2 x 30 mL), re-extracting the aqueous layer with DCM (2 x 30 mL), washing the combined organic layers with sat. aqueous NaHCO₃ solution (30 mL), drying over MgSO₄, filtration and concentration *in vacuo* to furnish the desired product as a white powder (907 mg, 74%). M.p.: 242.1 - 243.7 °C (lit.^[219]: 211 - 212 °C). ¹H NMR (300.1 MHz, d₆-DMSO): δ_H 11.18 (s, 1H, NH), 8.41 (dd, 1H, *J* = 4.7, 0.9 Hz, Ar CH), 8.33 (d, *J* = 8.8 Hz, 2H, Ar CH), 8.22 (d, *J* = 9.0 Hz, 2H, Ar CH), 8.20-8.16 (m, 1H, Ar CH), 7.90-7.84 (m, 1H, Ar CH), 7.20 (dd, *J* = 6.7, 5.0 Hz, 1H, Ar CH). ¹³C NMR (75.5 MHz, d₆-DMSO): δ_C 164.6 (quat. C), 151.8 (quat. C), 149.3 (quat. C), 148.0 (CH), 139.9 (quat. C), 138.3 (CH), 129.6 (CH), 123.4 (CH), 120.2 (CH), 114.8 (CH). MS (ES⁻) *m/z* 242 (100%, [M-H]⁻).

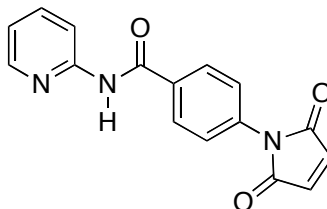
(*Z*)-4-oxo-4-(4-(pyridin-2-ylcarbamoyl)phenylamino)but-2-enoic acid **115**



4-nitro-*N*-(pyridin-2-yl)benzamide **114** (200 mg, 822 μmol) was dissolved in THF (15 mL). Palladium (20 mg, 10 wt.-% on carbon, dry) was added carefully. The solution was purged with hydrogen and kept under a hydrogen atmosphere overnight using hydrogen filled balloons. The following day, the solution was filtered through celite, maleic anhydride (98.1 mg, 1.00 mmol) was added to the filtrate and the solution was stirred overnight. Filtration of the precipitate yielded the desired product as a white solid (114 mg, 45% over two steps). M.p.: 188.1 - 188.4 °C. ¹H NMR (300.1 MHz d₆-DMSO): δ_H 10.73 (s, 1H, NH), 10.63 (s, 1H, NH), 8.39 (s, 1H, Ar CH), 8.18 (d, *J* = 8.3 Hz, 1H, Ar CH), 8.04 (d, *J* = 8.7 Hz, 2H, Ar CH), 7.86 (t, *J* = 7.3 Hz, 1H, Ar CH), 7.76 (d, *J* = 8.6 Hz, 2H, Ar CH), 7.18 (dd, *J* = 6.6, 5.2 Hz, 1H, Ar CH), 6.52 (d, *J* = 12.0 Hz, 1H, CH), 6.34 (d, *J* = 12.0 Hz, 1H, CH). ¹³C NMR (75.5 MHz, d₆-DMSO): δ 172.0 (quat. C), 166.9 (quat. C), 165.4 (quat. C), 163.6 (quat. C), 152.1 (quat. C),

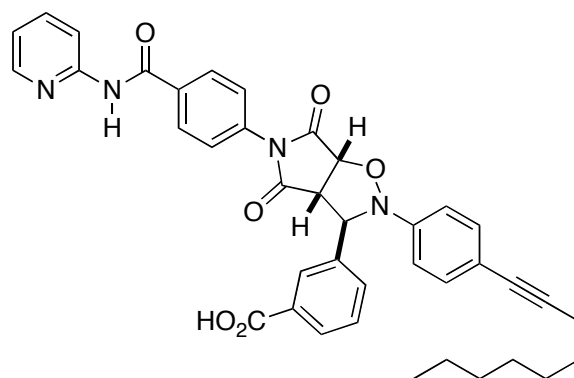
147.4 (CH), 142.1 (quat. C), 138.5 (CH), 131.6 (CH), 130.3 (CH), 129.1 (CH), 119.8 (CH), 118.6 (CH), 114.8 (CH). MS (ES+) m/z 312 (100%, [M+H]⁺). HRMS (ES+) calc. for C₁₆H₁₄N₃O₄ 312.0984, found 312.0992.

4-(2,5-dioxo-2,5-dihydro-1H-pyrrol-1-yl)-N-(pyridin-2-yl)benzamide 101



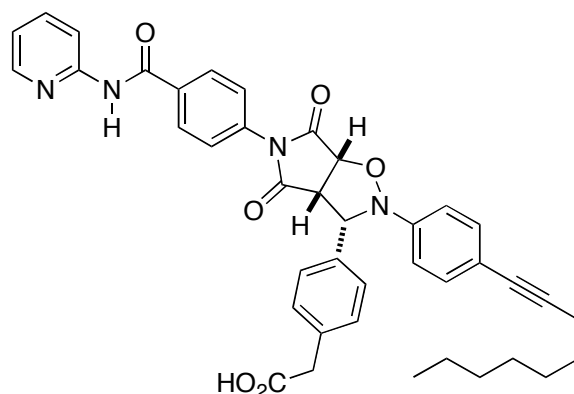
(Z)-4-oxo-4-(4-(pyridin-2-ylcarbamoyl) phenylamino)but-2-enoic acid **115** (114 mg, 367 μ mol) was suspended in dry MeCN (10 mL). Zinc bromide (83.3 mg, 367 μ mol) and HMDS (296 mg, 1.84 mmol) were added at room temperature and the mixture was refluxed at 85 °C for 1 hour. After cooling to room temperature, the precipitate was filtered and the filtrate was reduced to roughly 10% of its original volume. Water (25 mL) was added and a pH of 1 was adjusted using 1M HCl. The solution was extracted with DCM (3 x 50 mL). The combined organic layers were subsequently treated with an aqueous 0.1M EDTA solution (2 x 50 mL), H₂O (2 x 50 mL) and brine (50 mL), dried over MgSO₄, filtered and concentrated to yield the desired product as a light yellow solid (89 mg, 83%). M.p.: 256.0 - 256.5 °C. ¹H NMR (300.1 MHz, CDCl₃): δ_{H} 8.73 (s, 1H, NH), 8.42 (d, J = 8.4 Hz, 1H, Ar CH), 8.31 (ddd, J = 5.0, 1.8, 0.9 Hz, 1H, Ar CH), 8.05 (d, J = 8.9 Hz, 2H, Ar CH), 7.80 (ddd, J = 8.4, 7.4, 1.9 Hz, 1H, Ar CH), 7.59 (d, J = 8.9 Hz, 2H, Ar CH), 7.11 (ddd, J = 7.4, 5.0, 1.0 Hz, 1H, Ar CH), 6.91 (s, 2H, 2 x CH). ¹³C NMR (75.5 MHz, d₆-DMSO): δ_{C} 169.6 (quat. C), 165.3 (quat. C), 152.1 (quat. C), 147.9 (CH), 138.1 (CH), 134.8 (CH), 134.7 (quat. C), 133.0 (quat. C), 128.7 (CH), 126.0 (CH), 119.9 (CH), 114.7 (CH). MS (ES+) m/z 348 (40%), 316 (100%, [M+Na]⁺).

Template *trans*-104



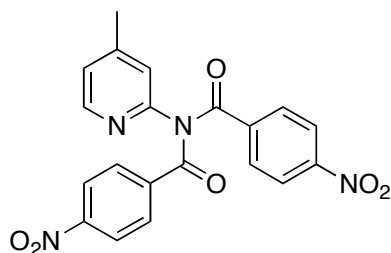
In an NMR tube, maleimide **101** (4.69 mg, 16.0 μmol) in CDCl_3 (400 μL) was combined with a solution of nitrone **70** (5.81 mg, 16.0 μmol) in CDCl_3 (400 μmol). After 48 hours at 0 $^\circ\text{C}$, the reaction showed complete conversion of the starting materials and proved sufficiently pure for characterisation (*trans/cis* > 15:1). ^1H NMR (300.1 MHz CDCl_3): δ_{H} 11.77 (s, 1H, NH), 8.60 (d, $J = 8.5$ Hz, 1H, Ar CH), 8.28 (ddd, $J = 5.2, 1.8, 0.7$ Hz, 1H, Ar CH), 8.20 (s, 1H, Ar CH), 8.17 (d, $J = 8.7$ Hz, 2H, Ar CH), 8.05 (d, $J = 7.8$ Hz, 1H, Ar CH), 7.91 (ddd, $J = 8.7, 7.2, 1.7$ Hz, 1H, Ar CH), 7.64 (d, $J = 7.5$ Hz, 1H, Ar CH), 7.46 (t, $J = 7.7$ Hz, 1H, Ar CH), 7.28 (d, $J = 8.9$ Hz, 2H, Ar CH), 7.20 (ddd, $J = 7.3, 5.2, 1.0$ Hz, 1H, Ar CH), 7.05 (d, $J = 8.9$ Hz, 2H, Ar CH), 7.04 (d, $J = 8.7$ Hz, 2H, Ar CH), 5.76 (s, 1H, CH), 5.22 (d, $J = 7.3$ Hz, 1H, CH), 4.21 (d, $J = 7.4$ Hz, 1H, CH), 2.35 (t, $J = 7.1$ Hz, 2H, CH_2), 1.61-1.52 (m, 2H, CH_2), 1.45-1.38 (m, 2H, CH_2), 1.31-1.23 (m, 6H, $3 \times \text{CH}_2$), 0.90-0.83 (m, 3H, CH_3). ^{13}C NMR (75.5 MHz, CDCl_3): δ_{C} 174.1 (quat. C), 173.2 (quat. C), 171.3 (quat. C), 166.4 (quat. C), 152.4 (quat. C), 147.2 (quat. C), 145.4 (CH), 140.5 (CH), 138.0 (quat. C), 135.0 (quat. C), 134.3 (quat. C), 133.0 (CH), 132.7 (CH), 131.4 (quat. C), 129.7 (CH), 129.6 (CH), 129.0 (CH), 128.5 (CH), 126.0 (CH), 120.0 (CH), 119.3 (quat. C), 116.3 (CH), 115.0 (CH), 90.4 (quat. C), 79.8 (quat. C), 77.5 (CH), 69.6 (CH), 56.0 (CH), 31.9 (CH_2), 29.9 (CH_2), 29.1 (CH_2), 29.0 (CH_2), 22.8 (CH_2), 19.6 (CH_2), 14.2 (CH_3). MS (ES $^-$) m/z 669 (5%), 655 (40%, $[\text{M}-\text{H}]^-$), 362 (100%). HRMS (ES $^-$) calc. for $\text{C}_{39}\text{H}_{35}\text{N}_4\text{O}_6$ 655.2557, found 655.2570.

Template *cis*-107



In an NMR tube, maleimide **101** (4.69 mg, 16.0 μmol) in CDCl_3 (400 μL) was combined with a solution of nitrone **71** (6.03 mg, 16.0 μmol) in CDCl_3 (400 μmol). After 48 hours at 0 $^\circ\text{C}$, the reaction showed complete conversion of the starting materials and proved sufficiently pure for characterisation of the *cis*-isomer (*cis/trans* = 1.3:1). ^1H NMR (300.1 MHz, CDCl_3): δ_{H} 10.84 (s, 1H, NH), 8.47 (d, J = 8.5 Hz, 1H, Ar CH), 8.20 (d, J = 4.9 Hz, 1H, Ar CH), 7.92 (d, J = 8.6 Hz, 2H, Ar CH), 7.87-7.84 (m, 1H, Ar CH), 7.36 (d, J = 8.1 Hz, 2H, Ar CH), 7.26 (d, J = 8.6 Hz, 2H, Ar CH), 7.21 (d, J = 8.1 Hz, 2H, Ar CH), 7.13 (d, J = 8.3 Hz, 2H, Ar CH), 7.16-7.10 (m, 1H, Ar CH), 6.99 (d, J = 8.6 Hz, 2H, Ar CH), 5.12 (d, J = 7.3 Hz, 2H, 2 \times CH), 4.13 (t, J = 8.6 Hz, 1H, CH), 3.65 (s, 2H, CH_2), 2.36 (t, J = 7.0 Hz, 2H, CH_2), 1.61-1.52 (m, 2H, CH_2), 1.45-1.38 (m, 2H, CH_2), 1.31-1.23 (m, 6H, 3 \times CH_2), 0.90-0.83 (m, 3H, CH_3). ^{13}C NMR (75.5 MHz, CDCl_3): δ_{C} 176.2 (quat. C), 172.5 (quat. C), 170.8 (quat. C), 166.2 (quat. C), 152.1 (quat. C), 147.5 (quat. C), 145.4 (CH), 140.4 (CH), 135.0 (quat. C), 134.2 (quat. C), 134.1 (quat. C), 133.3 (quat. C), 132.4 (CH), 130.6 (CH), 129.1 (CH), 127.9 (CH), 125.9 (CH), 120.4 (quat. C), 120.0 (CH), 117.0 (CH), 116.4 (CH), 90.7 (quat. C), 79.9 (quat. C), 77.4 (CH), 72.1 (CH), 54.5 (CH), 40.3 (CH_2), 31.9 (CH_2), 29.1 (CH_2), 29.0 (CH_2), 28.9 (CH_2), 22.8 (CH_2), 19.6 (CH_2), 14.2 (CH_3). MS (ES+) m/z 672 (7%), 671 (100%, $[\text{M}+\text{H}]^+$), 294 (80%). HRMS (ES+) calc. for $\text{C}_{40}\text{H}_{39}\text{N}_4\text{O}_6$ 671.2870, found 671.2869.

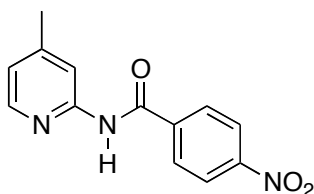
N-(4-methylpyridin-2-yl)-4-nitro-*N*-(4-nitrobenzoyl)benzamide **111**



4-nitrobenzoyl chloride (3.75 g, 19.9 mmol) was suspended in dry DCM (40 mL) and cooled to 0 $^\circ\text{C}$. A solution of 4,6-dimethylpyridin-2-amine (5.39 g, 49.8 mmol) in dry DCM (30 mL)

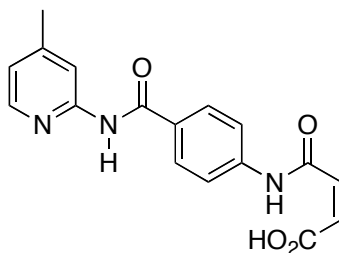
was slowly added dropwise. After stirring for 2 hours in which the solution was allowed to warm to room temperature, the occurring precipitate was filtered, redissolved in DCM (30 mL), washed with 1M HCl solution (2 x 40 mL), dried over MgSO₄ and concentrated to give the desired product as a white solid (3.65 g, 90%) which proved sufficiently pure for further conversion. ¹H NMR (400.1 MHz, CDCl₃): δ_H 8.24 (d, *J* = 8.9 Hz, 4H, 2 × Ar CH), 8.21 (d, *J* = 5.0 Hz, 1H, Ar CH), 7.90 (d, *J* = 8.9 Hz, 4H, 2 × Ar CH), 7.15 (s, 1H, 2 × Ar CH), 7.05 (d, *J* = 5.0 Hz, 1H, 2 × Ar CH), 2.39 (s, 3H, CH₃).

***N*-(4-methylpyridin-2-yl)-4-nitrobenzamide 112**



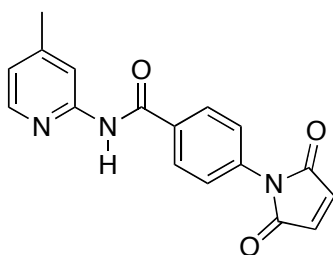
N-(4-methylpyridin-2-yl)-4-nitro-*N*-(4-nitrobenzoyl)benzamide **111** (450 mg, 1.11 mmol) was suspended in a mixture of methanol (10 mL) and dioxane (10 mL). Finely powdered sodium hydroxide (66.8 mg, 1.67 mmol) was added neat and the reaction was stirred for 2 hours at room temperature after which saturated aqueous NaHCO₃ solution (20 mL) was added. The reaction mixture was then extracted with DCM (2 x 20 mL). The combined organic layers were re-extracted with saturated aqueous NaHCO₃ solution (20 mL), dried over MgSO₄, filtered and concentrated to give a crude solid that was further purified by column chromatography (SiO₂, 300:100:4 Hex/EtOAc/Et₃N) to yield the desired product as a white solid (273 mg, 96%). M.p.: 194.2 - 196.3 °C (lit.^[220] 300 °C). ¹H NMR (300.1 MHz, CDCl₃): δ_H 9.17 (s, 1H, NH), 8.33 (d, *J* = 9.0 Hz, 2H, Ar CH), 8.21 (dt, *J* = 1.5, 0.7 Hz, 1H, Ar CH), 8.08 (d, *J* = 9.0 Hz, 2H, Ar CH), 8.02 (dd, *J* = 5.1, 0.5 Hz, 1H, Ar CH), 6.92 (ddd, *J* = 5.1, 1.5, 0.7 Hz, 1H, Ar CH), 2.42 (s, 3H, CH₃). ¹³C NMR (75.5 MHz, CDCl₃): δ_C 164.0 (quat. C), 151.3 (quat. C), 150.6 (quat. C), 150.0 (quat. C), 147.5 (CH), 140.1 (quat. C), 128.7 (CH), 124.1 (CH), 121.9 (CH), 115.3 (CH), 21.6 (CH₃). MS (ES⁺) *m/z* 685 (8%), 569 (9%), 258 (100%, [M+H]⁺), 195 (14%), 138 (9%).

(Z)-4-(4-(4-methylpyridin-2-yl)carbamoyl)phenylamino)-4-oxobut-2-enoic acid 113



N-(4-methylpyridin-2-yl)-4-nitrobenzamide **112** (1.42 g, 5.52 mmol) was dissolved in THF (60 mL). Palladium (142 mg, 10 wt.-% on carbon, dry) was added carefully. The solution was purged with hydrogen and kept under a hydrogen atmosphere overnight using hydrogen filled balloons. The following day, the solution was filtered through celite and concentrated to give crude amine intermediate which was directly dissolved in acetic acid (30 mL) without further purification. Maleic anhydride (650 mg, 6.62 mmol) was added neat and the solution was stirred overnight. Filtration of the precipitate yielded the desired product as a white solid (1.61 g, 90% over two steps). M.p.: 180.3 - 181.1 °C. ¹H NMR (300.1 MHz, d₆-DMSO): δ_H 10.59 (s, 2H, NH), 8.23 (dd, *J* = 5.1, 0.6 Hz, 1H, Ar CH), 8.04-8.03 (m, 1H, Ar CH), 8.03 (d, *J* = 8.8 Hz, 2H, Ar CH), 7.74 (d, *J* = 8.8 Hz, 2H, Ar CH), 7.00 (ddd, *J* = 5.1, 1.5, 0.6 Hz, 1H, Ar CH), 6.51 (d, *J* = 12.0 Hz, 1H, CH), 6.34 (d, *J* = 12.0 Hz, 1H, CH), 2.35 (s, 3H, CH₃). ¹³C NMR (75.5 MHz, d₆-DMSO): δ_C 172.0 (quat. C), 166.9 (quat. C), 165.2 (quat. C), 163.6 (quat. C), 152.2 (quat. C), 149.0 (quat. C), 147.3 (CH), 142.0 (quat. C), 131.7 (CH), 130.2 (CH), 129.0 (CH), 120.7 (CH), 118.6 (CH), 115.1 (CH), 21.0 (CH₃). MS (ES⁺) *m/z* 326 (100%, [M+H]⁺). HRMS (ES⁺) calc. for C₁₇H₁₆N₃O₄ 326.1141, found 326.1130.

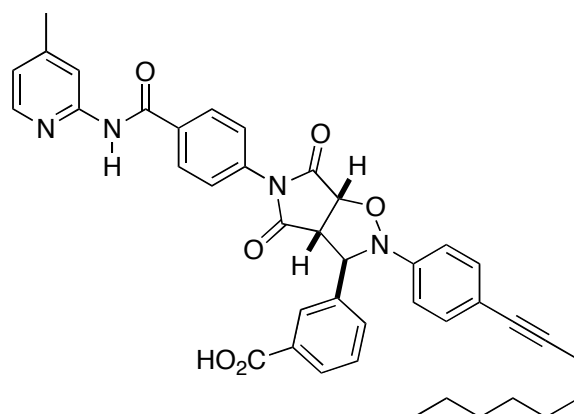
4-(2,5-dioxo-2,5-dihydro-1H-pyrrol-1-yl)-N-(4-methylpyridin-2-yl)benzamide 100



(*Z*)-4-(4-(4-methylpyridin-2-yl)carbamoyl)phenylamino)-4-oxobut-2-enoic acid (976 mg, 3.00 mmol) was suspended in dry MeCN (80 mL). Zinc bromide (676 mg, 3.00 mmol) and HMDS (1.45 g, 9.00 mmol) were added at room temperature and the mixture was refluxed at 90 °C for 1 hour. After cooling to room temperature, the precipitate was filtered and the filtrate was reduced to roughly 10% of its original volume. Water (150 mL) was added and a pH of 1 was adjusted using 1M HCl. The solution was extracted with DCM (3 x 150 mL). The combined

organic layers were subsequently treated with an aqueous 0.1M EDTA solution (2 x 50 mL), H₂O (2 x 50 mL) and brine (50 mL), dried over MgSO₄, filtered and concentrated to yield the desired product as a light yellow solid (749 mg, 81%). M.p.: 265.3 - 266.2 °C. ¹H NMR (300.1 MHz, CDCl₃): δ_H 8.60 (s, 1H, NH), 8.26 (s, 1H, Ar CH), 8.17 (d, *J* = 6.0 Hz, 1H, Ar CH), 8.04 (d, *J* = 8.7 Hz, 2H, Ar CH), 7.58 (d, *J* = 8.7 Hz, 2H, Ar CH), 6.93 (d, *J* = 6.0 Hz, 1H, Ar CH), 6.91 (s, 2H, 2 x CH), 2.35 (s, 3H, CH₃). ¹³C NMR (75.5 MHz, d₆-DMSO): δ_C 169.6 (quat. C), 165.2 (quat. C), 152.1 (quat. C), 149.0 (quat. C), 147.5 (CH), 134.8 (CH), 134.6 (quat. C), 133.0 (quat. C), 128.6 (CH), 126.1 (CH), 120.9 (CH), 115.1 (CH), 20.9 (CH₃). MS (CI⁺) *m/z* 308 (100%, [M + H]⁺). HRMS (ES⁺) calc. for C₁₇H₁₄N₃O₃ 308.1035, found 308.1035.

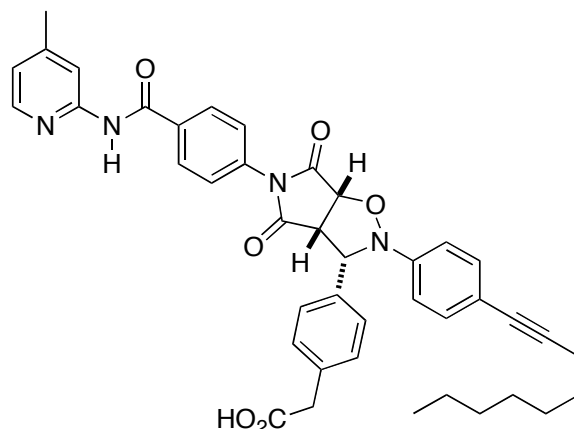
Template *trans*-103



In an NMR tube, maleimide **100** (4.92 mg, 16.0 μmol) in CDCl₃ (400 μL) was combined with a solution of nitrone **70** (5.81 mg, 16.0 μmol) in CDCl₃ (400 μmol). After 48 hours at 0 °C, the reaction showed complete conversion of the starting materials and proved sufficiently pure for characterisation (*trans/cis* > 15:1). ¹H NMR (499.9 MHz, CDCl₃): δ_H 11.85 (s, 1H, NH), 8.47 (s, 1H, Ar CH), 8.21 (s, 1H, Ar CH), 8.18 (d, *J* = 8.4 Hz, 2H, Ar CH), 8.13 (d, *J* = 5.4 Hz, 1H, Ar CH), 8.05 (d, *J* = 7.7 Hz, 1H, Ar CH), 7.65-7.64 (m, 1H, Ar CH), 7.46 (t, *J* = 7.7 Hz, 1H, Ar CH), 7.28 (d, *J* = 8.7 Hz, 2H, Ar CH), 7.05 (d, *J* = 8.9 Hz, 2H, Ar CH), 7.03 (d, *J* = 8.4 Hz, 2H, Ar CH), 7.03-7.01 (m, 1H, Ar CH), 5.76 (s, 1H, CH), 5.23 (d, *J* = 7.3 Hz, 1H, CH), 4.21 (d, *J* = 7.4 Hz, 1H, CH), 2.49 (s, 3H, CH₃), 2.35 (t, *J* = 7.2 Hz, 2H, CH₂), 1.62-1.52 (m, 2H, CH₂), 1.43-1.37 (m, 2H, CH₂), 1.32-1.22 (m, 6H, 3 x CH₂), 0.89-0.84 (m, 3H, CH₃). ¹³C NMR (75.5 MHz, CDCl₃): δ_C 174.1 (quat. C), 173.2 (quat. C), 171.4 (quat. C), 166.4 (quat. C), 152.7 (quat. C), 152.0 (quat. C), 147.2 (quat. C), 144.5 (CH), 138.0 (quat. C), 135.0 (quat. C), 134.3 (quat. C), 132.8 (CH), 132.7 (CH), 131.7 (quat. C), 129.7 (CH), 129.6 (CH), 129.0 (CH), 128.4 (CH), 126.1 (CH), 121.2 (CH), 119.3 (quat. C), 116.6 (CH), 115.0 (CH), 90.4 (quat. C), 79.8 (quat. C), 77.5 (CH), 69.6 (CH), 56.0 (CH), 31.9 (CH₂), 29.9 (CH₂), 29.1 (CH₂), 29.0 (CH₂), 22.8 (CH₂), 22.0 (CH₃), 19.6 (CH₂), 14.2

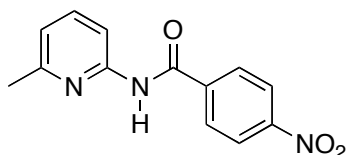
(CH₃). MS (ES+) *m/z* 671 (100%, [M+H]⁺), 308 (12%). HRMS (ES+) calc. for C₄₀H₃₉N₄O₆ 671.2870, found 671.2864.

Template *cis*-106



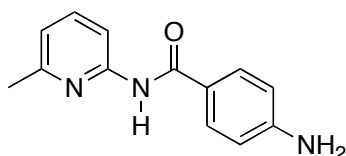
In an NMR tube, maleimide **100** (4.92 mg, 16.0 μ mol) in CDCl₃ (400 μ L) was combined with a solution of nitrone **71** (6.03 mg, 16.0 μ mol) in CDCl₃ (400 μ mol). After 48 hours at 0 °C, the reaction showed complete conversion of the starting materials and proved sufficiently pure for characterisation of the *cis*-isomer (*cis/trans* = 1.5:1). ¹H NMR (300.1 MHz, CDCl₃): δ_{H} 10.95 (s, 1H, NH), 8.34 (s, 1H, Ar CH), 7.97 (d, *J* = 8.7 Hz, 2H, Ar CH), 7.53 (d, *J* = 8.2 Hz, 1H, Ar CH), 7.39 (d, *J* = 8.2 Hz, 2H, Ar CH), 7.28 (d, *J* = 8.9 Hz, 2H, Ar CH), 7.22 (d, *J* = 8.2 Hz, 2H, Ar CH), 7.13 (d, *J* = 8.6 Hz, 2H, Ar CH), 6.98 (d, *J* = 8.8 Hz, 2H, Ar CH), 6.97-6.95 (m, 1H, Ar CH), 5.07 (d, *J* = 8.0 Hz, 1H, CH), 4.96 (d, *J* = 9.2 Hz, 1H, CH), 4.13 (dd, *J* = 9.2, 8.0 Hz, 1H, CH), 3.67 (d, *J* = 16.7 Hz, 1H, CH'H''), 3.62 (d, *J* = 16.9 Hz, 1H, CH'H''), 2.43 (s, 3H, CH₃), 2.36 (t, *J* = 7.0 Hz, 2H, CH₂), 1.61-1.52 (m, 2H, CH₂), 1.45-1.38 (m, 2H, CH₂), 1.31-1.23 (m, 6H, 3 \times CH₂), 0.90-0.83 (m, 3H, CH₃). ¹³C NMR (75.5 MHz, CDCl₃): δ_{C} 176.4 (quat. C), 172.6 (quat. C), 170.8 (quat. C), 166.0 (quat. C), 152.9 (quat. C), 151.5 (quat. C), 147.4 (quat. C), 144.2 (CH), 135.2 (quat. C), 134.3 (quat. C), 134.2 (quat. C), 133.2 (quat. C), 132.4 (CH), 130.6 (CH), 129.0 (CH), 127.9 (CH), 125.9 (CH), 121.2 (CH), 120.5 (quat. C), 117.2 (CH), 116.5 (CH), 90.7 (quat. C), 79.9 (quat. C), 77.3 (CH), 72.2 (CH), 54.5 (CH), 40.5 (CH₂), 31.9 (CH₂), 29.1 (CH₂), 29.0 (CH₂), 28.9 (CH₂), 22.8 (CH₂), 21.9 (CH₃), 19.6 (CH₂), 14.2 (CH₃). MS (ES+) *m/z* 685 (15%, [M+H]⁺), 308 (100%), 200 (4%). HRMS (ES+) calc. for C₄₁H₄₁N₄O₆ 685.3026, found 685.3026.

Synthesis of *N*-(6-methylpyridin-2-yl)-4-nitrobenzamide **110**



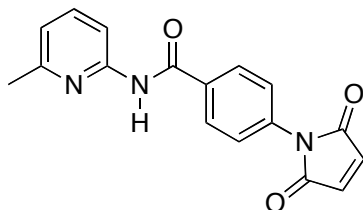
4-Nitrobenzoyl chloride (5.57 g, 30.0 mmol) in dry DCM (100 mL) was slowly reacted with a solution of 6-methylpyridin-2-amine (9.73 g, 90.0 mmol) in dry DCM (100 mL) at 0 °C. The reaction mixture was stirred overnight while warming up to room temperature. After quenching with H₂O (100 mL), the aqueous layer was extracted into DCM (3 x 80 mL). The combined organic layers were dried over MgSO₄, filtered and the solvent was evaporated to yield a yellow solid that was further purified by column chromatography (SiO₂; Hex:EtOAc, 3:2) to furnish a white powder (7.50 g, 97%). M.p.: 132.0 - 133.8 °C (lit.^[193] 130.0 - 132.0 °C). ¹H NMR (400.1 MHz, CDCl₃): δ_H 8.53 (bs, 1H, NH), 8.35 (d, *J* = 8.9 Hz, 2H, Ar CH), 8.16 (d, *J* = 8.2 Hz, 1H, Ar CH), 8.10 (d, *J* = 8.2 Hz, 2H, Ar CH), 7.68 (dd, *J* = 8.2, 7.5 Hz, 1H, Ar CH), 7.00 (d, *J* = 7.5 Hz, 1H, Ar CH), 2.49 (s, 3H, CH₃). ¹³C NMR (75.5 MHz, CDCl₃): δ_C 163.6 (quat. C), 157.1 (quat. C), 150.3 (quat. C), 150.0 (quat. C), 139.9 (quat. C), 139.0 (CH), 128.5 (CH), 124.0 (CH), 120.2 (CH), 111.2 (CH), 23.9 (CH₃). MS (ES+) *m/z* 256 (100%, [M+H]⁺).

Synthesis of 4-amino-*N*-(6-methylpyridin-2-yl)benzamide **45**



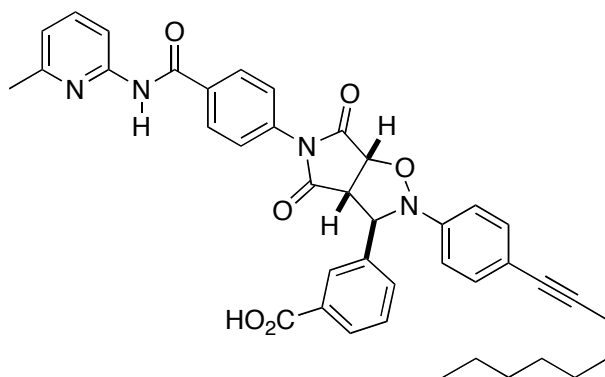
N-(6-methylpyridin-2-yl)-4-nitrobenzamide **110** (7.00 g, 27.2 mmol) was dissolved in a 5:1 THF/MeOH mixture (150 mL). Palladium (350 mg, 10% on carbon, dry) was added carefully. The solution was purged with hydrogen and kept under a hydrogen atmosphere overnight using hydrogen filled balloons. The following day, the solution was filtered through celite and concentrated *in vacuo* to yield the desired product (6.11 g, 99%). M.p.: 166.8 - 168.2 °C (lit.^[193] 169.0 - 170.0 °C). ¹H NMR (400.1 MHz, CDCl₃): δ_H 10.05 (bs, 1H, NH), 7.97 (d, *J* = 8.3 Hz, 1H, Ar CH), 7.78 (d, *J* = 8.7 Hz, 2H, Ar CH), 7.66 (dd, *J* = 8.3, 7.4 Hz, 1H, Ar CH), 6.95 (d, *J* = 7.4 Hz, 1H, Ar CH), 6.56 (d, *J* = 8.7 Hz, 2H, Ar CH), 5.80 (bs, 2H, NH), 2.42 (s, CH₃). ¹³C NMR (100.6 MHz, CDCl₃): δ_C 165.5 (quat. C), 156.3 (quat. C), 152.5 (quat. C), 152.1 (quat. C), 138.1 (CH), 129.8 (CH), 120.2 (quat. C), 118.3 (CH), 112.5 (CH), 111.4 (CH), 23.6 (CH₃). MS (ES+) *m/z* 250 (100%, [M+Na]⁺).

4-(2,5-dioxo-2,5-dihydro-1H-pyrrol-1-yl)-N-(6-methylpyridin-2-yl)benzamide **66**



4-amino-*N*-(6-methylpyridin-2-yl)benzamide **45** (5.45 g, 24.0 mmol) was dissolved in acetic acid (200 mL) and reacted with maleic anhydride (2.35 g, 24.0 mmol) to give a cloudy solution which was kept at room temperature for 2 hours, refluxed for 3 hours and stirred at room temperature overnight. The following day, the mixture was again refluxed for another 2 hours. Removal of the solvent yielded a crude product which was purified by column chromatography (SiO₂; DCM:AcOH, 19:1) to give pure product (5.31 g, 72%). M.p.: 239.9 - 241.1 °C (lit.^[193] >239 °C decomp.). ¹H NMR (400.1 MHz, d₆-DMSO): δ_H 10.81 (s, 1H, NH), 8.13 (d, *J* = 8.7 Hz, 2H, Ar CH), 8.02 (d, *J* = 8.2 Hz, 1H, Ar CH), 7.73 (dd, *J* = 8.2, 7.4 Hz, 1H, Ar CH), 7.49 (d, *J* = 8.7 Hz, 2H, Ar CH), 7.23 (s, 2H, 2 × CH), 7.04 (d, *J* = 7.4 Hz, 1H, Ar CH), 2.46 (s, 3H, CH₃). ¹³C NMR (100.6 MHz, d₆-DMSO): δ_C 169.7 (quat. C), 165.2 (quat. C), 156.6 (quat. C), 151.5 (quat. C), 138.4 (CH), 134.9 (CH), 134.6 (quat. C), 133.0 (quat. C), 128.7 (CH), 126.0 (CH), 119.2 (CH), 111.7 (CH), 23.6 (CH₃). MS (ES⁺) *m/z* 308 (100%, [M+H]⁺).

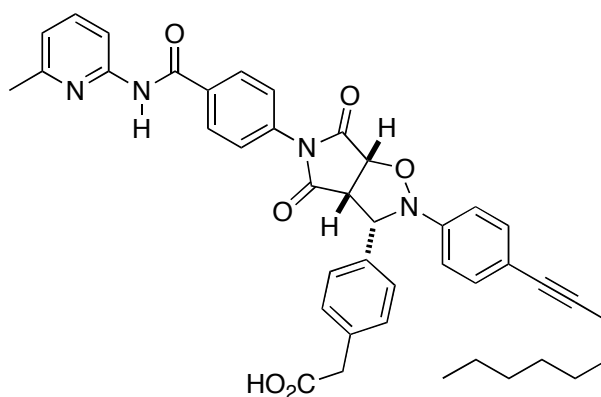
Template *trans*-102



In an NMR tube, maleimide **66** (4.92 mg, 16.0 μmol) in CDCl₃ (400 μL) was combined with a solution of nitrone **70** (5.81 mg, 16.0 μmol) in CDCl₃ (400 μmol). After 48 hours at 0 °C, the reaction showed complete conversion of the starting materials and proved sufficiently pure for characterisation (*trans/cis* > 15:1). ¹H NMR (400.1 MHz, CDCl₃): δ_H 11.71 (s, 1H, NH), 8.37 (d, *J* = 8.3 Hz, 1H, Ar CH), 8.16 (s, 1H, Ar CH), 8.12 (d, *J* = 8.5 Hz, 2H, Ar CH), 8.06 (d, *J* = 7.8 Hz, 1H, Ar CH), 7.76 (t, *J* = 8.0 Hz, 1H, Ar CH), 7.62 (d, *J* = 7.7 Hz, 1H, Ar CH), 7.44 (t, *J* = 7.7 Hz, 1H, Ar CH), 7.27 (d, *J* = 8.7 Hz, 2H, Ar CH), 7.04 (d, *J* = 8.9 Hz, 2H, Ar CH), 7.00 (d, *J* = 8.9 Hz, 2H, Ar CH), 6.99 (d, *J* = 7.2 Hz, 1H, Ar CH), 5.74 (s, 1H, CH), 5.18 (d, *J* = 7.4 Hz, 1H, CH),

4.19 (d, $J = 7.3$ Hz, 1H, CH), 2.58 (s, 3H, CH₃), 2.35 (t, $J = 7.2$ Hz, 2H, CH₂), 1.60-1.53 (m, 2H, CH₂), 1.42-1.37 (m, 2H, CH₂), 1.33-1.20 (m, 6H, 3 × CH₂), 0.89-0.82 (m, 3H, CH₃). ¹³C NMR (100.6 MHz, CDCl₃): δ_C 174.2 (quat. C), 173.2 (quat. C), 171.1 (quat. C), 166.4 (quat. C), 155.9 (quat. C), 151.9 (quat. C), 147.2 (quat. C), 140.6 (CH), 138.0 (quat. C), 135.1 (quat. C), 134.2 (quat. C), 132.8 (CH), 132.7 (CH), 131.4 (quat. C), 129.9 (CH), 129.6 (CH), 128.9 (CH), 128.4 (CH), 125.9 (CH), 120.0 (CH), 119.2 (quat. C), 114.9 (CH), 113.3 (CH), 90.4 (quat. C), 79.8 (quat. C), 77.6 (CH), 69.5 (CH), 56.0 (CH), 31.8 (CH₂), 29.1 (CH₂), 29.0 (CH₂), 28.9 (CH₂), 22.8 (CH₂), 22.2 (CH₃), 19.5 (CH₂), 14.2 (CH₃). MS (ES⁻) m/z 669 (100%, [M-H]⁻). HRMS (ES⁻) calc. for C₄₀H₃₇N₄O₆ 669.2713, found 669.2725.

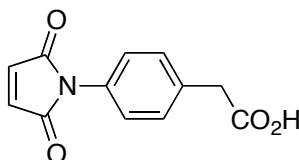
Template *cis*-105



In an NMR tube, maleimide **66** (4.92 mg, 16.0 μmol) in CDCl₃ (400 μL) was combined with a solution of nitrone **71** (6.03 mg, 16.0 μmol) in CDCl₃ (400 μmol). After 48 hours at 0 °C, the reaction showed complete conversion of the starting materials and proved sufficiently pure for characterisation of the *cis*-isomer (*cis/trans* = 2.5:1). ¹H NMR (300.1 MHz, CDCl₃): δ_H 10.97 (s, 1H, NH), 8.22 (d, $J = 8.4$ Hz, 1H, Ar CH), 7.93 (d, $J = 8.6$ Hz, 2H, Ar CH), 7.70 (t, $J = 8.0$ Hz, 1H, Ar CH), 7.38 (d, $J = 8.2$ Hz, 1H, Ar CH), 7.26 (d, $J = 8.7$ Hz, 2H, Ar CH), 7.20 (d, $J = 8.2$ Hz, 2H, Ar CH), 7.13 (d, $J = 8.7$ Hz, 2H, Ar CH), 6.97 (d, $J = 8.8$ Hz, 2H, Ar CH), 6.94 (d, $J = 8.3$ Hz, 2H, Ar CH), 5.02 (d, $J = 8.0$ Hz, 1H, CH), 4.94 (d, $J = 9.2$ Hz, 1H, CH), 4.12 (dd, $J = 8.9, 8.3$ Hz, 1H, CH), 3.65 (d, $J = 4.4$ Hz, 2H, CH), 2.45 (s, 3H, CH₃), 2.36 (t, $J = 7.0$ Hz, 2H, CH₂), 1.60-1.53 (m, 2H, CH₂), 1.42-1.37 (m, 2H, CH₂), 1.33-1.20 (m, 6H, 3 × CH₂), 0.89-0.82 (m, 3H, CH₃). ¹³C NMR (75.5 MHz, CDCl₃): δ_C 176.5 (quat. C), 172.7 (quat. C), 170.9 (quat. C), 166.1 (quat. C), 155.9 (quat. C), 151.4 (quat. C), 147.4 (quat. C), 140.4 (CH), 135.1 (quat. C), 134.2 (quat. C), 134.1 (quat. C), 133.2 (quat. C), 132.4 (CH), 130.5 (CH), 129.0 (CH), 127.9 (CH), 125.9 (CH), 120.5 (quat. C), 120.0 (CH), 117.3 (CH), 113.2 (CH), 90.8 (quat. C), 79.9 (quat. C), 77.2 (CH), 72.2 (CH), 54.5 (CH), 40.4 (CH₂), 31.9 (CH₂), 29.0 (CH₂), 29.0 (CH₂), 28.9 (CH₂), 22.8 (CH₂),

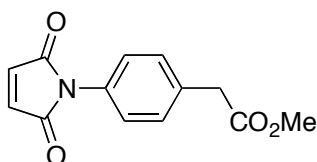
22.3 (CH₃), 19.6 (CH₂), 14.2 (CH₃). MS (ES+) *m/z* 685 (50%, [M+H]⁺), 308 (100%). HRMS (ES+) calc. for C₄₁H₄₁N₄O₆ 685.3026, found 685.3041.

Synthesis of 2-(4-(2,5-dioxo-2,5-dihydro-1H-pyrrol-1-yl)phenyl)ethanoic acid 33



2-(4-aminophenyl)ethanoic acid (13.6 g, 90.0 mmol) and maleic anhydride (8.83 g, 90.0 mmol) were dissolved in acetic acid (350 mL). The reaction mixture was stirred at room temperature for 5 hours, refluxed for 3 hours and kept to stir overnight at room temperature. Following, the solvent was removed *in vacuo* and the crude residue was purified using a short silica column with 5% acetic acid in DCM as eluent. The obtained crude product was recrystallised in hot chloroform to obtain a bright yellow solid (16.2 g, 70%). M.p.: 152.4 - 154.4 °C (lit.^[221] 151.7 - 153.1 °C). ¹H NMR (400.1 MHz, CDCl₃): δ_H 7.41 (d, *J* = 8.6 Hz, 2H, Ar CH), 7.33 (d, *J* = 8.6 Hz, 2H, Ar CH), 6.85 (s, 2H, 2 × CH), 3.69 (s, 2H, CH₂). ¹³C NMR (75.5 MHz, d₆-DMSO): δ_C 172.5 (quat. C), 169.9 (quat. C), 134.7 (quat. C), 134.6 (CH), 130.0 (quat. C), 129.9 (CH), 126.6 (CH), 40.1 (CH₂). MS (ES+) *m/z* 231 (10%, [M+H]), 186 (100%).

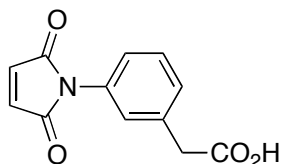
Synthesis of methyl 2-(4-(2,5-dioxo-2,5-dihydro-1H-pyrrol-1-yl)phenyl)ethanoate 57



2-(4-(2,5-dioxo-2,5-dihydro-1H-pyrrol-1-yl)phenyl) ethanoic acid (1.15 g, 4.97 mmol) was dissolved in DMF (20 mL) and methyl iodide (1.14 g, 8.00 mmol) was added carefully. Caesium carbonate (0.81 g, 2.50 mmol) was added and the reaction mixture was stirred for 16 hours under nitrogen and absence of light. The following day, the reaction was quenched with H₂O (50 mL) and extracted into EtOAc (3 × 50 mL). The combined organic fractions were washed with 3M HCl and ice water, dried over MgSO₄, filtered and solvent was removed *in vacuo*. The crude product was further purified by column chromatography (SiO₂; Hex:EtOAc, 1:2) to furnish the desired methyl ester (682 mg, 56%). M.p.: 88.0 - 88.7 °C (lit.^[197] 86.7 - 87.6 °C). ¹H NMR (300.1 MHz, CDCl₃): δ_H 7.39 (d, *J* = 8.5 Hz, 2H, Ar CH), 7.30 (d, *J* = 8.5 Hz, 2H, Ar CH), 6.85 (s, 2H, 2 × CH), 3.70 (s, 3H, CH₃), 3.65 (s, 2H, CH₂). ¹³C NMR (100.6 MHz, d₆-DMSO): δ_C 171.5 (quat. C), 170.0 (quat. C), 134.7 (CH), 134.0 (quat. C), 130.3 (quat.

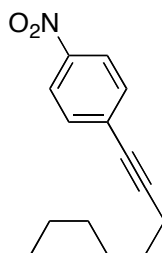
C), 129.9 (CH), 126.7 (CH), 51.8 (CH₃), 39.7 (CH₂). MS (ES+) *m/z* 245 (40%, [M+H]⁺), 186 (100%).

2-(3-(2,5-dioxo-2,5-dihydro-1H-pyrrol-1-yl)phenyl)acetic acid 120



3-aminophenylacetic acid 178 (5.00 g, 33.1 mmol) and maleic anhydride 126 (3.20 g, 32.7 mmol) was dissolved in glacial acetic acid (200 mL). The solution was stirred at room temperature under nitrogen for 12 h, followed by heating to reflux for further 5 h. The solvent was removed *in vacuo* and the residue was purified on silica gel chromatography column (hexane:EtOAc, 3:1) affording the desired product as a yellow solid which was recrystallised from DCM (3.53 g, 46%). M.p.: 114.3 - 115.0 °C. ¹H NMR (300.1 MHz, d₆-DMSO): δ_H 12.46 (s, 1H, C(O)OH), 7.46-7.41 (m, 1H, Ar CH), 7.32-7.28 (m, 1H, Ar CH), 7.24-7.20 (m, 2H, Ar CH), 7.16 (s, 2H, 2 × CH), 3.63 (s, 2H, CH₂). ¹³C NMR (75.5 MHz, d₆-DMSO): δ_C 172.8 (quat. C), 170.3 (quat. C), 136.3 (quat. C), 135.0 (CH), 131.8 (quat. C), 129.3 (CH), 129.1 (CH), 128.0 (CH), 125.5 (CH), 40.7 (CH₂). MS (CI+): *m/z* 231 (15%, [M+H]⁺), 214 (15%), 186 (100%). HRMS (CI+) calc. for C₁₂H₉NO₄ 231.0532, found 231.0540.

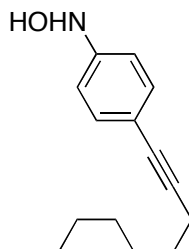
1-nitro-4-(oct-1-ynyl)benzene 130^[222]



1-iodo-4-nitrobenzene (3.74 g, 15.0 mmol) was suspended in Et₃N (100 mL). Triphenylphosphine (421 mg, 1.61 mmol), copper iodide (245 mg, 1.29 mmol) and dichlorobis(triphenylphosphine)-palladium (563 mg, 800 μmol) were added and the mixture was degassed with argon for 30 min. 1-Octyne (2.20 g, 20.0 mmol) was added *via* syringe under a protective argon atmosphere and the mixture was stirred overnight. The occurring brown solution was filtered through celite, concentrated and purified by column chromatography over silica using hexane as eluent to obtain the desired product as a dark yellow liquid (3.82 g, 83%). ¹H NMR (400.1 MHz, CDCl₃): δ_H 8.15 (d, *J* = 9.0 Hz, 2H, Ar CH), 7.51 (d, *J* = 9.0 Hz, 2H, Ar CH), 2.44 (t, *J* = 7.1 Hz, 2H, CH₂), 1.66-1.58 (m, 2H, CH₂), 1.49-1.42 (m, 2H, CH₂),

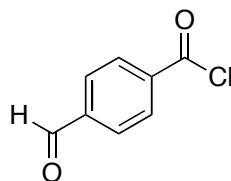
1.35-1.31 (m, 4H, 2 × CH₂), 0.93-0.89 (m, 3H, CH₃). ¹³C NMR (75.5 MHz, CDCl₃): δ_C 146.7 (quat. C), 132.4 (CH), 131.4 (quat. C), 123.6 (CH), 97.0 (quat. C), 79.4 (quat. C), 31.5 (CH₂), 28.8 (CH₂), 28.5 (CH₂), 22.7 (CH₂), 19.7 (CH₂), 14.2 (CH₃). MS (ES⁺): m/z 254 ([M+Na]⁺, 100%). HRMS (ES⁺) calc. for C₁₄H₁₇NO₂Na [M⁺] 254.1157, found 254.1158.

N-(4-(oct-1-ynyl)phenyl)hydroxylamine



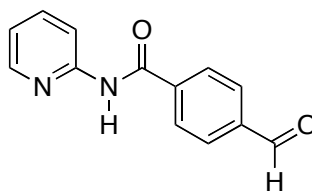
1-nitro-4-(oct-1-ynyl)benzene **130** (925 mg, 4.00 mmol) was dissolved in THF (20 mL). Rhodium (200 mg, 5 wt.-% on carbon, wet) and hydrazine monohydrate (206 mg, 4.12 mmol) were added and the reaction was followed by tlc (Hex:EtOAc, 1:1). After completion, the solution was filtered through celite and concentrated *in vacuo* to obtain the desired intermediate product as a dark brown liquid, which was directly used in the next step without further purification. ¹H NMR (300.1 MHz, CDCl₃): δ_H 7.32 (d, *J* = 8.6 Hz, 2H, Ar CH), 6.91 (d, *J* = 8.6 Hz, 2H, Ar CH), 2.38 (t, *J* = 7.0 Hz, 2H, CH₂), 1.65-1.57 (m, 2H, CH₂), 1.49-1.42 (m, 2H, CH₂), 1.38-1.26 (m, 4H, 2 × CH₂), 0.93-0.88 (m, 3H, CH₃).

4-formylbenzoyl chloride^[223]



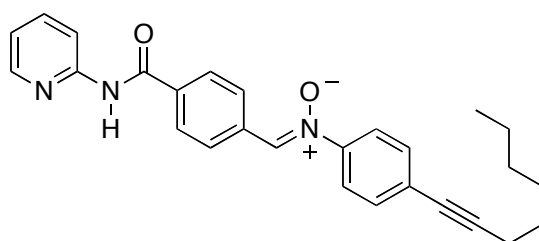
4-formylbenzoic acid (5 g, 33.3 mmol) was suspended in a mixture of thionyl chloride (10 mL) and toluene (80 mL). The reaction was refluxed at 110 °C overnight to form a clear solution. Removing all solvents *in vacuo* yielded the desired product as a grey solid that was used directly without further purification (5.45 g, 97%). The obtained spectra is in accordance with the literature. ¹H NMR (300.1 MHz, CDCl₃): δ_H 10.14 (s, 1H, C(O)H), 8.27 (d, *J* = 8.6 Hz, 2H, Ar CH), 8.01 (d, *J* = 8.7 Hz, 2H, Ar CH).

4-formyl-N-(pyridin-2-yl)benzamide 135



2-aminopyridine (600 mg, 6.38 mmol) was dissolved in a mixture of pyridine (15 mL) and dry DCM (15 mL). Neat DMAP (77.9 mg, 638 μ mol) was added and the solution was cooled to -30 $^{\circ}$ C. 4-formylbenzoyl chloride (900 mg, 5.34 mmol) in dry DCM (15 mL) was added slowly over two hours. The reaction mixture was stirred overnight allowing to warm to room temperature before it was reduced to dryness *in vacuo*. The residue was redissolved in DCM (30 mL) and extracted with saturated aqueous NaHCO_3 solution (2 x 30 mL). The organic fraction was dried over MgSO_4 , filtered and concentrated. The crude product was purified by column chromatography (SiO_2 , 3:1 Hexanes/EtOAc) to give the desired product as a white solid (884 mg, 73%). M.p.: $154.4 - 154.9$ $^{\circ}$ C. ^1H NMR (300.1 MHz, CDCl_3): δ_{H} 10.10 (s, 1H, C(O)H), 9.14 (s, 1H, NH), 8.38 (dt, $J = 8.4, 1.0$ Hz, 1H, Ar CH), 8.18 (ddd, $J = 4.9, 1.9, 0.9$ Hz, 2H, Ar CH), 8.08 (d, $J = 8.2$ Hz, 2H, Ar CH), 7.98 (d, $J = 8.2$ Hz, 2H, Ar CH), 7.77 (ddd, $J = 8.4, 7.4, 1.9$ Hz, 1H, Ar CH), 7.07 (ddd, $J = 7.4, 4.9, 1.0$ Hz, 1H, Ar CH). ^{13}C NMR (75.5 MHz, CDCl_3): δ_{C} 191.5 (C(O)H), 164.9 (quat. C), 151.4 (quat. C), 148.0 (CH), 139.5 (quat. C), 138.8 (CH), 138.7 (quat. C), 130.1 (CH), 128.1 (CH), 120.5 (CH), 114.6 (CH). MS (ES $^-$) m/z 225 (100%, $[\text{M}-\text{H}]^-$). HRMS (ES $^+$) calc. for $\text{C}_{13}\text{H}_{11}\text{N}_2\text{O}_2$ 227.0821, found 227.0818.

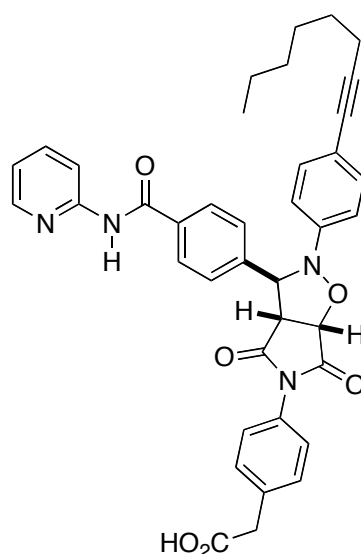
(Z)-4-(oct-1-ynyl)-N-(4-(pyridin-2-ylcarbamoyl)benzylidene)aniline oxide 119



N-(4-(oct-1-ynyl)phenyl) hydroxylamine (217 mg, 1.00 mmol) was dissolved in EtOH (5 mL) and 4-formyl-*N*-(pyridin-2-yl)benzamide (150 mg, 663 μ mol) was added neat. The solution was left to stand in the dark overnight before the precipitate was filtered to give the desired product as a light yellow solid (159 mg, 56%). M.p.: $159.5 - 159.9$ $^{\circ}$ C. ^1H NMR (300.1 MHz, CDCl_3): δ_{H} 8.80 (s, 1H, NH), 8.51 (d, $J = 8.5$ Hz, 2H, Ar CH), 8.42 (dt, $J = 8.4, 1.0$ Hz, 1H, Ar CH), 8.31 (ddd, $J = 5.0, 1.9, 0.9$ Hz, 1H, Ar CH), 8.04 (d, $J = 8.5$ Hz, 2H, Ar CH), 8.01 (s, 1H, CH), 7.79 (ddd, $J = 8.4, 7.4, 1.9$ Hz, 1H, Ar CH), 7.73 (d, $J = 8.8$ Hz, 2H, Ar CH), 7.50 (d, $J = 8.8$ Hz, 2H, Ar CH), 7.11 (ddd, $J = 7.4, 5.0, 1.0$ Hz, 1H, Ar CH), 2.43 (t, $J = 7.1$ Hz, 2H, CH_2),

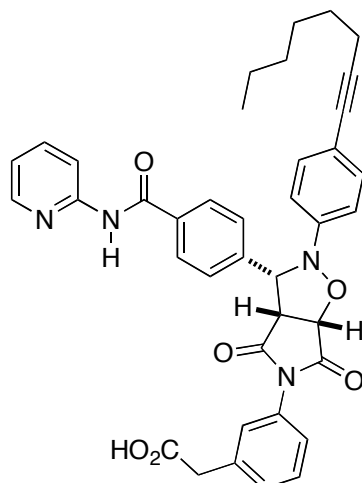
1.67-1.58 (m, 2H, CH₂), 1.51-1.41 (m, 2H, CH₂), 1.40-1.28 (m, 4H, 2 × CH₂), 0.95-0.87 (m, 3H, CH₃). ¹³C NMR (75.5 MHz, CDCl₃): δ_C 164.8 (quat. C), 151.5 (quat. C), 147.8 (CH), 147.7 (quat. C), 138.9 (CH), 135.6 (quat. C), 134.1 (quat. C), 133.3 (CH), 132.5 (CH), 129.3 (CH), 127.7 (CH), 126.8 (quat. C), 121.7 (CH), 120.3 (CH), 114.5 (CH), 93.7 (quat. C), 79.6 (quat. C), 31.5 (CH₂), 28.8 (CH₂), 28.7 (CH₂), 22.7 (CH₂), 19.6 (CH₂), 14.2 (CH₃). MS (ES⁺) *m/z* 873 (80%), 448 (100%, [M+Na]⁺). HRMS (ES⁺) calc. for C₂₇H₂₇N₃O₂Na 448.2001, found 448.1996.

Template *trans*-124



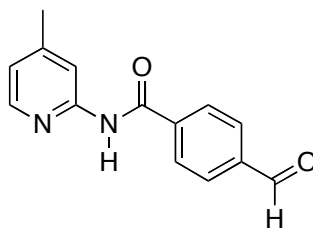
In an NMR tube, nitron **119** (8.50 mg, 16.0 μmol) in CDCl₃ (400 μL) was combined with a solution of maleimide **33** (4.62 mg, 16.0 μmol). After 48 hours at 0 °C, the reaction showed complete conversion of the starting materials and proved sufficiently pure for characterisation (*trans/cis* > 30:1). ¹H NMR (400.1 MHz, CDCl₃): δ_H 11.13 (s, 1H, NH), 8.60 (d, *J* = 8.5 Hz, 1H, Ar CH), 8.16 (d, *J* = 4.4 Hz, 1H, Ar CH), 7.97 (d, *J* = 8.2 Hz, 2H, Ar CH), 7.88 (t, *J* = 7.8 Hz, 1H, Ar CH), 7.43 (d, *J* = 8.1 Hz, 2H, Ar CH), 7.33 (d, *J* = 8.2 Hz, 2H, Ar CH), 7.30 (d, *J* = 8.6 Hz, 2H, Ar CH), 7.16 (t, *J* = 6.1 Hz, 1H, Ar CH), 7.10 (d, *J* = 8.5 Hz, 2H, Ar CH), 6.71 (d, *J* = 8.1 Hz, 2H, Ar CH), 5.78 (s, 1H, CH), 4.99 (d, *J* = 7.3 Hz, 1H, CH), 3.94 (d, *J* = 7.3 Hz, 1H, CH), 3.74 (s, 2H, CH₂), 2.37 (t, *J* = 7.0 Hz, 2H, CH₂), 1.63-1.50 (m, 2H, CH₂), 1.48-1.36 (m, 2H, CH₂), 1.35-1.18 (m, 4H, 2 × CH₂), 0.94-0.84 (m, 3H, CH₃). ¹³C NMR (100.6 MHz, CDCl₃): δ_C 177.0 (quat. C), 174.6 (quat. C), 173.2 (quat. C), 166.5 (quat. C), 152.2 (quat. C), 147.9 (quat. C), 145.1 (CH), 142.4 (quat. C), 140.5 (CH), 135.6 (quat. C), 133.7 (quat. C), 132.8 (CH), 130.9 (CH), 130.0 (quat. C), 129.0 (CH), 126.8 (CH), 126.2 (CH), 119.9 (CH), 119.0 (quat. C), 116.2 (CH), 114.5 (CH), 90.1 (quat. C), 80.0 (quat. C), 77.5 (CH), 68.9 (CH), 57.1 (CH), 40.2 (CH₂), 31.5 (CH₂), 28.9 (CH₂), 28.8 (CH₂), 22.7 (CH₂), 19.6 (CH₂), 14.2 (CH₃). MS (ES⁺) *m/z* 657 (100%, [M+H]⁺). HRMS (ES⁺) calc. for C₃₉H₃₇N₄O₆ 657.2713, found 657.2730.

Template *cis*-128



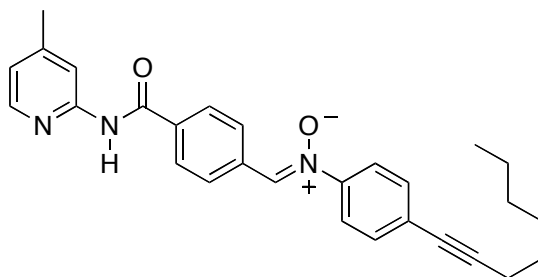
In an NMR tube, nitrone **119** (8.50 mg, 16.0 μmol) in CDCl_3 (400 μL) was combined with a solution of maleimide **120** (4.62 mg, 16.0 μmol). After 48 hours at 0 $^\circ\text{C}$, the reaction showed complete conversion of the starting materials and proved sufficiently pure for characterisation (*cis/trans* > 50:1). ^1H NMR (300.1 MHz, CDCl_3): δ_{H} 11.39 (s, 1H, NH), 8.45 (d, $J = 8.5$ Hz, 1H, Ar CH), 8.16 (ddd, $J = 5.2, 1.9, 0.9$ Hz, 1H, Ar CH), 8.01 (d, $J = 8.5$ Hz, 2H, Ar CH), 7.87 (ddd, $J = 8.5, 7.4, 1.9$ Hz, 1H, Ar CH), 7.64 (d, $J = 8.3$ Hz, 2H, Ar CH), 7.54 (s, 1H, Ar CH), 7.35 (t, $J = 7.8$ Hz, 1H, Ar CH), 7.27 (d, $J = 8.9$ Hz, 2H, Ar CH), 7.20-7.12 (m, 3H, Ar CH), 6.99 (d, $J = 8.9$ Hz, 2H, Ar CH), 5.32 (d, $J = 7.8$ Hz, 1H, CH), 4.99 (d, $J = 9.7$ Hz, 1H, CH), 4.14 (dd, $J = 9.7, 7.8$ Hz, 1H, CH), 3.79 (d, $J = 18.1$ Hz, 1H, CH'H''), 3.72 (d, $J = 18.1$ Hz, 1H, CH'H''), 2.36 (t, $J = 7.0$ Hz, 2H, CH_2), 1.62-1.52 (m, 2H, CH_2), 1.48-1.36 (m, 2H, CH_2), 1.35-1.24 (m, 4H, $2 \times \text{CH}_2$), 0.93-0.85 (m, 3H, CH_3). ^{13}C NMR (75.5 MHz, CDCl_3): δ_{C} 176.5 (quat. C), 173.5 (quat. C), 171.0 (quat. C), 167.3 (quat. C), 152.2 (quat. C), 146.3 (quat. C), 145.4 (CH), 140.3 (CH), 139.0 (quat. C), 135.5 (quat. C), 135.2 (quat. C), 132.2 (CH), 131.3 (quat. C), 130.1 (CH), 129.5 (CH), 129.0 (CH), 127.2 (CH), 126.8 (CH), 124.3 (CH), 120.3 (quat. C), 119.9 (CH), 118.0 (CH), 116.2 (CH), 90.6 (quat. C), 80.1 (quat. C), 77.2 (CH), 70.3 (CH), 54.8 (CH), 38.9 (CH_2), 31.5 (CH_2), 28.9 (CH_2), 28.7 (CH_2), 22.7 (CH_2), 19.6 (CH_2), 14.2 (CH_3). MS (ES $^-$) m/z 656 (7%), 655 (100%, $[\text{M}+\text{H}]^+$). HRMS (ES $^+$) calc. for $\text{C}_{39}\text{H}_{35}\text{N}_4\text{O}_6$ 655.2557, found 655.2545.

4-formyl-N-(4-methylpyridin-2-yl)benzamide 134



4-methyl-2-aminopyridine (690 mg, 6.38 mmol) was dissolved in a mixture of pyridine (15 mL) and dry DCM (15 mL). Neat DMAP (77.9 mg, 638 μ mol) was added and the solution was cooled to $-30\text{ }^{\circ}\text{C}$. 4-formylbenzoyl chloride (900 mg, 5.34 mmol) in dry DCM (15 mL) was added slowly over two hours. The reaction mixture was stirred overnight allowing to warm to room temperature before it was reduced to dryness *in vacuo*. The residue was redissolved in DCM (30 mL) and extracted with saturated aqueous NaHCO_3 solution (2 x 30 mL). The organic fraction was dried over MgSO_4 , filtered and concentrated. The crude product was purified by column chromatography (SiO_2 , 3:1 Hexanes/EtOAc) to give the desired product as a white solid (925 mg, 72%). M.p.: $147.3 - 148.0\text{ }^{\circ}\text{C}$. ^1H NMR (300.1 MHz, CDCl_3): δ_{H} 10.09 (s, 1H, C(O)H), 9.25 (s, 1H, NH), 8.23 (dt, $J = 1.5, 0.7\text{ Hz}$, 1H, Ar CH), 8.07 (d, $J = 8.2\text{ Hz}$, 2H, Ar CH), 8.00-7.98 (m, 1H, Ar CH), 7.98 (d, $J = 8.2\text{ Hz}$, 2H, Ar CH), 6.88 (ddd, $J = 5.1, 1.5, 0.7\text{ Hz}$, 1H, Ar CH), 2.40 (s, 3H, CH_3). ^{13}C NMR (75.5 MHz, CDCl_3): δ 191.5 (C(O)H), 164.9 (quat. C), 151.5 (quat. C), 150.4 (quat. C), 147.5 (CH), 139.7 (quat. C), 138.7 (quat. C), 130.1 (CH), 128.1 (CH), 121.6 (CH), 115.1 (CH), 21.6 (CH_3). MS (ES+) m/z 295 (100%), 263 (34%, $[\text{M}+\text{Na}]^+$). HRMS (ES+) calc. for $\text{C}_{14}\text{H}_{13}\text{N}_2\text{O}_2$ 241.0977, found 241.0974.

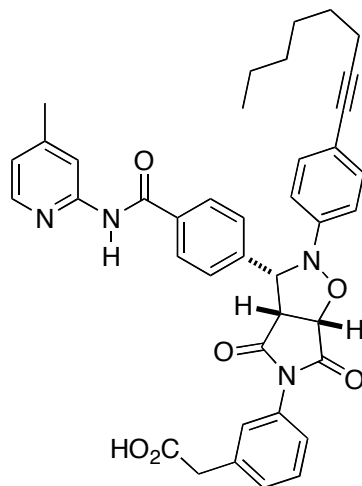
(Z)-N-(4-(4-methylpyridin-2-ylcarbamoyl)benzylidene)-4-(oct-1-ynyl)aniline oxide 118



N-(4-(oct-1-ynyl)phenyl) hydroxylamine (217 mg, 1.00 mmol) was dissolved in EtOH (5 mL) and 4-formyl-*N*-(4-methylpyridin-2-yl)benzamide (150 mg, 624 μ mol) was added neat. The solution was left to stand in the dark overnight before the precipitate was filtered to give the desired product as a light yellow solid (177 mg, 65%). ^1H NMR (300.1 MHz, CDCl_3): δ_{H} 8.79 (s, 1H, NH), 8.51 (d, $J = 8.4\text{ Hz}$, 2H, Ar CH), 8.27 (dt, $J = 1.5, 0.7\text{ Hz}$, 1H, Ar CH), 8.15 (dd, $J = 5.1, 0.5\text{ Hz}$, 1H, Ar CH), 8.04 (d, $J = 8.6\text{ Hz}$, 2H, Ar CH), 8.01 (s, 1H, CH), 7.73 (d, $J = 8.8\text{ Hz}$,

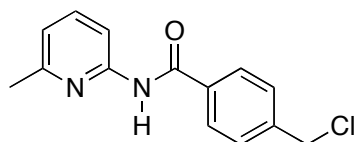
(CH₂), 22.7 (CH₂), 21.9 (CH₃), 19.6 (CH₂), 14.2 (CH₃). MS (ES⁺) *m/z* 671 (100%, [M+H]⁺). HRMS (ES⁺) calc. for C₄₀H₃₉N₄O₆ 671.2870, found 671.2869.

Template *cis*-127



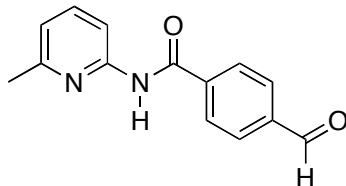
In an NMR tube, nitrone **118** (8.78 mg, 16.0 μ mol) in CDCl₃ (400 μ L) was combined with a solution of maleimide **120** (4.62 mg, 16.0 μ mol). After 48 hours at 0 °C, the reaction showed complete conversion of the starting materials and proved sufficiently pure for characterisation (*cis/trans* > 50:1). ¹H NMR (300.1 MHz, CDCl₃): δ_{H} 11.39 (s, 1H, NH), 8.29 (s, 1H, Ar CH), 8.00 (d, *J* = 8.3 Hz, 2H, Ar CH), 8.00 (d, *J* = 6.5 Hz, 1H, Ar CH), 7.63 (d, *J* = 8.3 Hz, 2H, Ar CH), 7.54 (s, 1H, Ar CH), 7.35 (t, *J* = 7.8 Hz, 1H, Ar CH), 7.27 (d, *J* = 8.9 Hz, 2H, Ar CH), 7.18 (d, *J* = 7.7 Hz, 1H, Ar CH), 7.15 (d, *J* = 7.8 Hz, 1H, Ar CH), 7.00 (d, *J* = 8.8 Hz, 2H, Ar CH), 6.97 (d, *J* = 6.5 Hz, 1H, Ar CH), 5.32 (d, *J* = 7.8 Hz, 1H, CH), 4.99 (d, *J* = 9.7 Hz, 1H, CH), 4.13 (dd, *J* = 9.7, 7.8 Hz, 1H, CH), 3.78 (d, *J* = 17.8 Hz, 1H, CH'H''), 3.70 (d, *J* = 17.8 Hz, 1H, CH'H''), 2.45 (s, 3H, CH₃), 2.36 (t, *J* = 7.0 Hz, 2H, CH₂), 1.62-1.52 (m, 2H, CH₂), 1.47-1.37 (m, 2H, CH₂), 1.36-1.27 (m, 4H, 2 \times CH₂), 0.92-0.85 (m, 3H, CH₃). ¹³C NMR (75.5 MHz, CDCl₃): δ_{C} 176.7 (quat. C), 173.5 (quat. C), 171.0 (quat. C), 167.3 (quat. C), 152.4 (quat. C), 151.9 (quat. C), 146.3 (quat. C), 144.7 (CH), 139.0 (quat. C), 135.6 (quat. C), 135.4 (quat. C), 132.3 (CH), 131.3 (quat. C), 130.1 (CH), 129.5 (CH), 129.0 (CH), 127.1 (CH), 126.8 (CH), 124.3 (CH), 121.1 (CH), 120.3 (quat. C), 118.0 (CH), 116.5 (CH), 90.6 (quat. C), 80.1 (quat. C), 77.3 (CH), 70.3 (CH), 54.8 (CH), 39.0 (CH₂), 31.5 (CH₂), 28.9 (CH₂), 28.7 (CH₂), 22.7 (CH₂), 21.9 (CH₃), 19.6 (CH₂), 14.2 (CH₃). MS (ES⁺) *m/z* 671 (100%, [M+H]⁺), 273 (10%), 241 (7%). HRMS (ES⁺) calc. for C₄₀H₃₉N₄O₆ 671.2870, found 671.2870.

Synthesis of 4-(chloromethyl)-N-(6-methylpyridin-2-yl)benzamide



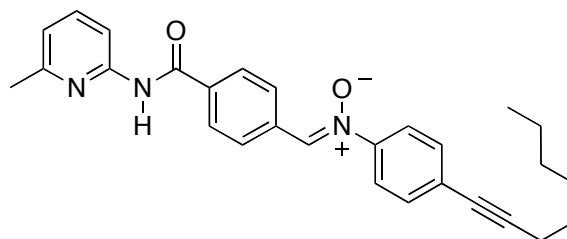
6-methylpyridin-2-amine (6.17 g, 57.0 mmol) in dry DCM (75 mL) was slowly reacted with a solution of 4-(chloromethyl)benzoyl chloride (4.90 g, 25.9 mmol) in dry DCM (75 mL) at 0 °C. The reaction was left to stir for 6 hours at room temperature before being quenched with H₂O (100 mL). The organic layer was washed with 1M HCl (75 mL) and the combined aqueous layer was extracted with DCM (3 x 75 mL). The combined organic layers were dried over MgSO₄, filtered and reduced *in vacuo* to yield pure product (6.71 g, 99%). M.p.: 125.5 - 126.4 °C. ¹H NMR (400.1 MHz, CDCl₃): δ_H 11.02 (s, 1H, NH), 8.58 (d, *J* = 8.6 Hz, 1H, Ar CH), 8.19 (d, *J* = 8.5 Hz, 2H, Ar CH), 7.97 (dd, *J* = 8.6, 7.6 Hz, 1H, Ar CH), 7.55 (d, *J* = 8.5 Hz, 2H, Ar CH), 7.09 (d, *J* = 7.6 Hz, 1H, Ar CH), 4.62 (s, 2H, CH₂), 2.68 (s, 3H, CH₃). ¹³C NMR (75.5 MHz, d₆-DMSO): δ_C 165.4 (quat. C), 152.9 (quat. C), 149.0 (quat. C), 143.6 (CH), 142.4 (quat. C), 132.5 (quat. C), 129.0 (CH), 128.6 (CH), 120.4 (CH), 113.2 (CH), 45.2 (CH₂), 20.9 (CH₃).

Synthesis of 4-formyl-N-(6-methylpyridin-2-yl)benzamide 133



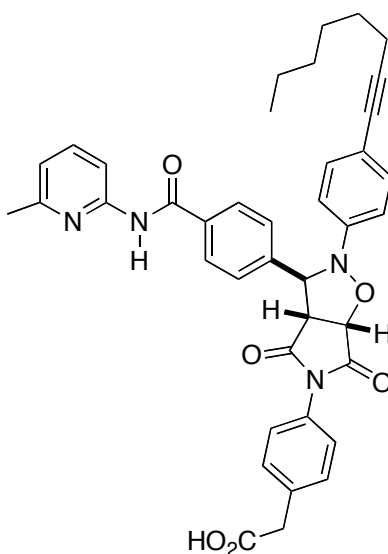
4-(chloromethyl)-N-(6-methylpyridin-2-yl)benzamide (3.00 g, 11.5 mmol) was dissolved in a 1:1 mixture of EtOH/H₂O (40 mL) and hexamethylenetetramine (4.80 g, 34.2 mmol) was added. The suspension was heated to reflux for 4 hours. Concentrated HCl (5 mL) was added and the solution was refluxed for another 0.5 hour. H₂O (100 mL) was added and the solution was extracted with DCM (3 x 100 mL). The combined organic layers were washed with brine, dried over MgSO₄, filtered and concentrated *in vacuo* to give sufficiently pure product (2.76 g, 99%). M.p.: 225.3 - 227.0 °C. ¹H NMR (400.1 MHz, CDCl₃): δ_H 12.49 (s, 1H, NH), 10.13 (s, 1H, C(O)H), 8.81 (d, *J* = 8.8 Hz, 1H, Ar CH), 8.50 (d, *J* = 8.5 Hz, 2H, Ar CH), 8.18 (dd, *J* = 8.8, 7.7 Hz, 1H, Ar CH), 8.07 (d, *J* = 8.5 Hz, 2H, Ar CH), 7.23 (d, *J* = 7.7 Hz, 1H, Ar CH), 2.83 (s, 3H, CH₃). ¹³C NMR (100.6 MHz, d₆-DMSO): δ_C 192.9 (C(O)H), 165.1 (quat. C), 153.5 (quat. C), 149.1 (quat. C), 143.1 (CH), 138.7 (quat. C), 137.8 (quat. C), 129.5 (CH), 128.9 (CH), 120.5 (CH), 113.2 (CH), 21.3 (CH₃).

(Z)-N-(4-(6-methylpyridin-2-ylcarbamoyl)benzylidene)-4-(oct-1-ynyl)aniline oxide 117



N-(4-(oct-1-ynyl)phenyl) hydroxylamine (217 mg, 1.00 mmol) was dissolved in EtOH (5 mL) and 4-formyl-*N*-(6-methylpyridin-2-yl)benzamide **133** (150 mg, 624 μ mol) was added neat. The solution was left to stand in the dark overnight before the precipitate was filtered to give the desired product as a light yellow solid (195 mg, 71%). M.p. 155.5 - 155.9 °C. ^1H NMR (300.1 MHz, CDCl_3): δ_{H} 8.67 (s, 1H, NH), 8.50 (d, $J = 8.4$ Hz, 2H, Ar CH), 8.21 (d, $J = 8.2$ Hz, 1H, Ar CH), 8.04 (d, $J = 8.6$ Hz, 2H, Ar CH), 8.01 (s, 1H, CH), 7.73 (d, $J = 8.8$ Hz, 2H, Ar CH), 7.68 (dd, $J = 8.1, 7.7$ Hz, 1H, Ar CH), 7.50 (d, $J = 8.8$ Hz, 2H, Ar CH), 6.96 (d, $J = 7.3$ Hz, 1H, Ar CH), 2.50 (s, 3H, CH_3), 2.43 (t, $J = 7.1$ Hz, 2H, CH_2), 1.67-1.58 (m, 2H, CH_2), 1.49-1.41 (m, 2H, CH_2), 1.36-1.31 (m, 4H, 2 \times CH_2), 0.94-0.89 (m, 3H, CH_3). ^{13}C NMR (75.5 MHz, CDCl_3): δ_{C} 164.8 (quat. C), 156.9 (quat. C), 150.7 (quat. C), 147.7 (quat. C), 139.2 (CH), 135.7 (quat. C), 134.0 (quat. C), 133.3 (CH), 132.5 (CH), 129.2 (CH), 127.7 (CH), 126.8 (quat. C), 121.7 (CH), 119.8 (CH), 111.3 (CH), 93.7 (quat. C), 79.6 (quat. C), 31.5 (CH_2), 28.8 (CH_2), 28.7 (CH_2), 24.0 (CH_3), 22.7 (CH_2), 19.6 (CH_2), 14.2 (CH_3). MS (ES+) m/z 901 (15%), 462 (100%, $[\text{M}+\text{Na}]^+$). HRMS (ES+) calc. for $\text{C}_{28}\text{H}_{30}\text{N}_3\text{O}_2$ 440.2338, found 440.2335.

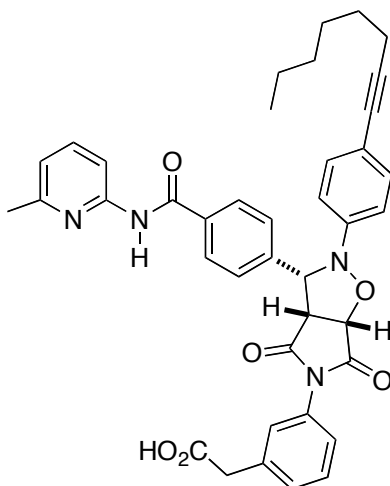
Template *trans*-122



In an NMR tube, nitrone **117** (8.78 mg, 16.0 μ mol) in CDCl_3 (400 μ L) was combined with a solution of maleimide **33** (4.62 mg, 16.0 μ mol). After 48 hours at 0 °C, the reaction showed

complete conversion of the starting materials and proved sufficiently pure for characterisation (*trans/cis* > 30:1). ¹H NMR (300.1 MHz, CDCl₃): δ_H 11.10 (s, 1H, NH), 8.38 (d, *J* = 8.4 Hz, 1H, Ar CH), 7.92 (d, *J* = 8.4 Hz, 2H, Ar CH), 7.75 (t, *J* = 8.0 Hz, 1H, Ar CH), 7.39 (d, *J* = 8.4 Hz, 2H, Ar CH), 7.32 (d, *J* = 8.4 Hz, 2H, Ar CH), 7.29 (d, *J* = 8.8 Hz, 2H, Ar CH), 7.10 (d, *J* = 8.8 Hz, 2H, Ar CH), 6.97 (d, *J* = 7.5 Hz, 1H, Ar CH), 6.71 (d, *J* = 8.3 Hz, 2H, Ar CH), 5.74 (s, 1H, CH), 4.97 (d, *J* = 7.4 Hz, 1H, CH), 3.90 (d, *J* = 7.4 Hz, 1H, CH), 3.74 (s, 2H, CH₂), 2.50 (s, 3H, CH₃), 2.37 (t, *J* = 7.0 Hz, 2H, CH₂), 1.62-1.51 (m, 2H, CH₂), 1.46-1.38 (m, 2H, CH₂), 1.37-1.18 (m, 4H, 2 × CH₂), 0.92-0.85 (m, 3H, CH₃). ¹³C NMR (75.5 MHz, CDCl₃): δ_C 176.8 (quat. C), 174.7 (quat. C), 173.2 (quat. C), 166.6 (quat. C), 155.8 (quat. C), 151.8 (quat. C), 147.9 (quat. C), 142.3 (quat. C), 140.6 (CH), 135.6 (quat. C), 133.9 (quat. C), 132.8 (CH), 130.8 (CH), 129.9 (quat. C), 129.0 (CH), 126.7 (CH), 126.2 (CH), 120.0 (CH), 119.0 (quat. C), 114.5 (CH), 113.4 (CH), 90.1 (quat. C), 80.0 (quat. C), 77.4 (CH), 68.9 (CH), 57.2 (CH), 40.3 (CH₂), 31.5 (CH₂), 28.9 (CH₂), 28.8 (CH₂), 22.7 (CH₂), 22.2 (CH₃), 19.6 (CH₂), 14.2 (CH₃). MS (ES⁺) *m/z* 671 (100%, [M+H]⁺). HRMS (ES⁺) calc. for C₄₀H₃₉N₄O₆ 671.2870, found 671.2863.

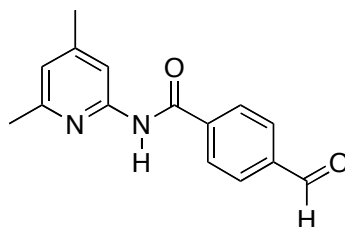
Template *cis*-126



In an NMR tube, nitron **117** (8.78 mg, 16.0 μmol) in CDCl₃ (400 μL) was combined with a solution of maleimide **120** (4.62 mg, 16.0 μmol). After 48 hours at 0 °C, the reaction showed complete conversion of the starting materials and proved sufficiently pure for characterisation (*cis/trans* > 50:1). ¹H NMR (300.1 MHz, CDCl₃): δ_H 11.32 (s, 1H, NH), 8.24 (d, *J* = 8.3 Hz, 1H, Ar CH), 8.00 (d, *J* = 8.5 Hz, 2H, Ar CH), 7.74 (dd, *J* = 8.3, 7.6 Hz, 1H, Ar CH), 7.63 (d, *J* = 8.3 Hz, 2H, Ar CH), 7.46 (s, 1H, Ar CH), 7.35 (t, *J* = 7.9 Hz, 1H, Ar CH), 7.26 (d, *J* = 8.9 Hz, 2H, Ar CH), 7.20 (d, *J* = 9.0 Hz, 1H, Ar CH), 7.15 (d, *J* = 8.1 Hz, 1H, Ar CH), 6.99 (d, *J* = 8.9 Hz, 2H, Ar CH), 6.96 (d, *J* = 7.6 Hz, 1H, Ar CH), 5.32 (d, *J* = 7.8 Hz, 1H, CH), 5.00 (d, *J* = 9.7 Hz, 1H, CH), 4.14 (dd, *J* = 9.8, 7.8 Hz, 1H, CH), 3.78 (d, *J* = 17.8 Hz, 1H, CH'H''), 3.73 (d, *J*

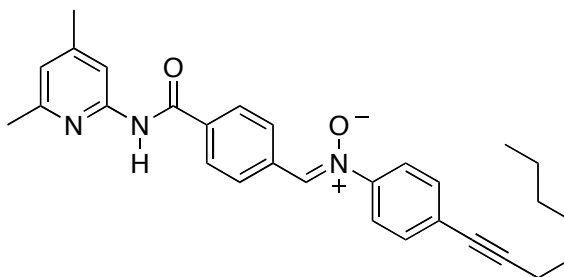
= 17.8 Hz, 1H, CH'H''), 2.49 (s, 3H, CH₃), 2.36 (t, *J* = 7.0 Hz, 2H, CH₂), 1.62-1.52 (m, 2H, CH₂), 1.47-1.37 (m, 2H, CH₂), 1.33-1.25 (m, 4H, 2 × CH₂), 0.91-0.86 (m, 3H, CH₃). ¹³C NMR (75.5 MHz, CDCl₃): δ_C 176.4 (quat. C), 173.4 (quat. C), 171.0 (quat. C), 167.2 (quat. C), 155.9 (quat. C), 151.7 (quat. C), 146.3 (quat. C), 140.4 (CH), 138.9 (quat. C), 135.6 (quat. C), 135.2 (quat. C), 132.2 (CH), 131.3 (quat. C), 130.0 (CH), 129.5 (CH), 129.0 (CH), 127.1 (CH), 126.7 (CH), 124.2 (CH), 120.2 (quat. C), 119.9 (CH), 117.9 (CH), 113.3 (CH), 90.6 (quat. C), 80.1 (quat. C), 77.4 (CH), 70.3 (CH) 54.7 (CH), 39.0 (CH₂), 31.5 (CH₂), 28.9 (CH₂), 28.7 (CH₂), 22.7 (CH₂), 22.2 (CH₃), 19.6 (CH₂), 14.2 (CH₃). MS (ES⁺) *m/z* 671 (100%, [M+H]⁺), 440 (18%), 241 (4%). HRMS (ES⁺) calc. for C₄₀H₃₉N₄O₆ 671.2870, found 671.2863.

***N*-(4,6-dimethylpyridin-2-yl)-4-formylbenzamide 132^[59]**



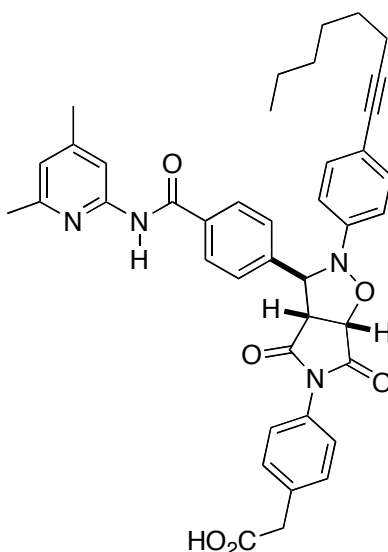
4-formylbenzoyl chloride (1.39 g, 8.25 mmol) was dissolved in dry DCM (15 mL) and triethylamine (1.01 g, 10.0 mmol) was added dropwise at 0 °C. A solution of 4,6-dimethyl-2-aminopyridine (1.22 g, 10.0 mmol) in dry DCM (15 mL) was added slowly over 2 hours and the reaction was left to stir overnight allowing to warm to room temperature. The mixture was then diluted with DCM (25 mL), extracted with saturated aqueous NH₄Cl solution (2 × 30 mL), the organic fraction was furthermore washed with saturated aqueous NaHCO₃ solution (2 × 30 mL) and H₂O (2 × 30 mL), dried over MgSO₄, filtered and concentrated *in vacuo*. The crude material was purified by column chromatography (SiO₂, Hexanes/EtOAc 3:1) to yield the desired product as a white solid (1.83 g, 87%). M.p.: 130.3 - 131.0 °C. ¹H NMR (300.1 MHz, CDCl₃): δ_H 10.09 (s, 1H, C(O)H), 8.79 (s, 1H, NH), 8.06 (d, *J* = 8.2 Hz, 2H, Ar CH), 8.02 (s, 1H, Ar CH), 7.98 (d, *J* = 8.2 Hz, 2H, Ar CH), 6.78 (s, 1H, Ar CH), 2.38 (s, 3H, CH₃), 2.36 (s, 3H, CH₃). ¹³C NMR (75.5 MHz, CDCl₃): δ_C 191.5 (C(O)H), 164.6 (quat. C), 156.6 (quat. C), 150.6 (quat. C), 150.5 (quat. C), 139.7 (quat. C), 138.7 (quat. C), 130.1 (CH), 128.0 (CH), 121.2 (CH), 112.0 (CH), 23.8 (CH₃), 21.5 (CH₃). MS (ES⁻) *m/z* 253 (100%, [M-H]⁻).

(Z)-N-(4-(4,6-dimethylpyridin-2-yl)carbamoyl)benzylidene)-4-(oct-1-ynyl)aniline oxide 116



N-(4-(oct-1-ynyl)phenyl) hydroxylamine (217 mg, 1.00 mmol) was dissolved in EtOH (5 mL) and 4-formyl-*N*-(4,6-dimethylpyridin-2-yl) benzamide (150 mg, 590 μ mol) was added neat. The solution was left to stand in the dark overnight before the precipitate was filtered to give the desired product as a light yellow solid (202 mg, 75%). M.p.: 157.0 - 158.0 $^{\circ}$ C. 1 H NMR (300.1 MHz, CDCl_3): δ_{H} 8.53 (s, 1H, NH), 8.50 (d, $J = 8.4$ Hz, 2H, Ar CH), 8.04 (s, 1H, Ar CH), 8.02 (d, $J = 8.8$ Hz, 2H, Ar CH), 8.00 (s, 1H, CH), 7.73 (d, $J = 8.8$ Hz, 2H, Ar CH), 7.50 (d, $J = 8.8$ Hz, 2H, Ar CH), 6.79 (s, 1H, Ar CH), 2.43 (s, 3H, CH_3), 2.43 (t, $J = 7.1$ Hz, 2H, CH_2), 2.37 (s, 3H, CH_3), 1.68-1.57 (m, 2H, CH_2), 1.53-1.40 (m, 2H, CH_2), 1.38-1.29 (m, 4H, $2 \times \text{CH}_2$), 0.94-0.88 (m, 3H, CH_3). ^{13}C NMR (75.5 MHz, CDCl_3): δ 164.7 (quat. C), 156.7 (quat. C), 150.8 (quat. C), 150.4 (quat. C), 147.7 (quat. C), 135.9 (quat. C), 133.9 (quat. C), 133.3 (CH), 132.5 (CH), 129.2 (CH), 127.6 (CH), 126.8 (quat. C), 121.7 (CH), 121.0 (CH), 111.8 (CH), 93.7 (quat. C), 79.6 (quat. C), 31.5 (CH_2), 28.8 (CH_2), 28.7 (CH_2), 24.0 (CH_3), 22.7 (CH_2), 21.5 (CH_3), 19.6 (CH_2), 14.2 (CH_3). MS (ES+) m/z 929 (50%), 476 (100%), 454 (100%, $[\text{M}+\text{H}]^+$). HRMS (ES+) calc. for $\text{C}_{29}\text{H}_{32}\text{N}_3\text{O}_2$ 454.2495, found 454.2489.

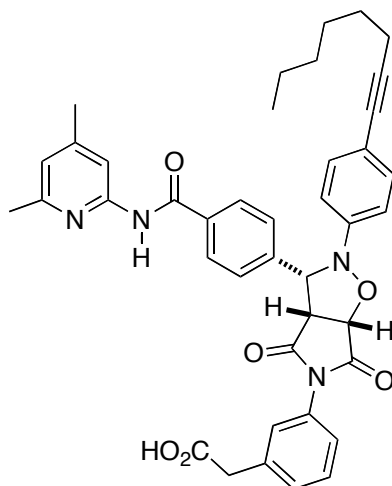
Template *trans*-121



In an NMR tube, nitron **116** (9.06 mg, 16.0 μ mol) in CDCl_3 (400 μ L) was combined with a solution of maleimide **33** (4.62 mg, 16.0 μ mol). After 48 hours at 0 $^{\circ}$ C, the reaction showed

complete conversion of the starting materials and proved sufficiently pure for characterisation (*trans/cis* > 30:1). ¹H NMR (300.1 MHz, CDCl₃): δ_H 11.20 (s, 1H, NH), 8.24 (s, 1H, Ar CH), 7.91 (d, *J* = 8.3 Hz, 2H, Ar CH), 7.38 (d, *J* = 8.3 Hz, 2H, Ar CH), 7.30 (d, *J* = 8.2 Hz, 2H, Ar CH), 7.29 (d, *J* = 8.7 Hz, 2H, Ar CH), 7.09 (d, *J* = 8.8 Hz, 2H, Ar CH), 6.80 (s, 1H, Ar CH), 6.70 (d, *J* = 8.3 Hz, 2H, Ar CH), 5.73 (s, 1H, CH), 4.95 (d, *J* = 7.4 Hz, 1H, CH), 3.89 (d, *J* = 7.4 Hz, 1H, CH), 3.70 (s, 2H, CH₂), 2.44 (s, 3H, CH₃), 2.40 (s, 3H, CH₃), 2.35 (t, *J* = 7.1 Hz, 2H, CH₂), 1.62-1.51 (m, 2H, CH₂), 1.46-1.38 (m, 2H, CH₂), 1.37-1.18 (m, 4H, 2 × CH₂), 0.92-0.85 (m, 3H, CH₃). ¹³C NMR (75.5 MHz, CDCl₃): δ_C 177.0 (quat. C), 174.7 (quat. C), 173.2 (quat. C), 166.6 (quat. C), 154.9 (quat. C), 152.7 (quat. C), 151.5 (quat. C), 147.9 (quat. C), 142.3 (quat. C), 135.9 (quat. C), 133.9 (quat. C), 132.8 (CH), 130.8 (CH), 129.9 (quat. C), 129.0 (CH), 126.7 (CH), 126.1 (CH), 121.2 (CH), 119.0 (quat. C), 114.5 (CH), 113.9 (CH), 90.1 (quat. C), 80.0 (quat. C), 77.4 (CH), 68.9 (CH), 57.2 (CH), 40.5 (CH₂), 31.5 (CH₂), 28.9 (CH₂), 28.8 (CH₂), 22.7 (CH₂), 21.7 (2 × CH₃), 19.6 (CH₂), 14.2 (CH₃). MS (ES⁺) *m/z* 685 (100%, [M+H]⁺). HRMS (ES⁺) calc. for C₄₁H₄₁N₄O₆ 685.3026, found 685.3036.

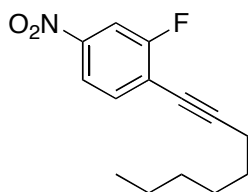
Template *cis*-125



In an NMR tube, nitrone **116** (9.06 mg, 16.0 μmol) in CDCl₃ (400 μL) was combined with a solution of maleimide **120** (4.62 mg, 16.0 μmol). After 48 hours at 0 °C, the reaction showed complete conversion of the starting materials and proved sufficiently pure for characterisation (*cis/trans* > 50:1). ¹H NMR (400.1 MHz, CDCl₃): δ_H 11.37 (s, 1H, NH), 8.08 (s, 1H, Ar CH), 8.00 (d, *J* = 8.4 Hz, 2H, Ar CH), 7.63 (d, *J* = 8.3 Hz, 2H, Ar CH), 7.46 (s, 1H, Ar CH), 7.35 (d, *J* = 7.8 Hz, 1H, Ar CH), 7.27 (d, *J* = 8.8 Hz, 2H, Ar CH), 7.19 (d, *J* = 7.6 Hz, 1H, Ar CH), 7.15 (d, *J* = 7.6 Hz, 1H, Ar CH), 6.99 (d, *J* = 8.8 Hz, 2H, Ar CH), 6.79 (s, 1H, Ar CH), 5.32 (d, *J* = 7.8 Hz, 1H, CH), 5.00 (d, *J* = 7.8 Hz, 1H, CH), 4.13 (dd, *J* = 9.7, 7.8 Hz, 1H, CH), 3.77 (d, *J* = 17.8 Hz, 1H, CH'H''), 3.71 (d, *J* = 17.8 Hz, 1H, CH'H''), 2.44 (s, 3H, CH₃), 2.39 (s, 3H, CH₃),

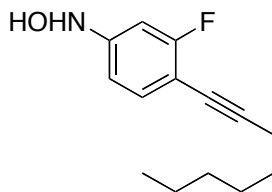
2.36 (t, $J = 7.1$ Hz, 2H, CH₂), 1.60-1.53 (m, 2H, CH₂), 1.46-1.38 (m, 2H, CH₂), 1.34-1.27 (m, 4H, 2 × CH₃), 0.91-0.86 (m, 3H, CH₃). ¹³C NMR (100.6 MHz, CDCl₃): δ_C 176.6 (quat. C), 173.4 (quat. C), 171.0 (quat. C), 167.3 (quat. C), 155.1 (quat. C), 152.5 (quat. C), 151.4 (quat. C), 146.4 (quat. C), 138.9 (quat. C), 135.7 (quat. C), 135.4 (quat. C), 132.2 (CH), 131.2 (quat. C), 130.0 (CH), 129.5 (CH), 129.0 (CH), 127.1 (CH), 126.8 (CH), 124.2 (CH), 121.1 (CH), 120.2 (quat. C), 117.8 (CH), 113.8 (CH), 90.5 (quat. C), 80.1 (quat. C), 77.4 (CH), 70.3 (CH), 54.7 (CH), 39.2 (CH₂), 31.5 (CH₂), 28.9 (CH₂), 28.7 (CH₂), 22.7 (CH₂), 21.9 (CH₃), 21.7 (CH₃), 19.6 (CH₂), 14.2 (CH₃). MS (ES⁺) m/z 685 (100%, [M+H]⁺). HRMS (ES⁺) calc. for C₄₁H₄₁N₄O₆ 685.3026, found 685.3019.

Synthesis of 2-fluoro-4-nitro-1-(oct-1-yn-1-yl)benzene 144



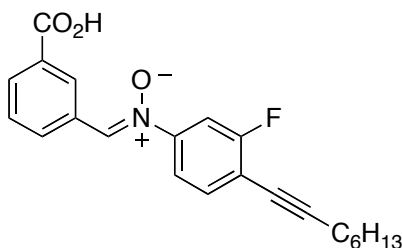
1-bromo-2-fluoro-4-nitrobenzene (1.32 mg, 6.00 mmol) was suspended in Et₃N (60 mL). Triphenylphosphine (168 mg, 644 μmol), copper iodide (98.0 mg, 516 μmol) and dichlorobis(triphenylphosphine)palladium (225 mg, 320 μmol) were added and the mixture was degassed with argon for 30 min. 1-Octyne (992 mg, 9.00 mmol) was added *via* syringe under a protective argon atmosphere and the mixture was stirred for two days at 85 °C. After cooling to room temperature, the brown solution was filtered through celite, concentrated and purified by column chromatography over silica using hexane as eluent to obtain the desired product as a dark yellow liquid (1.41 g, 94%). ¹H NMR (400.1 MHz, CDCl₃): δ_H 7.97 (ddd, $J = 8.5, 2.3, 0.8$ Hz, 1H, Ar CH), 7.93 (dd, $J = 8.8, 2.2$ Hz, 1H, Ar CH), 7.53 (dd, $J = 8.5, 7.0$ Hz, 1H, Ar CH), 2.49 (t, $J = 7.1$ Hz, 2H, CH₂), 1.67-1.60 (m, 2H, CH₂), 1.50-1.43 (m, 2H, CH₂), 1.35-1.30 (m, 4H, 2 × CH₂), 0.92-0.89 (m, 3H, CH₃). ¹³C NMR (100.6 MHz, CDCl₃): δ 162.4 (d, $J = 254.7$ Hz, quat. C), 147.3 (d, $J = 8.2$ Hz, quat. C), 134.0 (d, $J = 2.0$ Hz, CH), 120.1 (d, $J = 16.4$ Hz, quat. C), 119.2 (d, $J = 3.7$ Hz, CH), 111.4 (d, $J = 26.4$ Hz, CH), 102.5 (d, $J = 3.6$ Hz, quat. C), 73.0 (quat. C), 31.4 (CH₂), 28.7 (CH₂), 28.4 (CH₂), 22.7 (CH₂), 19.9 (CH₂), 14.2 (CH₃). ¹⁹F NMR (376.5 MHz, CDCl₃): δ_F -107.3. MS (ES⁺) m/z 250 (100%, [M+H]⁺), 251 (15%). HRMS (ES⁺) calc. for C₁₄H₁₇NO₂F 250.1243, found 250.1242.

Synthesis of *N*-(3-fluoro-4-(oct-1-yn-1-yl)phenyl)hydroxylamine 145



2-fluoro-4-nitro-1-(oct-1-yn-1-yl)benzene (498 mg, 2.00 mmol) was dissolved in THF (20 mL). Rhodium (50 mg, 5 wt.-% on carbon, wet) and hydrazine monohydrate (129 mg, 2.58 mmol) were added and the reaction was followed by tlc (Hex:EtOAc, 3:2). After completion, the solution was filtered through celite and concentrated *in vacuo* to obtain the desired intermediate product as a dark brown liquid, which was directly used in the next step without further purification. ^1H NMR (400.1 MHz, CDCl_3): δ_{H} 7.26 (d, $J = 8.1$ Hz, 1H, Ar CH), 6.80 (s, 1H, N(OH)H), 6.75 (dd, $J = 11.0, 2.1$ Hz, 1H, Ar CH), 6.62 (dd, $J = 8.4, 2.1$ Hz, 1H, Ar CH), 5.17 (d, $J = 2.2$ Hz, 1H, N(H)OH), 2.42 (t, $J = 7.1$ Hz, 2H, CH_2), 1.62 (m, 2H, CH_2), 1.49-1.42 (m, 2H, CH_2), 1.32 (m, 4H, $2 \times \text{CH}_2$), 0.90 (m, 3H, CH_3). ^{19}F NMR (376.5 MHz, CDCl_3): δ_{F} -110.2.

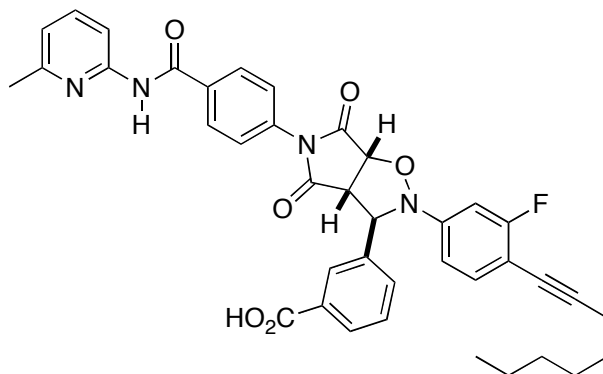
Synthesis of (*Z*)-*N*-(3-carboxybenzylidene)-3-fluoro-4-(oct-1-yn-1-yl)aniline oxide 141



Crude *N*-(3-fluoro-4-(oct-1-yn-1-yl)phenyl)hydroxylamine (2.00 mmol) was dissolved in EtOH (10 mL) and 3-carboxybenzaldehyde (270 mg, 1.80 mmol) was added neat. The solution was left to stand in the freezer for three days. The occurring precipitate was filtered, washed with copious amounts of hexanes to yield the desired compound as a white solid (289 mg, 44% over two steps). M.p.: 185.4 - 185.8 °C. ^1H NMR (300.1 MHz, $\text{d}_6\text{-DMSO}$): δ_{H} 9.10 (s, 1H, Ar CH), 8.75 (s, 1H, CH), 8.70 (d, $J = 8.1$ Hz, 1H, Ar CH), 8.05 (dt, $J = 7.8, 1.4$ Hz, 1H, Ar CH), 7.97 (dd, $J = 10.4, 2.2$ Hz, 1H, Ar CH), 7.84 (dd, $J = 8.5, 2.3$ Hz, 1H, Ar CH), 7.64 (t, $J = 8.0$ Hz, 2H, Ar CH), 2.50 (t, $J = 6.9$ Hz, 2H, CH_2), 1.61-1.51 (m, 2H, CH_2), 1.48-1.37 (m, 2H, CH_2), 1.35-1.24 (m, 4H, $2 \times \text{CH}_2$), 0.90-0.85 (m, 3H, CH_3). ^{13}C NMR (75.5 MHz, $\text{d}_6\text{-DMSO}$): δ 166.9 (quat. C), 161.6 (d, $J = 249.4$ Hz, quat. C), 148.2 (d, $J = 8.6$ Hz, quat. C), 133.7 (d, $J = 1.8$ Hz, CH), 133.6 (CH), 132.9 (CH), 131.4 (CH), 131.08 (quat. C), 131.05 (quat. C), 130.1 (CH), 128.9 (CH), 117.5 (d, $J = 3.4$ Hz, CH), 113.1 (d, $J = 16.3$ Hz, quat. C), 109.4 (d, $J = 26.3$ Hz, CH), 98.6 (d, $J = 3.2$ Hz, quat. C), 73.1 (quat. C), 30.7 (CH_2), 27.9 (CH_2), 27.8 (CH_2), 22.0 (CH_2), 18.9

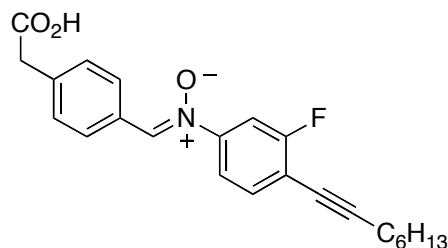
(CH₂), 13.9 (CH₃). ¹⁹F NMR (282 MHz, d₆-DMSO): δ_F -109.9. MS (ES⁻) *m/z* 366 (100%, [M-H]⁻). HRMS (ES⁺) calc. for C₂₂H₂₁NO₃F 366.1505, found 366.1515.

Template *trans*-161



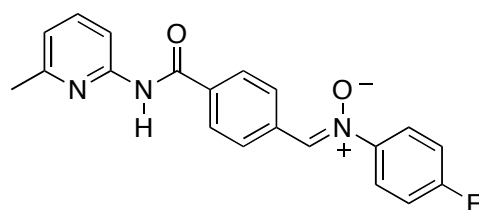
In an NMR tube, maleimide **66** (4.92 mg, 16.0 μmol) in CDCl₃ (400 μL) was combined with a solution of nitrone **141** (5.86 mg, 16.0 μmol) in CDCl₃ (400 μmol). After 48 hours at 0 °C, the reaction showed complete conversion of the starting materials and proved sufficiently pure for characterisation (*trans/cis* > 15:1). ¹H NMR (400.1 MHz, d₆-DMSO): δ_H 10.86 (s, 1H, NH), 8.12 (s, 1H, Ar CH), 8.05 (d, *J* = 8.5 Hz, 2H, Ar CH), 8.00 (d, *J* = 8.2 Hz, 1H, Ar CH), 7.91 (d, *J* = 7.7 Hz, 1H, Ar CH), 7.77 (d, *J* = 8.0 Hz, 1H, Ar CH), 7.73 (t, *J* = 7.9 Hz, 1H, Ar CH), 7.56 (t, *J* = 7.7 Hz, 1H, Ar CH), 7.33 (t, *J* = 8.3 Hz, 1H, Ar CH), 7.15 (dd, *J* = 11.8, 2.1 Hz, 1H, Ar CH), 7.04 (d, *J* = 7.9 Hz, 2H, Ar CH), 6.91 (d, *J* = 8.5 Hz, 2H, Ar CH), 6.10 (s, 1H, CH), 5.49 (d, *J* = 7.3 Hz, 1H, CH), 4.20 (d, *J* = 7.4 Hz, 1H, CH), 2.45 (s, 3H, CH₃), 2.41 (t, *J* = 6.9 Hz, 2H, CH₂), 1.55-1.46 (m, 2H, CH₂), 1.43-1.34 (m, 2H, CH₂), 1.26-1.20 (m, 4H, 2 × CH₂), 0.84-0.78 (m, 3H, CH₃). ¹³C NMR (100.6 MHz, d₆-DMSO): δ_C 173.8 (quat. C), 172.7 (quat. C), 166.8 (quat. C), 166.1 (d, *J* = 203.6 Hz, quat. C), 163.6 (quat. C), 156.5 (quat. C), 151.4 (quat. C), 149.8 (d, *J* = 9.6 Hz, quat. C), 139.0 (quat. C), 138.5 (CH), 134.4 (quat. C), 134.1 (quat. C), 133.9 (d, *J* = 1.9 Hz, CH), 131.4 (CH), 131.1 (quat. C), 129.1 (CH), 128.9 (CH), 128.7 (CH), 128.0 (CH), 125.8 (CH), 119.2 (CH), 111.6 (CH), 110.6 (d, *J* = 2.1 Hz, CH), 105.0 (d, *J* = 16.1 Hz, quat. C), 102.0 (d, *J* = 26.9 Hz, CH), 95.1 (d, *J* = 2.8 Hz, quat. C), 77.9 (CH), 73.4 (quat. C), 67.9 (CH), 56.4 (CH), 30.7 (CH₂), 28.0 (CH₂), 27.8 (CH₂), 23.5 (CH₃), 22.0 (CH₂), 18.8 (CH₂), 13.8 (CH₃). ¹⁹F NMR (375.5 MHz, d₆-DMSO): δ_F -110.3. MS (ES⁺) *m/z* 675 (40%, [M+H]⁺), 308 (100%). HRMS (ES⁺) calc. for C₃₉H₃₆N₄O₆F 675.2619, found 675.2643.

(Z)-N-(4-(carboxymethyl)benzylidene)-3-fluoro-4-(oct-1-yn-1-yl)aniline oxide 142



Crude *N*-(3-fluoro-4-(oct-1-yn-1-yl)phenyl)hydroxyl-amine (2.00 mmol) was dissolved in EtOH (10 mL) and 2-(4-formylphenyl)acetic acid (295 mg, 1.80 mmol) was added neat. The solution was left to stand in the freezer for three days. The occurring precipitate was filtered, washed with copious amounts of hexanes to yield the desired compound as a yellow solid (330 mg, 48% over two steps). M.p.: 159.9 - 160.3 °C. ¹H NMR (400.1 MHz, CDCl₃): δ_H 8.26 (d, *J* = 8.3 Hz, 2H, Ar CH), 7.93 (s, 1H, CH), 7.58 (dd, *J* = 9.5, 1.6 Hz, 1H, Ar CH), 7.51-7.44 (m, 2H, Ar CH), 7.33 (d, *J* = 8.3 Hz, 2H, Ar CH), 3.63 (s, 2H, CH₂), 2.47 (t, *J* = 7.1 Hz, 2H, CH₂), 1.74-1.57 (m, 2H, CH₂), 1.54-1.41 (m, 2H, CH₂), 1.41-1.28 (m, 4H, 2 × CH₂), 0.99-0.82 (m, 3H, CH₃). ¹³C NMR (100.6 MHz, CDCl₃): δ_C 174.7 (quat. C), 162.7 (d, *J* = 253.0 Hz, quat. C), 148.1 (d, *J* = 8.4 Hz, quat. C), 138.1 (quat. C), 136.6 (CH), 133.9 (d, *J* = 2.2 Hz, CH), 130.1 (CH), 129.8 (CH), 128.9 (quat. C), 117.0 (d, *J* = 3.6 Hz, CH), 115.0 (d, *J* = 16.3 Hz, quat. C), 110.0 (d, *J* = 26.2 Hz, CH), 99.0 (d, *J* = 3.2 Hz, quat. C), 73.1 (quat. C), 41.5 (CH₂), 31.5 (CH₂), 28.7 (CH₂), 28.5 (CH₂), 22.7 (CH₂), 19.8 (CH₂), 14.2 (CH₃). MS (ES⁺) *m/z* 763 (15%), 404 (33%), 382 (100%, [M + H]⁺). HRMS (ES⁺) calc. for C₂₃H₂₅NO₃F 382.1818, found 382.1813.

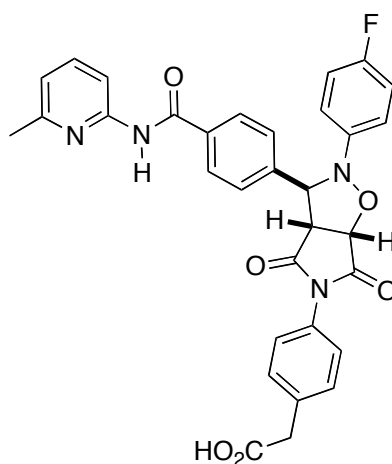
(Z)-4-fluoro-N-(4-(6-methylpyridin-2-yl)carbamoyl)benzylidene)aniline oxide 55



1-Fluoro-4-nitrobenzene (1.13 g, 8.00 mmol) was dissolved in EtOH (40 mL) and H₂O (12 mL). Bismuth trichloride (505 mg, 1.60 mmol) was added and potassium borohydride (518 mg, 9.60 mmol) was slowly added over a period of 5 minutes. After complete addition, the reaction mixture was stirred for 15 minutes, neutralised with 0.5M HCl and extracted into Et₂O (2 × 40 mL). The combined organic layers were washed with brine, dried over MgSO₄, filtered and the volume was reduced *in vacuo*. The crude product was dissolved in EtOH (15 mL) and reacted with 4-formyl-*N*-(6-methylpyridin-2-yl)benzamide (1.44 g, 6.00 mmol) in EtOH (15 mL). The solution was stirred overnight and kept in the freezer for

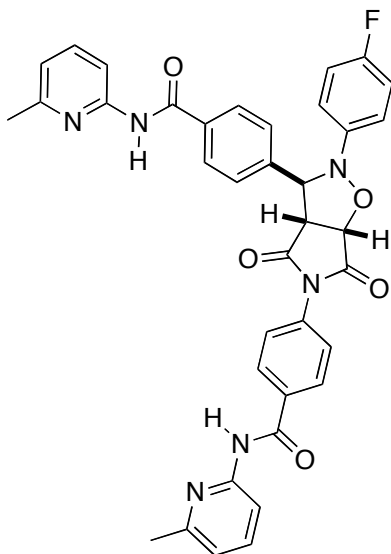
another night. Filtration of the occurring precipitate yielded pure product (964 mg, 46%). M.p.: 219.9 - 221.0 °C (lit.^[197] 217.2 – 218.3 °C). ¹H NMR (300.1 MHz, CDCl₃): δ_H 8.60 (s, 1H, NH), 8.49 (d, *J* = 8.5 Hz, 2H, Ar CH), 8.19 (d, *J* = 8.2 Hz, 1H, Ar CH), 8.03 (d, *J* = 8.6 Hz, 2H, Ar CH), 7.97 (s, 1H, CH), 7.83-7.78 (m, 2H, Ar CH), 7.67 (t, *J* = 7.9 Hz, 1H, Ar CH), 7.22-7.16 (m, 2H, Ar CH), 6.96 (d, *J* = 7.5 Hz, 1H, Ar CH), 2.49 (s, 3H, CH₃). ¹³C NMR (75.5 MHz, CDCl₃): δ_C 164.6 (quat. C), 163.5 (d, *J* = 251.5 Hz, quat. C), 157.1 (quat. C), 150.7 (quat. C), 145.3 (d, *J* = 3.1 Hz, quat. C), 139.0 (CH), 135.9 (quat. C), 133.9 (quat. C), 133.4 (CH), 129.2 (CH), 127.7 (CH), 123.9 (d, *J* = 8.9 Hz, CH), 119.8 (CH), 116.3 (d, *J* = 23.3 Hz, CH), 111.2 (CH), 24.1 (CH₃). ¹⁹F NMR (CDCl₃, 376.5 MHz) = δ_F -110.1. MS (ES+) *m/z* 372 (100%, [M+Na]⁺).

Template *trans*-59b^[197]



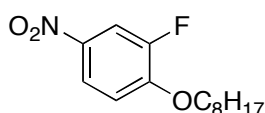
Maleimide **33** (13.9 mg, 48.0 μmol) in CDCl₃ (1.20 mL) was combined with a solution of nitrene **55** (20.9 mg, 48.0 μmol) in CDCl₃ (1.20 mL). After 48 hours at room temperature the solvent was removed, the remaining solid was washed intensively with hexanes, dried and was found to be sufficiently pure for characterisation (*trans/cis* > 50:1). ¹H NMR (400.1 MHz, CDCl₃): δ_H 11.11 (s, 1H, NH), 8.37 (d, *J* = 8.4 Hz, 1H, Ar CH), 7.91 (d, *J* = 8.5 Hz, 2H, Ar CH), 7.75 (dd, *J* = 8.4, 7.6 Hz, 1H, Ar CH), 7.36 (dd, *J* = 8.2, 5.9 Hz, 4H, 2 × Ar CH), 7.15-7.11 (m, 2H, Ar CH), 6.99-6.94 (m, 3H, Ar CH), 6.83 (d, *J* = 8.5 Hz, 2H, Ar CH), 5.67 (s, 1H, CH), 5.00 (d, *J* = 7.3 Hz, 1H, CH), 3.92 (d, *J* = 7.6 Hz, 1H, CH), 3.76 (s, 2H, CH₂), 2.51 (s, 3H, CH₃). ¹³C NMR (75.5 MHz, d₆-DMSO): δ_C 174.3 (quat. C), 173.2 (quat. C), 172.4 (quat. C), 165.4 (quat. C), 157.9 (d, *J* = 238.9 Hz, quat. C), 156.6 (quat. C), 151.5 (quat. C), 145.0 (d, *J* = 2.2 Hz, quat. C), 142.5 (quat. C), 138.4 (CH), 135.8 (quat. C), 133.6 (quat. C), 129.9 (CH), 129.9 (quat. C), 128.3 (CH), 127.1 (CH), 126.0 (CH), 119.1 (CH), 116.3 (d, *J* = 7.7 Hz, CH), 115.6 (d, *J* = 22.5 Hz, CH), 111.7 (CH), 77.7 (CH), 68.5 (CH), 56.4 (CH), 39.7 (CH₂), 23.6 (CH₃). ¹⁹F NMR (CDCl₃, 376.5 MHz) = δ_F -122.1. MS (ES+) *m/z* 581 (100%, [M+H]⁺).

Template *trans*-69



A solution of maleimide **66** (103 mg, 500 μmol) and nitrone **55** (125 mg, 500 μmol) in CHCl_3 (8 mL) was stirred for three days at room temperature in the absence of light. After evaporation of the solvent, the crude mixture of isomers was purified by column chromatography (SiO_2 ; Hex:EtOAc, 3:1) to give pure *trans*-isomer product (115 mg, 50%). ^1H NMR (400.1 MHz, CDCl_3): δ_{H} 8.71 (s, 1H, NH), 8.67 (s, 1H, NH), 8.16 (t, $J = 8.0$ Hz, 2H, Ar CH), 7.97-7.93 (m, 4H, Ar CH), 7.67-7.61 (m, 4H, Ar CH), 7.11-7.06 (m, 2H, Ar CH), 6.99-6.91 (m, 6H, Ar CH), 5.68 (s, 1H, CH), 5.17 (d, $J = 7.6$ Hz, 1H, CH), 4.05 (d, $J = 7.6$ Hz, 1H, CH), 2.46 (s, 3H, CH_3), 2.45 (s, 3H, CH_3). ^{13}C NMR (100.6 MHz, CDCl_3): δ_{C} 173.5 (quat. C), 172.0 (quat. C), 165.0 (quat. C), 164.5 (quat. C), 159.1 (d, $J = 243.5$ Hz, quat. C), 157.1 (quat. C), 157.0 (quat. C), 150.8 (quat. C), 150.7 (quat. C), 144.2 (d, $J = 2.7$ Hz, quat. C), 142.1 (quat. C), 139.1 (CH), 139.0 (CH), 134.9 (quat. C), 134.5 (quat. C), 134.1 (quat. C), 128.2 (CH), 128.1 (CH), 127.4 (CH), 126.2 (CH), 119.8 (d, $J = 6.2$ Hz, CH), 116.7 (CH), 116.7 (CH), 116.2 (d, $J = 22.6$ Hz, CH), 111.2 (CH), 111.2 (CH), 77.1 (CH), 70.3 (CH), 57.3 (CH), 24.0 (CH_3 , 2C). ^{19}F NMR (376.5 MHz, CDCl_3): δ_{F} -120.3. MS (ES+) m/z 657 (100%, $[\text{M}+\text{H}]^+$). HRMS (ES+) calc. for $\text{C}_{37}\text{H}_{30}\text{N}_6\text{O}_5\text{F}$ 657.2262, found 657.2260.

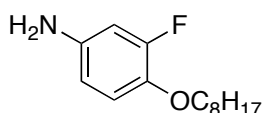
Synthesis of 2-fluoro-4-nitro-1-(octyloxy)benzene **158**^[224]



2-fluoro-4-nitrophenol (5.00 g, 31.8 mmol) was dissolved in acetone (250 mL). To this mixture was then added neat K_2CO_3 (8.81 g, 63.6 mmol) and bromooctane (6.59 mL, 38.2 mmol) *via* syringe. The solution was refluxed at 60 $^\circ\text{C}$ overnight while kept under a nitrogen atmosphere. After cooling to room temperature, the solution was poured into water

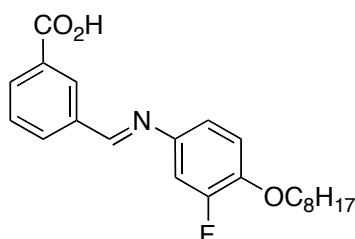
(300 mL), acidified with 3M HCl until disappearance of the yellow colour and extracted into DCM (3 x 100 mL). The combined organic layers were dried over MgSO₄, filtered and concentrated. The residue was redissolved in hexanes and all solids were filtered off. The resulting solution was concentrated and the obtained oil was purified by column chromatography (Hex:EtOAc, 20:1) to yield the desired product as a light yellow liquid (7.04 g, 82%). ¹H NMR (300.1 MHz, CDCl₃): δ_H 8.03 (ddd, *J* = 9.0, 2.7, 1.4 Hz, 1H, Ar CH), 7.97 (dd, *J* = 10.7, 2.7 Hz, 1H, Ar CH), 7.01 (t, *J* = 8.5 Hz, 1H, Ar CH), 4.12 (t, *J* = 6.6 Hz, 2H, CH₂), 1.91-1.80 (m, 2H, CH₂), 1.52-1.42 (m, 2H, CH₂), 1.38-1.23 (m, 8H, 4 x CH₂), 0.90-0.86 (m, 3H, CH₃). ¹³C NMR (75.5 MHz, CDCl₃): δ 153.2 (d, *J* = 10.6 Hz, quat. C), 151.5 (d, *J* = 251.3 Hz, quat. C), 140.7 (d, *J* = 7.2 Hz, quat. C), 121.0 (d, *J* = 3.4 Hz, CH), 113.0 (d, *J* = 2.4 Hz, CH), 112.4 (d, *J* = 22.9 Hz, CH), 70.1 (CH₂), 31.9 (CH₂), 29.4 (CH₂), 29.3 (CH₂), 29.0 (CH₂), 25.9 (CH₂), 22.8 (CH₂), 14.2 (CH₃). ¹⁹F NMR (282 MHz, CDCl₃): δ -131.0. MS (ES+) *m/z* 292 (100%, [M+Na]⁺).

Synthesis of 3-fluoro-4-(octyloxy)aniline 155



2-fluoro-4-nitro-1-(octyloxy)benzene (700 mg, 2.60 mmol) was dissolved in EtOH (30 mL). Palladium (70 mg, 10 wt.-% on carbon, dry) was added carefully. The solution was purged with hydrogen and kept under a hydrogen atmosphere overnight using hydrogen filled balloons. The following day, the solution was filtered through celite and concentrated *in vacuo* to yield the desired product in sufficient quality for further conversion. ¹H NMR (400.1 MHz, CDCl₃): δ_H 6.79 (t, *J* = 8.9 Hz, 1H, Ar CH), 6.46 (dd, *J* = 12.6, 2.7 Hz, 1H, Ar CH), 6.37 (ddd, *J* = 8.6, 2.7, 1.3 Hz, 1H, Ar CH), 3.93 (t, *J* = 6.7 Hz, 2H, CH₂), 3.56 (s, 2H, 2 x NH), 1.80-1.69 (m, 2H, CH₂), 1.47-1.40 (m, 2H, CH₂), 1.36-1.24 (m, 8H, 4 x CH₂), 0.91-0.84 (m, 3H, CH₃). ¹⁹F NMR (282 MHz, CDCl₃): δ_F -133.2.

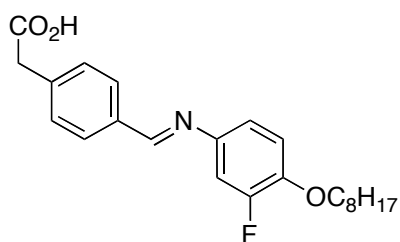
Synthesis of (E)-3-(((3-fluoro-4-(octyloxy)phenyl)imino)methyl)benzoic acid 151



Crude 3-fluoro-4-(octyloxy)aniline (264 mg, 1.10 mmol) was dissolved in a minimum amount of EtOH (4 mL). 3-carboxybenzaldehyde (166 mg, 1.10 mmol) was added neat and the

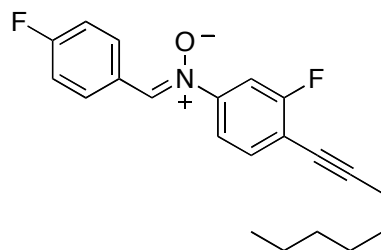
solution was sonicated and left to stand in the dark overnight. The resulting precipitate was filtered, washed with hexanes and dried to give the desired imine as a white solid (245 mg, 60% over two steps). M.p.: 143.0 - 143.5 °C. ¹H NMR (400.1 MHz, CDCl₃): δ_H 8.59 (s, 1H, CH), 8.53 (s, 1H, Ar CH), 8.23-8.19 (m, 2H, Ar CH), 7.60 (t, *J* = 7.7 Hz, 1H, Ar CH), 7.11 (dd, *J* = 12.2, 2.4 Hz, 1H, Ar CH), 7.05 (dd, *J* = 9.0, 2.2 Hz, 1H, Ar CH), 6.99 (t, *J* = 8.6 Hz, 1H, Ar CH), 4.06 (t, *J* = 6.6 Hz, 2H, CH₂), 1.83-1.79 (m, 2H, CH₂), 1.53-1.46 (m, 2H, CH₂), 1.38-1.30 (m, 8H, 4 × CH₂), 0.92-0.86 (m, 3H, CH₃). ¹³C NMR (75.5 MHz, CDCl₃): δ_C 171.4 (quat. C), 157.9 (CH), 153.1 (d, *J* = 247.1 Hz, quat. C), 146.3 (d, *J* = 11.1 Hz, quat. C), 144.4 (d, *J* = 7.2 Hz, quat. C), 136.7 (quat. C), 133.4 (CH), 132.9 (CH), 131.0 (CH), 130.2 (quat. C), 129.2 (CH), 117.5 (d, *J* = 3.2 Hz, CH), 115.2 (d, *J* = 2.8 Hz, CH), 109.3 (d, *J* = 19.5 Hz, CH), 69.9 (CH₂), 32.0 (CH₂), 29.5 (CH₂), 29.4 (CH₂), 29.4 (CH₂), 26.1 (CH₂), 22.8 (CH₂), 14.25 (CH₃). ¹⁹F NMR (282 MHz, CDCl₃): δ -133.4. MS (ES+) *m/z* 372 (100%, [M+H]⁺). HRMS (ES+) calc. for C₂₂H₂₇NO₃F 372.1975, found 372.1974.

Synthesis of (*E*)-2-(4-(((3-fluoro-4-(octyloxy)phenyl)imino)methyl)phenyl)acetic acid 152



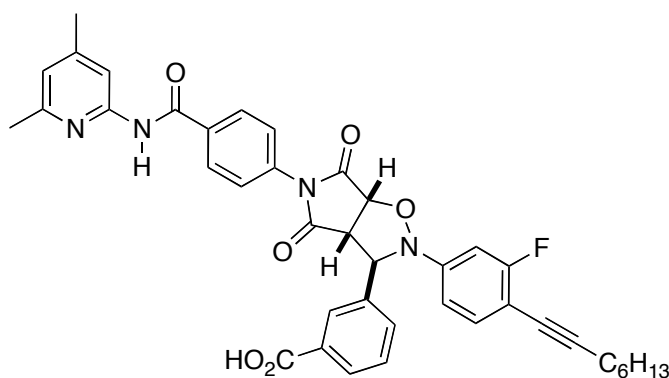
Crude 3-fluoro-4-(octyloxy)aniline (264 mg, 1.10 mmol) was dissolved in a minimum amount of EtOH (4 mL). 2-(4-formylphenyl)acetic acid (166 mg, 1.10 mmol) was added neat and the solution was sonicated and left to stand in the dark overnight. The resulting precipitate was filtered, washed with hexanes and dried to give the desired imine as a white solid (223 mg, 53% over two steps). M.p.: 130.8 - 131.5 °C. ¹H NMR (400.1 MHz, CDCl₃): δ_H 8.46 (s, 1H, CH), 7.88 (d, *J* = 8.1 Hz, 2H, Ar CH), 7.42 (d, *J* = 8.1 Hz, 2H, Ar CH), 7.09 (dd, *J* = 6.1, 2.1 Hz, 1H, Ar CH), 7.05-6.98 (m, 2H, Ar CH), 4.07 (t, *J* = 6.6 Hz, 2H, CH₂), 3.75 (s, 2H, CH₂), 1.90-1.81 (m, 2H, CH₂), 1.55-1.45 (m, 2H, CH₂), 1.41-1.32 (m, 8H, 4 × CH₂), 0.94-0.89 (m, 3H, CH₃). ¹³C NMR (75.5 MHz, CDCl₃): δ_C 176.7 (quat. C), 159.1 (CH), 153.0 (d, *J* = 246.9 Hz, quat. C), 146.0 (d, *J* = 11.1 Hz, quat. C), 144.9 (d, *J* = 7.1 Hz, quat. C), 136.9 (quat. C), 135.24 (quat. C), 130.0 (CH), 129.2 (CH), 117.3 (d, *J* = 3.2 Hz, CH), 115.3 (d, *J* = 2.8 Hz, CH), 109.2 (d, *J* = 19.6 Hz, CH), 70.0 (CH₂), 41.2 (CH₂), 32.0 (CH₂), 29.5 (CH₂), 29.4 (CH₂), 29.4 (CH₂), 26.1 (CH₂), 22.8 (CH₂), 14.2 (CH₃). ¹⁹F NMR (282 MHz, CDCl₃): δ_F -133.5. MS (ES+) *m/z* 386 (100%, [M+H]⁺). HRMS (ES+) calc. for C₂₃H₂₉NO₃F 386.2131, found 386.2129.

Synthesis of (Z)-3-fluoro-N-(4-fluorobenzylidene)-4-(oct-1-yn-1-yl)aniline oxide 150



Crude *N*-(3-fluoro-4-(oct-1-yn-1-yl)phenyl)hydroxyl-amine (2.00 mmol) was dissolved in EtOH (10 mL) and 4-fluorobenzaldehyde (223 mg, 1.80 mmol) was added neat. The solution was left to stand in the freezer for three days. The occurring precipitate was filtered, washed with copious amounts of hexanes to yield the desired compound as a white solid (376 mg, 61% over two steps). M.p.: 99.1 - 99.5 °C. ¹H NMR (300.1 MHz, CDCl₃): δ_H 8.44 (dd, *J* = 8.9, 5.6 Hz, 2H, Ar CH), 7.90 (s, 1H, CH), 7.60-7.56 (m, 1H, Ar CH), 7.52-7.45 (m, 2H, Ar CH), 7.17 (d, *J* = 8.7 Hz, 2H, Ar CH), 2.47 (t, *J* = 7.0 Hz, 2H, CH₂), 1.68-1.59 (m, 2H, CH₂), 1.51-1.42 (m, 2H, CH₂), 1.37-1.30 (m, 4H, 2 × CH₂), 0.92-0.87 (m, *J* = 7.6 Hz, 3H, CH₃). ¹³C NMR (75.5 MHz, CDCl₃): δ_C 164.2 (d, *J* = 254.5 Hz, quat. C), 162.9 (d, *J* = 253.1 Hz, quat. C), 148.5 (d, *J* = 8.2 Hz, quat. C), 133.9 (d, *J* = 2.2 Hz, CH), 133.5 (s, CH), 131.7 (d, *J* = 8.4 Hz, CH), 126.9 (d, *J* = 3.3 Hz, quat. C), 116.8 (d, *J* = 3.7 Hz, CH), 116.1 (d, *J* = 21.9 Hz, CH), 114.9 (d, *J* = 16.4 Hz, quat. C), 109.8 (d, *J* = 26.1 Hz, CH), 99.0 (d, *J* = 3.4 Hz, quat. C), 73.1 (quat. C), 31.5 (CH₂), 28.7 (CH₂), 28.5 (CH₂), 22.7 (CH₂), 19.8 (CH₂), 14.18 (CH₃). ¹⁹F NMR (282 MHz, CDCl₃): δ_F -106.3, -108.2. MS (ES⁺) *m/z* 364 (100%, [M+Na]⁺), 365 (8%), 705 (28%). HRMS (ES⁺) calc. for C₂₁H₂₁NOF₂Na 364.1489, found 364.1484.

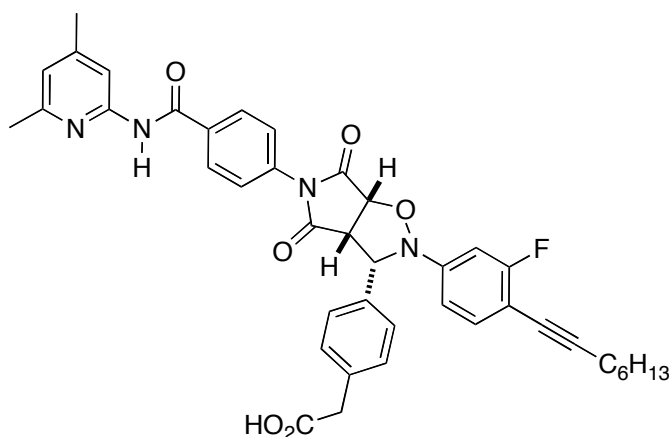
Template *trans*-146



In an NMR tube, maleimide **72** (5.94 mg, 16.0 μmol) in CDCl₃ (400 μL) was combined with a solution of nitrone **141** (5.87 mg, 16.0 μmol) in CDCl₃ (400 μL). After 48 hours at 0 °C, the reaction showed complete conversion. Removal of the solvent provided sufficiently pure material (*trans/cis* > 25:1). ¹H NMR (300.1 MHz, CDCl₃): δ_H 11.90 (s, 1H, NH), 8.25 (s, 1H, Ar

CH), 8.17 (d, $J = 8.7$ Hz, 2H, Ar CH), 8.15 (s, 1H, Ar CH), 8.06 (d, $J = 7.8$ Hz, 1H, Ar CH), 7.58 (d, $J = 7.9$ Hz, 1H, Ar CH), 7.43 (t, $J = 7.7$ Hz, 1H, Ar CH), 7.22 (d, $J = 8.0$ Hz, 1H, Ar CH), 7.18 (d, $J = 8.6$ Hz, 2H, Ar CH), 6.84-6.76 (m, 3H, Ar CH), 5.65 (s, 1H, CH), 5.22 (d, $J = 7.3$ Hz, 1H, CH), 4.21 (d, $J = 7.4$ Hz, 1H, CH), 2.56 (s, 3H, CH₃), 2.42 (s, 3H, CH₃), 2.39 (t, $J = 7.1$ Hz, 2H, CH₂), 1.63-1.53 (m, 2H, CH₂), 1.46-1.39 (m, 2H, CH₂), 1.34-1.25 (m, 4H, 2 × CH₂), 0.89-0.85 (m, 3H, CH₃). ¹³C NMR (75.5 MHz, CDCl₃): δ_c 173.9 (quat. C), 173.0 (quat. C), 171.3 (quat. C), 166.5 (quat. C), 163.2 (d, $J = 250.9$ Hz, quat. C), 155.0 (quat. C), 152.9 (quat. C), 151.5 (quat. C), 148.5 (d, $J = 8.6$ Hz, quat. C), 137.2 (quat. C), 135.2 (quat. C), 134.2 (d, $J = 2.5$ Hz, CH), 134.2 (quat. C), 132.7 (CH), 132.0 (quat. C), 129.9 (CH), 129.8 (CH), 128.9 (CH), 128.4 (CH), 125.7 (CH), 121.3 (CH), 114.0 (CH), 110.7 (d, $J = 2.4$ Hz, CH), 107.3 (d, $J = 16.3$ Hz, quat. C), 103.1 (d, $J = 26.3$ Hz, CH), 95.6 (d, $J = 3.0$ Hz, quat. C), 77.4 (CH), 73.3 (quat. C), 69.8 (CH), 56.0 (CH), 31.5 (CH₂), 28.7 (CH₂), 28.7 (CH₂), 22.7 (CH₂), 21.8 (2 × CH₃), 19.8 (CH₂), 14.2 (CH₃). ¹⁹F NMR (282 MHz, CDCl₃): δ_F -108.8. MS (ES⁺) m/z 689 (90%, [M+H]⁺), 322 (100%). HRMS (ES⁺) calc. for C₄₀H₃₈N₄O₆F 689.2775, found 689.2789.

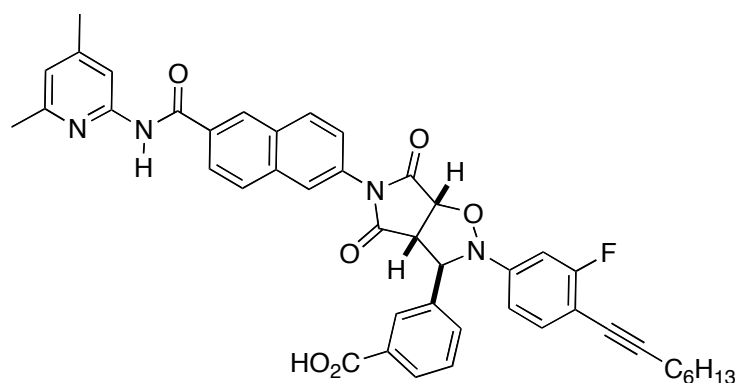
AB product *cis*-148



In an NMR tube, maleimide **72** (5.14 mg, 16.0 μ mol) in CDCl₃ (400 μ L) was combined with a solution of nitrone **142** (6.09 mg, 16.0 μ mol) in CDCl₃ (400 μ mol). After 48 hours at 0 °C, the reaction showed complete conversion of the starting materials and the *cis*-isomer could be characterised (*cis/trans* = 3:1). ¹H NMR (400.1 MHz, CDCl₃): δ_H 10.81 (s, 1H, NH), 8.00 (s, 1H, Ar CH), 7.81 (d, $J = 8.4$ Hz, 2H, Ar CH), 7.31 (d, $J = 8.0$ Hz, 2H, Ar CH), 7.16-7.12 (m, 3H, Ar CH), 7.01 (d, $J = 8.3$ Hz, 2H, Ar CH), 6.78 (dd, $J = 10.9, 1.9$ Hz, 1H, Ar CH), 6.70 (s, 1H, Ar CH), 6.62 (dd, $J = 8.5, 1.8$ Hz, 1H, Ar CH), 5.08 (d, $J = 8.0$ Hz, 1H, CH), 4.95 (d, $J = 8.9$ Hz, 1H, CH), 4.08 (t, $J = 8.7$ Hz, 1H, CH), 3.56 (s, 2H, CH₂), 2.33 (s, 3H, CH₃), 2.33 (t, $J = 4.7$ Hz, 2H, CH₂), 2.30 (s, 3H, CH₃), 1.63-1.53 (m, 2H, CH₂), 1.46-1.39 (m, 2H, CH₂), 1.34-1.25 (m, 4H, 2 × CH₂), 0.89-0.85 (m, 3H, CH₃). ¹³C NMR (100.6 MHz, CDCl₃): δ_c 176.5 (quat. C), 172.1 (quat.

C), 170.5 (quat. C), 166.3 (quat. C), 163.0 (d, $J = 250.8$ Hz, quat. C), 155.1 (quat. C), 152.5 (quat. C), 151.2 (quat. C), 149.2 (d, $J = 8.9$ Hz, quat. C), 135.5 (quat. C), 134.5 (quat. C), 134.4 (quat. C), 134.0 (d, $J = 2.8$ Hz, CH), 133.9 (quat. C), 132.8 (quat. C), 130.6 (CH), 128.9 (CH), 127.8 (CH), 125.7 (CH), 121.2 (CH), 113.6 (CH), 112.3 (d, $J = 3.0$ Hz, CH), 108.4 (d, $J = 16.2$ Hz, quat. C), 104.5 (d, $J = 26.2$ Hz, CH), 96.0 (d, $J = 3.2$ Hz, quat. C), 77.4 (CH), 72.0 (CH), 54.4 (CH), 40.6 (CH₂), 31.5 (CH₂), 28.7 (CH₂), 28.7 (CH₂), 22.7 (CH₂), 22.0 (CH₃), 21.7 (CH₃), 19.8 (CH₂), 14.2 (CH₃). ¹⁹F NMR (375.5 MHz, CDCl₃): δ_F -108.9. MS (ES+) m/z 703 (25%, [M+H]⁺), 322 (100%). HRMS (ES+) calc. for C₄₁H₄₀N₄O₆F 703.2932, found 703.2947.

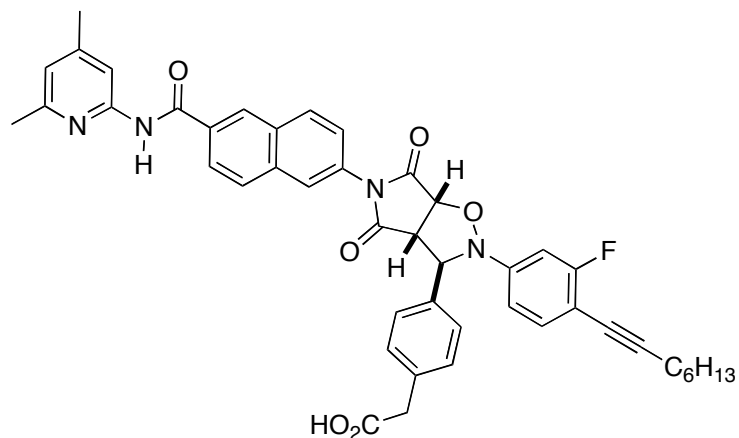
Template *trans*-147



In an NMR tube, maleimide **74** (5.94 mg, 16.0 μ mol) in CDCl₃ (400 μ L) was combined with a solution of nitrone **141** (5.86 mg, 16.0 μ mol) in CDCl₃ (400 μ L). After 48 hours at 0 °C, the reaction showed complete conversion. Removal of the solvent provided sufficiently pure cycloadduct (*trans/cis* > 30:1). ¹H NMR (400.1 MHz, d₆-DMSO): δ_H 10.83 (s, 1H, NH), 8.73 (s, 1H, Ar CH), 8.16 (s, 1H, Ar CH), 8.12-8.09 (m, 2H, Ar CH), 7.98-7.92 (m, 3H, Ar CH), 7.81 (d, $J = 8.0$ Hz, 1H, Ar CH), 7.58 (t, $J = 7.7$ Hz, 1H, Ar CH), 7.41 (t, $J = 8.3$ Hz, 1H, Ar CH), 7.24 (dd, $J = 11.8, 2.2$ Hz, 1H, Ar CH), 7.13 (dd, $J = 8.6, 2.2$ Hz, 1H, Ar CH), 7.08 (dd, $J = 8.7, 1.9$ Hz, 1H, Ar CH), 7.01 (s, 1H, Ar CH), 6.90 (s, 1H, Ar CH), 6.17 (s, 1H, CH), 5.52 (d, $J = 7.3$ Hz, 1H, CH), 4.26 (d, $J = 7.3$ Hz, 1H, CH), 2.46 (t, $J = 7.0$ Hz, 2H, CH₂), 2.42 (s, 3H, CH₃), 2.33 (s, 3H, CH₃), 1.58-1.48 (m, 2H, CH₂), 1.45-1.38 (m, 2H, CH₂), 1.31-1.21 (m, 4H, 2 \times CH₂), 0.88-0.80 (m, 3H, CH₃). ¹³C NMR (100.6 MHz, d₆-DMSO): δ_C 174.1 (quat. C), 172.9 (quat. C), 167.1 (quat. C), 165.6 (quat. C), 162.3 (d, $J = 247.7$ Hz, quat. C), 156.2 (quat. C), 151.6 (quat. C), 150.2 (d, $J = 9.5$ Hz, quat. C), 149.0 (quat. C), 139.1 (quat. C), 134.0 (d, $J = 1.9$ Hz, CH), 133.7 (quat. C), 132.5 (quat. C), 131.4 (quat. C), 131.3 (CH), 131.1 (quat. C), 130.6 (quat. C), 130.2 (CH), 129.1 (CH), 128.8 (CH), 128.5 (CH), 127.9 (CH), 127.8 (CH), 125.5 (CH), 124.7 (CH), 124.5 (CH), 120.1 (CH), 112.1 (CH), 110.6 (d, $J = 2.9$ Hz, CH), 105.1 (d, $J = 16.2$ Hz, quat. C), 102.0 (d, $J = 26.9$ Hz, quat. C), 95.3 (d, $J = 2.8$ Hz, quat. C), 78.2 (CH), 73.4 (quat. C), 68.0 (CH), 56.4 (CH), 30.8

(CH₂), 28.1 (CH₂), 27.9 (CH₂), 23.4 (CH₃), 22.0 (CH₂), 20.9 (CH₃), 18.8 (CH₂), 13.8 (CH₃). ¹⁹F NMR (282 MHz, CDCl₃): δ_F -108.6. HRMS (MALDI) calc. for C₄₄H₄₀N₄O₆F 739.2926, found 739.2632.

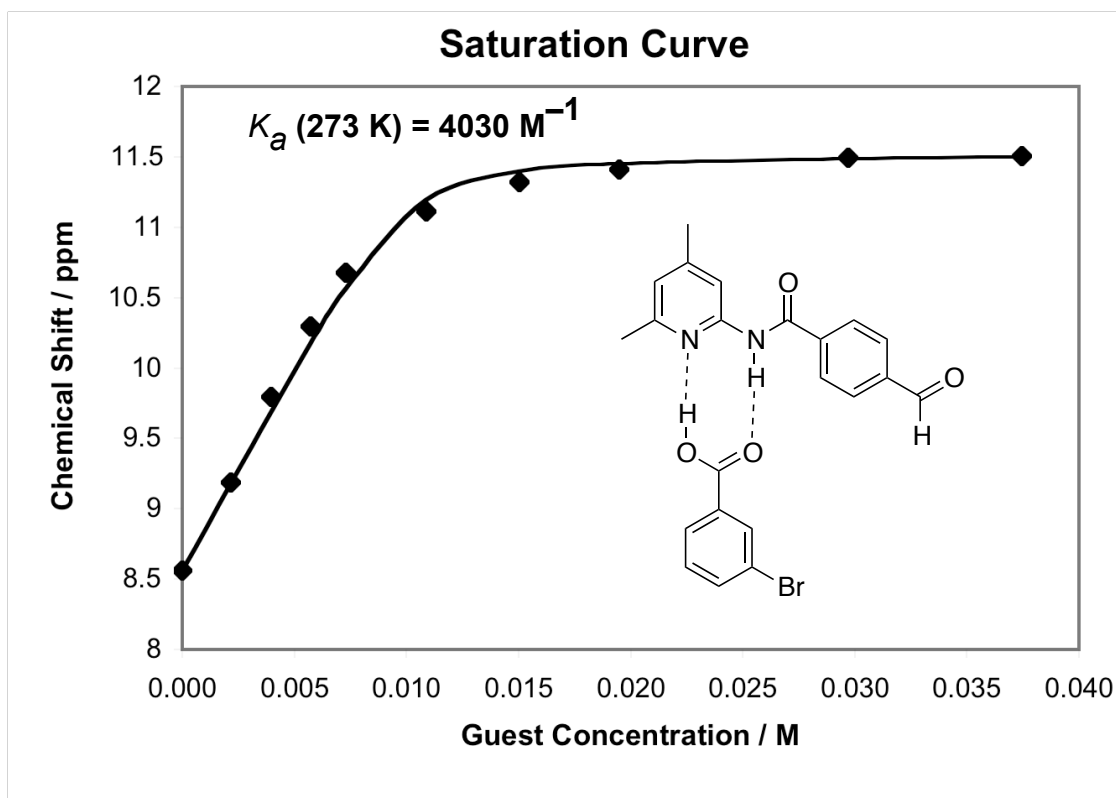
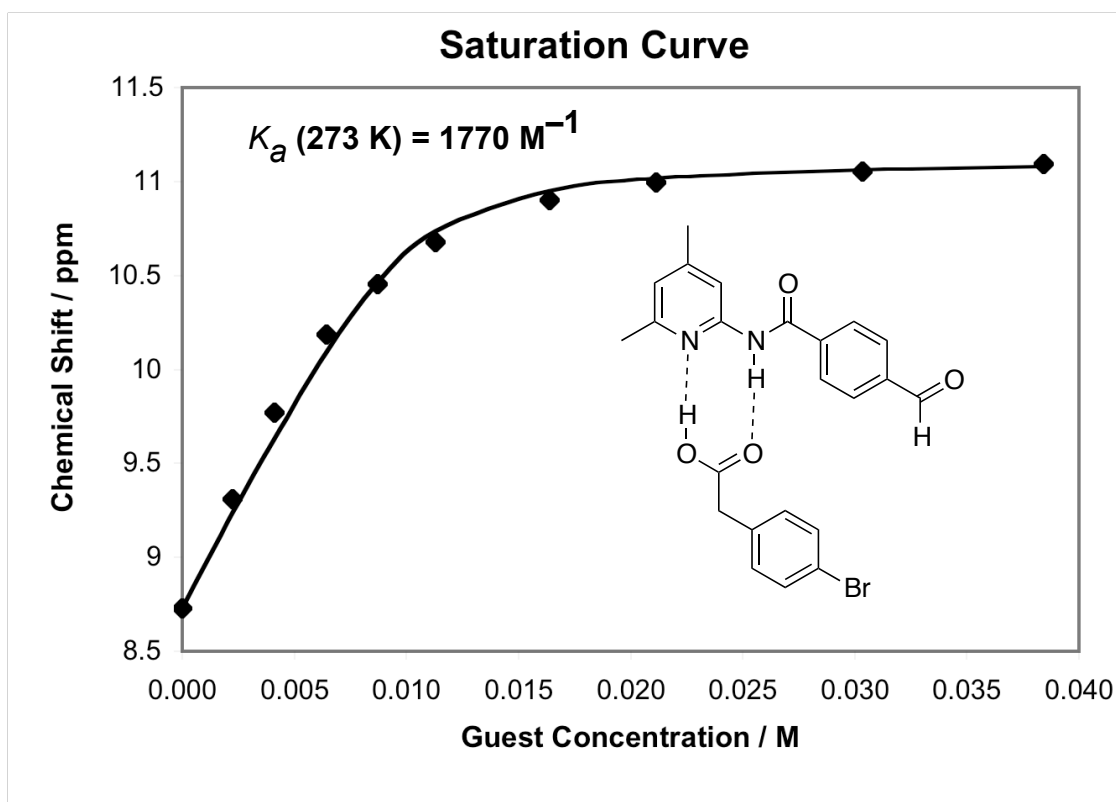
Template *trans*-149



In an NMR tube, maleimide **74** (5.94 mg, 16.0 μmol) in CDCl₃ (400 μL) was combined with a solution of nitrone **142** (6.09 mg, 16.0 μmol) in CDCl₃ (400 μL). After 48 hours at 0 °C, the reaction showed complete conversion of the starting materials and proved sufficiently pure for characterisation (*trans/cis* > 20:1). ¹H NMR (300.1 MHz, CDCl₃): δ_H 11.28 (s, 1H, NH), 8.58 (s, 1H, Ar CH), 8.29 (s, 1H, Ar CH), 8.11 (dd, *J* = 8.6, 1.4 Hz, 1H, Ar CH), 7.85 (d, *J* = 8.5 Hz, 1H, Ar CH), 7.46 (t, *J* = 8.8 Hz, 1H, Ar CH), 7.32-7.21 (m, 1H, Ar CH), 7.30 (d, *J* = 8.4 Hz, 2H, Ar CH), 7.22 (d, *J* = 8.3 Hz, 2H, Ar CH), 7.01-6.92 (m, 3H, Ar CH), 6.86 (dd, *J* = 8.5, 2.1 Hz, 1H, Ar CH), 6.82 (s, 1H, Ar CH), 5.65 (s, 1H, CH), 5.05 (d, *J* = 7.4 Hz, 1H, CH), 3.92 (d, *J* = 7.4 Hz, 1H, CH), 3.75 (s, 2H, CH₂), 2.49 (s, 3H, CH₃), 2.45 (t, *J* = 7.2 Hz, 2H, CH₂), 2.42 (s, 3H, CH₃), 1.68-1.57 (m, 2H, CH₂), 1.52-1.42 (m, 2H, CH₂), 1.34-1.25 (m, 4H, 2 × CH₂), 0.91-0.84 (m, 3H, CH₃). ¹³C NMR (100.6 MHz, d₆-DMSO): δ_C 174.4 (quat. C), 173.1 (quat. C), 172.6 (quat. C), 165.6 (quat. C), 162.3 (d, *J* = 247.6 Hz, quat. C), 156.1 (quat. C), 151.5 (quat. C), 150.2 (d, *J* = 9.6 Hz, quat. C), 149.3 (quat. C), 136.8 (quat. C), 134.9 (quat. C), 134.0 (d, *J* = 1.9 Hz, CH), 133.8 (quat. C), 132.5 (quat. C), 131.5 (quat. C), 130.6 (quat. C), 130.1 (CH), 129.7 (CH), 128.5 (CH), 127.9 (CH), 127.0 (CH), 125.5 (CH), 124.9 (CH), 124.6 (CH), 120.2 (CH), 112.2 (CH), 110.6 (d, *J* = 2.4 Hz, CH), 104.9 (d, *J* = 16.1 Hz, quat. C), 102.0 (d, *J* = 26.9 Hz, CH), 95.2 (d, *J* = 2.8 Hz, quat. C), 78.1 (CH), 73.5 (quat. C), 68.2 (CH), 56.3 (CH), 40.3 (CH₂), 30.8 (CH₂), 28.1 (CH₂), 27.9 (CH₂), 23.3 (CH₃), 22.0 (CH₂), 20.9 (CH₃), 18.8 (CH₂), 13.9 (CH₃). ¹⁹F NMR (375.5 MHz, d₆-DMSO): δ_F -110.2. HRMS (MALDI) calc. for C₄₅H₄₂N₄O₆F 753.3083, found 753.3088.

Appendix

A1. Examples of saturation curves



A2. SimFit scripts

A2.1 Example for a bimolecular reaction

```
=====
* Benzene Maleimide + Control Nitroene
=====
* Bimolecular Model - trans and cis product
=====
* rate constant for trans: 1.77E-4 ; cis: 6.97E-5 ; R = 7.5%
=====

DIM (2)

* Bimolecular routes to TRANS

REACTION (A + B --> TRANS) CONSTANT (1, 1.72E-6, 1, 1, 1000)

* Bimolecular routes to CIS

REACTION (A + B --> CIS) CONSTANT (2, 0.61E-6, 2, 1, 1000)

REACTION (COMPILE)

REACTION (SHOW)
CONSTANT (SHOW)

DEFINE (1, TRANS, P, 1) SCALE (3,1)
DEFINE (2, CIS, P, 4) SCALE (3,1)

SELECT (TRANS, CIS)

READ (BIMOLECULAR)
REACTION (DOC)
CONSTANT (DOC)

TIME (SEC)
WIN (0, 60000, 20000, 200, 0, 3e-3, 5e-3, 1e-4)

ASSIGN (OBS, TRANS = TRANS)
ASSIGN (OBS, CIS = CIS)
ASSIGN (SPEC, A = #10e-3)
ASSIGN (SPEC, B = #10e-3)

CHOOSE (EXP1)

INTEG (STIFF, 1E-9, 1, 0.075, 100, 50)

PLOT (OBS, RES)

*Optimise rate constants using simplex

SIMPLEX (PLOT)
SIMPLEX (PLOT)
SIMPLEX (PLOT)
SIMPLEX (PLOT)
SIMPLEX (PLOT)

PLOT (OBS, RES)
```

A2.2 Example for a self-replicating reaction

```

=====
* Carboxy Nitron + Dimethyl Benzene
=====
*
* Replication Model including all bimolecular
*
* Cis = --
* Trans = SR
*
=====
*
* A = Benzene Maleimide
* C = Carboxy Nitron
*
* Best Fit ( R = 1.62 %)
* k1 = 1.556E-02
* k2 = 3.363E-01
* 33 = 70
*
=====

DIM (2)

* Bimolecular routes to TRANS
REACTION (A + C --> TRANS )          CONSTANT ( 1, 2.23E-4, 0)

* Bimolecular routes to CIS
REACTION (A + C --> CIS )            CONSTANT ( 2, 1.14E-4, 0)

* Formation of binary complexes
REACTION (A + TRANS ==> ATRANS )     CONSTANT ( 3, 1E9, 0) CONSTANT ( 4, 2.50E+5, 0)
REACTION (C + TRANS ==> CTRANS )     CONSTANT ( 5, 1E9, 0) CONSTANT ( 6, 2.50E+5, 0)
REACTION (A + CTRANS ==> ACTRANS )    CONSTANT ( 7, 1E9, 0) CONSTANT ( 8, 2.50E+5, 0)
REACTION (C + ATRANS ==> ACTRANS )    CONSTANT ( 9, 1E9, 0) CONSTANT (10, 2.50E+5, 0)
REACTION (A + CIS ==> ACIS )          CONSTANT (11, 1E9, 0) CONSTANT (12, 2.50E+5, 0)
REACTION (C + CIS ==> CCIS )          CONSTANT (13, 1E9, 0) CONSTANT (14, 2.50E+5, 0)
REACTION (A + CCIS ==> ACCIS )        CONSTANT (15, 1E9, 0) CONSTANT (16, 2.50E+5, 0)
REACTION (C + ACIS ==> ACCIS )        CONSTANT (17, 1E9, 0) CONSTANT (18, 2.50E+5, 0)

* Ternary complex reaction
REACTION (ACTRANS --> TRANSTRANS )    CONSTANT (19, 2E-4, 1, 1, 1000)

* Product duplexes - only [TRANS*TRANS] is stable beyond one Pyr*COOH association
REACTION (TRANS + TRANS ==> TRANSTRANS ) CONSTANT (20, 1E9, 0) CONSTANT (21, 1E+1, 2, 1,
100000)
REACTION (CIS + CIS ==> CISCIS )      CONSTANT (22, 1E9, 0) CONSTANT (23, 2.50E+5, 0)
REACTION (TRANS + CIS ==> TRANSCIS )   CONSTANT (24, 1E9, 0) CONSTANT (25, 2.50E+5, 0)

* AB reaction gives CIS
REACTION (A + C ==> AC)               CONSTANT (26, 1E9, 0) CONSTANT (27, 2.50E+5, 0)

*Bimolecular Reactions of Complexes

REACTION (ACIS + C --> TRANS + CIS )   CONSTANT (28, 2.23E-4, 0)
REACTION (CCIS + A --> TRANS + CIS )   CONSTANT (29, 2.23E-4, 0)
REACTION (ATRANS + C --> TRANS + TRANS ) CONSTANT (30, 2.23E-4, 0)
REACTION (CTRANS + A --> TRANS + TRANS ) CONSTANT (31, 2.23E-4, 0)

REACTION (AC + A --> TRANS + A )       CONSTANT (32, 2.23E-4, 0)
REACTION (AC + C --> TRANS + C )       CONSTANT (33, 2.23E-4, 0)
REACTION (AC + AC --> TRANS + A + C )   CONSTANT (34, 2.23E-4, 0)

REACTION (ACIS + CCIS --> TRANS + CIS + CIS ) CONSTANT (35, 2.23E-4, 0)
REACTION (ACIS + CTRANS --> TRANS + TRANS + CIS ) CONSTANT (36, 2.23E-4, 0)
REACTION (ATRANS + CCIS --> TRANS + TRANS + CIS ) CONSTANT (37, 2.23E-4, 0)
REACTION (ATRANS + CTRANS --> TRANS + TRANS + TRANS ) CONSTANT (38, 2.23E-4, 0)

```

```

REACTION (ACIS + C      --> CIS + CIS      )      CONSTANT (39, 1.14E-4, 0)
REACTION (CCIS + A     --> CIS + CIS      )      CONSTANT (40, 1.14E-4, 0)
REACTION (ATRANS + C   --> CIS + TRANS    )      CONSTANT (41, 1.14E-4, 0)
REACTION (CTrans + A   --> CIS + TRANS    )      CONSTANT (42, 1.14E-4, 0)

REACTION (AC + A       --> CIS + A        )      CONSTANT (43, 1.14E-4, 0)
REACTION (AC + C       --> CIS + C        )      CONSTANT (44, 1.14E-4, 0)
REACTION (AC + AC      --> CIS + A + C    )      CONSTANT (45, 1.14E-4, 0)

REACTION (ACIS + CCIS  --> CIS + CIS + CIS  )      CONSTANT (46, 1.14E-4, 0)
REACTION (ACIS + CTRANS --> CIS + TRANS + CIS )      CONSTANT (47, 1.14E-4, 0)
REACTION (ATRANS + CCIS --> CIS + TRANS + CIS )      CONSTANT (48, 1.14E-4, 0)
REACTION (ATRANS + CTRANS --> CIS + TRANS + TRANS )      CONSTANT (49, 1.14E-4, 0)

REACTION (AC + ACIS    --> TRANS + A + CIS  )      CONSTANT (50, 2.23E-4, 0)
REACTION (AC + CCIS    --> TRANS + C + CIS  )      CONSTANT (51, 2.23E-4, 0)
REACTION (AC + ATRANS  --> TRANS + A + TRANS )      CONSTANT (52, 2.23E-4, 0)
REACTION (AC + CTRANS  --> TRANS + C + TRANS )      CONSTANT (53, 2.23E-4, 0)

REACTION (AC + ACIS    --> CIS + A + CIS  )      CONSTANT (54, 1.14E-4, 0)
REACTION (AC + CCIS    --> CIS + C + CIS  )      CONSTANT (55, 1.14E-4, 0)
REACTION (AC + ATRANS  --> CIS + A + TRANS )      CONSTANT (56, 1.14E-4, 0)
REACTION (AC + CTRANS  --> CIS + C + TRANS )      CONSTANT (57, 1.14E-4, 0)

REACTION (ACCIS + A    --> CIS + A + TRANS )      CONSTANT (58, 2.23E-4, 0)
REACTION (ACCIS + C    --> CIS + C + TRANS )      CONSTANT (59, 2.23E-4, 0)
REACTION (ACTRANS + A  --> TRANS + A + TRANS )      CONSTANT (60, 2.23E-4, 0)
REACTION (ACTRANS + C  --> TRANS + C + TRANS )      CONSTANT (61, 2.23E-4, 0)

REACTION (ACCIS + A    --> CIS + A + CIS  )      CONSTANT (62, 1.14E-4, 0)
REACTION (ACCIS + C    --> CIS + C + CIS  )      CONSTANT (63, 1.14E-4, 0)
REACTION (ACTRANS + A  --> TRANS + A + CIS  )      CONSTANT (64, 2.23E-4, 0)
REACTION (ACTRANS + C  --> TRANS + C + CIS  )      CONSTANT (65, 2.23E-4, 0)

REACTION (AC + ACCIS   --> CIS + A + C + CIS  )      CONSTANT (66, 1.14E-4, 0)
REACTION (AC + ACCIS   --> TRANS + A + C + CIS )      CONSTANT (67, 2.23E-4, 0)
REACTION (AC + ACTRANS --> CIS + A + C + TRANS )      CONSTANT (68, 1.14E-4, 0)
REACTION (AC + ACTRANS --> TRANS + A + C + TRANS )      CONSTANT (69, 2.23E-4, 0)

REACTION (COMPILE)

REACTION (SHOW)
CONSTANT (SHOW)

DEFINE (1, TRANS, P, 1) SCALE (3,1)
DEFINE (2, CIS , P, 4) SCALE (3,1)

SELECT (TRANS, CIS)

READ (BENZCAR)
REACTION (DOC)
CONSTANT (DOC)

TIME (SEC)
WIN (0, 80000, 20000, 200, 0, 10E-3, 2E-3, 1E-4)

ASSIGN (OBS, TRANS = TRANS + ATRANS + CTRANS + ACTRANS + 2 TRANSTRANS + TRANSCIS)
ASSIGN (OBS, CIS = CIS + ACIS + CCIS + ACCIS + 2 CISCIS + TRANSCIS)
ASSIGN (SPEC, A = #10e-3 )
ASSIGN (SPEC, C = #10e-3 )

CHOOSE (EXP1)

INTEG (STIFF, 1E-9, 4, 0.05, 200, 100)

PLOT (OBS, RES)

* 10 rounds of Simplex optimizer without screen
* update

OPAR (1E16)

```

SIMPLEX (PLOT)
SIMPLEX (PLOT)
SIMPLEX (PLOT)
SIMPLEX (PLOT)
NEWTON (PLOT)

PLOT (FILE)
PLOT (SPEC)

*SCAN (1.02, 20, 20)

A2.3 Script for the reaction of maleimide 72 with 71

```

=====
* Phenylacetic Nitroene + Dimethyl Benzene
=====
* Replication Model including all bimolecular
*
* Cis   = AB
* Trans = SR
*
=====
*
* A = Benzene Maleimide
* P = Phenylacetic Nitroene
*
* Best Fit ( R = 4.56 % )
*
* k1 = 5.0936 E -3
* k2 = 29.33
* k3 = 6.4765 E -5
*
=====

DIM (3)

* Bimolecular routes to TRANS
REACTION (A + P --> TRANS )          CONSTANT ( 1, 1.84E-4, 0)

* Bimolecular routes to CIS
REACTION (A + P --> CIS   )          CONSTANT ( 2, 1.03E-4, 0)

* Formation of binary complexes
REACTION (A + TRANS ==> ATRANS )     CONSTANT ( 3, 1E9, 0) CONSTANT ( 4, 5.55E+5, 0)
REACTION (P + TRANS ==> PTRANS  )     CONSTANT ( 5, 1E9, 0) CONSTANT ( 6, 5.55E+5, 0)
REACTION (A + PTRANS ==> APTRANS )    CONSTANT ( 7, 1E9, 0) CONSTANT ( 8, 5.55E+5, 0)
REACTION (P + ATRANS ==> APTRANS )    CONSTANT ( 9, 1E9, 0) CONSTANT (10, 5.55E+5, 0)
REACTION (A + CIS   ==> ACIS   )     CONSTANT (11, 1E9, 0) CONSTANT (12, 5.55E+5, 0)
REACTION (P + CIS   ==> PCIS   )     CONSTANT (13, 1E9, 0) CONSTANT (14, 5.55E+5, 0)
REACTION (A + PCIS  ==> APCIS  )     CONSTANT (15, 1E9, 0) CONSTANT (16, 5.55E+5, 0)
REACTION (P + ACIS  ==> APCIS  )     CONSTANT (17, 1E9, 0) CONSTANT (18, 5.55E+5, 0)

* Ternary complex reaction
REACTION (APTRANS      --> TRANSTRANS )  CONSTANT (19, 2E-4, 1, 1, 1000)

* Product duplexes - only [TRANS*TRANS] is stable beyond one Pyr*COOH association
REACTION (TRANS + TRANS ==> TRANSTRANS )  CONSTANT (20, 1E9, 0) CONSTANT (21, 1E+4, 2, 1, 1000)
REACTION (CIS  + CIS   ==> CISCIS   )    CONSTANT (22, 1E9, 0) CONSTANT (23, 5.55E+5, 0)
REACTION (TRANS + CIS  ==> TRANSCIS  )    CONSTANT (24, 1E9, 0) CONSTANT (25, 5.55E+5, 0)

* AB reaction gives CIS
REACTION (A + P          ==> AP)        CONSTANT (26, 1E9, 0) CONSTANT (27, 5.55E+5, 0)

*Bimolecular Reactions of Complexes

REACTION (ACIS + P      --> TRANS + CIS )          CONSTANT (28, 1.84E-4, 0)
REACTION (PCIS + A     --> TRANS + CIS )          CONSTANT (29, 1.84E-4, 0)
REACTION (ATrans + P   --> TRANS + TRANS )        CONSTANT (30, 1.84E-4, 0)
REACTION (PTRANS + A   --> TRANS + TRANS )        CONSTANT (31, 1.84E-4, 0)

REACTION (AP + A       --> TRANS + A )            CONSTANT (32, 1.84E-4, 0)
REACTION (AP + P       --> TRANS + P )            CONSTANT (33, 1.84E-4, 0)
REACTION (AP + AP      --> TRANS + A + P )        CONSTANT (34, 1.84E-4, 0)

REACTION (ACIS + PCIS  --> TRANS + CIS + CIS )    CONSTANT (35, 1.84E-4, 0)
REACTION (ACIS + PTRANS --> TRANS + TRANS + CIS ) CONSTANT (36, 1.84E-4, 0)
REACTION (ATrans + PCIS --> TRANS + TRANS + CIS ) CONSTANT (37, 1.84E-4, 0)
REACTION (ATrans + PTRANS --> TRANS + TRANS + TRANS ) CONSTANT (38, 1.84E-4, 0)

```

```

REACTION (ACIS + P --> CIS + CIS ) CONSTANT (39, 1.03E-4, 0)
REACTION (PCIS + A --> CIS + CIS ) CONSTANT (40, 1.03E-4, 0)
REACTION (ATRANS + P --> CIS + TRANS ) CONSTANT (41, 1.03E-4, 0)
REACTION (PTRANS + A --> CIS + TRANS ) CONSTANT (42, 1.03E-4, 0)

REACTION (AP + A --> CIS + A ) CONSTANT (43, 1.03E-4, 0)
REACTION (AP + P --> CIS + P ) CONSTANT (44, 1.03E-4, 0)
REACTION (AP + AP --> CIS + A + P ) CONSTANT (45, 1.03E-4, 0)

REACTION (ACIS + PCIS --> CIS + CIS + CIS ) CONSTANT (46, 1.03E-4, 0)
REACTION (ACIS + PTRANS --> CIS + TRANS + CIS ) CONSTANT (47, 1.03E-4, 0)
REACTION (ATRANS + PCIS --> CIS + TRANS + CIS ) CONSTANT (48, 1.03E-4, 0)
REACTION (ATRANS + PTRANS --> CIS + TRANS + TRANS ) CONSTANT (49, 1.03E-4, 0)

REACTION (AP + ACIS --> TRANS + A + CIS ) CONSTANT (50, 1.84E-4, 0)
REACTION (AP + PCIS --> TRANS + P + CIS ) CONSTANT (51, 1.84E-4, 0)
REACTION (AP + ATRANS --> TRANS + A + TRANS ) CONSTANT (52, 1.84E-4, 0)
REACTION (AP + PTRANS --> TRANS + P + TRANS ) CONSTANT (53, 1.84E-4, 0)

REACTION (AP + ACIS --> CIS + A + CIS ) CONSTANT (54, 1.03E-4, 0)
REACTION (AP + PCIS --> CIS + P + CIS ) CONSTANT (55, 1.03E-4, 0)
REACTION (AP + ATRANS --> CIS + A + TRANS ) CONSTANT (56, 1.03E-4, 0)
REACTION (AP + PTRANS --> CIS + P + TRANS ) CONSTANT (57, 1.03E-4, 0)

REACTION (APCIS + A --> CIS + A + TRANS ) CONSTANT (58, 1.84E-4, 0)
REACTION (APCIS + P --> CIS + P + TRANS ) CONSTANT (59, 1.84E-4, 0)
REACTION (APTRANS + A --> TRANS + A + TRANS ) CONSTANT (60, 1.84E-4, 0)
REACTION (APTRANS + P --> TRANS + P + TRANS ) CONSTANT (61, 1.84E-4, 0)

REACTION (APCIS + A --> CIS + A + CIS ) CONSTANT (62, 1.03E-4, 0)
REACTION (APCIS + P --> CIS + P + CIS ) CONSTANT (63, 1.03E-4, 0)
REACTION (APTRANS + A --> TRANS + A + CIS ) CONSTANT (64, 1.84E-4, 0)
REACTION (APTRANS + P --> TRANS + P + CIS ) CONSTANT (65, 1.84E-4, 0)

REACTION (AP + APCIS --> CIS + A + P + CIS ) CONSTANT (66, 1.03E-4, 0)
REACTION (AP + APCIS --> TRANS + A + P + CIS ) CONSTANT (67, 1.84E-4, 0)
REACTION (AP + APTRANS --> CIS + A + P + TRANS ) CONSTANT (68, 1.03E-4, 0)
REACTION (AP + APTRANS --> TRANS + A + P + TRANS ) CONSTANT (69, 1.84E-4, 0)

REACTION (AP --> CIS ) CONSTANT (70, 5.55E-3, 3, 1, 1000 )

REACTION (COMPILE)

REACTION (SHOW)
CONSTANT (SHOW)

DEFINE (1, TRANS, P, 1) SCALE (3,1)
DEFINE (2, CIS , P, 4) SCALE (3,1)

SELECT (TRANS, CIS)

READ (BENZPAA)
REACTION (DOC)
CONSTANT (DOC)

TIME (SEC)
WIN (0, 60000, 20000, 200, 0, 7.5E-3, 2.5E-3, 1E-4)

ASSIGN (OBS, TRANS = TRANS + ATRANS + PTRANS + APTRANS + 2 TRANSTRANS + TRANSCIS)
ASSIGN (OBS, CIS = CIS + ACIS + PCIS + APCIS + 2 CISCIS + TRANSCIS)
ASSIGN (SPEC, A = #10e-3 )
ASSIGN (SPEC, P = #10e-3 )

CHOOSE (EXP1)

INTEG (STIFF, 1E-9, 4, 0.05, 200, 100)

PLOT (OBS, RES)

* 10 rounds of Simplex optimizer without screen
* update

```

OPAR (1E16)

SIMPLEX (PLOT)
SIMPLEX (PLOT)
SIMPLEX (PLOT)
SIMPLEX (PLOT)
NEWTON (PLOT)

PLOT (FILE)

*SCAN (1.02, 20, 20)

A2.4 Script for the simulation of SR vs AB competition

```

=====
* Phenylacetic Nitron + Carboxy Nitron + Dimethyl Benzene
=====
*
* A      = Benzene Maleimide
* C      = Carboxy Nitron
* P      = Phenylacetic Nitron
* TRANS  = SR - Phenylacetic
* CIS    = AB - Phenylacetic
* TRANSC = SR - Carboxy
* CISC   = -- - Carboxy
*
=====

MODE (ISOSIM)

* Bimolecular routes to TRANS and TRANSC
REACTION (A + P --> TRANS , 1.84E-4 )
REACTION (A + C --> TRANSC , 2.45E-4 )

* Bimolecular routes to CIS and CISC
REACTION (A + P --> CIS , 1.03E-4 )
REACTION (A + C --> CISC , 1.25E-4 )

* Formation of binary complexes
REACTION (A + TRANS ==> ATRANS , 1E9, 5.55E+5 )
REACTION (C + TRANS ==> CTRANS , 1E9, 2.50E+5 )
REACTION (P + TRANS ==> PTRANS , 1E9, 5.55E+5 )

REACTION (A + CIS ==> ACIS , 1E9, 5.55E+5 )
REACTION (C + CIS ==> CCIS , 1E9, 2.50E+5 )
REACTION (P + CIS ==> PCIS , 1E9, 5.55E+5 )

REACTION (A + TRANSC ==> ATRANSC , 1E9, 2.50E+5 )
REACTION (C + TRANSC ==> CTRANSC , 1E9, 2.50E+5 )
REACTION (P + TRANSC ==> PTRANSC , 1E9, 5.55E+5 )

REACTION (A + CISC ==> ACISC , 1E9, 2.50E+5 )
REACTION (C + CISC ==> CCISC , 1E9, 2.50E+5 )
REACTION (P + CISC ==> PCISC , 1E9, 5.55E+5 )

REACTION (A + PTRANS ==> APTRANS , 1E9, 5.55E+5 )
REACTION (A + CTRANS ==> ACTRANS , 1E9, 5.55E+5 )
REACTION (P + ATRANS ==> APTRANS , 1E9, 5.55E+5 )
REACTION (C + ATRANS ==> ACTRANS , 1E9, 2.50E+5 )

REACTION (A + PCIS ==> APCIS , 1E9, 5.55E+5 )
REACTION (A + CCIS ==> ACCIS , 1E9, 5.55E+5 )
REACTION (P + ACIS ==> APCIS , 1E9, 5.55E+5 )
REACTION (C + ACIS ==> ACCIS , 1E9, 2.50E+5 )

REACTION (A + PTRANSC ==> APTRANSC , 1E9, 2.50E+5 )
REACTION (A + CTRANSC ==> ACTRANSC , 1E9, 2.50E+5 )
REACTION (P + ATRANSC ==> APTRANSC , 1E9, 5.55E+5 )
REACTION (C + ATRANSC ==> ACTRANSC , 1E9, 2.50E+5 )

REACTION (A + PCISC ==> APCISC , 1E9, 2.50E+5 )
REACTION (A + CCISC ==> ACCISC , 1E9, 2.50E+5 )
REACTION (P + ACISC ==> APCISC , 1E9, 5.55E+5 )
REACTION (C + ACISC ==> ACCISC , 1E9, 2.50E+5 )

* Ternary complex reaction
REACTION (APTRANS --> TRANSTRANS , 9.18E-4 )
REACTION (ACTRANSC --> TRANSCTRANSC , 1.15E-2 )

* AB reaction gives CIS
REACTION (A + P ==> AP , 1E9, 5.55E+5 )
REACTION (AP --> CIS , 7.65E-5 )

```


* AB reaction gives unreactive AC complex

REACTION (A + C ==> AC , 1E9, 2.50E+5)

* Product duplexes - only [TRANS*TRANS] and [TRANSC*TRANSC] are stable beyond one Pyr*COOH association

REACTION (TRANS + TRANS ==> TRANSTRANS , 1E9, 1.02E+3)

REACTION (TRANS + CIS ==> TRANSCIS , 1E9, 5.55E+5)

REACTION (TRANS + TRANSC ==> TRANSTRANSC , 1E9, 5.55E+5)

REACTION (TRANS + CISC ==> TRANSCISC , 1E9, 5.55E+5)

REACTION (TRANSC + TRANSC ==> TRANSCTRANSC , 1E9, 2.86E-1)

REACTION (TRANSC + CIS ==> TRANSCCIS , 1E9, 2.50E+5)

REACTION (TRANSC + CISC ==> TRANSCCISC , 1E9, 2.50E+5)

REACTION (CIS + CIS ==> CISCIS , 1E9, 5.55E+5)

REACTION (CIS + CISC ==> CISCISC , 1E9, 5.55E+5)

REACTION (CISC + CISC ==> CISCCISC , 1E9, 2.50E+5)

* Bimolecular Reactions of Complexes

REACTION (AP + A --> TRANS + A , 1.84E-4)

REACTION (AP + P --> TRANS + P , 1.84E-4)

REACTION (AP + AP --> TRANS + A + P , 1.84E-4)

REACTION (AP + A --> CIS + A , 1.03E-4)

REACTION (AP + P --> CIS + P , 1.03E-4)

REACTION (AP + AP --> CIS + A + P , 1.03E-4)

REACTION (AC + A --> TRANSC + A , 2.45E-4)

REACTION (AC + C --> TRANSC + C , 2.45E-4)

REACTION (AC + AC --> TRANSC + A + C , 2.45E-4)

REACTION (AC + A --> CISC + A , 1.25E-4)

REACTION (AC + C --> CISC + C , 1.25E-4)

REACTION (AC + AC --> CISC + A + C , 1.25E-4)

REACTION (AP + C --> TRANSC + P , 2.45E-4)

REACTION (AP + AC --> TRANSC + A + P , 2.45E-4)

REACTION (AP + C --> CISC + P , 1.25E-4)

REACTION (AP + AC --> CISC + A + P , 1.25E-4)

REACTION (AP + ATRANS --> TRANS + TRANS + A , 1.84E-4)

REACTION (AP + CTRANS --> TRANS + TRANSC + P , 2.45E-4)

REACTION (AP + PTRANS --> TRANS + TRANS + P , 1.84E-4)

REACTION (AP + ATRANS --> TRANS + CIS + A , 1.03E-4)

REACTION (AP + CTRANS --> TRANS + CISC + P , 1.25E-4)

REACTION (AP + PTRANS --> TRANS + CIS + P , 1.03E-4)

REACTION (AC + ATRANS --> TRANS + TRANSC + A , 2.45E-4)

REACTION (AC + CTRANS --> TRANS + TRANSC + C , 2.45E-4)

REACTION (AC + PTRANS --> TRANS + TRANS + C , 1.84E-4)

REACTION (AC + ATRANS --> TRANS + CISC + A , 1.25E-4)

REACTION (AC + CTRANS --> TRANS + CISC + C , 1.25E-4)

REACTION (AC + PTRANS --> TRANS + CIS + C , 1.03E-4)

REACTION (AP + ACIS --> CIS + TRANS + A , 1.84E-4)

REACTION (AP + CCIS --> CIS + TRANSC + P , 2.45E-4)

REACTION (AP + PCIS --> CIS + TRANS + P , 1.84E-4)

REACTION (AP + ACIS --> CIS + CIS + A , 1.03E-4)

REACTION (AP + CCIS --> CIS + CISC + P , 1.25E-4)

REACTION (AP + PCIS --> CIS + CIS + P , 1.03E-4)

REACTION (AC + ACIS --> CIS + TRANSC + A , 2.45E-4)

REACTION	(AC	+	CCIS	-->	CIS	+	TRANSC	+	C	,	2.45E-4)
REACTION	(AC	+	PCIS	-->	CIS	+	TRANS	+	C	,	1.84E-4)
REACTION	(AC	+	ACIS	-->	CIS	+	CISC	+	A	,	1.25E-4)
REACTION	(AC	+	CCIS	-->	CIS	+	CISC	+	C	,	1.25E-4)
REACTION	(AC	+	PCIS	-->	CIS	+	CIS	+	C	,	1.03E-4)
REACTION	(AP	+	ATRANS	-->	TRANSC	+	TRANS	+	A	,	1.84E-4)
REACTION	(AP	+	CTRANS	-->	TRANSC	+	TRANSC	+	P	,	2.45E-4)
REACTION	(AP	+	PTRANS	-->	TRANSC	+	TRANS	+	P	,	1.84E-4)
REACTION	(AP	+	ATRANS	-->	TRANSC	+	CIS	+	A	,	1.03E-4)
REACTION	(AP	+	CTRANS	-->	TRANSC	+	CISC	+	P	,	1.25E-4)
REACTION	(AP	+	PTRANS	-->	TRANSC	+	CIS	+	P	,	1.03E-4)
REACTION	(AC	+	ATRANS	-->	TRANSC	+	TRANSC	+	A	,	2.45E-4)
REACTION	(AC	+	CTRANS	-->	TRANSC	+	TRANSC	+	C	,	2.45E-4)
REACTION	(AC	+	PTRANS	-->	TRANSC	+	TRANS	+	C	,	1.84E-4)
REACTION	(AC	+	ATRANS	-->	TRANSC	+	CISC	+	A	,	1.25E-4)
REACTION	(AC	+	CTRANS	-->	TRANSC	+	CISC	+	C	,	1.25E-4)
REACTION	(AC	+	PTRANS	-->	TRANSC	+	CIS	+	C	,	1.03E-4)
REACTION	(AP	+	ACISC	-->	CISC	+	TRANS	+	A	,	1.84E-4)
REACTION	(AP	+	CCISC	-->	CISC	+	TRANSC	+	P	,	2.45E-4)
REACTION	(AP	+	PCISC	-->	CISC	+	TRANS	+	P	,	1.84E-4)
REACTION	(AP	+	ACISC	-->	CISC	+	CIS	+	A	,	1.03E-4)
REACTION	(AP	+	CCISC	-->	CISC	+	CISC	+	P	,	1.25E-4)
REACTION	(AP	+	PCISC	-->	CISC	+	CIS	+	P	,	1.03E-4)
REACTION	(AC	+	ACISC	-->	CISC	+	TRANSC	+	A	,	2.45E-4)
REACTION	(AC	+	CCISC	-->	CISC	+	TRANSC	+	C	,	2.45E-4)
REACTION	(AC	+	PCISC	-->	CISC	+	TRANS	+	C	,	1.84E-4)
REACTION	(AC	+	ACISC	-->	CISC	+	CISC	+	A	,	1.25E-4)
REACTION	(AC	+	CCISC	-->	CISC	+	CISC	+	C	,	1.25E-4)
REACTION	(AC	+	PCISC	-->	CISC	+	CIS	+	C	,	1.03E-4)
REACTION	(AP	+	APTRANS	-->	TRANS	+	TRANS	+	A	+	P , 1.84E-4)
REACTION	(AP	+	ACTRANS	-->	TRANS	+	TRANSC	+	A	+	P , 2.45E-4)
REACTION	(AP	+	ACTRANS	-->	TRANS	+	TRANS	+	A	+	C , 1.84E-4)
REACTION	(AP	+	APTRANS	-->	TRANS	+	CIS	+	A	+	P , 1.03E-4)
REACTION	(AP	+	ACTRANS	-->	TRANS	+	CISC	+	A	+	P , 1.25E-4)
REACTION	(AP	+	ACTRANS	-->	TRANS	+	CIS	+	A	+	C , 1.03E-4)
REACTION	(AC	+	APTRANS	-->	TRANS	+	TRANS	+	A	+	C , 1.84E-4)
REACTION	(AC	+	APTRANS	-->	TRANS	+	TRANSC	+	A	+	P , 2.45E-4)
REACTION	(AC	+	ACTRANS	-->	TRANS	+	TRANSC	+	A	+	C , 2.45E-4)
REACTION	(AC	+	APTRANS	-->	TRANS	+	CIS	+	A	+	P , 1.03E-4)
REACTION	(AC	+	APTRANS	-->	TRANS	+	CISC	+	A	+	P , 1.25E-4)
REACTION	(AC	+	ACTRANS	-->	TRANS	+	CISC	+	A	+	C , 1.25E-4)
REACTION	(AP	+	APCIS	-->	CIS	+	TRANS	+	A	+	P , 1.84E-4)
REACTION	(AP	+	ACCIS	-->	CIS	+	TRANSC	+	A	+	P , 2.45E-4)
REACTION	(AP	+	ACCIS	-->	CIS	+	TRANS	+	A	+	C , 1.84E-4)
REACTION	(AP	+	APCIS	-->	CIS	+	CIS	+	A	+	P , 1.03E-4)
REACTION	(AP	+	ACCIS	-->	CIS	+	CISC	+	A	+	P , 1.25E-4)
REACTION	(AP	+	ACCIS	-->	CIS	+	CIS	+	A	+	C , 1.03E-4)
REACTION	(AC	+	APCIS	-->	CIS	+	TRANS	+	A	+	C , 1.84E-4)
REACTION	(AC	+	APCIS	-->	CIS	+	TRANSC	+	A	+	P , 2.45E-4)
REACTION	(AC	+	ACCIS	-->	CIS	+	TRANSC	+	A	+	C , 2.45E-4)
REACTION	(AC	+	APCIS	-->	CIS	+	CIS	+	A	+	P , 1.03E-4)
REACTION	(AC	+	APCIS	-->	CIS	+	CISC	+	A	+	P , 1.25E-4)
REACTION	(AC	+	ACCIS	-->	CIS	+	CISC	+	A	+	C , 1.25E-4)
REACTION	(AP	+	APTRANS	-->	TRANSC	+	TRANS	+	A	+	P , 1.84E-4)

REACTION	(AP	+	ACTRANS	-->	TRANSC	+	TRANSC	+	A	+	P	, 2.45E-4)
REACTION	(AP	+	ACTRANS	-->	TRANSC	+	TRANS	+	A	+	C	, 1.84E-4)
REACTION	(AP	+	APTRANS	-->	TRANSC	+	CIS	+	A	+	P	, 1.03E-4)
REACTION	(AP	+	ACTRANS	-->	TRANSC	+	CISC	+	A	+	P	, 1.25E-4)
REACTION	(AP	+	ACTRANS	-->	TRANSC	+	CIS	+	A	+	C	, 1.03E-4)
REACTION	(AC	+	APTRANS	-->	TRANSC	+	TRANS	+	A	+	C	, 1.84E-4)
REACTION	(AC	+	APTRANS	-->	TRANSC	+	TRANSC	+	A	+	P	, 2.45E-4)
REACTION	(AC	+	ACTRANS	-->	TRANSC	+	TRANSC	+	A	+	C	, 2.45E-4)
REACTION	(AC	+	APTRANS	-->	TRANSC	+	CIS	+	A	+	P	, 1.03E-4)
REACTION	(AC	+	APTRANS	-->	TRANSC	+	CISC	+	A	+	P	, 1.25E-4)
REACTION	(AC	+	ACTRANS	-->	TRANSC	+	CISC	+	A	+	C	, 1.25E-4)
REACTION	(AP	+	APCISC	-->	CISC	+	TRANS	+	A	+	P	, 1.84E-4)
REACTION	(AP	+	ACCISC	-->	CISC	+	TRANSC	+	A	+	P	, 2.45E-4)
REACTION	(AP	+	ACCISC	-->	CISC	+	TRANS	+	A	+	C	, 1.84E-4)
REACTION	(AP	+	APCISC	-->	CISC	+	CIS	+	A	+	P	, 1.03E-4)
REACTION	(AP	+	ACCISC	-->	CISC	+	CISC	+	A	+	P	, 1.25E-4)
REACTION	(AP	+	ACCISC	-->	CISC	+	CIS	+	A	+	C	, 1.03E-4)
REACTION	(AC	+	APCISC	-->	CISC	+	TRANS	+	A	+	C	, 1.84E-4)
REACTION	(AC	+	APCISC	-->	CISC	+	TRANSC	+	A	+	P	, 2.45E-4)
REACTION	(AC	+	ACCISC	-->	CISC	+	TRANSC	+	A	+	C	, 2.45E-4)
REACTION	(AC	+	APCISC	-->	CISC	+	CIS	+	A	+	P	, 1.03E-4)
REACTION	(AC	+	APCISC	-->	CISC	+	CISC	+	A	+	P	, 1.25E-4)
REACTION	(AC	+	ACCISC	-->	CISC	+	CISC	+	A	+	C	, 1.25E-4)
REACTION	(CTRANS	+	A	-->	TRANSC	+	TRANS					, 2.45E-4)
REACTION	(PTRANS	+	A	-->	TRANS	+	TRANS					, 1.84E-4)
REACTION	(ATRANS	+	C	-->	TRANSC	+	TRANS					, 2.45E-4)
REACTION	(ATRANS	+	P	-->	TRANS	+	TRANS					, 1.84E-4)
REACTION	(CTRANS	+	A	-->	CISC	+	TRANS					, 1.25E-4)
REACTION	(PTRANS	+	A	-->	CIS	+	TRANS					, 1.03E-4)
REACTION	(ATRANS	+	C	-->	CISC	+	TRANS					, 1.25E-4)
REACTION	(ATRANS	+	P	-->	CIS	+	TRANS					, 1.03E-4)
REACTION	(CCIS	+	A	-->	TRANSC	+	CIS					, 2.45E-4)
REACTION	(PCIS	+	A	-->	TRANS	+	CIS					, 1.84E-4)
REACTION	(ACIS	+	C	-->	TRANSC	+	CIS					, 2.45E-4)
REACTION	(ACIS	+	P	-->	TRANS	+	CIS					, 1.84E-4)
REACTION	(CCIS	+	A	-->	CISC	+	CIS					, 1.25E-4)
REACTION	(PCIS	+	A	-->	CIS	+	CIS					, 1.03E-4)
REACTION	(ACIS	+	C	-->	CISC	+	CIS					, 1.25E-4)
REACTION	(ACIS	+	P	-->	CIS	+	CIS					, 1.03E-4)
REACTION	(CTRANS	+	A	-->	TRANSC	+	TRANSC					, 2.45E-4)
REACTION	(PTRANS	+	A	-->	TRANS	+	TRANSC					, 1.84E-4)
REACTION	(ATRANS	+	C	-->	TRANSC	+	TRANSC					, 2.45E-4)
REACTION	(ATRANS	+	P	-->	TRANS	+	TRANSC					, 1.84E-4)
REACTION	(CTRANS	+	A	-->	CISC	+	TRANSC					, 1.25E-4)
REACTION	(PTRANS	+	A	-->	CIS	+	TRANSC					, 1.03E-4)
REACTION	(ATRANS	+	C	-->	CISC	+	TRANSC					, 1.25E-4)
REACTION	(ATRANS	+	P	-->	CIS	+	TRANSC					, 1.03E-4)
REACTION	(CCISC	+	A	-->	TRANSC	+	CISC					, 2.45E-4)
REACTION	(PCISC	+	A	-->	TRANS	+	CISC					, 1.84E-4)
REACTION	(ACISC	+	C	-->	TRANSC	+	CISC					, 2.45E-4)
REACTION	(ACISC	+	P	-->	TRANS	+	CISC					, 1.84E-4)
REACTION	(CCISC	+	A	-->	CISC	+	CISC					, 1.25E-4)
REACTION	(PCISC	+	A	-->	CIS	+	CISC					, 1.03E-4)
REACTION	(ACISC	+	C	-->	CISC	+	CISC					, 1.25E-4)
REACTION	(ACISC	+	P	-->	CIS	+	CISC					, 1.03E-4)
REACTION	(APTRANS	+	A	-->	TRANS	+	TRANS	+	A			, 1.84E-4)

```
REACTION (ACTRANS + A --> TRANS + TRANSC + A , 2.45E-4 )
REACTION (APTRANS + C --> TRANS + TRANSC + P , 2.45E-4 )
REACTION (ACTRANS + C --> TRANS + TRANSC + C , 2.45E-4 )
REACTION (APTRANS + P --> TRANS + TRANS + P , 1.84E-4 )
REACTION (ACTRANS + P --> TRANS + TRANS + C , 1.84E-4 )
```

```
REACTION ( COMPILE )
REACTION ( SHOW )
```

```
INIT ( A , 0.01000 , 1)
INIT ( C , 0.01000 , 2)
INIT ( P , 0.01000 , 3)
INIT ( CIS , 0.00000 , 4)
INIT ( TRANS , 0.00000 , 5)
INIT ( CISC , 0.00000 , 6)
INIT ( TRANSC , 0.00000 , 7)
```

```
INTEG (STIFF, 1E-9, 8, 0.05, 200, 100)
```

```
NUMPLOT ( 100 )
```

```
TIME ( SEC )
```

```
WIN (0, 240000, 24000, 0.1, 0, 10E-3, 2E-3, 1E-4)
```

```
PLOT (FILE)
```

```
PLOT
```

A2.5 Script for the reciprocal system between

```
=====
* Formation of Bisamido naphtha template from Naphtha Maleimide and Elef Nitrone
=====
* Bimolecular Model - trans and cis product
=====
*
* rate constant for trans: 1.31E-4; cis: 6.12E-5 ; R = 5.9%
*
=====

DIM (2)

* Bimolecular routes to TRANS

REACTION (A + B --> TRANS) CONSTANT (1, 1.72E-6, 1, 1, 1000)

* Bimolecular routes to CIS

REACTION (A + B --> CIS) CONSTANT (2, 0.61E-6, 2, 1, 1000)

REACTION (COMPILE)

REACTION (SHOW)
CONSTANT (SHOW)

DEFINE (1, TRANS, P, 1) SCALE (3,1)
DEFINE (2, CIS, P, 4) SCALE (3,1)

SELECT (TRANS, CIS)

READ (BANT)
REACTION (DOC)
CONSTANT (DOC)

TIME (SEC)
WIN (0, 60000, 20000, 200, 0, 3e-3, 5e-3, 1e-4)

ASSIGN (OBS, TRANS = TRANS)
ASSIGN (OBS, CIS = CIS)
ASSIGN (SPEC, A = #10e-3)
ASSIGN (SPEC, B = #10e-3)

CHOOSE (EXP1)

INTEG (STIFF, 1E-9, 1, 0.075, 100, 50)

PLOT (OBS, RES)

*Optimise rate constants using simplex

SIMPLEX (PLOT)
SIMPLEX (PLOT)
SIMPLEX (PLOT)
SIMPLEX (PLOT)
SIMPLEX (PLOT)

PLOT (OBS, RES)
```

A2.6 Simulation script for the recycling experiment in Figure 7.19

```

=====
* Reciprocal and Self-Replicating Systems -
* Simulation of Complete System
*
* A = Amidopyridine Nitrone
* B = Acid Maleimide
* C = Acid Nitorne
* D = Amidopyridine Maleimide
* T1 = Reciprocal Replicator 1
* T2 = Reciprocal Replicator 2
* R1 = Self-Replicator 1
* R2 = Self-Replicator 2
=====

MODE      ( ISOSIM )

=====
* Make the binary complexes and reactions
=====

REACTION (A + B      ==> AB      , 1.00E9, 1.00E+6 )
REACTION (C + D      ==> CD      , 1.00E9, 1.00E+6 )
REACTION (A + C      ==> AC      , 1.00E9, 1.00E+6 )
REACTION (B + D      ==> BD      , 1.00E9, 1.00E+6 )

REACTION (AB + A     --> R1 + A   , 5.00E-5 )
REACTION (AB + B     --> R1 + B   , 5.00E-5 )

REACTION (CD + C     --> R2 + C   , 5.00E-5 )
REACTION (CD + D     --> R2 + D   , 5.00E-5 )

REACTION (      2 AB --> R1 + A + B , 5.00E-5 )
REACTION (      2 CD --> R2 + C + D , 5.00E-5 )
REACTION ( AC + BD   --> T2 + B + C , 5.00E-5 )
REACTION ( AC + BD   --> T1 + A + D , 5.00E-5 )
REACTION ( AC + BD   --> R1 + C + D , 5.00E-5 )
REACTION ( AC + BD   --> R2 + A + B , 5.00E-5 )

REACTION (AC + B     --> T1 + A   , 5.00E-5 )
REACTION (AC + D     --> R2 + A   , 5.00E-5 )
REACTION (AC + B     --> R1 + C   , 5.00E-5 )
REACTION (AC + D     --> T2 + C   , 5.00E-5 )

REACTION (BD + C     --> T1 + D   , 5.00E-5 )
REACTION (BD + A     --> T2 + B   , 5.00E-5 )
REACTION (BD + C     --> R2 + B   , 5.00E-5 )
REACTION (BD + A     --> R1 + D   , 5.00E-5 )

=====
* Make the R1 Replicator
=====

REACTION (A + B      --> R1      , 5.00E-5 )

REACTION (A + R1     ==> AR1     , 1.00E9, 1.00E+6 )
REACTION (B + R1     ==> BR1     , 1.00E9, 1.00E+6 )
REACTION (A + BR1    ==> ABR1    , 1.00E9, 1.00E+6 )
REACTION (B + AR1    ==> ABR1    , 1.00E9, 1.00E+6 )

REACTION (R1 + R1    ==> R1R1    , 1.00E9, 1.00E+3 )

REACTION (ABR1      --> R1R1    , 0.85E-3 )

=====
* Make the R2 Replicator
=====

REACTION (C + D      --> R2      , 5.00E-5 )

```

```

REACTION ( C + R2      ==> CR2      , 1.00E9, 1.00E+6 )
REACTION ( D + R2      ==> DR2      , 1.00E9, 1.00E+6 )
REACTION ( C + DR2     ==> CDR2     , 1.00E9, 1.00E+6 )
REACTION ( D + CR2     ==> CDR2     , 1.00E9, 1.00E+6 )

REACTION ( R2 + R2     ==> R2R2     , 1.00E9, 1.00E+3 )

REACTION ( CDR2        --> R2R2        , 1.00E-3 )

*=====
* Make the T2 Reciprocal Replicator
*=====

REACTION ( A + D      --> T2          , 4.00E-5 )

REACTION ( A + T1     ==> AT1        , 1.00E+9 , 1.00E+6 )
REACTION ( D + T1     ==> DT1        , 1.00E+9 , 1.00E+6 )
REACTION ( A + AT1    ==> AAT1       , 1.00E+9 , 1.00E+6 )
REACTION ( D + AT1    ==> ADT1       , 1.00E+9 , 1.00E+6 )
REACTION ( A + DT1    ==> ADT1       , 1.00E+9 , 1.00E+6 )
REACTION ( D + DT1    ==> DDT1       , 1.00E+9 , 1.00E+6 )

REACTION ( ADT1       --> T1T2       , 1.05E-3 )

REACTION ( A + DT1    --> T1 + T2     , 4.00E-5 )
REACTION ( DT1 + A    --> T1 + T2     , 4.00E-5 )

*=====
* Make the T1 Reciprocal Replicator
*=====

REACTION ( B + C      --> T1          , 4.00E-5 )

REACTION ( C + T2     ==> CT2        , 1.00E+9 , 1.00E+6 )
REACTION ( B + T2     ==> BT2        , 1.00E+9 , 1.00E+6 )
REACTION ( C + CT2    ==> CCT2       , 1.00E+9 , 1.00E+6 )
REACTION ( B + CT2    ==> BCT2       , 1.00E+9 , 1.00E+6 )
REACTION ( C + BT2    ==> BCT2       , 1.00E+9 , 1.00E+6 )
REACTION ( B + BT2    ==> BBT2       , 1.00E+9 , 1.00E+6 )

REACTION ( BCT2       --> T1T2       , 1.35E-3 )

REACTION ( C + BT2    --> T1 + T2     , 4.00E-5 )
REACTION ( CT2 + B    --> T1 + T2     , 4.00E-5 )

REACTION ( T1 + T2    ==> T1T2       , 1.00E+9 , 1.00E+3 )

REACTION ( COMPILER )
REACTION ( SHOW      )

INIT ( A , 0.01000 , 1 )
INIT ( B , 0.01000 , 2 )
INIT ( C , 0.01000 , 3 )
INIT ( D , 0.01000 , 4 )
INIT ( R1 , 0.00000 , 6 )
INIT ( R2 , 0.00000 , 7 )
INIT ( T1 , 0.00000 , 8 )
INIT ( T2 , 0.00000 , 9 )

INTEG (STIFF, 1E-9, 8, 0.05, 200, 200)

NUMPLOT ( 100 )

TIME ( SEC )

WIN (0, 500000, 100000, 0.1, 0, 25E-3, 5E-3, 3E-4)

PLOT (FILE)

PLOT

```

References

- [1] J. D. Watson, F. H. C. Crick, *Nature* **1953**, *171*, 737-738.
- [2] J. D. Watson, F. H. C. Crick, *Nature* **1953**, *171*, 964-967.
- [3] D. Nelkin, M. S. Lindee, *The DNA Mystique: The Gene As a Cultural Icon*, University of Michigan Press, **2004**.
- [4] T. Krude, *DNA: Changing Science and Society*, Cambridge University Press, **2003**.
- [5] A. Eschenmoser, *Tetrahedron* **2007**, *63*, 12821-12844.
- [6] B. M. Rode, D. Fitz, T. Jakschitz, *Chem. Biodivers.* **2007**, *4*, 2674-2702.
- [7] P. A. Lindahl, *Orig. Life Evol. Biosph.* **2004**, *34*, 2674-2702.
- [8] I. Fry, *The Emergence of Life on Earth: A Scientific Overview*, Rutgers University Press, New Brunswick, NJ (USA), **2000**.
- [9] L. E. Orgel, *The Origins of Life: Molecules and Natural Selection*, John Wiley & Sons, Inc., New York, **1973**.
- [10] S. F. Mason, *Chemical Evolution Origin of the Elements, Molecules and Living Systems*, Clarendon Press, Oxford, **1991**.
- [11] G. Zubay, *Origins of Life on the Earth and in the Cosmos*, 2nd ed., Academic Press, San Diego, **2000**.
- [12] B. Alberts, A. Johnson, J. Lewis, M. Raff, K. Roberts, P. Walter, in *Molecular Biology of the Cell*, 5th ed., Garland Science, **2007**, pp. 263-329.
- [13] I. Hubscher, G. Maga, S. Spadari, *Annu. Rev. Biochem.* **2002**, *71*, 133-163.
- [14] E. R. Barry, S. D. Bell, *Microbiol. Mol. Biol. Rev.* **2006**, *70*, 876-887.
- [15] K. Kruger, *Cell* **1982**, *31*, 147-157.
- [16] F. H. Westheimer, *Nature* **1986**, *319*, 534-536.
- [17] J. A. Doudna, T. R. Cech, *Nature* **2002**, *418*, 222-228.
- [18] T. R. Cech, *Bioscience Reports* **2004**, *24*, 363-385.
- [19] J. Demongeota, A. Moreirab, *J. Theor. Biol.* **2007**, *249*, 314-324.
- [20] A. Luptak, J. W. Szostak, *Ribozymes and Catalysis* **2008**, 123-133.
- [21] M. M. Yusupov, G. Z. Yusupova, A. Baucom, K. Lieberman, T. N. Earnest, J. H. D. Cate, H. F. Noller, *Science* **2001**, *292*, 883-896.
- [22] W. Gilbert, *Nature* **1986**, *319*, 618.
- [23] G. F. Joyce, L. E. Orgel, in *The RNA World* (Eds.: R. F. Gesteland, T. R. Cech, J. F. Atkins), Cold Spring Harbor Laboratory Press, New York, **1999**, pp. 49-77.
- [24] D. P. Bartel, P. J. Unrau, *Trends Biochem. Sci.* **1999**, *24*, 9-13.
- [25] G. F. Joyce, *Nature* **1989**, *338*, 217-224.

- [26] L. E. Orgel, *Orig. Life Evol. Biosph.* **2003**, *33*, 211-218.
- [27] A. Eschenmoser, *Science* **1999**, *284*, 2118-2124.
- [28] M. Beier, F. Reck, T. Wagner, R. Krishnamurthy, A. Eschenmoser, *Science* **1999**, *283*, 699-703.
- [29] M. Ferencic, G. Reddy, X. Wu, S. Guntha, J. Nandy, R. Krishnamurthy, A. Eschenmoser, *Chem. Biodivers.* **2004**, *1*, 939-979.
- [30] C. Anastasi, F. E. Buchet, M. A. Crowe, M. Helliwell, J. Raftery, J. D. Sutherland, *Chem. Eur. J.* **2008**, *14*, 2375-2388.
- [31] M. W. Powner, B. Gerland, J. D. Sutherland, *Nature* **2009**, *459*, 239-242.
- [32] M. W. Powner, J. D. Sutherland, *ChemBioChem* **2008**, *9*, 2386-2387.
- [33] M. W. Powner, J. D. Sutherland, *Angew. Chem. Int. Ed.* **2010**, *49*, 4641-4643.
- [34] M. W. Powner, J. D. Sutherland, J. W. Szostak, *J. Am. Chem. Soc.* **2010**, *132*, 16677-16688.
- [35] J. W. Szostak, *Nature* **2009**, *459*, 171-172.
- [36] R. Rohatgi, D. P. Bartel, J. W. Szostak, *J. Am. Chem. Soc.* **1996**, *118*, 3332-3339.
- [37] R. Rohatgi, D. P. Bartel, J. W. Szostak, *J. Am. Chem. Soc.* **1996**, *118*, 3340-3344.
- [38] O. Taran, O. Thoennessen, K. Achilles, G. von Kiedrowski, *J. Sys. Chem.* **2010**, *1:9*, 1-16.
- [39] G. Ertem, *Orig. Life Evol. Biosph.* **2004**, *34*, 549-570.
- [40] A. G. Cairns-Smith, *Chem. Eur. J.* **2008**, *14*, 3830-3839.
- [41] J. P. Ferris, *Orig. Life Evol. Biosph.* **2002**, *32*, 311-332.
- [42] J. P. Ferris, *Philos. Trans. R. Soc. London, Ser. B* **2006**, *361*, 1777-1786.
- [43] A. J. Hager, J. D. Pollard, J. W. Szostak, *Chem. Biol.* **1996**, *3*, 717-725.
- [44] R. K. Saiki, D. H. Gelfand, S. Stoffel, S. J. Scharf, R. Higuchi, G. T. Horn, K. B. Mullis, H. A. Erlich, *Science* **1988**, *239*, 487-491.
- [45] K. B. Mullis, *Sci. Am.* **1990**, *262*, 56-65.
- [46] J. W. Szostak, D. P. Bartel, P. L. Luisi, *Nature* **2001**, *409*, 387-390.
- [47] P. Stanó, P. L. Luisi, *Chem. Comm.* **2010**, *46*, 3639-3653.
- [48] P. Walde, *BioEssays* **2010**, *32*, 296-303.
- [49] W. K. Johnston, P. J. Unrau, M. S. Lawrence, M. E. Glasner, D. P. Bartel, *Science* **2001**, *292*, 1319-1325.
- [50] J. Rogers, G. F. Joyce, *RNA* **2001**, *7*, 395-404.
- [51] N. Paul, G. F. Joyce, *PNAS* **2002**, *99*, 12733-12740.
- [52] B. J. Lam, G. F. Joyce, *Nat. Biotechnol.* **2009**, *27*, 288-292.
- [53] D.-E. Kim, G. F. Joyce, *Chem. Biol.* **2004**, *11*, 1505-1512.
- [54] T. A. Lincoln, G. F. Joyce, *Science* **2009**, *323*, 1229-1232.

- [55] L. E. Orgel, *Nature* **1992**, 358, 203-209.
- [56] S. Hoffmann, *Angew. Chem. Int. Ed.* **1992**, 31, 1013-1016.
- [57] J. Burmeister, in *Molecular Origins of Life*, Cambridge University Press, **1998**, pp. 295-311.
- [58] P. L. Luisi, in *The Emergence of Life*, Cambridge University Press, **2006**, pp. 129-153.
- [59] A. Vidonne, D. Philp, *Tetrahedron* **2008**, 64, 8464-8475.
- [60] G. von Kiedrowski, J. Helbing, B. Wlotzka, S. Jordan, M. Mathen, T. Achilles, D. Sievers, A. Terfort, B. C. Kahrs, *Nachr. Chem. Tech. Lab.* **1992**, 40, 578-588.
- [61] M. Famulok, J. S. Nowick, J. R. Jr., *Acta Chem. Scand.* **1992**, 46, 315-324.
- [62] D. Sievers, T. Achilles, J. Burmeister, S. Jordan, A. Terfort, G. von Kiedrowski, *NATO ASI Ser., Ser. C* **1994**, 446, 46-64.
- [63] B. G. Bag, G. von Kiedrowski, *Pure & Appl. Chem.* **1996**, 68, 2145-2152.
- [64] D. H. Lee, K. Severin, M. R. Ghadiri, *Curr. Opin. Chem. Biol.* **1997**, 1, 491-496.
- [65] E. K. Wilson, *Chem. Eng. News* **1998**, 76.
- [66] A. Robertson, A. J. Sinclair, D. Philp, *Chem. Soc. Rev.* **2000**, 29, 141-152.
- [67] N. Paul, G. F. Joyce, *Curr. Opin. Chem. Biol.* **2004**, 8, 634-639.
- [68] V. Patzke, G. von Kiedrowski, *ARKIVOC* **2007**, 5, 293-310.
- [69] G. von Kiedrowski, *Bioorg. Chem. Front.* **1993**, 3, 113-146.
- [70] K. Soai, T. Shibata, I. Sato, *Acc. Chem. Res.* **2000**, 33, 382-390.
- [71] D. G. Blackmond, *Asymmetric Synthesis* **2007**, 181-185.
- [72] T. R. Kelly, C. Zhao, G. J. Bridger, *J. Am. Chem. Soc.* **1989**, 111, 3744-3745.
- [73] T. R. Kelly, G. J. Bridger, C. Zhao, *J. Am. Chem. Soc.* **1990**, 112, 8024-8034.
- [74] I. Stahl, G. von Kiedrowski, *J. Am. Chem. Soc.* **2006**, 128, 14014-14015.
- [75] D. N. Reinhoudt, D. M. Rudkevich, F. de Jong, *J. Am. Chem. Soc.* **1996**, 118, 6880-6889.
- [76] G. von Kiedrowski, *Angew. Chem. Int. Ed.* **1986**, 25, 932-935.
- [77] T. Inoue, G. F. Joyce, K. Grzeskowiak, L. E. Orgel, J. M. Brown, C. B. Reese, *J. Mol. Biol.* **1984**, 669-676.
- [78] G. von Kiedrowski, B. Wlotzka, J. Helbing, *Angew. Chem. Int. Ed.* **1989**, 28, 1235-1237.
- [79] W. S. Zielinski, L. E. Orgel, *Nature* **1987**, 327, 346-347.
- [80] G. von Kiedrowski, B. Wlotzka, J. Helbing, M. Matzen, S. Jordan, *Angew. Chem. Int. Ed.* **1991**, 30, 423-426.
- [81] T. Li, K. C. Nicolaou, *Nature* **1994**, 369, 218-221.
- [82] A. Luther, R. Brandtsch, G. von Kiedrowski, *Nature* **1998**, 396, 245-248.
- [83] T. Achilles, G. von Kiedrowski, *Angew. Chem. Int. Ed.* **1993**, 32, 1198-1201.
- [84] D. Sievers, G. von Kiedrowski, *Nature* **1994**, 369, 221-224.

- [85] D. Sievers, G. von Kiedrowski, *Chem. Eur. J.* **1998**, *4*, 629-641.
- [86] I. Ghosh, J. Chmielewski, *Curr. Opin. Chem. Biol.* **2004**, *8*, 640-644.
- [87] X. Li, J. Chmielewski, *Org. Biomol. Chem.* **2003**, *1*, 901-904.
- [88] D. H. Lee, J. R. Granja, J. A. Martinez, K. Severin, M. R. Ghadiri, *Nature* **1996**, *382*, 525-528.
- [89] K. Severin, D. H. Lee, J. A. Martinez, M. R. Ghadiri, *Chem. Eur. J.* **1997**, *3*, 1017-1024.
- [90] P. E. Dawson, T. W. Muir, I. Clark-Lewis, S. B. H. Kent, *Science* **1994**, *266*, 776-779.
- [91] K. Severin, D. H. Lee, A. J. Kennan, M. R. Ghadiri, *Nature* **1997**, *389*, 706-709.
- [92] S. Yao, I. Ghosh, R. Zutshi, J. Chmielewski, *J. Am. Chem. Soc.* **1997**, *119*, 10559-10560.
- [93] S. Yao, I. Ghosh, R. Zutshi, J. Chmielewski, *Angew. Chem. Int. Ed.* **1998**, *37*, 478-481.
- [94] S. Yao, I. Ghosh, R. Zutshi, J. Chmielewski, *Nature* **1998**, *396*, 447-450.
- [95] R. Issac, J. Chmielewski, *J. Am. Chem. Soc.* **2002**, *124*, 6808-6809.
- [96] X. Li, J. Chmielewski, *J. Am. Chem. Soc.* **2003**, *125*, 11820-11821.
- [97] D. H. Lee, K. Severin, Y. Yokobayashi, M. R. Ghadiri, *Nature* **1997**, *390*, 591-594.
- [98] M. Eigen, P. Schuster, *Naturwissenschaften* **1971**, *58*, 465-523.
- [99] B.-O. Küppers, *Information and the Origin of Life*, MIT Press, Cambridge, MA (USA), **1990**.
- [100] M. Eigen, P. Schuster, *The Hypercycle: A Principle of Natural Self-Organization*, Springer Verlag, New York, NY (USA), **1979**.
- [101] K. Severin, D. H. Lee, J. A. Martinez, M. Vieth, M. R. Ghadiri, *Angew. Chem. Int. Ed.* **1998**, *37*, 126-128.
- [102] V. Avetisov, *Orig. Life Evol. Biosph.* **2007**, *37*, 367-370.
- [103] F. C. Frank, *Biochim. Biophys. Acta* **1953**, *11*, 459-463.
- [104] D. G. Blackmond, M. Klussmann, *AIChE J.* **2007**, *53*, 2-8.
- [105] M. Levine, C. S. Kenesky, D. Mazori, R. Breslow, *Org. Lett.* **2008**, *10*, 2433-2436.
- [106] D. G. Blackmond, *Angew. Chem. Int. Ed.* **2009**, *48*, 2648-2654.
- [107] D. G. Blackmond, *PNAS* **2004**, *101*, 5732-5736.
- [108] A. Saghatelian, Y. Yokobayashi, K. Soltani, M. R. Ghadiri, *Nature* **2001**, *409*, 797-801.
- [109] G. Ashkenasy, R. Jagasia, M. Yadav, M. R. Ghadiri, *PNAS* **2004**, *101*, 10872-10877.
- [110] G. Ashkenasy, M. R. Ghadiri, *J. Am. Chem. Soc.* **2004**, *126*, 11140-11141.
- [111] B. Rubinov, N. Wagner, H. Rapaport, G. Ashkenasy, *Angew. Chem. Int. Ed.* **2009**, *48*, 6683-6686.
- [112] J. Rebek Jr., *NATO Sci. Ser. I* **2005**, *364*, 91-105.
- [113] A. Vidonne, D. Philp, *Eur. J. Org. Chem.* **2009**, 593-610.
- [114] T. Tjivikua, P. Ballester, J. Rebek Jr., *J. Am. Chem. Soc.* **1990**, *112*, 1249-1250.

- [115] D. S. Kemp, K. S. Petrakis, *J. Org. Chem.* **1989**, *46*, 5140-5143.
- [116] J. S. Nowick, Q. Feng, T. Tjivikua, P. Ballester, J. Rebek Jr., *J. Am. Chem. Soc.* **1991**, *113*, 8831-8839.
- [117] F. M. Menger, A. V. Eliseev, N. A. Khanjin, M. J. Sherrod, *J. Org. Chem.* **1995**, *60*, 2870-2878.
- [118] E. A. Wintner, B. Tsao, J. Rebek Jr., *J. Org. Chem.* **1995**, *60*, 7997-8001.
- [119] F. M. Menger, A. V. Eliseev, N. A. Khanjin, *J. Am. Chem. Soc.* **1994**, *116*, 3613-3614.
- [120] M. Morgan Conn, E. A. Wintner, J. Rebek Jr., *J. Am. Chem. Soc.* **1994**, *116*, 8823-8824.
- [121] V. Rotello, J.-I. Hong, J. Rebek Jr., *J. Am. Chem. Soc.* **1991**, *113*, 9422-9423.
- [122] E. A. Wintner, M. Morgan Conn, J. Rebek Jr., *J. Am. Chem. Soc.* **1994**, *116*, 8877-8884.
- [123] M. Morgan Conn, E. A. Wintner, J. Rebek Jr., *Angew. Chem. Int. Ed.* **1994**, *33*, 1577-1579.
- [124] I. Huc, R. J. Pieters, J. Rebek Jr., *J. Am. Chem. Soc.* **1994**, *116*, 10296-10297.
- [125] R. J. Pieters, I. Huc, J. Rebek Jr., *Angew. Chem. Int. Ed.* **1994**, *33*, 1579-1581.
- [126] R. J. Pieters, I. Huc, J. Rebek Jr., *Tetrahedron* **1995**, *51*, 485-498.
- [127] J.-I. Hong, Q. Feng, V. Rotello, J. Rebek Jr., *Science* **1992**, *255*, 848-850.
- [128] T. K. Park, Q. Feng, J. Rebek Jr., *J. Am. Chem. Soc.* **1992**, *114*, 4529-4532.
- [129] T. K. Park, J. Schroeder, J. Rebek Jr., *J. Am. Chem. Soc.* **1991**, *113*, 5125-5128.
- [130] S. Kamioka, D. Ajami, J. Rebek Jr., *Chem. Comm.* **2009**, 7324-7326.
- [131] S. Kamioka, D. Ajami, J. Rebek Jr., *PNAS* **2010**, *107*, 541-544.
- [132] Q. Feng, T. K. Park, J. Rebek Jr., *Science* **1992**, *256*, 1179-1180.
- [133] A. Terfort, G. von Kiedrowski, *Angew. Chem. Int. Ed.* **1992**, *31*, 654-656.
- [134] B. Wang, I. O. Sutherland, *Chem. Comm.* **1997**, 1495-1496.
- [135] M. Kindermann, I. Stahl, M. Reimold, W. M. Pankau, G. von Kiedrowski, *Angew. Chem. Int. Ed.* **2005**, *44*, 6750-6755.
- [136] V. C. Allen, D. Philp, N. Spencer, *Org. Lett.* **2001**, *3*, 777-780.
- [137] E. Kassianidis, R. J. Pearson, D. Philp, *Org. Lett.* **2005**, *7*, 3833-3836.
- [138] E. Kassianidis, D. Philp, *Chem. Comm.* **2006**, 4072-4074.
- [139] E. Kassianidis, R. J. Pearson, E. A. Wood, D. Philp, *Faraday Discuss.* **2010**, *145*, 235-254.
- [140] E. Kassianidis, D. Philp, *Angew. Chem. Int. Ed.* **2006**, *45*, 6344-6348.
- [141] R. J. Pearson, E. Kassianidis, A. M. Z. Slawin, D. Philp, *Org. Biomol. Chem.* **2004**, *2*, 3434-3441.
- [142] R. J. Pearson, E. Kassianidis, A. M. Z. Slawin, D. Philp, *Chem. Eur. J.* **2006**, *12*, 6829-6840.
- [143] E. Kassianidis, R. J. Pearson, D. Philp, *Chem. Eur. J.* **2006**, *12*, 8798-8812.
- [144] J. R. Nitschke, *Acc. Chem. Res.* **2007**, *40*, 103-112.

- [145] R. F. Ludlow, S. Otto, *Chem. Soc. Rev.* **2008**, *37*, 101-108.
- [146] L. J. Prins, P. Scrimin, *Angew. Chem. Int. Ed.* **2009**, *48*, 2288-2306.
- [147] J. Stankiewicz, L. H. Eckardt, *Angew. Chem. Int. Ed.* **2006**, *45*, 342-344.
- [148] J. J. P. Peyralans, S. Otto, *Curr. Opin. Chem. Biol.* **2009**, *13*, 1-9.
- [149] J. R. Nitschke, *Nature* **2009**, *462*, 736-738.
- [150] A. Dieckmann, S. Beniken, C. Lorenz, N. L. Doltsinis, G. von Kiedrowski, *J. Syst. Chem.* **2010**, *1:10*, 1-6.
- [151] A. Dieckmann, S. Beniken, C. D. Lorenz, N. L. Doltsinis, G. von Kiedrowski, *Chem. Eur. J.* **2011**, *17*, 468-480.
- [152] M. N. Stojanovic, T. E. Mitchell, D. Stefanovic, *J. Am. Chem. Soc.* **2002**, *124*, 3555-3561.
- [153] B. M. Frezza, S. L. Cockroft, M. R. Ghadiri, *J. Am. Chem. Soc.* **2007**, *129*, 14875-14879.
- [154] N. Wagner, G. Ashkenasy, *Chem. Eur. J.* **2009**, *2009*, 1765-1775.
- [155] V. C. Allen, C. C. Robertson, S. M. Turega, D. Philp, *Org. Lett.* **2010**, *12*, 1920-1923.
- [156] I. R. Epstein, J. A. Pojman, O. Steinbock, *Chaos* **2006**, *16*, 037101.
- [157] A. F. Taylor, M. R. Tinsley, F. Wang, Z. Y. Huang, K. Showalter, *Science* **2009**, *323*, 614-617.
- [158] J. Horvath, I. Szalai, P. de Kepper, *Science* **2009**, *324*, 772-775.
- [159] V. E. Campbell, J. R. Nitschke, *Synlett.* **2008**, *20*, 3077-3090.
- [160] J. W. Sadownik, R. V. Ulijn, *Curr. Opin. Biotechnol.* **2010**, *21*, 401-411.
- [161] G. Gasparini, M. Dal Molin, L. J. Prins, *Eur. J. Org. Chem.* **2010**, *13*, 2429-2440.
- [162] S. Mirtschin, A. Slabon-Turski, R. Scopelliti, A. H. Velders, K. Severin, *J. Am. Chem. Soc.* **2010**, *132*, 14004-14005.
- [163] P. T. Corbett, J. Leclaire, L. Vial, K. R. West, J.-L. Wietor, J. K. M. Sanders, S. Otto, *Chem. Rev.* **2006**, *106*, 3652-3711.
- [164] S. Ladame, *Org. Biomol. Chem.* **2008**, *6*, 219-226.
- [165] S. Otto, R. L. E. Furlan, J. K. M. Sanders, *Curr. Opin. Chem. Biol.* **2002**, *6*, 321-327.
- [166] C. D. Meyer, C. S. Joiner, J. F. Stoddart, *Chem. Soc. Rev.* **2007**, *36*, 1705-1723.
- [167] S. Otto, K. Severin, *Top. Curr. Chem.* **2007**, *277*, 267-288.
- [168] P. T. Corbett, L. H. Tong, J. K. M. Sanders, S. Otto, *J. Am. Chem. Soc.* **2005**, *127*, 8902-8903.
- [169] S. Otto, S. Kubik, *J. Am. Chem. Soc.* **2003**, *125*, 7804-7805.
- [170] R. F. Ludlow, S. Otto, *J. Am. Chem. Soc.* **2008**, *130*, 12218-12219.
- [171] O. Ramström, J.-M. Lehn, *Nat. Rev. Drug Discovery* **2002**, *1*, 26-36.
- [172] S. Hiraoka, M. Fujita, *J. Am. Chem. Soc.* **1999**, *121*, 10239-10240.

- [173] K. S. Chichak, S. J. Cantrill, A. R. Pease, S.-H. Chiu, G. W. V. Cave, J. L. Atwood, J. F. Stoddart, *Science* **2004**, *304*, 1308-1312.
- [174] Q.-F. Sun, J. Iwasa, D. Ogawa, Y. Ishido, S. Sato, T. Ozeki, Y. Sei, K. Yamaguchi, M. Fujita, *Science* **2010**, *328*, 1144-1147.
- [175] B. Icli, N. Christinat, J. Tönnemann, C. Schüttler, R. Scopelliti, K. Severin, *J. Am. Chem. Soc.* **2009**, *131*, 3154-3155.
- [176] M. Hochgürtel, H. Kroth, D. Piecha, M. Hofmann, C. Nicolau, S. Krause, O. Schaaf, G. Sonnenmoser, A. V. Eliseev, *PNAS* **2002**, *99*, 3382-3391.
- [177] B. Shi, R. Stevenson, D. J. Campopiano, M. F. Greaney, *J. Am. Chem. Soc.* **2006**, *128*, 8459-8467.
- [178] L. Milanesi, C. A. Hunter, S. E. Sedelinkova, J. P. Waltho, *Chem. Eur. J.* **2006**, *12*, 1081-1087.
- [179] D. Schultz, J. R. Nitschke, *Angew. Chem. Int. Ed.* **2006**, *45*, 2453-2456.
- [180] P. Mal, D. Schultz, K. Beyeh, K. Rissanen, J. R. Nitschke, *Angew. Chem. Int. Ed.* **2008**, *47*, 8297-8301.
- [181] P. Mal, B. Breiner, K. Rissanen, J. R. Nitschke, *Science* **2009**, *324*, 1697-1699.
- [182] S. Xu, N. Giuseppone, *J. Am. Chem. Soc.* **2008**, *130*, 1826-1827.
- [183] V. del Amo, D. Philp, *Chem. Eur. J.* **2010**.
- [184] M. Angelin, A. Fischer, O. Ramström, *J. Org. Chem.* **2008**, *73*, 3593-3595.
- [185] V. del Amo, A. M. Z. Slawin, D. Philp, *Org. Lett.* **2008**, *10*, 4589-4592.
- [186] V. del Amo, *Unpublished Results*.
- [187] S. M. Turega, C. Lorenz, J. Sadownik, D. Philp, *Chem. Comm.* **2008**, 4076-4078.
- [188] J. Sadownik, D. Philp, *Angew. Chem. Int. Ed.* **2008**, *47*, 9965-9970.
- [189] F. Garcia-Tellado, S. Goswami, S.-K. Chang, S. J. Geib, A. D. Hamilton, *J. Am. Chem. Soc.* **1990**, *112*, 7393-7394.
- [190] F. Garcia-Tellado, J. Albert, A. D. Hamilton, *J. Chem. Soc., Chem. Commun.* **1991**, 1761-1764.
- [191] M. S. Goodman, J. Weiss, A. D. Hamilton, *Tetrahedron Lett.* **1994**, *35*, 8943-8946.
- [192] A. Vidonne, PhD thesis, University of St Andrews **2009**.
- [193] E. Wood, PhD thesis, University of St Andrews **2007**.
- [194] N. Coskun, A. Öztürk, *Tetrahedron* **2007**, *63*, 1402-1410.
- [195] K. V. Gothelf, K. A. Jørgensen, *Chem. Rev.* **1998**, *98*, 863-909.
- [196] D. A. Ball, S. G. Diaz, V. M. Lynch, E. V. Anslyn, *Tetrahedron Lett.* **1995**, *36*, 4155-4158.
- [197] J. Sadownik, PhD thesis, University of St Andrews **2009**.

- [198] H. C. Brown, *Determination of Organic Structures by Physical Methods*, Academic Press, New York, **1955**.
- [199] S. Hoops, S. Sahle, R. Gauges, C. Lee, J. Pahle, N. Simus, M. Singhal, L. Xu, P. Mendes, U. Kummer, *Bioinformatics* **2006**, *22*, 3067-3074.
- [200] S. M. Turega, D. Philp, *Chem. Comm.* **2006**, *35*, 3684-3686.
- [201] D. Bray, *Nature* **1995**, *376*, 307-312.
- [202] J. E. Dueber, B. J. Yeh, K. Chak, W. A. Lim, *Science* **2003**, *301*, 1904-1908.
- [203] T. Konry, D. R. Walt, *J. Am. Chem. Soc.* **2009**, *131*, 13232-13233.
- [204] E. Szathmary, I. Gladkih, *J. Theor. Biol.* **1989**, *138*, 55-58.
- [205] E. Szathmary, *J. Theor. Biol.* **1997**, *187*, 555-571.
- [206] E. Szathmary, *Philos. Trans. R. Soc. London, Ser. B* **2006**, *361*, 1761-1776.
- [207] G. J. Bauer, J. S. McCaskill, H. Otten, *PNAS* **1989**, *86*, 7937-3941.
- [208] J. S. McCaskill, G. J. Bauer, *PNAS* **1993**, *90*, 4191-4195.
- [209] I. Bottero, *Unpublished Results*.
- [210] W. L. F. Armarego, D. D. Perrin, *Purification of Laboratory Chemicals*, Butterworth-Heinemann, Oxford (UK), **1997**.
- [211] S. J. Cantrill, M. C. T. Fyfe, F. M. Raymo, J. F. Stoddart, in *NMR in Supramolecular Chemistry* (Ed.: M. Pons), Kluwer Academic Publishers, Alphen aan den Rijn (The Netherlands), **1999**, pp. 1-18.
- [212] K. Hirose, in *Analytical Methods in Supramolecular Chemistry* (Ed.: C. A. Schalley), Wiley-VCH, Weinheim (Germany), **2007**, pp. 17-54.
- [213] A. Gea, N. Farcy, N. Roque i Rossell, J. Martins, P. J. De Clercq, A. Madder, *Eur. J. Org. Chem.* **2006**, 4135-4146.
- [214] Y. Chiang, K. Kolmakov, A. J. Kreske, *Can. J. Chem.* **2008**, *86*, 101-104.
- [215] S. Ung, A. Falguieres, A. Guy, C. Ferroud, *Tetrahedron Lett.* **2005**, *46*, 5913-5917.
- [216] S. Bouhayat, S. Piessard, G. Le Baut, L. Sparfel, J.-Y. Petit, F. Piriou, L. Welin, *J. Med. Chem.* **1985**, *28*, 555-559.
- [217] S. Tsuneo, *Bull. Chem. Soc. Jpn.* **1985**, *58*, 2821-2825.
- [218] H. Erlenmeyer, W. Grubenmann, H. Bloch, *Helv. Chim. Acta* **1948**, *31*, 75-77.
- [219] M. J. Zacuto, F. Xu, *J. Org. Chem.* **2007**, *72*, 6298-6300.
- [220] W.-H. Sun, W. Zhang, T. Gao, X. Tang, L. Chen, Y. Li, X. Jin, *J. Organomet. Chem.* **2004**, *689*, 917-929.
- [221] M. Yoshizawa, T. Kusakawa, M. Fujita, K. Yamaguchi, *J. Am. Chem. Soc.* **2000**, *122*, 6311-6312.
- [222] F. Monnier, F. Turtaut, L. Duroure, M. Taillefer, *Org. Lett.* **2008**, *10*, 3203-3206.

- [223] T. Komatsu, Y. Urano, Y. Fujikawa, T. Kobayashi, H. Kojima, T. Terai, K. Hanaoka, T. Nagano, *Chem. Comm.* **2009**, *45*, 7015-7017.
- [224] S. Coco, P. Espinet, J. Martin-Alvarez, A.-M. Levelut, *J. Mater. Chem.* **1997**, *7*, 19-23.